

# UC Berkeley

## UC Berkeley Electronic Theses and Dissertations

### Title

C—C Bond Cleavage of Carvone-Derived Cyclobutanols En Route to Abscisic Acid Analogs and Taxoid Natural Products

### Permalink

<https://escholarship.org/uc/item/0xg40658>

### Author

Wang, Brian S

### Publication Date

2019

Peer reviewed|Thesis/dissertation

C–C Bond Cleavage of Carvone-Derived Cyclobutanols En Route to Abscisic Acid Analogs  
and Taxoid Natural Products

By

Brian S Wang

A dissertation submitted in partial satisfaction of the  
requirements for the degree of  
Doctor of Philosophy  
in  
Chemistry  
in the  
Graduate Division  
of the  
University of California, Berkeley

Committee in charge:

Professor Richmond Sarpong, Chair  
Professor Thomas Maimone  
Professor Zinmay Renee Sung

Fall 2019

C–C Bond Cleavage of Carvone-Derived Cyclobutanols En Route to Abscisic Acid Analogs  
and Taxoid Natural Products

Copyright 2019  
by  
Brian S Wang

## Abstract

### C–C Bond Cleavage of Carvone-Derived Cyclobutanols En Route to Abscisic Acid Analogs and Taxoid Natural Products

by

Brian S Wang

Doctor of Philosophy in Chemistry

University of California, Berkeley

Professor Richmond Sarpong, Chair

This dissertation describes our application of C–C bond cleavage methodology on carvone-derived cyclobutanols to access functionalized cyclohexenones, which have been utilized toward 1) the syntheses of analogs of the plant hormone abscisic acid, and 2) syntheses of the taxagifine-like natural products, a subclass of the taxoid family of natural products. In Chapter 1, we review the most recent applications of transition metal-catalyzed C–C single bond cleavage in natural product synthesis, highlighting how the strategic use of C–C bond cleavage can streamline retrosynthetic efforts. Ten total syntheses from 2014–2019 are discussed, with examples including the use of C–C bond cleavage on both the core and the periphery of synthetic intermediates.

In Chapter 2, we discuss our efforts toward the syntheses of rationally designed analogs of abscisic acid. This chapter first outlines the biology of and previous synthetic efforts toward abscisic acid and its analogs; our computation-aided design of 5',5'-spirocyclic ABA analogs with higher expected potency and metabolic stability, informed by this background, is then described. Our synthetic strategy toward these analogs involves the C–C bond cleavage/olefination of a carvone-derived cyclobutanol to yield a cyclohexenone with various functional groups in place to facilitate further derivatization. We describe the implementation of this strategy to a late stage at the end of this chapter.

In Chapter 3, we review the history, biology, and previous syntheses of the taxoid natural products. While, of the taxoid natural products, taxol has historically been the focus of both biological studies and synthetic work, special emphasis is placed in this chapter on the taxagifine-like natural products, which possess an additional bridging ether ring between C12 and C17. The high *in vitro* bioactivity of originally isolated member taxagifine, despite its myriad structural differences with taxol, suggest that the mechanism of action of the taxagifine-like natural products may involve their adoption of a distinct orientation in the binding site of tubulin; trying to understand this alternative binding yet comparable activity provides a motivation for the pursuit of syntheses of these natural products, which to date have not been reported.

In Chapter 4, we detail the construction of a highly oxygenated 6/8/6/5 tetracyclic core of taxagifine, with C–C bond cleavage/cross-coupling and aldol addition reactions forming two key C–C bonds between two carvone-derived A- and C-ring precursor fragments. Our

investigations of numerous alternative cross-coupling partners and cyclization strategies are also described.

Finally, in Chapter 5, we describe our efforts toward the late-stage functionalization of the tetracyclic core of taxagifine. Specifically, we describe our efforts to 1) introduce the C9,C10-*trans*-diol motif found in taxagifine, 2) install oxidation at C5 and C2, and 3) transpose the C3–C4 alkene while stereoselectively placing a hydrogen atom at C3. Our investigations have culminated in the synthesis of a C10,C2-oxidized late-stage intermediate, whose conversion to natural products taxagifine III and 4-deacetyltaxagifine III in large part involves synthetic transformations that we have studied on model systems. Our examination of methods to introduce C14 and C19 oxidation, as well as to convert the tetracyclic core of taxagifine to other, less oxidized taxoid cores, is also discussed.

# Contents

Acknowledgements	iv
<b>1 Transition Metal-Mediated C–C Single Bond Cleavage: Making the Cut in Total Synthesis</b>	<b>1</b>
1.1 Introduction	1
1.2 Core C–C Single Bond Cleavage in Total Synthesis	3
1.2.1 Phomactin Terpenoids (Sarpong, 2018)	4
1.2.2 (–)-Xishacorene B (Sarpong, 2018)	6
1.2.3 (–)-Cycloclavine (Dong, 2018)	8
1.2.4 (–)-Lingzhiol (Lan, Gong, and Yang, 2014)	10
1.2.5 (±)-Rhodomolleins XX and XXII (Ding, 2019)	12
1.2.6 (±)-GB22 (Shenvi, 2019)	15
1.3 Peripheral C–C Single Bond Cleavage in Total Synthesis	17
1.3.1 (–)-Aspewentins A, B, and C (Grubbs and Stoltz, 2015)	17
1.3.2 (–)-Chromodorolide B (Overman, 2018, second-generation)	19
1.3.3 Pyrone Diterpenes (±)-Subglutinol A, (±)-Subglutinol B, (±)-Sesquicillin A, and (±)-Higginsianin A (Baran, 2018)	22
1.3.4 (+)-Longirabdiol, (–)-Longirabdolactone, and (–)-Effusin (Li, 2019)	25
1.4 Conclusion and Outlook	27
1.5 References	29
<b>2 The History and Biology of Abscisic Acid and Attempted Syntheses of Rationally Designed Analogs</b>	<b>32</b>
2.1 A Brief History of Abscisic Acid: Initial Discovery To Current Agricultural Relevance	32
2.2 The Biology of Abscisic Acid	33
2.2.1 Mechanism of Action	33
2.2.2 Biosynthesis and Catabolism	35
2.3 Previous Investigations of Abscisic Acid Analogs	37
2.3.1 8 <sup>3</sup> -Functionalized ABA Analogs	37
2.3.2 Structure-Activity Relationships of ABA	39
2.3.3 Rational Design of an ABA Receptor Antagonist	40
2.4 Computationally-Guided Design of 5 <sup>3</sup> -Functionalized Abscisic Acid Analogs	41
2.5 Synthetic Approach to 5 <sup>3</sup> ,5 <sup>3</sup> -Spirocyclic Abscisic Acid Analogs	45
2.5.1 Retrosynthesis	45

2.5.2	Synthesis of Common Cyclohexenone Intermediate . . . . .	45
2.5.3	Synthesis of Dichlorocyclopropanated Cyclohexenones . . . . .	46
2.5.4	Late-Stage Progress Toward 5',5'-Spirocyclic ABA Analogs . . . . .	48
2.6	Conclusion and Outlook . . . . .	53
2.7	Experimental Contributors . . . . .	53
2.8	Experimental Methods and Procedures . . . . .	54
2.8.1	General Methods . . . . .	54
2.8.2	Experimental Procedures . . . . .	55
2.8.3	Supplementary Figures . . . . .	65
2.9	References . . . . .	65
	Appendix 2a: NMR Spectra Relevant to Chapter 2 . . . . .	93
	Appendix 2b: X-Ray Crystallographic Data Relevant to Chapter 2 . . . . .	93
<b>3</b>	<b>The History, Biology, and Previous Syntheses of the Taxoid Natural Products</b>	
	<i>With Special Emphasis on the Taxagifine-Like Natural Products</i>	<b>93</b>
3.1	A Brief History of the Taxoid Natural Products: Isolation and Development as Pharmaceuticals . . . . .	93
3.2	The Biological Activities of Taxol and Taxagifine . . . . .	95
3.2.1	Mechanism of Action of Taxol . . . . .	95
3.2.2	Clinical Challenges for Taxol Treatment . . . . .	97
3.2.3	Biological Studies of the Taxagifine-Like Natural Products . . . . .	99
3.3	Biosynthesis of the Taxoid Natural Products . . . . .	102
3.4	Previous Syntheses of Taxoid Natural Products . . . . .	104
3.4.1	Nicolaou's Total Synthesis of Taxol . . . . .	104
3.4.2	Other Total Syntheses of Taxol . . . . .	107
3.4.3	The Two-Phase Synthetic Strategy for Taxoid Natural Products . . . . .	110
3.5	Conclusion and Outlook . . . . .	116
3.6	References . . . . .	116
<b>4</b>	<b>Synthesis of a Highly Oxidized Tetracyclic Core of the Taxagifine-Like Natural Products</b>	<b>121</b>
4.1	Prior Exploratory Studies and Retrosynthesis . . . . .	121
4.2	Synthesis of Northern and Southern Coupling Partners . . . . .	124
4.3	Cross-Coupling Studies and Synthesis of Tetracyclic Cores . . . . .	127
4.4	Alternative Strategies for B-Ring Closure . . . . .	134
4.4.1	Aldol Condensation . . . . .	134
4.4.2	Cyclization of $\alpha$ -Functionalized Methyl Ketones . . . . .	135
4.4.3	Pinacol Coupling . . . . .	138
4.4.4	Brook Rearrangement . . . . .	139
4.4.5	Carbonyl–Olefin Metathesis . . . . .	139
4.5	Conclusion . . . . .	140
4.6	Experimental Contributors . . . . .	140
4.7	Experimental Methods and Procedures . . . . .	140
4.7.1	General Methods . . . . .	140

4.7.2	Experimental Procedures . . . . .	142
4.7.3	Supplementary Figures . . . . .	163
4.8	References . . . . .	163
	Appendix 4a: NMR Spectra Relevant to Chapter 4 . . . . .	232
	Appendix 4b: X-Ray Crystallographic Data Relevant to Chapter 4 . . . . .	232
<b>5</b>	<b>Late-Stage Progress Toward the Total Syntheses of Taxagifine-Like Natural Products</b>	<b>232</b>
5.1	Installation of C10 Oxygenation . . . . .	232
5.1.1	Initial Attempts at Enolate C10-Oxidation . . . . .	232
5.1.2	Initial Attempts at C11-OH Elimination . . . . .	234
5.1.3	Miscellaneous C10 Oxidation Attempts . . . . .	235
5.1.4	<i>s</i> -BuLi-based C10 Oxidation . . . . .	236
5.2	Strategies for Accessing C9,C10- <i>trans</i> -Diol Motifs . . . . .	239
5.2.1	Hydroboration of Enol Ethers . . . . .	239
5.2.2	Direct Reduction of C10-Oxidized Compounds . . . . .	240
5.2.3	Attempted C9,C10- <i>trans</i> -Diol Synthesis via Alkene Dihydroxylations . . . . .	244
5.2.4	Attempted C9- or C11-Hydroxy-Directed C10-Oxidations . . . . .	246
5.3	Installation of C5 Oxygenation . . . . .	248
5.4	Installation of C2 Oxygenation . . . . .	251
5.4.1	Attempts at Radical C2-H Abstraction . . . . .	251
5.4.2	Attempts at C2 Functionalization via Formal Ene/Allylic Transposition . . . . .	252
5.4.3	C5-Tether-Assisted C2 Functionalization . . . . .	254
5.4.4	Successful C2 Functionalization via Formal Ene/Allylic Transposition . . . . .	256
5.5	Transposition of the C3-C4 Alkene and Setting of the C3 Stereocenter . . . . .	261
5.5.1	Non-Directed C3-C4 Alkene Functionalization . . . . .	261
5.5.2	Pd-Catalyzed C3-C4 Alkene Reductive Transposition . . . . .	262
5.5.3	Allylic Diazene Rearrangement . . . . .	263
5.5.4	Allylsulfinic Acid Rearrangement . . . . .	267
5.6	Model System Studies of Future Transformations . . . . .	270
5.6.1	Oxetane Formation . . . . .	270
5.6.2	Protecting Group Cleavages . . . . .	271
5.6.3	Stereoselective C13 Carbonyl Reduction . . . . .	273
5.6.4	Selective C7-OH and/or C4-OH Acetylations . . . . .	274
5.7	Studies Toward Other Taxoid Cores and Other Oxidation Patterns . . . . .	275
5.7.1	C14 and C19 Oxidation . . . . .	275
5.7.2	Access to Unnatural and Other Natural Taxoid Cores . . . . .	276
5.8	Conclusion and Outlook . . . . .	279
5.9	Experimental Contributors . . . . .	282
5.10	Experimental Methods and Procedures . . . . .	282
5.10.1	General Methods . . . . .	282
5.10.2	Experimental Procedures . . . . .	283
5.11	References . . . . .	308



## Acknowledgements

I'd like to first thank Professor Richmond Sarpong for providing such an excellent laboratory environment, and for all his advice and support over the years. Thank you especially for granting me the freedom to pursue all my whims, whether rational or irrational, chemistry-related or otherwise. It's rare and underappreciated for a mentor to sit back and provide space for exploration rather than simply lead by the hand or pressure for results, and I think you struck the balance just right.

Thanks to everyone I've ever worked with on a project, in no particular order: Mel Perea, Dr. Nick O'Connor, Dr. Ben Wyler, Dr. Shota Nagasawa, Johny Nguyen, Yuto Kimura, and Max Scheruebl. It was a pleasure working with all of you through the highs (e.g., C10), lows (e.g., also C10), and everything in between.

I'd also like to thank everyone I've shared a lab with over the years for always providing a supportive and encouraging research environment. I'd like to especially thank Drs. Ahmad Masarwa, Lana Kulyk, and Danilo Pereira de Santana—the original 844 crew—for being the absolute most welcoming group of people a clueless incoming first year could've asked for. Thanks for fielding all my questions about interpreting NMRs and basic lab techniques. Thanks also to the newest 844 crew—Jose Roque, Ian Bakanas, and Jinsu Ham—for constant chemistry discussions and for your infectious curiosity; you've made me a better chemist for it. Even as the “senior grad student,” in conversations with each of you I often felt like the least knowledgeable about any given topic, and that's the most valuable feeling of all.

Thanks to all in the group that have provided friendship over the years, especially: Sid Hill, Jason Pflueger, Paul Leger, Kyle Owens, Becca Johnson, and Jose Roque. You all lightened up the daily routine of labwork and helped make grad school more enjoyable, and you've each inspired me in your own way.

Finally, thanks to all the friends and family that have provided me love and support from afar. It's a wonderful thing to know that I can count on so many people scattered around the world to have my back no matter what, and it's not something I'll ever take for granted.

# Chapter 1

## Transition Metal-Mediated C–C Single Bond Cleavage: Making the Cut in Total Synthesis

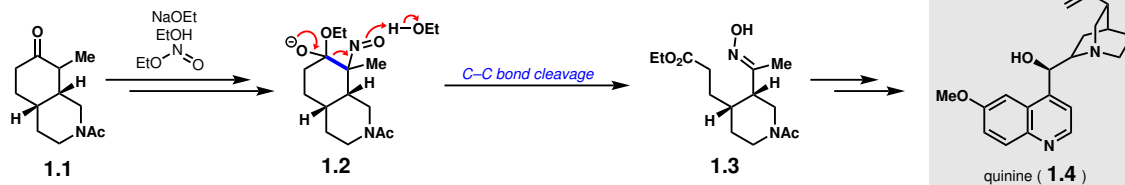
### 1.1 Introduction

For over half a century, natural products have served as prime targets of chemical synthesis. The structural complexity of natural products continues to inspire the development of new strategies and methods for synthesis, and their oft-medicinally relevant biological activity motivates efficient synthesis design to access larger amounts of these compounds or their derivatives. Historically, a major focus in the development of synthetic strategies and methods has been the forging of C–C single bonds to construct the unique carbon frameworks associated with complex natural products; indeed, the pattern and prevalence of C–C single bonds is often the predominant distinction between these natural products and simple chemical building block precursors. As a result, some of the most practiced reactions in total synthesis—e.g., the Diels–Alder reaction, the aldol reaction, and Pd-catalyzed cross-couplings—have featured the formation of C–C single bonds.

While the progressive formation of C–C single bonds constitutes a logical approach for efficient syntheses of natural products from commercially available starting materials, chemists have also long recognized the potential for C–C single bond cleavage to streamline syntheses.<sup>1</sup> Indeed, Woodward’s landmark synthesis of quinine (**1.4**) in 1944 featured a C–C single bond cleavage of a cyclohexanone by treatment with ethyl nitrite (**1.1** to **1.3**, Scheme 1.1A).<sup>2</sup> Beyond fully organic processes such as that employed in the Woodward synthesis, the development of transition metal-mediated C–C single bond cleavage processes has enabled access to an even fuller palette of chemical reactivity. Specifically, transition metal-mediated C–C single bond cleavage events often precede the formation of a reactive organometallic intermediate, which offers the opportunity for further functionalization across the cleaved C–C bond through two-electron elementary steps. Showcasing this mode of reactivity is Trost’s synthesis of (+)-frondosin A (**1.10**), where a key ruthenium-catalyzed vinylcyclopropane [5 + 2] cycloaddition proceeds via ruthenacyclopentene intermediate **1.7**; C–C single bond cleavage then generates reactive organoruthenium intermediate **1.8**, enabling subsequent C–

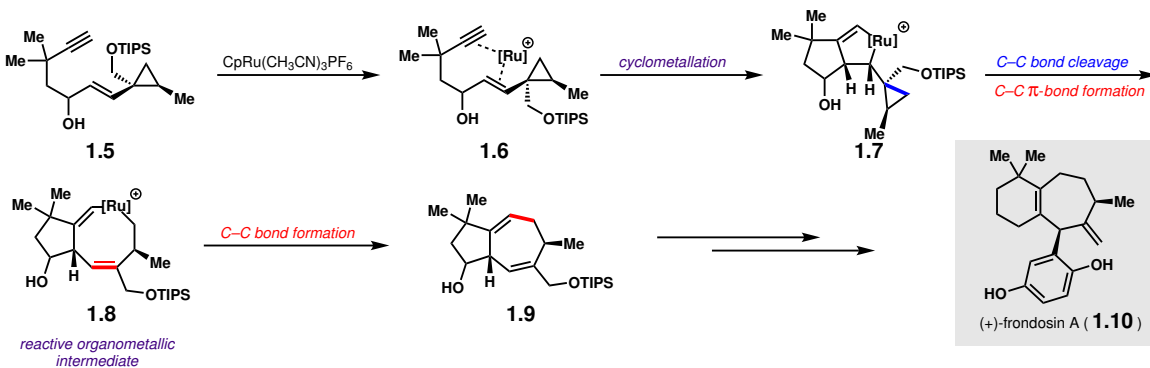
### A. Non-Transition Metal-Mediated C–C Cleavage

Woodward's synthesis of quinine (1944):



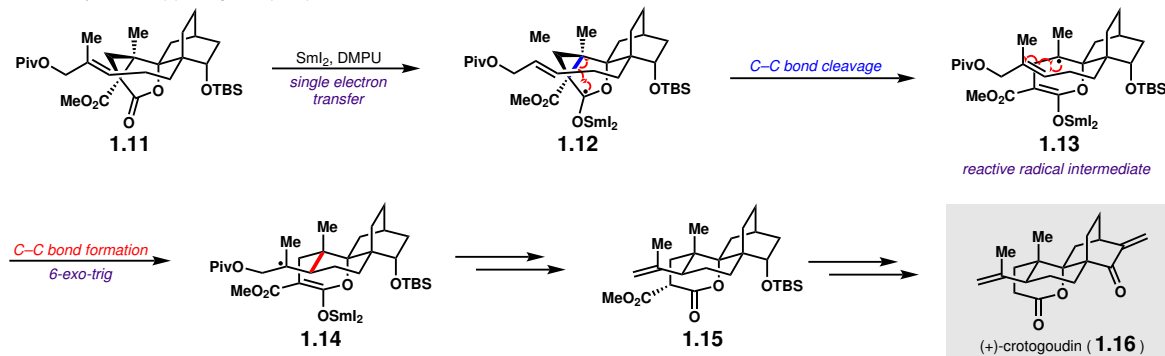
### B. Transition Metal-Mediated C–C Cleavage: Two-Electron Reactivity

Trost's synthesis of (+)-frondosin A (2007):



### C. Transition Metal-Mediated C–C Cleavage: One-Electron Reactivity

Carreira's synthesis of (+)-crotagoudin (2013):



**Scheme 1.1:** Examples of previous syntheses highlighting non-transition metal-mediated C–C bond cleavage (1A), transition metal-mediated C–C single bond cleavage resulting in a reactive organometallic intermediate (two-electron reactivity, 1B), and transition metal-mediated C–C single bond cleavage resulting in a reactive radical intermediate (one-electron reactivity, 1C).

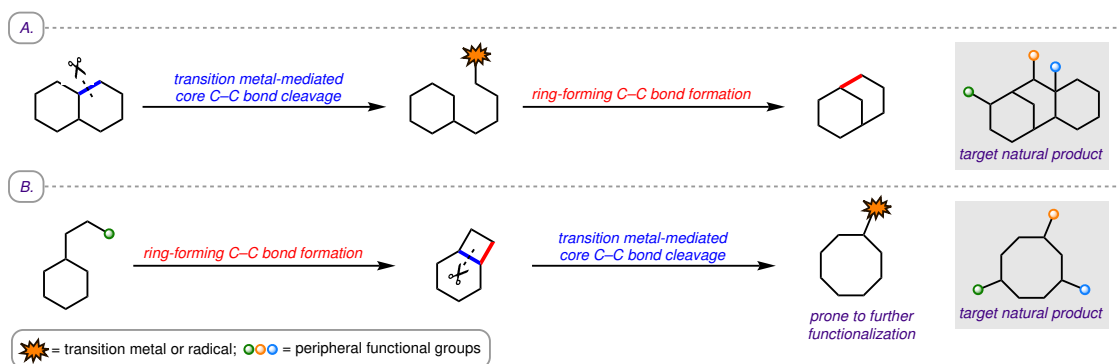
C single bond formation via reductive elimination (Scheme 1.1B).<sup>3</sup> Overall, the exploitation of transition metal two-electron reactivity permitted functionalization across a strained C–C single bond, generating an additional C–C single bond and a C–C double bond.

As an alternative mode of reactivity, the redox-activity of transition metals may facilitate their participation in a single electron transfer event with a substrate; subsequent cleavage of a C–C bond would result in the formation of a reactive radical intermediate, which may recombine with a metal complex or engage in further radical processes.<sup>4</sup> Car-

reira's synthesis of (+)-crotoougoudin (**1.16**) serves as a prime example; in the course of the synthesis, SmI<sub>2</sub>-mediated single electron reduction of lactone **1.11** yields ketyl radical **1.12** (Scheme 1.1C). Cyclopropane C–C bond cleavage then occurs to generate reactive radical intermediate **1.13**, facilitating subsequent C–C bond formation via a 6-*exo-trig* radical cyclization to yield intermediate **1.14**. Reduction, elimination of the pivalate group, and protonation then delivered compound **1.15**, which was elaborated to the natural product. Overall, the installation of a C–C single bond in the core of crotoougoudin was accomplished by the cleavage/functionalization of a cyclopropane C–C bond via one-electron transition metal reactivity.<sup>6</sup>

The accessibility of these multiple modes of reactivity upon transition metal-mediated C–C single bond cleavage has increasingly inspired synthetic chemists to consider C–C single bonds as functional groups in retrosynthetic analysis. Recently, there has been a profusion of methods involving transition metal-mediated C–C single bond cleavage/functionalization, resulting in increased applications of both novel and established C–C bond cleavage tactics to comprise new strategies for total synthesis. While others have recently reviewed mechanistic aspects and methodological applications of C–C single bond cleavage processes<sup>7–13</sup> or transition metal-catalyzed C–C single bond cleavage in total syntheses prior to 2015,<sup>14</sup> here we focus on selected total syntheses utilizing transition metal-mediated C–C single bond cleavage from 2014–2019. We will highlight how the cleavage of C–C single bonds in either the core or on the periphery of synthetic intermediates has enabled access to both two-electron and one-electron transition metal reactivity manifolds, facilitating new retrosynthetic opportunities for each natural product discussed.

## 1.2 Core C–C Single Bond Cleavage in Total Synthesis



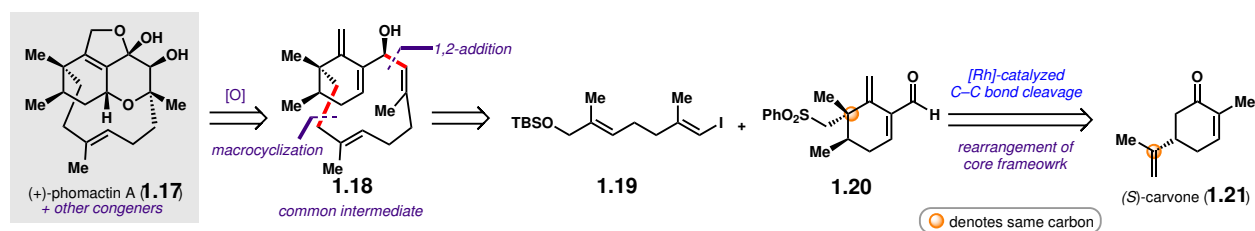
**Scheme 1.2:** Conceptual examples of paired core C–C single bond cleavage and ring-forming C–C bond formation events, with core C–C single bond cleavage occurring either before (2A) or after (2B) ring-forming C–C bond formation.

For the purposes of this chapter, we will define “core” C–C single bonds as those that occur within a central ring of a synthetic intermediate. Thus, the cleavage of such a core C–C single bond would transform a monocyclic system to a linear system, a bicyclic system to a monocyclic system, etc. When paired with ring-forming processes, core C–C single

bond cleavage events can result in the rapid remodeling of synthetic intermediates to more closely resemble the molecular architecture of the target natural product. This may be the case whether a C–C single bond cleavage event immediately precedes or succeeds a ring-forming event (e.g., compare Scheme 1.2A and Scheme 1.2B). As a result, synthetic tactics involving core C–C single bond cleavage and ring-forming events occurring in rapid succession may enable novel, counterintuitive retrosynthetic disconnections resulting in proposed synthetic intermediates that may not “map on” well to the target natural product. These tactics therefore expand the synthetic toolbox, extending the boundaries of retrosynthesis and inviting the creativity of the synthetic practitioner to develop new strategies. Following are discussions of selected recent total syntheses employing core C–C single bond cleavage as a strategic transform.

## 1.2.1 Phomactin Terpenoids (Sarpong, 2018)

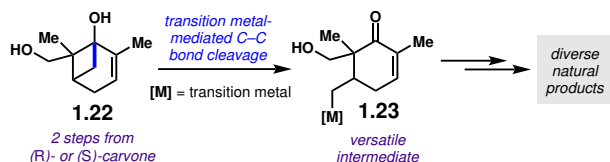
The phomactin natural products are a family of highly oxygenated diterpenoids first isolated in 1991 from fungi of the genus *Phoma*.<sup>15</sup> Through early studies, (+)-phomactin A (**1.17**, Scheme 1.3) was shown to be a platelet activating factor receptor (PAFR) antagonist, with potential implications in cancer therapy. Aside from this interesting bioactivity, the phomactins also contain a unique bicyclo[9.3.1]pentadecane core comprised of a cyclohexenyl fragment and a macrocyclic strap, presenting a formidable synthetic challenge. Despite this challenge, Sarpong and coworkers successfully established the first unified approach to several congeners of the phomactin family. Key to their strategy was the design of a versatile common intermediate (**1.18**) with functionality that could guide an array of downstream oxidation events necessary to obtain different congeners (Scheme 1.3). Retrosynthetically, this intermediate could arise from two fragments, a highly functionalized cyclohexenyl ring (**1.20**) and vinyl iodide **1.19**, which in the forward sense could undergo a fragment coupling followed by macrocyclization. Finally, cyclohexene **1.20** could be rapidly synthesized from (*S*)-carvone (**1.21**) through the application of a C–C bond cleavage tactic.



**Scheme 1.3:** Sarpong and coworkers’ retrosynthesis of phomactins.

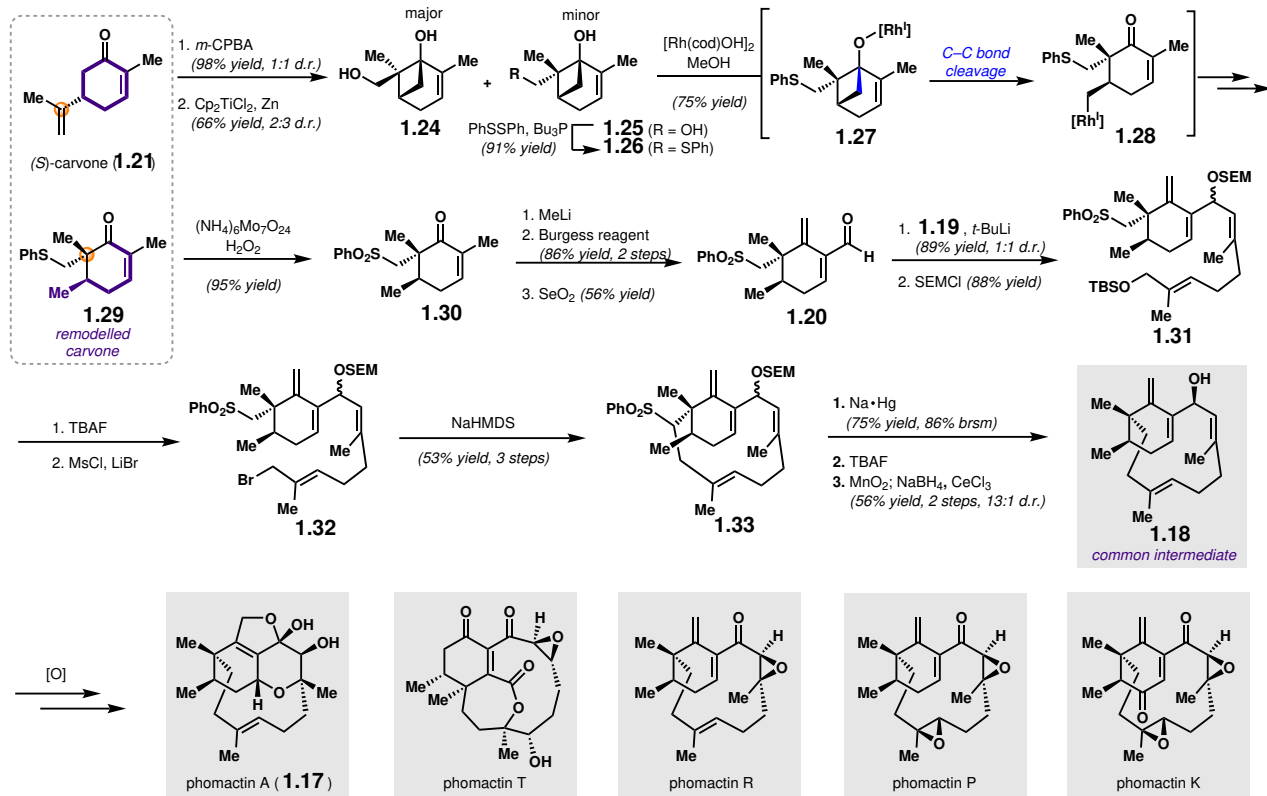
While efficient access to the macrocyclic strap has been well established in previous syntheses, accessing highly functionalized cyclohexenyl fragments such as **1.20** has been a particularly laborious endeavor in previous work, adding greatly to overall step counts.<sup>16,17</sup> To address the challenge of accessing fragments of this nature more efficiently, Sarpong and coworkers envisioned obtaining this cyclohexenyl fragment from chiral pool terpene (*S*)-carvone by employing a C–C bond cleavage event, which would result in a substantial

remodeling of the carvone core framework and enable efficient access to **1.20**. Previously, building on work pioneered by others on the C–C cleavage/functionalization of cyclobutanols,<sup>18–20</sup> Sarpong and coworkers had established a powerful strategy that entailed using enantioenriched cyclobutanols (**1.22**) derived from carvone in a transition metal-mediated C–C bond cleavage reaction to produce a versatile organometallic intermediate (**1.23**) prone to further functionalization, including C–C bond-forming processes<sup>21</sup> (Scheme 1.4). Overall, this strategy provides efficient access to a variety of stereochemically rich cyclohexenones that can be elaborated to diverse natural product-like scaffolds.



**Scheme 1.4:** Cyclobutanol C–C bond cleavage strategy employed by Sarpong and coworkers.

To carry out this strategy in the context of the phomactins, Sarpong and coworkers' synthetic studies began with the synthesis of cyclohexene **1.20** (Scheme 1.5). Following a known sequence by Bermejo and coworkers, the isopropenyl group of (*S*)-carvone was subjected to epoxidation followed by a Ti(III)-mediated reductive coupling of the epoxide and carbonyl to afford diastereomeric cyclobutanols **1.24** and **1.25**.<sup>22</sup> Mitsunobu displacement of the primary hydroxy group of the minor diastereomer furnished phenyl sulfide **1.26**, which then set the stage for the key C–C bond cleavage event. Treatment of **1.26** with sub-stoichiometric amounts of  $[\text{Rh}(\text{cod})\text{OH}]_2$  promoted a ligand exchange with the tertiary hydroxy group to provide Rh-alkoxide **1.27**, followed by  $\beta$ -carbon elimination of the less substituted C–C bond to yield alkyl-Rh species **1.28**, which readily afforded cyclohexenone **1.29**. The sequence of events involving formation of a strained cyclobutanol from carvone followed by strain-releasing C–C bond cleavage overall engendered a rearrangement of the carvone skeleton, resulting in the integration of the isopropenyl group into the core framework (Scheme 1.3B, dashed box). Following this key sequence was oxidation of the sulfide to the sulfone to afford **1.30**; subsequent MeLi addition to the carbonyl followed by a Burgess elimination of the resulting alcohol then installed an *exo*-methylene moiety. Allylic oxidation of the vinylic methyl group delivered aldehyde **1.20**. Lithiation of **1.19** promoted 1,2-addition to the aldehyde with subsequent protection of the resulting alcohol to afford **1.31**. Cleavage of the TBS group followed by conversion of the hydroxy group to an allylic bromide provided **1.32**, which underwent macrocyclization upon treatment with NaHMDS to give **1.33**. Removal of the sulfone, cleavage of the SEM group, and oxidation of the unveiled hydroxy group to the carbonyl with subsequent diastereoselective reduction furnished **1.18**, which served as a common intermediate. From this intermediate, several congeners of the phomactin family, including phomactin A (**1.17**), were efficiently obtained through various oxidation tactics. From their work on the phomactins, Sarpong and coworkers effectively demonstrated the power of ring formation/C–C bond cleavage in remodeling the core framework of chiral pool molecules such as carvone, thus enabling efficient access to traditionally challenging motifs.



Scheme 1.5: Synthesis of key common intermediate **1.18**.

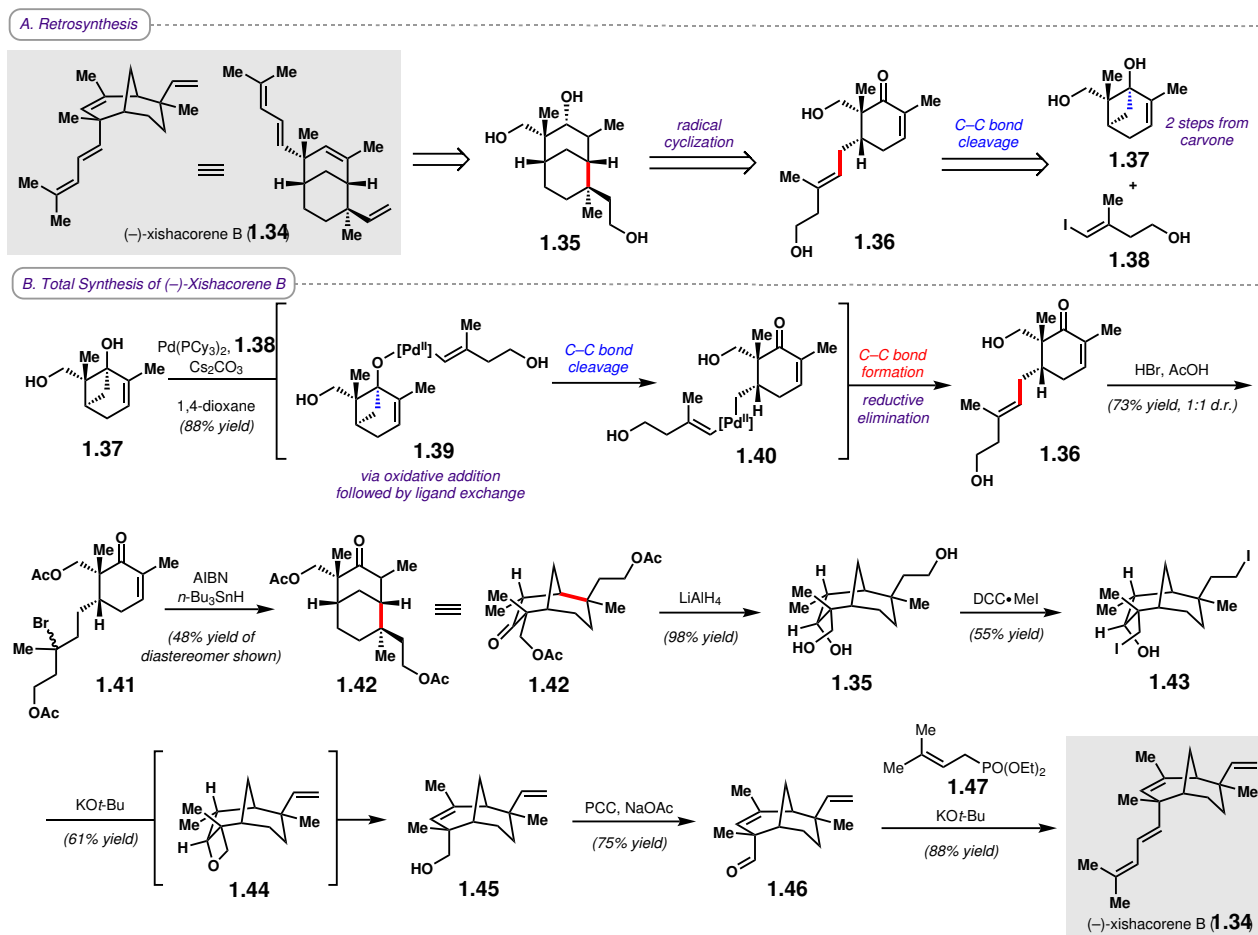
## 1.2.2 (–)-Xishacorene B (Sarpong, 2018)

In addition to their work on the phomactins, Sarpong and coworkers showcased the utility of C–C bond cleavage in 2018 with the first total synthesis of xishacorene B (**1.34**, Scheme 1.6A).<sup>23</sup> The xishacorene diterpenes, hydrocarbon natural products first isolated in 2017 from the soft coral *Sinularia polydactyla* off the coast of China, exhibit immunopotentiating activity and contain a unique bicyclo[3.3.1]nonane core. Retrosynthetically, xishacorene B could arise from triol **1.35**, which in turn could be constructed from cyclohexenone **1.36** through a radical cyclization, with the reactive enone serving as a radical acceptor. This cyclohexenone was proposed to arise from cyclobutanol **1.37** and vinyl iodide **1.38** through a Pd-catalyzed C–C bond cleavage/cross-coupling reaction. Cyclobutanol **1.37** was synthesized in two steps from (*R*)-carvone (see Scheme 1.5).<sup>22</sup>

The forward synthesis commenced with treatment of cyclobutanol **1.37** and vinyl iodide **1.38** with a Pd(0) catalyst, which formed Pd-alkoxide **1.39** after oxidative addition of the vinyl iodide and ligand exchange with the tertiary alcohol (Scheme 1.6B). The Pd-alkoxide then underwent  $\beta$ -carbon elimination to afford alkyl-Pd intermediate **1.40**, which after reductive elimination yielded the desired cross-coupled product (**1.36**). This strategy, in which C–C bond cleavage of a carvone-derived cyclobutanol facilitated the synthesis of a highly functionalized cyclohexenone, was also employed in Sarpong and coworkers' syntheses of phomactin terpenoids (see Scheme 1.5); however, in contrast to the syntheses of the

phomactins, in which an alkyl-Rh intermediate underwent protodemetalation, the alkyl-Pd intermediate **1.40** was primed to undergo reductive elimination, enabling the formation of an additional C–C bond. Bromination of the trisubstituted olefin group of **1.36** with concomitant acetylation of the hydroxy groups provided alkyl bromide **1.41**. Treatment with AIBN and *n*-Bu<sub>3</sub>SnH then promoted the formation of a tertiary radical, which underwent 6-*exo-trig* cyclization to the enone, forging the [3.3.1] bicyclic core of xishacorene B. Notably, by employing various cross-coupling partners in place of **1.38** in the Pd-catalyzed C–C cleavage/cross-coupling and continuing with radical cyclization, a variety of different [3.3.1] and [3.2.1] bicycles could be obtained.

Global reduction of **1.42** with LiAlH<sub>4</sub> afforded triol **1.35**, which was then iodinated with DCC·MeI to yield bisiodinated alcohol **1.43**. Treatment with KO*t*-Bu led to alcohol **1.45** via oxetane **1.44**, which upon oxidation with PCC afforded aldehyde **1.46**. Finally, Horner–Wadsworth–Emmons olefination with phosphonate ester **1.47** provided (–)-xishacorene B in a total of 10 steps from (*R*)-carvone. Overall, Sarpong and coworkers were able to demonstrate a new strategy for preparing bicyclic compounds by performing a C–C bond cleavage/cross-coupling reaction with subsequent radical cyclization, showcasing the versa-



**Scheme 1.6:** Retrosynthesis (A) and total synthesis (B) of (–)-xishacorene B.



tility of C–C bond cleavage for remodeling chiral pool molecules to provide unconventional access to complex frameworks.

### 1.2.3 (–)-Cycloclavine (Dong, 2018)

The ergot alkaloids are a large family of polycyclic indole alkaloids that exhibit a range of biological activities (Figure 1.1). Cycloclavine (**1.48**), isolated from seeds of the flowering plant *Ipomoea hildebrandtii* in 1969, exhibits insecticidal and antiparasitic activities. Structurally, cycloclavine is unique among the ergot alkaloids as the only member that contains a cyclopropane ring. In addition, cycloclavine exhibits a pentacyclic core with three contiguous stereocenters, two of which are vicinal quaternary centers. These synthetic challenges, along with its biological activity, have made cycloclavine an intriguing target for synthetic chemists. Herein, we discuss the 2018 asymmetric total synthesis of (–)-cycloclavine by Dong and coworkers, which was accomplished through an enantioselective C–C activation/functionalization strategy.<sup>24</sup> For clarity, C–C activation in this chapter will be defined as a specific form of C–C bond cleavage that is accomplished by an oxidative addition of a transition metal into a C–C bond.

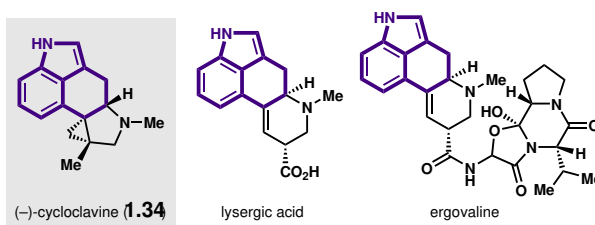
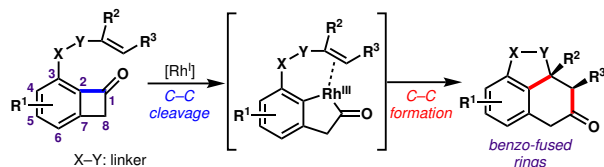


**Figure 1.1:** Selected ergot alkaloids.

While transition metal-catalyzed C–C activation of cyclobutanones is well established,<sup>10</sup> there continues to be an ongoing effort to leverage this powerful reactivity in new and interesting ways as a strategy for accessing natural product-like scaffolds. One prominent recent advancement in cyclobutanone C–C activation is the Rh-catalyzed carboacylation of olefins developed by Dong and coworkers, which provides efficient access to benzo-fused ring systems from benzocyclobutenones (Scheme 1.7). This specific C–C activation approach, first reported in 2012,<sup>25</sup> begins with oxidative addition of a Rh-complex into the C1–C2 bond of a strained cyclobutenone, followed by migratory insertion of the proximal olefin group and reductive elimination to forge two new bonds, giving rise to the desired benzo-fused ring system. It should be noted that while oxidative addition of the Rh-complex into the less-substituted C1–C8 bond is kinetically favored (and usually observed in traditional methods), the tethered double bond in this case serves as a directing group for the desired C1–C2 cleavage. This “cut-and-sew” approach therefore leads to novel benzo-fused tricycles, a key structural component in a number of biologically active natural products, including cycloclavine.

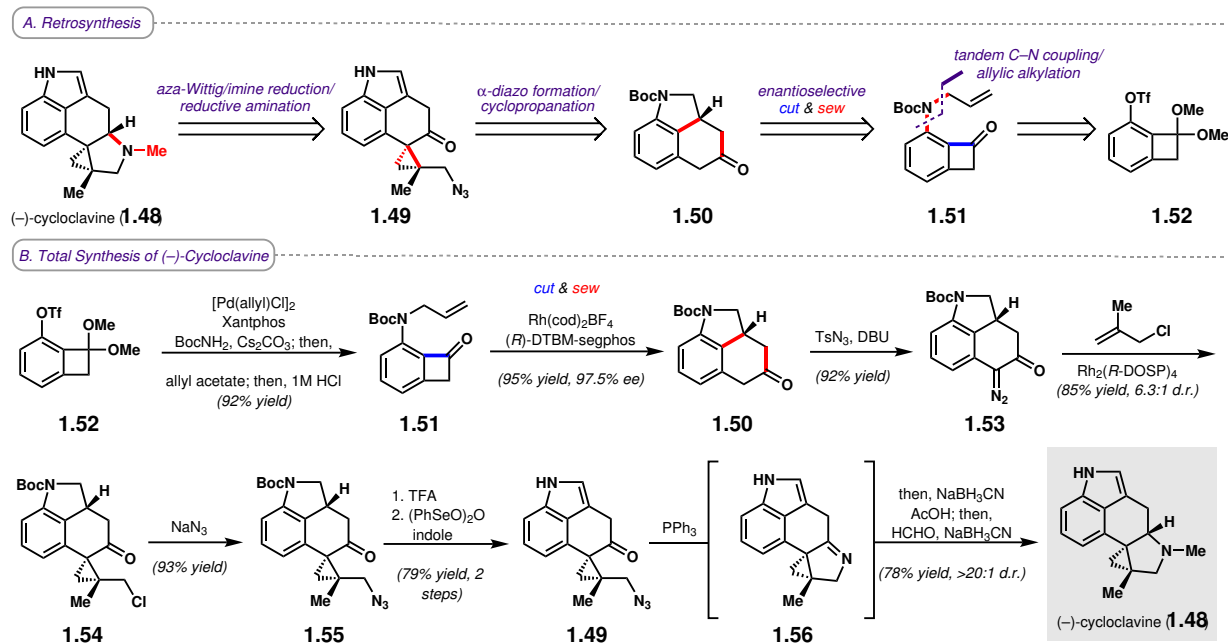
In a retrosynthetic sense, it was proposed that cycloclavine (**1.48**) could arise from tetra-cycle **1.49** through an aza-Wittig/imine reduction/reductive amination sequence, which in the forward sense would forge the pyrrolidine moiety in the natural product (Scheme 1.8A).



**Scheme 1.7:** “Cut and sew” C–C activation strategy by Dong and coworkers.

This tetracycle would arise from benzo-fused tricycle **1.50** through diazo formation  $\alpha$  to the ketone followed by a diastereoselective Rh-catalyzed cyclopropanation. Tricycle **1.50** would then be constructed from benzocyclobutenone **1.51** via the key asymmetric Rh-catalyzed C–C activation reaction. Finally, benzocyclobutenone **1.51** could be constructed from triflate **1.52** via a tandem C–N coupling/allylic alkylation reaction.

The synthesis of cycloclavine (Scheme 1.8B) commenced with a known two step sequence to obtain triflate **1.52**. Initial efforts focused on coupling **1.52** directly with allylamine; however, this proved to be infeasible. As an alternative, **1.52** was first coupled to *tert*-butyl carbamate using a Pd-catalyzed C–N cross-coupling, which was followed by an allylic alkylation catalyzed by the same Pd complex. Subsequent cleavage of the acetal upon acidic workup furnished benzocyclobutenone **1.51**. After attempting conditions initially developed for the cut-and-sew of benzocyclobutenones with an allylic ether linkage<sup>26</sup>, which gave substandard results (i.e., low yields and enantioselectivities), Dong and coworkers determined that the added bulkiness and rigidity of the amine linker required the use of a less bulky and more electron-deficient Rh-complex. The use of the cationic Rh(I) precatalyst  $\text{Rh}(\text{cod})_2\text{BF}_4$  proved to be effective in enhancing olefin coordination, and, when paired with (*R*)-DTBM-segphos as the ligand, provided the desired product in excellent yield and *ee* (95% yield,



**Scheme 1.8:** Retrosynthesis (A) and total synthesis (B) of (–)-cycloclavine.

97.5% *ee*). With benzo-fused tricycle **1.50** in hand, Dong and coworkers turned their attention to constructing the [3.1.0] bicycle in the southern portion of the molecule. Treatment of **1.50** with  $\text{TsN}_3$  afforded the  $\alpha$ -diazo ketone (**1.53**), which then underwent a Rh-catalyzed diastereoselective cyclopropanation with 2-methylallyl chloride to yield tetracycle **1.54**. Azidation of the alkyl chloride moiety with  $\text{NaN}_3$  provided azide **1.55**. Cleavage of the Boc protecting group followed by dehydrogenation afforded indole **1.49**, which was converted to (–)-cycloclavine via an aza-Wittig/imine reduction/reductive amination sequence. While transition metal-catalyzed C–C bond activation of strained ring systems has been an active field of research since the 1990s, there have been surprisingly few examples of its application in total synthesis. The synthesis of cycloclavine serves as a prime example of how C–C bond activation strategies can be designed and implemented to build complex polycyclic ring systems efficiently and showcases the power that these strategies have in complex molecule synthesis.

### 1.2.4 (–)-Lingzhiol (Lan, Gong, and Yang, 2014)

Certain structural motifs occur frequently in a variety of diverse natural products; these conserved moieties often inspire synthetic chemists to develop strategies and methods for their preparation, which can ultimately facilitate entries into an array of natural products. Two examples of common scaffolds include [4.3.0] and [3.3.0] bicycles bearing vicinal quaternary centers, which appear in several natural products isolated from different sources that exhibit a range of biological activities (Figure 1.2).<sup>27</sup> One such natural product is (–)-lingzhiol (**1.57**), a [4.3.0] bicycle-containing meroterpenoid isolated in 2013 from the mushroom *Ganoderma lucidum*.<sup>28</sup> Herein, we discuss the total synthesis of (–)-lingzhiol by Yang and coworkers, who demonstrated a highly versatile Rh-catalyzed formal (3+2) cycloaddition (facilitated by a C–C bond cleavage event) as the key step to efficiently access the [4.3.0] core for lingzhiol. Additionally, this cycloaddition method could be extended for the formation of [3.3.0] bicycles, thus expanding the applicability of this method to other natural product classes.

The proposed mechanism of the Rh-catalyzed formal (3+2) cycloaddition begins with formation of the alkyne-bound Rh-alkoxide (**1.59**), which then undergoes a retro-propargylation, resulting in the C–C bond cleavage and the formation of an allenyl-Rh intermediate (**1.60**).

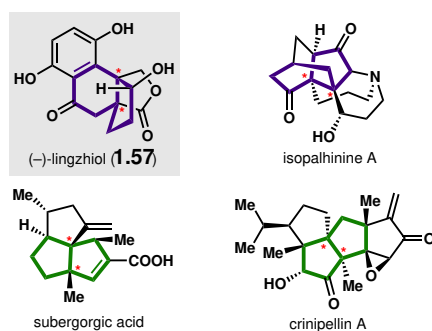
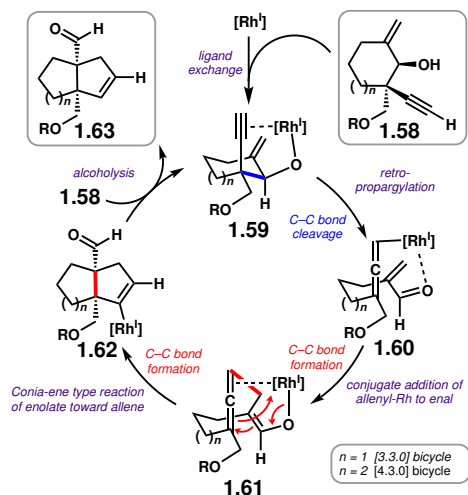


**Figure 1.2:** Representative natural products containing [4.3.0] (purple) and [3.3.0] (green) bicycles with vicinal quaternary stereocenters (red asterisk).

Conjugate addition of the allenyl-Rh species to the resulting enal forms the first C–C bond leading to an oxygen-bound Rh-enolate (**1.61**). This enolate then likely undergoes a Conia-ene-type reaction with the allene to afford bicycle **1.62**, forming the second C–C bond. Alcoholysis then leads to the desired bicyclic product (**1.63**) with concomitant regeneration of Rh-alkoxide **1.59**. Notably, this process proved to be highly versatile as the ring size in the starting material dictates the product outcome, with seven-membered rings yielding [4.3.0] bicycles and six-membered rings yielding [3.3.0] bicycles. Additionally, in contrast to examples discussed thus far which leverage ring strain, this strategy can effect C–C bond cleavage in more thermodynamically stable six-membered rings.

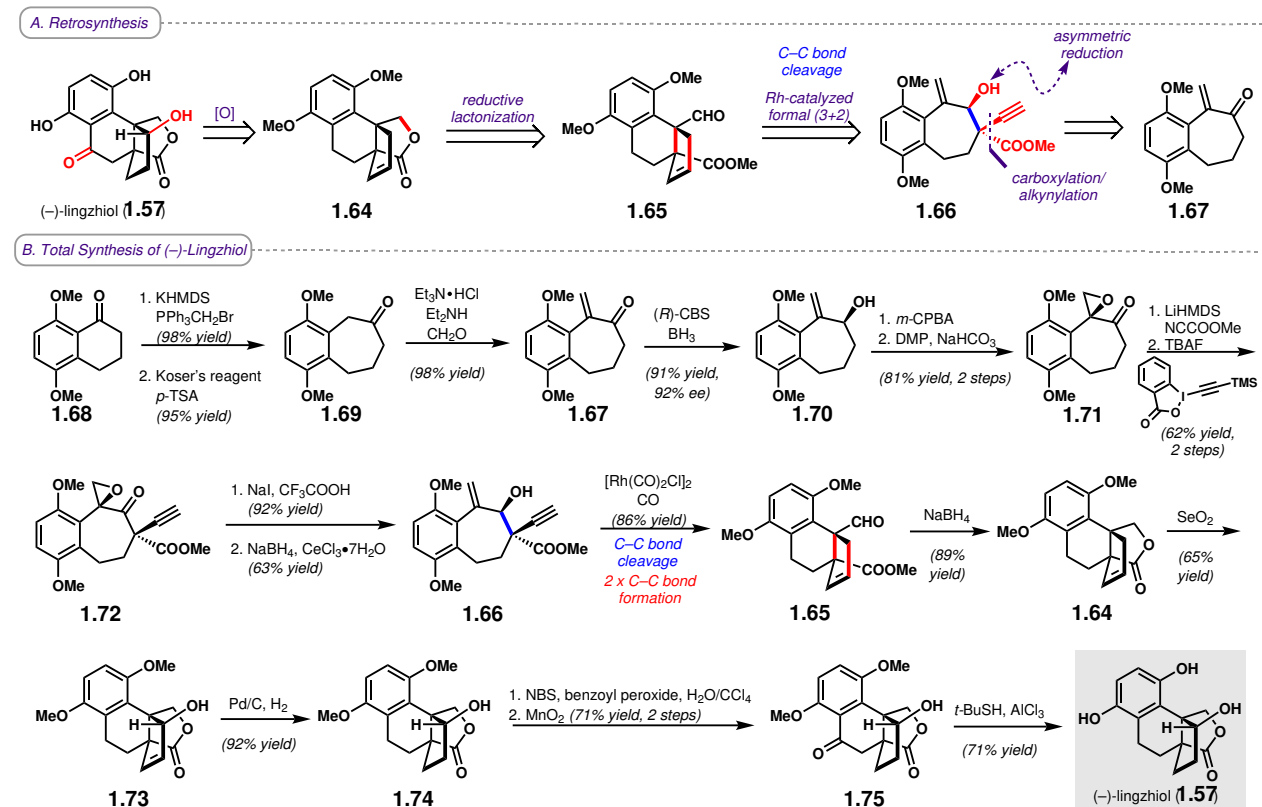


**Scheme 1.9:** Rh-catalyzed formal (3+2) cycloaddition.

Retrosynthetically, it was envisioned that lingzhiol could arise from lactone **1.64** via late-stage allylic and benzylic oxidations (Scheme 1.10). Lactone **1.64** could be synthesized from tricycle **1.65**, which, in turn, could arise from **1.66** using the key Rh-catalyzed formal (3+2) sequence. Finally, **1.66** would arise from enone **1.67** through a series of functionalizations, including asymmetric reduction of the carbonyl group followed by a carboxylation/propargylation sequence.

Beginning from **1.68**, Wittig olefination followed by a Koser's reagent-mediated ring expansion afforded **1.69**, which was subsequently converted to enone **1.67** upon treatment with *in situ*-generated Eschenmoser's salt. CBS reduction then afforded enantioenriched **1.70**, which underwent epoxidation of the *exo*-methylene with *m*-CPBA followed by oxidation of the hydroxy group to the carbonyl with DMP to deliver  $\beta$ -epoxy ketone **1.71**. Carboxylation followed by propargylation afforded **1.72**, which was then converted to allylic alcohol **1.66**. Treatment with  $[\text{Rh}(\text{CO})_2\text{Cl}]_2$  converted **1.66** to tricyclic compound **1.65** via the key formal (3+2) cycloaddition with formation of two new C–C bonds.  $\text{NaBH}_4$  reduction of the more reactive aldehyde followed by lactonization of the resulting hydroxy group furnished lactone **1.64**, which subsequently underwent allylic oxidation with  $\text{SeO}_2$  to provide allylic alcohol **1.73**. Hydrogenation with Pd/C and  $\text{H}_2$  furnished **1.74**, which was followed by a two-step sequence to effect a benzylic oxidation, yielding the fully oxidized core (**1.75**). Finally, deprotection of the bisphenol moiety by cleavage of the methoxy groups completed the

synthesis of (–)-lingzhiol (**1.57**). The total synthesis of (–)-lingzhiol represents a unique example of C–C bond cleavage as the only example in this chapter highlighting core cleavage that is not strain-promoted. This specific type of C–C bond cleavage expedites the overall process of remodeling a core framework by not requiring initial formation of a strained ring, benefiting instead from the formation of a  $\pi$ -allenyl intermediate.



**Scheme 1.10:** Retrosynthesis (A) and total synthesis (B) of (–)-lingzhiol.

### 1.2.5 (±)-Rhodomolleins XX and XXII (Ding, 2019)

Rhodomollein XX (**1.76**) and rhodomollein XXII (**1.77**) are gryanane diterpenoids isolated from *Rhododendron molle* from the Ericaceae family of flowering plants (Figure 1.3). The gryanoid natural products exhibit a range of biological activities, including insecticidal, antifeedant, and analgesic activities and contain a characteristic 5/7/6/5 tetracyclic carbon

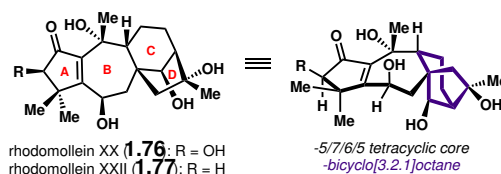
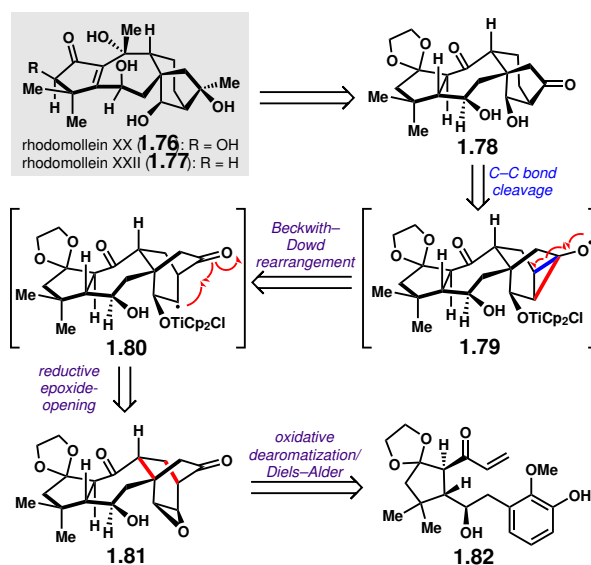


**Figure 1.3:** Rhodomollein XX and rhodomollein XXII.

skeleton. Many of these natural products are also densely functionalized with numerous stereogenic centers and oxygenation. Biosynthetically, the gryanoid natural products are thought to be related to the *ent*-kauranoid family of natural products due to the presence of the *ent*-kauranoid-like bicyclo[3.2.1]octane moiety (C/D rings). Adding to their previous work in *ent*-kauranoid natural product synthesis,<sup>29</sup> Ding and coworkers sought to prepare the structurally similar gryanoid natural products, focusing on establishing new strategies for accessing the bicyclo[3.2.1]octane moiety, which culminated in the first total syntheses of rhodomolleins XX and XXII.<sup>30</sup>

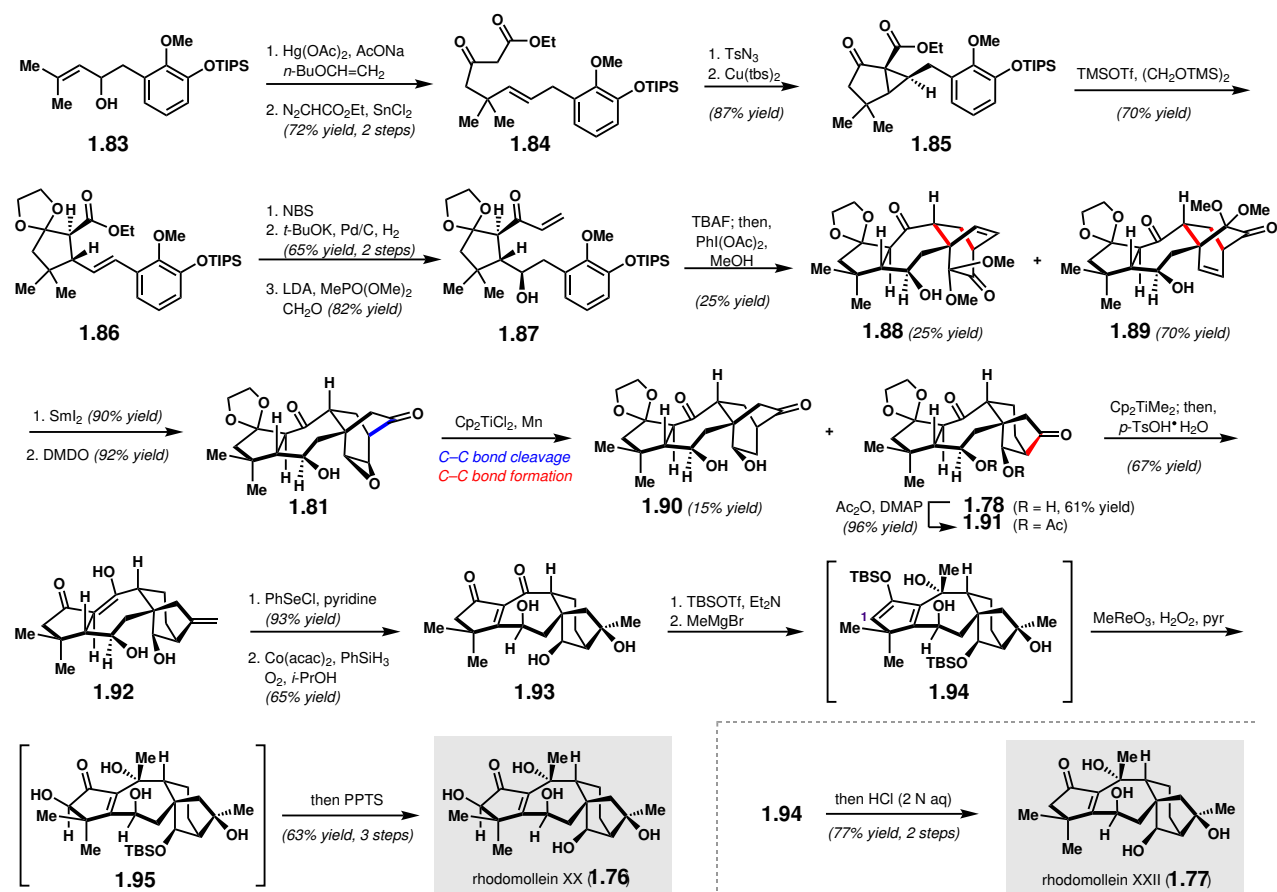
Ding and coworkers envisioned obtaining rhodomolleins XX and XXII in a divergent fashion from intermediate **1.78** via late-stage manipulations of the core framework (Scheme 1.11). [3.2.1] Bicycle-containing **1.78** was anticipated to arise from epoxide **1.81** through the key Ti(III)-mediated reductive radical cascade that would forge the key [3.2.1] bicycle. In the forward sense, this process would begin with Ti(III)-mediated epoxide ring opening to generate radical intermediate **1.80**, followed by radical cyclization to the proximal carbonyl to yield alkoxy radical **1.79**. This Beckwith–Dowd rearrangement would terminate with C–C bond cleavage, forging the [3.2.1] bicycle in the process. Overall, this process would effect a rearrangement of the [2.2.2] bicycle to a [3.2.1] bicycle, representing a substantial reorganization of the rhodomollein core framework. Finally, epoxide **1.81** would be obtained from phenol **1.82**, which in the forward sense would undergo a tandem oxidative dearomatization/Diels–Alder sequence to build the [2.2.2] bicycle of **1.81**.



**Scheme 1.11:** Retrosynthesis of rhodomollein XX and XXII.

The total synthesis (Scheme 1.12) began with treatment of **1.83** with *n*-butylvinyl ether and Hg(OAc)<sub>2</sub>, which promoted formation of a vinyl ether intermediate that underwent Claisen rearrangement followed by formation of  $\beta$ -ketoester **1.84** via a Roskamp reaction. Diazo formation with subsequent Cu-catalyzed cyclopropanation furnished cyclopropane **1.85**, which then underwent Noyori ketalization<sup>31</sup> with concomitant ring opening of the cyclopropane to give ketal **1.86**. Epoxidation of the benzylic olefin with NBS/H<sub>2</sub>O followed by a hydrogenative epoxide opening and Horner–Wadsworth–Emmons olefination with an

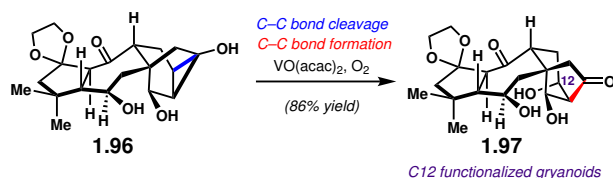
*in situ*-generated phosphonate ester provided enone **1.87**. Cleavage of the TIPS group unveiled the phenolic hydroxy group that, upon treatment with PIDA, underwent the oxidative dearomatization/Diels–Alder cascade to give the [2.2.2] bicycle as a mixture of diastereomers (**1.88** + **1.89**), with the the desired bicycle as the major diastereomer (**1.89**). Demethoxylation with  $\text{SmI}_2$  followed by epoxidation with DMDO afforded the key step precursor, epoxide **1.81**. Subjecting this epoxide to  $\text{Cp}_2\text{TiCl}_2$  and Mn proved effective for the key Ti-mediated cascade reaction, with the reaction affording a mixture of **1.90** and the desired [3.2.1] bicycle product (**1.78**), which was subsequently acetylated to give **1.91**. Olefination with subsequent deacetylation provided triol **1.92**, which was converted to **1.93** through  $\alpha$ -selenide elimination followed by Mukaiyama hydration of the *exo*-methylene. Protection of the left-hand ketone as the silyl enol ether, methyl Grignard addition into the central ketone, and hydroxylation of the C1 position with  $\text{MeReO}_3$  afforded **1.94**, which was elaborated to rhodomollein XX (**1.76**) following cleavage of the silyl ether. Likewise, rhodomollein XXII (**1.77**) was obtained from **1.94** after cleavage of the silyl enol ether and silyl ether with 2N HCl. Through their total synthesis of the rhodomollein natural products, Ding and coworkers effectively demonstrated the power of pairing robust ring-forming processes, such as the tandem oxidative dearomatization/Diels–Alder, with strategic C–C bond cleavage events, such as the



Scheme 1.12: Total synthesis of rhodomollein XX and XXII.



Ti(III)-mediated radical cascade, which can provide new opportunities for topological reorganization, enabling efficient transition between complex bicyclic scaffolds. Notably, while the key C–C bond cleavage step in the total syntheses terminated with reduction of the C12 position, through further studies, Ding and coworkers demonstrated that treatment of cyclopropanol **1.96** with VO(acac)<sub>3</sub> could afford the C–C bond cleavage product with subsequent C12 hydroxylation (**1.97**), potentially providing access to the C12 oxygenated congeners of the gryanoid family of natural products (Scheme 1.13).



**Scheme 1.13:** C–C bond cleavage with subsequent C12 functionalization.

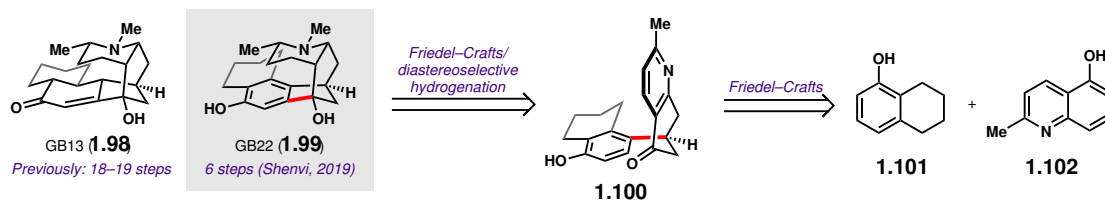
### 1.2.6 (±)-GB22 (Shenvi, 2019)

The bark of *Galbulimima belgraveana* and *G. baccata* exhibits hallucinogenic effects when chewed, and has therefore been used in traditional medicine in Papua New Guinea, Malaysia, and Northern Australia, where these tropical flowering plants are found.<sup>32</sup> However, the constituent natural products present in the bark—collectively named the GB alkaloids—have not been extensively tested for bioactivity, in part because their complex structures have made their chemical syntheses challenging, limiting the supply of material for biological study. For example, the most concise syntheses of GB13 (**1.98**) required 18–19 steps;<sup>33</sup> the related compound GB22 (**1.99**) had not been synthesized prior to 2019 (Scheme 1.14). Here, we discuss the synthesis of GB22 by Shenvi and coworkers utilizing a key Ir/Ni dual-catalytic siloxycyclopropane C–C bond cleavage/arylation, enabling access to GB22 in six steps in the longest linear sequence.<sup>34</sup>

Shenvi and coworkers originally envisioned that GB22 could arise through a phenol-ketone intramolecular Friedel–Crafts addition of **1.100** followed by diastereoselective hydrogenation of the pyridine ring; **1.100** in turn could be constructed by a Friedel–Crafts addition of phenol **1.101** and cyclohexadienone **1.102**. It was hypothesized that cyclohexadienone **1.102** might yield an  $\alpha,\beta$ -unsaturated oxocarbenium ion under acidic conditions to provide a reactive site for conjugate addition. However, all attempts to effect this Friedel–Crafts addition under Brønsted or Lewis acidic conditions failed, presumably because of the preferential Lewis acid coordination/protonation, and hence deactivation, of **1.101** over **1.102**. As a result, Shenvi and coworkers turned to an alternative method for forging this first C–C bond by exploiting C–C bond cleavage.

To prepare a precursor substrate for C–C bond cleavage, commercially available **1.103** was first converted to the silyl enol ether; Simmons–Smith cyclopropanation then delivered siloxycyclopropane **1.104** (Scheme 1.15). It was discovered that under iridium photocatalysis, single electron oxidation of siloxycyclopropane **1.104** yielded radical cation **1.106**, which prompted C–C bond cleavage to deliver radical intermediate **1.107**. Nickel-catalyzed

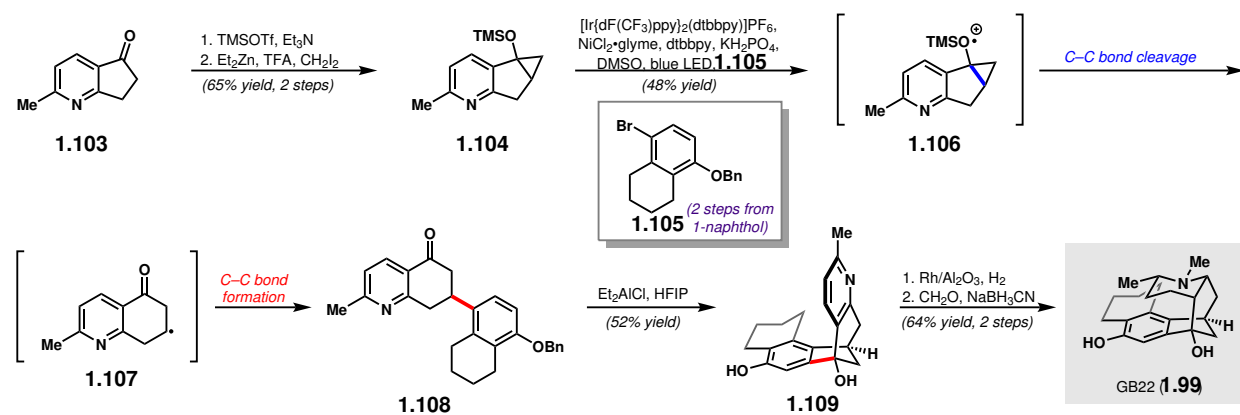




**Scheme 1.14:** GB alkaloids GB13 and GB22 and Shenvi and coworkers' original retrosynthesis of GB22.

cross-coupling with bromoarene **1.105** (available in two steps from 1-naphthol) then afforded **1.108**. Notably, this *endo*-selective siloxycyclopropane ring-opening can be contrasted with the *exo*-selective cyclopropanol ring-opening typically observed under two-electron Pd-catalysis, highlighting the complementarity of two-electron and one-electron transition metal reactivity manifolds. In addition, these siloxycyclopropane arylation conditions could be successfully implemented to couple a variety of siloxycyclopropanes, haloarenes, and haloalkenes.

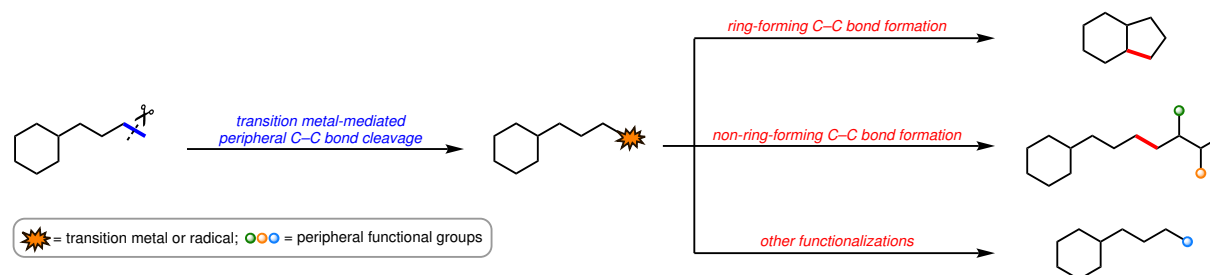
To forge the second C–C bond (i.e., **1.108** → **1.109**), several Lewis and Brønsted acids were screened, resulting only in retro-Friedel–Crafts additions. Ultimately, it was discovered that the combination of Et<sub>2</sub>AlCl and HFIP was uniquely capable of effecting the desired Friedel–Crafts addition. It was hypothesized that a complex such as Al[OCH(CF<sub>3</sub>)<sub>2</sub>]<sub>2</sub>Cl may be formed in situ, which could serve as a hydrogen bonding catalyst or a strong Lewis acid. After diastereoselective hydrogenation of the pyridine ring from the convex face and reductive amination with formaldehyde, the total synthesis of (±)-GB22 was completed in a total of six steps in the longest linear sequence. The brevity of the synthesis was enabled by a transition metal-mediated C–C bond cleavage/C–C bond formation event, where the formed C–C bond was otherwise difficult to install using more traditional methods.



**Scheme 1.15:** Shenvi and coworkers' synthesis of GB22.

## 1.3 Peripheral C–C Single Bond Cleavage in Total Synthesis

In contrast to core C–C single bond cleavage processes, “peripheral” C–C single bond cleavage, as defined here, takes place outside the central ring(s) of a synthetic intermediate, with subsequent functionalizations potentially leading to an array of diverse products (Scheme 16). As a result, peripheral C–C single bond cleavage does not inherently transform the core architecture of an intermediate; therefore, peripheral C–C single bond cleavage, unlike core C–C single bond cleavage, does not tend to be employed in counterintuitive retrosynthetic strategies. In fact, the cleavage and functionalization of peripheral C–C bonds tends to replicate processes that are already achievable with traditional reactive functional groups (e.g., a C–X bond, where X is a halogen). Nevertheless, peripheral C–C single bond cleavage events can present new retrosynthetic opportunities by 1) expanding the pool of starting materials to include building blocks with extra carbon atoms and 2) enabling the use of synthetic strategies and tactics that may have been infeasible with more traditional reactive functional groups, either as a result of the synthetic inaccessibility or instability of intermediates containing these moieties. Following are discussions of recent total syntheses that highlight the utility of employing peripheral C–C single bond cleavage as a strategic transform.

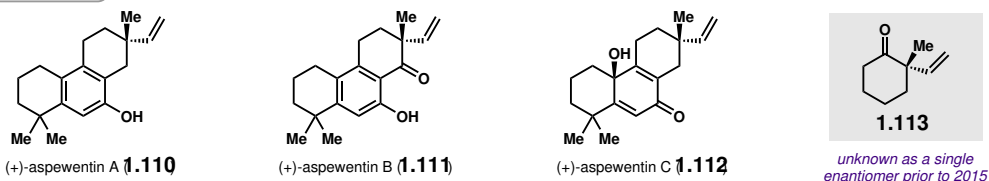


**Scheme 1.16:** Conceptual examples of peripheral C–C bond cleavage and functionalization.

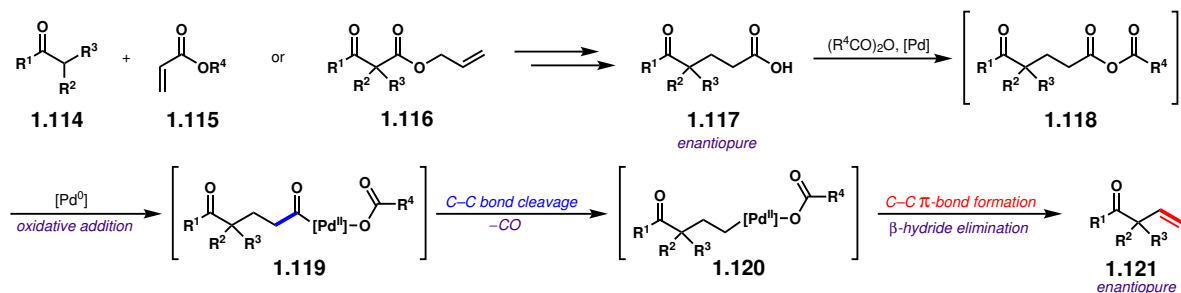
### 1.3.1 (–)-Aspewentins A, B, and C (Grubbs and Stoltz, 2015)

Norditerpenoid natural products (+)-aspewentins A (**1.110**), B (**1.111**), and C (**1.112**) were first isolated from marine-derived fungus *Aspergillus wentii* in 2014 and were determined to exhibit potent growth inhibition activities against marine plankton species (Scheme 1.17A).<sup>35</sup> Aspewentin B in particular possesses an all-carbon quaternary stereocenter bearing a vinyl group  $\alpha$  to a carbonyl, a structural motif that has been challenging for synthetic chemists to access enantioselectively. Indeed, even simple cyclohexanone **1.113** was unknown in the literature as a single enantiomer prior to 2015. In order to address this gap in synthetic methodology, Stoltz and coworkers developed a strategy for accessing  $\alpha$ -vinyl carbonyl compounds bearing an  $\alpha$ -quaternary stereocenter via Pd-catalyzed decarbonylative dehydration.<sup>36,37</sup> Specifically, carboxylic acids such as **1.117** could be obtained as a single enantiomer by enantioselective Michael addition of  $\alpha,\alpha$ -disubstituted enolates derived from carbonyl compounds **1.114** to acrylate acceptors (**1.115**); they could be alternatively accessed using

A. *Aspewentin Natural Products*



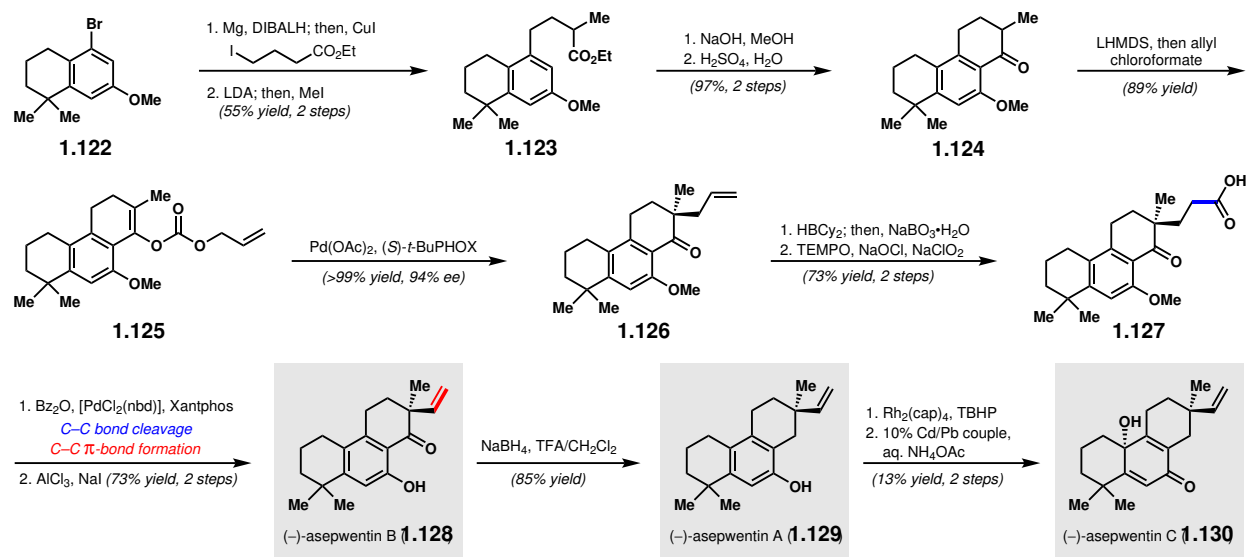
B. *Strategy for Accessing Enantiopure  $\alpha$ -Vinyl,  $\alpha$ -Quaternary Carbonyl Compounds*



**Scheme 1.17:** (+)-Aspewentins A–C and cyclohexanone **1.113** (A), and the strategy for accessing enantiopure  $\alpha$ -vinyl,  $\alpha$ -quaternary carbonyl compounds via Pd-catalyzed decarboxylative dehydration (B).

enantioselective Pd-catalyzed allylic alkylation of  $\beta$ -ketoesters **1.116** (Scheme 1.17B). Pd-catalyzed decarbonylative dehydration of carboxylic acids **1.117** then afforded enantiopure  $\alpha$ -vinyl,  $\alpha$ -quaternary carbonyl compounds **1.121**; this process presumably occurs through the in situ formation of mixed anhydrides **1.118**, followed by oxidative addition (**1.119**), decarbonylation (**1.120**), and  $\beta$ -hydride elimination. Stoltz and coworkers were able to implement this strategy on a variety of simple substrates to obtain the corresponding  $\alpha$ -vinyl,  $\alpha$ -quaternary carbonyl-containing products.

In order to further highlight the utility of this strategy, Stoltz and coworkers turned to the total synthesis of (–)-aspewentin B.<sup>36</sup> The Grignard reagent derived from aryl bromide **1.122** was alkylated with 4-iodobutyrate; subsequent  $\alpha$ -methylation afforded **1.123**. Saponification and acid-mediated cyclization then delivered tricyclic ketone **1.124**. Formation of the lithium enolate of **1.124** was followed by trapping with allyl chloroformate, yielding enol carbonate **1.125**. At this point, the aforementioned strategy for accessing  $\alpha$ -vinyl carbonyl compounds was implemented. First, Pd-catalyzed decarboxylative allylic alkylation of **1.125** with chiral ligand (*S*)-*t*-Bu-PHOX afforded  $\alpha$ -quaternary carbonyl compound **1.126** in 94% *ee*. Hydroboration-oxidation then transformed the terminal alkene to a primary hydroxy group, which was further oxidized to deliver carboxylic acid **1.127**. Finally, the key Pd-catalyzed decarbonylative dehydration yielded an  $\alpha$ -vinyl carbonyl compound through peripheral C–C bond cleavage, which was followed by phenyl methyl ether cleavage to complete the synthesis of (–)-aspewentin B (**1.128**). Benzylic carbonyl reduction of (–)-aspewentin B provided (–)-aspewentin A (**1.129**), which, in turn, could be transformed to (–)-aspewentin C (**622**) via oxidative dearomatization. The syntheses of (–)-aspewentins A–C highlight the ability of peripheral C–C bond cleavage/functionalization tactics to enable processes—namely, the enantiocontrolled formation of an all-carbon quaternary center bearing a vinyl group  $\alpha$  to a carbonyl—that had otherwise been synthetically challenging.



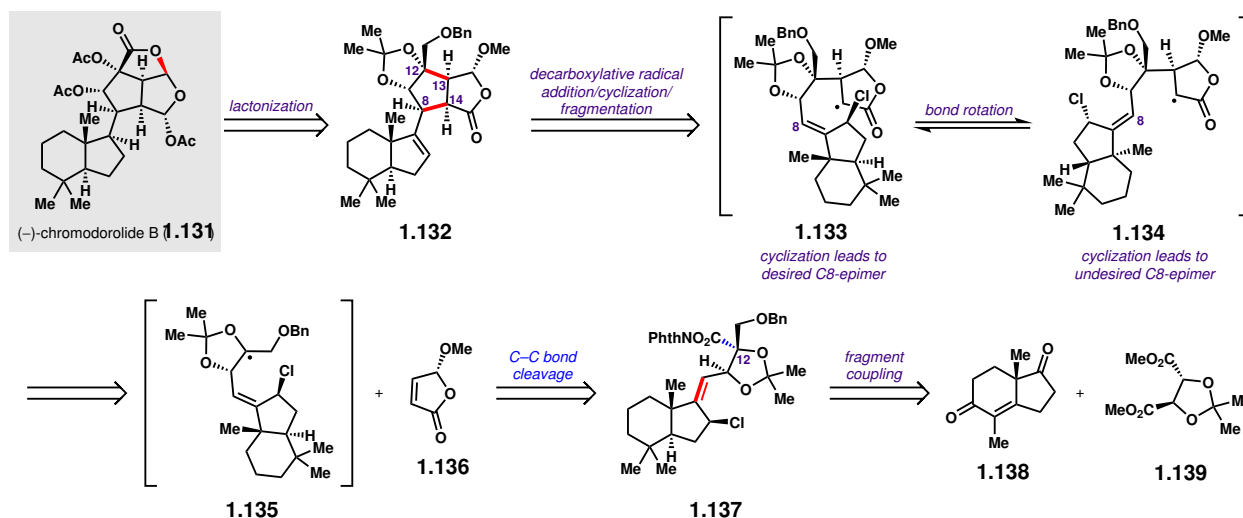
Scheme 1.18: Stoltz and coworkers' syntheses of (-)-asepwentins A–C.

### 1.3.2 (–)-Chromodorolide B (Overman, 2018, second-generation)

The chromodorolides are diterpenoid natural products originally isolated from nudibranchs in the genus *Chromodoris* and are hypothesized to originate from the sponges consumed by these nudibranchs.<sup>38</sup> Their structural analogy to other spongian diterpenes with potent effects on the Golgi apparatus suggests that the chromodorolides may also possess Golgi-modifying activity. In particular, the structure of (–)-chromodorolide B (**1.131**, Scheme 1.19) is characterized by a highly oxygenated 5/5/5 all-*cis*-fused tricyclic fragment linked to a second *trans*-hydrindane fragment; this complex pentacyclic skeleton and its associated ten contiguous stereocenters establish (–)-chromodorolide B as a highly challenging synthetic target. Herein, we discuss Overman and coworkers' second-generation synthesis of (–)-chromodorolide B using a transition metal-photocatalyzed decarboxylative radical addition/cyclization/fragmentation cascade, which proved to be highly effective in constructing the *cis*-oxabicyclo[3.3.0]octane ring system of the chromodorolides.<sup>39</sup>

Overman and coworkers hypothesized that (–)-chromodorolide B could arise through lactonization and other functional group manipulations from hydrindene **1.132**. Hydrindene **1.132** was, in turn, envisioned to arise from a decarboxylative radical addition / cyclization / fragmentation cascade ultimately beginning from *N*-acyloxyphthalimide fragment **1.137** and known butenolide fragment **1.136**. In the forward sense, this process was envisioned to proceed with formation of an  $\alpha$ -oxy radical (**1.135**) followed by conjugate addition to **1.136** to yield intermediate **1.133**; a final radical cyclization would complete the oxabicyclo[3.3.0] ring system. Notably, four stereocenters (at carbons 8, 12, 13, and 14) would have to be set with high levels of selectivity for this retrosynthetic disconnection to be reasonable. In particular, the bond rotation of intermediate **1.133** to rotamer **1.134** and subsequent cyclization could afford an undesired C8-epimer of **1.132**. It should be mentioned that the proposal of such a cascade sequence was enabled by the existence of decarboxylative methods for generating an  $\alpha$ -oxy radical, as alternative radical precursors (e.g., C12 halides) would likely be

unstable. To complete the retrosynthesis, *N*-acyloxyphthalimide **1.137** could ultimately be constructed from the coupling of two fragments derived from commercially available enedione **1.138** and tartaric acid-derived diester **1.139**, both known as single enantiomers.



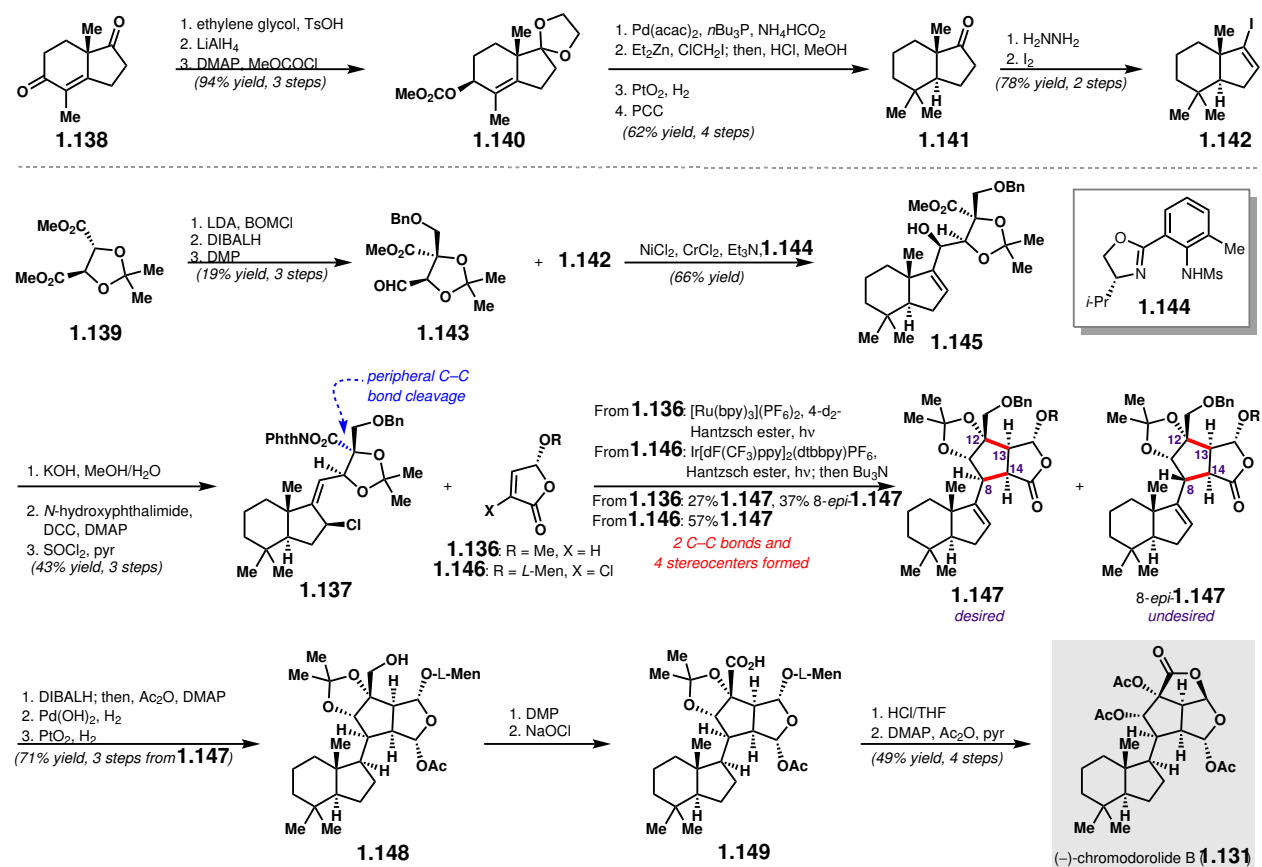
**Scheme 1.19:** Overman and coworkers' retrosynthesis of (-)-chromodorolide B.

Overman and coworkers began with the nine-step preparation of *trans*-hydrindenyl iodide fragment **1.142** from (*S*)-enedione **1.138** (Scheme 1.20). Protection of the cyclopentanone carbonyl as the ethylene glycol acetal, 1,2-reduction of the cyclohexenone, and acylation of the resulting secondary hydroxy group yielded allylic carbonate **1.140**. Pd-catalyzed reductive transposition provided a *trans*-hydrindene; subsequent cyclopropanation of the trisubstituted alkene, acetal hydrolysis, hydrogenolysis of the cyclopropane, and oxidation of the resulting secondary alcohol afforded *trans*-hydrindanone **1.141**. Finally, **1.141** was converted to vinyl iodide **1.142** over two steps by Barton iodination.<sup>40</sup> Notably, while vinyl iodide **1.142** had been reported before, previous routes were relatively inefficient and did not easily scale.

A second fragment, **1.143**, was synthesized in three steps from tartrate-derived diester **1.139**. Coupling of the two fragments (**1.143** and **1.142**) was then attempted. After some experimentation, it was discovered that Nozaki-Hiyama-Kishi coupling conditions with added oxazoline ligand **1.144** was optimal for the synthesis of allylic alcohol **1.145** as a single diastereomer; in contrast, similar reaction conditions without added ligand **1.144** or vinyl lithium-generating coupling conditions resulted only in low to modest diastereoselectivity. Saponification of **1.145** and esterification of the resulting acid with *N*-hydroxyphthalimide provided an *N*-acyloxyphthalimide compound; allylic OH → Cl transposition then yielded allylic chloride **1.137**.

Initial attempts at executing the key decarboxylative radical addition / cyclization / fragmentation sequence with *N*-acyloxyphthalimide **1.137** and butenolide **1.136** yielded a maximum of 27% of desired product **1.147** along with 37% of its C8-epimer, with the latter arising from cyclization of conformer **1.134** (Scheme 1.20). Notably, a deuterated Hantzsch ester was used to disfavor premature quenching of the reactive  $\alpha$ -acyl radical before the

subsequent C–C bond formation; however, small quantities of a product resulting from this premature quenching was still isolated under the optimized conditions. While the yield of the desired adduct (i.e., **1.147**) was low, the favorable diastereoselectivity of 5.5:1 with respect to the stereocenters generated at C12, C13, and C14 suggested that the coupling could be rendered efficient if the process resulting in 8-*epi*-**1.147** could be disfavored. Computational analysis of the transition states leading to **1.147** and 8-*epi*-**1.147** led to a hypothesis that the addition of a chlorine substituent to the  $\alpha$  position of the butenolide would favor the formation of **1.147** by enhancing steric interactions between this chlorine substituent and the allylic chlorine of fragment **1.137** in the transition state leading to 8-*epi*-**1.147**. This hypothesis was borne out experimentally, as the treatment of fragment **1.137** and chlorine-containing butenolide **1.146** under optimized photoredox-catalyzed conditions afforded desired product **1.147** exclusively in 57% yield, with dechlorination occurring in the same pot; notably, 8-*epi*-**1.147** was not detected in the crude reaction mixture. Additionally, under these reaction conditions, replacing Hantzsch ester with deuterated Hantzsch ester was found to be unnecessary. Overall, the key addition/cyclization/fragmentation sequence, initiated by peripheral C–C bond cleavage in the form of iridium photocatalyzed decarboxylation, resulted in the formation of two new C–C bonds and formed four stereocenters with high selectivity.



Scheme 1.20: Overman and coworkers' synthesis of (–)-chromodorolide B.

For the completion of the natural product, the lactone carbonyl of **1.147** was reduced diastereoselectively to the aluminum hemiacetal, which was acetylated *in situ*; hydrogenolysis of the benzyl ether followed by diastereoselective alkene reduction delivered primary alcohol **1.148**. Oxidation to the carboxylic acid over two steps afforded **1.149**, after which treatment with HCl triggered formation of the lactone and acetonide cleavage. Finally, global acetylation completed the synthesis of (–)-chromodorolide B (**1.131**). The rapid generation of target-relevant complexity associated with the key addition/cyclization/fragmentation sequence in this synthesis exemplifies the power of radical reactivity manifolds, entry into which may be facilitated by—or, in some situations, may even require—transition metal-mediated C–C bond cleavage.

### 1.3.3 Pyrone Diterpenes (±)-Subglutinol A, (±)-Subglutinol B, (±)-Sesquicillin A, and (±)-Higginsianin A (Baran, 2018)

Pyrone diterpenes are a class of natural products that have become the subject of increasing study in recent years as additional members of the subclass possessing interesting bioactivity continue to be discovered. Their bioactivity includes immunomodulatory, anti-infective, and cytotoxic activities.<sup>41</sup> In particular, subglutinol A (**1.150**), subglutinol B (**1.151**), and sesquicillin A (**1.152**) have been the targets of several previous synthetic efforts, resulting in completed syntheses in 21–27 steps (Figure 1.4).<sup>42</sup> The related compound higginsianin A (**1.153**), on the other hand, had not been the subject of total synthetic efforts prior to 2018. Herein, we discuss the syntheses of these four pyrone diterpenes by Baran and coworkers, which were completed in 15–17 steps by relying productively on transition metal-mediated peripheral C–C bond cleavage tactics.<sup>43</sup>

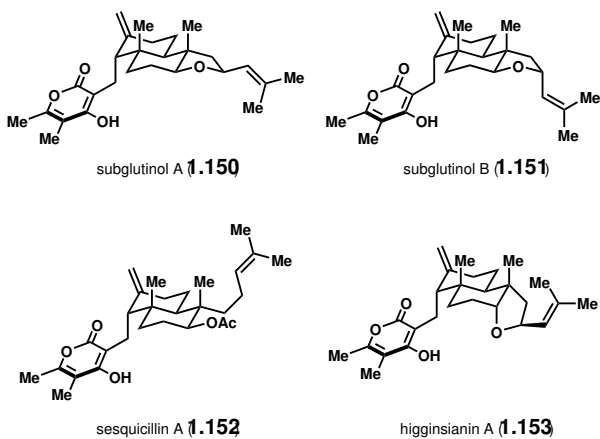
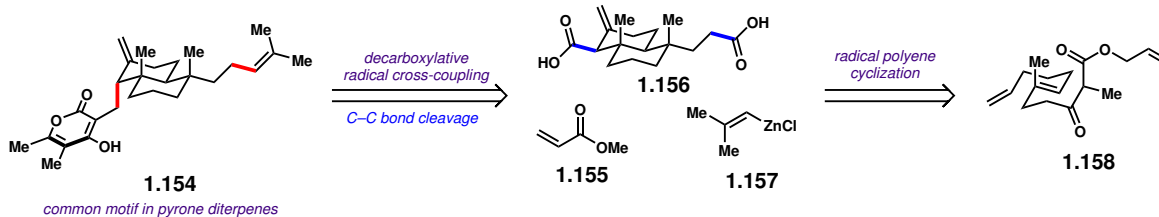


**Figure 1.4:** Pyrone diterpenes.

Previous syntheses of subglutinol A, subglutinol B, and sesquicillin A relied mainly on two-electron chemistry, requiring multiple protecting group, redox, and functional group manipulations in order to avoid functional group incompatibilities. In an attempt to avoid the high step counts associated with carrying out these manipulations, Baran and coworkers investigated one-electron chemistry to assemble the pyrone diterpene carbon skeletons.



Specifically, they envisioned that the carbon skeletons of these natural products (conceptually represented as **1.154**, Scheme 1.21) could arise from consecutive decarboxylative radical cross couplings between carboxylic acids (conceptually represented as **1.156**) and simple coupling partners **1.155** and **1.157**. The decalin system of compounds such as **1.156** could, in turn, arise from a radical polyene cyclization of linear  $\beta$ -ketoester **1.158**.

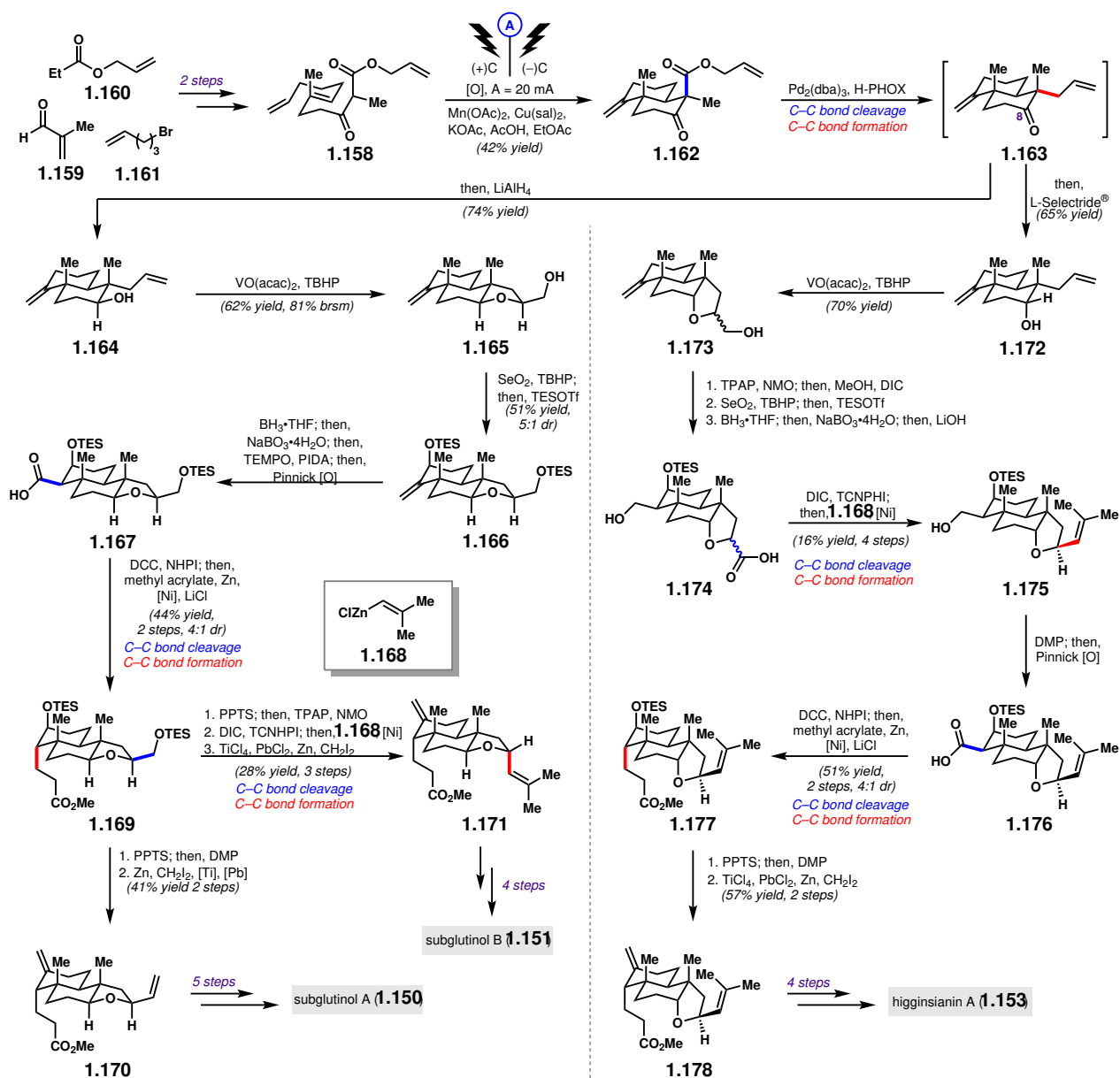


**Scheme 1.21:** Baran and coworkers' strategy for the synthesis of pyrone diterpenes.

Baran and coworkers began with polyene cyclization precursor **1.158**, available in two steps from simple building blocks **1.159**–**1.161** (Scheme 1.22). Extensive optimization efforts culminated in an electrochemically-assisted Mn-mediated radical polycyclization to furnish decalin system **1.162**. Tsuji allylation constituted the first peripheral C–C bond cleavage/C–C bond formation event, yielding intermediate **1.163**; at this point, the synthetic route diverged toward the various pyrone diterpenes. For the syntheses of subglutinols A and B, reduction of the carbonyl group from the  $\alpha$ -face was desired; this could be accomplished by treatment of intermediate **1.163** with  $\text{LiAlH}_4$ . Vanadium-catalyzed hydroxy-directed epoxidation of the terminal alkene of **1.164** triggered THF ring-closure, affording primary alcohol **1.165**. Allylic oxidation and silyl ether formation provided **1.166**, the alkene of which was converted to a carboxylic acid to deliver **1.167**. A decarboxylative Giese reaction of **1.167** with methyl acrylate then yielded **1.169**. Finally, silyl ether cleavage with PPTS, oxidation of the primary and secondary hydroxy groups by one oxidation state, and Takai–Lombardo olefination of both resulting carbonyl groups<sup>44</sup> afforded compound **1.170**, completing a formal synthesis of subglutinol A (5 steps from **1.170**). Alternatively, from **1.169**, silyl ether cleavage, oxidation of the primary hydroxy group to the carboxylic acid and the secondary hydroxy group to the ketone, and decarboxylative alkenylation with alkenylzinc species **1.168** resulted in diastereoselective installation of an isopropenyl group; Takai–Lombardo olefination then provided **1.171**, completing the formal synthesis of subglutinol B (4 steps from **1.171**).

Compared to subglutinols A and B, higginsianin A is epimeric at C8; the desired stereoconfiguration for the synthesis of higginsianin A was established by L-Selectride® reduction of intermediate **1.163** to give **1.172**. Vanadium-catalyzed epoxidation and THF ring-closure afforded primary alcohol **1.173** as a mixture of diastereomers; subsequent oxidation of the primary hydroxy group to the carboxylic acid was followed by methyl esterification. Allylic oxidation, triethylsilyl ether formation, hydroboration-oxidation, and methyl ester saponification then delivered carboxylic acid **1.174** as a mixture of diastereomers. Diastereoselective isopropenyl group installation again could be accomplished via decarboxylative alkenylation with alkenylzinc species **1.168**, yielding primary alcohol **1.175**. After oxidation to carboxylic acid **1.176**, a decarboxylative Giese reaction with methyl acrylate afforded **1.177** as the major diastereomer. Silyl ether cleavage, oxidation of the resulting secondary hydroxy group to

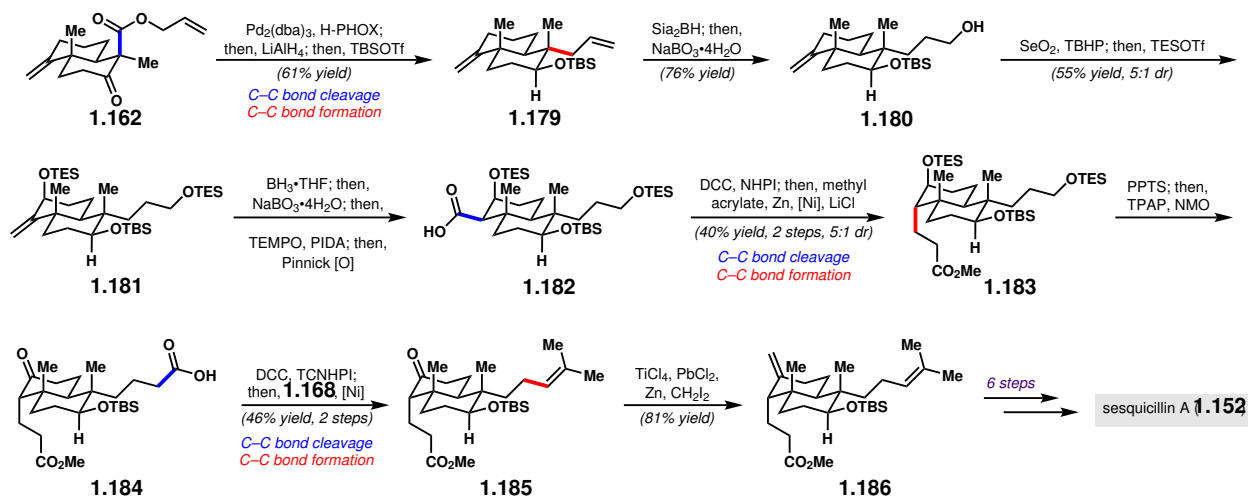




**Scheme 1.22:** Baran and coworkers' synthesis of subglutinol A (**1.150**), subglutinol B (**1.151**), and higginsianin A (**1.153**).

the ketone, and Takai–Lombardo olefination delivered **1.178**; in a four-step sequence analogous to that required for the syntheses of subglutinols A and B, **1.178** could be transformed to higginsianin A (**1.153**).

Finally, sesquicillin A, which lacks a THF ring, was synthesized using a similar strategy (Scheme 1.23). Decarboxylative Tsuji allylation of **1.162**, reduction of the carbonyl, and protection of the resulting hydroxy group as the TBS ether afforded compound **1.179**. Hydroboration-oxidation, allylic oxidation, and triethylsilyl ether formation then delivered protected triol **1.181**. Conversion of the alkene to a carboxylic acid provided **1.182**, which



**Scheme 1.23:** Baran and coworkers' synthesis of sesquicillin A (**1.152**).

underwent a decarboxylative Giese reaction to yield **1.183** as the major diastereomer. Silyl ether cleavage and global oxidation then afforded carboxylic acid **1.184**, which underwent decarboxylative alkenylation with alkenylzinc species **1.168** to yield isopropenyl-containing compound **1.185**. Finally, Takai–Lombardo olefination provided **1.186**, completing the formal synthesis of sesquicillin A (6 steps from **1.186**).

Across the four syntheses of these pyrone diterpenes by Baran and coworkers, eleven peripheral C–C bond cleavage/C–C bond formation events were executed. In particular, the decarboxylative alkenylation events for the installation of isopropenyl groups deserve further comment, as they powerfully highlight the advantages of transition metal-mediated C–C bond cleavage/functionalization: 1) the precursor carboxylic acids are located  $\alpha$  to an ethereal oxygen, rendering alternative radical precursors (e.g., alkyl halides) potentially unstable; and 2) in comparison to decarboxylative Giese reactions, decarboxylative alkenylations take further advantage of transition metal reactivity, as the transition metals guide C–C bond formation after re-engaging with the initially formed radical species. Overall, the four syntheses of pyrone diterpenes discussed here illustrate the power of retrosynthetic disconnections involving peripheral C–C bond cleavage/functionalization.

### 1.3.4 (+)-Longirabdiol, (–)-Longirabdolactone, and (–)-Effusin (Li, 2019)

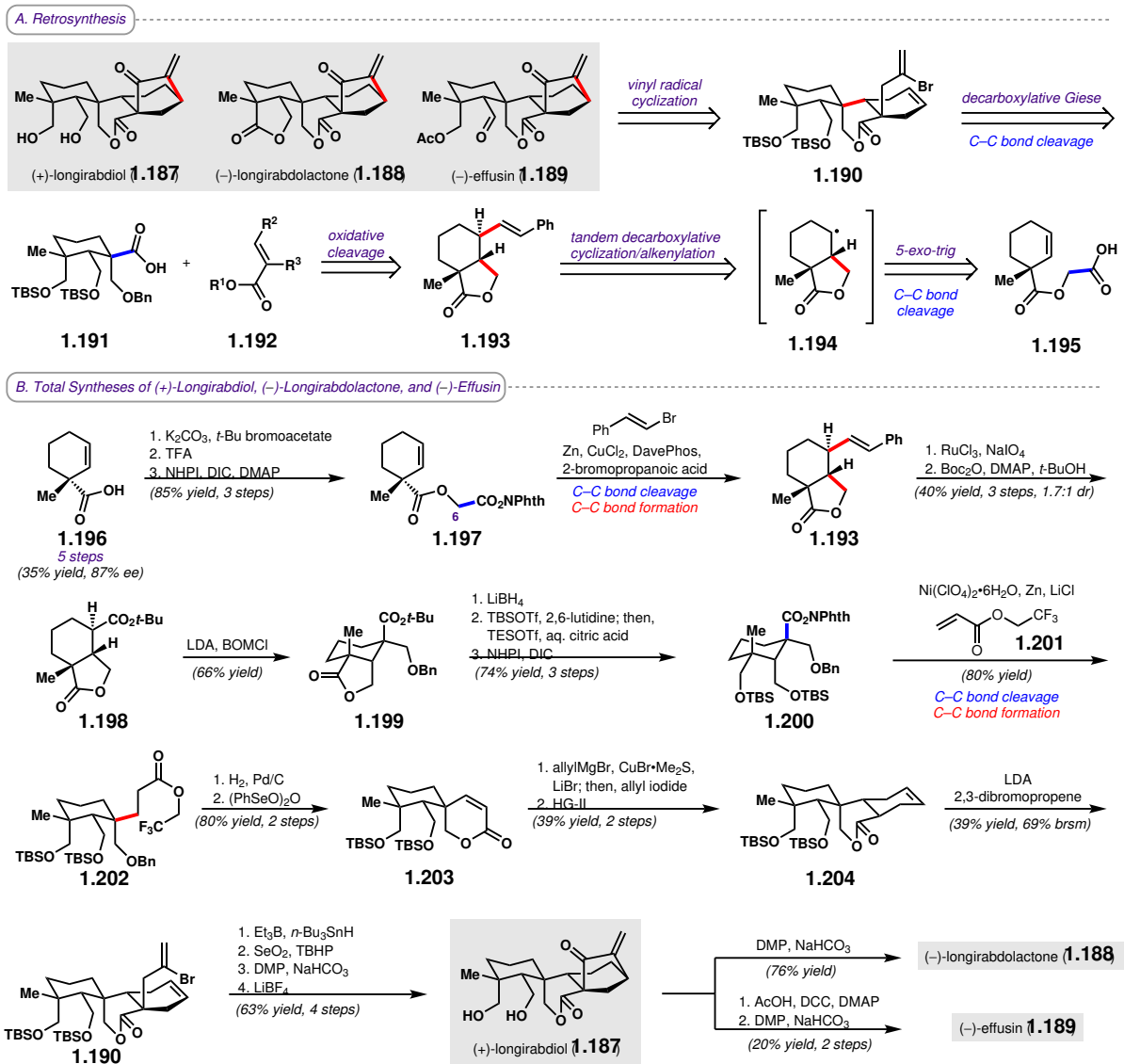
The *ent*-kauranoid natural products, a family of diterpenoids isolated from the *Isodon* genus of flowering plants, have exhibited a wide range of bioactivities, including antibacterial, antitumor, anti-inflammatory, and antifedant activities.<sup>45</sup> Their biological activities, in addition to their intricate carbon skeletons, have made them the subject of intense synthetic interest over the years. However, syntheses of spiro-lactone *ent*-kauranoids (+)-longirabdiol (**1.187**, Scheme 1.24A), (–)-longirabdolactone (**1.188**), and (–)-effusin (**1.189**), as well as their specific bioactivities, had not been reported prior to 2019. Here, we discuss the first syntheses of these natural products by Li and coworkers, which made use of decarboxylative

tactics for the formation of key C–C bonds.<sup>46</sup> Specifically, Li and coworkers envisioned that the bicyclo[3.2.1]octane of the three natural products could be furnished through a vinyl radical cyclization from vinyl bromide **1.190**; **1.190** could in turn arise from a decarboxylative Giese reaction between acid **1.191** and a suitable  $\alpha,\beta$ -unsaturated ester radical acceptor (**1.192**). The carboxylic acid of **1.191** would be obtained from oxidative cleavage of alkene **1.193**, two carbon-carbon bonds of which would be forged in a novel tandem decarboxylative cyclization/alkenylation sequence from acid **1.195** via radical intermediate **1.194**.

Li and coworkers began their synthesis with a known five-step sequence, converting commercially available ethyl 2-cyclohexanonecarboxylate enantioselectively to carboxylic acid **1.196**; in an additional three steps, *N*-acyloxyphthalimide **1.197** was synthesized, serving as a precursor for the key tandem decarboxylative cyclization/alkenylation sequence (Scheme 1.24B). After extensive optimization, it was found that reductive cross-coupling conditions with CuCl<sub>2</sub> as catalyst, DavePhos as ligand, and 2-bromopropanoic acid as additive were optimal for decarboxylative cyclization/alkenylation with  $\beta$ -bromostyrene, delivering lactone **1.193** in 60% yield by <sup>1</sup>H NMR as a mixture of diastereomers. These conditions were found to be adequate for the syntheses of several other  $\gamma$ -lactones as well. Mechanistic studies indicated that both a radical addition-fragmentation pathway as well as a copper-catalyzed radical cross-coupling pathway may be operative. It should be noted that the construction of  $\gamma$ -lactones by C <sub>$\gamma$</sub>  to C <sub>$\beta$</sub>  radical cyclization had not been previously achieved because of the relative rarity of alternative radical precursors (e.g.,  $\alpha$ -oxy halides); carboxylic acid derivatives are thus uniquely enabling in this regard. Oxidative cleavage of the alkene in **1.193** followed by esterification afforded **1.198** in 40% isolated yield over three steps.

$\alpha$ -Alkylation of ester **1.198** with BOMCl provided benzyl ether **1.199** as a single diastereomer, suggesting that electrophile addition occurred exclusively from the  $\alpha$ -face to avoid 1,3-diaxial interactions with the axial methyl group. As this diastereoselectivity would be undesired for the subsequent decarboxylative Giese reaction, efforts were taken to hinder the  $\alpha$ -face. Thus, the lactone of **1.199** was reduced, and the resulting hydroxy groups were protected as bulky TBS ethers; esterification then yielded *N*-acyloxyphthalimide **1.200**. While efforts to install a tethered radical acceptor followed by effecting an intramolecular decarboxylative Giese were unfruitful, an intermolecular decarboxylative Giese with **1.201** successfully provided product **1.202** as a single diastereomer, validating the hypothesis that the bulky TBS ethers would drive radical addition from the  $\beta$ -face. Hydrogenolysis of the benzyl ether triggered spontaneous lactonization, after which oxidation with benzeneseleninic anhydride afforded unsaturated lactone **1.203**.

Initial attempts to introduce an additional six-membered ring by a Diels–Alder cycloaddition with 1,3-butadiene were unsuccessful; therefore, a two-step alternative was performed instead, whereby allyl cuprate conjugate addition followed by treatment with allyl iodide yielded a diolefin, and subsequent ring-closing metathesis delivered **1.204**.  $\alpha$ -Allylation with 2,3-dibromopropene provided vinyl bromide **1.190**, which cyclized upon treatment with Et<sub>3</sub>B and *n*-Bu<sub>3</sub>SnH to furnish a bicyclo[3.2.1]octane. Sequential treatment with SeO<sub>2</sub> and DMP afforded an allylic ketone intermediate, which after silyl ether cleavage yielded (+)-longirabdiol. (–)-Longirabdolactone and (–)-effusin could be accessed from (+)-longirabdiol in one and two steps, respectively. The completion of the first total syntheses of these natural products, enabled by peripheral decarboxylative C–C bond cleavage/C–C bond formation tactics, provided material for biological study, wherein each of the three natural products



**Scheme 1.24:** Retrosynthesis (A) and total syntheses of (+)-longirabdiol, (-)-longirabdolactone, and (-)-effusin (B).

were found to exhibit low micromolar activity in cell viability assays against ten different cancer cell lines.

## 1.4 Conclusion and Outlook

The syntheses described above highlight the retrosynthetic disconnections uniquely enabled by transition metal-mediated C–C single bond cleavage tactics. In several cases, C–C bond cleavage-based synthetic strategies resulted in shorter synthetic routes than had been accomplished thus far with more traditional strategies, often as a result of facilitating the formation of organometallic or radical intermediates that would otherwise be difficult to

access. Despite the potential advantages of incorporating C–C bond cleavage tactics into synthetic strategies, it remains a relatively rare phenomenon in total synthesis. At least two reasons can be offered to explain why this is the case. First, as highlighted in this review, the use of a combination of core C–C bond cleavage and ring-forming events tends to result in counterintuitive synthetic routes, challenging the creative capabilities of synthetic planners; therefore, it may be that the inability to “map on” carbon frameworks in natural products to those in starting materials when using core C–C bond cleavage tactics has limited their use thus far in total synthesis. Second, there has historically been a paucity of transition metal-mediated C–C bond cleavage/functionalization methods relative to those that are purely bond-constructive.

To the extent that these two reasons account for the relative lack of C–C bond cleavage in total synthesis, there is much reason to believe that C–C bond cleavage will see increasing use in total synthesis in the future. First, much attention has been given recently to the increasing capabilities of computer-assisted retrosynthetic planners;<sup>47</sup> it may be that these planners will have a comparative advantage in discovering routes employing C–C bond cleavage tactics, which would otherwise be counterintuitive for a human synthetic planner to devise. Second, there has been a profusion of C–C bond cleavage methodologies in recent years, setting the stage for bond constructions beyond those employed in the syntheses covered in this review. As a result, opportunities abound for the innovative total synthetic chemist. One area ripe for innovation is the C–C bond cleavage of unstrained rings, for which a number of impactful methodologies have been published recently<sup>48</sup> but whose use in total synthesis has so far been limited (the synthesis of (–)-lingzhiol described above being the sole exception highlighted in this review). As compared to the use of strained ring C–C bond cleavage tactics, we anticipate that the use of unstrained ring C–C bond cleavage tactics in total synthesis would both enable myriad retrosynthetic opportunities—as unstrained rings are far more common in simple chemical building blocks than strained rings—as well as help further curtail the lengths of syntheses, given that synthetic steps often must be expended to construct strained rings before subsequent C–C bond cleavage. In addition, there remain opportunities for advancement in the use of peripheral C–C bond cleavage in total synthesis, moving beyond decarboxylative strategies; for example, the use of newly-published methods for C–C bond cleavage on substrates at a lower oxidation state than the carboxylic acid (e.g., at the alcohol or aldehyde oxidation state)<sup>49</sup> promises to streamline syntheses that often spend multiple steps on oxidation to the carboxylic acid, and, in some cases, further esterification.

Between the dual trends of 1) the increasing capabilities of computer-assisted retrosynthetic planners, which may more easily discover counterintuitive synthetic routes employing C–C bond cleavage tactics, and 2) the increasing abundance of C–C bond cleavage methodologies, there is much reason to believe that the use of transition metal-mediated C–C bond cleavage in total synthesis will only become more prominent in the future. The complexity of natural products generally makes them ideal “proving grounds” for synthetic strategies and tactics; therefore, the increasing utility of transition metal-mediated C–C single bond cleavage in natural product synthesis may be a harbinger of its more widespread application in other synthetic fields. This development, if it comes to pass, may have welcome impacts on drug discovery, materials synthesis, and chemical biology.

## 1.5 References

- (1) Drahl, M. A.; Manpadi, M.; Williams, L. J. *Angew. Chem. Int. Ed.* **2013**, *52*, 11222–11251.
- (2) (a) Woodward, R. B.; Doering, W. E. *J. Am. Chem. Soc.* **1944**, *66*, 849–849; (b) Woodward, R. B.; Doering, W. E. *J. Am. Chem. Soc.* **1945**, *67*, 860–874.
- (3) Trost, B. M.; Hu, Y.; Horne, D. B. *J. Am. Chem. Soc.* **2007**, *129*, 11781–11790.
- (4) C–C bond cleavage followed by further radical reactivity can, of course, be initiated without a transition metal as well. For examples of recent total syntheses employing C–C bond cleavage followed by radical reactivity without a transition metal, see ref. [5].
- (5) (a) Imamura, Y.; Yoshioka, S.; Nagatomo, M.; Inoue, M. *Angew. Chem. Int. Ed.* **2019**, *58*, 12159–12163; (b) Fujino, H.; Nagatomo, M.; Paudel, A.; Panthee, S.; Hamamoto, H.; Sekimizu, K.; Inoue, M. *Angew. Chem. Int. Ed.* **2017**, *56*, 11865–11869; (c) W. M. Crossley, S.; Tong, G.; Lambrecht, M. J.; Burdge, H. E.; Shenvi, R. **2019**, DOI: 10.26434/chemrxiv.9275318.v1; (d) Renata, H.; Zhou, Q.; Dünstl, G.; Felding, J.; Merchant, R. R.; Yeh, C.-H.; Baran, P. S. *J. Am. Chem. Soc.* **2015**, *137*, 1330–1340.
- (6) Breitler, S.; Carreira, E. M. *Angew. Chem. Int. Ed.* **2013**, *52*, 11168–11171.
- (7) Fumagalli, G.; Stanton, S.; Bower, J. F. *Chem. Rev.* **2017**, *117*, 9404–9432.
- (8) Chen, P.-h.; Billett, B. A.; Tsukamoto, T.; Dong, G. *ACS Catal.* **2017**, *7*, 1340–1360.
- (9) Marek, I.; Masarwa, A.; Delaye, P.-O.; Leibeling, M. *Angew. Chem. Int. Ed.* **2015**, *54*, 414–429.
- (10) Souillart, L.; Cramer, N. *Chem. Rev.* **2015**, *115*, 9410–9464.
- (11) Sivaguru, P.; Wang, Z.; Zanoni, G.; Bi, X. *Chem. Soc. Rev.* **2019**, *48*, 2615–2656.
- (12) Nairoukh, Z.; Cormier, M.; Marek, I. *Nat. Rev. Chem.* **2017**, *1*, 1–17.
- (13) Morcillo, S. P. *Angew. Chem. Int. Ed.* **2019**, *58*, 14044–14054.
- (14) Murakami, M.; Ishida, N. *Cleavage of Carbon-Carbon Single Bonds by Transition Metals* **2015**, 253–272.
- (15) Kuroda, Y. et al. *Nature Chem.* **2018**, *10*, 938–945.
- (16) Miyaoka, H.; Saka, Y.; Miura, S.; Yamada, Y. *Tetrahedron Lett.* **1996**, *37*, 7107–7110.
- (17) Mohr, P. J.; Halcomb, R. L. *J. Am. Chem. Soc.* **2003**, *125*, 1712–1713.
- (18) (a) Matsumura, S.; Maeda, Y.; Nishimura, T.; Uemura, S. *J. Am. Chem. Soc.* **2003**, *125*, 8862–8869; (b) Nishimura, T.; Uemura, S. *J. Am. Chem. Soc.* **1999**, *121*, 11010–11011; (c) Nishimura, T.; Ohe, K.; Uemura, S. *J. Am. Chem. Soc.* **1999**, *121*, 2645–2646.
- (19) (a) Seiser, T.; Cramer, N. *J. Am. Chem. Soc.* **2010**, *132*, 5340–5341; (b) Seiser, T.; Cramer, N. *Angew. Chem. Int. Ed.* **2008**, *47*, 9294–9297.
- (20) Ishida, N.; Sawano, S.; Masuda, Y.; Murakami, M. *J. Am. Chem. Soc.* **2012**, *134*, 17502–17504.

- (21) (a) Masarwa, A.; Weber, M.; Sarpong, R. *J. Am. Chem. Soc.* **2015**, *137*, 6327–6334; (b) Weber, M.; Owens, K.; Masarwa, A.; Sarpong, R. *Org. Lett.* **2015**, *17*, 5432–5435.
- (22) (a) Bermejo, F. A.; Fernández Mateos, A.; Marcos Escribano, A.; Martín Lago, R.; Mateos Burón, L.; Rodríguez López, M.; Rubio González, R. *Tetrahedron* **2006**, *62*, 8933–8942; (b) Martín-Rodríguez, M.; Galán-Fernández, R.; Marcos-Escribano, A.; Bermejo, F. A. *J. Org. Chem.* **2009**, *74*, 1798–1801.
- (23) Kerschgens, I.; Rovira, A. R.; Sarpong, R. *J. Am. Chem. Soc.* **2018**, *140*, 9810–9813.
- (24) Deng, L.; Chen, M.; Dong, G. *J. Am. Chem. Soc.* **2018**, *140*, 9652–9658.
- (25) Xu, T.; Dong, G. *Angew. Chem. Int. Ed.* **2012**, *51*, 7567–7571.
- (26) Xu, T.; Dong, G. *Angew. Chem. Int. Ed.* **2014**, *53*, 10733–10736.
- (27) Long, R.; Huang, J.; Shao, W.; Liu, S.; Lan, Y.; Gong, J.; Yang, Z. *Nat. Commun.* **2014**, *5*, 1–10.
- (28) Yan, Y.-M.; Ai, J.; Zhou, L.; Chung, A. C.; Li, R.; Nie, J.; Fang, P.; Wang, X.-L.; Luo, J.; Hu, Q.; Hou, F.-F.; Cheng, Y.-X. *Org. Lett.* **2013**, *15*, 5488–5491.
- (29) He, C.; Hu, J.; Wu, Y.; Ding, H. *J. Am. Chem. Soc.* **2017**, *139*, 6098–6101.
- (30) Yu, K.; Yang, Z.-N.; Liu, C.-H.; Wu, S.-Q.; Hong, X.; Zhao, X.-L.; Ding, H. *Angew. Chem. Int. Ed.* **2019**, *58*, 8556–8560.
- (31) Noyori, R.; Murata, S.; Suzuki, M. *Tetrahedron* **1981**, *37*, 3899–3910.
- (32) Rinner, U.; Lentsch, C.; Aichinger, C. *Synthesis* **2010**, *2010*, 3763–3784.
- (33) (a) Movassaghi, M.; Hunt, D. K.; Tjandra, M. *J. Am. Chem. Soc.* **2006**, *128*, 8126–8127; (b) Zi, W.; Yu, S.; Ma, D. *Angew. Chem. Int. Ed.* **2010**, *49*, 5887–5890; (c) Larson, K. K.; Sarpong, R. *J. Am. Chem. Soc.* **2009**, *131*, 13244–13245.
- (34) Burdge, H. E.; Oguma, T.; Kawajiri, T.; Shenvi, R. **2019**, DOI: 10.26434/chemrxiv.8263415.v1.
- (35) Miao, F.-P.; Liang, X.-R.; Liu, X.-H.; Ji, N.-Y. *J. Nat. Prod.* **2014**, *77*, 429–432.
- (36) Liu, Y.; Virgil, S. C.; Grubbs, R. H.; Stoltz, B. M. *Angew. Chem. Int. Ed.* **2015**, *54*, 11800–11803.
- (37) Liu, Y.; Kim, K. E.; Herbert, M. B.; Fedorov, A.; Grubbs, R. H.; Stoltz, B. M. *Adv. Synth. Catal.* **2014**, *356*, 130–136.
- (38) Dumdei, E. J.; De Silva, E. D.; Andersen, R. J.; Choudhary, M. I.; Clardy, J. *J. Am. Chem. Soc.* **1989**, *111*, 2712–2713.
- (39) (a) Tao, D. J.; Slutskyy, Y.; Muuronen, M.; Le, A.; Kohler, P.; Overman, L. E. *J. Am. Chem. Soc.* **2018**, *140*, 3091–3102; (b) Tao, D. J.; Slutskyy, Y.; Overman, L. E. *J. Am. Chem. Soc.* **2016**, *138*, 2186–2189.
- (40) Barton, D. H. R.; Bashirdes, G.; Fourrey, J.-L. *Tetrahedron Lett.* **1983**, *24*, 1605–1608.
- (41) Al-Khdhairawi, A. A. Q.; Cordell, G. A.; Thomas, N. F.; Nagojappa, N. B. S.; Weber, J.-F. F. *Org. Biomol. Chem.* **2019**, DOI: 10.1039/C9OB01501A.

- (42) (a) Zhang, F.; Danishefsky, S. J. *Angew. Chem. Int. Ed.* **2002**, *41*, 1434–1437; (b) Katoh, T.; Oguchi, T.; Watanabe, K.; Abe, H. *Heterocycles* **2010**, *80*, 229; (c) Kim, H.; Baker, J. B.; Lee, S.-U.; Park, Y.; Bolduc, K. L.; Park, H.-B.; Dickens, M. G.; Lee, D.-S.; Kim, Y.; Kim, S. H.; Hong, J. *J. Am. Chem. Soc.* **2009**, *131*, 3192–3194; (d) Kikuchi, T.; Mineta, M.; Ohtaka, J.; Matsumoto, N.; Katoh, T. *Eur. J. Org. Chem.* **2011**, *2011*, 5020–5030; (e) Kim, H.; Baker, J. B.; Park, Y.; Park, H.-B.; DeArmond, P. D.; Kim, S. H.; Fitzgerald, M. C.; Lee, D.-S.; Hong, J. *Chem. Asian J.* **2010**, *5*, 1902–1910.
- (43) Merchant, R. R.; Oberg, K. M.; Lin, Y.; Novak, A. J. E.; Felding, J.; Baran, P. S. *J. Am. Chem. Soc.* **2018**, *140*, 7462–7465.
- (44) Takai, K.; Kakiuchi, T.; Kataoka, Y.; Utimoto, K. *J. Org. Chem.* **1994**, *59*, 2668–2670.
- (45) Sun, H.-D.; Huang, S.-X.; Han, Q.-B. *Nat. Prod. Rep.* **2006**, *23*, 673–698.
- (46) Zhang, J.; Li, Z.; Zhuo, J.; Cui, Y.; Han, T.; Li, C. *J. Am. Chem. Soc.* **2019**, *141*, 8372–8380.
- (47) Coley, C. W.; Green, W. H.; Jensen, K. F. *Acc. Chem. Res.* **2018**, *51*, 1281–1289.
- (48) (a) Roque, J. B.; Kuroda, Y.; Göttemann, L. T.; Sarpong, R. *Science* **2018**, *361*, 171–174; (b) Roque, J. B.; Kuroda, Y.; Göttemann, L. T.; Sarpong, R. *Nature* **2018**, *564*, 244–248; (c) Xia, Y.; Lu, G.; Liu, P.; Dong, G. *Nature* **2016**, *539*, 546–550; (d) Zhao, K.; Yamashita, K.; Carpenter, J. E.; Sherwood, T. C.; Ewing, W. R.; Cheng, P. T. W.; Knowles, R. R. *J. Am. Chem. Soc.* **2019**, *141*, 8752–8757; (e) Hu, A.; Chen, Y.; Guo, J.-J.; Yu, N.; An, Q.; Zuo, Z. *J. Am. Chem. Soc.* **2018**, *140*, 13580–13585; (f) Guo, J.-J.; Hu, A.; Chen, Y.; Sun, J.; Tang, H.; Zuo, Z. *Angew. Chem. Int. Ed.* **2016**, *55*, 15319–15322.
- (49) (a) Xu, Y.; Qi, X.; Zheng, P.; Berti, C. C.; Liu, P.; Dong, G. *Nature* **2019**, *567*, 373–378; (b) Murphy, S. K.; Park, J.-W.; Cruz, F. A.; Dong, V. M. *Science* **2015**, *347*, 56–60; (c) Wu, X.; Cruz, F. A.; Lu, A.; Dong, V. M. *J. Am. Chem. Soc.* **2018**, *140*, 10126–10130; (d) Zhang, K.; Chang, L.; An, Q.; Wang, X.; Zuo, Z. *J. Am. Chem. Soc.* **2019**, *141*, 10556–10564.



## Chapter 2

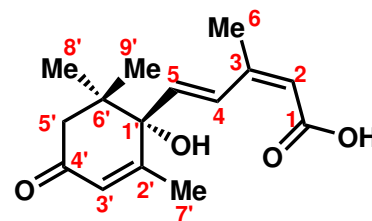
# The History and Biology of Abscisic Acid and Attempted Syntheses of Rationally Designed Analogs

### 2.1 A Brief History of Abscisic Acid: Initial Discovery To Current Agricultural Relevance

Abscisic acid (**2.1**, Figure 2.1), as one of the five “classical” phytohormones,<sup>1</sup> has been a subject of intense study by both plant biologists and synthetic chemists since its initial isolation by Addicott and Lyon from cotton fruit in 1963.<sup>2</sup> Since it was believed to promote the abscission, or shedding, of plant leaves, it was initially given the name “abscisin II.” A compound inducing dormancy in woody plants was isolated that same year and was referred to as a “dormin”;<sup>3</sup> it was later shown that this compound was identical to abscisin II.<sup>4</sup> After its structure was confirmed by chemical synthesis<sup>5</sup>—with the absolute configuration of the natural compound later determined to be the (*S*)-enantiomer<sup>6–8</sup>—the name of abscisin II/dormin was revised to abscisic acid (ABA) in order to prevent further confusion.<sup>9</sup> The name has persisted despite the gradual discovery that ABA does not play a major role in regulating abscission for most plant species.

Today, ABA is known to be a ubiquitous plant hormone found in virtually all plant species.<sup>10,11</sup> It plays a regulatory role for a variety of plant functions, including but not limited to seed dormancy and germination<sup>12</sup>; plant responses to abiotic stresses such as drought, salinity, and cold temperatures<sup>13–15</sup>; and fruit ripening.<sup>13</sup> The importance of ABA to plant function has motivated its thorough study over the past 50 years, resulting in an increased understanding of its mechanism of action, biosynthesis, and catabolism, and in synthetic routes to the natural product or its analogs (*vide infra*).

The importance of ABA has not been lost on the agricultural industry, with Valent BioSciences Corporation in particular having commercialized ABA for its exogenous ap-



(*S*)-abscisic acid (**2.1**)

**Figure 2.1:** Structure of (*S*-abscisic acid (ABA) (**2.1**).

plication to crop plants. Specifically, Valent BioSciences has marketed ABA formulations for increasing the drought tolerance of flowers (Contego™),<sup>16</sup> delaying corn seed germination (BioNik®),<sup>17</sup> and promoting the ripening of red table grapes (ProTone®).<sup>18</sup> Given the potential opportunities for the advancement of agriculture, ABA analogs with greater potency and/or metabolic stability, as well as enhanced synthetic accessibility, warrant further study (*vide infra*). Rational design of these analogs requires a proper understanding of the mechanism of action of ABA at the molecular level.

## 2.2 The Biology of Abscisic Acid

### 2.2.1 Mechanism of Action

While many intermediates involved in ABA signal transduction had been identified previously, elucidation of the early events in signal transduction had been hampered by the lack of identification of an ABA receptor until relatively recently. In 2009, two groups simultaneously discovered the class of receptors responsible for the initial binding of ABA; Park et al. named these *Pyrabactin Resistance/Pyrabactin Resistance 1-Like* (PYR/PYL) receptors,<sup>20</sup> while Ma et al. referred to them as the *Regulatory Component of ABA Receptor* (RCAR) class of receptors.<sup>21</sup> The identification of these receptors led to the proposal of a central signaling module for ABA signaling (Figure 2.2). Upon ABA binding, PYR/PYL/RCAR receptors (“PYR” in Figure 2.2; dimeric receptors shown, although many members of the

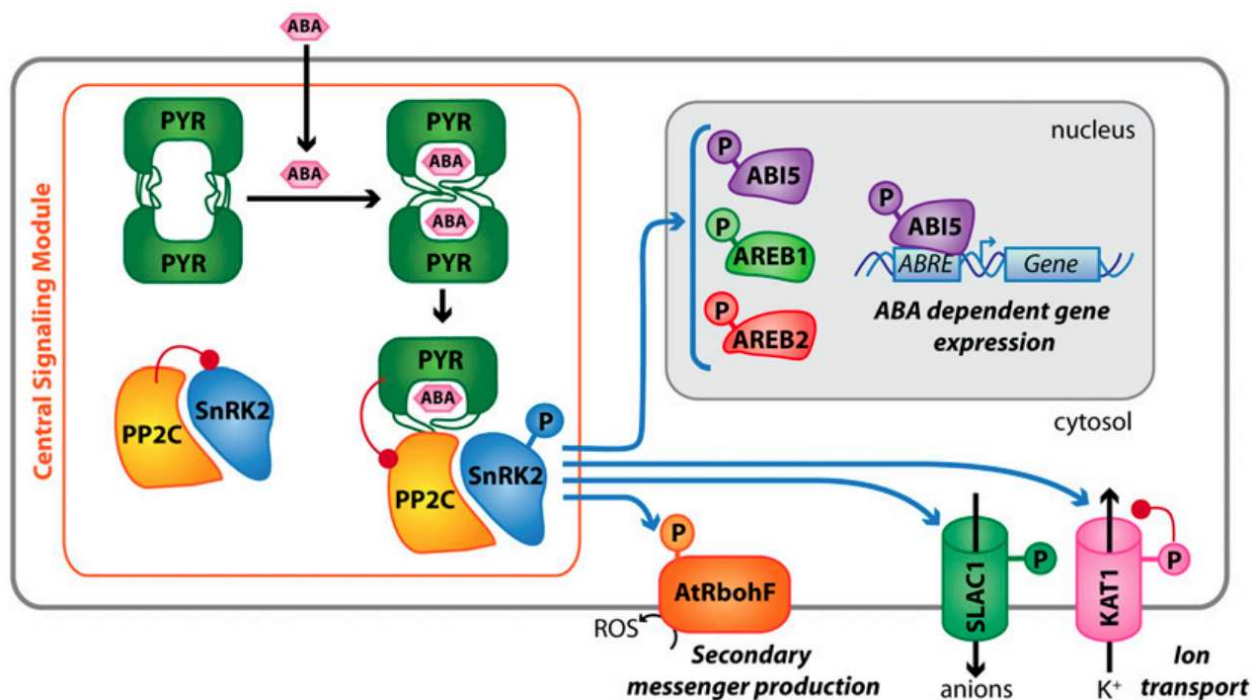


**Figure 2.2:** Central signaling module for ABA signaling. Figure reproduced from ref. [19]. Copyright 2010 Cold Spring Harbor Laboratory Press. Licensed under CC BY-NC 4.0 (<https://creativecommons.org/licenses/by-nc/4.0/legalcode>).

class exist as monomers) undergo a conformational change and can then bind to a member of the protein phosphatase 2C (PP2C) class. The PP2C—which, in the absence of ABA, dephosphorylates and therefore inactivates an SNF1-related protein kinase 2 (SnRK2)—is inhibited by its participation in the PYR/PYL/RCAR–ABA–PP2C ternary complex. Phosphorylated SnRK2s are then able to accumulate and phosphorylate enzymes, transcription factors, and ion channels to modulate metabolism, gene expression, and ion transport, respectively. The existence of 14 PYR/PYL/RCARs, 9 PP2Cs, 3 SnRK2s, and numerous downstream SnRK2 targets speaks to the complexity of the regulatory network controlled by ABA.<sup>19,22,23</sup>

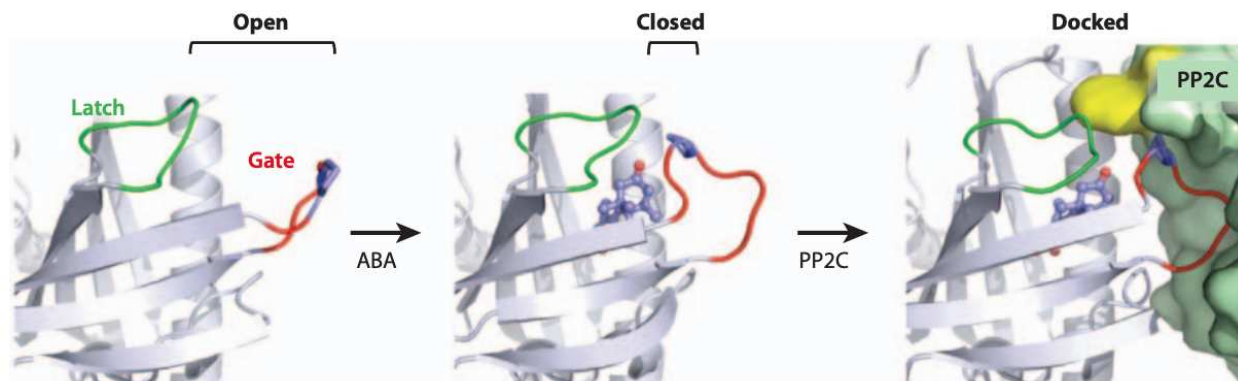


**Figure 2.3:** “Gate-latch-lock” mechanism of ABA signal transduction. Republished with permission of Her Majesty the Queen in Right of Canada, as represented by the Minister of Innovation, Science, and Economic Development, 2010, from ref. [22]; permission conveyed through Copyright Clearance Center, Inc.

A number of X-ray crystallographic studies published soon after the discovery of the PYR/PYL/RCAR receptors have illuminated the details of the events that immediately follow ABA binding.<sup>24</sup> Specifically, a “gate-latch-lock” mechanism is proposed, whereby the initial binding of ABA to the PYR/PYL/RCAR receptor induces a conformational change such that a loop (the “gate”) covers the newly bound ABA (Figure 2.3), along with a separate “latch” loop. In the PYR/PYL/RCAR–ABA complex, the carboxylic acid, hydroxy, and carbonyl groups of ABA are especially important for making water-mediated hydrogen bonds to polar residues in the binding pocket; a number of hydrophobic contacts between ABA and hydrophobic residues in the binding pocket are also important (Figure 2.4). Once ABA is bound, the folded gate loop then forms a hydrophobic surface that can recruit the binding of a PP2C (Figure 2.3). The indole ring of a tryptophan residue of the PP2C inserts between the gate and latch loops and forms a water-mediated hydrogen bond to ABA, “locking” the ternary complex in place.<sup>24e</sup>

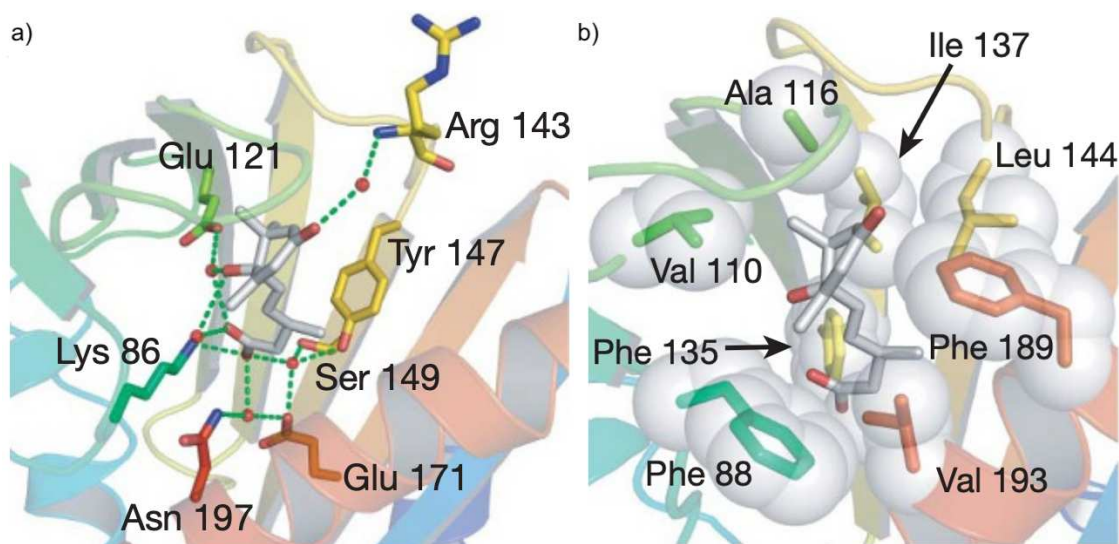
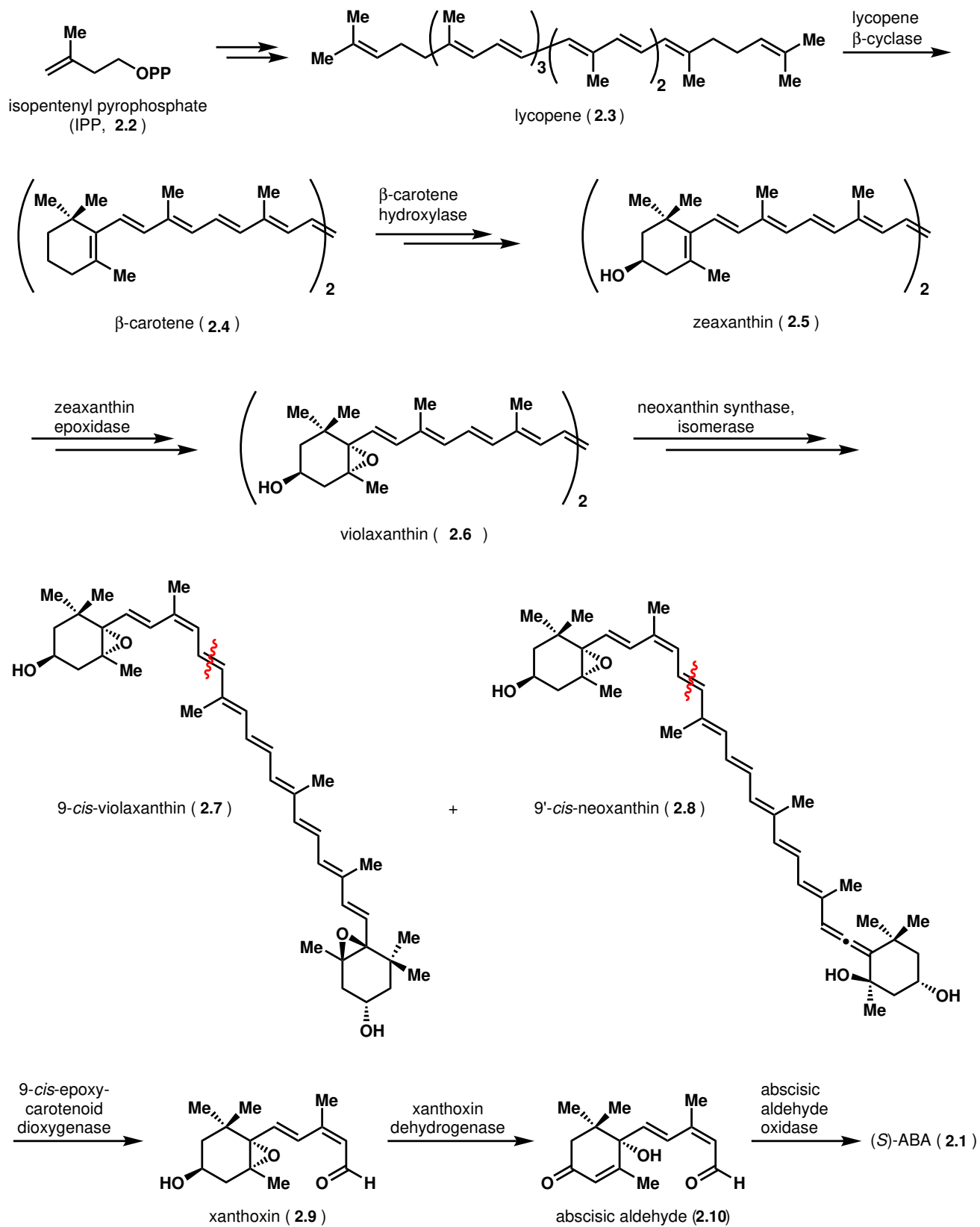


**Figure 2.4:** a) Hydrogen bond network between ABA and PYL1. b) Hydrophobic interactions between ABA and PYL1. Reprinted by permission from Springer Nature Customer Service Centre GmbH: Springer Nature, ref. [24c], Copyright 2009.

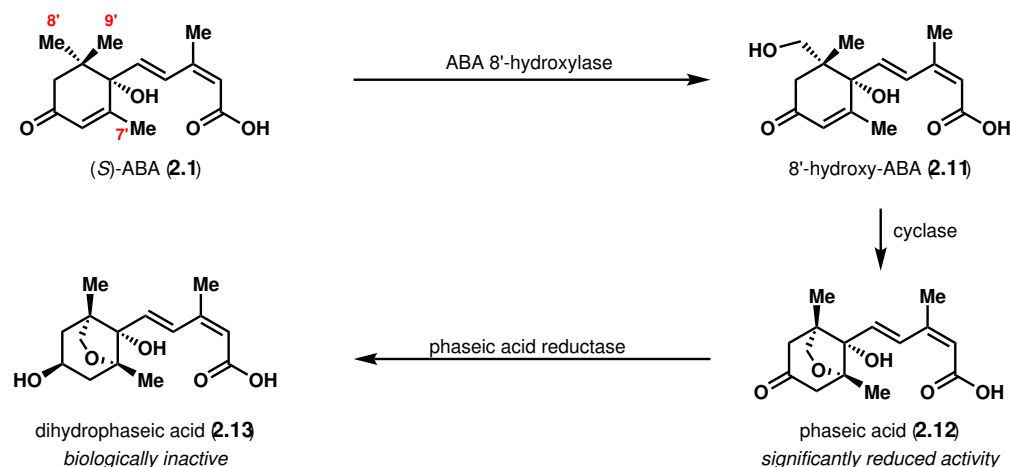
### 2.2.2 Biosynthesis and Catabolism

The levels of ABA in a plant cell are regulated by the relative rates of biosynthesis and catabolism. The biosynthesis of ABA begins with isopentenyl phosphate (IPP, **2.2**) synthesized via the non-mevalonate pathway (Scheme 2.1).<sup>25,26</sup> Sequential condensations and dehydrogenations yield the C<sub>40</sub> carotenoid lycopene (**2.3**), which is then cyclized by lycopene  $\beta$ -synthase to  $\beta$ -carotene (**2.4**). Hydroxylation, epoxidation, and isomerization then delivers isomers 9-*cis*-violaxanthin (**2.7**) and 9'-*cis*-neoxanthin (**2.8**) via intermediates zeaxanthin (**2.5**) and violaxanthin (**2.6**). Oxidative cleavage releases the C<sub>15</sub> aldehyde xanthoxin (**2.9**; subsequent oxidation yields first abscisic aldehyde (**2.10**) and finally abscisic acid (**2.1**).

The catabolism of ABA occurs via hydroxylation and/or glucosyl conjugation.<sup>25,26</sup> While hydroxylation at the 7' and 9' positions have been reported, enzymatic hydroxylation at the 8' position is typically thought to be the predominant method of ABA catabolism via hydroxylation (Scheme 2.2). 8'-hydroxy-ABA (**2.11**) then isomerizes to phaseic acid (**2.12**) in a step that has been postulated to be catalyzed enzymatically.<sup>27</sup> Phaseic acid shows significantly reduced bioactivity in general, although this varies among bioassays. The further reduction of phaseic acid to dihydrophaseic acid (**2.13**) results in complete abrogation of bioactivity. The carboxy and hydroxy groups on ABA or any of its catabolites can also be conjugated to glucose and then exported from the cell, with the glucosyl ester of ABA being the most common glucosylated catabolite. In general, phaseic acid and dihydrophaseic acid have been observed to be the most abundant catabolites, suggesting that 8'-hydroxylation is the predominant catabolic pathway. Accordingly, the preparation of ABA analogs with reduced propensity for oxidation at the 8'-position has previously been investigated, with the aim of increasing metabolic stability (*vide infra*).



Scheme 2.1: Biosynthesis of (*S*)-abscisic acid (2.1).



**Scheme 2.2:** Catabolism of (*S*)-abscisic acid (**2.1**) via 8'-hydroxylation.

## 2.3 Previous Investigations of Abscisic Acid Analogs

While several syntheses of racemic<sup>5,28,29</sup> and enantiopure<sup>6,8,30–32</sup> ABA exist, chemical synthesis has not been able to provide ABA in as efficient a manner as fungal fermentation, which is used industrially.<sup>33</sup> Therefore, the role of synthetic chemists has primarily been to investigate the structure-activity relationships of ABA via the synthesis of analogs that are not accessible biosynthetically.

### 2.3.1 8'-Functionalized ABA Analogs

As of 2002, over 100 ABA analogs had been synthesized and investigated for their bioactivities.<sup>34</sup> Of these, many were 8'-functionalized analogs investigated for their ability to slow the oxidation at the 8' position largely responsible for ABA catabolism (e.g., **2.14–2.21**, Figure 2.5).<sup>35</sup> Those that retained higher bioactivity than ABA in long-term assays could potentially be used as metabolically stable ABA analogs for agricultural use.

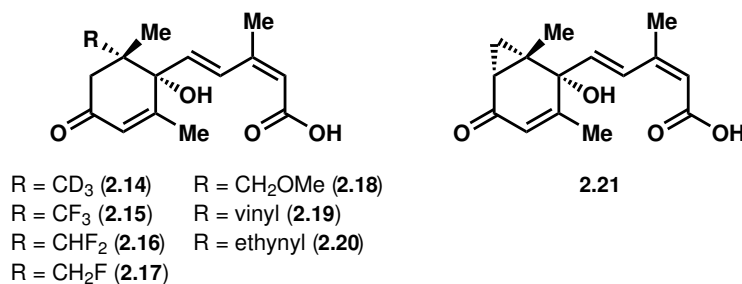


**Figure 2.5:** 8'-functionalized ABA analogs.

Todoroki and coworkers synthesized enantiopure 8'-functionalized ABA analogs **2.14–2.21** and tested their bioactivity in two separate assays: 1) an assay measuring the extent of stomatal opening of the epidermal strips of spiderwort, and 2) an assay measuring the elongation of the second leaf sheath of rice seedlings.<sup>35</sup> The stomatal opening assay was

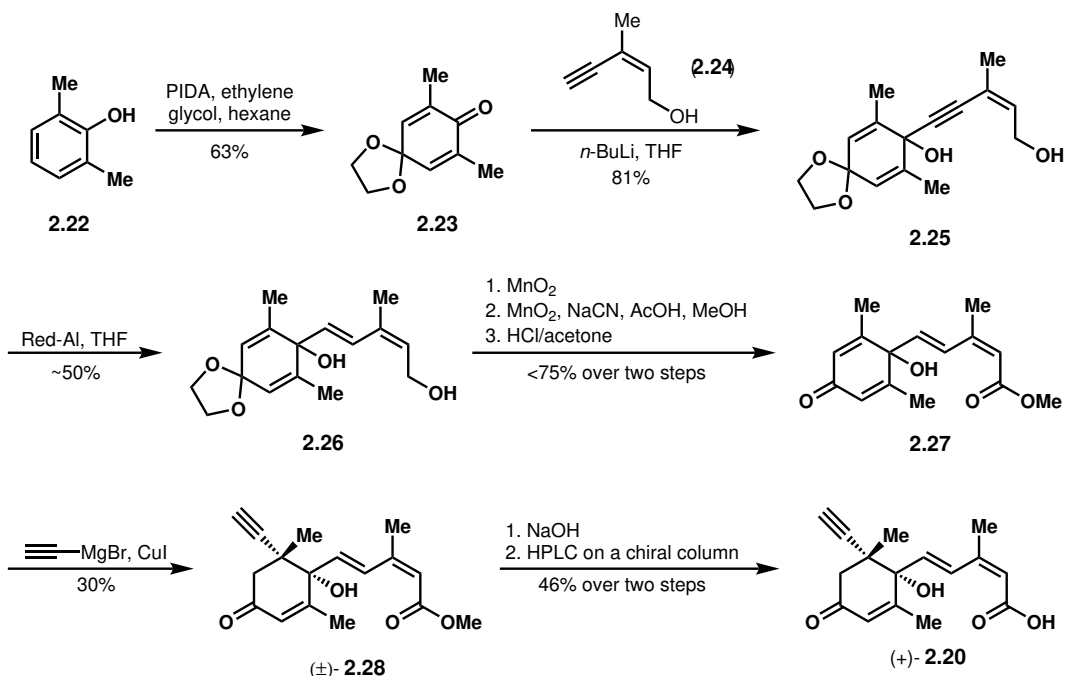


conducted over 3 h, whereas the rice elongation assay was measured over 7 d; as a result, the extent of inhibition of stomatal opening was taken purely as a measure of compound binding affinities to the ABA receptors, whereas the extent of inhibition of rice elongation accounted for metabolic stability as well. The activities of the 8'-functionalized analogs were compared to that of (*S*-ABA) in the same assays. As seen in Table 2.1, on the whole, the 8'-functionalized analogs were similarly active to ABA in the short-term stomatal opening assay, but were more potent than ABA in the long-term rice elongation assay, suggesting that 8'-functionalization did not significantly interfere with ABA binding to its receptor, but was effective at curtailing catabolism via 8'-hydroxylation. Particularly striking are the examples of **2.15**, **2.20**, and **2.21** (entries 2, 7, and 8), which were >30 times more potent than ABA in the long-term rice elongation assay while retaining comparable activity in the short-term stomatal opening assay. These results are in accordance with the hypothesis that 8'-functionalized ABA analogs are less competent substrates for ABA 8'-hydroxylase,<sup>36</sup> although it is also possible that these compounds act as suicide inhibitors of ABA 8'-hydroxylase.<sup>37</sup>

**Table 2.1:** Biological activities of ABA analogs **2.14**–**2.21** in a short-term stomatal opening assay and in a long-term rice elongation assay. <sup>a</sup>IC<sub>50</sub> Ratio refers to the IC<sub>50</sub> value of the ABA analog divided by the IC<sub>50</sub> value of (*S*)-ABA.

Entry	Compound	IC <sub>50</sub> Ratio <sup>a</sup> (stomatal opening)	IC <sub>50</sub> Ratio <sup>a</sup> (rice elongation)
1	<b>2.14</b>	0.88	0.34
2	<b>2.15</b>	0.92	0.03
3	<b>2.16</b>	1.16	0.17
4	<b>2.17</b>	1.15	1.25
5	<b>2.18</b>	6.21	0.22
6	<b>2.19</b>	1.50	0.30
7	<b>2.20</b>	1.18	0.03
8	<b>2.21</b>	0.94	0.03

The syntheses of these 8'-functionalized ABA analogs is not trivial, typically requiring 10–15 steps from readily available starting materials, including resolution of racemic material by HPLC with a chiral column. The synthesis of ethynyl-bearing analog **2.20** is shown below as an instructive example. The synthesis commences with oxidative dearomatization of 2,6-dimethylphenol (**2.22** with ethylene glycol, yielding benzoquinone acetal **2.23** (Scheme 2.3).<sup>38</sup> Acetylide addition of **2.24** produces diol **2.25**, after which tertiary hydroxy group-directed Red-Al® reduction of the alkyne delivers *trans*-alkene **2.26**. Oxidation of the primary hydroxy group to the aldehyde, Corey–Gilman–Ganem oxidation to the methyl ester, and hydrolysis of the acetal affords compound **2.27**. Ethynyl cuprate addition in a 1,4-fashion to the doubly  $\alpha$ ,  $\beta$ -unsaturated ketone yields alkyne **2.28** as a racemic mixture; finally, saponification of the ester and separation of the enantiomers by HPLC on a chiral column affords enantiopure ABA analog **2.20**.<sup>35f</sup>



Scheme 2.3: Synthesis of 8'-methylidyne-ABA (2.20).

### 2.3.2 Structure-Activity Relationships of ABA

Based on the numerous ABA analogs synthesized and tested for biological activity, a qualitative account of the structure-activity relationships of ABA can be given, and is briefly discussed here (Figure 2.6). The C8' and C9' methyl groups are considered to be important for engaging in hydrophobic interactions with the binding pocket, as the removal of both methyl groups results in a decrease in activity. The C6 and C7' methyl groups are more important still, as removal of either results in complete abrogation of bioactivity. The orientation of the *Z*-double bond is essential, and is presumed to be important for positioning the carboxylic acid to properly make hydrogen bonding interactions; the importance of the hydrogen bonding capacity of the carboxylic acid group, as well as that of the 4'-carbonyl group and 1'-hydroxyl group, has been confirmed by X-ray crystallographic studies of ABA bound to its receptor (*vide supra*). Finally, the C2'-C3' double bond can be reduced to a single bond without substantially diminishing bioactivity, although only if the 7' methyl

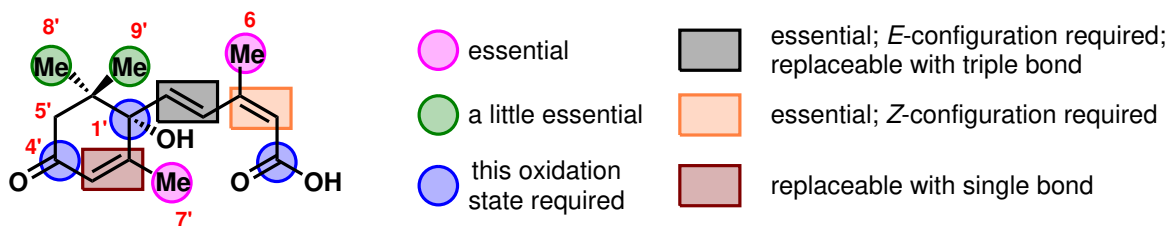


Figure 2.6: Qualitative summary of ABA structure-activity relationships. Reproduced from ref. [34], Copyright 2002, with permission from Elsevier.



group is placed *cis* to the dienolic acid side chain; the *trans* isomer is inactive, presumably as a result of a change in the conformation of the molecule. Notably, 5'-functionalized ABA analogs have not been studied in detail to-date.

### 2.3.3 Rational Design of an ABA Receptor Antagonist

Most ABA analogs were synthesized and tested for biological activity before the identities of the ABA receptors were established; the discovery of the PYR/PYL/RCAR class of receptors, and the existence of crystal structures of these receptors with ABA bound, has introduced new opportunities for the rational design of ABA analogs. Most pertinently, Takeuchi et al. described in 2014 the rational design of ABA analogs as antagonists of the PYR/PYL/RCAR-PP2C interaction.<sup>39</sup> Antagonists of ABA-induced signal transduction could find applications in agriculture, given that ABA inhibits seed germination; the careful application of antagonists to seeds could enable the finer control of seed germination rates.

ABA analog design by Takeuchi et al. began with the observation that a small, solvent-exposed tunnel formed by conserved hydrophobic residues in the PYR/PYL/RCAR receptors resided near the 3' position of ABA. Such a tunnel could potentially accommodate an alkyl chain; in addition, protrusion of an alkyl substituent through the tunnel would interfere with PP2C docking, therefore inhibiting the downstream effects of normal ABA-induced signal transduction. To test this hypothesis, Takeuchi et al. designed and synthesized "AS6" (**2.29**, Figure 2.7), a 3'-hexylsulfanyl ABA analog expected to act as an antagonist.

Both *in vitro* and *in vivo* assays bore out this prediction. When co-applied with ABA, AS6 effectively suppressed the normally inhibitory effect of ABA on *Arabidopsis* seed germination, resulting in faster-germinating seeds (Figure 2.8); the same trend was observed for lettuce seed germination. AS6-treated radish seedlings wilted more readily than ABA-treated seedlings, consistent with AS6 exhibiting antagonism toward ABA promotion of drought tolerance. Expression of ABA-responsive genes by qRT-PCR was detected in ABA-treated *Arabidopsis*, but not in AS6-treated specimens. Finally, in an enzyme inhibition assay, PP2C activity was reduced by PYL/PYR/RCAR receptors in the presence of ABA, but was reduced significantly less in the presence of AS6.

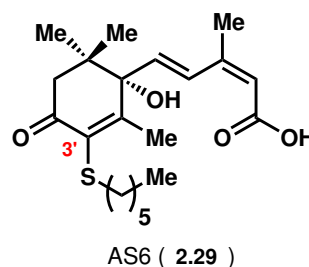


**Figure 2.7:** Structure of AS6 (**2.29**).

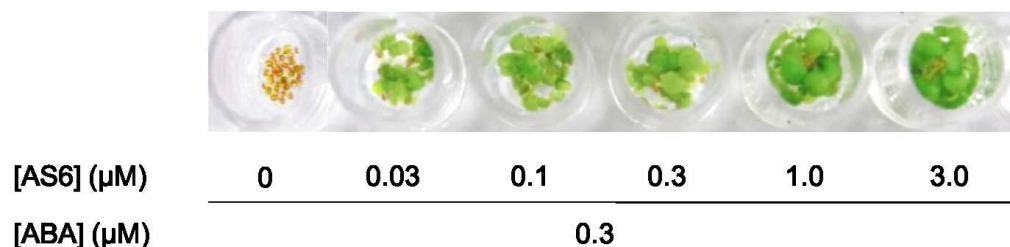


**Figure 2.8:** *Arabidopsis* seed germination assay with co-application of 0.3 μM ABA and varying concentrations of AS6 for 10 d. Reprinted by permission from Springer Nature Customer Service Centre GmbH: Springer Nature, from ref. [39], Copyright 2014.

Each of these observations is consistent with AS6 binding to a PYR/PYL/RCAR receptor, but without subsequent docking of a PP2C as a result of the 3'-alkylsulfanyl chain.

In order to characterize the nature of AS6 binding to the PYR/PYL/RCAR receptors, a crystal structure of AS6 bound to PYR1 (a PYR/PYL/RCAR receptor) was obtained. The crystal structure confirmed the 3'-alkylsulfanyl group passing through the 3' tunnel; in addition, superposition of the crystal structure on that of the PYR1-ABA-HAB1 ternary complex (where HAB1 is a member of the PP2C class) indicated that the 3'-alkylsulfanyl group would interfere with the docking of HAB1 (Figure 2.9a). Specifically, the terminus of the 3'-alkylsulfanyl chain was predicted to occupy the same space as a valine residue well-conserved among the PP2Cs (Figure 2.9b).

The rational design of AS6 provides an illustration of how structural knowledge of ligand-receptor interactions can guide the design of ABA analogs with novel properties *in vivo* in accordance with predictions. We used the case of AS6 as a motivating example for our computationally guided design of 5'-functionalized ABA analogs.

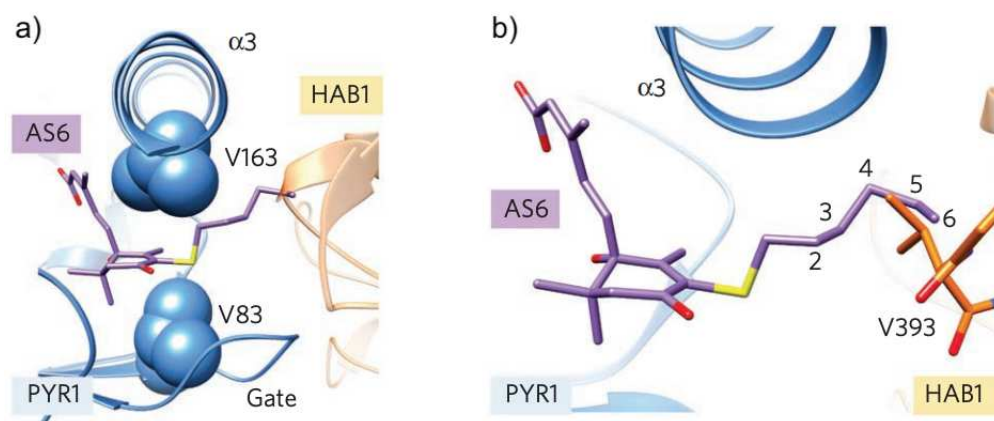


**Figure 2.9:** a) Crystal structure of AS6 bound to PYR1, a PYR/PYL/RCAR receptor. Superimposed on the PYR1-ABA-HAB1 ternary complex in order to show interaction with HAB1, a PP2C. b) Interaction between the 3'-alkylsulfanyl side chain of AS6 with a conserved valine residue of the PP2Cs. Reprinted by permission from Springer Nature Customer Service Centre GmbH: Springer Nature, from ref. [39], Copyright 2014.

## 2.4 Computationally-Guided Design of 5'-Functionalized Abscisic Acid Analogs

Considering the pre-existing structure-activity relationships known for ABA (see Figure 2.6), we noticed that the 5' position has been conspicuously unexplored, despite the large number of ABA analogs that have been synthesized and tested for bioactivity to date. With structural knowledge of PYR/PYL/RCAR-ABA and PYR/PYL/RCAR-ABA-PP2C interactions available to us, we anticipated that we could rationally design 5'-functionalized ABA analogs with improved properties as compared to both natural ABA and analogs synthesized to date. For example, we hoped that we could design both 1) 5'-functionalized ABA analogs

with more potent binding to the PYR/PYL/RCAR receptors, which would act as agonists, and 2) 5'-functionalized ABA analogs with potent binding to the PYR/PYL/RCAR receptors, but with less potent binding to the PYR/PYL/RCAR-ABA-PP2C ternary complex, which would act as antagonists. In addition, these 5'-functionalized ABA analogs could incorporate 8'-functionalization for improved metabolic stability (see section 2.3.1), with 8'-methylidyne analogs particularly attractive for reasons of synthetic accessibility.

We envisioned that we could use Prime MM-GBSA<sup>40</sup>, a method for minimizing receptor-ligand complexes and calculating binding energies of ligands to their receptors, to calculate the binding energies of various 5'-functionalized ABA analogs in both the PYR/PYL/RCAR receptors and the PYR/PYL/RCAR-ABA-PP2C ternary complex. Given the highly conserved nature of the relevant residues in the PYR/PYL/RCAR receptors and in the PP2Cs, only PYR1 and HAB1 were used in these calculations as representative of the PYR / PYL / RCAR receptors and the PP2Cs, respectively. Beginning with the structures of the PYR1-ABA and PYR1-ABA-HAB1 complexes from the Protein Data Bank (accession numbers 3K90 and 3QN1, respectively), we would manually replace the ABA ligand with the desired ABA analog, followed by execution of the Prime MM-GBSA energy calculations.

In order to validate that the Prime MM-GBSA-returned binding energies would correlate with experimentally determined bioactivities, we first carried out Prime MM-GBSA calculations on a number of ABA analogs with known bioactivities (Figure 2.10). Overall, the calculated energies were in accordance with the known experimental data. *trans, trans*-ABA (**2.30**) and 6-nor-ABA (**2.31**), analogs known to possess little to no bioactivity,<sup>41,42</sup> were predicted to bind much more weakly to PYR1. Similarly, less biologically active ABA catabolites phaseic acid (**2.12**) and dihydrophaseic acid (**2.13**) were predicted to bind more weakly to PYR1. Finally, AS6 (**2.29**) was predicted to bind more strongly to PYR1, but

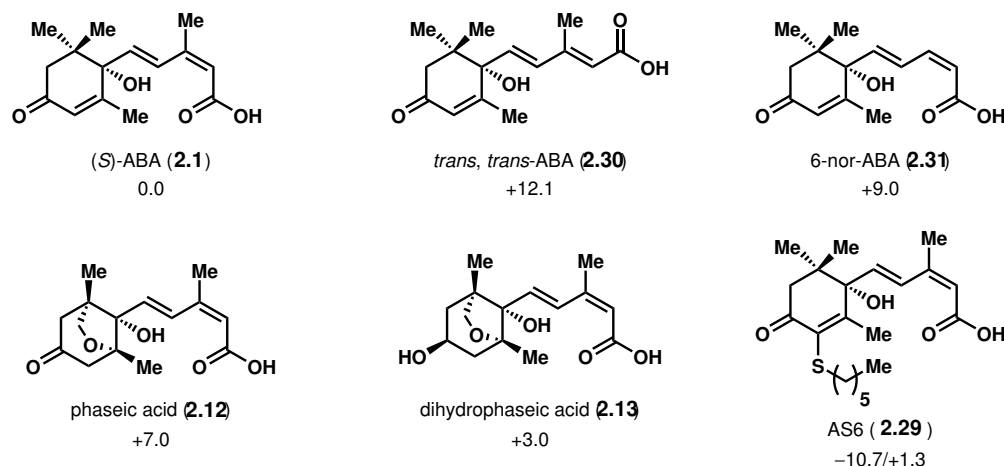


**Figure 2.10:** Prime MM-GBSA-calculated binding energies. First number provided is the binding energy of the ABA analog in the PYR1-ABA analog complex; second number, if provided, is the binding energy of the ABA analog in the PYR1-ABA analog-HAB1 complex. All energies provided are relative to the calculated binding energy of ABA in the PYR1-ABA or PYR1-ABA-HAB1 complexes in kcal/mol, with positive numbers indicating weaker binding than ABA and negative numbers indicating stronger binding than ABA.

to bind less strongly to the PYR1–AS6–HAB1 complex, consistent with its performance as an antagonist of the PYR/PYL/RCAR–PP2C interaction. While these comparisons overall validated Prime MM-GBSA-calculated energies as a proxy for *in vivo* activities, they also provided reason to interpret the calculated binding energies with caution. For example, dihydrophaseic acid is known to be less biologically active compared to phaseic acid, yet it was predicted to bind more strongly to PYR1 than phaseic acid. In addition, in isothermal titration calorimetry experiments, Takeuchi et al. found the apparent dissociation constants of ABA and AS6 for two separate PYR/PYL/RCAR receptors to be similar, whereas Prime MM-GBSA calculations predicted that AS6 would bind much more strongly to PYR1 than ABA.<sup>39</sup> These apparent differences between experimental predictions based on Prime MM-GBSA-calculated binding energies and actual experimental results may be a result of either 1) the imprecision of the Prime MM-GBSA calculations, or 2) the multitude of inputs beyond PYR1–ABA analog binding affinity that would affect experimentally measured *in vivo* bioactivities (e.g., cell permeability, rate of catabolism, off-target binding, etc.). Nevertheless, this initial set of data suggested to us that Prime MM-GBSA calculations could serve as a rough guide to identifying 5'-functionalized ABA analogs that were most likely to exhibit desired types and levels of bioactivity.

We continued with the virtual screening of a small library of 5'-functionalized ABA analogs; in total, over 60 5'-functionalized ABA analogs—chosen on the dual bases of synthetic accessibility and expected interactions with residues in PYR1 near the 5' position—were screened for their binding energies in a PYR1–ABA analog complex and in a PYR1–ABA analog–HAB1 complex (see Table S2.1 in section 2.8.3). Of these, 5',5'-spirocyclic ABA analogs (**2.32–2.37**) tended to be high-performing agonists (Figure 2.11), with the exception of thiirane compounds **2.34**, which were predicted to be antagonists of the PYR1–HAB1 interaction. Interestingly, 5',5'-spirocyclopropane analog **2.38** was predicted to possess much lower binding affinities in the PYR1–ABA analog and PYR1–ABA analog–HAB1 complexes than heteroatom-bearing 5',5'-spirocyclic analogs, suggesting that hydrogen bonding may contribute significantly to the greater binding affinities of these analogs. Given that both compounds in pairs of diastereomers consistently displayed greater binding energies than ABA, hydrogen bonding opportunities may exist on both faces of the ABA analog. Aside from the epoxide-bearing ABA analogs, those diastereomers that placed the heteroatoms on the  $\alpha$ -face typically had greater predicted binding energies, suggesting that hydrogen bonding on the  $\alpha$ -face may be more significant. Notably, the much lower predicted potencies of similar, non-spirocyclic 5',5'-disubstituted analogs (e.g., compare **2.39** to **2.32a**) suggest that the interactions responsible for the predicted binding energies of the 5',5'-spirocyclic analogs are very sensitive to small conformational changes.

The 8'-methyldiyne-bearing variants of these 5',5'-spirocyclic ABA analogs (**2.40–2.45**) were also screened, yielding similar predicted binding affinities to their 8'-H counterparts, consistent with Todoroki and coworkers' finding that 8'-methyldiyne-ABA performed similarly to ABA in a short-term stomatal opening bioassay (see Table 2.1, entry 7); these analogs could potentially serve as metabolically stable agonists (Figure 2.12).

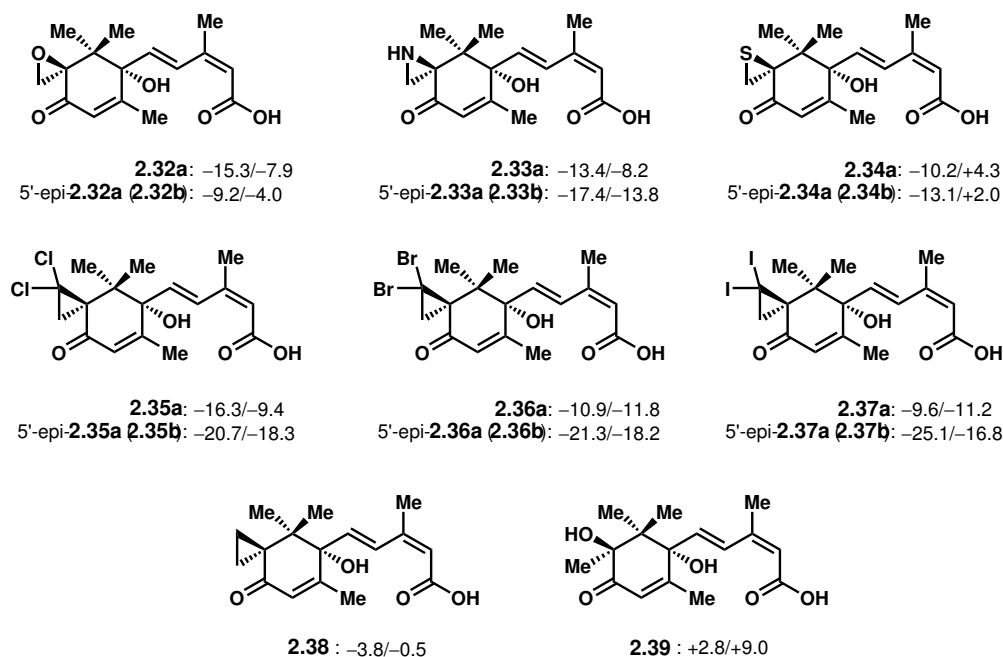


**Figure 2.11:** Prime MM-GBSA-calculated binding energies of 5',5'-difunctionalized ABA analogs. First number provided is the binding energy of the ABA analog in the PYR1-ABA analog complex; second number is the binding energy of the ABA analog in the PYR1-ABA analog-HAB1 complex. All energies provided are relative to the calculated binding energy of ABA in the PYR1-ABA or PYR1-ABA-HAB1 complexes in kcal/mol, with positive numbers indicating weaker binding than ABA and negative numbers indicating stronger binding than ABA.

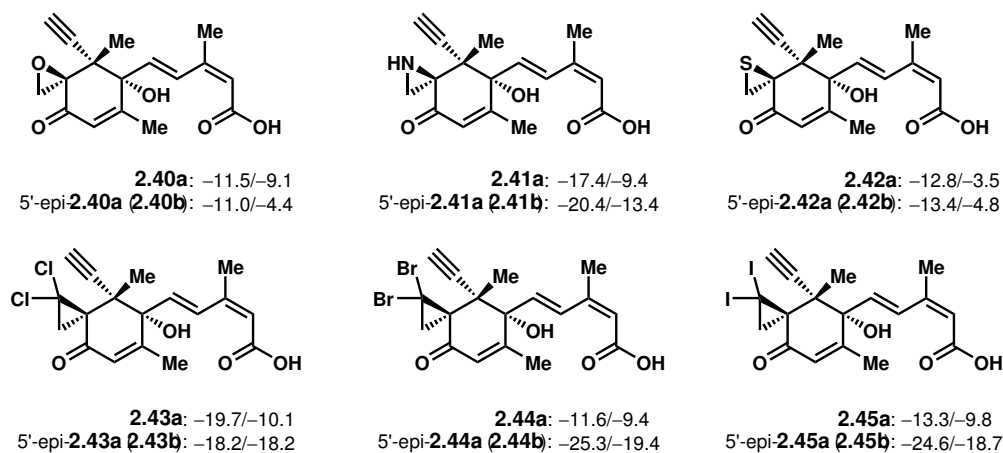
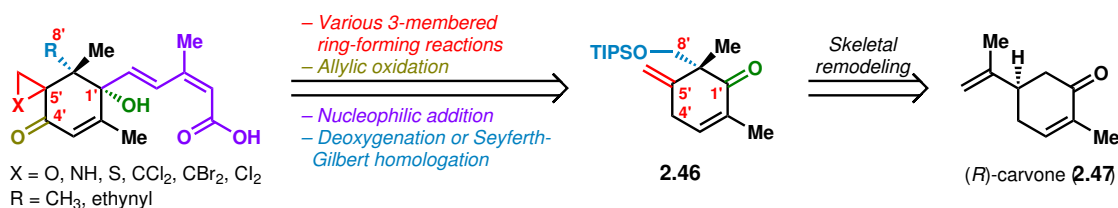


**Figure 2.12:** Prime MM-GBSA-calculated binding energies of 5',5'-spirocyclic 8'-methylidyne ABA analogs. First number provided is the binding energy of the ABA analog in the PYR1-ABA analog complex; second number is the binding energy of the ABA analog in the PYR1-ABA analog-HAB1 complex. All energies provided are relative to the calculated binding energy of ABA in the PYR1-ABA or PYR1-ABA-HAB1 complexes in kcal/mol, with positive numbers indicating weaker binding than ABA and negative numbers indicating stronger binding than ABA.

## 2.5 Synthetic Approach to 5',5'-Spirocyclic Abscisic Acid Analogs

### 2.5.1 Retrosynthesis

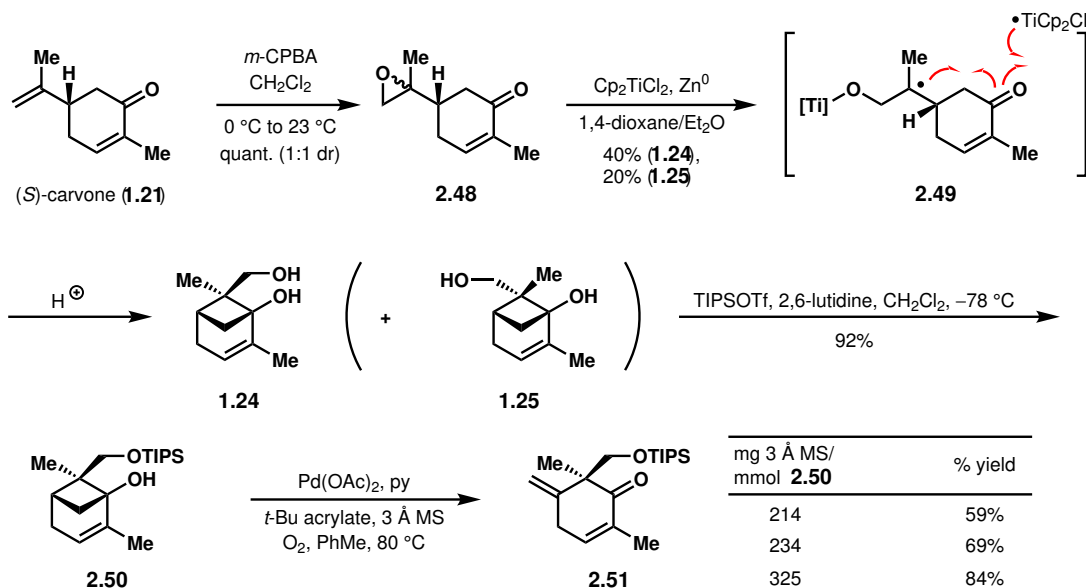
In order to test the designed 5',5'-spirocyclic ABA analogs for enhanced biological activities, a synthetic route for their access was needed. Given the similarities in structure between the designed analogs, we envisioned that each analog could potentially be accessed from a common intermediate. Specifically, we anticipated that the 5',5'-spirocyclic ABA analogs with or without an 8'-methylidyne group could be accessed from *exo*-methylene-containing cyclohexenone **2.46** by sequential functionalizations of the cyclohexenone core (Scheme 2.4). In the forward direction, the *exo*-methylene could be functionalized via various three-membered ring-forming reactions (e.g., epoxidation, aziridination, episulfidation, dihalocyclopropanation). Allylic oxidation at C4 would install the C4' carbonyl. The dienoic acid side chain could be introduced via nucleophilic addition at C1'; finally, the 8' position could be either deoxygenated to yield the 8'-H ABA analogs or subjected to Seyferth-Gilbert homologation of the corresponding aldehyde to yield the 8'-methylidyne ABA analogs. The central cyclohexenone **2.46** could be accessed from (*R*)-carvone (**2.47**) through a short skeletal remodeling sequence.



**Scheme 2.4:** Retrosynthesis of 5',5'-spirocyclic ABA analogs via common cyclohexenone intermediate **2.46**.

### 2.5.2 Synthesis of Common Cyclohexenone Intermediate

While a complete synthesis of the ABA analogs would begin from (*R*)-carvone, due to considerations of material availability, exploratory work was carried out on the *ent*-series beginning from (*S*)-carvone. In a known two-step sequence, (*S*)-carvone (**1.21**) was first epoxidized with *m*-CPBA to deliver epoxy-carvone (**2.48**) as a 1:1 mixture of diastereomers; subjecting to a Ti(III) species generated *in situ* triggered a reductive epoxide opening/radical 4-*exo*-trig cyclization (see **2.49**), yielding diastereomeric cyclobutanols **1.24** and **1.25** (Scheme 2.5).<sup>43</sup> Major diastereomer **1.24** was then protected as the TIPS silyl ether (**2.50**). Under the optimized conditions, subsequent Pd(II)-catalyzed oxidative C–C cleavage proceeded smoothly to deliver cyclohexenone **2.51** in 84% yield. Optimization efforts revealed the importance of the amount of molecular sieves added to the reaction, with higher amounts resulting in higher conversions; since water is a byproduct of the reoxidation of Pd(0) to Pd(II), scavenging of water drives this reoxidation and accelerates the reaction.<sup>44</sup>



**Scheme 2.5:** Synthesis of cyclohexenone intermediate **2.51**.

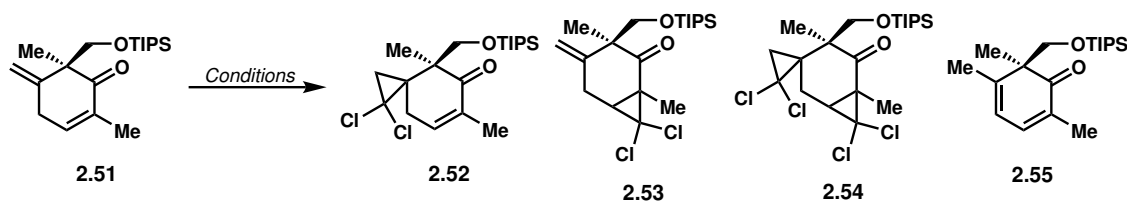
Interestingly, two very similar sets of peaks were observed in the pure  $^1\text{H}$  NMRs of cyclobutanol **2.50** and cyclohexenone **2.51**, in a  $\sim 5$ – $10$ : $1$  ratio, with run-to-run variability in the ratio. Dual sets of peaks were observed for several compounds further in the synthetic sequence as well. Notably, TBS and TBDPS ethers of cyclobutanol **2.50** exhibited only one set of peaks in the  $^1\text{H}$  NMR. Conversion of the TIPS ether **2.50** back to diol **1.24** yielded only one set of peaks in the crude  $^1\text{H}$  NMR, suggesting that the second set of peaks did not arise from inseparable side products or contamination. It was hypothesized that the TIPS ethers consisted of two distinct stereo- or atropisomers. Variable temperature NMR experiments conducted on compound **2.50** up to  $84$  °C revealed no convergence of the sets of peaks, suggesting a barrier to interconversion of at least  $18.0$  kcal/mol at room temperature, and perhaps much higher.<sup>45</sup> We speculate that, similar to what is observed with molecular propellers,<sup>46</sup> the TIPS ethers possess chirality with respect to the three isopropyl groups positioned around the central silicon atom,<sup>47,48</sup> and that the two sets of peaks observed in the  $^1\text{H}$  NMR correspond to two diastereomeric compounds which differ with respect to this additional element of chirality. To our knowledge, TIPS silyl ethers are not typically reported to be mixtures of diastereomers when used in synthesis, suggesting that this phenomenon is uncommon and may be enabled by particularities of our system.

### 2.5.3 Synthesis of Dichlorocyclopropanated Cyclohexenones

From common intermediate **2.51**, the synthetic route could diverge towards various 5',5'-spirocyclic ABA analogs depending on the particular spirocyclic ring-forming reaction performed next. Based on a combination of 1) high predicted potency, 2) anticipated relative inertness to ring-opening processes, both chemically and *in vivo*, and 3) synthetic accessibility, the two diastereomeric 5',5'-dichlorocyclopropanated ABA analogs were targeted first. Selective dichlorocyclopropanation of the *exo*-methylene of **2.51** was attempted as

described in Table 2.2. Initial conditions with 60 equivalents of  $\text{CHCl}_3$  and 190 equivalents of  $\text{NaOH}$  (50 wt% aq.) in the presence of phase transfer catalyst triethylbenzylammonium chloride (TEBAC) yielded mostly over-dichlorocyclopropanated product **2.54**, along with desired product **2.52** and undesired dichlorocyclopropanated product **2.53** (entry 1); these products were chromatographically inseparable. Lower amounts of  $\text{CHCl}_3$  and  $\text{NaOH}$  resulted in higher ratios of desired product **2.52** to undesired products (entry 2), although much lower amounts (and therefore much higher concentrations) resulted exclusively in isomerization of the starting material to dienone **2.55** (entry 3). Dilution of the conditions in entry 3 yielded no conversion (entry 4). The use of additional phase-transfer catalysts thought to promote mono-dichlorocyclopropanation<sup>49,50</sup> did not improve the ratio of desired to undesired products (entries 5 and 6). Finally, the use of alternative dichlorocarbene precursor sodium trichloroacetate consistently resulted in no conversion (entries 7–9).

**Table 2.2:** Attempted optimization of selective dichlorocyclopropanation of cyclohexenone **2.51**. <sup>a</sup>Ratios based on crude <sup>1</sup>H NMR.



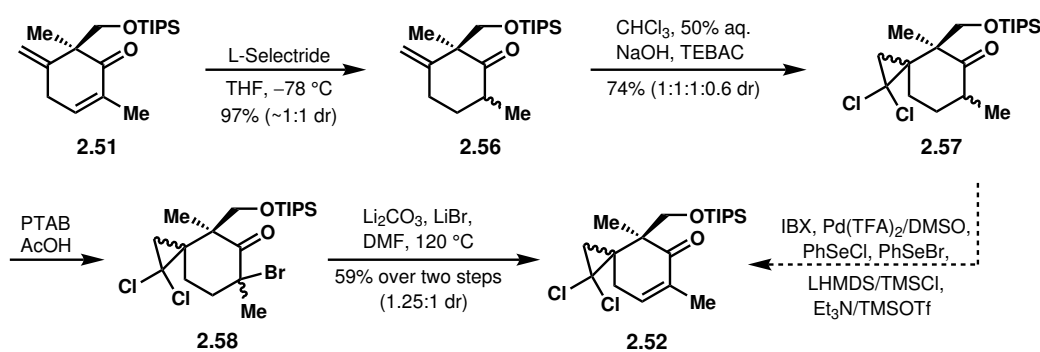
Entry	Conditions	Results
1	$\text{CHCl}_3$ (60 equiv.), 50 wt% aq. $\text{NaOH}$ (190 equiv.), TEBAC (0.1 equiv), 23 °C	2:1:6 <sup>a</sup> <b>2.52</b> : <b>2.53</b> : <b>2.54</b>
2	$\text{CHCl}_3$ (30 equiv.), 30 wt% aq. $\text{NaOH}$ (30 equiv.), TEBAC (0.1 equiv), 23 °C	6:4:3 <sup>a</sup> <b>2.52</b> : <b>2.53</b> : <b>2.54</b>
3	$\text{CHCl}_3$ (4 equiv.), 50 wt% aq. $\text{NaOH}$ (4 equiv.), TEBAC (0.1 equiv), 23 °C	<b>2.55</b>
4	$\text{CHCl}_3$ (4 equiv.), 50 wt% aq. $\text{NaOH}$ (4 equiv.), TEBAC (0.1 equiv), diluted with $\text{CH}_2\text{Cl}_2/\text{H}_2\text{O}$ to 0.03 M, 23 °C	No conversion
5	$\text{CHCl}_3$ (30 equiv.), 30 wt% aq. $\text{NaOH}$ (30 equiv.), benzyltriethyl(2-hydroxyethyl)-ammonium chloride (0.1 equiv), 40 °C	Similar to entry 2
6	$\text{CHCl}_3$ (30 equiv.), 30 wt% aq. $\text{NaOH}$ (30 equiv.), tetramethylammonium chloride (0.1 equiv), 40 °C	No conversion
7	sodium trichloroacetate, DME, 85 °C	No conversion
8	sodium trichloroacetate, TEBAC, tetrachloroethylene/diglyme, 115 °C	No conversion
9	sodium trichloroacetate, Adogen 464, $\text{CHCl}_3$ , 80 °C	No conversion

Given our difficulties with selective dichlorocyclopropanation, we decided to remove the competing site of dichlorocyclopropanation via a conjugate reduction of the enone. Thus, treating cyclohexenone **2.51** with L-Selectride yielded cyclohexanone **2.56** as a mixture of diastereomers in 97% yield (Scheme 2.6). Dichlorocyclopropanation of this compound proceeded smoothly, providing **2.57** in 74% yield as a mixture of four diastereomers. At this point, in order to reinstall the alkene, we attempted  $\alpha$ ,  $\beta$ -dehydrogenation of the ketone. Attempted one-step dehydrogenations were unsuccessful; both IBX oxidation<sup>51</sup> and aerobic Pd(II)-catalyzed dehydrogenation<sup>52</sup> resulted in no conversion, even at elevated temperatures. In order to carry out a Saegusa-Ito oxidation, we attempted to form the silyl enol ether; however, no conversion was observed under either hard or soft enolization conditions, perhaps as a result of steric hindrance. In preparation for a Reich-type selenide oxidation-elimination,



we treated **2.57** with PhSeCl and PhSeBr; however, no  $\alpha$ -selenide product was observed. Finally, we turned to  $\alpha$ -bromination; while no conversion was observed upon treatment with LHMDS and NBS, we did observe formation of **2.58** with pyridinium tribromide in acetic acid. Screening of other brominating agents (e.g., NBS, CuBr<sub>2</sub>, Meldrum's acid dibromide<sup>53</sup>) revealed phenyltrimethylammonium tribromide (PTAB)<sup>54</sup> to be optimal. Notably, while brominations with PTAB have been reported to be greatly retarded by the presence of water and are typically carried out in anhydrous THF, we found that the bromination of **2.58** was extremely slow in anhydrous THF, with very little conversion after 16 h. On the other hand, brominations with PTAB in AcOH typically reached completion in under 2 h. We speculate that the AcOH assists in enolization of the ketone, either through hydrogen bonding or by the generation of HBr upon reaction with PTAB.

From  $\alpha$ -bromide **2.58**, while attempted elimination with DBU yielded multiple side products alongside desired enone **2.52**, treatment with Li<sub>2</sub>CO<sub>3</sub> and LiBr at elevated temperatures cleanly afforded the desired product. Under the optimized conditions, the  $\alpha$ -bromination-elimination sequence was carried out in two steps without purification of any intermediates in a 59% overall yield.

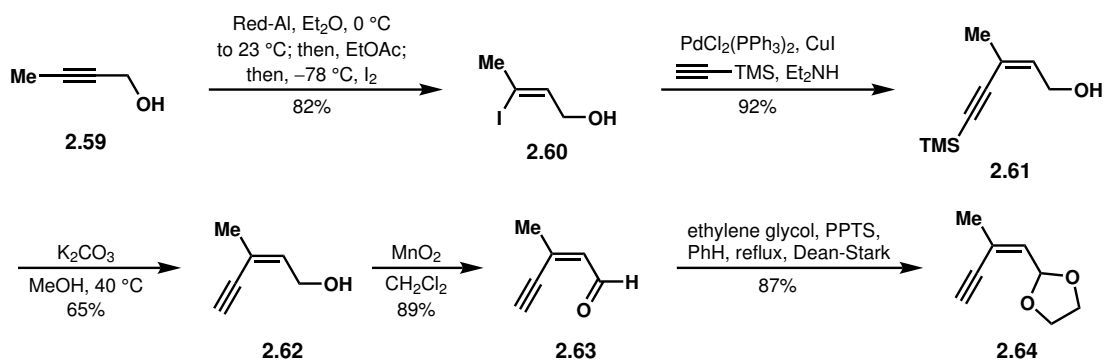


**Scheme 2.6:** Synthesis of dichlorocyclopropanated enone **2.52**.

## 2.5.4 Late-Stage Progress Toward 5',5'-Spirocyclic ABA Analogs

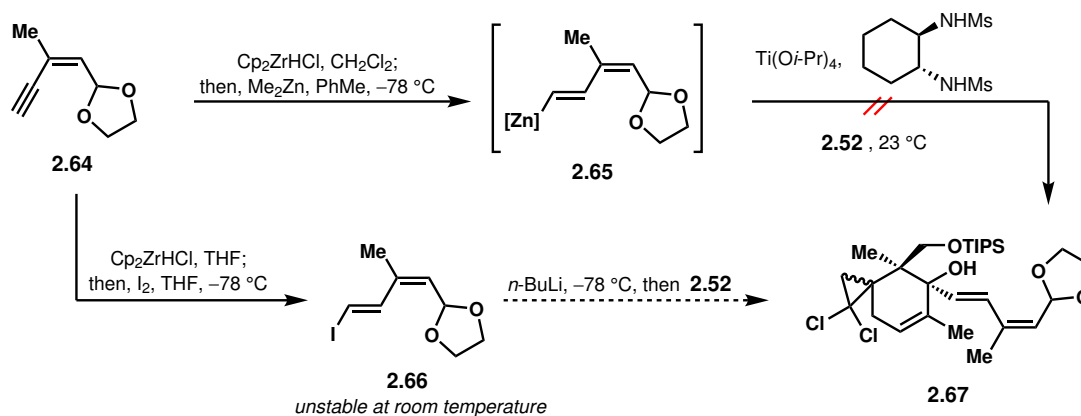
With **2.52** in hand, we set out to install the dienolic acid side chain via nucleophilic addition. Inspired by a previous synthesis of phaseic acid in which the same dienolic acid side chain was installed,<sup>55</sup> we envisioned deriving a nucleophile from known enyne compound **2.64** (Scheme 2.7). This enyne was synthesized in five known steps. First, propargylic alcohol **2.59** was reduced stereoselectively with Red-Al, followed by trapping of the vinylaluminumate with iodine to yield vinyl iodide **2.60**.<sup>56</sup> Sonogashira coupling with trimethylsilylacetylene then afforded silylated enyne **2.61**.<sup>57</sup> Cleavage of the trimethylsilyl group provided **2.62**<sup>58</sup>; oxidation of the allylic alcohol to aldehyde **2.63**<sup>59</sup> was followed by acetalization to deliver **2.64**.<sup>55</sup>

Given the requirement of a *trans*, *trans*-alkene in the desired ABA analogs, we hoped to perform an addition of a *trans*, *trans*-dienyl nucleophile derived from enyne **2.64**. We first attempted addition of a dienylzinc species (**2.65**) in the presence of a titanium catalyst and chiral ligand, on the basis of the precedent of Li and Walsh (Scheme 2.8).<sup>60</sup> However, no



Scheme 2.7: Synthesis of enyne **2.64**.

conversion of **2.52** was observed, and we recovered only the diene derived from **2.65**. We then attempted to prepare vinyl iodide **2.66** in hopes that the corresponding vinyl lithium could be added to **2.52** to yield **2.67**; these efforts were stymied by the rapid decomposition of vinyl iodide **2.66** upon standing at room temperature.

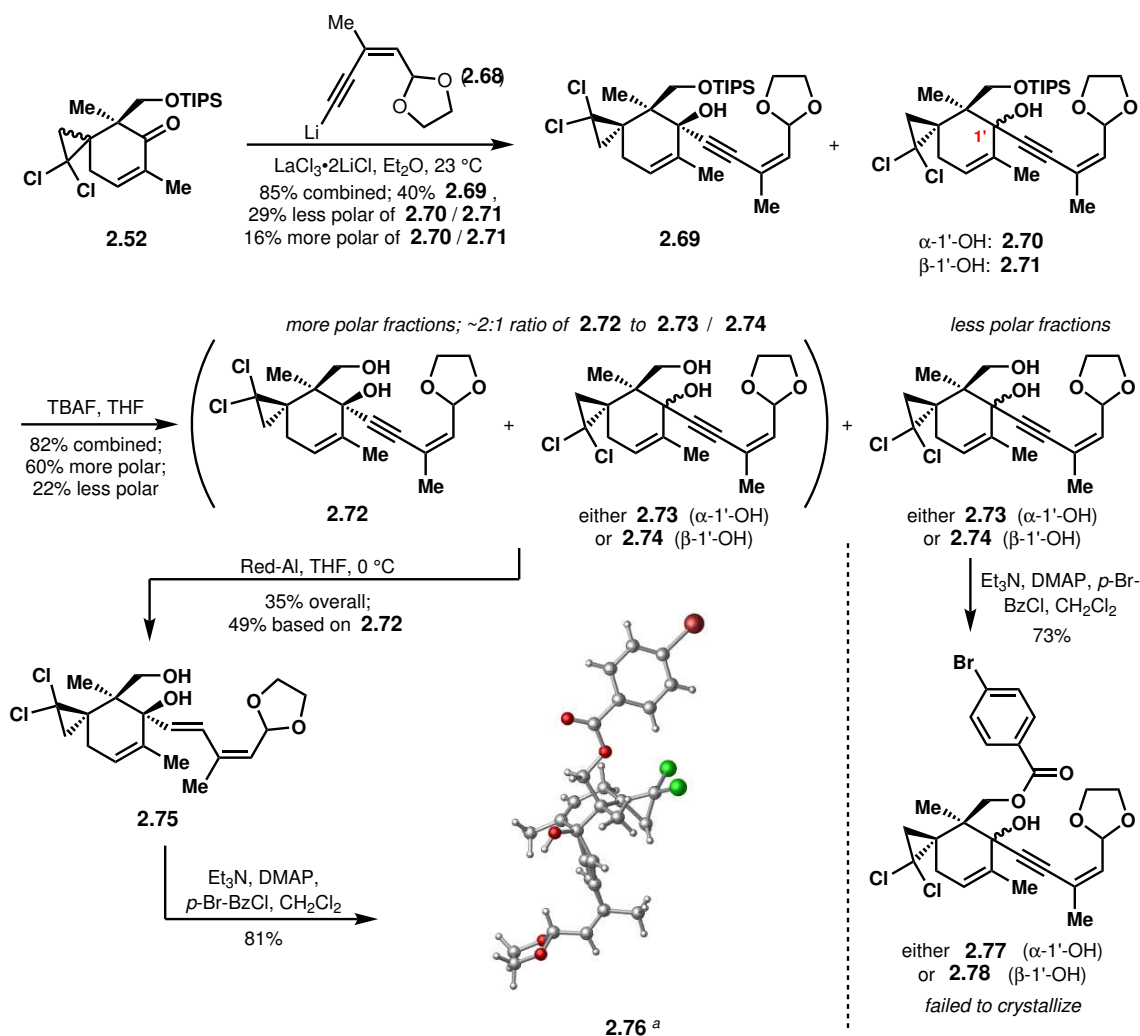


Scheme 2.8: Attempted additions of a dienyl nucleophile to **2.52**.

Faced with difficulties associated with addition of a dienyl nucleophile, we began investigating acetylide addition, anticipating that we could subsequently reduce the alkyne to the *trans*-alkene. Initial attempts at nucleophilic addition of the alkynyllithium of **2.64** (**2.68**), formed by stirring **2.64** with *n*-BuLi, in THF were unsuccessful, resulting in no conversion even at elevated temperatures (Scheme 2.9). Adding the alkynyllithium or alkynylmagnesiates of **2.64** to a pre-stirred mixture of **2.52** and  $\text{LaCl}_3 \cdot 2\text{LiCl}^{61}$ , or addition of the alkynylcerium formed from the reaction of **2.64** and  $\text{CeCl}_3^{62}$  to **2.52**, resulted in no conversion as well. Finally, after a solvent screen that included PhMe,  $\text{CH}_2\text{Cl}_2$ , MTBE, diglyme, and dioxane, it was discovered that the use of diethyl ether was critical for the conversion of one of the diastereomers of **2.52** diastereoselectively to desired product **2.69** (stereochemistry identified later, *vide infra*). Under the optimized conditions, which included the pre-stirring of **2.52** with  $\text{LaCl}_3 \cdot 2\text{LiCl}$  and the use of 2.5 equivalents of the alkynyllithium of **2.64**, we were able to fully convert both diastereomers of **2.52** to tertiary alcohol products, albeit with less than complete diastereoselectivity for the less reactive diastereomer, resulting in three diastere-

omeric products in a combined 85% yield (40% **2.69**, 29% **2.70/2.71**, and 16% **2.70/2.71** based on integral ratios in the  $^1\text{H}$  NMR).

We then set out to confirm the stereochemistry of each the three diastereomers. After TBAF-mediated TIPS ether cleavage, three diastereomeric diols were isolated. A ~2:1 mixture of the diol derived from **2.69** (**2.72**) and the diol derived from the more minor of **2.70/2.71** (**2.73/2.74**)—the more polar fractions—could be chromatographically separated from the diol derived from the more major of **2.70/2.71** (**2.73/2.74**, the less polar fractions). This 2:1 mixture was then reduced to the *trans*-alkene with Red-Al; only the major product **2.75**, derived from **2.72**, could be isolated. Esterification with *p*-bromobenzoyl chloride provided crystalline product **2.76**, whose structure was confirmed by X-ray crystallography. In particular, the desired stereochemical configuration at C1' was confirmed, as well as the

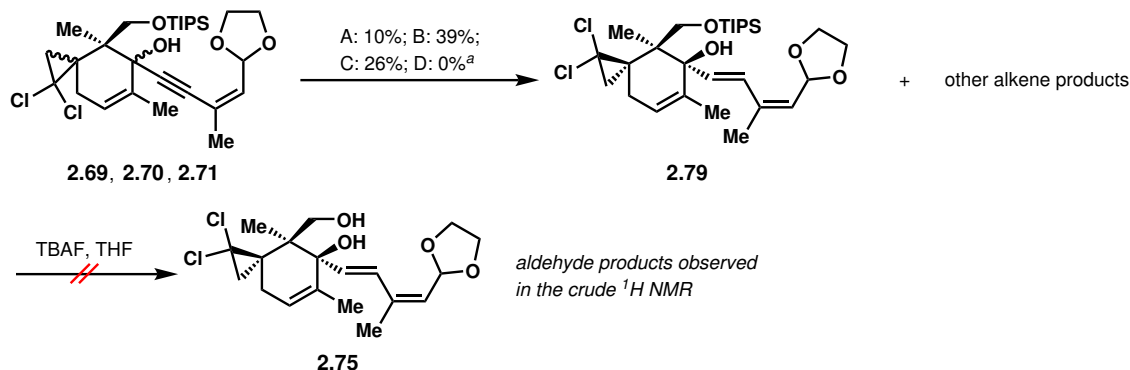


**Scheme 2.9:** Acetylide addition and attempted stereochemical confirmation of diastereomeric products. <sup>a</sup>X-ray crystal structure of **2.76** Note that contamination of the crystallized sample with alkyne **2.72** complicates the observed bond order of the C4–C5 alkene; however, the *trans*-configuration can still be identified.

configuration at C5' of the major product of the nucleophilic addition.

The product contained in the less polar fractions after the TIPS ether cleavage, either **2.73** or **2.74**, was also esterified with *p*-bromobenzoyl chloride. Unfortunately, this product failed to crystallize, and its structure could not be unambiguously confirmed.

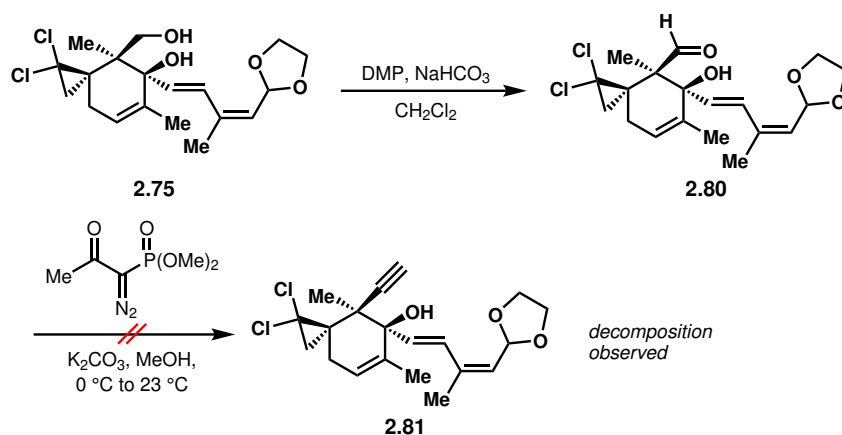
While confirming the stereochemistry of the nucleophilic addition products, we were simultaneously experimenting with the later steps in the synthesis. We imagined that a Red-Al reduction of the alkyne to the *trans*-alkene in the next step would minimize functional group incompatibilities and/or protecting group manipulations later on in the synthesis. Subjection of the mixture of acetylide addition adducts **2.69**–**2.71** to Red-Al initially resulted in a very messy crude reaction mixture with four or more products, the major product of which was presumed to arise from the major constituent of the starting material (i.e. **2.69** to **2.79**) (condition A, Scheme 2.10). Altogether, these largely inseparable products were isolated with 10% mass recovery. After extensive optimization, including changes to reaction temperature and workup procedure, we were able to increase the mass recovery of these various products to 39% on a 20 mg scale (condition B); however, the success of these reaction conditions was not maintained upon increasing scale, with the mass recovery falling to 26% on a 60 mg scale (condition C). We also attempted the *trans*-hydrosilylation of the alkyne,<sup>63</sup> with the expectation that the vinylsilane product could be easily converted to *trans*-alkene **2.79**; however, we did not observe the formation of the desired vinylsilane under these conditions (condition D). The mixture of alkene products, including **2.79**, that we were able to obtain from Red-Al reductions was subjected to TBAF in an effort to access diol **2.75**; unfortunately, we observed aldehyde peaks in the crude <sup>1</sup>H NMR, indicating hydrolysis



**Scheme 2.10:** Attempted reductions of alkynes **2.69**–**2.71** to their corresponding *trans*-alkenes. <sup>a</sup>Condition A: 19 mg scale; 2 equiv. Red-Al added as a 0.35 M solution in PhMe to starting materials at 0 °C in THF and warmed to 23 °C; 0.07 M; 4 h; worked up with Rochelle's salt. Condition B: 20 mg scale; starting materials dried via azeotropic distillation with PhH; 3 equiv. Red-Al added as a 0.35 M solution in THF to starting materials at –78 °C in THF and warmed to 0 °C; 0.036 M; 2 h; worked up with Glauber's salt. Condition C: 61 mg scale; starting materials dried via azeotropic distillation with PhH; 3 equiv. Red-Al added as a 0.35 M solution in THF to starting materials at –78 °C in THF and warmed to 0 °C; 0.025 M; 2 h; worked up with Glauber's salt. Condition D: 1.2 equiv. Et<sub>3</sub>SiH, 0.05 equiv. [Cp\**Ru*Cl]<sub>4</sub>, CH<sub>2</sub>Cl<sub>2</sub>, 0.07 M, 2.5 h. All percentages express mass recovery of alkene products relative to starting material mass.

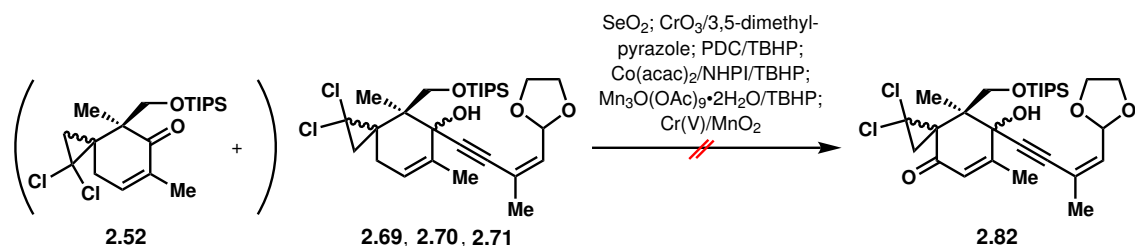
of the sensitive acetal moiety.

Our difficulties with alkyne reduction immediately following acetylide addition prompted us to reconsider an alternative order of events. Specifically, we attempted to move forward with diol **2.75**, formed by initial TIPS ether cleavage followed by Red-Al reduction of the alkyne (see Scheme 2.9, **2.69–2.71** to **2.75**). We hoped that transformation of the primary hydroxy group to the desired methylidyne group would minimize protecting group manipulations before subsequent allylic oxidation. To this end, we oxidized the primary hydroxy group to the aldehyde, yielding compound **2.80**, which was carried forward without purification (Scheme 2.11). Attempted execution of the Ohira-Bestmann modification of the Seyferth-Gilbert homologation to yield alkyne **2.81** afforded only decomposition, perhaps initiated by a retro-aldol reaction.



**Scheme 2.11:** Attempted transformation of diol **2.75** to 8'-methylidyne compound **2.81**.

Finally, we carried out preliminary investigations for allylic oxidation at the 4' position. Due to reasons of material constraint, we typically carried out these allylic oxidations on 1:1.7 mixtures of cyclohexenone **2.52** and tertiary alcohols **2.69–2.71** recovered from acetylide additions that failed to reach full conversion (Scheme 2.12). For this reason, we are hesitant to reach definite conclusions about the viability of this allylic oxidation on the basis of these investigations; however, our difficulties with this allylic oxidation are consistent with our expectations that tertiary alcohols **2.69–2.71** would prove to be challenging substrates for allylic oxidation, given the plethora of functional groups that may be reactive under a number of different allylic oxidation conditions. We subjected **2.69–2.71** to allylic oxidation conditions falling under a variety of mechanistic categories, including 1) pericyclic (SeO<sub>2</sub>, CrO<sub>3</sub>/3,5-dimethylpyrazole<sup>64</sup>), 2) transition metal-mediated hydrogen atom abstraction (PDC/TBHP,<sup>65</sup> Co(acac)<sub>2</sub>/NHPI/TBHP,<sup>66,67</sup> Mn<sub>3</sub>O(OAc)<sub>9</sub>·2H<sub>2</sub>O,<sup>68</sup>), and 3) transition metal-mediated single electron transfer (Cr(V) reagent/MnO<sub>2</sub><sup>69</sup>). Under no reaction conditions were we able to observe formation of desired enone products **2.82**; we observed mainly starting material or decomposition. Further investigations with pure starting materials are needed to establish the feasibility of this allylic oxidation, and it is possible that the allylic oxidation will need to be carried out at an earlier stage.



**Scheme 2.12:** Attempted allylic oxidations of allylic alcohols **2.69–2.71**.

## 2.6 Conclusion and Outlook

Given the major regulatory role it plays in many plant functions, the plant hormone ABA has garnered much attention from both synthetic chemists and plant biologists, attested to by the over one hundred ABA analogs synthesized to date as well as the thousands of research papers published on the study of ABA. As evidenced by the agricultural industry's interest in the exogenous application of ABA to crops to influence their seed germination rates, drought tolerance, and propensities for fruit ripening, further insights into the function of ABA is a project with major potential practical benefits. Since the PYR/PYL/RCAR receptors responsible for initial binding of ABA in the plant were only discovered 10 years ago, this is a project whose biggest developments are likely yet to come. The seminal discovery of these receptors has in particular enabled synthetic chemists to contribute to this project through the computationally-guided rational design of ABA analogs, in contrast to the majority of ABA analogs that were synthesized prior.

In this chapter, we have investigated a synthetic route towards 5',5'-spirocyclic, 8'-methylidyne ABA analogs, whose 5',5'-spirocycle has been predicted by binding energy calculations to impart greater potency, and whose 8'-methylidyne should impart metabolic stability based on previous study. We have developed a four-step method from carvone for the preparation of a common cyclohexenone intermediate (**2.51**), from which the synthetic route could hypothetically be diverged toward a number of 5',5'-spirocyclic, 8'-methylidyne ABA analogs. As a first manifestation of this plan, we investigated the synthesis of two diastereomeric 5',5'-dichlorocyclopropanated ABA analogs. In seven steps, we were able to transform cyclohexenone **2.51** to late-stage intermediate **2.75**, bearing both the 5',5'-dichlorocyclopropane and a dienyl side chain, leaving only 8'-methylidyne installation and 4'-allylic oxidation as the major remaining transformations. While the dense functionality of **2.75** may make the remainder of the synthesis challenging, we hope that the work described in this chapter provides a useful foundation upon which future syntheses of 5',5'-spirocyclic ABA analogs can be built.

## 2.7 Experimental Contributors

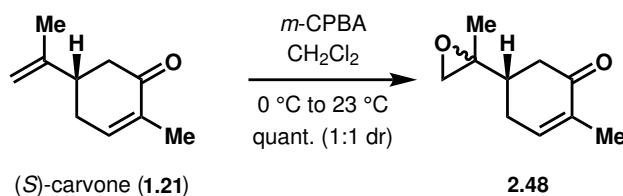
All experimental and computational work discussed in sections 2.4–2.5.4 was completed by Brian Wang.

## 2.8 Experimental Methods and Procedures

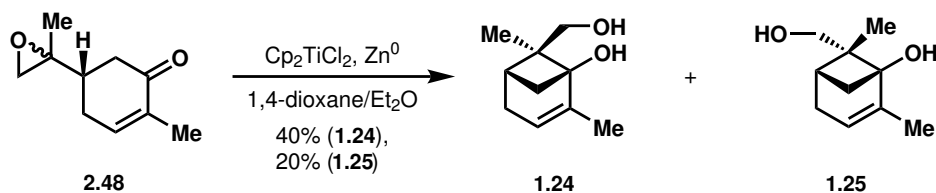
### 2.8.1 General Methods

Unless otherwise stated, all reactions were stirred with Teflon<sup>TM</sup>-coated magnetic stir bars and were conducted in flame- or oven-dried glassware under an N<sub>2</sub> atmosphere following standard Schlenk technique. Anhydrous THF, Et<sub>2</sub>O, PhMe, PhH, MeCN, Et<sub>3</sub>N, and MeOH were obtained by sparging with Ar followed by passage through a column of activated alumina, and were kept under an Ar atmosphere. Anhydrous CH<sub>2</sub>Cl<sub>2</sub> was obtained by distilling over CaH<sub>2</sub> under an N<sub>2</sub> atmosphere. All other solvents and reagents were purchased from commercial suppliers and used without further purification, unless otherwise stated. All reactions were monitored by thin layer chromatography on Silicycle Siliaplate<sup>TM</sup> 250 µm silica gel (indicator F-254), with visualization by UV irradiation (254 nm) and staining by *p*-anisaldehyde. Reaction mixture temperatures above 23 °C were controlled by an IKA<sup>®</sup> temperature modulator. When stated, non-standard reaction mixture temperatures were obtained using a Thermo Scientific<sup>TM</sup> EK45/90 Immersion Cooler. Evaporation of solvents under reduced pressure was carried out on rotary evaporators. Purification by manual flash chromatography was conducted with Sorbent Technologies 60 Å silica gel of particle size 40–63 µm. Automated flash column chromatography was performed on a Yamazen<sup>®</sup> Smart Flash EPCLC W-Prep 2XY automated flash chromatography system, with Universal Columns (60 Å silica gel of particle size 40 µm) or Universal Column Premiums (60 Å silica gel of particle size 30 µm). NMR spectra were acquired in deuterated solvents purchased from Cambridge Isotope Laboratories, Inc. NMR spectra were recorded on Bruker spectrometers at the UC Berkeley College of Chemistry NMR Facility, operating at 300, 400, 500, 600, or 700 MHz for <sup>1</sup>H NMR, and at 75, 100, 125, 150, or 175 MHz for <sup>13</sup>C NMR. <sup>1</sup>H NMR spectra are calibrated to the residual solvent peak CDCl<sub>3</sub> (δ = 7.260 ppm) or C<sub>6</sub>D<sub>6</sub> (δ = 7.160 ppm), and <sup>13</sup>C NMR spectra are calibrated to the residual solvent peak CDCl<sub>3</sub> (δ = 77.16 ppm). <sup>1</sup>H NMR data are reported as follows: chemical shift (multiplicity, coupling constant, number of protons). Abbreviations of multiplicity patterns are as follows: d = doublet, t = triplet, br = broad, s = singlet, q = quartet, m = multiplet, dd = doublet of doublets, dt = doublet of triplets, dq = doublet of quartets, dp = doublet of pentets, ddd = doublet of doublet of doublets, dtd = doublet of triplet of doublets, tt = triplet of triplets. IR spectra were acquired on a Bruker ALPHA Platinum ATR spectrometer (neat), and select IR peaks are reported as frequency of absorption in cm<sup>-1</sup>. High resolution mass spectrometry data was obtained from the Mass Spectral Facility at the University of California, Berkeley on a Finnigan/Thermo LTQ-FT instrument (ESI or EI) or from the Catalysis Facility of Lawrence Berkeley National Laboratory on a PerkinElmer AxION 2 UHPLC-TOF system (ESI or APCI). Data acquisition and processing were performed using Xcalibur<sup>TM</sup> software. Optical rotations were measured with a Perkin-Elmer 241 polarimeter with a Na D-line lamp (path length 1 dm, cell volume 1 mL, c in g/100 mL). X-ray data was collected on a Bruker APEX-II CCD diffractometer with Mo-Kα radiation (λ = 0.71073 Å) or a MicroStar-H X8 APEX-II diffractometer with Cu-Kα radiation (λ = 1.54178 Å). CYLview was used for graphic rendering.

## 2.8.2 Experimental Procedures



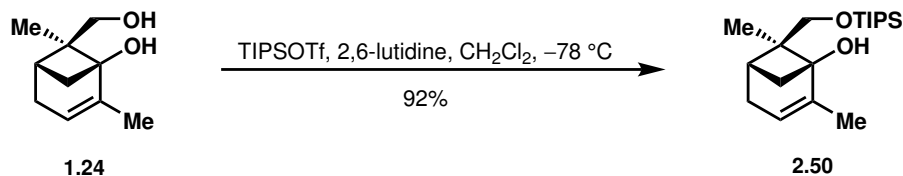
This procedure was adapted from ref. [70] To a solution of (*S*)-carvone (26.0 mL, 166 mmol, 1 equiv) in ACS grade CH<sub>2</sub>Cl<sub>2</sub> (not dried prior to use) (550 mL, 0.3 M) at 0 °C was added *m*-CPBA (70%, 45.1 g, 183 mmol, 1.1 equiv) portionwise over 30 min while the reaction was stirred. The resulting milky suspension was warmed to 23 °C and stirred for 19 h under air. The reaction was then quenched by the addition of sat. aq. Na<sub>2</sub>S<sub>2</sub>O<sub>3</sub> (100 mL) and the resulting mixture was stirred for an additional 30 min. Sat. aq. Na<sub>2</sub>S<sub>2</sub>O<sub>3</sub> (300 mL) was then added, and the organic and aqueous layers were separated. The aqueous phase was extracted with CH<sub>2</sub>Cl<sub>2</sub> (2 x 200 mL). The combined organic layers were washed with 1 M NaOH (3 x 100 mL), washed with brine (200 mL), dried over Na<sub>2</sub>SO<sub>4</sub>, filtered, and concentrated *in vacuo* to give **2.48** (29.0 g, quant., 1:1 dr) as a yellow oil. This material was sufficiently pure by <sup>1</sup>H NMR analysis and was carried on to the next step without purification. The spectral data is consistent with that reported in the literature.<sup>70</sup>



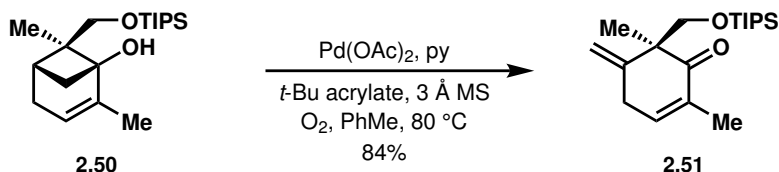
This procedure was adapted from ref. [43]. To a 1 L three-neck flask was added Zn (13.0 g, 199 mmol, 6.6 equiv) and Cp<sub>2</sub>TiCl<sub>2</sub> (16.5 g, 66.2 mmol, 2.2 equiv). The 1 L flask was equipped with a 250 mL addition funnel, evacuated and backfilled with N<sub>2</sub>, and the addition funnel was filled with 1,4-dioxane (100 mL) and Et<sub>2</sub>O (100 mL). The solvents were sparged with N<sub>2</sub> for 30 min in the addition funnel, added to the flask, and the reaction mixture was stirred at 23 °C for 3.5 h. The addition funnel was then charged with **2.48** (5.0 g, 30 mmol, 1 equiv), 1,4-dioxane (100 mL), and Et<sub>2</sub>O (100 mL). This solution was sparged just as before and added to the flask over 1 h. After stirring the reaction mixture for 14 h at 23 °C, the reaction was quenched with sat. aq. NaH<sub>2</sub>PO<sub>4</sub> (200 mL) and brine (200 mL), and the resulting solution was diluted with EtOAc (200 mL). After stirring the mixture vigorously for an additional 5.5 h, the mixture was filtered through Celite with EtOAc, and the organic and aqueous layers were separated. The aqueous phase was extracted with EtOAc (3 x 200 mL), and the combined organic layers were washed with brine (400 mL), dried over Na<sub>2</sub>SO<sub>4</sub>, filtered, and concentrated *in vacuo*. The crude product was purified by Yamazen automated flash column chromatography (20% EtOAc/hexanes to 60% EtOAc/hexanes) to afford impure **1.24** as a thick yellow oil and **1.25** (1.01 g, 20% yield) as a white solid. Impure **1.24** was re-purified by Yamazen automated flash column chromatography (10% EtOAc/CH<sub>2</sub>Cl<sub>2</sub> to 30% EtOAc/CH<sub>2</sub>Cl<sub>2</sub>) to afford mostly pure **1.24** as a colorless oil. Trituration with pen-



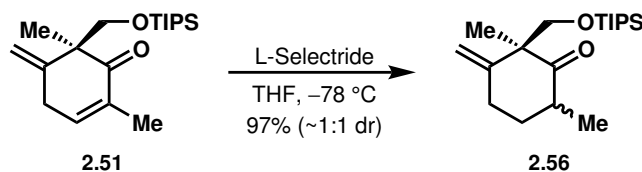
tanones afforded pure **1.24** (2.01 g, 40% yield) as a white solid. The spectral data of **1.24** and **1.25** are consistent with that reported in the literature.<sup>43</sup>



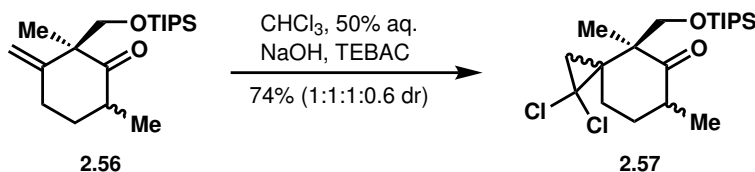
To a solution of **1.24** (2.01 g, 12.0 mmol, 1 equiv.) in  $\text{CH}_2\text{Cl}_2$  (55 mL, 0.22 M) at  $-78\text{ }^\circ\text{C}$ , 2,6-lutidine (4.2 mL, 35.8 mmol, 3 equiv.) and TIPSOTf (4.2 mL, 15.5 mmol, 1.3 equiv.) were added. After 15 min, the reaction mixture was poured into  $\text{H}_2\text{O}$  (100 mL) and  $\text{CH}_2\text{Cl}_2$  (50 mL). The aqueous and organic layers were separated, and the aqueous layer was extracted with  $\text{CH}_2\text{Cl}_2$  (3 x 50 mL). The combined organic layers were dried over  $\text{Na}_2\text{SO}_4$ , filtered, and concentrated *in vacuo* to reveal a crude yellow liquid. The crude product was purified by Yamazen automated flash column chromatography (2% EtOAc/hexanes) to afford **2.50** (3.56 g, 92% yield) as a colorless oil. **<sup>1</sup>H NMR** (500 MHz,  $\text{CDCl}_3$ ) *Major set of peaks*:  $\delta$  4.41 (s, 1H), 4.38 (d,  $J = 10.0$  Hz, 1H), 3.85 (d,  $J = 10.0$  Hz, 3H). *Minor set of peaks*:  $\delta$  4.42 (s, 1H), 4.33 (d,  $J = 10.0$  Hz, 1H), 3.79 (d,  $J = 10.0$  Hz, 1H). *Major + minor sets of peaks*:  $\delta$  5.18 (s, 1H), 2.37 (dd,  $J = 8.6, 7.0$  Hz, 1H), 2.20–2.00 (m, 2H), 1.98–1.87 (m, 1H), 1.76 (d,  $J = 2.1$  Hz, 3H), 1.68 (d,  $J = 8.6$  Hz, 1H), 1.20–1.01 (m, 24H).



A 50 mL round-bottomed flask was charged with 3 Å molecular sieves (504 g, crushed into a powder with mortar and pestle) and flame-dried under high vacuum. In a separate flask, a solution of **2.50** (503 mg, 1.55 mmol, 1 equiv), anhydrous pyridine (0.25 mL, 3.10 mmol, 2.0 equiv), and *t*-Bu acrylate (0.57 mL, 3.88 mmol, 2.5 equiv) in toluene (30 mL, 0.05 M) was prepared under  $\text{N}_2$ , and after being thoroughly mixed, the solution was uncapped and added to the reaction flask.  $\text{Pd}(\text{OAc})_2$  (34.8 mg, 0.155 mmol, 0.1 equiv) was added and the flask was equipped with a reflux condenser sealed with a septum. The flask was evacuated and backfilled with  $\text{O}_2$  (5x) using an  $\text{O}_2$  balloon, and the reaction mixture was stirred at  $80\text{ }^\circ\text{C}$  for 24 h. The solution was then allowed to cool to  $23\text{ }^\circ\text{C}$  and the beige suspension was filtered over a plug of silica, washed with PhMe, and concentrated *in vacuo*. The filtrate was purified by Yamazen automated flash chromatography (1%  $\text{Et}_2\text{O}$ /hexanes) to afford **2.51** (420 mg, 84% yield) as a cloudy-white oil. **<sup>1</sup>H NMR** (500 MHz,  $\text{CDCl}_3$ ) *Major set of peaks*:  $\delta$  3.84 (d,  $J = 9.0$  Hz, 1H), 3.72 (d,  $J = 9.0$  Hz, 1H), 1.29 (s, 3H). *Minor set of peaks*:  $\delta$  3.80 (d,  $J = 9.1$  Hz, 1H), 3.66 (d,  $J = 9.1$  Hz, 1H), 1.27 (s, 3H). *All sets of peaks*:  $\delta$  6.71–6.66 (m, 1H), 4.97–4.95 (m, 1H), 4.95–4.93 (m, 1H), 3.38–3.28 (m, 1H), 3.08–2.98 (m, 1H), 1.79–1.75 (m, 3H), 1.56 (s, 3H), 1.09–0.92 (m, 21H).

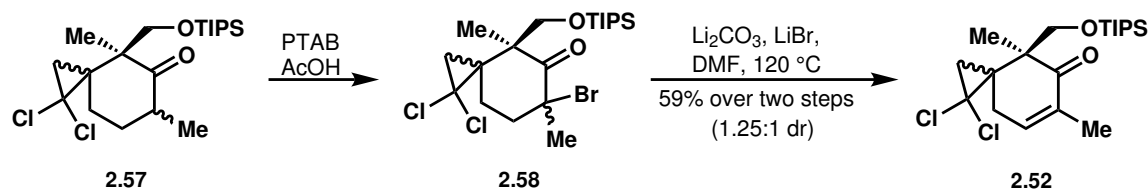


To a solution of **2.51** (690 mg, 2.14 mmol, 1 equiv) in anhydrous THF (30 mL, 0.07 M) at  $-78\text{ }^\circ\text{C}$ , L-Selectride (1.0 M in THF, 6.4 mL, 6.4 mmol, 3 equiv) was added over 2 min. After 1 h, the reaction mixture was poured into  $\text{H}_2\text{O}$  (15 mL), sat. aq.  $\text{NH}_4\text{Cl}$  (15 mL), and  $\text{Et}_2\text{O}$  (30 mL). The aqueous and organic layers were separated, and the aqueous layer was extracted with  $\text{Et}_2\text{O}$  (3 x 30 mL). The combined organic layers were dried over  $\text{Na}_2\text{SO}_4$ , filtered, and concentrated *in vacuo*. The crude product was purified by Yamazen automated flash column chromatography (1%  $\text{Et}_2\text{O}$ /hexanes) to afford **2.56** (671 mg, 97% yield) as a colorless oil.  $^1\text{H NMR}$  (500 MHz,  $\text{CDCl}_3$ ) *Major set of peaks (diastereomer one)*:  $\delta$  4.14 (d,  $J = 9.2$  Hz, 1H), 3.61 (d,  $J = 9.2$  Hz, 1H), 1.26 (s, 3H). *Major set of peaks (diastereomer two)*:  $\delta$  4.04 (d,  $J = 9.5$  Hz, 1H), 3.79 (d,  $J = 9.5$  Hz, 1H), 1.22 (s, 3H). *Minor set of peaks (diastereomer one)*:  $\delta$  4.07 (d,  $J = 9.4$  Hz, 1H), 3.55 (d,  $J = 9.3$  Hz, 1H), 1.24 (s, 3H). *Minor set of peaks (diastereomer two)*:  $\delta$  4.93–4.92 (m, 1H), 3.98 (d,  $J = 9.5$  Hz, 1H), 3.73 (d,  $J = 9.5$  Hz, 1H), 1.21 (s, 3H). *All sets of peaks; normalized such that for one  $^1\text{H}$ : major set of peaks (diastereomer one) = 1.00, major set of peaks (diastereomer two) = 0.89, minor set of peaks (diastereomer one) = 0.11, minor set of peaks (diastereomer two) = 0.12*:  $\delta$  4.98–4.95 (m, 1H), 4.95–4.94 (m, 1H), 4.89–4.88 (m, 1H), 4.85–4.82 (m, 1H), 2.79–2.64 (m, 2H), 2.60–2.46 (m, 3H), 2.44–2.35 (m, 1H), 2.11–1.92 (m, 2H), 1.49–1.39 (m, 1H), 1.34–1.29 (m, 1H), 1.12–0.94 (m, 51H).

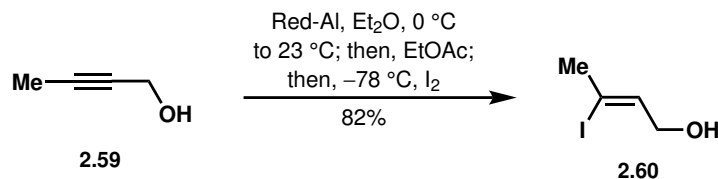


To a solution of **2.56** (354 mg, 1.09 mmol, 1 equiv) in  $\text{CHCl}_3$  (5.2 mL, 65.4 mmol, 60 equiv), triethylbenzylammonium chloride (TEBAC) (24.8 mg, 0.109 mmol, 0.1 equiv) was added. While stirring vigorously, aq.  $\text{NaOH}$  (50 wt%, 1.7 mL, 65.4 mmol, 60 equiv) was added. The reaction mixture was stirred vigorously open to air for 15 h, after which  $\text{H}_2\text{O}$  (10 mL) and  $\text{CH}_2\text{Cl}_2$  (10 mL) were added. The aqueous and organic layers were separated. The aqueous layer was extracted with  $\text{CH}_2\text{Cl}_2$  (3 x 10 mL), and the combined organic layers were dried over  $\text{Na}_2\text{SO}_4$ , filtered, and concentrated *in vacuo* to reveal a crude orange oil. The crude product was purified by Yamazen automated flash column chromatography (1%  $\text{Et}_2\text{O}$ /hexanes) to afford **2.57** (327 mg, 74% yield) as a cloudy-white oil.  $^1\text{H NMR}$  (500 MHz,  $\text{CDCl}_3$ ) *Major set of peaks (diastereomer one)*:  $\delta$  4.50 (d,  $J = 9.6$  Hz, 1H), 3.94 (d,  $J = 9.6$  Hz, 1H). *Major set of peaks (diastereomer two)*:  $\delta$  4.34 (d,  $J = 9.5$  Hz, 1H), 4.22 (d,  $J = 9.5$  Hz, 1H). *Major set of peaks (diastereomers three and four)*:  $\delta$  4.12 (d,  $J = 10.1$  Hz, 1H), 4.08 (d,  $J = 10.1$  Hz, 1H), 3.87 (d,  $J = 10.1$  Hz, 1H), 3.59 (d,  $J = 10.1$  Hz, 1H). *Minor set of peaks (all diastereomers)*:  $\delta$  4.43 (d,  $J = 9.6$  Hz, 1H), 4.28 (d,  $J = 9.4$  Hz, 1H), 4.15 (d,  $J = 9.5$  Hz, 1H), 4.07 (d,  $J = 10.1$  Hz, 1H), 4.03 (d,  $J = 10.5$  Hz, 1H), 3.86 (d,  $J = 9.7$  Hz), 3.81

(d,  $J = 10.1$  Hz, 1H), 3.53 (d,  $J = 10.2$  Hz, 1H). All sets of peaks; normalized such that for one  $^1\text{H}$ : major set of peaks (diastereomer one) = 1.00, major set of peaks (diastereomer two) = 0.58, major set of peaks (diastereomer three, diastereomer four) = 1.02, 1.03, minor set of peaks (each diastereomer) = range from 0.06–0.20:  $\delta$  2.99–2.89 (m, 1.0H), 2.86–2.61 (m, 3.4H), 2.46–2.36 (m, 1.1H), 2.32 (dd,  $J = 7.8, 1.6$  Hz, 1.0H), 2.30–1.95 (m, 7.9H), 1.78–1.67 (m, 4.3H), 1.62 (ddd,  $J = 14.2, 9.1, 2.8$  Hz, 0.8H), 1.58–1.56 (m, 1.5H), 1.55–1.31 (m, 9.1H), 1.30–1.27 (m, 7.4H), 1.17 (s, 2.9H), 1.17–0.93 (m, 106.4H), 0.91 (s, 2.4H).

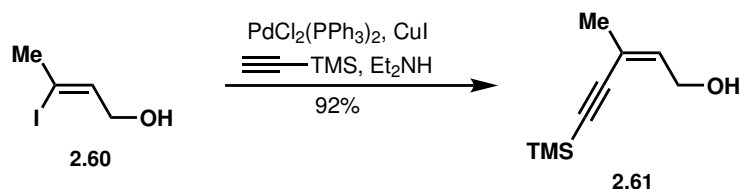


To a solution of **2.57** (891 mg, 2.19 mmol, 1 equiv) in AcOH (20 mL, 0.11 M), phenyltrimethylammonium perbromide (PTAB) (1.23 g, 3.28 mmol, 1.5 equiv) was added, and the reaction was stirred at 23 °C under air. After 2 h, the reaction mixture was poured into sat. aq.  $\text{Na}_2\text{CO}_3$  (50 mL) and  $\text{Et}_2\text{O}$  (50 mL). The aqueous and organic layers were separated, and the aqueous layer was extracted with  $\text{Et}_2\text{O}$  (3 x 50 mL). The combined organic layers were washed with brine (150 mL), then dried over  $\text{Na}_2\text{SO}_4$ , filtered, and concentrated *in vacuo* to reveal a crude light orange liquid. DMF (20 mL, 0.11 M) was added, followed by  $\text{Li}_2\text{CO}_3$  (485 mg, 6.56 mmol, 3 equiv) and LiBr (570 mg, 6.56 mmol, 3 equiv). The reaction mixture was stirred at 120 °C for 1 h, after which to the reaction mixture was added  $\text{Et}_2\text{O}$  (100 mL) and brine (50 mL). The aqueous and organic layers were separated, and the organic layer was washed with brine (3 x 50 mL). The organic layer was dried over  $\text{Na}_2\text{SO}_4$ , filtered, and concentrated *in vacuo*. The crude product was purified by Yamazen automated flash column chromatography (1%  $\text{Et}_2\text{O}$ /hexanes) to afford **2.52** (519 mg, 59% yield) as a cloudy-white oil.  $^1\text{H}$  NMR (500 MHz,  $\text{CDCl}_3$ ) Major diastereomer:  $\delta$  4.16 (d,  $J = 10.0$  Hz, 1H), 4.01 (d,  $J = 10.1$  Hz, 1H), 2.94–2.85 (m, 1H), 2.40 (dd,  $J = 8.2, 0.9$  Hz, 1H), 2.22 (ddd,  $J = 18.6, 6.2, 1.4$  Hz, 1H), 1.40 (d,  $J = 8.2$  Hz, 1H), 1.26 (s, 3H) Minor diastereomer:  $\delta$  4.25 (d,  $J = 9.2$  Hz, 1H), 3.93 (d,  $J = 9.2$  Hz, 1H), 3.47–3.41 (m, 1H), 2.02 (ddd,  $J = 19.0, 6.4, 1.4$  Hz, 1H), 1.23 (d,  $J = 7.9$  Hz, 1H), 1.15 (s, 3H). Major + minor diastereomer; normalized such that for one  $^1\text{H}$ : major diastereomer = 1.25, minor diastereomer = 1.00:  $\delta$  6.69–6.63 (m, 2H), 1.83–1.79 (m, 8H), 1.12–0.93 (m, 47H).

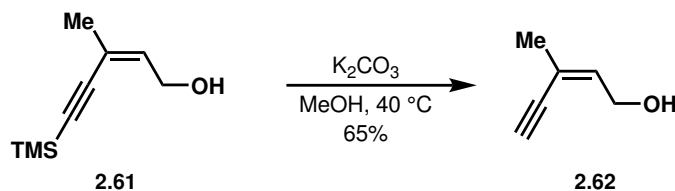


This procedure was adapted from ref. [56]. To a solution of Red-Al (70 wt% in PhMe, 16.7 mL, 60.2 mmol, 1.5 equiv) in  $\text{Et}_2\text{O}$  (80 mL) in a flame-dried 250 mL round-bottomed flask, **2.59** (3.0 mL, 40.1 mmol, 1 equiv) was added dropwise at 0 °C, and the reaction mixture was warmed to 23 °C. After 26 h, the reaction mixture was cooled to 0 °C, and EtOAc (4

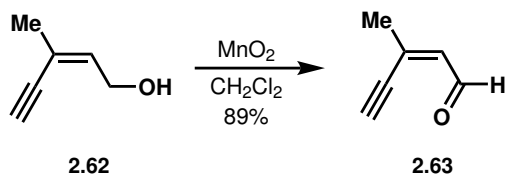
mL) was added. The reaction mixture was stirred for 10 min and then cooled to  $-78\text{ }^{\circ}\text{C}$ .  $\text{I}_2$  (15.3 g, 60.2 mmol, 1.5 equiv) was added and the reaction mixture was stirred for 1 h, after which it was warmed to  $23\text{ }^{\circ}\text{C}$ ; the reaction mixture turned dark red while warming. After 1.5 h, the reaction mixture was poured into a stirred solution of sat. aq.  $\text{Na}_2\text{S}_2\text{O}_3$  (40 mL) and sat. aq. Rochelle's salt (40 mL), and EtOAc (30 mL) was added. The mixture was stirred vigorously for 1 h, and then the aqueous and organic layers were separated. The aqueous layer was extracted with EtOAc (3 x 100 mL), and the combined organic layers were dried over  $\text{Na}_2\text{SO}_4$ , filtered, and concentrated *in vacuo* to reveal a crude red liquid. The crude product was purified by Yamazen automated flash column chromatography (20% EtOAc/hexanes) to afford **2.60** (6.52 g, 82% yield) as an orange oil. The spectral data is consistent with that reported in the literature.<sup>56</sup>



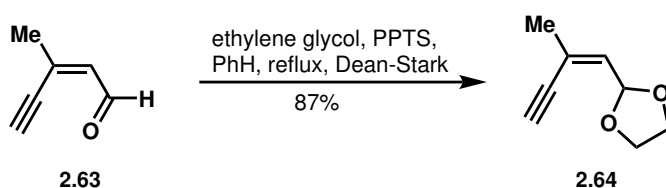
This procedure was adapted from ref. [57]. A solution of **2.60** (6.51 g, 32.9 mmol, 1 equiv) in  $\text{Et}_2\text{NH}$  (60 mL, 0.55M) was added to  $\text{PdCl}_2(\text{Ph}_3\text{P})_2$  (462 mg, 0.66 mmol, 0.02 equiv) and  $\text{CuI}$  (62.6 mg, 0.33 mmol, 0.01 equiv) at  $23\text{ }^{\circ}\text{C}$ . The reaction mixture was stirred for 10 min, after which trimethylsilylacetylene (5.5 mL, 39.5 mmol, 1.2 equiv) was added dropwise. The reaction mixture was stirred for 13 h, after which it was poured into  $\text{Et}_2\text{O}$  (120 mL) and quenched with sat. aq.  $\text{NH}_4\text{Cl}$  (50 mL). The aqueous and organic layers were separated, and the aqueous layer was extracted with  $\text{Et}_2\text{O}$  (3 x 100 mL). The combined organic layers were washed with  $\text{H}_2\text{O}$  (250 mL), then with brine (250 mL). The combined organic layers were dried over  $\text{Na}_2\text{SO}_4$ , filtered, and concentrated *in vacuo* to afford a crude red oil. The crude product was purified by Yamazen automated flash column chromatography (15% EtOAc/hexanes) to afford **2.61** (5.11 g, 92% yield) as an orange oil. The spectral data is consistent with that reported in the literature.<sup>57</sup>



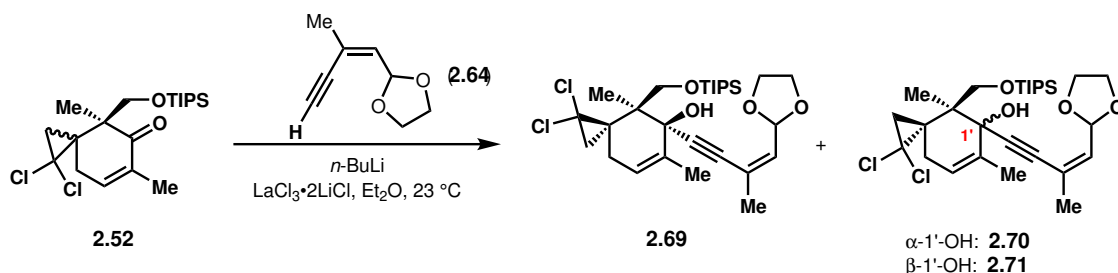
This procedure was adapted from ref. [58]. To a solution of **2.61** (2.58 g, 15.3 mmol, 1 equiv) in anhydrous MeOH (25 mL, 0.61 M),  $\text{K}_2\text{CO}_3$  (31.7 mg, 0.229 mmol, 0.015 equiv) was added. The reaction mixture was warmed to  $40\text{ }^{\circ}\text{C}$  for 2 h, after which it was concentrated *in vacuo*. The crude product was purified by Yamazen automated flash column chromatography (20% EtOAc/hexanes) to afford **2.62** (0.962 g, 65% yield based on  $^1\text{H}$  NMR) as a yellow-orange liquid. Solvent from purification was not fully removed *in vacuo* before the next reaction in order to avoid loss of product as a result of its volatility. The spectral data is consistent with that reported in the literature.<sup>58</sup>



This procedure was adapted from ref. [59]. To a solution of **2.62** (0.962 g, 10.0 mmol, 1 equiv) in  $\text{CH}_2\text{Cl}_2$  (30 mL, 0.33 M),  $\text{MnO}_2$  (9.66 g, 100 mmol, 10 equiv) was added. The reaction mixture was stirred at 23 °C for 21 h, after which it was filtered through Celite and concentrated *in vacuo* to afford **2.63** (840 mg, 89% yield by  $^1\text{H}$  NMR) as a yellow-orange liquid. Solvent was not fully removed *in vacuo* before the next reaction in order to avoid loss of product as a result of its volatility. The spectral data is consistent with that reported in the literature.<sup>59</sup>

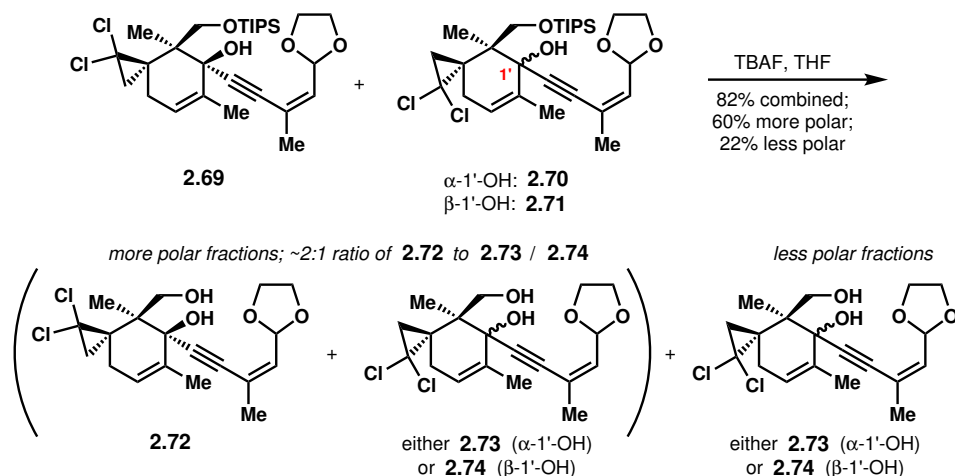


This procedure was adapted from ref. [55]. To a solution of **2.63** (840 mg, 8.92 mmol, 1 equiv) in benzene (30 mL, 0.30 M), non-anhydrous ethylene glycol (0.65 mL, 11.6 mmol, 1.3 equiv) and PPTS (247 mg, 0.98 mmol, 0.11 equiv) were added. A Dean-Stark apparatus and reflux condenser were attached, and the reaction was heated to reflux. After 1 h, brine (30 mL) was added to the reaction mixture, and the aqueous and organic layers were separated. The aqueous layer was extracted with  $\text{Et}_2\text{O}$  (3 x 20 mL). The combined organic layers were dried over  $\text{Na}_2\text{SO}_4$ , filtered, and concentrated *in vacuo* to reveal a crude amber liquid. Kugelrohr distillation (55 °C, 0.8 torr) afforded **2.64** (1.07 g, 87% yield) as a light yellow liquid. The spectral data is consistent with that reported in the literature.<sup>55</sup>



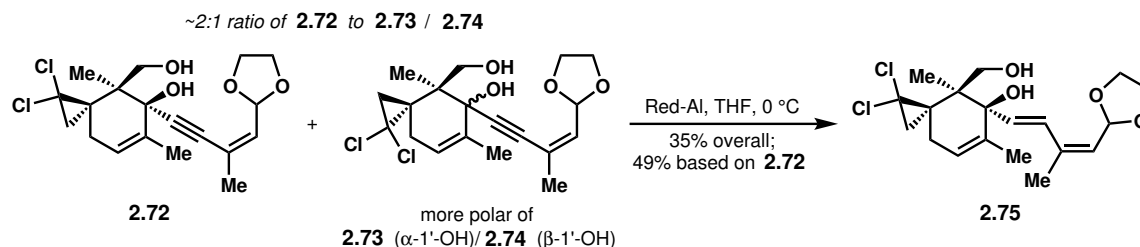
Both **2.52** (323 mg, 0.796 mmol, 1 equiv) and **2.64** (280 mg, 2.03 mmol, 2.55 equiv) were dried via azeotropic distillation with PhH. To a solution of **2.52** in  $\text{Et}_2\text{O}$  (6.8 mL) at 23 °C,  $\text{LaCl}_3 \cdot \text{LiCl}$  (0.57 M in THF, 1.4 mL, 0.796 mmol, 1 equiv) was added over 2 min; white solids precipitated out of solution. The mixture was stirred for 80 min. Meanwhile, to a solution of **2.64** in  $\text{Et}_2\text{O}$  (5.7 mL) at  $-78$  °C,  $n\text{-BuLi}$  (1.6 M in hexane, 1.2 mL, 1.99 mmol, 2.5 equiv) was added over 1.5 min. The mixture was stirred for 20 min, after which it was added to the mixture of **2.52** and  $\text{LaCl}_3 \cdot \text{LiCl}$  in  $\text{Et}_2\text{O}$  over 15 min, resulting in a cloudy orange solution. After 4 h, the reaction was quenched with sat. aq.  $\text{NH}_4\text{Cl}$  (15 mL) and

Et<sub>2</sub>O (15 mL), and the aqueous and organic layers were separated. The aqueous layer was extracted with Et<sub>2</sub>O (3 x 10 mL), and the combined organic layers were dried over Na<sub>2</sub>SO<sub>4</sub>, filtered, and concentrated *in vacuo*. The crude product was purified by Yamazen automated flash column chromatography (12% EtOAc/hexanes with 1% Et<sub>3</sub>N) to afford a mixture of diastereomers **2.69**–**2.71** contaminated with **2.64**. If desired, the less polar of **2.70/2.71** could be separated from the other two diastereomers. The mixture was heated to 40 °C under high vacuum for 48 h to remove **2.64**, affording **2.69**–**2.71** (366 mg, 85% yield) as a viscous cloudy-white oil. **<sup>1</sup>H NMR of the less polar of 2.70/2.71, pure** (500 MHz, CDCl<sub>3</sub>): δ 5.63 (dd, *J* = 7.6, 1.5 Hz, 1H), 5.63 (br s, 1H), 5.57 (d, *J* = 7.7 Hz, 1H), 5.37 (br s, 1H), 4.48 (br d, *J* = 8.7 Hz, 1H), 4.13 (br d, *J* = 9.3 Hz, 1H), 4.04–3.95 (m, 2H), 3.93–3.83 (m, 2H), 2.85 (br d, *J* = 18.7 Hz, 1H), 1.97 (d, *J* = 8.4 Hz, 1H), 1.89 (d, *J* = 1.5 Hz, 3H), 1.86 (br s, 3H), 1.71 (br d, *J* = 18.1 Hz, 1H), 1.44 (s, 3H), 1.32 (d, *J* = 8.4 Hz, 1H), 1.20–0.98 (m, 21H). **<sup>1</sup>H NMR of mixture of all diastereomers** (500 MHz, CDCl<sub>3</sub>) **2.69**: δ 5.57 (d, *J* = 7.7 Hz, 1H), 5.43–5.39 (m, 1H), 4.99 (s, 1H), 4.35 (d, *J* = 9.6 Hz, 1H), 3.93 (d, *J* = 9.6 Hz, 1H), 2.72–2.65 (m, 1H), 2.15 (d, *J* = 8.3 Hz, 1H), 1.81–1.72 (m, 1H), 1.51 (s, 3H), 1.32 (d, *J* = 8.4 Hz, 1H). *Less polar of 2.70/2.71*: δ 5.58 (d, *J* = 7.7 Hz, 1H), 5.37 (br s, 1H), 4.48 (br d, *J* = 8.7 Hz, 1H), 4.13 (br d, *J* = 9.3 Hz, 1H), 2.85 (br d, *J* = 18.7 Hz, 1H), 1.98 (d, *J* = 8.4 Hz, 1H), 1.71 (br d, *J* = 18.1 Hz, 1H), 1.44 (s, 3H), 1.33 (d, *J* = 8.4 Hz, 1H). *More polar of 2.70/2.71*: δ 5.54 (s, 1H), 4.64 (d, *J* = 11.1 Hz, 1H), 4.25 (d, *J* = 11.2 Hz, 1H), 2.84–2.76 (m, 1H), 2.64 (d, *J* = 7.9 Hz, 1H), 1.56 (s, 3H), 1.41 (d, *J* = 7.8 Hz, 1H). *All diastereomers: normalized such that for one <sup>1</sup>H: 2.69 = 1.00, less polar of 2.70/2.71 = 0.67, more polar of 2.70/2.71 = 0.39*: δ 5.69–5.60 (m, 3.4H), 4.04–3.96 (m, 4.5H), 3.91–3.84 (m, 4.2H), 1.97–1.91 (m, 6.0H), 1.91–1.87 (m, 5.4H), 1.87–1.84 (br s, 2.3H), 1.23–0.99 (m, 46.6H).

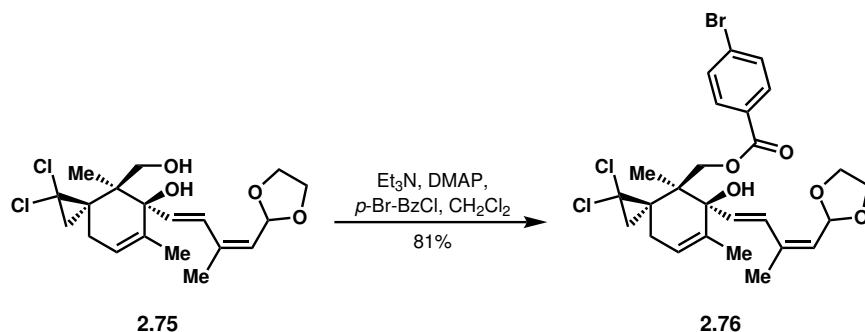


To a solution of **2.69**–**2.71** (57.7 mg, 0.106 mmol, 1 equiv) in THF (0.5 mL, 0.21 M) at 0 °C, TBAF (1.0 M in THF, 0.21 mL, 0.21 mmol, 2 equiv) was added, and the reaction mixture was warmed to 23 °C. After 4.5 h, H<sub>2</sub>O (2 mL) and EtOAc (3 mL) were added to the reaction mixture. The aqueous and organic layers were separated, and the aqueous layer was extracted with EtOAc (3 x 2 mL). The combined organic layers were dried over Na<sub>2</sub>SO<sub>4</sub>, filtered, and concentrated *in vacuo* to reveal a crude yellow liquid. The crude product was purified by Yamazen automated flash column chromatography (35% EtOAc/hexanes with

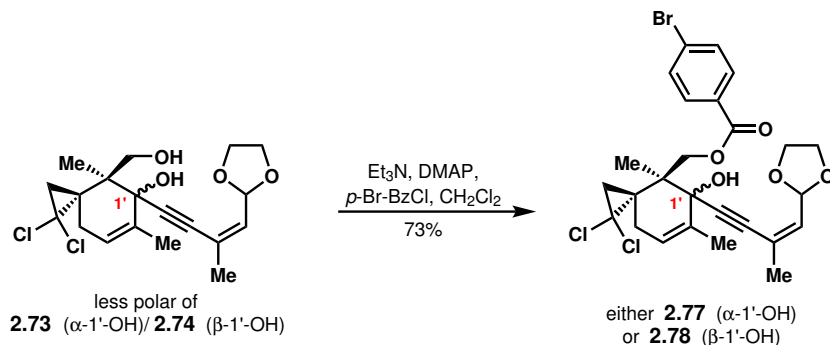
1% Et<sub>3</sub>N) to afford a mixture of **2.72** and the more polar of **2.73/2.74** (24.6 mg, 60% yield), and the less polar of **2.73/2.74** (9.0 mg, 22% yield). <sup>1</sup>H NMR of a mixture of **2.72** and the more polar of **2.73/2.74** (400 MHz, CDCl<sub>3</sub>) **2.72**: δ 5.56 (d, *J* = 7.5 Hz, 1H), 5.50–5.45 (s, 1H), 4.19 (d, *J* = 11.2 Hz, 1H), 3.19 (br s, 1H), 2.75–2.67 (m, 1H), 2.44 (br s, 1H), 2.06 (dd, *J* = 8.1, 1.0 Hz, 1H), 1.90 (d, *J* = 1.6 Hz, 6H), 1.82–1.75 (m, 1H), 1.28 (d, *J* = 8.2 Hz, 1H), 1.43 (s, 3H). More polar of **2.73/2.74**: δ 5.60–5.56 (m, 1H), 4.45 (br d, *J* = 12.0 Hz, 1H), 3.80 (br d, *J* = 11.3 Hz, 1H), 4.18 (d, *J* = 12.3 Hz, 1H), 2.94 (br s, 1H), 2.86–2.76 (m, 1H), 2.68 (d, *J* = 7.4 Hz, 1H), 1.95 (d, *J* = 1.5 Hz, 6H), 1.89–1.82 (m, 1H), 1.35 (d, *J* = 7.7 Hz, 1H), 1.14 (s, 1H). Both diastereomers; normalized such that for one <sup>1</sup>H: **2.72** = 1.00, more polar of **2.73/2.74** = 0.50: δ 5.74–5.64 (m, 2H), 4.05–3.96 (m, 3H), 3.96–3.87 (m, 3H). <sup>1</sup>H NMR of the less polar of **2.73/2.74** (500 MHz, CDCl<sub>3</sub>) δ 5.73 (dq, *J* = 6.6, 1.6 Hz, 1H), 5.64 (d, *J* = 6.6 Hz, 1H), 5.46–5.38 (m, 1H), 5.04 (br s, 1H), 4.25 (d, *J* = 10.6 Hz, 1H), 4.07–3.94 (m, 3H), 3.94–3.87 (m, 2H), 3.09 (br s, 1H), 2.82 (d, *J* = 18.8 Hz, 1H), 2.00 (dd, *J* = 8.3, 1.2 Hz, 1H), 1.91 (d, *J* = 1.6 Hz, 3H), 1.88–1.85 (m, 3H), 1.81–1.72 (m, 1H), 1.42 (s, 3H), 1.31 (d, *J* = 8.3 Hz, 1H).



A mixture of **2.72** and the more polar of **2.73/2.74** (4.9 mg, 0.013 mmol, 1 equiv) was dried via azeotropic distillation with PhH. To a solution of the mixture of **2.72** and the more polar of **2.73/2.74** in THF (0.3 mL, 0.04 M) at 0 °C, Red-Al (0.35 M in PhMe, 10.8  $\mu$ L, 0.038 mmol, 3 equiv) was added. The reaction mixture was stirred for 1 h, after which the reaction was quenched with H<sub>2</sub>O (5  $\mu$ L), then aq. NaOH (15 wt%, 5  $\mu$ L), then H<sub>2</sub>O (5  $\mu$ L). The reaction mixture was warmed to 23 °C and stirred for 30 min, after which it was filtered through Celite and concentrated *in vacuo*. The crude product was purified by flash column chromatography (35% EtOAc/hexanes with 1% Et<sub>3</sub>N) to afford **2.75** (1.7 mg, 35% yield, 49% yield based on **2.72**). <sup>1</sup>H NMR (500 MHz, CDCl<sub>3</sub>): δ 6.67 (d, *J* = 15.6 Hz, 1H), 5.70 (d, *J* = 7.2 Hz, 1H), 5.66 (d, *J* = 15.5 Hz, 1H), 5.50–5.44 (m, 1H), 5.37 (d, *J* = 7.2 Hz, 1H), 4.32 (d, *J* = 10.8 Hz, 1H), 4.06–3.97 (m, 2H), 3.95–3.87 (m, 2H), 3.87 (d, *J* = 10.8 Hz, 1H), 3.61 (s, 1H), 2.78–2.71 (m, 1H), 2.29 (br s, 1H), 1.86 (d, *J* = 1.4 Hz, 3H), 1.82–1.74 (m, 1H), 1.80 (d, *J* = 7.6 Hz, 1H), 1.69 (d, *J* = 2.0 Hz, 3H), 1.31 (d, *J* = 7.9 Hz, 1H), 1.18 (s, 3H).



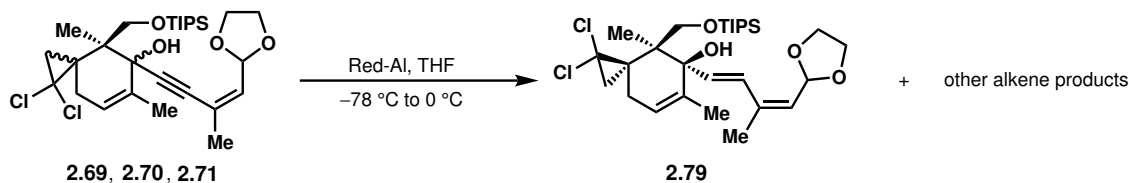
To a solution of **2.75** (5.4 mg, 0.014 mmol, 1 equiv) in  $\text{CH}_2\text{Cl}_2$  (0.3 mL, 0.05 M),  $\text{Et}_3\text{N}$  (7.8  $\mu\text{L}$ , 0.056 mmol, 4 equiv), DMAP (0.4 mg, 0.003 mmol, 0.23 equiv), and  $p\text{-Br-BzCl}$  (6.1 mg, 0.028 mmol, 2 equiv) were added. The reaction mixture was stirred at 23 °C for 2.5 h, after which  $\text{CH}_2\text{Cl}_2$  (1 mL) and  $\text{H}_2\text{O}$  (1 mL) were added. The aqueous and organic layers were separated, and the aqueous layer was extracted with  $\text{CH}_2\text{Cl}_2$  (3 x 1 mL). The combined organic layers were dried over  $\text{Na}_2\text{SO}_4$ , filtered, and concentrated *in vacuo* to afford a crude yellow-white solid. The crude product was purified by flash column chromatography (25%  $\text{EtOAc}$ /hexanes with 1%  $\text{Et}_3\text{N}$ ) to afford **2.76** (6.4 mg, 81% yield) as a crystalline solid.  $^1\text{H NMR}$  (600 MHz,  $\text{CDCl}_3$ ):  $\delta$  8.06 (d,  $J = 8.6$  Hz, 2H), 7.60 (d,  $J = 8.6$  Hz, 2H), 6.68 (d,  $J = 15.7$  Hz, 1H), 5.73 (d,  $J = 15.7$  Hz, 1H), 5.69 (d,  $J = 7.1$  Hz, 1H), 5.47–5.43 (m, 1H), 5.41 (d,  $J = 6.8$  Hz, 1H), 4.73 (d,  $J = 11.6$  Hz, 1H), 4.56 (d,  $J = 11.6$  Hz, 1H), 4.06–3.99 (m, 2H), 3.95–3.88 (m, 2H), 2.89 (d,  $J = 19.3$  Hz, 1H), 2.45 (s, 1H), 1.87 (d,  $J = 1.3$  Hz, 3H), 1.87–1.81 (m, 1H), 1.73 (d,  $J = 7.9$  Hz, 1H), 1.37 (d,  $J = 7.7$  Hz, 1H), 1.14 (s, 3H).



To a solution of the less polar of **2.73/2.74** (5.8 mg, 0.015 mmol, 1 equiv) in  $\text{CH}_2\text{Cl}_2$  (0.3 mL, 0.05 M),  $\text{Et}_3\text{N}$  (8.3  $\mu\text{L}$ , 0.060 mmol, 4 equiv), DMAP (0.2 mg, 0.001 mmol, 0.1 equiv), and  $p\text{-Br-BzCl}$  (3.6 mg, 0.016 mmol, 1.1 equiv) were added. The reaction mixture was stirred at 23 °C for 21 h, after which DMAP (1.3 mg, 0.011 mmol, 0.7 equiv) and  $p\text{-Br-BzCl}$  (5.0 mg, 0.023 mmol, 1.5 equiv) were added. The reaction mixture was stirred for another 4 h, after which  $p\text{-Br-BzCl}$  (4.6 mg, 0.021 mmol, 1.4 equiv) was added. The reaction mixture was stirred for another 1.5 h, after which  $\text{H}_2\text{O}$  (1 mL) and  $\text{CH}_2\text{Cl}_2$  (1 mL) were added. The aqueous and organic layers were separated, and the aqueous layer was extracted with  $\text{CH}_2\text{Cl}_2$  (3 x 1 mL). The combined organic layers were dried over  $\text{Na}_2\text{SO}_4$ , filtered, and concentrated *in vacuo* to reveal a crude white solid. The crude product was purified by flash column chromatography (20%  $\text{EtOAc}$ /hexanes with 1%  $\text{Et}_3\text{N}$ ) to afford **2.77/2.78** (6.2 mg, 73% yield) as an oil.  $^1\text{H NMR}$  (500 MHz,  $\text{CDCl}_3$ ):  $\delta$  7.84 (d,  $J = 8.6$  Hz, 2H), 7.60 (d,  $J$



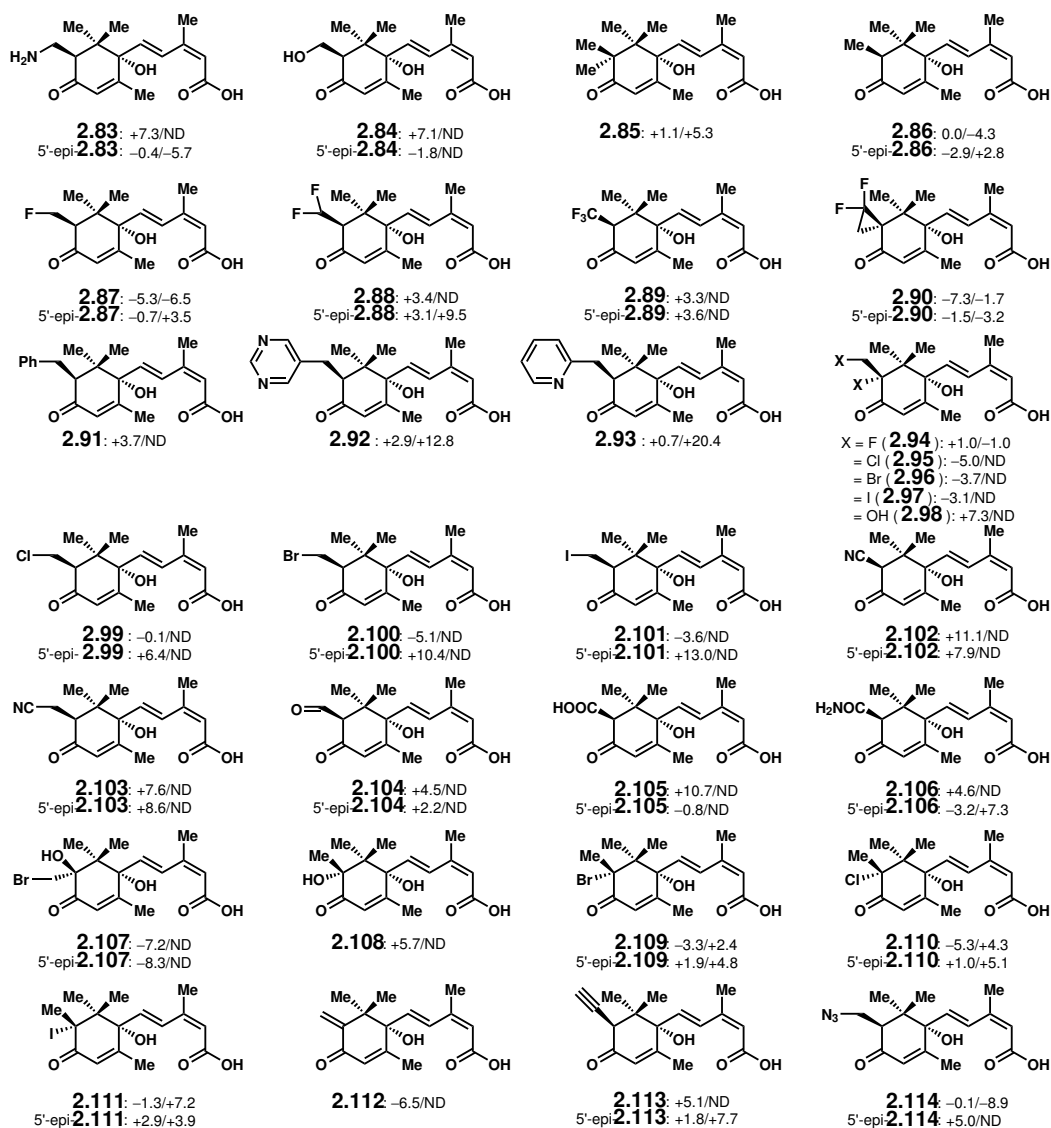
= 8.6 Hz, 2H), 5.67 (d,  $J = 7.1$  Hz, 1H), 5.58 (d,  $J = 7.3$  Hz, 2H), 4.77 (br d,  $J = 11.7$  Hz, 1H), 4.54 (br d,  $J = 11.7$  Hz, 1H), 4.03–3.94 (m, 2H), 3.94–3.85 (m, 2H), 2.76 (br s, 1H), 2.61 (br d,  $J = 19.2$  Hz, 1H), 2.22 (br s, 1H), 2.07 (br d,  $J = 8.5$  Hz, 1H), 1.96 (s, 3H), 1.84 (s, 3H), 1.46 (s, 3H), 1.37 (d,  $J = 8.1$  Hz, 1H).



A mixture of diastereomers **2.69–2.71** (19.8 mg, 0.036 mmol, 1 equiv) was dried via azeotropic distillation with PhH. To a solution of **2.69–2.71** in THF (1.0 mL, 0.036 M) at  $-78$  °C, Red-Al (10:1 dilution in THF of 70 wt% in toluene, 31.0  $\mu$ L, 0.109 mmol, 3 equiv) was added over 4 min, and the reaction mixture was warmed to  $0$  °C. The reaction mixture was stirred for 1 h, after which the reaction was quenched with Glauber's salt (20 mg) and the reaction mixture was warmed to  $23$  °C. The mixture was stirred for 15 min, after which it was filtered through Celite and concentrated *in vacuo*. The crude product was purified by flash column chromatography (8% EtOAc/hexanes with 1% Et<sub>3</sub>N) to afford **2.79** and other alkene products (7.8 mg, 39% mass recovery). **<sup>1</sup>H NMR of major product 2.79, mostly pure** (400 MHz, CDCl<sub>3</sub>):  $\delta$  6.71 (d,  $J = 15.4$  Hz, 1H), 5.73 (d,  $J = 7.5$  Hz, 1H), 5.63 (d,  $J = 15.5$  Hz, 1H), 5.45–5.38 (m, 1H), 5.33 (d,  $J = 7.6$  Hz, 1H), 5.04 (d,  $J = 1.2$  Hz, 1H), 4.43 (d,  $J = 9.4$  Hz, 1H), 4.06–3.96 (m, 2H), 3.95–3.84 (m, 3H), 2.77–2.67 (m, 1H), 1.85 (d,  $J = 7.9$  Hz), 1.84 (d,  $J = 1.3$  Hz, 3H), 1.80–1.72 (m, 1H), 1.69 (d,  $J = 1.7$  Hz, 3H), 1.30 (d,  $J = 7.9$  Hz, 1H), 1.21 (s, 3H), 1.11–1.01 (m, 21H).

## 2.8.3 Supplementary Figures

**Table S2.1:** Prime MM-GBSA-calculated binding energies. First number provided is the binding energy of the ABA analog in the PYR1–ABA analog complex; second number, if provided, is the binding energy of the ABA analog in the PYR1–ABA analog–HAB1 complex. All energies provided are relative to the calculated binding energy of ABA in the PYR1–ABA or PYR1–ABA–HAB1 complexes in kcal/mol, with positive numbers indicating weaker binding than ABA and negative numbers indicating stronger binding than ABA. ND = not determined.



## 2.9 References

- (1) Kende, H.; Zeevaart, J. A. D. *The Plant Cell* **1997**, *9*, 1197–1210.

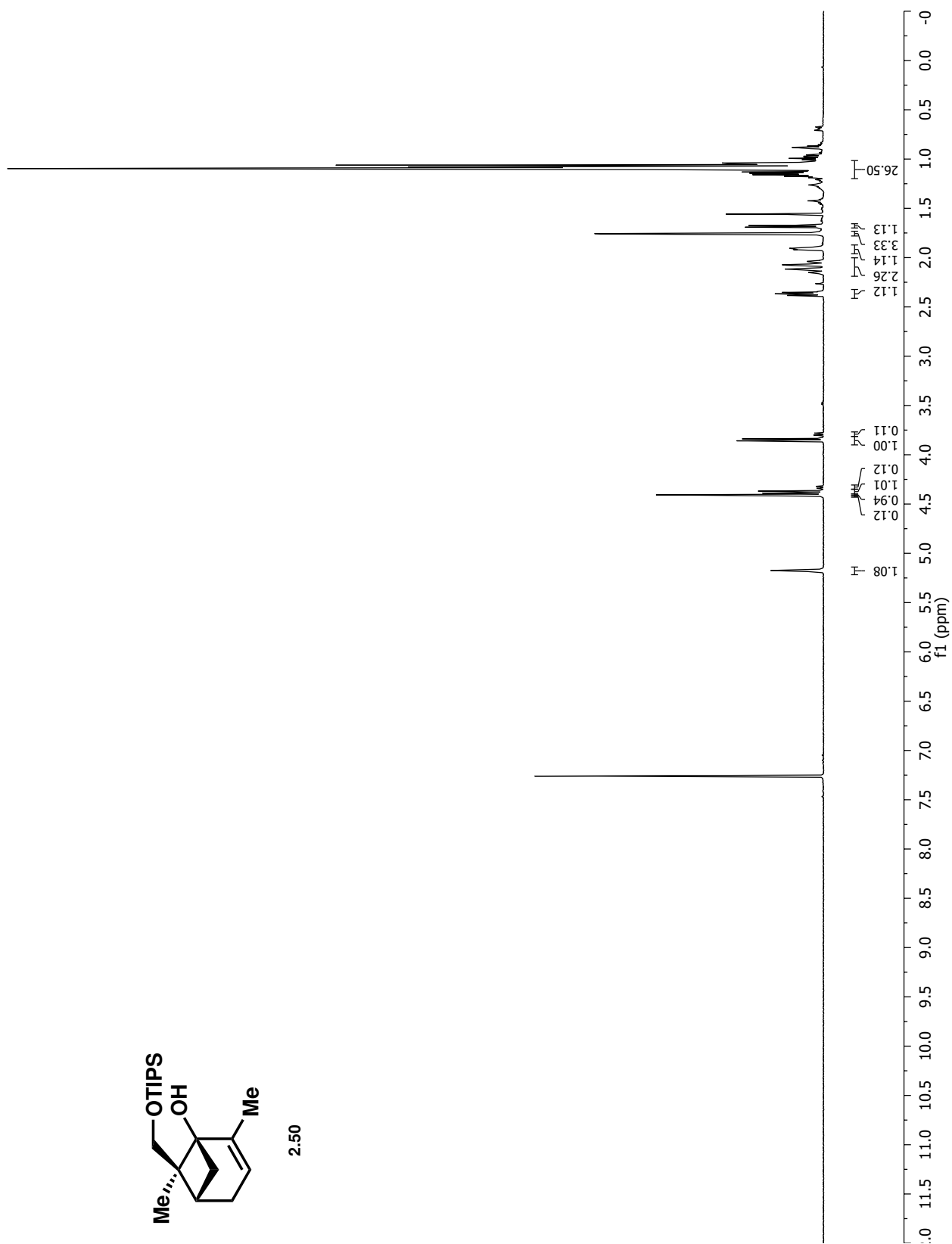
- (2) Ohkuma, K.; Lyon, J. L.; Addicott, F. T.; Smith, O. E. *Science* **1963**, *142*, 1592–1593.
- (3) Eagles, C. F.; Wareing, P. F. *Nature* **1963**, *199*, 874–875.
- (4) Cornforth, J. W.; Milborrow, B. V.; Ryback, G.; Wareing, P. F. *Nature* **1965**, *205*, 1269–1270.
- (5) Cornforth, J. W.; Milborrow, B. V.; Ryback, G. *Nature* **1965**, *206*, 715–715.
- (6) Cornforth, J. W.; Draber, W.; Milborrow, B. V.; Ryback, G. *Chem. Commun. (London)* **1967**, 114–116.
- (7) Ryback, G. *J. Chem. Soc., Chem. Commun.* **1972**, *0*, 1190–1191.
- (8) Koreeda, M.; Weiss, G.; Nakanishi, K. *J. Am. Chem. Soc.* **1973**, *95*, 239–240.
- (9) Addicott, F. T.; Lyon, J. L.; Ohkuma, K.; Thiessen, W. E.; Carns, H. R.; Smith, O. E.; Cornforth, J. W.; Milborrow, B. V.; Ryback, G.; Wareing, P. F. *Science* **1968**, *159*, 1493–1493.
- (10) Li, J.; Wu, Y.; Xie, Q.; Gong, Z. In *Hormone Metabolism and Signaling in Plants*, Li, J., Li, C., Smith, S. M., Eds.; Academic Press: 2017, pp 161–202.
- (11) ABA has also been discovered in a variety of other non-plant organisms including humans, although for these other organisms it does not play as central a role as in plants.<sup>71</sup>.
- (12) Nambara, E.; Okamoto, M.; Tatematsu, K.; Yano, R.; Seo, M.; Kamiya, Y. *Seed Sci. Res.* **2010**, *20*, 55–67.
- (13) Leng, P.; Yuan, B.; Guo, Y. *J. Exp. Bot.* **2014**, *65*, 4577–4588.
- (14) Sah, S. K.; Reddy, K. R.; Li, J. *Front. Plant Sci.* **2016**, *7*, DOI: 10.3389/fpls.2016.00571.
- (15) Vishwakarma, K.; Upadhyay, N.; Kumar, N.; Yadav, G.; Singh, J.; Mishra, R. K.; Kumar, V.; Verma, R.; Upadhyay, R. G.; Pandey, M.; Sharma, S. *Front. Plant Sci.* **2017**, *8*, DOI: 10.3389/fpls.2017.00161.
- (16) Waterland, N. L.; Campbell, C. A.; Finer, J. J.; Jones, M. L. *HortScience* **2010**, *45*, 409–413.
- (17) BioNik – Valent BioSciences – Biorational Crop Enhancement., <https://www.valentbiosciences.com/cropenhancement/products/bionik/> (accessed 09/22/2019).
- (18) Valent BioSciences ProTone Plant Growth Regulator., <http://www.protonepgr.com/> (accessed 09/22/2019).
- (19) Hubbard, K. E.; Nishimura, N.; Hitomi, K.; Getzoff, E. D.; Schroeder, J. I. *Genes Dev.* **2010**, *24*, 1695–1708.
- (20) Park, S.-Y. et al. *Science* **2009**, *324*, 1068–1071.
- (21) Ma, Y.; Szostkiewicz, I.; Korte, A.; Moes, D.; Yang, Y.; Christmann, A.; Grill, E. *Science* **2009**, *324*, 1064–1068.
- (22) Cutler, S. R.; Rodriguez, P. L.; Finkelstein, R. R.; Abrams, S. R. *Annu. Rev. Plant Biol.* **2010**, *61*, 651–679.

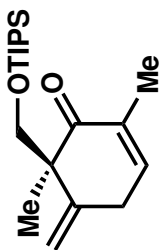
- (23) Klingler, J. P.; Batelli, G.; Zhu, J.-K. *J. Exp. Bot.* **2010**, *61*, 3199–3210.
- (24) (a) Yin, P.; Fan, H.; Hao, Q.; Yuan, X.; Wu, D.; Pang, Y.; Yan, C.; Li, W.; Wang, J.; Yan, N. *Nat. Struct. Mol. Biol.* **2009**, *16*, 1230–1236; (b) Santiago, J.; Rodrigues, A.; Saez, A.; Rubio, S.; Antoni, R.; Dupeux, F.; Park, S.-Y.; Márquez, J. A.; Cutler, S. R.; Rodriguez, P. L. *Plant J.* **2009**, *60*, 575–588; (c) Miyazono, K.-i.; Miyakawa, T.; Sawano, Y.; Kubota, K.; Kang, H.-J.; Asano, A.; Miyauchi, Y.; Takahashi, M.; Zhi, Y.; Fujita, Y.; Yoshida, T.; Kodaira, K.-S.; Yamaguchi-Shinozaki, K.; Tanokura, M. *Nature* **2009**, *462*, 609–614; (d) Nishimura, N.; Sarkeshik, A.; Nito, K.; Park, S.-Y.; Wang, A.; Carvalho, P. C.; Lee, S.; Caddell, D. F.; Cutler, S. R.; Chory, J.; Yates, J. R.; Schroeder, J. I. *Plant J.* **2010**, *61*, 290–299; (e) Melcher, K. et al. *Nature* **2009**, *462*, 602–608.
- (25) Nambara, E.; Marion-Poll, A. *Annu. Rev. Plant Biol.* **2005**, *56*, 165–185.
- (26) Finkelstein, R. *The Arabidopsis Book* **2013**, *2013*, DOI: 10.1199/tab.0166.
- (27) Milborrow, B. V.; Carrington, N. J.; Vaughan, G. T. *Phytochemistry* **1988**, *27*, 757–759.
- (28) Roberts, D. L.; Heckman, R. A.; Hege, B. P.; Bellin, S. A. *J. Org. Chem.* **1968**, *33*, 3566–3569.
- (29) Constantino, M. G.; Losco, P.; Castellano, E. E. *J. Org. Chem.* **1989**, *54*, 681–683.
- (30) Kienzle, F.; Mayer, H.; Minder, R. E.; Thommen, H. *Helv. Chim. Acta* **1978**, *61*, 2616–2627.
- (31) Rose, P. A.; Abrams, S. R.; Shaw, A. C. *Tetrahedron: Asymmetry* **1992**, *3*, 443–450.
- (32) Smith, T. R.; Clark, A. J.; Clarkson, G. J.; Taylor, P. C.; Marsh, A. *Org. Biomol. Chem.* **2006**, *4*, 4186–4192.
- (33) Shi, T.-Q.; Peng, H.; Zeng, S.-Y.; Ji, R.-Y.; Shi, K.; Huang, H.; Ji, X.-J. *Bioengineered* **2016**, *8*, 124–128.
- (34) Todoroki, Y.; Hirai, N. In *Studies in Natural Products Chemistry*, Atta-ur-Rahman, Ed.; Bioactive Natural Products (Part H), Vol. 27; Elsevier: 2002, pp 321–360.
- (35) (a) Todoroki, Y.; Hirai, N.; Koshimizu, K. *Biosci. Biotech. Biochem.* **1994**, *58*, 707–715; (b) Todoroki, Y.; Hirai, N.; Koshimizu, K. *Phytochemistry* **1995**, *38*, 561–568; (c) Todoroki, Y.; Hirai, N.; Koshimizu, K. *Phytochemistry* **1995**, *40*, 633–641; (d) Todoroki, Y.; Nakano, S.-i.; Hirai, N.; Ohigashi, H. *Tetrahedron* **1996**, *52*, 8081–8098; (e) Todoroki, Y.; Nakano, S.-i.; Hirai, N.; Mitsui, T.; Ohigashi, H. *Biosci. Biotech. Biochem.* **1997**, *61*, 1872–1876; (f) Todoroki, Y.; Nakano, S.-i.; Arai, S.; Hirai, N.; Ohigashi, H. *Biosci. Biotech. Biochem.* **1997**, *61*, 2043–2045.
- (36) Ueno, K.; Araki, Y.; Hirai, N.; Saito, S.; Mizutani, M.; Sakata, K.; Todoroki, Y. *Bioorg. Med. Chem.* **2005**, *13*, 3359–3370.
- (37) Cutler, A. J.; Rose, P. A.; Squires, T. M.; Loewen, M. K.; Shaw, A. C.; Quail, J. W.; Krochko, J. E.; Abrams, S. R. *Biochemistry* **2000**, *39*, 13614–13624.
- (38) Lei, B.; Abrams, S. R.; Ewan, B.; Gusta, L. V. *Phytochemistry* **1994**, *37*, 289–296.

- (39) Takeuchi, J.; Okamoto, M.; Akiyama, T.; Muto, T.; Yajima, S.; Sue, M.; Seo, M.; Kanno, Y.; Kamo, T.; Endo, A.; Nambara, E.; Hirai, N.; Ohnishi, T.; Cutler, S. R.; Todoroki, Y. *Nature Chem. Biol.* **2014**, *10*, 477–482.
- (40) Prime, version 4.0, Schrödinger, LLC, New York, NY, 2015.
- (41) Brabham, D. E.; Biggs, R. H. *Photochem. Photobiol.* **1981**, *34*, 33–37.
- (42) Yamashita, K.; Watanabe, T.; Watanabe, M.; Oritani, T. *Agric. Biol. Chem.* **1982**, *46*, 3069–3073.
- (43) (a) Bermejo, F. A.; Fernández Mateos, A.; Marcos Escribano, A.; Martín Lago, R.; Mateos Burón, L.; Rodríguez López, M.; Rubio González, R. *Tetrahedron* **2006**, *62*, 8933–8942; (b) Martín-Rodríguez, M.; Galán-Fernández, R.; Marcos-Escribano, A.; Bermejo, F. A. *J. Org. Chem.* **2009**, *74*, 1798–1801.
- (44) Nishimura, T.; Ohe, K.; Uemura, S. *J. Am. Chem. Soc.* **1999**, *121*, 2645–2646.
- (45) Shanan-Atidi, H.; Bar-Eli, K. H. *J. Phys. Chem.* **1970**, *74*, 961–963.
- (46) Mislow, K. *Acc. Chem. Res.* **1976**, *9*, 26–33.
- (47) Gloaguen, B.; Astruc, D. *J. Am. Chem. Soc.* **1990**, *112*, 4607–4609.
- (48) Anderson, J. E.; Casarini, D.; Lunazzi, L.; Mazzanti, A. *J. Org. Chem.* **2000**, *65*, 1729–1737.
- (49) Dehmlow, E. V.; Prashad, M. *J. Chem. Res., Synop.* **1982**, 354.
- (50) Hiyama, T.; Sawada, H.; Tsukanaka, M.; Nozaki, H. *Tetrahedron Lett.* **1975**, *16*, 3013–3016.
- (51) Nicolaou, K. C.; Zhong, Y.-L.; Baran, P. S. *J. Am. Chem. Soc.* **2000**, *122*, 7596–7597.
- (52) Diao, T.; Stahl, S. S. *J. Am. Chem. Soc.* **2011**, *133*, 14566–14569.
- (53) Bloch, R. *Synthesis* **1978**, *1978*, 140–142.
- (54) Jacques, J.; Marquet, A. *Org. Synth.* **1973**, *53*, 111.
- (55) Abrams, G. D.; Abrams, S. R.; Nelson, L. A. K.; Gusta, L. V. *Tetrahedron* **1990**, *46*, 5543–5554.
- (56) Hayashi, Y.; Shoji, M.; Ishikawa, H.; Yamaguchi, J.; Tamura, T.; Imai, H.; Nishigaya, Y.; Takabe, K.; Kakeya, H.; Osada, H. *Angew. Chem. Int. Ed.* **2008**, *47*, 6657–6660.
- (57) Odedra, A.; Wu, C.-J.; Madhushaw, R. J.; Wang, S.-L.; Liu, R.-S. *J. Am. Chem. Soc.* **2003**, *125*, 9610–9611.
- (58) Kulyk, S.; Dougherty, W. G.; Kassel, W. S.; Zdilla, M. J.; Sieburth, S. M. *Org. Lett.* **2011**, *13*, 2180–2183.
- (59) Seiller, B.; Bruneau, C.; Dixneuf, P. H. *Tetrahedron* **1995**, *51*, 13089–13102.
- (60) Li, H.; Walsh, P. J. *J. Am. Chem. Soc.* **2005**, *127*, 8355–8361.
- (61) Krasovskiy, A.; Kopp, F.; Knochel, P. *Angew. Chem. Int. Ed.* **2006**, *45*, 497–500.
- (62) Imamoto, T.; Takiyama, N.; Nakamura, K.; Hatajima, T.; Kamiya, Y. *J. Am. Chem. Soc.* **1989**, *111*, 4392–4398.

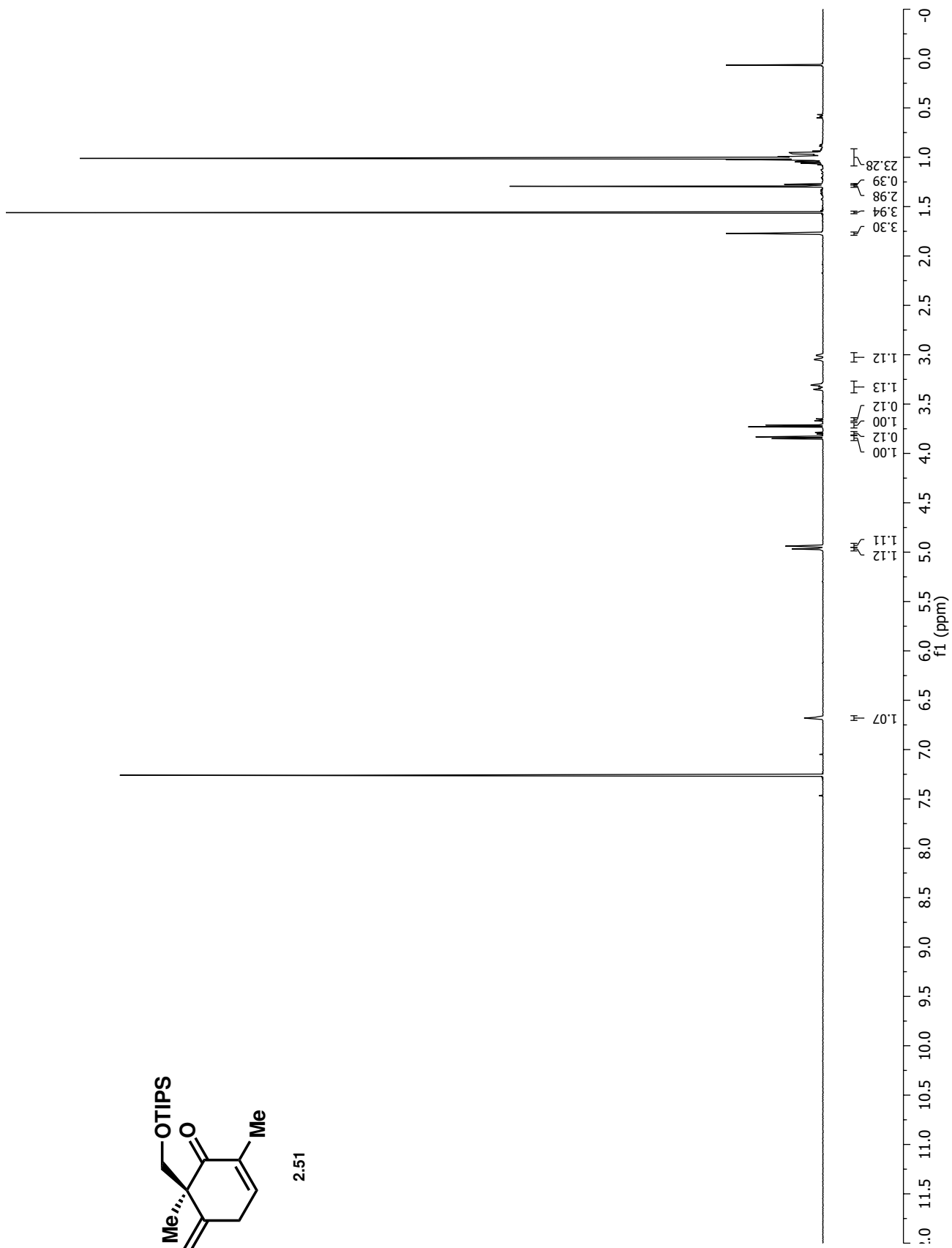
- (63) Rummelt, S. M.; Radkowski, K.; Roşca, D.-A.; Fürstner, A. *J. Am. Chem. Soc.* **2015**, *137*, 5506–5519.
- (64) Salmond, W. G.; Barta, M. A.; Havens, J. L. *J. Org. Chem.* **1978**, *43*, 2057–2059.
- (65) Chidambaram, N.; Chandrasekaran, S. *J. Org. Chem.* **1987**, *52*, 5048–5051.
- (66) Ishii, Y.; Iwahama, T.; Sakaguchi, S.; Nakayama, K.; Nishiyama, Y. *J. Org. Chem.* **1996**, *61*, 4520–4526.
- (67) Zhao, Q.; Qian, C.; Chen, X.-Z. *Steroids* **2015**, *94*, 1–6.
- (68) Shing, T. K. M.; Yeung, Su, P. L. *Org. Lett.* **2006**, *8*, 3149–3151.
- (69) Wilde, N. C.; Isomura, M.; Mendoza, A.; Baran, P. S. *J. Am. Chem. Soc.* **2014**, *136*, 4909–4912.
- (70) Mori, K.; Igarashi, Y. *Liebigs Ann.* **1988**, *1988*, 93–95.
- (71) Li, H.-H.; Hao, R.-L.; Wu, S.-S.; Guo, P.-C.; Chen, C.-J.; Pan, L.-P.; Ni, H. *Biochem. Pharmacol.* **2011**, *82*, 701–712.

# Appendix 2a: NMR Spectra Relevant to Chapter 2

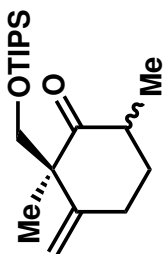




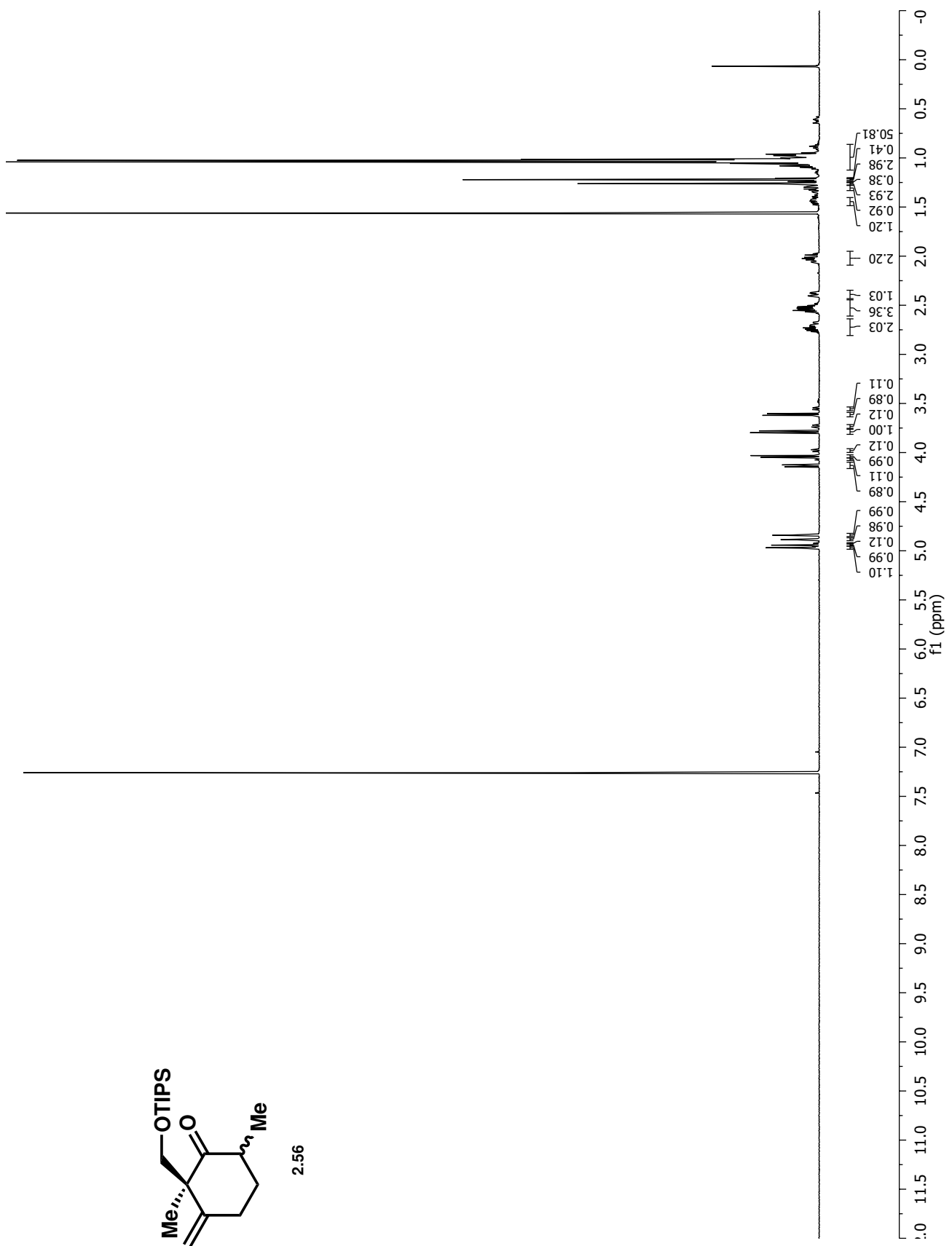
2.51

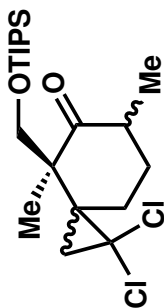




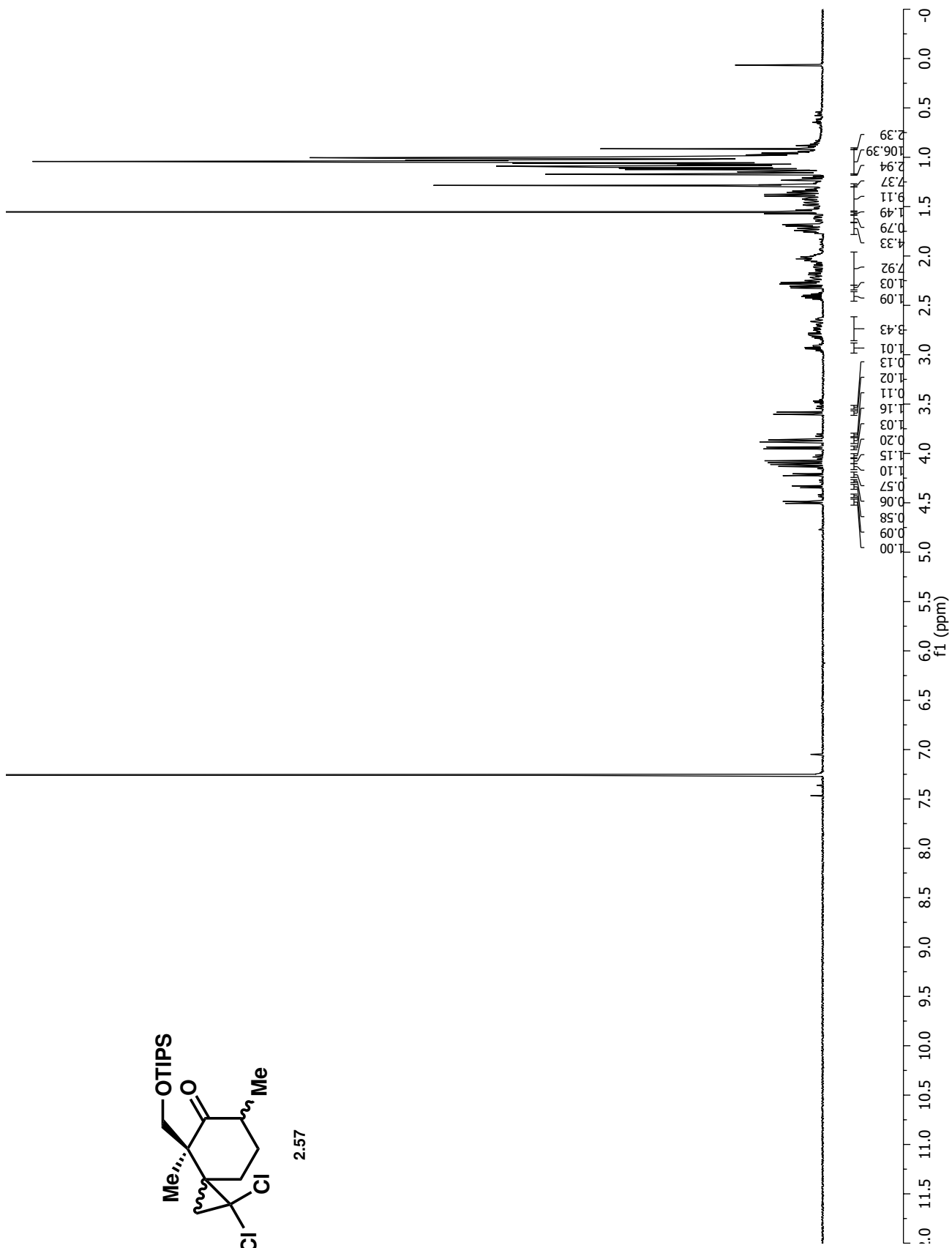


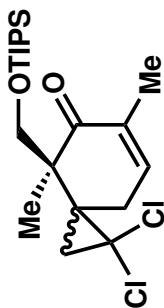
2.56



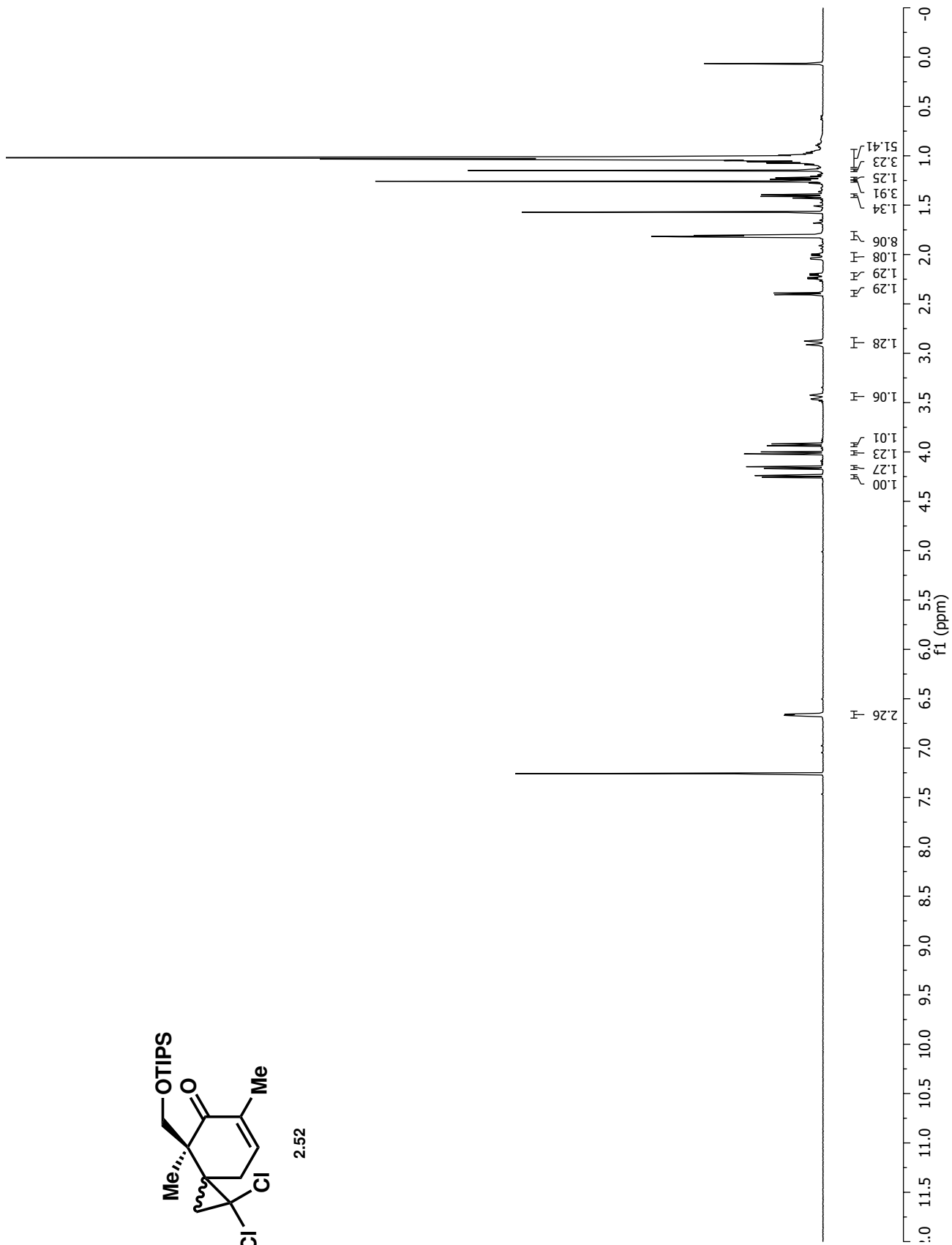


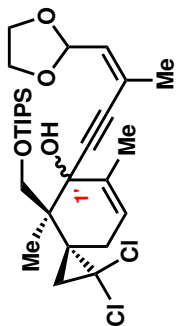
2.57



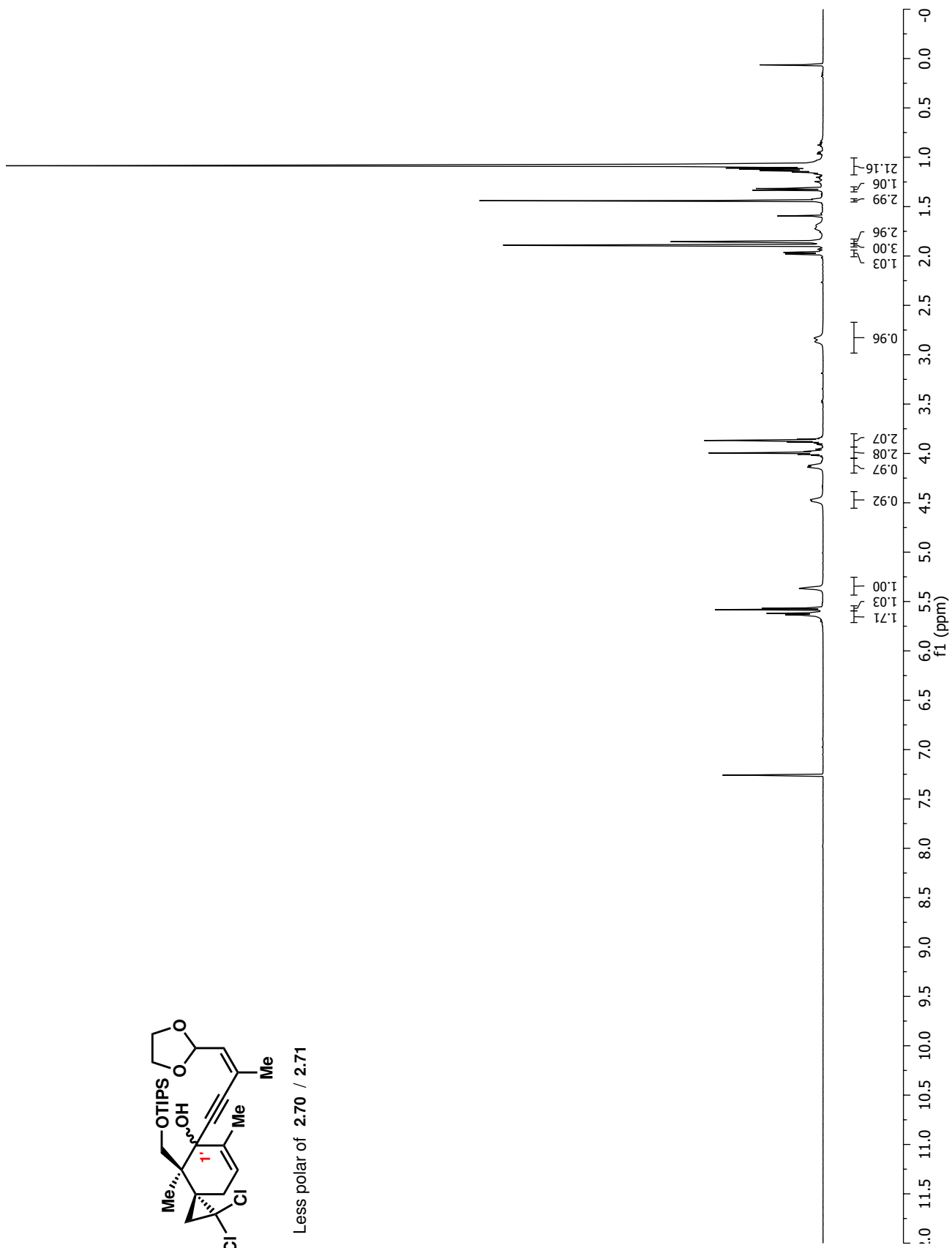


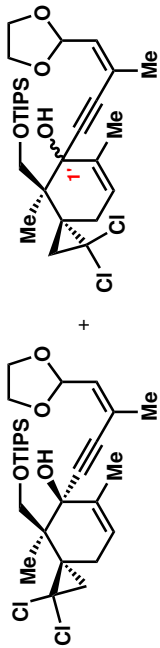
2.52





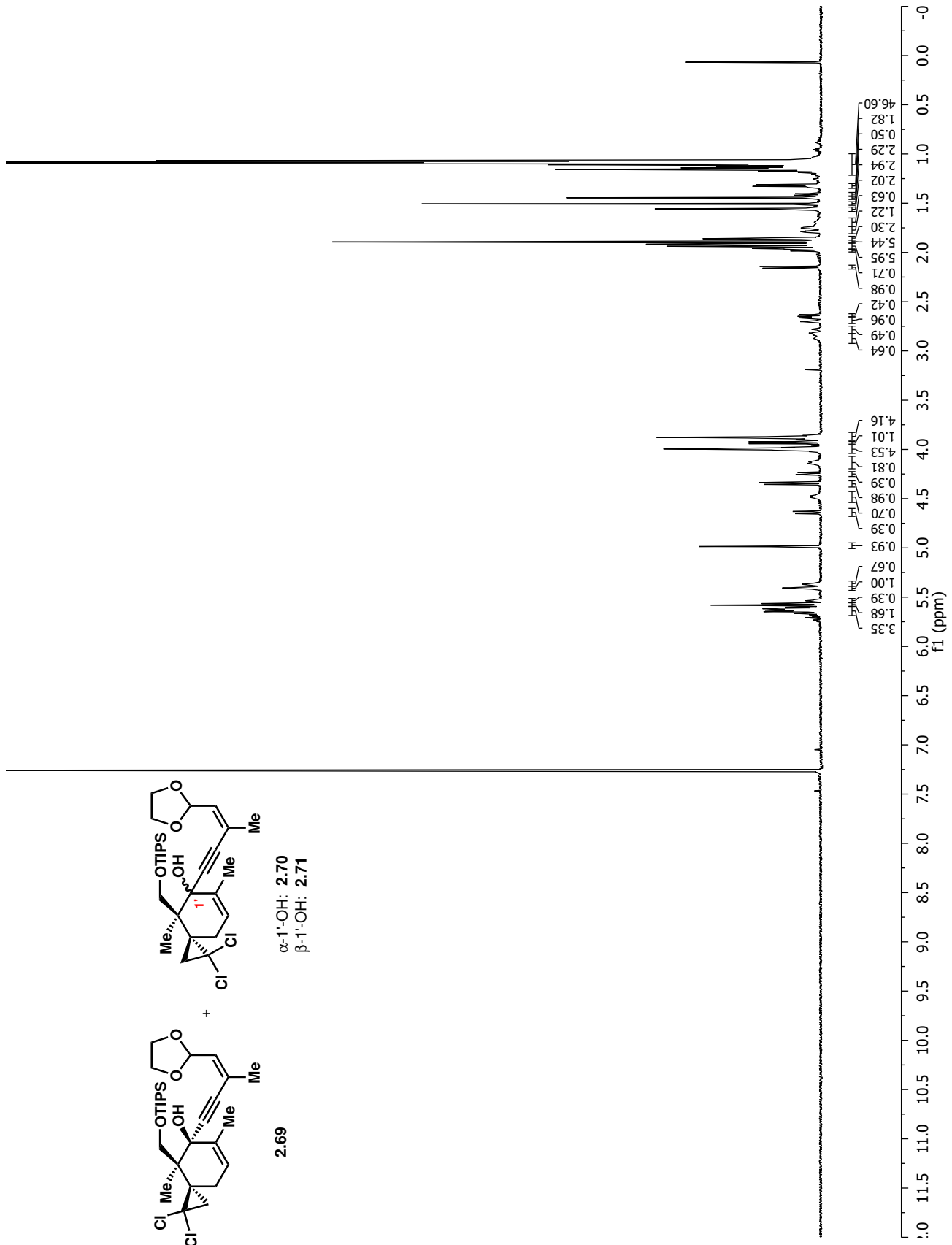
Less polar of 2.70 / 2.71

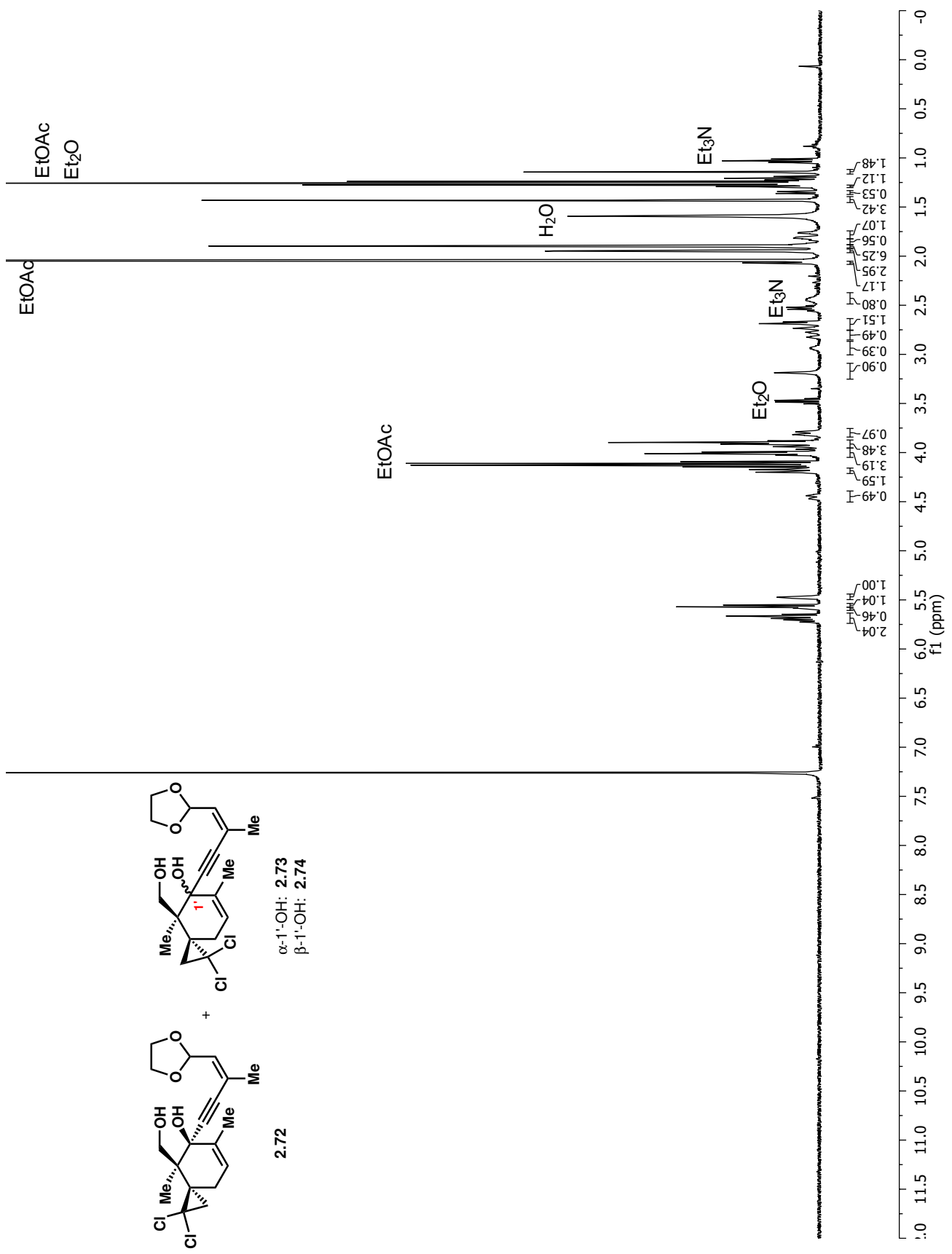
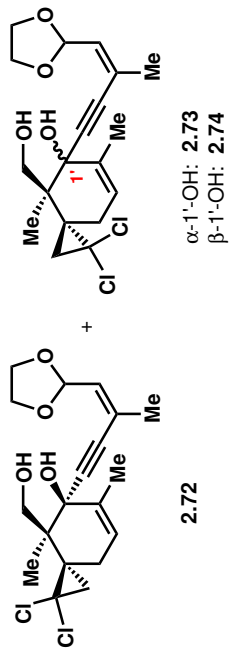


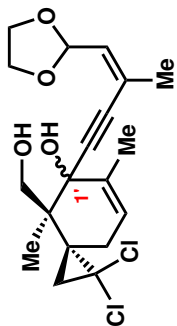


2.69

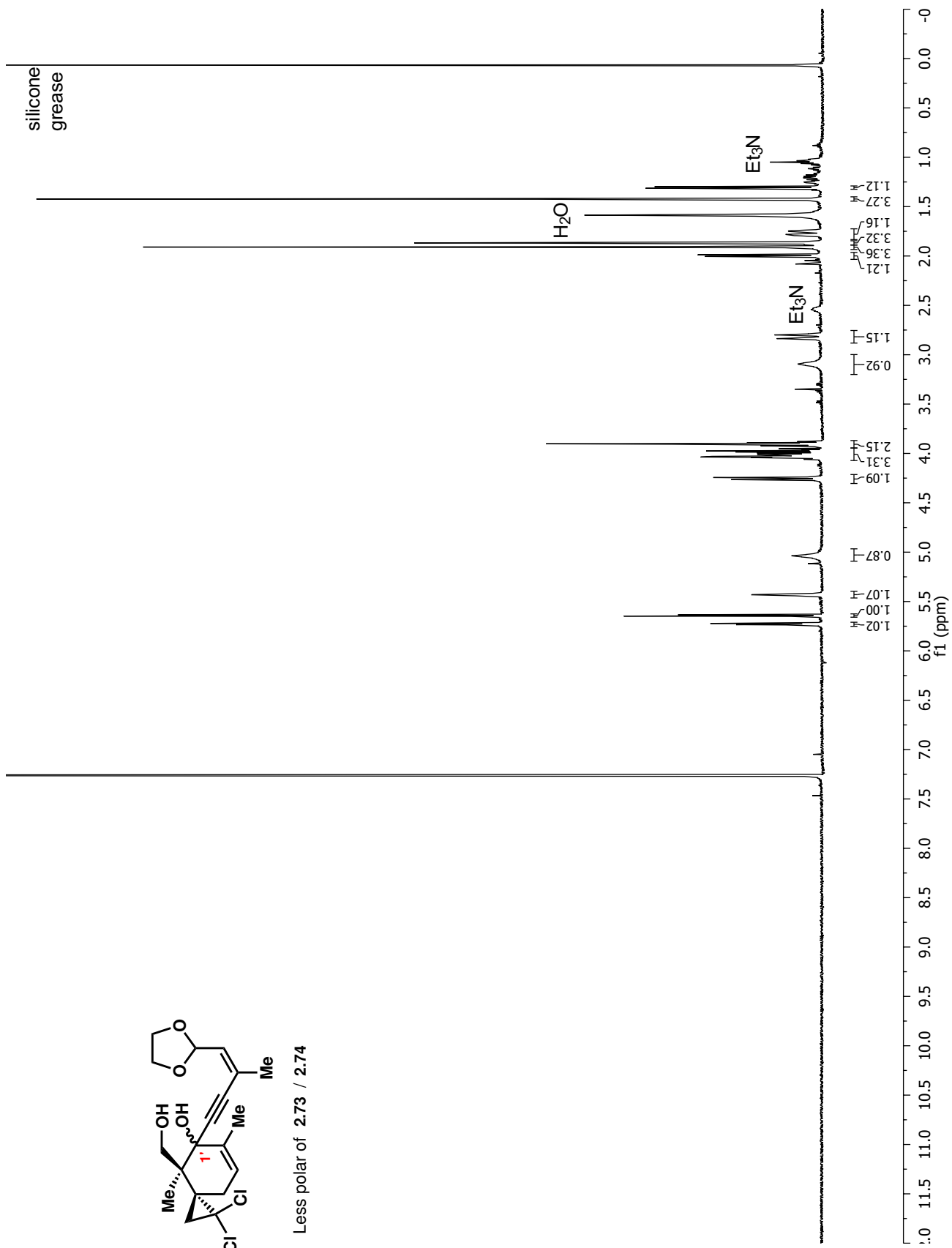
$\alpha$ -1'-OH: 2.70  
 $\beta$ -1'-OH: 2.71

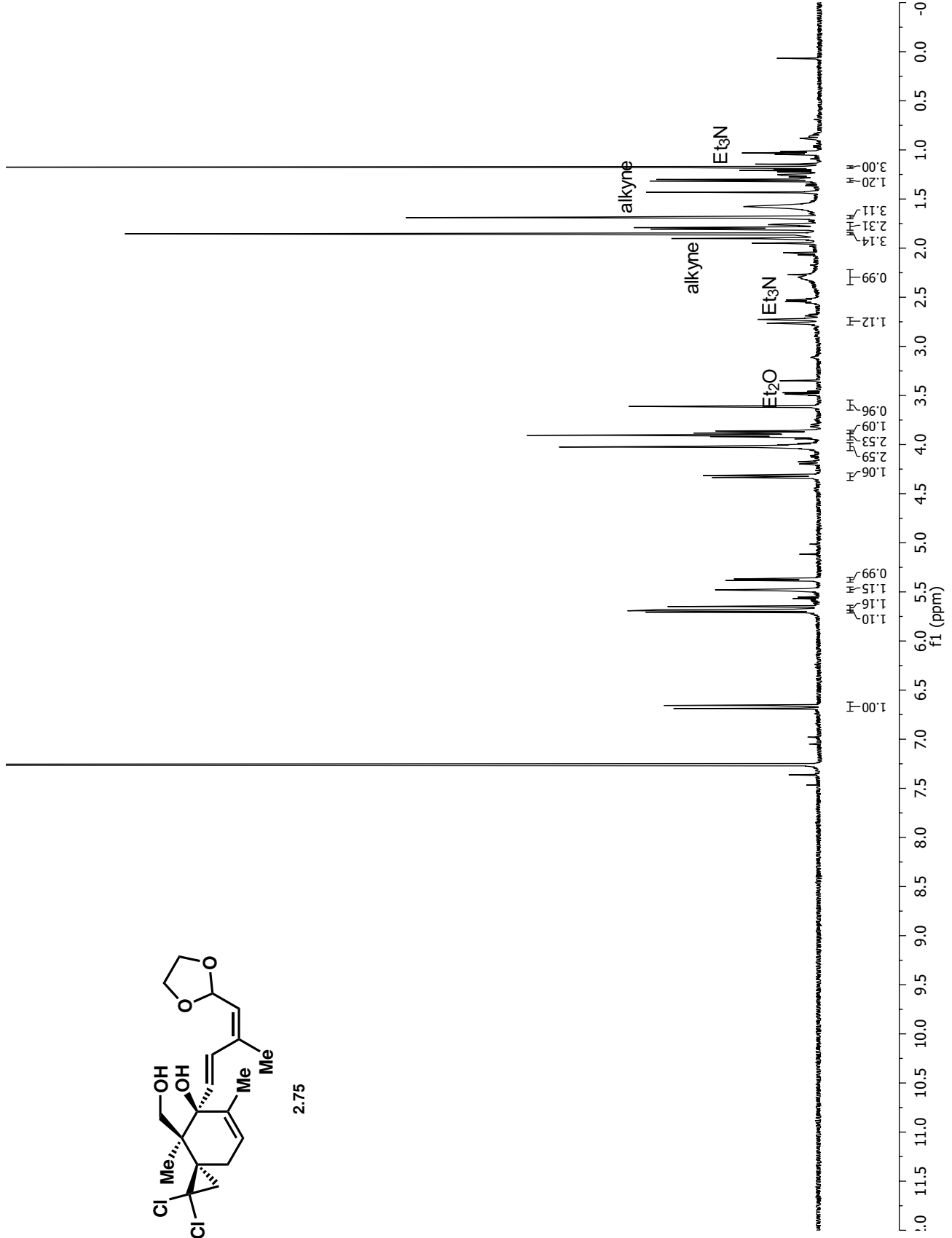
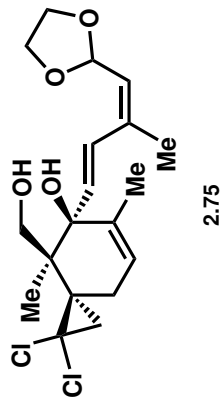




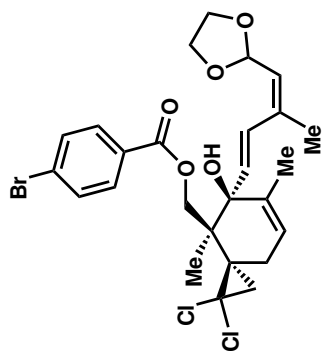


Less polar of 2.73 / 2.74

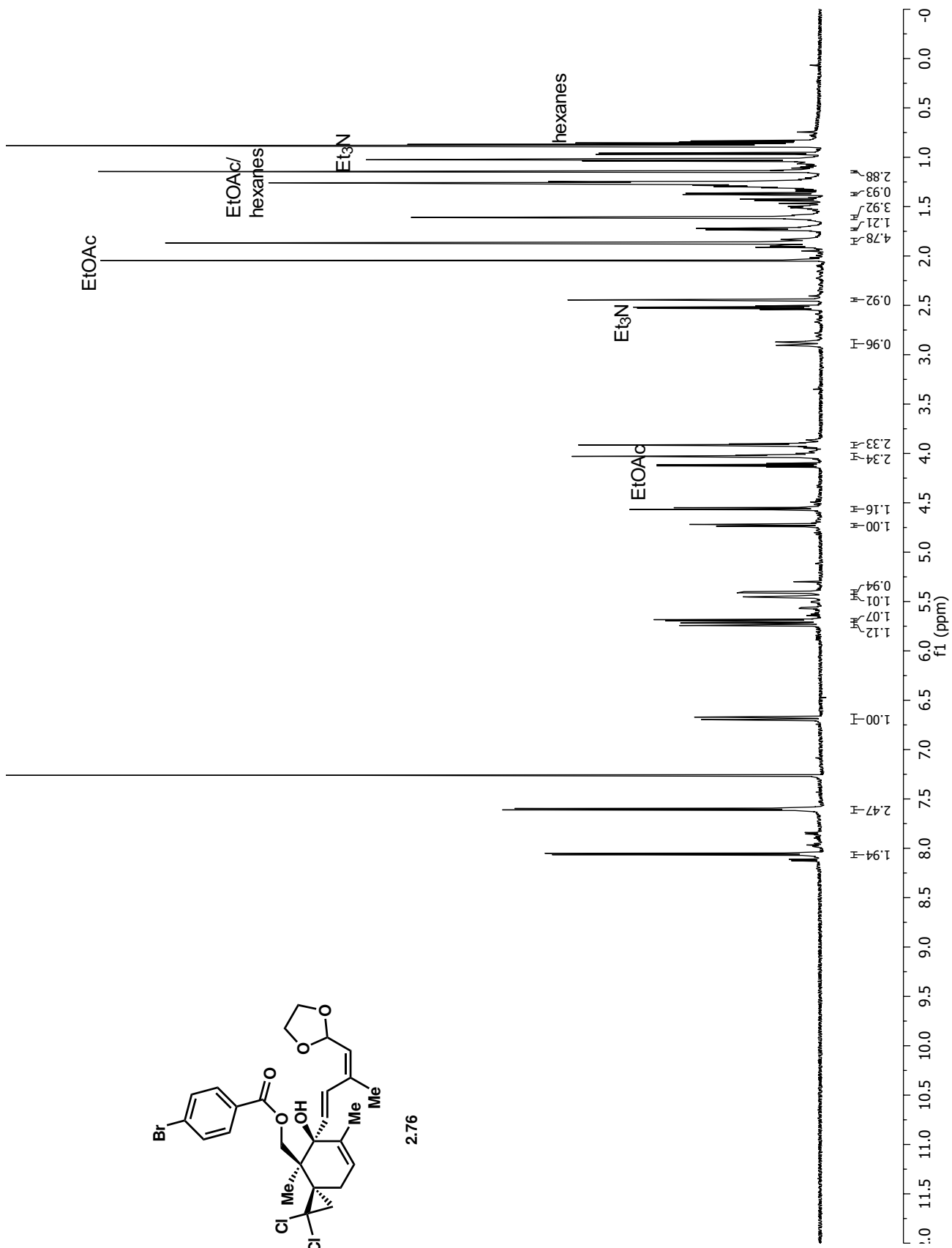


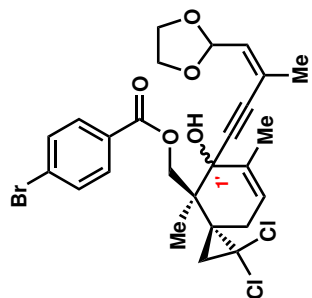




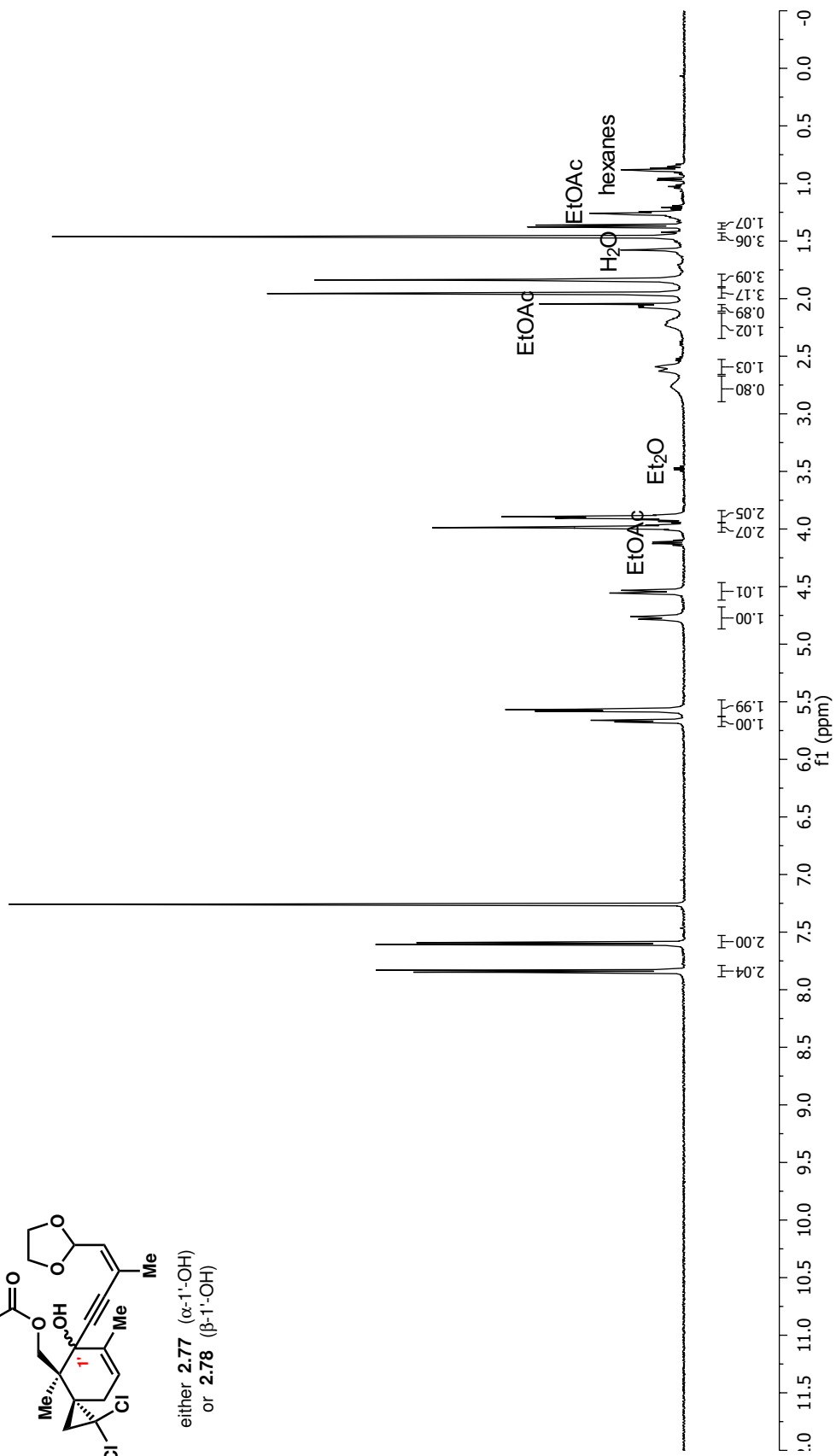


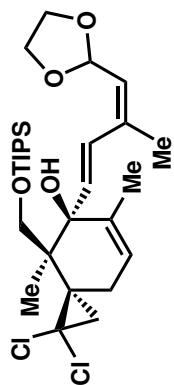
2.76



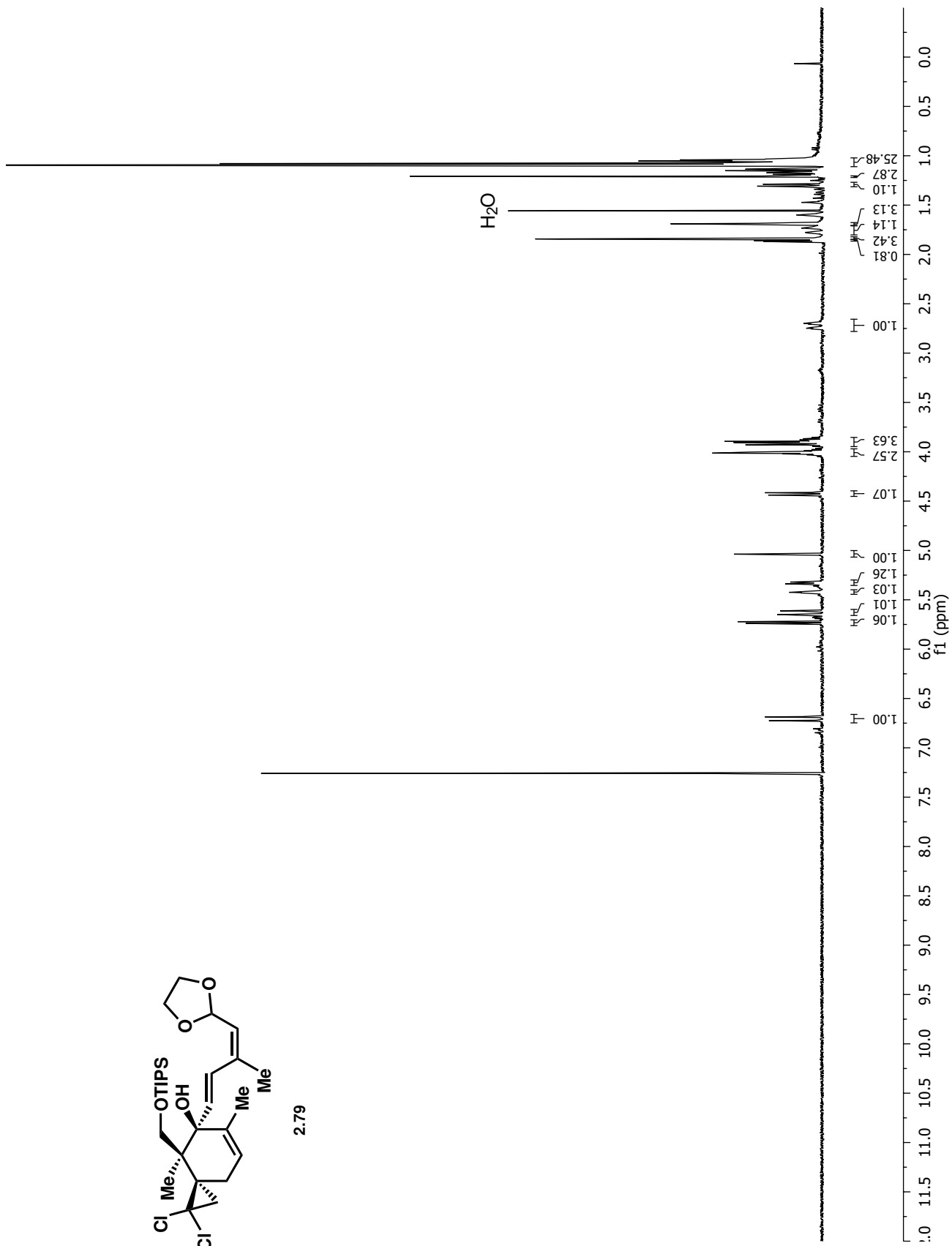


either 2.77 ( $\alpha$ -1'-OH)  
or 2.78 ( $\beta$ -1'-OH)



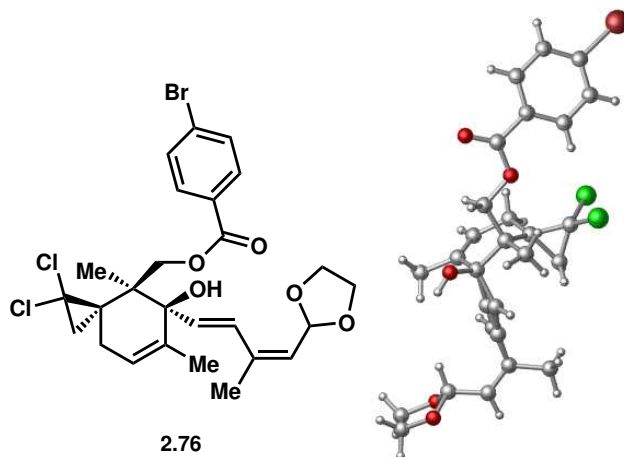


2.79



## Appendix 2b: X-Ray Crystallographic Data Relevant to Chapter 2

### X-ray crystallographic analysis of 2.76



A colorless plate 0.060 x 0.040 x 0.020 mm in size was mounted on a Cryoloop with Paratone oil. Data were collected in a nitrogen gas stream at 100(2) K using and scans. Crystal-to-detector distance was 60 mm and exposure time was 10 seconds per frame using a scan width of 2.0°. Data collection was 99.9% complete to 67.000° in  $\theta$ . A total of 35056 reflections were collected covering the indices,  $-13 \leq h \leq 13$ ,  $-11 \leq k \leq 11$ ,  $-14 \leq l \leq 14$ . 4491 reflections were found to be symmetry independent, with an  $R_{\text{int}}$  of 0.0732. Indexing and unit cell refinement indicated a primitive, monoclinic lattice. The space group was found to be P 21 (No. 4). The data were integrated using the Bruker SAINT software program and scaled using the SADABS software program. Solution by iterative methods (SHELXT-2014) produced a complete heavy-atom phasing model consistent with the proposed structure. All non-hydrogen atoms were refined anisotropically by full-matrix least-squares (SHELXL-2014). All hydrogen atoms were placed using a riding model. Their positions were constrained relative to their parent atom using the appropriate HFIX command in SHELXL-2014. Absolute stereochemistry was unambiguously determined to be *S* at C9 and C10, respectively.

Table 1. Crystal data and structure refinement for sarpong129.

X-ray ID	sarpong129	
Sample/notebook ID	BW3-3	
Empirical formula	C <sub>26</sub> H <sub>28.42</sub> Br Cl <sub>2</sub> O <sub>5</sub>	
Formula weight	571.72	
Temperature	100(2) K	
Wavelength	1.54178 Å	
Crystal system	Monoclinic	
Space group	P 21	
Unit cell dimensions	a = 11.1738(5) Å	a = 90°.
	b = 9.4462(4) Å	b = 107.965(3)°.
	c = 12.3863(6) Å	g = 90°.
Volume	1243.63(10) Å <sup>3</sup>	
Z	2	
Density (calculated)	1.527 Mg/m <sup>3</sup>	
Absorption coefficient	4.528 mm <sup>-1</sup>	
F(000)	587	
Crystal size	0.060 x 0.040 x 0.020 mm <sup>3</sup>	
Theta range for data collection	3.751 to 68.609°.	
Index ranges	-13 ≤ h ≤ 13, -11 ≤ k ≤ 11, -14 ≤ l ≤ 14	
Reflections collected	35056	
Independent reflections	4491 [R(int) = 0.0732]	
Completeness to theta = 67.000°	99.9 %	
Absorption correction	Semi-empirical from equivalents	
Max. and min. transmission	0.929 and 0.732	
Refinement method	Full-matrix least-squares on F <sup>2</sup>	
Data / restraints / parameters	4491 / 1 / 308	
Goodness-of-fit on F <sup>2</sup>	1.113	
Final R indices [I > 2σ(I)]	R1 = 0.0509, wR2 = 0.1228	
R indices (all data)	R1 = 0.0550, wR2 = 0.1257	
Absolute structure parameter	0.046(11)	
Extinction coefficient	n/a	
Largest diff. peak and hole	1.085 and -0.333 e.Å <sup>-3</sup>	

Table 2. Atomic coordinates ( $\times 10^4$ ) and equivalent isotropic displacement parameters ( $\text{\AA}^2 \times 10^3$ ) for sarpong129.  $U(\text{eq})$  is defined as one third of the trace of the orthogonalized  $U^{ij}$  tensor.

	x	y	z	$U(\text{eq})$
C(1)	12068(5)	8276(7)	-2309(5)	27(1)
C(2)	11399(6)	9436(7)	-2079(5)	31(1)
C(3)	10673(6)	9248(8)	-1379(6)	34(1)
C(4)	10609(5)	7951(8)	-914(4)	30(1)
C(5)	11265(6)	6801(7)	-1114(6)	32(1)
C(6)	12002(6)	6965(7)	-1826(6)	31(1)
C(7)	12873(5)	8432(7)	-3074(5)	27(1)
C(8)	13406(5)	9929(7)	-4379(5)	28(1)
C(9)	13155(5)	11464(6)	-4809(5)	26(1)
C(10)	11729(5)	11773(7)	-5198(5)	25(1)
C(11)	10987(5)	10677(7)	-6037(5)	30(1)
C(12)	11602(7)	10282(8)	-6902(5)	35(2)
C(13)	12752(7)	10634(8)	-6867(6)	38(2)
C(14)	13567(6)	11584(8)	-5910(6)	35(2)
C(15)	13981(5)	12450(7)	-3874(6)	38(2)
C(16)	11255(6)	13293(7)	-5419(6)	31(1)
C(17)	11016(5)	12466(6)	-4481(5)	29(1)
C(18)	13343(9)	10154(10)	-7737(8)	52(2)
C(19)	13350(20)	12860(30)	-6620(30)	27(2)
C(20)	13250(30)	13980(30)	-7070(20)	28(2)
C(19A)	13551(9)	13142(12)	-6244(12)	27(2)
C(20A)	13012(10)	13624(14)	-7263(9)	28(2)
C(21)	13046(6)	15166(7)	-7654(6)	30(1)
C(22)	12497(6)	16285(9)	-7064(6)	40(2)
C(23)	13470(6)	15474(8)	-8518(6)	33(1)
C(24)	14068(7)	14436(9)	-9087(6)	39(2)
C(25)	14364(9)	13930(13)	-10761(8)	61(3)
C(26)	15543(10)	14440(30)	-9971(9)	127(8)
O(1)	13542(4)	7501(5)	-3235(4)	31(1)
O(2)	12726(4)	9697(5)	-3576(3)	27(1)
O(3)	14867(4)	11115(6)	-5572(5)	44(1)

O(4)	13438(5)	14360(7)	-10265(4)	48(1)
O(5)	15317(5)	14914(8)	-8992(4)	53(2)
Cl(1)	11656(2)	13066(2)	-3066(1)	38(1)
Cl(2)	9456(1)	11890(2)	-4666(2)	36(1)
Br(1)	9587(1)	7767(1)	65(1)	44(1)

---

Table 3. Bond lengths [Å] and angles [°] for sarpong129.

C(1)-C(6)	1.387(9)	C(15)-H(15A)	0.9800
C(1)-C(2)	1.404(9)	C(15)-H(15B)	0.9800
C(1)-C(7)	1.501(8)	C(15)-H(15C)	0.9800
C(2)-C(3)	1.370(9)	C(16)-C(17)	1.491(8)
C(2)-H(2)	0.9500	C(16)-H(16A)	0.9900
C(3)-C(4)	1.365(10)	C(16)-H(16B)	0.9900
C(3)-H(3)	0.9500	C(17)-Cl(1)	1.769(7)
C(4)-C(5)	1.375(10)	C(17)-Cl(2)	1.772(6)
C(4)-Br(1)	1.912(5)	C(18)-H(18A)	0.9800
C(5)-C(6)	1.390(9)	C(18)-H(18B)	0.9800
C(5)-H(5)	0.9500	C(18)-H(18C)	0.9800
C(6)-H(6)	0.9500	C(19)-C(20)	1.18(4)
C(7)-O(1)	1.210(8)	C(20)-C(21)	1.31(3)
C(7)-O(2)	1.333(8)	C(19A)-C(20A)	1.302(17)
C(8)-O(2)	1.443(7)	C(19A)-H(19A)	0.9500
C(8)-C(9)	1.540(9)	C(20A)-C(21)	1.539(14)
C(8)-H(8A)	0.9900	C(20A)-H(20A)	0.9500
C(8)-H(8B)	0.9900	C(21)-C(23)	1.330(9)
C(9)-C(10)	1.544(7)	C(21)-C(22)	1.518(10)
C(9)-C(15)	1.549(9)	C(22)-H(22A)	0.9800
C(9)-C(14)	1.573(8)	C(22)-H(22B)	0.9800
C(10)-C(17)	1.513(8)	C(22)-H(22C)	0.9800
C(10)-C(11)	1.519(9)	C(23)-C(24)	1.482(10)
C(10)-C(16)	1.526(9)	C(23)-H(23)	0.9500
C(11)-C(12)	1.488(9)	C(24)-O(4)	1.413(9)
C(11)-H(11A)	0.9900	C(24)-O(5)	1.437(9)
C(11)-H(11B)	0.9900	C(24)-H(24)	1.0000
C(12)-C(13)	1.314(10)	C(25)-O(4)	1.416(9)
C(12)-H(12)	0.9500	C(25)-C(26)	1.461(17)
C(13)-C(18)	1.497(10)	C(25)-H(25A)	0.9900
C(13)-C(14)	1.541(11)	C(25)-H(25B)	0.9900
C(14)-O(3)	1.451(7)	C(26)-O(5)	1.386(12)
C(14)-C(19)	1.47(3)	C(26)-H(26A)	0.9900
C(14)-C(19A)	1.528(12)	C(26)-H(26B)	0.9900



O(3)-H(3A)	0.8400		
C(6)-C(1)-C(2)	120.4(6)	C(17)-C(10)-C(16)	58.8(4)
C(6)-C(1)-C(7)	118.8(5)	C(11)-C(10)-C(16)	115.6(5)
C(2)-C(1)-C(7)	120.8(5)	C(17)-C(10)-C(9)	125.3(5)
C(3)-C(2)-C(1)	119.0(6)	C(11)-C(10)-C(9)	112.2(5)
C(3)-C(2)-H(2)	120.5	C(16)-C(10)-C(9)	120.1(5)
C(1)-C(2)-H(2)	120.5	C(12)-C(11)-C(10)	112.8(5)
C(4)-C(3)-C(2)	120.1(6)	C(12)-C(11)-H(11A)	109.0
C(4)-C(3)-H(3)	119.9	C(10)-C(11)-H(11A)	109.0
C(2)-C(3)-H(3)	119.9	C(12)-C(11)-H(11B)	109.0
C(3)-C(4)-C(5)	122.2(5)	C(10)-C(11)-H(11B)	109.0
C(3)-C(4)-Br(1)	117.9(5)	H(11A)-C(11)-H(11B)	107.8
C(5)-C(4)-Br(1)	119.9(5)	C(13)-C(12)-C(11)	125.2(7)
C(4)-C(5)-C(6)	118.7(6)	C(13)-C(12)-H(12)	117.4
C(4)-C(5)-H(5)	120.7	C(11)-C(12)-H(12)	117.4
C(6)-C(5)-H(5)	120.7	C(12)-C(13)-C(18)	122.9(8)
C(1)-C(6)-C(5)	119.6(6)	C(12)-C(13)-C(14)	120.8(6)
C(1)-C(6)-H(6)	120.2	C(18)-C(13)-C(14)	116.3(7)
C(5)-C(6)-H(6)	120.2	O(3)-C(14)-C(19)	112.8(9)
O(1)-C(7)-O(2)	124.6(5)	O(3)-C(14)-C(19A)	107.4(6)
O(1)-C(7)-C(1)	123.6(5)	O(3)-C(14)-C(13)	110.2(6)
O(2)-C(7)-C(1)	111.7(5)	C(19)-C(14)-C(13)	94.2(15)
O(2)-C(8)-C(9)	107.6(5)	C(19A)-C(14)-C(13)	113.5(7)
O(2)-C(8)-H(8A)	110.2	O(3)-C(14)-C(9)	105.2(5)
C(9)-C(8)-H(8A)	110.2	C(19)-C(14)-C(9)	122.7(12)
O(2)-C(8)-H(8B)	110.2	C(19A)-C(14)-C(9)	108.8(7)
C(9)-C(8)-H(8B)	110.2	C(13)-C(14)-C(9)	111.3(5)
H(8A)-C(8)-H(8B)	108.5	C(9)-C(15)-H(15A)	109.5
C(8)-C(9)-C(10)	110.3(5)	C(9)-C(15)-H(15B)	109.5
C(8)-C(9)-C(15)	107.7(5)	H(15A)-C(15)-H(15B)	109.5
C(10)-C(9)-C(15)	116.1(5)	C(9)-C(15)-H(15C)	109.5
C(8)-C(9)-C(14)	107.3(5)	H(15A)-C(15)-H(15C)	109.5
C(10)-C(9)-C(14)	105.4(5)	H(15B)-C(15)-H(15C)	109.5
C(15)-C(9)-C(14)	109.8(5)	C(17)-C(16)-C(10)	60.2(4)
C(17)-C(10)-C(11)	114.9(5)	C(17)-C(16)-H(16A)	117.8

C(10)-C(16)-H(16A)	117.8	C(21)-C(22)-H(22B)	109.5
C(17)-C(16)-H(16B)	117.8	H(22A)-C(22)-H(22B)	109.5
C(10)-C(16)-H(16B)	117.8	C(21)-C(22)-H(22C)	109.5
H(16A)-C(16)-H(16B)	114.9	H(22A)-C(22)-H(22C)	109.5
C(16)-C(17)-C(10)	61.0(4)	H(22B)-C(22)-H(22C)	109.5
C(16)-C(17)-Cl(1)	119.3(5)	C(21)-C(23)-C(24)	124.2(6)
C(10)-C(17)-Cl(1)	126.5(4)	C(21)-C(23)-H(23)	117.9
C(16)-C(17)-Cl(2)	117.7(4)	C(24)-C(23)-H(23)	117.9
C(10)-C(17)-Cl(2)	117.8(4)	O(4)-C(24)-O(5)	105.2(5)
Cl(1)-C(17)-Cl(2)	107.9(3)	O(4)-C(24)-C(23)	111.7(6)
C(13)-C(18)-H(18A)	109.5	O(5)-C(24)-C(23)	108.8(7)
C(13)-C(18)-H(18B)	109.5	O(4)-C(24)-H(24)	110.3
H(18A)-C(18)-H(18B)	109.5	O(5)-C(24)-H(24)	110.3
C(13)-C(18)-H(18C)	109.5	C(23)-C(24)-H(24)	110.3
H(18A)-C(18)-H(18C)	109.5	O(4)-C(25)-C(26)	104.1(8)
H(18B)-C(18)-H(18C)	109.5	O(4)-C(25)-H(25A)	110.9
C(20)-C(19)-C(14)	172(4)	C(26)-C(25)-H(25A)	110.9
C(19)-C(20)-C(21)	174(4)	O(4)-C(25)-H(25B)	110.9
C(20A)-C(19A)-C(14)	124.2(16)	C(26)-C(25)-H(25B)	110.9
C(20A)-C(19A)-H(19A)	117.9	H(25A)-C(25)-H(25B)	109.0
C(14)-C(19A)-H(19A)	117.9	O(5)-C(26)-C(25)	108.8(8)
C(19A)-C(20A)-C(21)	125.9(15)	O(5)-C(26)-H(26A)	109.9
C(19A)-C(20A)-H(20A)	117.1	C(25)-C(26)-H(26A)	109.9
C(21)-C(20A)-H(20A)	117.1	O(5)-C(26)-H(26B)	109.9
C(20)-C(21)-C(23)	125.7(12)	C(25)-C(26)-H(26B)	109.9
C(20)-C(21)-C(22)	111.0(13)	H(26A)-C(26)-H(26B)	108.3
C(23)-C(21)-C(22)	122.1(6)	C(7)-O(2)-C(8)	116.2(5)
C(23)-C(21)-C(20A)	120.7(7)	C(14)-O(3)-H(3A)	109.5
C(22)-C(21)-C(20A)	117.1(6)	C(24)-O(4)-C(25)	105.3(6)
C(21)-C(22)-H(22A)	109.5	C(26)-O(5)-C(24)	105.2(8)

---

Symmetry transformations used to generate equivalent atoms:

Table 4. Anisotropic displacement parameters ( $\text{\AA}^2 \times 10^3$ ) for sarpong129. The anisotropic displacement factor exponent takes the form:  $-2p^2 [ h^2 a^* U^{11} + \dots + 2 h k a^* b^* U^{12} ]$

	U <sup>11</sup>	U <sup>22</sup>	U <sup>33</sup>	U <sup>23</sup>	U <sup>13</sup>	U <sup>12</sup>
C(1)	24(2)	26(3)	28(3)	2(2)	6(2)	0(2)
C(2)	36(3)	22(3)	33(3)	5(2)	10(2)	0(2)
C(3)	40(3)	28(4)	37(3)	3(3)	18(3)	8(3)
C(4)	28(2)	36(4)	29(2)	-2(3)	13(2)	-5(3)
C(5)	34(3)	24(3)	41(3)	3(3)	13(2)	0(2)
C(6)	32(3)	24(3)	37(3)	2(3)	10(2)	5(2)
C(7)	27(3)	23(3)	28(3)	8(2)	6(2)	2(2)
C(8)	26(2)	26(3)	33(3)	4(2)	10(2)	2(2)
C(9)	24(3)	19(3)	35(3)	5(2)	8(2)	1(2)
C(10)	22(2)	19(3)	33(3)	3(2)	9(2)	0(2)
C(11)	25(3)	32(4)	33(3)	-2(3)	8(2)	-3(2)
C(12)	43(3)	29(4)	32(3)	-1(3)	8(3)	9(3)
C(13)	49(4)	28(4)	44(4)	16(3)	27(3)	13(3)
C(14)	25(3)	37(4)	46(3)	13(3)	17(2)	8(2)
C(15)	24(3)	27(4)	60(4)	-1(3)	6(3)	-1(2)
C(16)	28(3)	20(3)	47(3)	10(3)	17(3)	1(2)
C(17)	27(3)	20(3)	41(3)	3(2)	13(2)	-3(2)
C(18)	74(6)	37(4)	64(5)	10(4)	46(5)	14(4)
C(21)	25(3)	28(3)	32(3)	5(3)	4(2)	-2(2)
C(22)	36(3)	42(4)	45(4)	-1(3)	20(3)	-2(3)
C(23)	31(3)	29(4)	36(3)	7(3)	7(2)	3(2)
C(24)	42(3)	39(4)	41(4)	12(3)	18(3)	6(3)
C(25)	62(5)	81(7)	46(4)	-7(4)	26(4)	25(5)
C(26)	50(5)	290(30)	42(5)	-19(8)	20(4)	32(9)
O(1)	34(2)	19(2)	46(2)	7(2)	18(2)	6(2)
O(2)	31(2)	20(2)	30(2)	5(2)	9(2)	4(2)
O(3)	29(2)	46(3)	64(3)	26(3)	25(2)	12(2)
O(4)	39(3)	65(4)	40(3)	-5(3)	13(2)	12(2)
O(5)	37(3)	87(5)	36(3)	8(3)	15(2)	13(3)
Cl(1)	44(1)	27(1)	42(1)	-4(1)	11(1)	5(1)
Cl(2)	32(1)	30(1)	53(1)	2(1)	22(1)	0(1)

Br(1) 51(1) 42(1) 49(1) 8(1) 30(1) 5(1)

---

Table 5. Hydrogen coordinates ( $\times 10^4$ ) and isotropic displacement parameters ( $\text{\AA}^2 \times 10^3$ ) for sarpong129.

	x	y	z	U(eq)
H(2)	11448	10336	-2404	37
H(3)	10213	10021	-1216	40
H(5)	11215	5912	-772	39
H(6)	12459	6183	-1982	38
H(8A)	13116	9258	-5021	34
H(8B)	14318	9780	-4009	34
H(11A)	10886	9817	-5616	36
H(11B)	10137	11056	-6427	36
H(12)	11126	9733	-7530	42
H(15A)	13919	12159	-3134	58
H(15B)	13687	13428	-4031	58
H(15C)	14859	12386	-3867	58
H(16A)	11885	14064	-5210	37
H(16B)	10533	13478	-6104	37
H(18A)	13933	9381	-7424	79
H(18B)	13796	10946	-7942	79
H(18C)	12686	9820	-8413	79
H(19A)	13962	13803	-5671	33
H(20A)	12557	12963	-7816	34
H(22A)	12519	17207	-7420	59
H(22B)	12993	16330	-6260	59
H(22C)	11625	16039	-7132	59
H(23)	13384	16422	-8788	39
H(24)	14099	13480	-8732	47
H(25A)	14209	14361	-11520	73
H(25B)	14374	12887	-10835	73
H(26A)	16172	13669	-9784	152
H(26B)	15881	15225	-10322	152
H(3A)	15210	11397	-6049	66

## Chapter 3

# The History, Biology, and Previous Syntheses of the Taxoid Natural Products

*With Special Emphasis on the Taxagifine-Like Natural Products*

### 3.1 A Brief History of the Taxoid Natural Products: Isolation and Development as Pharmaceuticals

The taxoid natural products have long held the attention of both synthetic and medicinal chemists as a result of their structural complexity and biological activity.<sup>1</sup> Their history stretches back millennia; yew trees, the natural sources of the taxoid natural products, have been known to possess biological activity since at least the first century B.C.E. when Julius Caesar reported the poisoning of the king of Eburones with “juice of the yew.”<sup>2</sup> More recently, in 1856, in the first attempt to study the compounds responsible for this biological activity, a mixture of alkaloids was isolated for the first time from the English yew and given the name “taxine.”<sup>3</sup> However, only in the mid-20th century did the taxoid natural products begin to be thoroughly and systematically studied.

The initial discovery of taxol (**3.1**, Figure 3.1), the most well-studied taxoid natural product to-date, was prompted by the initiation of a National Cancer Institute program in 1960 to screen plant extracts for chemotherapeutic activity. In 1964, an extract from the bark of the Pacific yew was found to be cytotoxic toward KB cells; two years later, the first pure sample of taxol was isolated from Pacific yew bark. Despite the structural complexity of taxol as well as its low isolation yield from the Pacific yew bark, the structure of taxol was ultimately determined and published in 1971.<sup>4</sup> In 1979, taxol was established as an antimetabolic acting via the inhibition of microtubule depolymerization. The discovery of this unique mechanism of action heightened interest in taxol, given that many antimetabolic compounds at the time were known to act through the inhibition of tubulin polymerization rather than microtubule

depolymerization.<sup>5</sup> The 1980s saw the passage of taxol through Phase I and Phase II clinical trials, which revealed its remarkable efficacy against ovarian cancer<sup>6</sup> and spurred the development of semisynthetic approaches for accessing greater quantities of taxol.<sup>7</sup> Finally, in 1992, taxol received FDA approval for the treatment of refractory ovarian cancer; in the next six years, it received FDA approvals for the treatment of breast cancer, non-small cell lung cancer, and AIDS-related Kaposi's sarcoma. A synthetic analog of taxol, docetaxel (**3.2**), was also discovered in 1986 and has been used for the treatment of breast cancer, non-small cell lung cancer, prostate cancer, gastric cancer, head and neck cancer, and ovarian cancer.<sup>8</sup>

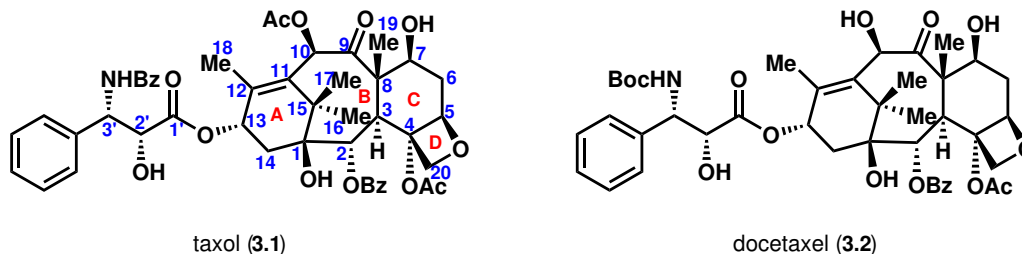


**Figure 3.1:** Structures of taxol (**3.1**) and docetaxel (**3.2**).

As a result of the success of taxol and docetaxel, scientific interest in the taxoid natural products increased dramatically in the 1990s. From 1992–1999, over 250 taxoid natural products had been isolated and characterized, more than tripling the total number of taxoid natural products that had been known before 1992<sup>1d</sup>; today, over 500 taxoid natural products

	<b>Name</b>	<b>R<sub>1</sub></b>	<b>R<sub>2</sub></b>	<b>R<sub>3</sub></b>	<b>R<sub>4</sub></b>	<b>R<sub>5</sub></b>	<b>R<sub>6</sub></b>
	taxagifine ( <b>3.3</b> )	Ac	H	H	Ac	H	Cinn
	taxumairol R ( <b>3.4</b> )	Ac	H	H	Ac	OBz	Ac
	5 $\alpha$ -[( <i>R</i> )-3'-dimethylamino-3'-phenylpropanoyloxy]taxinine M ( <b>3.5</b> )	Ac	H	H	Ac	OBz	Ra
	taxezopidine N ( <b>3.6</b> )	Ac	H	H	Ac	H	Ra
	2 $\alpha$ -deacetyl-5 $\alpha$ -decinnamoyltaxagifine ( <b>3.7</b> )	H	H	H	Ac	H	H
Cinn =	5 $\alpha$ -decinnamoyltaxagifine ( <b>3.8</b> )	Ac	H	H	Ac	H	H
Ra =	5 $\alpha$ -acetyl-5 $\alpha$ -decinnamoyltaxagifine ( <b>3.9</b> )	Ac	H	H	Ac	H	Ac
	5 $\alpha$ -decinnamoyl-11-acetyl-19-hydroxytaxagifine ( <b>3.10</b> )	Ac	H	Ac	Ac	OH	H
	19-debenzoyl-19-acetyltaxinine M ( <b>3.11</b> )	Ac	H	H	Ac	OAc	H
	taxinine M ( <b>3.12</b> )	Ac	H	H	Ac	OBz	H
	tasumatrol L ( <b>3.13</b> )	Ac	CH <sub>2</sub> OH	H	Ac	OBz	H
	taxuspine S ( <b>3.14</b> )	Ac	H	H	Ac	OH	Cinn
	taxuspine T ( <b>3.15</b> )	Ac	H	H	H	OAc	Cinn
	taxezopidine L ( <b>3.16</b> )	Ac	H	H	Ac	OAc	Cinn
	taxacin ( <b>3.17</b> )	Ac	H	H	Ac	OBz	Cinn

R = Ac: taxagifine III (**3.18**)  
R = H: 4-deacetyltaxagifine III (**3.19**)

**Figure 3.2:** Structures of the “taxagifine-like” natural products.

have been isolated.<sup>1e</sup> These include the “taxagifine-like” natural products—so-called herein paying homage to the originally isolated member taxagifine (**3.3**)—which contain a bridging ether ring between C12 and C17 and which receive special emphasis in this chapter (**3.3–3.19**; Figure 3.2). Despite the extensive efforts expended on the isolation of other taxoid natural products aside from taxol, there has been little in-depth investigation of their biological activities, presumably hindered by their typically low isolation yields. As a result, our knowledge of the biological activities of the taxoid natural products has been limited to that of taxol and its closely related analogs. Taxol remains the only taxoid natural product to have entered clinical trials.

## 3.2 The Biological Activities of Taxol and Taxagifine

### 3.2.1 Mechanism of Action of Taxol

In 1979, Horwitz and coworkers demonstrated that taxol promotes tubulin polymerization into microtubules, in contrast with a multitude of other anti-mitotic natural products (e.g., vincristine, vinblastine, colchicine, podophyllotoxin, etc.), which had been known at the time to inhibit microtubule assembly.<sup>5</sup> In addition, they discovered that taxol-treated microtubules were resistant to CaCl<sub>2</sub>-induced depolymerization *in vitro*, suggesting that a binding site existed for taxol on the intact microtubule rather than on the tubulin heterodimer. Given the importance of microtubule dynamics to the proper progression of mitosis, these initial studies suggested a mechanism of action to explain taxol’s antitumor properties.

Through photoaffinity labeling<sup>9</sup> and electron crystallography<sup>10</sup> studies, a hydrophobic pocket in  $\beta$ -tubulin has now been defined as the taxol-binding site. In addition, several models have been proposed for the bioactive conformation of taxol when bound to  $\beta$ -tubulin,<sup>10c,10d,11</sup>. One major proposal, in which taxol adopts a T-shaped conformation, is shown here for illustration (Figure 3.3). Three notable features of taxol-tubulin binding—pictured in Figure 3.3 but which also remain consistent across other major proposals for taxol-tubulin binding—include: a) the importance of the 2'-OH as either a hydrogen bond donor or acceptor, b) the prevalence of hydrophobic residues along the “southern” hemisphere of taxol to accommodate the 3'-benzamido phenyl, the 3'-phenyl, and the 2-benzoyl

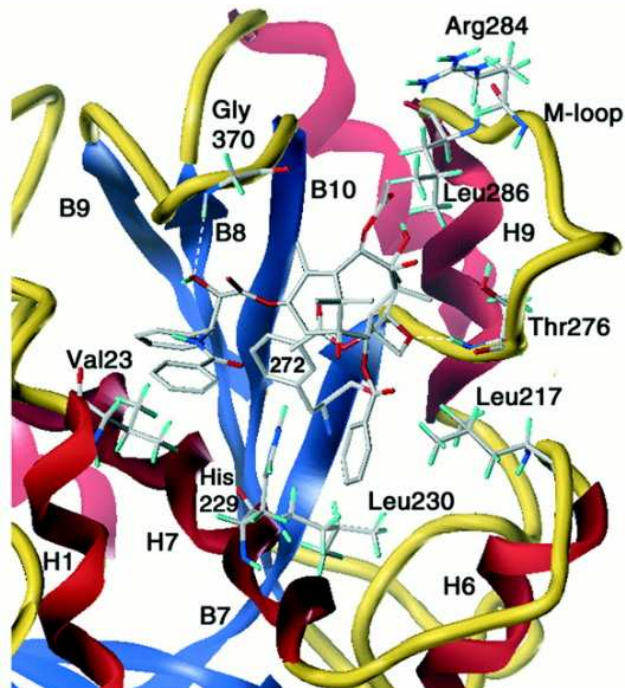


**Figure 3.3:** Taxol shown binding to  $\beta$ -tubulin. Figure reproduced from ref. [10c]. Copyright 2001 National Academy of Sciences.



phenyl, and c) the essentiality of the contacts between the “eastern” portion of taxol and the residues of the M-loop.

Recent cryo-EM studies have elucidated the means by which taxol binding to  $\beta$ -tubulin stabilizes the microtubule and inhibits depolymerization.<sup>12</sup> Microtubule depolymerization is typically induced by the hydrolysis of GTP, for which  $\beta$ - and  $\alpha$ -tubulin have a binding site. Upon GTP hydrolysis to GDP, a conformational change occurs in the tubulin heterodimer, inducing considerable strain (Figure 3.4). This strain can be relieved by the bending of the tubulin protofilament, ultimately leading to microtubule depolymerization. With taxol bound, however, conformation of the GDP-bound protofilament resembles that of the GTP-bound protofilament. The lack of strain in the GDP-bound protofilament prevents bending from taking place, inhibiting microtubule depolymerization.

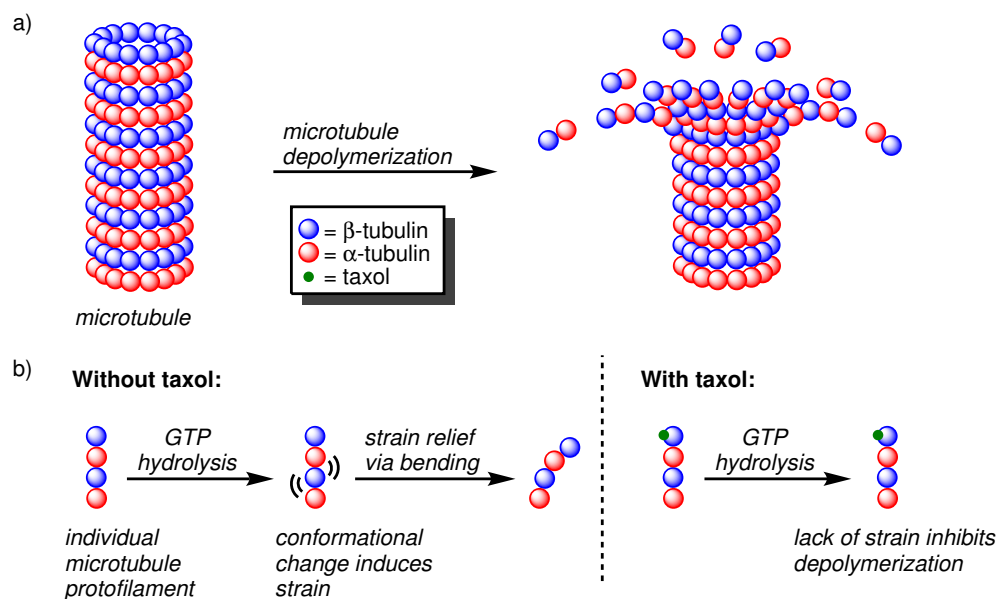


**Figure 3.4:** a) Microtubule depolymerization, showing the “peeling” of protofilaments. b) The difference between taxol-bound and free microtubule protofilament behavior upon GTP hydrolysis.

With the inhibition of microtubule depolymerization in taxol-treated cells, normal microtubule dynamics are disrupted. At least two models have been proposed to explain how this disruption of microtubule dynamics interferes with mitosis and ultimately results in cell death. In the first model, taxol-treated cells are arrested at the spindle assembly checkpoint, a checkpoint after metaphase that ensures proper attachment of the chromosomes to the mitotic spindle before progression to anaphase. Microtubule dynamics have been found to be important for the proper attachment of microtubules emanating from the mitotic spindle to the kinetochores of the chromosomes aligned along the metaphase plate. The loss of microtubule dynamicity results in either the loss of tension across the kinetochores<sup>13</sup> or the complete detachment of the kinetochores from the microtubules,<sup>14</sup> triggering the spindle assembly checkpoint (Figure 3.5a). Some mitotically arrested cells can then undergo apoptosis.

In a second model, the suppression of microtubule dynamics interferes with the ability

of microtubules to “search out” spindle pole components and focus them into a cohesive spindle pole. As a result, the microtubules become concentrated not just at two poles at separate ends of the cell, but around the periphery of the cell as well, ultimately resulting in the formation of multipolar spindles (Figure 3.5b).<sup>15</sup> Progression through anaphase results in segregation of chromosomes in multiple different directions; after cytokinesis, multiple daughter cells are formed, some of which are non-viable since they lack essential genes.<sup>16</sup> It has been proposed that the particular mechanism by which taxol disrupts mitosis is concentration-dependent, with mitotic arrest at the spindle assembly checkpoint occurring at higher concentrations, and with the induction of multipolar spindle formation occurring at lower, more clinically relevant concentrations.

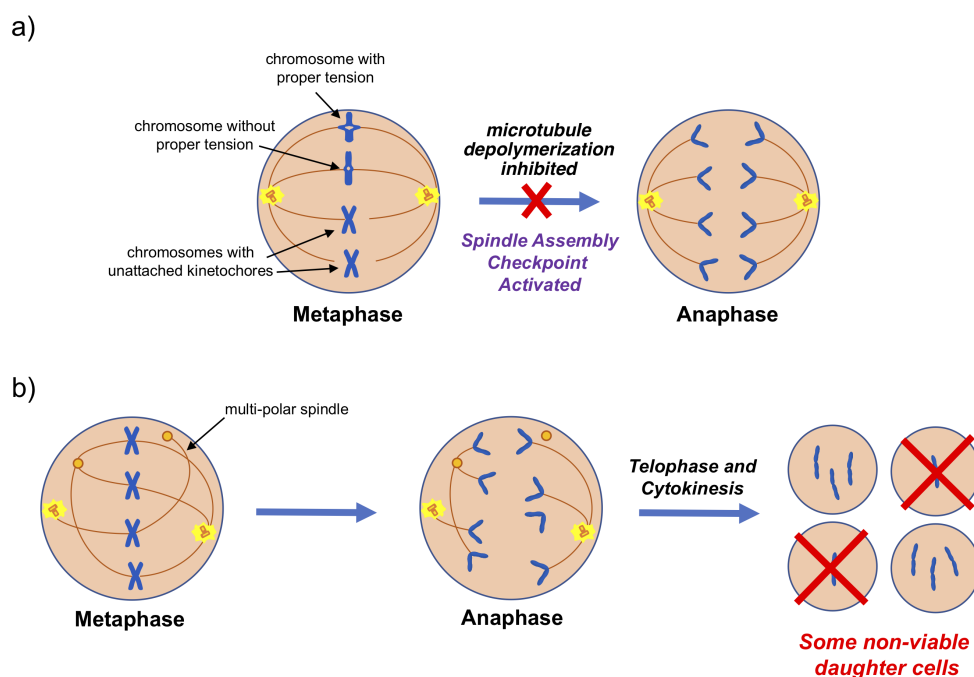


**Figure 3.5:** a) The spindle assembly checkpoint model of taxol’s antimitotic properties. b) The multi-polar spindle model of taxol’s antimitotic properties.

### 3.2.2 Clinical Challenges for Taxol Treatment

Multiple challenges have arisen regarding the clinical use of taxol since its discovery as a potent antitumor agent. First, taxol is poorly water-soluble, and so is often administered with the surfactant Cremophor EL. The high concentration of Cremophor EL required can result in potentially life-threatening acute hypersensitivity reactions in some patients, and has been associated with neurotoxicity as well.<sup>17</sup> Second, innate and/or acquired resistance to taxol treatment is common. For example, the time to progression in patients treated with taxol as a first-line chemotherapeutic for metastatic breast cancer is only 6 to 10 months.<sup>18</sup> Improvements in taxol formulation have lessened the impact of its poor water-solubility; most notably, a Cremophor EL-free, albumin-bound formulation of taxol (Abraxane®) has

been FDA-approved for breast cancer, pancreatic cancer, and non-small cell lung cancer. Comparatively, the issue of taxol resistance has been more challenging to overcome.

Multiple mechanisms have been proposed to explain taxol resistance, and the phenomenon of resistance is likely multifactorial, with patient-to-patient variation in the relative importance of each mechanism.<sup>20</sup> One major mechanism attributed to play a causal role in taxol resistance is the overexpression of isotypes of  $\beta$ -tubulin that bind taxol less effectively. At least seven isotypes of  $\beta$ -tubulin are known ( $\beta$ I,  $\beta$ II,  $\beta$ III,  $\beta$ IVa,  $\beta$ IVb,  $\beta$ V, and  $\beta$ VI); in non-neuronal cells,  $\beta$ I-tubulin is the dominant isotype, while the expression of  $\beta$ III-tubulin is typically low. Overexpression of  $\beta$ III-tubulin has been associated with taxol resistance in tumor cells.<sup>21</sup> It has been postulated that specific amino acid differences between  $\beta$ I- and  $\beta$ III-tubulin may weaken taxol binding in  $\beta$ III-tubulin. Specifically, it has been proposed that the disorganization of the M-loop caused by a substitution of serine for arginine at residue 277 may lower affinity for taxol in  $\beta$ III-tubulin (cf. Figure 3.6a and Figure 3.6b).<sup>19</sup> Additionally, Horwitz and coworkers have proposed that the substitution of a threonine for an alanine at residue 218 may influence the shape of the binding pocket and lessen taxol accessibility.<sup>22</sup> Scambia and coworkers have shown that the seco-taxane analog IDN5390 (**3.20**, Figure 3.6d)—whose structure is distinct from that of taxol in that it lacks a C-ring—was able to treat taxol-resistant cells with increased expression levels of  $\beta$ III-tubulin, and have

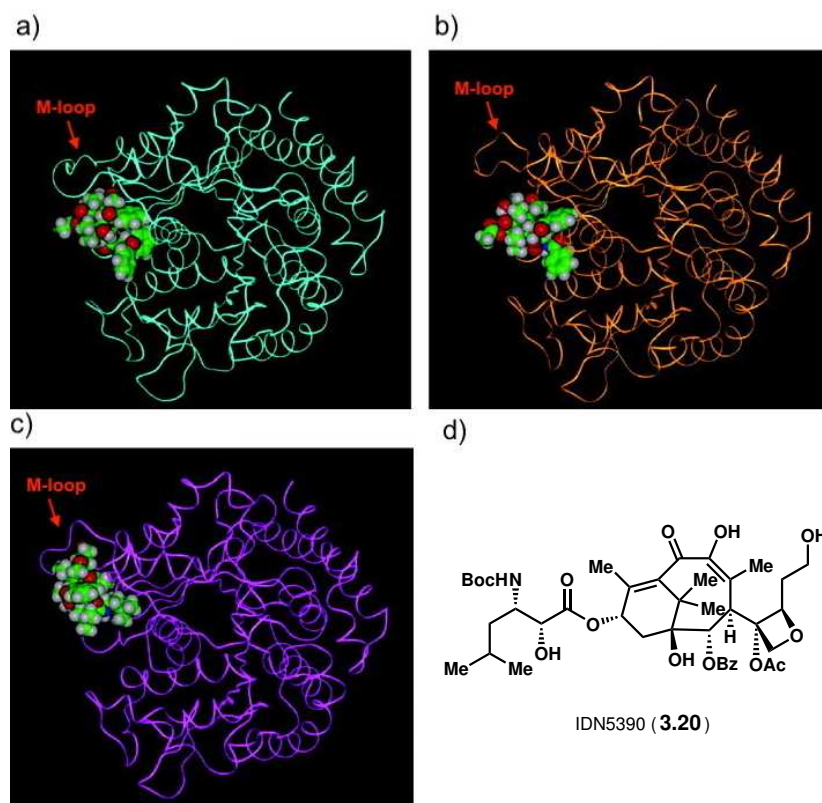


**Figure 3.6:** a)  $\beta$ I-tubulin in complex with taxol. b)  $\beta$ III-tubulin in complex with taxol. c)  $\beta$ III-tubulin in complex with seco-taxane IDN5390. d) Seco-taxane IDN5390 (**3.20**). Adapted from ref. [19], Copyright 2005, with permission from AACR.

suggested through molecular modeling that IDN5390 binds the binding site of  $\beta$ III-tubulin more effectively than taxol does (Figure 3.6c). In addition, the combination of IDN5390 and taxol exhibited a synergistic effect in promoting polymerization of tubulin with high  $\beta$ III-tubulin content. This result underscores the notion that structurally distinct taxoids may serve as valuable therapeutics in combination therapies with taxol in order to treat taxol-resistant tumors.

### 3.2.3 Biological Studies of the Taxagifine-Like Natural Products

Relative to taxol, the taxagifine-like natural products have been less studied. The earliest-known member, taxagifine (**3.3**), was isolated in 1982 from *Taxus baccata* and its structure was determined by X-ray crystallography.<sup>23</sup> Two structural differences between taxagifine and taxol—namely, taxagifine’s lack of an oxetane D ring, and its additional bridging ether ring between C12 and C17—have the effect of distorting the conformation of taxagifine relative to taxol, which may grant it unusual biological properties. Specifically, the A-ring, which adopts a boat-like conformation in taxol, is half-chair-like in taxagifine. Additionally, the C-ring, which is locked by the oxetane ring into an envelope in taxol, adopts a chair conformation in taxagifine. Both molecules possess a cupped or cage-like shape.

Notably, taxagifine lacks structural features typically associated with the potent bioactivity of taxol. Specifically, taxagifine lacks an ester side chain at C13—whose 2'-OH group in taxol has been implicated as essential for bioactivity due to its hydrogen-bonding capacity (see Figure 3.3 and ref. [24])—as well as the oxetane D-ring, which has been proposed to be important both as a hydrogen bond acceptor and as a conformational constraint on the C-ring.<sup>25</sup> In addition, aside from the cinnamoyl ester at C5, the lack of aromatic moieties calls into question the ability of taxagifine to interact favorably with the taxane binding site in tubulin via either  $\pi$ -stacking or hydrophobic interactions.

Nevertheless, taxagifine has showed promising bioactivity in a number of assays. In an *in vitro* assay, taxagifine was shown to inhibit the  $\text{Ca}^{2+}$ -induced depolymerization of microtubules with a potency of about one-third to one-half of that of taxol, and with activity greater than ~80% of the taxoid natural products tested (Figure 3.7).<sup>26</sup> Related compound taxezopidine L (**3.16**) shows similar activity in this assay. Taxagifine typically shows moderate activity in cell-based assays, as well. For example, taxagifine showed cytotoxic activity against murine leukemia L1210 cells ( $\text{IC}_{50} = 1.3 \mu\text{M}$ , cf. taxol  $\text{IC}_{50} = 0.33 \mu\text{M}$ ) and human epidermoid carcinoma KB cells ( $\text{IC}_{50} = 0.86 \mu\text{M}$ , cf. taxol  $\text{IC}_{50} = 8.8 \text{ nM}$ ),<sup>27,28</sup> and cell growth inhibitory activity against human cervical cancer HeLa cells ( $\text{IC}_{50} = 13.3 \mu\text{M}$ , cf. taxol  $\text{IC}_{50} = 7.9 \mu\text{M}$ ),<sup>29</sup> malignant lung tumor VA-13 cells ( $\text{IC}_{50} = 8.8 \mu\text{M}$ , cf. taxol  $\text{IC}_{50} = 5.0 \text{ nM}$ ), and human liver tumor HepG2 cells ( $\text{IC}_{50} = 11.9 \mu\text{M}$ , cf. taxol  $\text{IC}_{50} = 8.1 \mu\text{M}$ ).<sup>30</sup> The inactivity of  $5\alpha$ -decinnamoyltaxagifine (**3.8**) in several of these assays (VA-13 cells:  $\text{IC}_{50} = 49 \mu\text{M}$ ; L1210 cells:  $\text{IC}_{50} > 10 \mu\text{M}$ ; KB cells:  $\text{IC}_{50} > 10 \mu\text{M}$ ) highlights the importance of the cinnamoyl ester for the bioactivity of taxagifine.

The relatively potent bioactivity of taxagifine is surprising given its lack of oxetane ring and C13-ester side chain. In addition, appendage of the ester side chain found in docetaxel to taxagifine at C13, yielding compound **3.21**, abrogates its ability to inhibit microtubule depolymerization *in vitro* (Scheme 3.1).<sup>31</sup> Given these observations, we hypothesize that taxagifine’s biological activity is mediated by its binding to the taxol binding site in  $\beta$ -

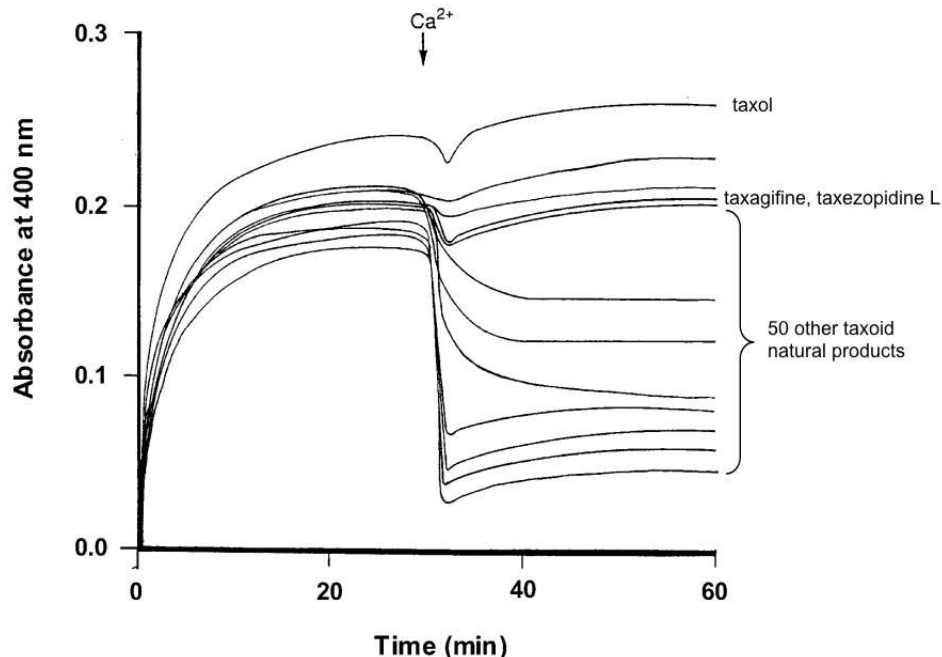
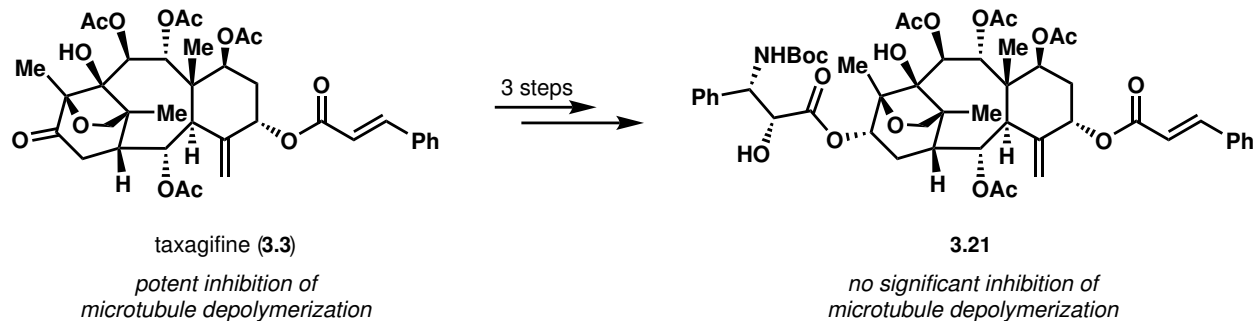


**Figure 3.7:** Microtubule depolymerization assay of 60 taxoid natural products, with extent of tubulin polymerization measured by turbidity. Reprinted (adapted from) with permission from ref. [26]. Copyright (2004) American Chemical Society.

tubulin, but that taxagifine binds in a different orientation than taxol, and therefore that a distinct set of interactions with the tubulin binding site are responsible for binding. For example, while the C13-ester side chain and the oxetane ring are no longer important for the binding of taxagifine to tubulin, the C5-cinnamoyl ester is essential.



**Scheme 3.1:** Synthesis of **3.21** via the appendage of docetaxel-like side chain onto taxagifine.

In order to probe this hypothesis, we conducted computational docking studies to determine the binding orientations of taxol and taxagifine in the taxol binding site of  $\beta$ -tubulin. We obtained the electron crystallographic structure of taxol in  $\beta$ -tubulin from the Protein Data Bank (accession number 1JFF) and docked both taxol and taxagifine with the ligand docking program Glide.<sup>32</sup> As seen in Figure 3.8, taxagifine was predicted to adopt an

orientation distinct from that of taxol. A detailed examination of the docked taxol orientation reveals that the significance of the 2'-OH group and of the three phenyl groups has been recapitulated, with the 2'-OH group acting as a hydrogen bond donor to an aspartate residue and with the three phenyl groups accommodated by a series of hydrophobic residues lining the binding pocket (Figure 3.9). In contrast, the docking of taxagifine anchors the C5-cinnamoyl ester near the hydrophobic residues, consistent with the observed importance of the cinnamoyl ester to the biological activity of taxagifine (Figure 3.10).

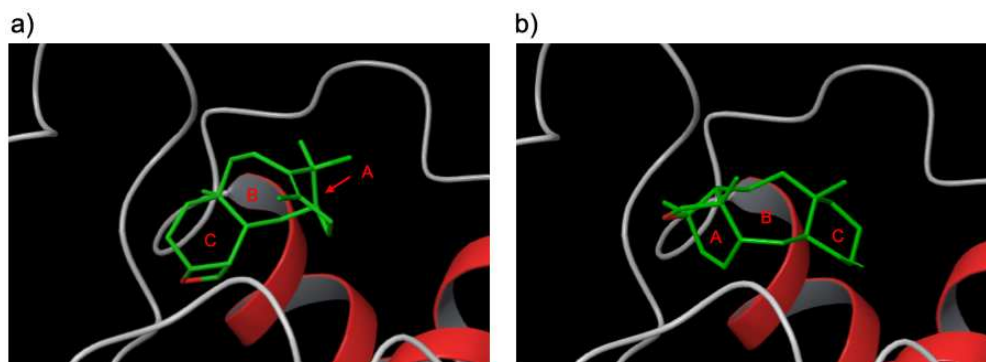


**Figure 3.8:** Results of docking of a) taxol, and b) taxagifine in  $\beta$ -tubulin (Glide, Schrödinger, LLC, New York, NY, 2018). While docking was carried out on the full natural products, only the carbon skeletons are shown here for clarity, with the ring identities highlighted.

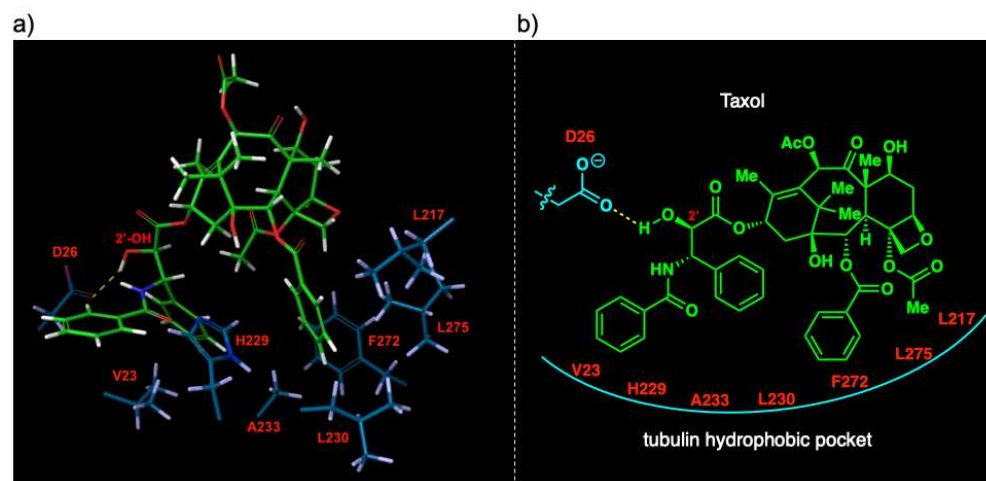


**Figure 3.9:** Results of docking of taxol in  $\beta$ -tubulin (Glide, Schrödinger, LLC, New York, NY, 2018). a) Ligand-protein interactions shown in detail. b) Cartoon version of ligand-protein interactions.

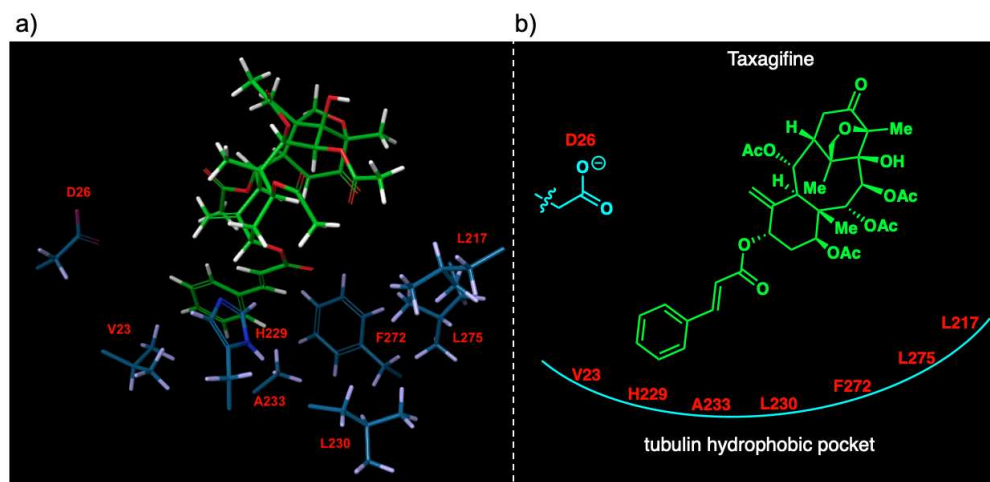


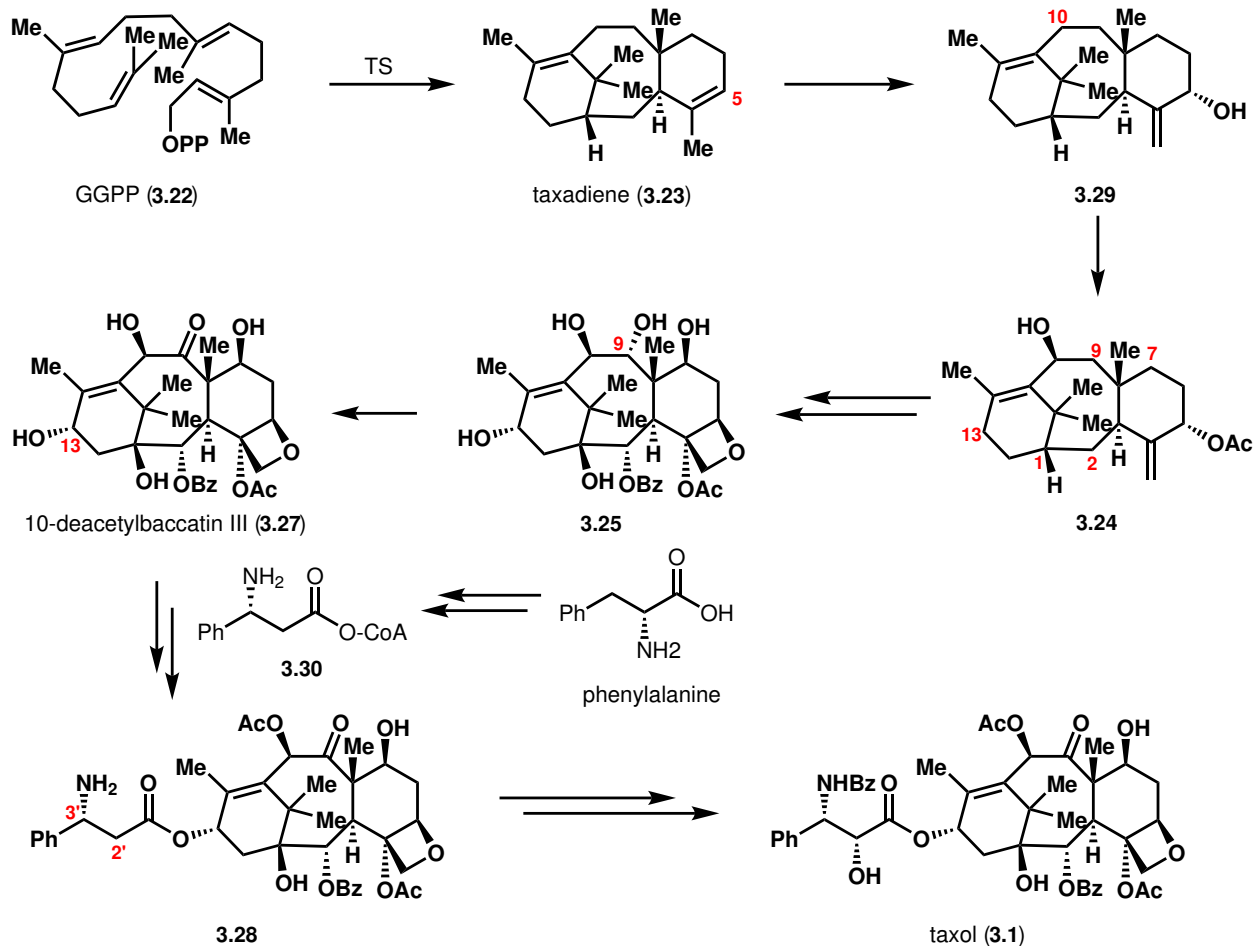
**Figure 3.10:** Results of docking of taxagifine in  $\beta$ -tubulin (Glide, Schrödinger, LLC, New York, NY, 2018). a) Ligand-protein interactions shown in detail. b) Cartoon version of ligand-protein interactions.

With the case of IDN5390 serving as precedent, it is possible that adoption of a different orientation in the binding site would allow taxagifine to exhibit increased binding affinity to  $\beta$ III-tubulin relative to taxol, and therefore to be potent against taxol-resistant cancer cells. In accordance with this possibility, Yin and coworkers discovered that taxagifine showed potent activity against taxol-resistant cells derived from the human ovarian carcinoma cell line A2780 ( $IC_{50} = 0.19 \mu\text{M}$ ; cf. taxol  $IC_{50} = 4.4 \mu\text{M}$ , docetaxel  $IC_{50} = 0.42 \mu\text{M}$ ).<sup>33</sup> Given these preliminary lines of evidence, we speculate that taxagifine—and, by extension, the taxagifine-like natural products at large, and derivatives thereof—could potentially serve as a molecular platform from which to discover new taxoid therapeutics with bioactivity profiles distinct from those typically attained with taxol-like scaffolds. Further investigation would be facilitated by access to these natural products in quantities greater than what can be easily achieved through natural isolation, and via methods that would permit easy diversification.

### 3.3 Biosynthesis of the Taxoid Natural Products

There have been many studies pertaining to the biosynthesis of taxol, in part motivated by the alternative production methods that would be enabled by a full understanding of the biosynthetic pathway. It is generally believed that the entire process requires 19 enzymatic steps from geranylgeranyl pyrophosphate (GGPP, **3.22**), beginning with the cationic cyclization of GGPP by taxadiene synthase (TS) to taxadiene (**3.23**) (Scheme 3.2).<sup>34,35</sup> Hydroxylation at C5 followed by acetylation of the C5–OH yields **3.24**. The order of the subsequent oxidations at C1, C2, C7, C9, and C13 is unknown, but hypothetical intermediate **3.25** is proposed to arise as a result. The oxetane is also hypothesized to arise during this sequence via an intermediate epoxide **3.26**; the oxetane synthesis is proposed to be catalyzed by an as-yet-unidentified oxomutase (OXM) enzyme (Scheme 3.3).<sup>36</sup> Oxidation of the C9–OH to

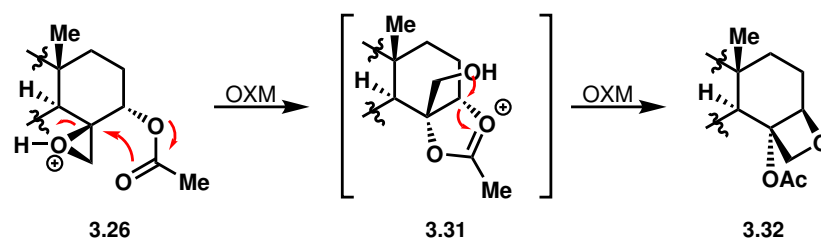




**Scheme 3.2:** The proposed biosynthetic pathway for taxol.

the carbonyl yields 10-deacetylbaccatin III (**3.27**), which has previously been an important precursor in the commercial semisynthesis of taxol. Acetylation of the C10–OH followed by esterification to append the phenylalanine-derived side chain yields compound **3.28**. Finally, 2'-hydroxylation and benzoylation of the 3'-NH<sub>2</sub> affords taxol.

The biosynthetic pathway for the taxagifine-like natural products, similar to the biosynthesis of most taxoid natural products apart from taxol, is mostly unknown. Given that taxagifine lacks hydroxylation at C1 and lacks the oxetane ring, it can be surmised that



**Scheme 3.3:** The proposed epoxide-to-oxetane biosynthetic transformation.



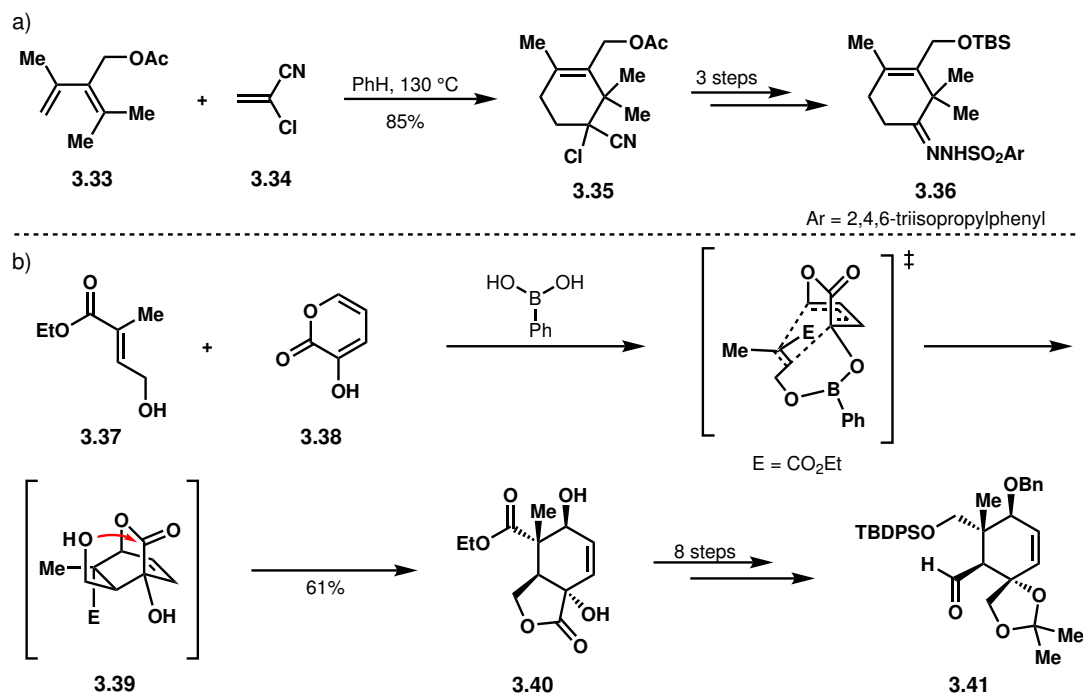
divergence from the taxol biosynthetic pathway occurs fairly early, but not much else can be presumed. Therefore, the biosynthesis or semisynthesis of taxagifine-like compounds is impractical at this stage for the provision of material for biological studies.

## 3.4 Previous Syntheses of Taxoid Natural Products

Given the relative obscurity of the taxagifine-like subfamily, there have been no reported attempts to synthesize these natural products to date. However, as a result of the demand for greater quantities of taxol for clinical use in the late 20th century, the synthetic community has devoted much effort to the synthesis of this natural product, resulting in six total syntheses,<sup>37–42</sup> three formal syntheses,<sup>43–45</sup> and many reports of studies toward taxol and syntheses of the 6/8/6 tricyclic taxane core.<sup>46</sup> Several syntheses of taxanes at lower oxidation states exist as well.<sup>47</sup> Only a few selected illustrative examples of these synthetic efforts, which provide useful insights into the synthesis of the taxagifine-like natural products, will be described here.

### 3.4.1 Nicolaou's Total Synthesis of Taxol

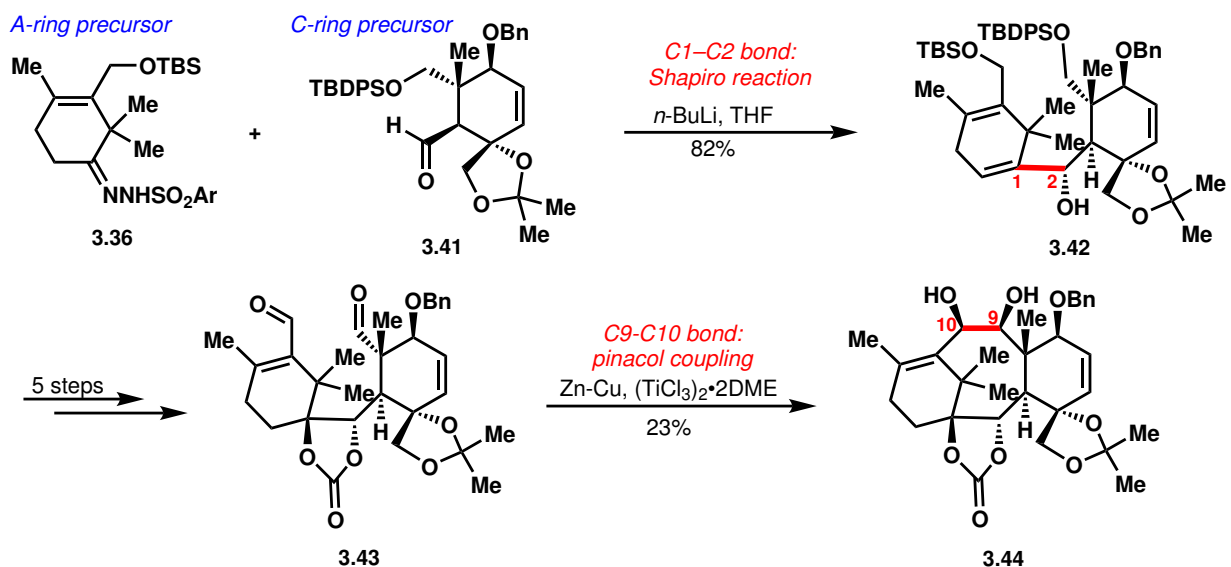
The Nicolaou group was one of the first to publish a total synthesis of taxol in 1994, and provides an illustrative example of a convergent total synthesis through the coupling of A-ring and C-ring fragments.<sup>40</sup> Synthesis of the A-ring fragment began with a Diels–Alder reaction between diene **3.33** and 2-chloroacrylonitrile (**3.34**), yielding cyclohexene **3.35** (Scheme 3.4a). A sequence of three steps then transformed **3.35** to hydrazone **3.36** as



**Scheme 3.4:** Nicolaou's synthesis of a) A-ring fragment **3.36** and b) C-ring fragment **3.41**.

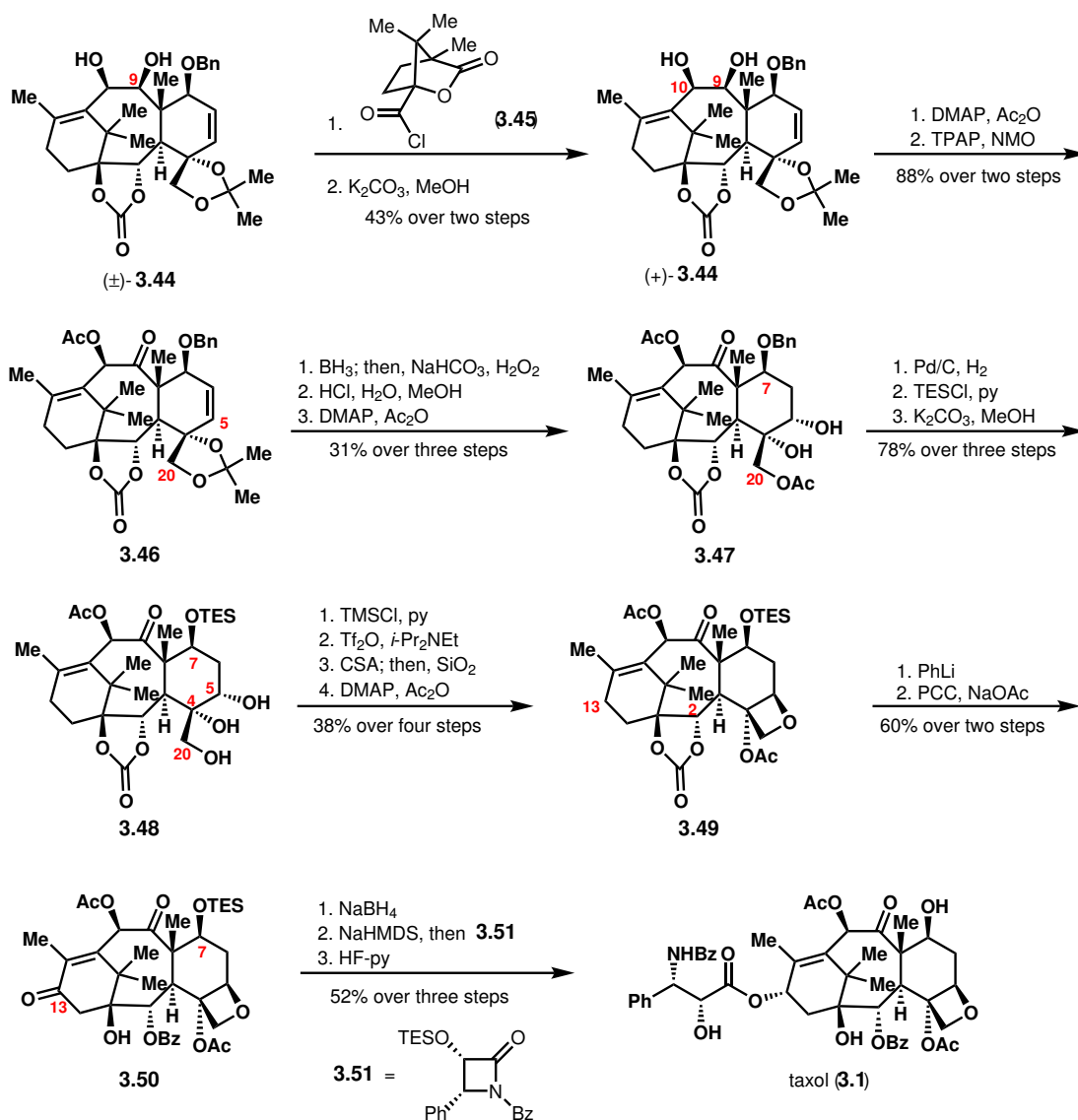
the A-ring precursor. Synthesis of the C-ring fragment began with a boronic acid-assisted Diels–Alder reaction between dienophile **3.37** and 3-hydroxy-2-pyrone **3.38** to provide intermediate **3.39**; trans-lactonization with the primary hydroxy group then yielded diol **3.40** (Scheme 3.4b). Further functional group manipulations then provided aldehyde **3.41** as the C-ring precursor.

Coupling of the A- and C-ring precursor fragments was accomplished by a Shapiro reaction to forge the C1–C2 bond, yielding alcohol **3.42** as a single diastereomer (Scheme 3.5). Further transformations, including the stereoselective introduction of oxygenation at C1, provided dialdehyde **3.43** as the precursor to the pinacol coupling. Subjecting dialdehyde **3.43** to titanium(III) chloride and a zinc-copper alloy triggered the pinacol coupling, which forged the C9–C10 bond to close the B-ring and afford diol **3.44**. This completed the 6/8/6 tricyclic core of taxol.



**Scheme 3.5:** Shapiro reaction and pinacol coupling as key bond-forming events in the synthesis of 6/8/6 tricycle **3.44**.

Up to this point, the synthesis was racemic. In order to provide access to enantiomerically enriched material, Nicolaou and coworkers resolved racemic **3.44** by acylation of the C9–OH with chiral acyl chloride **3.45**, yielding two separable diastereomers (Scheme 3.6). Methanolysis of the desired diastereomer afforded enantiopure **3.44** in 43% yield over two steps. Selective acylation of the C10-hydroxy group followed by Ley oxidation of the C9–OH yielded compound **3.46**. Hydroboration–oxidation delivered the C5-hydroxylated compound regioselectively; hydrolysis of the acetonide followed by selective acetylation of the primary C20–OH provided diol **3.47**. The benzyl group at the C7–OH was replaced by a triethylsilyl group by a two-step sequence, after which selective cleavage of the C20–OAc afforded triol **3.48**. Oxetane formation then commenced with selective trimethylsilylation of the primary C20-hydroxy group; triflation of the secondary C5-hydroxy group followed by treatment with mild acid triggered oxetane ring closure. Acetylation of the remaining tertiary hydroxy group at C4 yielded compound **3.49**. Addition of PhLi delivered the benzoate at C2, after which allylic oxidation with PCC provided C13 carbonyl compound **3.50**. Finally, stereoselective

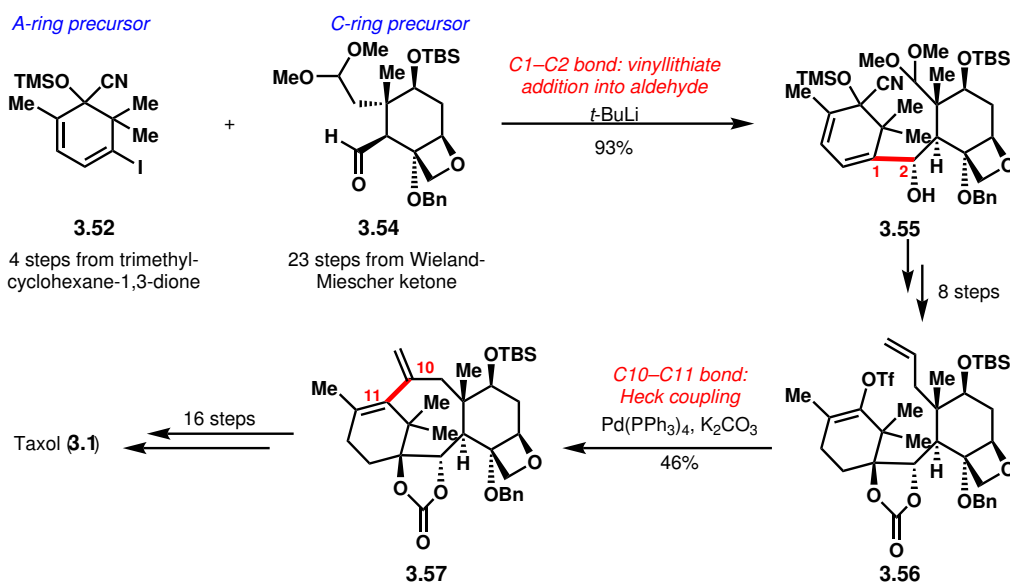


**Scheme 3.6:** Resolution of **3.44** and completion of Nicolaou's total synthesis of taxol.

reduction of the C13 carbonyl with  $\text{NaBH}_4$ , esterification with Ojima's  $\beta$ -lactam (**3.51**),<sup>7c</sup> and cleavage of the C7 silyl ether completed the Nicolaou synthesis of taxol in a total of 40 steps in the longest linear sequence.

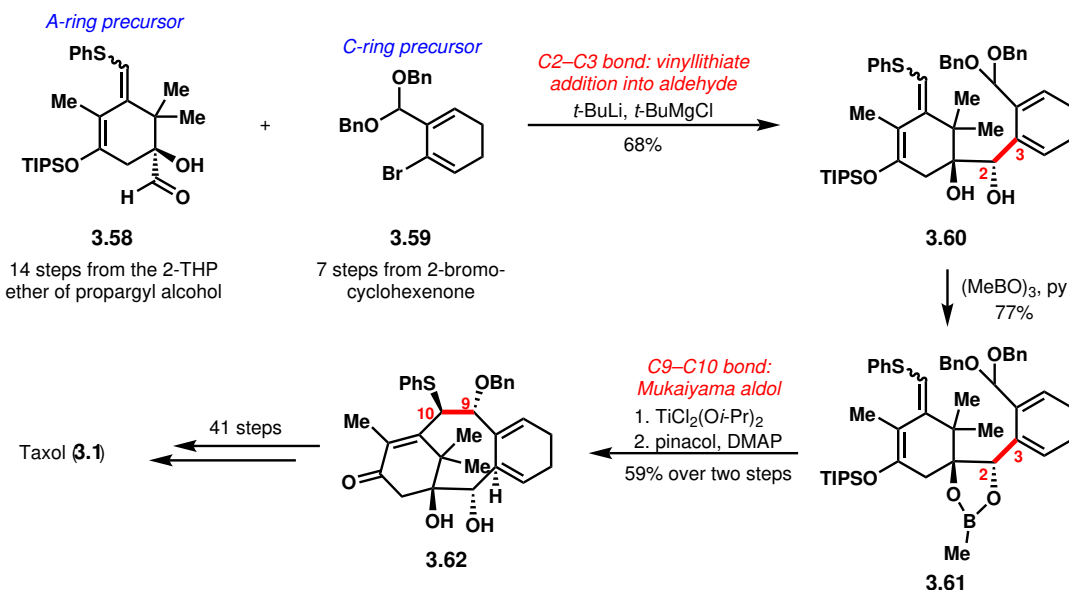
### 3.4.2 Other Total Syntheses of Taxol

Several total and formal syntheses follow a similar strategy to that of Nicolaou, with the syntheses of functionalized cyclohexyl A- and C-ring precursors followed by two sequential bond-forming events to forge the B-ring. The Danishefsky synthesis in 1996 involved the initial synthesis of A-ring precursor cyclohexadiene **3.52** and C-ring precursor aldehyde **3.53** from trimethylcyclohexane-1,3-dione and the Wieland-Miescher ketone, respectively (Scheme 3.7).<sup>41</sup> Notably, the C-ring precursor includes the oxetane ring, which was introduced much earlier in the Danishefsky synthesis relative to the other syntheses of taxol. Similar to Nicolaou's synthesis, the addition of a vinylolithiate derived from **3.52** to the aldehyde of **3.54** forges the C1–C2 bond and delivers alcohol **3.55**. After 8 additional steps, vinyl triflate **3.56** was synthesized as a suitable substrate for Heck coupling. Pd-catalyzed Heck coupling then afforded **3.57** by closure of the B-ring via formation of the C10–C11 bond. A further 16 steps completed the total synthesis of taxol in a total of 49 steps in the longest linear sequence.



**Scheme 3.7:** Summary of Danishefsky's synthesis of taxol.

The Kuwajima synthesis, published in 2000, began with the preparation of aldehyde **3.58** and vinyl bromide **3.59** from commercial building blocks (Scheme 3.8).<sup>39b</sup> The addition of the vinylolithiate derived from **3.59** to the magnesium alkoxide derived from **3.58** took place under chelation control, delivering diol **3.60** as a single diastereomer, which existed as two atropisomers. Protection of the diol delivered boronate ester **3.61** as a single isomer, whose conformation placed the terminus of the silyl dienol ether near the acetal, enhancing the prospects of subsequent cyclization attempts. Indeed, subjecting **3.61** to  $\text{TiCl}_2(\text{O}i\text{-Pr})_2$  as a Lewis acid triggered the vinylogous Mukaiyama aldol cyclization, providing **3.62** after cleavage of the boronate ester in a separate step. While this sequence provided ready access to a functionalized taxane core, an additional 41 steps were required to carry out the functional group transformations necessary to complete the synthesis of taxol, which was accomplished in a total of 59 steps in the longest linear sequence.



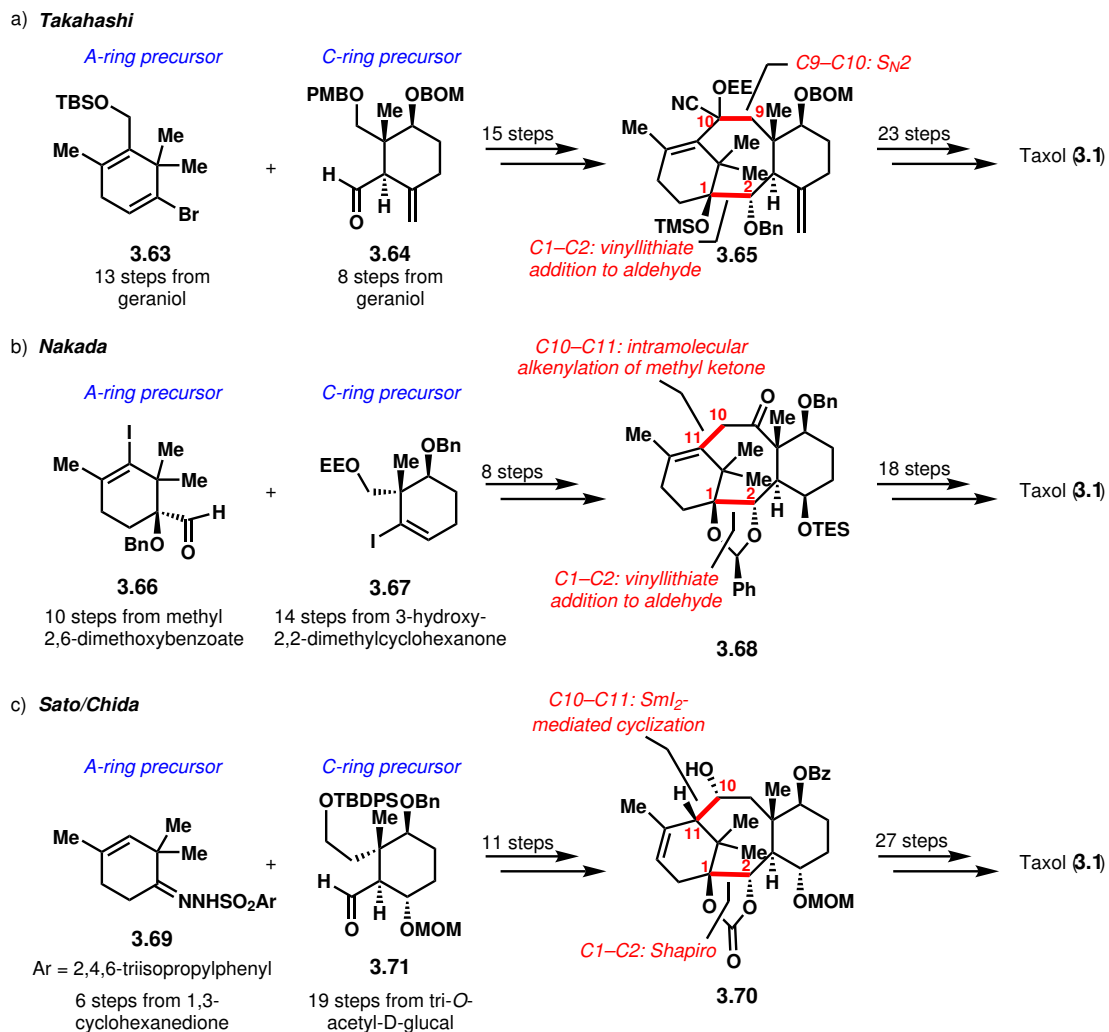
**Scheme 3.8:** Summary of Kuwajima's synthesis of taxol.

The three formal syntheses of taxol also follow a similar strategy. The Takahashi synthesis in 2006 involved the transformation of geraniol into both A-ring precursor vinyl bromide **3.63** and aldehyde **3.64** (Scheme 3.9).<sup>44</sup> Following addition of the vinylithiate derived from **3.63** into the aldehyde of **3.64** to form the C1–C2 bond, several functional group transformations, and an intramolecular  $\text{S}_{\text{N}}2$  reaction to forge the C9–C10 bond, tricyclic intermediate **3.65** was synthesized. Notably, the synthetic sequence to intermediate **3.65** could be fully carried out on an automated synthesizer. After an additional 16 steps, an intermediate from the Danishefsky synthesis of taxol was intercepted, which in another 7 steps would allow for the synthesis of taxol; the complete synthesis of taxol would require 51 steps in the longest linear sequence.

Nakada's synthesis in 2015 commenced with the preparation of A-ring precursor aldehyde **3.66** and C-ring precursor vinyl iodide **3.67**.<sup>45</sup> Nucleophilic addition of the vinylithiate derived from **3.67** to the aldehyde of **3.66** formed the C1–C2 bond; a subsequent Pd-catalyzed intramolecular alkenylation of a methyl ketone forged the C10–C11 bond to close the B-ring. Notably, while the B-ring-closing reaction of several previous syntheses of taxols were characterized by low to moderate yields, this transformation occurred in an extremely efficient 97% yield. An additional 14 steps converted **3.68** to an advanced intermediate in the Nicolaou synthesis; four more steps would convert that intermediate to taxol. In total, Nakada's synthetic route would enable the synthesis of taxol in 40 steps in the longest linear sequence.

Finally, Sato's and Chida's synthesis of taxol in 2015 involved the initial synthesis of A-ring precursor arylsulfonylhydrazone **3.69** and C-ring precursor aldehyde **3.70**.<sup>43</sup> Formation of the C1–C2 bond was accomplished by Shapiro coupling of these two fragments; a later  $\text{SmI}_2$ -mediated cyclization of an intermediate with a C10 aldehyde and a C12 allylic benzoate forged the C10–C11 bond, delivering intermediate **3.70**. After an additional 18 steps, an intermediate in Takahashi's synthesis was intercepted, after which another 9 steps would deliver taxol. In total, Sato and Chida's synthetic route would provide taxol in 57 steps

from commercially available starting materials.



**Scheme 3.9:** Summary of a) Takahashi's, b) Nakada's, and c) Sato/Chida's formal syntheses of taxol.

Overall, the six syntheses of taxol discussed here all follow the same strategy initially pioneered by Nicolaou, reinforcing the notion that a convergent approach involving the coupling of two similarly complex fragments is particularly attractive in the total synthesis of a natural product as complex as taxol. In addition, the continued success of the “A + C → AC → ABC” strategy for the construction of the 6/8/6 tricyclic core of taxol suggested that a similar strategy might work well in the context of the taxagifine-like natural products. However, given the differences in the cores of the two kinds of natural products—i.e., in taxagifine, the presence of the ether bridge between C12 and C17, the presence of a hydroxy group at C11, and the absence of a hydroxy group at C1—different bond-forming events would have to be proposed for the syntheses of the taxagifine-like natural products. In addition, we imagined that access to modern synthetic tools would enable a shorter and more efficient synthesis of the taxagifine-like natural products than has been achieved for taxol.

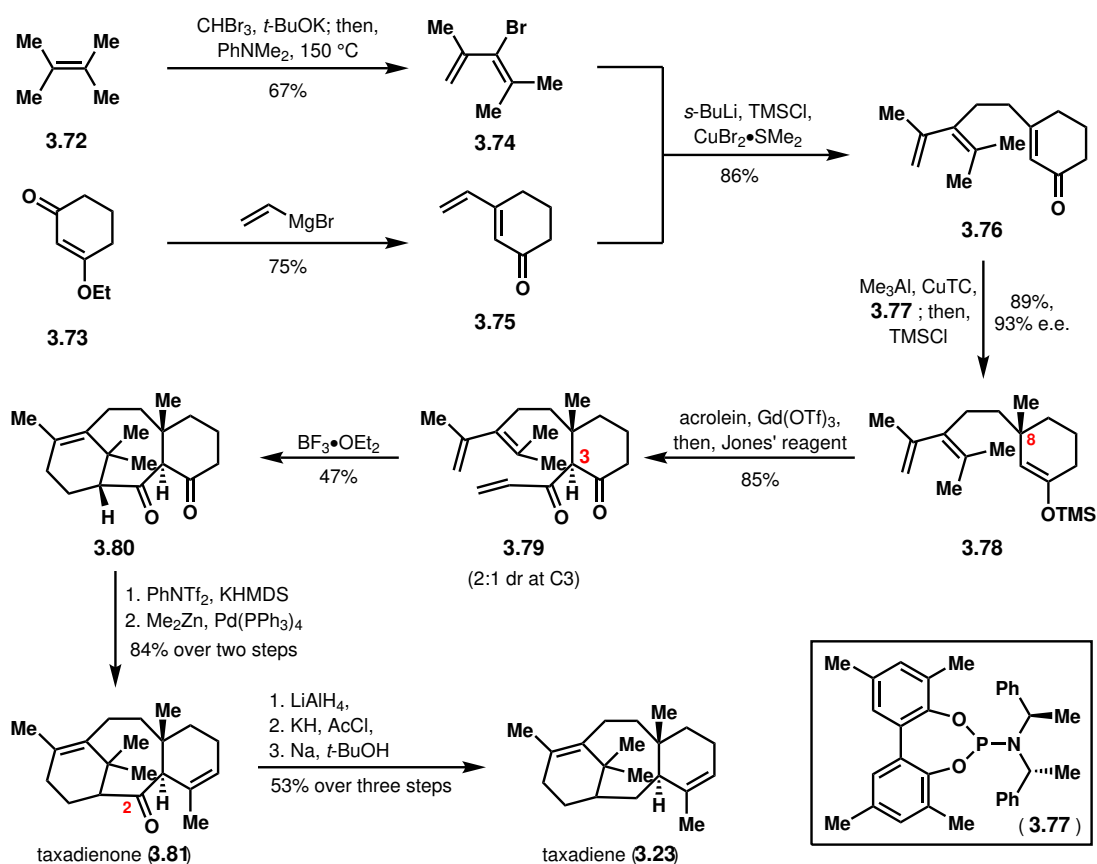
### 3.4.3 The Two-Phase Synthetic Strategy for Taxoid Natural Products

The continued development of site-selective C–H functionalization methodology has enabled a distinct strategy for the synthesis of the taxoid natural products. In particular, Baran has pioneered a bioinspired approach to the taxoid natural products that involves two phases: an initial “cyclase” phase consisting of C–C bond-forming events for the rapid construction of the 6/8/6 tricyclic core of the taxoid natural products; and a subsequent “oxidase” phase largely characterized by site-selective C–H oxidation events.<sup>46g,48</sup> The biosynthesis of taxol can be thought of as occurring in these two phases; however, it is a greater challenge to carry out site-selective C–H oxidations chemically than with tailored biosynthetic machinery, and attempts to do so can inspire new synthetic methodology. Given that our planned synthesis for the taxagifine-like natural products would require late-stage site-selective C–H oxidations on a taxane scaffold, it is instructive to review the Baran group’s two-phase synthetic strategy as applied to the taxoid natural products.

The Baran group’s two-phase taxoid synthesis program commenced with the selection of a suitable cyclase phase endpoint. While taxadiene, as the biosynthetic cyclase phase endpoint, was the most natural choice, other chemically accessible low-oxidation-level tricyclic scaffolds would also be appropriate. Ultimately, the Baran group was able to synthesize “taxadienone” (**3.81**) in seven steps in the longest linear sequence (Scheme 3.10).<sup>46f</sup> Under Baran’s terminology, taxadienone, harboring four units of oxidation, is a “level four” taxoid, whose strategically placed units of oxidation could be used to facilitate the introduction of further oxidation in the synthesis of more highly oxidized taxoids (e.g., taxol, a “level 11” taxoid).

The synthesis of taxadienone began with the one-step preparation of known dienyl bromide **3.74** and dienone **3.75** from known compounds **3.72** and **3.73**, respectively. The cuprate derived from **3.74** was added in a 1,6-fashion to **3.75** with TMSCl as a Lewis acid, delivering **3.76** in 86% yield. The quaternary center at C8 was set enantioselectively by cuprate addition of a methyl group in a 1,4-fashion to enone **3.76**, utilizing chiral phosphoramidite ligand **3.77**. The aluminum enolate was then trapped as the trimethylsilyl enol ether to afford **3.78**. After screening various Lewis acids and other reaction condition parameters, it was found that a Mukaiyama aldol could be effected with acrolein by use of Gd(OTf)<sub>3</sub> as Lewis acid, yielding compound **3.79** as a 2:1 inseparable mixture of diastereomers at C3. Subjection of the mixture to BF<sub>3</sub>-etherate triggered a Diels-Alder cyclization, providing tricyclic compound **3.80** as a single diastereomer after purification. Finally, chemoselective formation of a vinyl triflate followed by Negishi coupling installed the final carbon of taxadienone (**3.81**). While taxadienone would be a suitable cyclase phase endpoint for the synthesis of more highly oxidized taxoids, less oxidized taxoids without oxidation at C2 might require a less oxidized cyclase phase endpoint. Thus, taxadienone was also transformed into taxadiene (**3.23**, a “level two” taxane) in a three-step sequence involving reduction of the C2 carbonyl, acetylation of the resulting secondary hydroxy group, and dissolving metal reduction. Notably, the syntheses of taxadienone and taxadiene were carried out on gram scale, providing ready access to material that could be used for subsequent taxoid syntheses.

With two possible cyclase phase endpoint compounds in hand, higher-oxidation-state



**Scheme 3.10:** Baran's synthesis of taxadienone (3.81) and taxadiene (3.23).

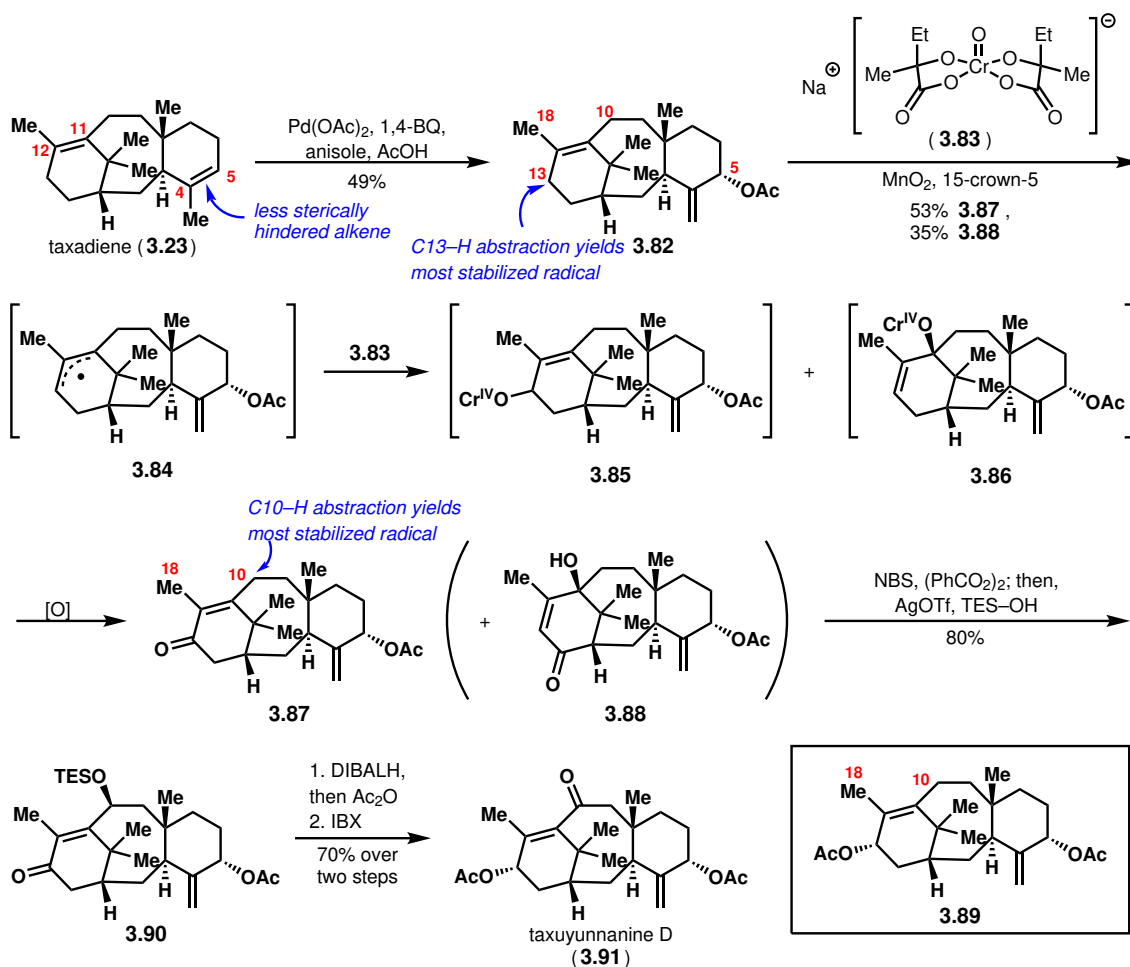
taxoid natural products could begin to be synthesized by the design and execution of an appropriate oxidase phase. As an initial testbed for oxidation chemistry on the taxane scaffold, Baran and coworkers approached the synthesis of taxuyunnanin D (3.91, a "level six" taxoid) (Scheme 3.11).<sup>47e</sup> Given the lack of oxidation at C2, taxadiene was chosen as the starting material for this synthesis. From taxadiene, additional oxidation would be required at C5, C10, and C13. Notably, each of these three positions is allylic and therefore activated for oxidation; in addition, these three positions are hypothesized to be the first to be oxidized in the biosynthesis of taxol, suggesting that the order of enzymatic oxidations is guided by the innate reactivity of taxadiene. The Baran group hypothesized that this innate reactivity profile might be harnessed to orchestrate a sequence of site-selective oxidations via chemical means as well.

Given the steric hindrance associated with the C11–C12 alkene as compared to the C4–C5 alkene, and given that oxidation occurs first at C5 in the biosynthesis of taxol, it was reasonable to assume that C5 was the most activated position for initial oxidation. Indeed, subjecting taxadiene to Pd-catalyzed allylic acetoxylation delivered exclusively C5-oxidized allylic acetate 3.82. Notably, the use of anisole as an additive was important for achieving higher yields, presumably to facilitate the re-oxidation of Pd(0) to Pd(II). At this point, allylic oxidation had to occur at either C10 or C13 selectively over the other, and selectively over C18. DFT calculations carried out on allylic radicals derived from 3.82 indicated



that C13–H abstraction would yield a radical more stabilized than C10–H abstraction or C18–H abstraction. Accordingly, treatment of **3.82** with Cr(V) oxidant **3.83** yielded enone compounds **3.87** and **3.88**, with no evidence of C10 or C18 oxidation. It is hypothesized that this Cr(V) oxidation occurs through a SET followed by deprotonation to deliver delocalized radical **3.84**, after which recombination with another Cr(V) species yields intermediates **3.85** and **3.86**. Further oxidation of these intermediates would afford observed products **3.87** and **3.88**. Notably, as is necessary for the plausibility of this mechanistic proposal, it was discovered that Cr(V) oxidant **3.83** was unable to effect oxidative transposition on simple tertiary allylic alcohols, in contrast with more traditional Cr(VI) species.

With compound **3.87** in hand, a final selective allylic oxidation of C10 over C18 remained. DFT calculations of allylic radicals derived from **3.87** suggested that the C10 allylic radical would be more stable than the C18 allylic radical. Interestingly, DFT calculations revealed that this stability profile was reversed when considering the C13- $\alpha$ -allylic acetate derived from the reduction of **3.87** (**3.89**). Thus, C10 oxidation was attempted with C13 at the ketone oxidation state. In accordance with the DFT calculations, treatment of **3.87** under radical



**Scheme 3.11:** Baran's synthesis of taxuyunnanine D (**3.91** via sequential site-selective oxidations).

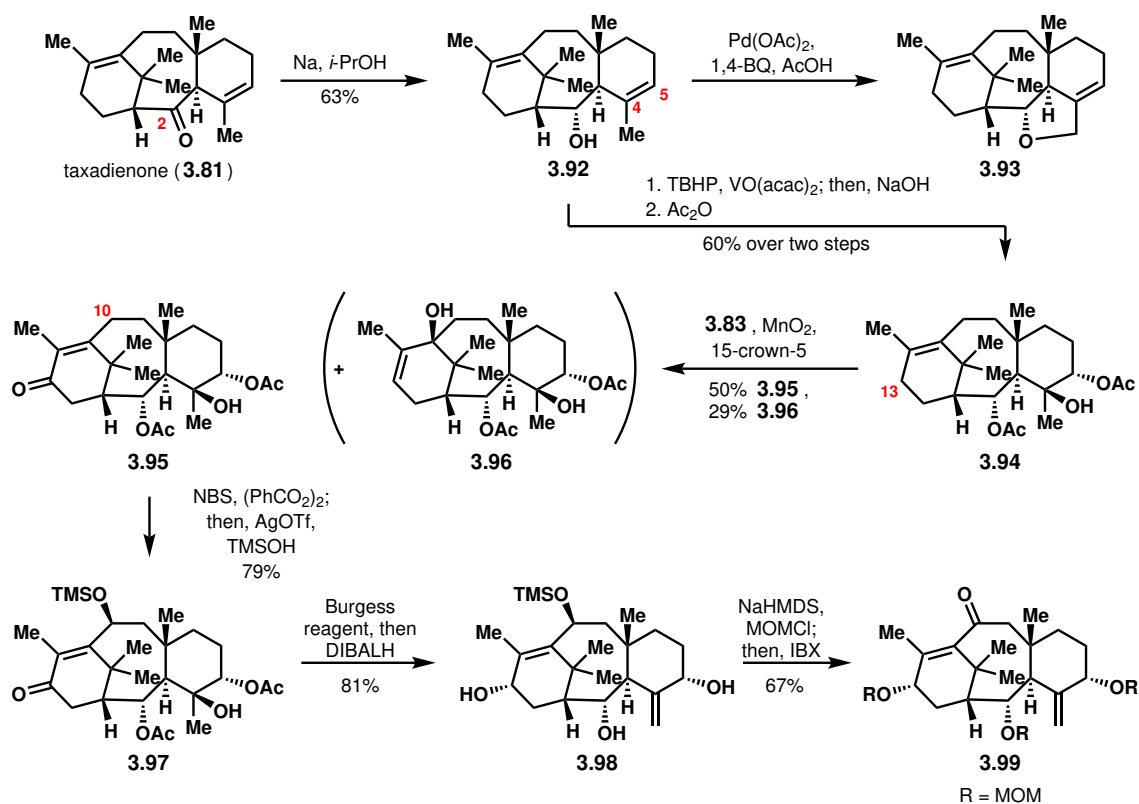
halogenation conditions (NBS, benzoyl peroxide) yielded predominantly the C10-bromide product, with C18-bromide observed only when larger quantities of NBS were used. Silver-mediated substitution with TES-OH then afforded silyl ether **3.89**. Notably, subjecting the C13- $\alpha$ -allylic acetate **3.89** to the same bromination conditions resulted in preferential bromination at C18, again corroborating the predictions made based on DFT calculations and underscoring the notion that remote functional groups can have subtle electronic and/or steric effects on taxoid systems with significant implications for reactivity profiles.

Finally, stereoselective reduction of the C13 carbonyl group, acetylation of the resulting secondary  $\alpha$ -hydroxy group, and oxidation of the silyl ether delivered taxuyunnanin D (**3.91**). The rapidity of the synthesis of taxuyunnanin D (five steps from taxadiene) testified that a detailed understanding of innate reactivity preferences can significantly streamline efforts toward the syntheses of oxidized natural products such as the taxoids. Importantly, the synthesis of taxuyunnanin D required oxidation reactions from a variety of categories, with ultimately only one category being fruitful for each site (i.e., oxidation via  $\pi$ -allyl metal complex for C5, oxidation via transition-metal-mediated SET for C13, oxidation via radical halogenation for C10), emphasizing that different categories of oxidation reaction provide different levels of site-selectivity depending on the molecular context, and that discovering the optimal category for any particular site may require extensive experimentation.

The synthesis of a highly oxidized taxoid natural product such as taxol would require familiarity with oxidation strategies for sites other than C5, C10, and C13. To this end, the Baran group next approached the syntheses of decinamoyltaxinin E (**3.107**) and taxabaccatin III (**3.108**), “level 7” taxoid natural products that additionally contained oxidation at C2 and C9 (Scheme 3.13).<sup>47f</sup> The presence of C2 oxidation in the natural products motivated the use of taxadienone as the starting point for these syntheses.

The syntheses of **3.107** and **3.108** commenced with the reduction of the C2 carbonyl of taxadienone under dissolving metal conditions, which delivered the C2-OH compound as a separable ~6:1 mixture of diastereomers (major diastereomer, **3.92**, shown) (Scheme 3.12). Notably, attempted reductions on substrates more advanced than taxadienone could not be accomplished stereoselectively to deliver the desired  $\alpha$ -isomer. With the desired configuration and oxidation level set at C2, the Baran group attempted to recapitulate the oxidation strategies used for the synthesis of taxuyunnanin D in order to install oxygenation at C5, C10, and C13. However, in another demonstration of the unexpected influence of remote functional groups in complex systems, the C2-OH interfered with the Pd-catalyzed allylic acetoxylation that had succeeded in the taxuyunnanin D synthesis; specifically, cyclic ether **3.93** was isolated instead. C2-hydroxy-protected variants of **3.92** also did not undergo the desired reaction. An alternative oxidation strategy was used instead, wherein an oxo-vanadium-complex-catalyzed epoxidation of the C4-C5 alkene and subsequent epoxide hydrolysis delivered a *trans*-diol at C4 and C5; acetylation of the secondary hydroxy groups then yielded compound **3.94**. Treatment of **3.94** with the Cr(V) complex **3.83** delivered a mixture of desired C13-oxidized enone **3.95** and undesired tertiary alcohol **3.96**, similar to what had been observed in the taxuyunnanin D synthesis. Interestingly, the presence of the tertiary hydroxy group was crucial for the success of this reaction, as the *exo*-methylene-containing variant of **3.94** failed to undergo C13 oxidation under identical conditions. Selective C10 radical halogenation and subsequent silver-mediated substitution afforded **3.97**; the tertiary hydroxy group was then eliminated with Burgess reagent, and

treatment with DIBALH simultaneously reduced the C13 carbonyl group and cleaved the acetyl protecting groups to yield free triol **3.98**. Protection of the hydroxy groups as the MOM ethers followed by IBX oxidation of the silyl ether afforded **3.99**.



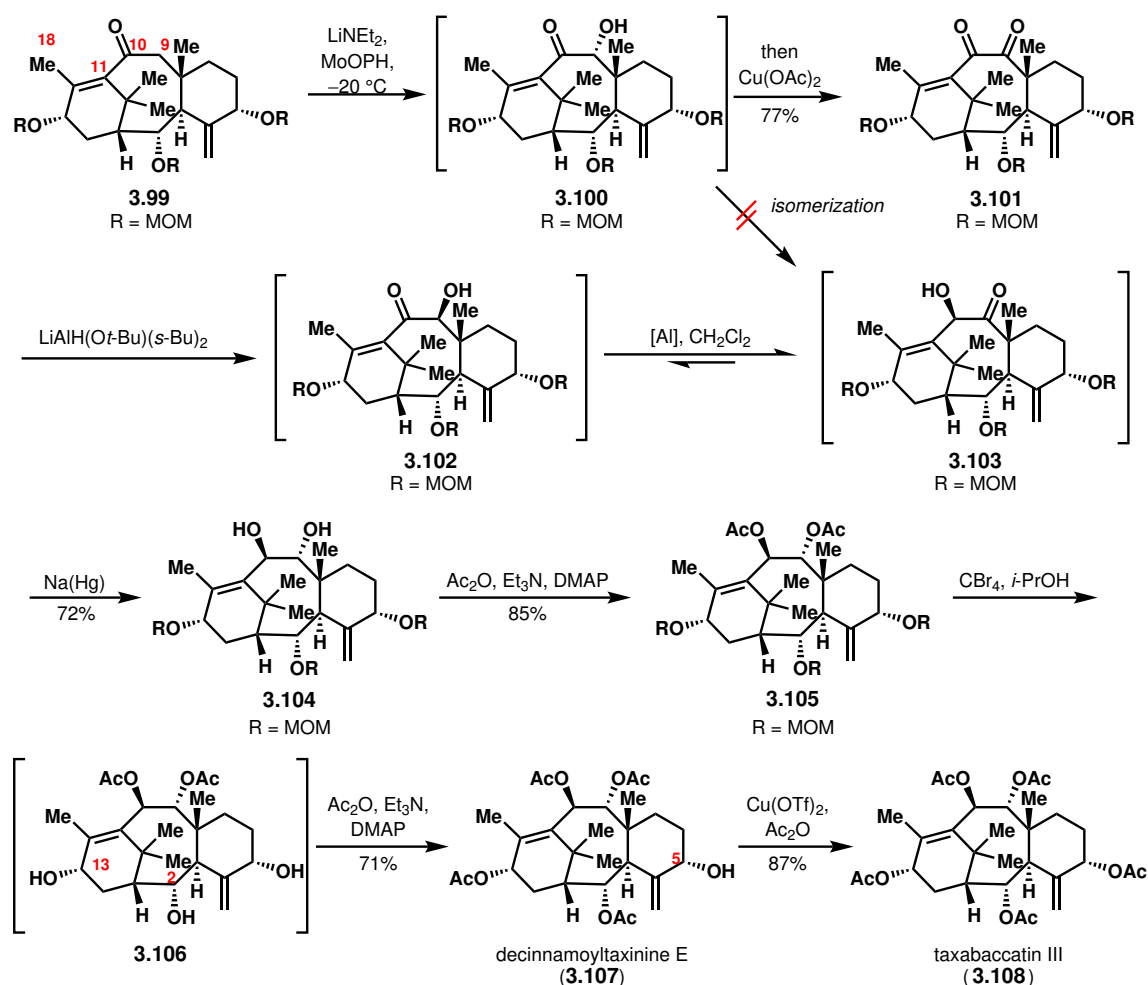
**Scheme 3.12:** Synthesis of intermediate **3.99** en route to decinnamoyltaxinine E and taxabaccatin III.

Compound **3.99** could be considered to be analogous to taxuyunnanine D, containing simply additional oxygenation at C2. Indeed, the synthetic sequence yielding **3.99** was adopted from that leading to taxuyunnanine D, with C2-containing taxadienone used as the starting point rather than taxadiene. However, while the chemistry developed for taxuyunnanine D was valuable in the synthesis of **3.99**, challenges encountered along the way also demonstrated that oxidation strategies developed in one molecular context may not always translate to other, even quite similar contexts.

At this point, only stereoselective oxidation at C9 and stereoselective reduction at C10 remained. C9 oxidation was accomplished by enolate formation followed by trapping with an oxidant to yield **3.100**; notably, the choices of  $\text{LiNEt}_2$  as base, MoOPH as oxidant, and  $-20^\circ\text{C}$  as reaction temperature were crucial to the success of the reaction, in particular to avoid competitive oxidation at either C11 or C18. From **3.100**, the direct stereoselective reduction of C10 proved infeasible, with the only identifiable products resulting from hydride, single-electron, and other types of reductions typically being undesired isomeric compounds (e.g., the undesired diastereomer at C9, or the 1,4-reduction product). Ultimately, it proved advantageous to first oxidize **3.100** to dione **3.101**, with subsequent reduction with  $\text{LiAlH}(\text{O}t\text{-Bu})(s\text{-Bu})_2$  site- and stereoselectively delivering  $\alpha$ -hydroxy ketone **3.102**. This reductant

was unique in providing desired levels of selectivity in comparison to attempts with other hydride reagents. Fortunately, **3.102** spontaneously isomerized to **3.103** in CH<sub>2</sub>Cl<sub>2</sub>, with the isomerization accelerated by the residual aluminum salts from the reduction. Attempts to directly access **3.103** from **3.100** via isomerization proved unsuccessful.

While the stereoselective reduction of the C10 carbonyl of **3.103** was challenging as well—with the undesired diastereomer at C9 and deoxygenated compounds being characteristic products of certain hydride and single electron transfer reductants—ultimately 5% sodium amalgam proved competent to provide the desired *trans*-diol **3.104**. At this point, only protecting group manipulations were required to complete the syntheses of the natural products. Acetylation of the C9 and C10 hydroxy groups yielded diacetate **3.105**; then, cleavage of the MOM ethers afforded triol **3.106**, the C13- and C2-hydroxy groups of which could be acetylated in the same pot to deliver decinnamoyltaxinine E (**3.107**). Further acetylation of the C5-hydroxy group provided taxabaccatin III (**3.108**), completing the first syntheses of these natural products.



**Scheme 3.13:** Completion of the syntheses of decinnamoyltaxinine E (**3.107**) and taxabaccatin III (**3.108**).

The lessons that the Baran group's two-phase taxoid natural product syntheses have

taught for the synthesis of the taxagifine-like natural products are manifold. First, if possible, a “cyclase phase” endpoint should be chosen such that late-stage oxidations would occur at activated positions, in order to facilitate endgame transformations. Second, given that multiple subtle steric and electronic factors affect the site-selectivities of oxidation reactions, oxidation reactions on model systems should not be treated as providing conclusive information about the promise of the same reactions on a real system. Finally, the sequence of late-stage oxidations would optimally be orchestrated in a manner that takes into serious consideration the innate reactivity preferences of the system in question.

### 3.5 Conclusion and Outlook

The taxoid natural products have a storied history, in which taxol in particular has been the central character. Taxol’s antitumor activity and success in the clinic has spurred multiple research programs aimed at understanding its mechanism of action, understanding and engineering its biosynthesis, and synthesizing both the natural product itself as well as derivatives thereof. On the basis of the immense amount of funding and research effort that has been expended on taxol, the other taxoid natural products appear understudied in comparison. It may have historically been the case that other taxoid natural products have not displayed promising enough bioactivity to justify the further procurement of material for biological studies, especially in the context of their typically low isolation yields. Gaining synthetic access to other taxoid natural products has been challenging as well, given that even relatively simple taxoid natural products require the stereoselective synthesis of a 6/8/6 tricyclic carbon skeleton with a specific oxidation pattern.

The taxagifine-like natural products may prove to be an exception. The surprisingly high level of bioactivity of taxagifine in spite of its lack of key structural elements implies that this natural product may adopt an orientation in the tubulin binding site distinct from that of taxol—a particularly intriguing hypothesis in light of the rise of resistance to cancer treatment with taxol. The other taxagifine-like natural products have received little to no study at all; further surprises may lie in these natural products as well. While these natural products all contain high levels of oxidation and may prove challenging to synthesize, the synthetic community has accrued over 20 years of experience synthesizing taxol and related natural products. Lessons learned from these efforts, as well as the application of modern synthetic methods, could be applied to facilitate the first syntheses of the taxagifine-like natural products. Our efforts to synthesize the tetracyclic core of these natural products is expounded upon in Chapter 4.

### 3.6 References

- (1) (a) Rowinsky, E. K.; Onetto, N.; Canetta, R. M.; Arbusk, S. G. *Semin. Oncol.* **1992**, *19*, 646–662; (b) Pazdur, R.; Kudelka, A. P.; Kavanagh, J. J.; Cohen, P. R.; Raber, M. N. *Cancer Treat. Rev.* **1993**, *19*, 351–386; (c) Kingston, D. G. I. *Trends Biotechnol.* **1994**, *12*, 222–227; (d) Baloglu, E.; Kingston, D. G. I. *J. Nat. Prod.* **1999**, *62*, 1448–1472; (e) Wang, Y.-F.; Shi, Q.-W.; Dong, M.; Kiyota, H.; Gu, Y.-C.; Cong, B. *Chem. Rev.* **2011**, *111*, 7652–7709.

- (2) Caesar, J.; Kennedy, E. C., *De bello Gallico VI*; Bristol Classical Press, Dept. of Classics, University of Bristol: Bristol, 1982.
- (3) Lucas, H. *Arch. Pharm.* **1856**, *135*, 145–149.
- (4) Wani, M. C.; Taylor, H. L.; Wall, M. E.; Coggon, P.; McPhail, A. T. *J. Am. Chem. Soc.* **1971**, *93*, 2325–2327.
- (5) Schiff, P. B.; Fant, J.; Horwitz, S. B. *Nature* **1979**, *277*, 665–667.
- (6) McGuire, W. P. *Ann. Intern. Med.* **1989**, *111*, 273.
- (7) (a) Denis, J. N.; Greene, A. E.; Guenard, D.; Gueritte-Voegelein, F.; Mangatal, L.; Potier, P. *J. Am. Chem. Soc.* **1988**, *110*, 5917–5919; (b) Holton, R. A. (University, F. S.). Method for preparation of taxol using  $\beta$ -lactam. US Patent, 5175315A, 1992; (c) Ojima, I.; Habus, I.; Zhao, M.; Zucco, M.; Park, Y. H.; Sun, C. M.; Brigaud, T. *Tetrahedron* **1992**, *48*, 6985–7012.
- (8) Guenard, D.; Gueritte-Voegelein, F.; Potier, P. *Acc. Chem. Res.* **1993**, *26*, 160–167.
- (9) (a) Rao, S.; Horwitz, S. B.; Ringel, I. *J. Natl. Cancer Inst.* **1992**, *84*, 785–788; (b) Rao, S.; Krauss, N. E.; Heerding, J. M.; Swindell, C. S.; Ringel, I.; Orr, G. A.; Horwitz, S. B. *J. Biol. Chem.* **1994**, *269*, 3132–3134; (c) Rao, S.; Orr, G. A.; Chaudhary, A. G.; Kingston, D. G. I.; Horwitz, S. B. *J. Biol. Chem.* **1995**, *270*, 20235–20238; (d) Rao, S.; He, L.; Chakravarty, S.; Ojima, I.; Orr, G. A.; Horwitz, S. B. *J. Biol. Chem.* **1999**, *274*, 37990–37994.
- (10) (a) Nogales, E.; Wolf, S. G.; Khan, I. A.; Ludueña, R. F.; Downing, K. H. *Nature* **1995**, *375*, 424–427; (b) Nogales, E.; Wolf, S. G.; Downing, K. H. *Nature* **1998**, *391*, 199–203; (c) Snyder, J. P.; Nettles, J. H.; Cornett, B.; Downing, K. H.; Nogales, E. *Proc. Natl. Acad. Sci. U.S.A.* **2001**, *98*, 5312–5316; (d) Löwe, J.; Li, H.; Downing, K. H.; Nogales, E. *J. Mol. Bio.* **2001**, *313*, 1045–1057; (e) Li, H.; DeRosier, D. J.; Nicholson, W. V.; Nogales, E.; Downing, K. H. *Structure* **2002**, *10*, 1317–1328.
- (11) Geney, R.; Sun, L.; Pera, P.; Bernacki, R. J.; Xia, S.; Horwitz, S. B.; Simmerling, C. L.; Ojima, I. *Chem. Biol.* **2005**, *12*, 339–348.
- (12) Alushin, G. M.; Lander, G. C.; Kellogg, E. H.; Zhang, R.; Baker, D.; Nogales, E. *Cell* **2014**, *157*, 1117–1129.
- (13) (a) Kelling, J.; Sullivan, K.; Wilson, L.; Jordan, M. A. *Cancer Res.* **2003**, *63*, 2794–2801; (b) Proudfoot, K. G.; Anderson, S. J.; Dave, S.; Bunning, A. R.; Sinha Roy, P.; Bera, A.; Gupta, M. L. *Cell Rep.* **2019**, *27*, 416–428.e4.
- (14) (a) Waters, J. C.; Chen, R.-H.; Murray, A. W.; Salmon, E. D. *J. Cell Biol.* **1998**, *141*, 1181–1191; (b) Magidson, V.; He, J.; Ault, J. G.; O’Connell, C. B.; Yang, N.; Tikhonenko, I.; McEwen, B. F.; Sui, H.; Khodjakov, A. *J. Cell Biol.* **2016**, *212*, 307–319.
- (15) Hornick, J. E.; Bader, J. R.; Tribble, E. K.; Trimble, K.; Breunig, J. S.; Halpin, E. S.; Vaughan, K. T.; Hinchcliffe, E. H. *Cell Motil. Cytoskeleton* **2008**, *65*, 595–613.
- (16) (a) Zasadil, L. M.; Andersen, K. A.; Yeum, D.; Rocque, G. B.; Wilke, L. G.; Tevaarwerk, A. J.; Raines, R. T.; Burkard, M. E.; Weaver, B. A. *Sci. Transl. Med.* **2014**, *6*, 229ra43–229ra43; (b) Weaver, B. A. *Mol. Biol. Cell* **2014**, *25*, 2677–2681.

- (17) Gelderblom, H.; Verweij, J.; Nooter, K.; Sparreboom, A. *Eur. J. Cancer* **2001**, *37*, 1590–1598.
- (18) Rivera, E. *Breast J.* **2010**, *16*, 252–263.
- (19) Ferlini, C.; Raspaglio, G.; Mozzetti, S.; Cicchillitti, L.; Filippetti, F.; Gallo, D.; Fattorusso, C.; Campiani, G.; Scambia, G. *Cancer Res.* **2005**, *65*, 2397–2405.
- (20) Orr, G. A.; Verdier-Pinard, P.; McDaid, H.; Horwitz, S. B. *Oncogene* **2003**, *22*, 7280–7295.
- (21) (a) Kamath, K.; Wilson, L.; Cabral, F.; Jordan, M. A. *J. Biol. Chem.* **2005**, *280*, 12902–12907; (b) Kavallaris, M.; Kuo, D. Y.; Burkhart, C. A.; Regl, D. L.; Norris, M. D.; Haber, M.; Horwitz, S. B. *J. Clin. Invest.* **1997**, *100*, 1282–1293.
- (22) Yang, C.-P. H.; Yap, E.-H.; Xiao, H.; Fiser, A.; Horwitz, S. B. *Proc. Natl. Acad. Sci. U.S.A.* **2016**, 201613286.
- (23) Chauvière, G.; Guénard, D.; Pascard, C.; Picot, F.; Potier, P.; Prangé, T. *J. Chem. Soc., Chem. Commun.* **1982**, 495–496.
- (24) Sharma, S.; Lagisetti, C.; Poliks, B.; Coates, R. M.; Kingston, D. G. I.; Bane, S. *Biochemistry* **2013**, *52*, 2328–2336.
- (25) Wang, M.; Cornett, B.; Nettles, J.; Liotta, D. C.; Snyder, J. P. *J. Org. Chem.* **2000**, *65*, 1059–1068.
- (26) Shigemori, H.; Kobayashi, J. *J. Nat. Prod.* **2004**, *67*, 245–256.
- (27) Kobayashi, J.; Inubushi, A.; Hosoyama, H.; Yoshida, N.; Sasaki, T.; Shigemori, H. *Tetrahedron* **1995**, *51*, 5971–5978.
- (28) Kobayashi, J.; Hosoyama, H.; Wang, X.-x.; Shigemori, H.; Koiso, Y.; Iwasaki, S.; Sasaki, T.; Naito, M.; Tsuruo, T. *Bioorg. Med. Chem. Lett.* **1997**, *7*, 393–398.
- (29) Liu, H.-S.; Gao, Y.-H.; Liu, L.-H.; Liu, W.; Shi, Q.-W.; Dong, M.; Suzuki, T.; Kiyota, H. *Biosci. Biotechnol. Biochem.* **2016**, *80*, 1883–1886.
- (30) Wang, L.; Bai, L.; Tokunaga, D.; Watanabe, Y.; Hasegawa, T.; Sakai, J.-i.; Tang, W.; Bai, Y.; Hirose, K.; Yamori, T.; Tomida, A.; Tsuruo, T.; Ando, M. *Journal of Wood Science* **2008**, *54*, 390–401.
- (31) Denis, J.-N.; Greene, A. E. *Nat. Prod. Lett.* **1996**, *8*, 27–32.
- (32) (a) Friesner, R. A.; Banks, J. L.; Murphy, R. B.; Halgren, T. A.; Klicic, J. J.; Mainz, D. T.; Repasky, M. P.; Knoll, E. H.; Shelley, M.; Perry, J. K.; Shaw, D. E.; Francis, P.; Shenkin, P. S. *J. Med. Chem.* **2004**, *47*, 1739–1749; (b) Halgren, T. A.; Murphy, R. B.; Friesner, R. A.; Beard, H. S.; Frye, L. L.; Pollard, W. T.; Banks, J. L. *J. Med. Chem.* **2004**, *47*, 1750–1759; (c) Friesner, R. A.; Murphy, R. B.; Repasky, M. P.; Frye, L. L.; Greenwood, J. R.; Halgren, T. A.; Sanschagrin, P. C.; Mainz, D. T. *J. Med. Chem.* **2006**, *49*, 6177–6196.
- (33) Sun, Z.-H.; Chen, Y.; Guo, Y.-Q.; Qiu, J.; Zhu, C.-G.; Jin, J.; Tang, G.-H.; Bu, X.-Z.; Yin, S. *Bioorg. Med. Chem. Lett.* **2015**, *25*, 1240–1243.

- (34) Croteau, R.; Ketchum, R. E. B.; Long, R. M.; Kaspera, R.; Wildung, M. R. *Phytochem. Rev.* **2006**, *5*, 75–97.
- (35) McElroy, C.; Jennewein, S. In *Biotechnology of Natural Products*, Schwab, W., Lange, B. M., Wüst, M., Eds.; Springer International Publishing: Cham, 2018, pp 145–185.
- (36) Guéritte-Voegelein, F.; Guénard, D.; Potier, P. *J. Nat. Prod.* **1987**, *50*, 9–18.
- (37) (a) Holton, R. A.; Somoza, C.; Kim, H. B.; Liang, F.; Biediger, R. J.; Boatman, P. D.; Shindo, M.; Smith, C. C.; Kim, S. *J. Am. Chem. Soc.* **1994**, *116*, 1597–1598; (b) Holton, R. A.; Kim, H. B.; Somoza, C.; Liang, F.; Biediger, R. J.; Boatman, P. D.; Shindo, M.; Smith, C. C.; Kim, S. *J. Am. Chem. Soc.* **1994**, *116*, 1599–1600.
- (38) (a) Wender, P. A. et al. *J. Am. Chem. Soc.* **1997**, *119*, 2755–2756; (b) Wender, P. A.; Badham, N. F.; Conway, S. P.; Floreancig, P. E.; Glass, T. E.; Houze, J. B.; Krauss, N. E.; Lee, D.; Marquess, D. G.; McGrane, P. L.; Meng, W.; Natchus, M. G.; Shuker, A. J.; Sutton, J. C.; Taylor, R. E. *J. Am. Chem. Soc.* **1997**, *119*, 2757–2758.
- (39) (a) Morihira, K.; Hara, R.; Kawahara, S.; Nishimori, T.; Nakamura, N.; Kusama, H.; Kuwajima, I. *J. Am. Chem. Soc.* **1998**, *120*, 12980–12981; (b) Kusama, H.; Hara, R.; Kawahara, S.; Nishimori, T.; Kashima, H.; Nakamura, N.; Morihira, K.; Kuwajima, I. *J. Am. Chem. Soc.* **2000**, *122*, 3811–3820.
- (40) Nicolaou, K. C.; Yang, Z.; Liu, J. J.; Ueno, H.; Nantermet, P. G.; Guy, R. K.; Claiborne, C. F.; Renaud, J.; Couladouros, E. A.; Paulvannan, K.; Sorensen, E. J. *Nature* **1994**, *367*, 630–634.
- (41) Danishefsky, S. J.; Masters, J. J.; Young, W. B.; Link, J. T.; Snyder, L. B.; Magee, T. V.; Jung, D. K.; Isaacs, R. C. A.; Bornmann, W. G.; Alaimo, C. A.; Coburn, C. A.; Di Grandi, M. J. *J. Am. Chem. Soc.* **1996**, *118*, 2843–2859.
- (42) Mukaiyama, T.; Shiina, I.; Iwadare, H.; Saitoh, M.; Nishimura, T.; Ohkawa, N.; Sakoh, H.; Nishimura, K.; Tani, Y.-i.; Hasegawa, M.; Yamada, K.; Saitoh, K. *Chem. Eur. J.* **1999**, *5*, 121–161.
- (43) (a) Fukaya, K. et al. *Org. Lett.* **2015**, *17*, 2570–2573; (b) Fukaya, K.; Kodama, K.; Tanaka, Y.; Yamazaki, H.; Sugai, T.; Yamaguchi, Y.; Watanabe, A.; Oishi, T.; Sato, T.; Chida, N. *Org. Lett.* **2015**, *17*, 2574–2577.
- (44) Doi, T.; Fuse, S.; Miyamoto, S.; Nakai, K.; Sasuga, D.; Takahashi, T. *Chem. Asian J.* **2006**, *1*, 370–383.
- (45) Hirai, S.; Utsugi, M.; Iwamoto, M.; Nakada, M. *Chem. Eur. J.* **2015**, *21*, 355–359.
- (46) (a) Kende, A. S.; Johnson, S.; Sanfilippo, P.; Hodges, J. C.; Jungheim, L. N. *J. Am. Chem. Soc.* **1986**, *108*, 3513–3515; (b) Swindell, C. S.; Patel, B. P. *J. Org. Chem.* **1990**, *55*, 3–5; (c) Kress, M. H.; Ruel, R.; Miller, W. H.; Kishi, Y. *Tetrahedron Lett.* **1993**, *34*, 5999–6002; (d) Rubenstein, S. M.; Williams, R. M. *J. Org. Chem.* **1995**, *60*, 7215–7223; (e) Guo, X.; Paquette, L. A. *J. Org. Chem.* **2005**, *70*, 315–320; (f) Mendoza, A.; Ishihara, Y.; Baran, P. S. *Nat. Chem.* **2012**, *4*, 21–25; (g) Ishihara, Y.; Mendoza, A.; Baran, P. S. *Tetrahedron* **2013**, *69*, 5685–5701; (h) Matoba, H.; Watanabe, T.; Nagatomo, M.; Inoue, M. *Org. Lett.* **2018**, *20*, 7554–7557.



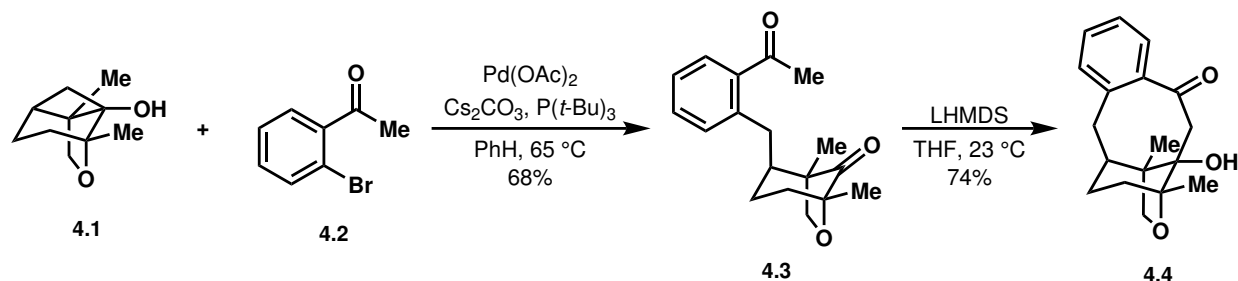
- (47) (a) Holton, R. A.; Juo, R. R.; Kim, H. B.; Williams, A. D.; Harusawa, S.; Lowenthal, R. E.; Yogai, S. *J. Am. Chem. Soc.* **1988**, *110*, 6558–6560; (b) Paquette, L. A.; Zhao, M. *J. Am. Chem. Soc.* **1998**, *120*, 5203–5212; (c) Paquette, L. A.; Wang, H.-L.; Su, Z.; Zhao, M. *J. Am. Chem. Soc.* **1998**, *120*, 5213–5225; (d) Hara, R.; Furukawa, T.; Horiguchi, Y.; Kuwajima, I. *J. Am. Chem. Soc.* **1996**, *118*, 9186–9187; (e) Wilde, N. C.; Isomura, M.; Mendoza, A.; Baran, P. S. *J. Am. Chem. Soc.* **2014**, *136*, 4909–4912; (f) Yuan, C.; Jin, Y.; Wilde, N. C.; Baran, P. S. *Angew. Chem. Int. Ed.* **2016**, *55*, 8280–8284; (g) Imamura, Y.; Yoshioka, S.; Nagatomo, M.; Inoue, M. *Angew. Chem. Int. Ed.* **2019**, *58*, 12159–12163.
- (48) Ishihara, Y.; Baran, P. S. *Synlett* **2010**, *2010*, 1733, 1733–1745.

# Chapter 4

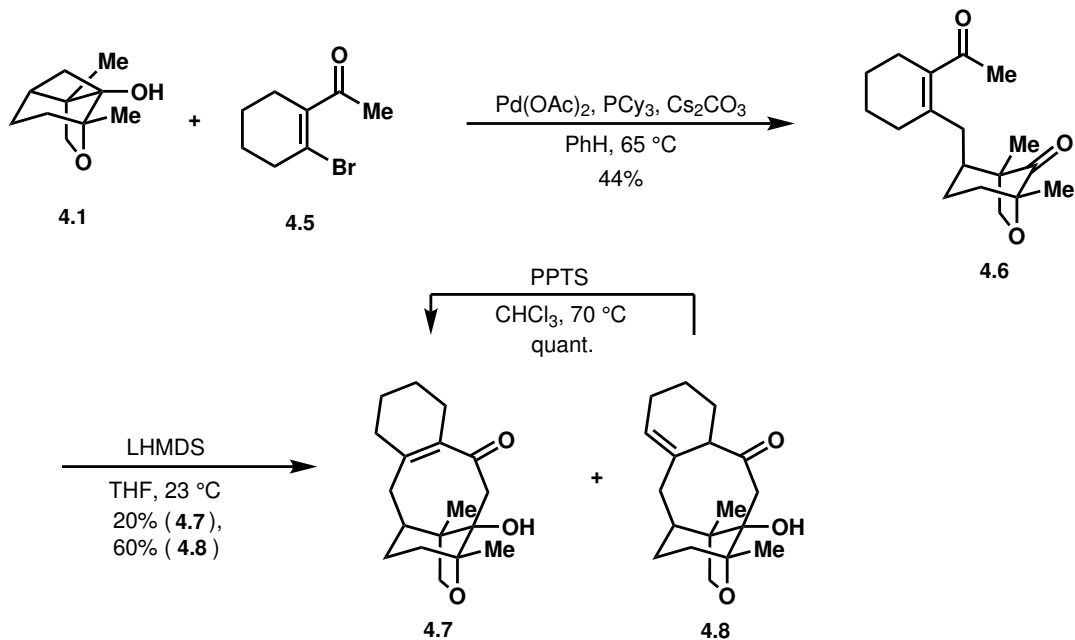
## Synthesis of a Highly Oxidized Tetracyclic Core of the Taxagifine-Like Natural Products

### 4.1 Prior Exploratory Studies and Retrosynthesis

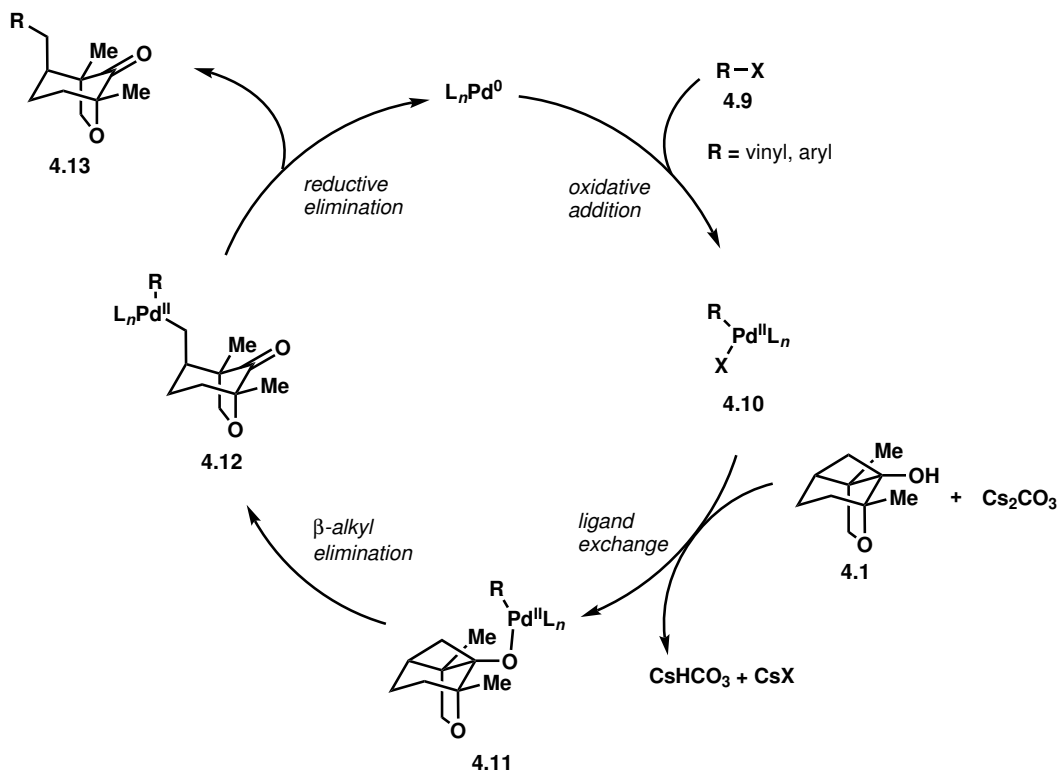
Prior to my efforts toward the taxagifine-like natural products, exploratory work toward the core of these natural products had been conducted. In 2015, building on Uemura's investigation of cyclobutanol arylation,<sup>1</sup> former members of the Sarpong group Dr. Kyle Owens, Dr. Manuel Weber, and Dr. Ahmad Masarwa reported a C–C cleavage/cross-coupling reaction of (*S*)-carvone-derived cyclobutanol **4.1**<sup>2a</sup> with aryl bromide **4.2** to yield methyl ketone-bearing cyclohexanone **4.3**; treatment of this methyl ketone with LHMDS then effected an aldol addition to deliver a simplified core of the taxagifine-like natural products (**4.4**, Scheme 4.1).<sup>3,4</sup> Subsequently, a former visiting scholar of the Sarpong group, Carolin Gerleve, investigated the cross-coupling of cyclobutanol **4.1** with cyclohexenyl electrophiles, including cyclohexenyl bromides, chlorides, and triflates. In particular, Carolin found that cyclobutanol **4.1** cross-coupled with cyclohexenyl bromide **4.5** to deliver methyl ketone **4.6**. Treatment of **4.6** with LHMDS yielded enone **4.7** and isomerized compound **4.8**, which could be converted to **4.7** under mildly acidic conditions (Scheme 4.2).



**Scheme 4.1:** Synthesis of a simplified core of the taxagifine-like natural products, utilizing an aryl bromide cross-coupling partner.



**Scheme 4.2:** Synthesis of a simplified core of the taxagifine-like natural products, utilizing a cyclohexenyl bromide cross-coupling partner.

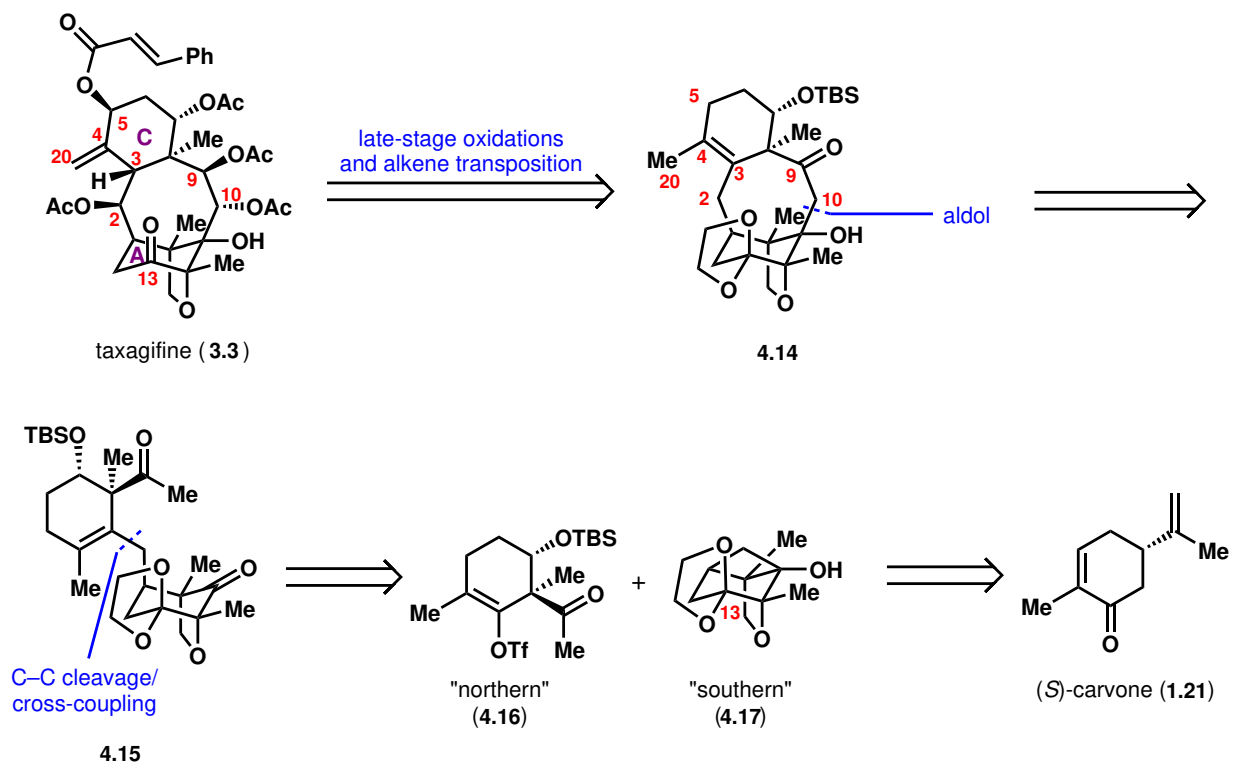


**Scheme 4.3:** Mechanism of the C–C cleavage/cross-coupling reaction.

Mechanistically, the cross-coupling of cyclobutanol **4.1** with a vinyl or aryl electrophile (**4.9**, Scheme 4.3) involves the initial oxidative addition of **4.9** into a Pd(0) species to yield Pd(II) species **4.10**; subsequent ligation with **4.1**, which yields Pd-alkoxide **4.11**, is followed by a strain-releasing  $\beta$ -alkyl elimination to generate alkyl-Pd intermediate **4.12**. Finally, reductive elimination affords cross-coupled product **4.13** and regenerates Pd(0).

While these initial studies validated that a C–C cleavage/cross-coupling/aldol sequence could be used as a method to construct the tetracyclic core of the taxagifine-like natural products, the cross-coupling of more complex fragments would be required in any potential synthesis of these natural products. To this end, my initial efforts on this project—which were carried out in concert with Dr. Benjamin Wyler—involved devising a retrosynthesis of the taxagifine-like natural products utilizing more complex cross-coupling partners. We imagined that early introduction of additional oxidation at C13 of A-ring precursor would obviate the need for a late-stage  $sp^3$  C–H oxidation of an unactivated position remote from possible directing groups (see Scheme 4.4 for numbering). In addition, we envisioned that a second coupling partner, which carries stereochemical information and bears all the core carbons found on the C-ring in the taxagifine-like natural products would minimize potentially difficult late-stage manipulations of the C-ring. With these ideas in mind, we proposed the retrosynthesis shown in Scheme 4.4.

We targeted taxagifine (**3.3**) as a representative member of the taxagifine-like natural products, and anticipated that a robust synthetic route to taxagifine would facilitate access

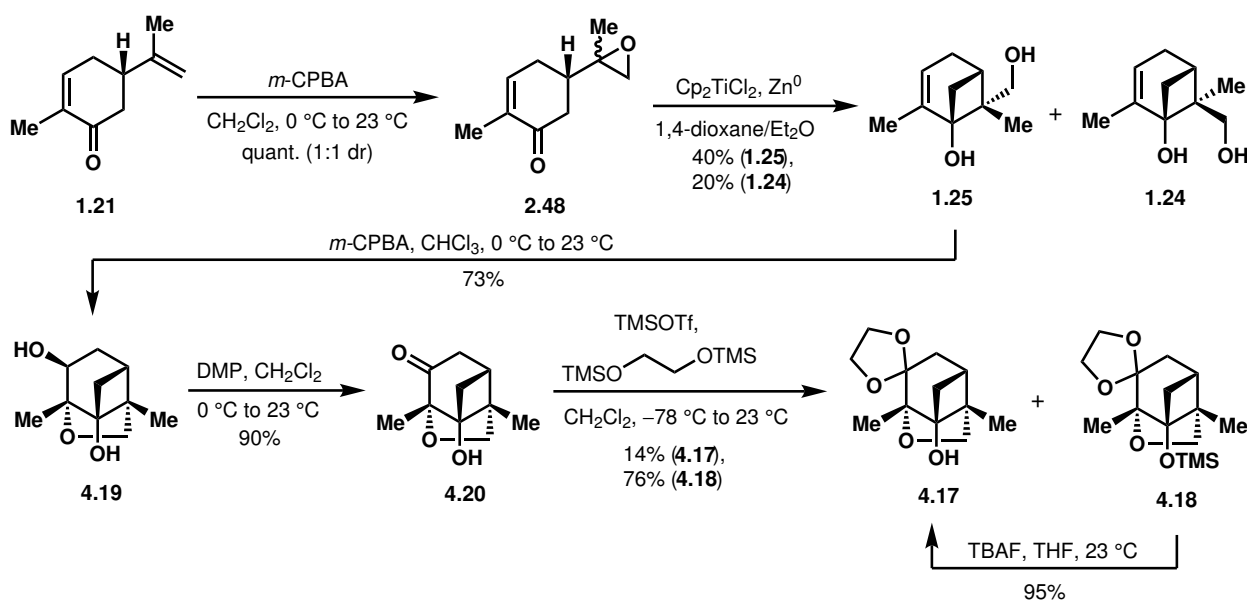


**Scheme 4.4:** Retrosynthetic plan for taxagifine utilizing complex coupling partners **4.16** and **4.17**.

to other taxagifine-like natural products, as well as derivatives thereof. We envisioned that taxagifine could be synthesized from tetracyclic core **4.14** via a series of late-stage oxidations at C2, C5, and C10. Strategic placement of functional groups was key to the conception of this stage of the retrosynthesis; we envisioned that the C3–C4 double bond would activate the C–H bonds at C2 and C5 towards oxidation, and that the carbonyl group at C9 would likewise activate the C–H bond at C10. Transposition of the tetrasubstituted C3–C4 double bond to the exocyclic C4–C20 position, with concomitant stereoselective placement of a hydrogen atom on the concave face of **4.14** at C3, would also be necessary. Tetracycle **4.14** could be constructed via an intramolecular aldol addition of methyl ketone **4.15**, which could, in turn, arise from a key C–C cleavage/cross-coupling reaction between “northern” coupling partner **4.16** and “southern” coupling partner **4.17**. Finally, we anticipated that each of these coupling partners could be synthesized from (*S*)-carvone.

## 4.2 Synthesis of Northern and Southern Coupling Partners

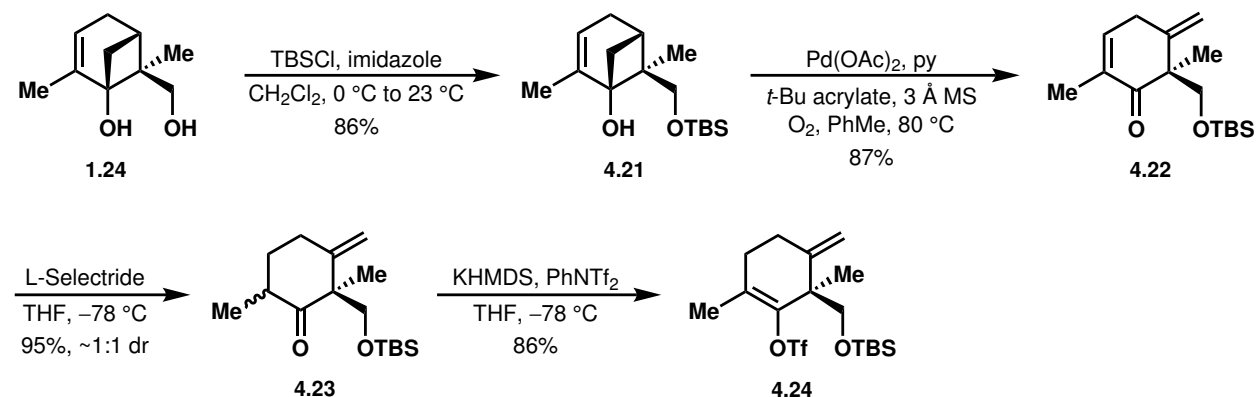
At this point, we set out to synthesize the northern and southern coupling partners. Beginning from (*S*)-carvone, we accessed known cyclobutanols **1.25** and **1.24** by epoxidation of the 1,1-disubstituted double bond, followed by Ti(III)-mediated reductive epoxide opening/radical 4-*exo-trig* cyclization, using a procedure adapted from Bermejo et al. (Scheme 4.5).<sup>2</sup> Epoxidation of the minor cyclobutanol diastereomer (**1.25**) with *m*-CPBA was followed by nucleophilic displacement of the epoxide by the pendant primary hydroxy group, yielding diol **4.19**<sup>5</sup>; subsequent Dess–Martin oxidation<sup>6</sup> of the secondary hydroxy group afforded ketone **4.20**. Finally, Noyori ketalization<sup>7</sup> delivered southern coupling partner **4.17** and silylated compound **4.18**, the silyl ether of which was readily cleaved to generate



Scheme 4.5: Synthesis of southern coupling partner **4.17**.

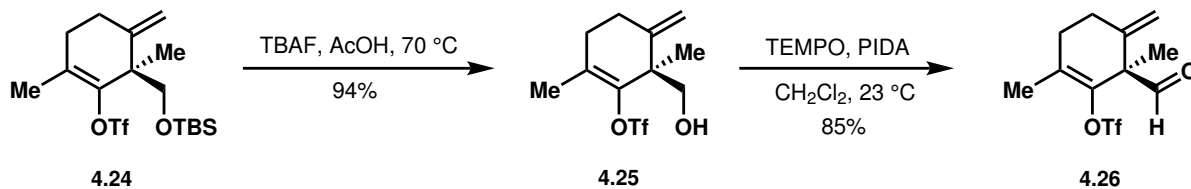
#### 4.17.

We continued with the synthesis of the northern coupling partner. The primary hydroxy group of cyclobutanol **1.24**—the major diastereomer from the Ti(III)-mediated reaction in Scheme 4.5—was first protected as TBS ether **4.21**. Subsequent subjection to conditions for Pd-catalyzed oxidative C–C cleavage<sup>1c</sup> yielded enone compound **4.22** (Scheme 4.6). Conjugate reduction with L-Selectride® afforded cyclohexanone **4.23** as an inconsequential mixture of diastereomers, which were then converted to vinyl triflate **4.24** under strongly basic conditions. Notably, the order and rate of addition strongly impacted the outcome of the triflation; it was found that rapid addition of KHMDS to a solution of PhNTf<sub>2</sub> and cyclohexanone **4.23** produced the product in the best yields. In contrast, treatment of the substrate first with KHMDS and then with PhNTf<sub>2</sub> consistently led to incomplete conversion. In addition, the conjugate reduction/triflation sequence, when performed in one pot, was not reproducible on scale (i.e., >500 mg). Taken together, these findings suggest that the reaction outcome depends on the counteraction to the generated enolate (boron enolates were likely formed under the one-pot conditions, instead of potassium enolates), on the reaction temperature (greater exotherms accompany more rapid addition of KHMDS), and/or on the concentrations of the reactive species throughout the reaction (higher concentrations of PhNTf<sub>2</sub> are present during the initial generation of the enolate under the successful reaction conditions).



**Scheme 4.6:** Synthesis of vinyl triflate **4.24** en route to the northern coupling partner.

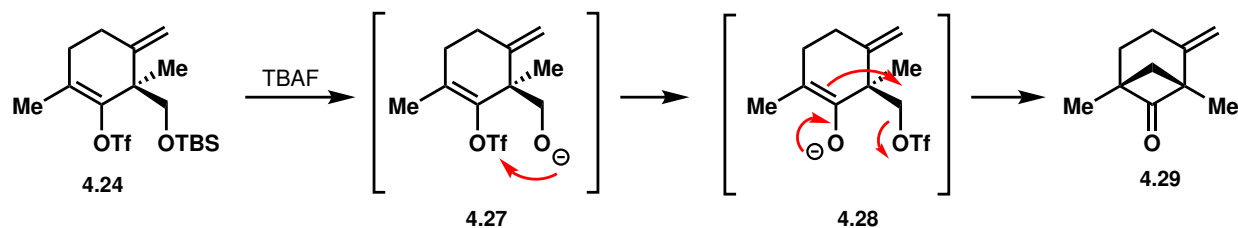
To obtain material to study the cross-coupling studies in a model system, we targeted aldehyde **4.26** (Scheme 4.7). Cleavage of the silyl ether with TBAF under mildly acidic conditions yielded primary alcohol **4.25**, which was oxidized to afford aldehyde **4.26**.<sup>8</sup>



**Scheme 4.7:** Synthesis of aldehyde **4.26** as model northern coupling partner.

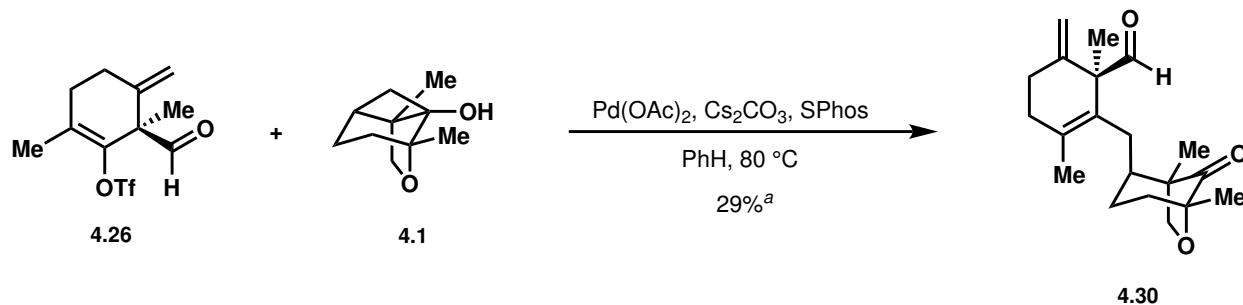
It should be noted that acetic acid was critical to the success of the desilylation reaction

to give alcohol **4.25**. Simply treating **4.25** with TBAF at 23 °C exclusively delivered an undesired product, whose apparent volatility precluded thorough characterization. Nevertheless, we speculate that without added acid, alkoxide **4.27** was generated initially, then converted to enolate **4.28** after transfer of the triflyl group; intramolecular nucleophilic displacement of the triflate moiety would then yield ketone **4.29** (Scheme 4.8). This hypothesis is in accordance with studies by Tanino et al.,<sup>9</sup> who reported the synthesis of [3.1.1]bicyclic ketones from cyclohexenyl triflates bearing a TBS-protected hydroxymethyl group, similar to **4.24**. The addition of acetic acid presumably prevents triflyl transfer.



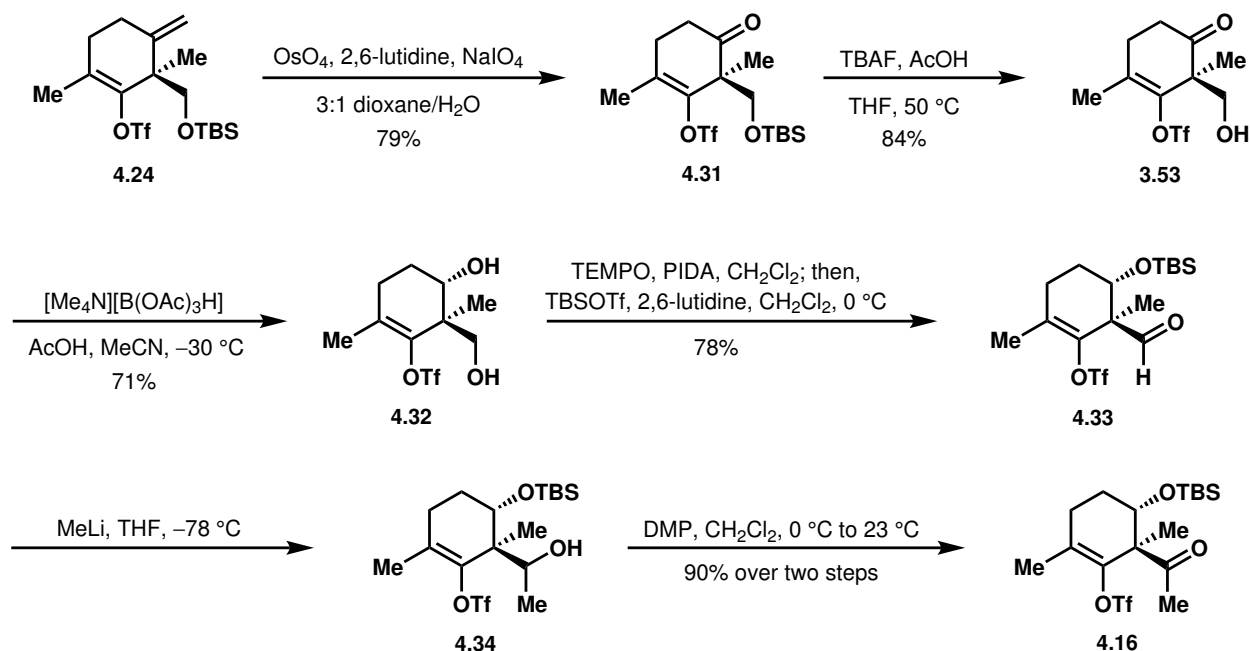
**Scheme 4.8:** Possible reaction mechanism for the undesired reaction observed upon simple treatment of **4.24** with TBAF.

With aldehyde **4.26** in hand, and lacking access to sufficient quantities of C13-oxidized southern coupling partner **4.17**, we attempted to cross-coupling it with model southern coupling partner **4.1**. We were gratified to observe formation of the desired cross-coupled product **4.30**, albeit in 29% yield by <sup>1</sup>H NMR.



**Scheme 4.9:** Cross-coupling of model northern coupling partner **4.26** with model southern coupling partner **4.1**. <sup>a</sup><sup>1</sup>H NMR yield with mesitylene as an internal standard.

Having shown that a complex cyclohexenyl triflate can serve as an electrophile in the key cross-coupling reaction, We then continued the synthesis of the northern coupling partner **4.16** from TBS ether **4.24** (Scheme 4.10). Lemieux–Johnson oxidative cleavage<sup>10</sup> of the *exo*-methylene with 2,6-lutidine as an additive<sup>11</sup> yielded ketone **4.31**, which was treated with TBAF and acetic acid to afford primary alcohol **3.53**. Evans–Saksena reduction<sup>12</sup> produced diol **4.32** as a single diastereomer. Selective oxidation of the primary hydroxy group to the carbonyl<sup>8</sup> and subsequent protection of the remaining secondary hydroxy group as a TBS ether in the same pot yielded aldehyde **4.33**. Finally, nucleophilic addition of methyl lithium to the aldehyde and Dess–Martin oxidation<sup>6</sup> of the resultant alcohol (**4.34**) yielded the northern coupling partner (**4.16**).



Scheme 4.10: Completion of synthesis of northern coupling partner **4.16**.

### 4.3 Cross-Coupling Studies and Synthesis of Tetracyclic Cores

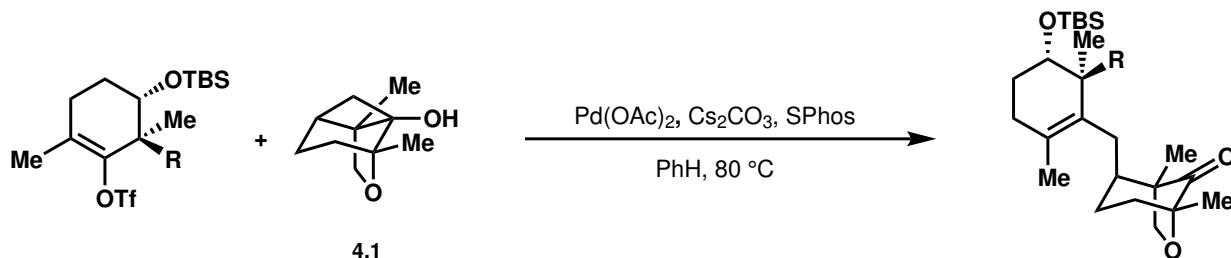
With **4.16** in hand, we commenced with studying the cross-coupling of **4.16** with model southern coupling partner **4.1** (Table 4.1). Upon subjection of **4.16** and **4.1** to the cross-coupling conditions, we did not observe formation of desired product **4.15**. The majority of cyclobutanol **4.1** was recovered; however, the vinyl triflate had been converted to  $\alpha$ -triflyl ketone **34.35**. Acting under the assumption that this was simply a base-mediated transformation, we attempted the cross-coupling with alternative inorganic bases  $\text{NaHCO}_3$  and  $\text{K}_3\text{PO}_4$ , but no conversion was observed under these conditions. Given the challenges associated with the coupling of **4.16**, we began to investigate the cross-coupling of alternative candidate northern coupling partners, which contained a pendant two-carbon unit, but lacked acidic  $\alpha$ -protons.

The alternative northern coupling partners **4.39** were each synthesized in one step from either methyl ketone **4.16**, secondary alcohol **4.34**, or aldehyde **4.33** under standard reaction conditions (see experimental methods and procedures for details). Subjection of silyl enol ether **4.39a** to the cross-coupling reaction conditions yielded only  $\alpha$ -triflyl ketone **4.35** (entry 1, Table 4.1). Protected secondary alcohols **4.39b** and **4.39c** gave only cyclohexene products, which were indicative of  $\beta$ -hydride elimination (*vide infra*), while TMS-protected secondary alcohol **4.39d** was desilylated to secondary alcohol **4.34**, which was subsequently oxidized to methyl ketone **4.16**. In contrast, cross-coupling using vinyl group-bearing coupling partner **4.39e** yielded 34% of the desired product (**4.40e**) by  $^1\text{H}$  NMR. Ethynyl group-bearing coupling partner **4.39f** instead appeared to decompose under the reaction conditions.

Upon the successful coupling of vinyl group-bearing compound **4.39e** with **4.1**, we began

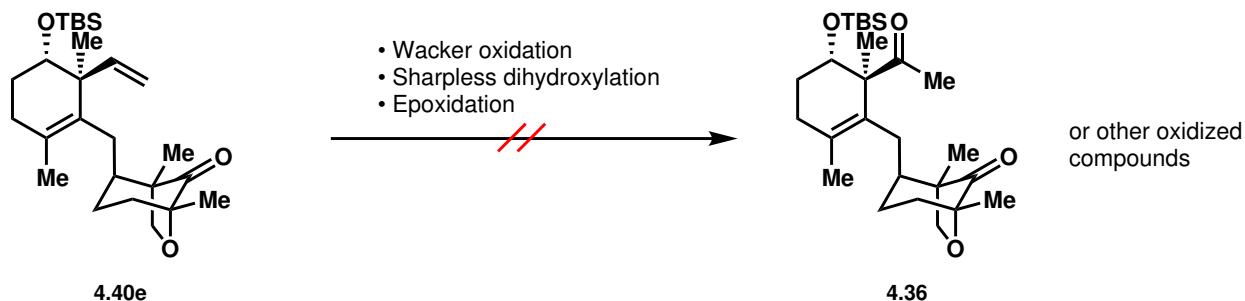


**Table 4.1:** Attempts at cross-coupling model southern coupling partner **4.1** with alternative northern coupling partners with pendant two-carbon units.  $^1\text{H}$  NMR yield with mesitylene as an internal standard.



Entry	R	Vinyl triflate	Cross-coupled product	Results
1		4.16	4.36	 (4.35)
2		4.39a	4.40a	4.35
3		4.39b (~1:1 dr)	4.40b	 (4.37)
4		4.39c (~1:1 dr)	4.40c	 (4.38)
5		4.39d (~1:1 dr)	4.40d	4.34 and 4.16
6		4.39e	4.40e	34% of 4.40e <sup>a</sup>
7		4.39f	4.40f	Decomposition of vinyl triflate

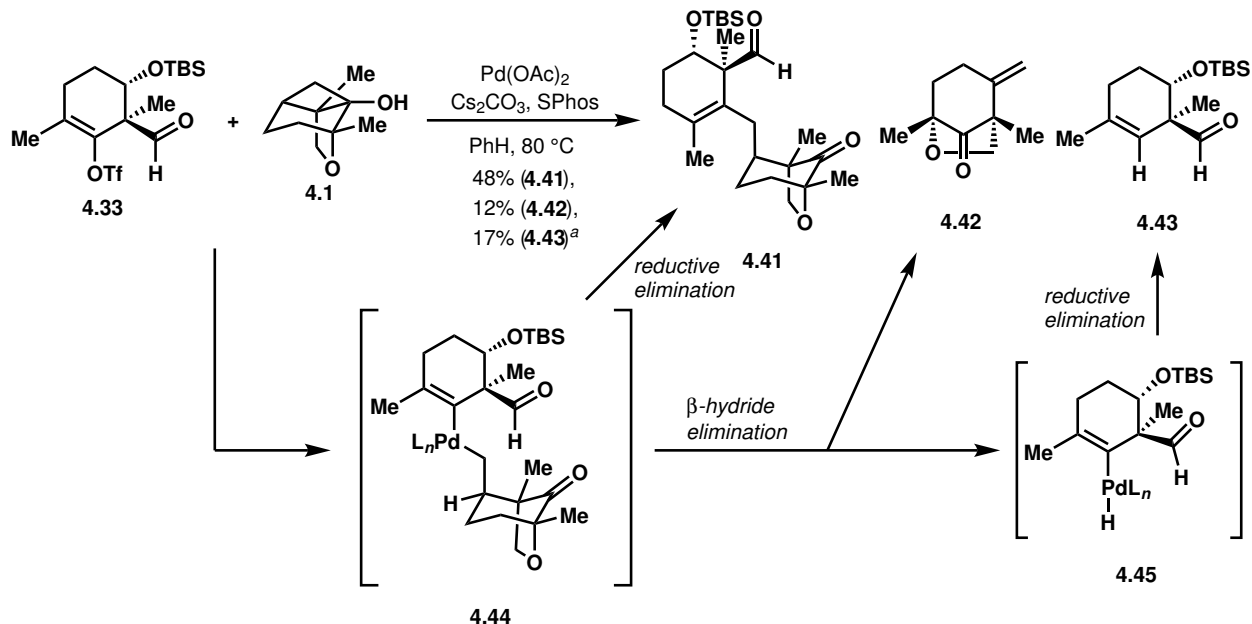
to investigate oxidation of the terminal alkene to the methyl ketone (**4.36**), which would be a suitable substrate for aldol cyclization (Scheme 4.11). Unfortunately, under any conditions investigated for Wacker oxidation, none of the methyl ketone was observed; in one instance, the isomeric aldehyde was observed instead. We were also unable to functionalize the alkene using alternative oxidation strategies (i.e., Sharpless dihydroxylation<sup>13</sup> or epoxidation), perhaps due to the demanding steric environment.



1

**Scheme 4.11:** Attempts to oxidize the vinyl group of **4.40e**.

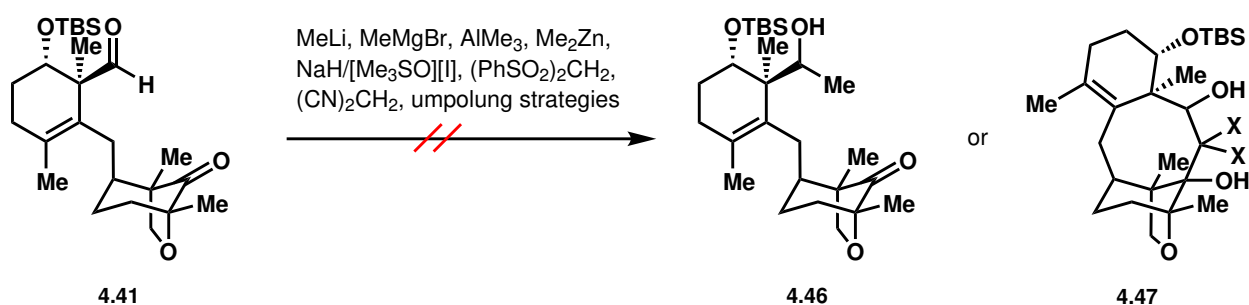
Given difficulties in cross-coupling with a northern coupling partner that bears a pendant two-carbon unit, we explored the possibility of using aldehyde **4.33** as a cross-coupling partner and introducing an additional carbon atom later. Reaction of aldehyde **4.33** with model southern coupling partner **4.1** afforded cross-coupled product **4.41** in 48% yield (Scheme 4.12). The major side products included cyclohexanone **4.42** and cyclohexene **4.43**, both of which presumably arise from  $\beta$ -hydride elimination from alkyl-Pd intermediate **4.44**.



**Scheme 4.12:** Cross-coupling between aldehyde **4.33** and model southern coupling partner **4.1**. <sup>a</sup><sup>1</sup>H NMR yields with mesitylene as an internal standard.

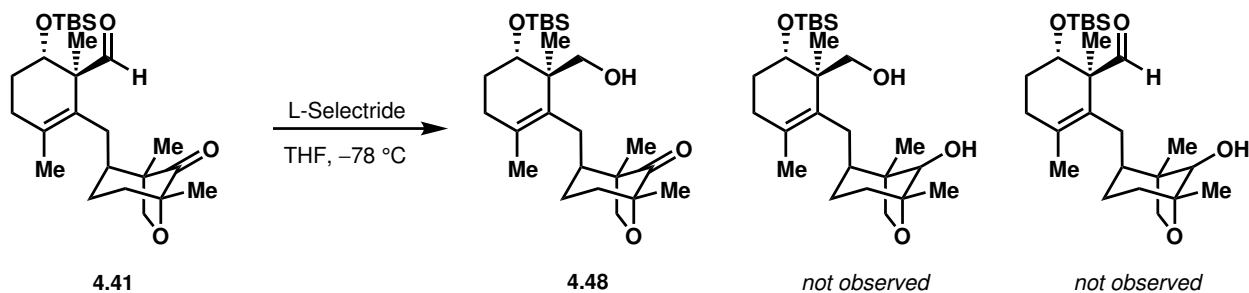
After extensive optimization, including screening electron-withdrawing ligands (*vide infra*), we were unable to increase either the ratio of the desired cross-coupled product to  $\beta$ -hydride elimination products, or the overall yield of the reaction (see Table S4.1, Section 4.7.3 for more details).

With aldehyde **4.41** in hand, we examined methods to install an additional one-carbon unit. Unfortunately, nucleophilic addition of MeLi to **4.41** was non-selective with respect to the aldehyde and the A-ring ketone groups, delivering similar quantities of the desired aldehyde addition product (**4.46**), a ketone addition product, and a double addition product (Scheme 4.13). Addition of other one-carbon nucleophiles—such as MeMgBr, AlMe<sub>3</sub>, Me<sub>2</sub>Zn, and TMSCHN<sub>2</sub><sup>14</sup>—also failed to yield the desired product; Corey–Chaykovsky epoxidation was selective for the A-ring ketone group. Efforts to add a methylene dianion surrogate, such as bis(phenylsulfonyl)methane or malononitrile, which would undergo nucleophilic addition to both the aldehyde and the A-ring ketone groups to forge the B-ring in one pot (i.e., to a compound of the type **4.47**), failed to convert the starting material. Umpolung strategies to install the extra carbon as a methyl electrophile (e.g., via conversion of the aldehyde to the 1,3-dithiane or the TMS-protected cyanhydrin) were similarly unfruitful.



**Scheme 4.13:** Attempted addition of a one-carbon unit to aldehyde **4.41**.

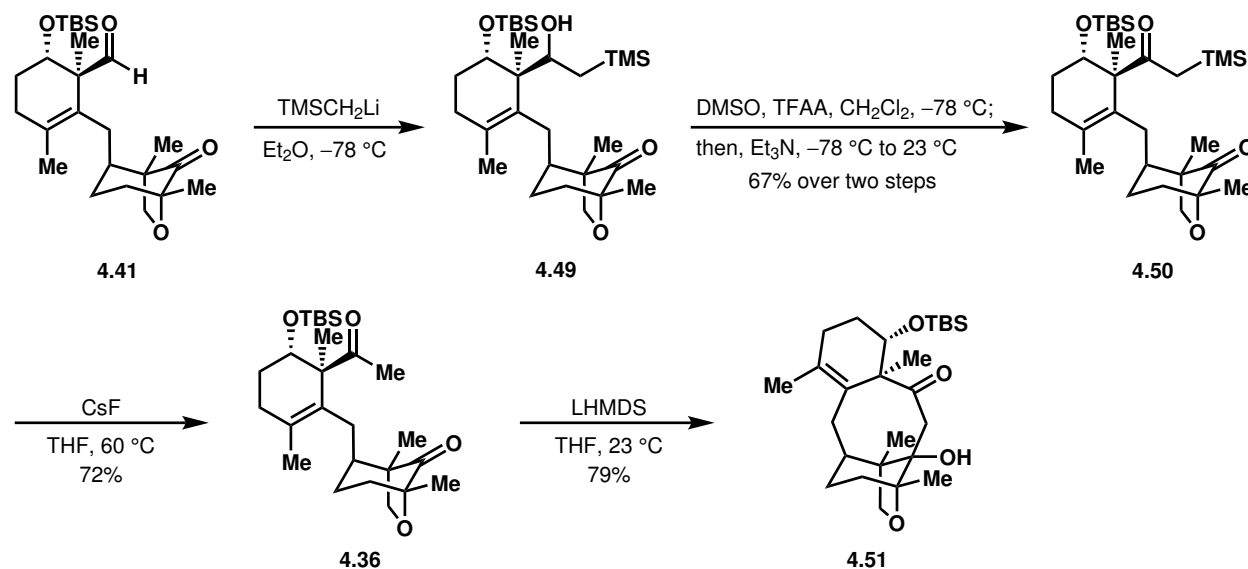
In the course of these studies, we discovered that L-Selectride® selectively reduced the aldehyde carbonyl of **4.41** to give alcohol **4.48** as a single chemoisomer (Scheme 4.14). We therefore hypothesized that sterically demanding nucleophiles might, in general, react selectively with the relatively more accessible aldehyde. Indeed, TMSCH<sub>2</sub>Li displayed increased selectivity for aldehyde addition relative to MeLi (Scheme 4.15). Upon solvent screening, we determined that replacing THF with Et<sub>2</sub>O further improved the selectivity for aldehyde addition. Finally, the rate of reagent addition was found to be important as well, with faster



**Scheme 4.14:** Chemoselective reduction of aldehyde **4.41**.

rates of addition giving higher levels of conversion. Ultimately, while results varied run-to-run, we were able to consistently achieve selectivities of ~2.5–4:1 of aldehyde addition to ketone addition and double addition products, at conversions of ~80%.

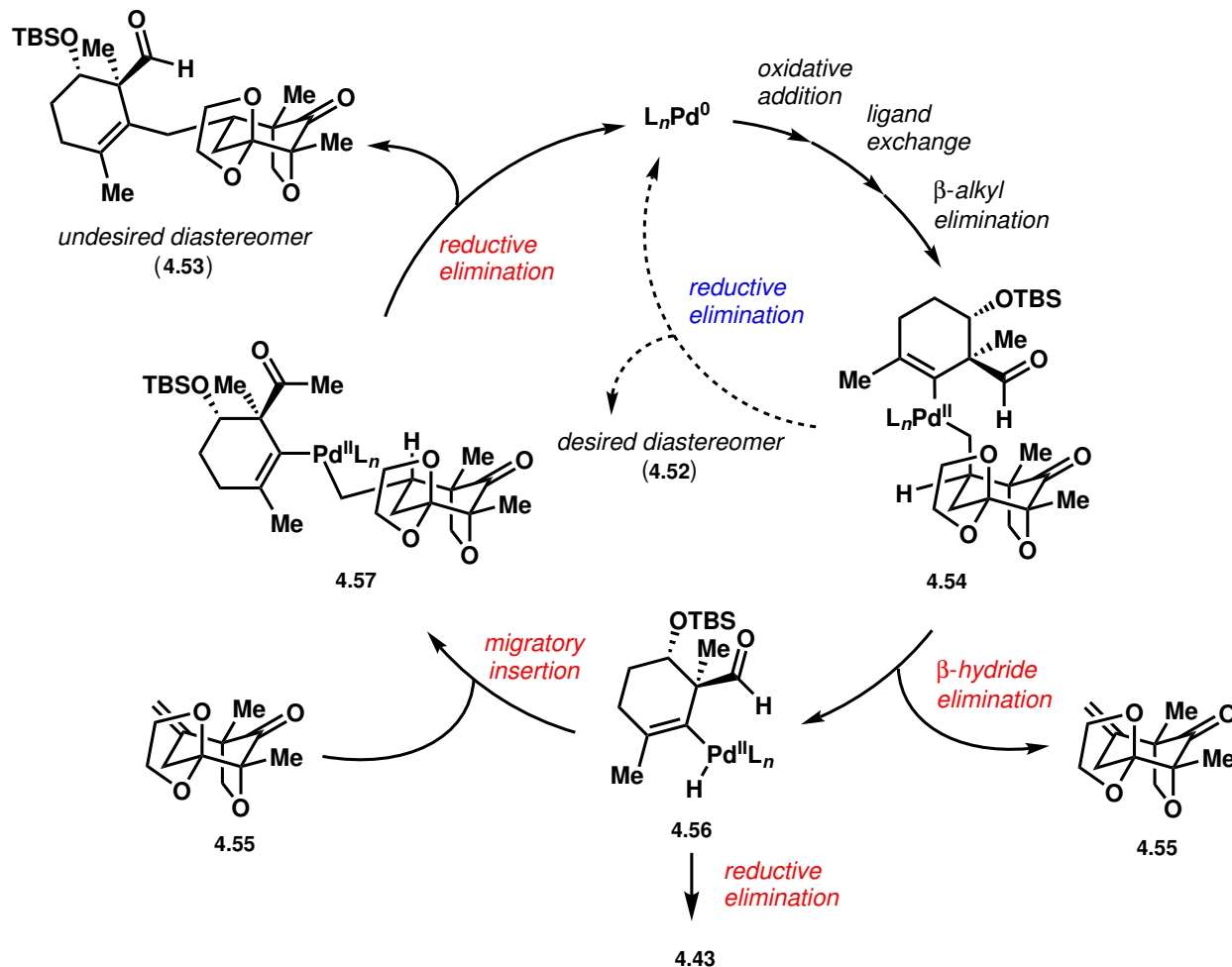
While the sterically demanding environment of the secondary hydroxy group of **4.49** rendered initial attempts at oxidation unsuccessful, we were ultimately able to efficiently synthesize ketone **4.50** via Omura–Sharma–Swern oxidation.<sup>15</sup> Subsequently, we selectively cleaved the trimethylsilyl group with CsF, then treated the resultant methyl ketone **4.36** with LHMDS to deliver model tetracyclic core **4.51**, thereby demonstrating the success of aldol cyclization as a method to forge the B-ring in a system with a more complex C-ring.



**Scheme 4.15:** Synthesis of model tetracyclic core **4.51**.

We then turned our attention to the synthesis of a more complex tetracyclic core **4.14** containing oxidation at C13, anticipating that lessons learned from our model studies synthesizing tetracyclic core **4.51** would be applicable to the synthesis of **4.14**. Synthesis of **4.14** would first involve the cross-coupling of northern coupling partner **4.33** with a more highly oxidized southern coupling partner (**4.17**). Intriguingly, attempted cross-coupling of **4.33** with **4.17** using the conditions found to be optimal on the model system delivered exclusively cross-coupled product **4.53**, which is epimeric at C1 with respect to desired product **4.52** (entry 1, Table 4.2).

Mechanistically, the formation of undesired diastereomer **4.53** may be explained by considering the fate of alkyl-Pd intermediate **4.54** (Scheme 4.16). Reductive elimination would afford the desired diastereomer **4.52**, while  $\beta$ -hydride elimination of alkyl-Pd species **4.54** would generate cyclohexanone **4.55** and Pd-hydride species **4.56**. Reductive elimination of **4.56** would deliver cyclohexene **4.43**; alternatively, diastereoselective insertion of the *exo*-methylene of cyclohexanone **4.55** into the Pd-hydride would yield alkyl-Pd species **4.57**, which is epimeric at C1 compared to alkylpalladium species **4.54**. Reductive elimination from **4.54** would afford undesired diastereomer **4.53**. Cyclohexanone **4.55** and cyclohexene **4.43** were observed in the crude reaction mixture, providing further evidence that alkylpalladium species **4.54** predominantly underwent  $\beta$ -hydride elimination, rather than the desired



**Scheme 4.16:** Mechanistic proposal for the formation of undesired diastereomer **4.53**.

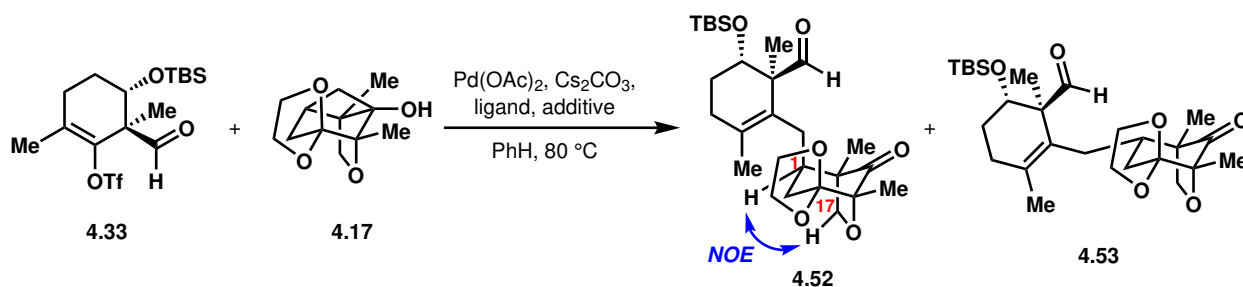
reductive elimination. We speculate that the decreased propensity for alkyl-Pd intermediate **4.54** to undergo reductive elimination—relative to the analogous intermediate generated upon cross-coupling with model southern coupling partner **4.1**—may be attributed to the presence of the ketal group, which would decrease electron density on the ligated A-ring.

On the basis of the proposed mechanism for formation of **4.53**, we hypothesized that the reaction outcome could be controlled by tuning the steric and electronic properties of the metal complex such that reductive elimination from alkyl-Pd species **4.54** would be more favorable than  $\beta$ -hydride elimination. Specifically, we imagined that the formation of a more electron-deficient metal complex would be beneficial, as this tends to increase the rate of reductive elimination and decrease the rate of  $\beta$ -hydride elimination.<sup>16</sup> Accordingly, we investigated electron-withdrawing ligands and additives.

We quickly identified  $AsPh_3$  as a ligand that provided some amount of the desired diastereomer, albeit with poor diastereoselectivity and overall yield. The identity of the product was confirmed by an NOE correlation between the methine proton at C1 and a methylene proton at C17 (entry 2, Table 4.2). The improved effectiveness of  $AsPh_3$  compared to more conventional phosphine ligands may be attributed to its poorer  $\sigma$ -donicity.<sup>17</sup> Consistent with

AsPh<sub>3</sub>-ligated Pd complexes being relatively electron-deficient, reactions with AsPh<sub>3</sub> exhibited low levels of conversion, presumably as a result of slow rates of oxidative addition; increasing the catalyst and ligand loading restored high levels of conversion and increased overall yield (entry 3). We next screened additives, cognizant of previous reports that 1,4-benzoquinone promotes reductive elimination.<sup>18</sup> Indeed, the addition of 1,4-benzoquinone radically improved diastereoselectivity and overall yield (entry 4). Interestingly, while more electron-deficient and/or more sterically hindered benzoquinones typically provided higher diastereoselectivity, overall yields did not improve (entries 5–10). Using the optimized conditions that employed AsPh<sub>3</sub> and 1,4-benzoquinone, we were able to perform the cross-coupling reaction on 1.5 g scale, observing increased yield and diastereoselectivity (entry 11) relative to the test reaction (entry 4). Notably, it was important to use rigorously degassed benzene to achieve high yields; trace amounts of oxygen were detrimental to the reaction.

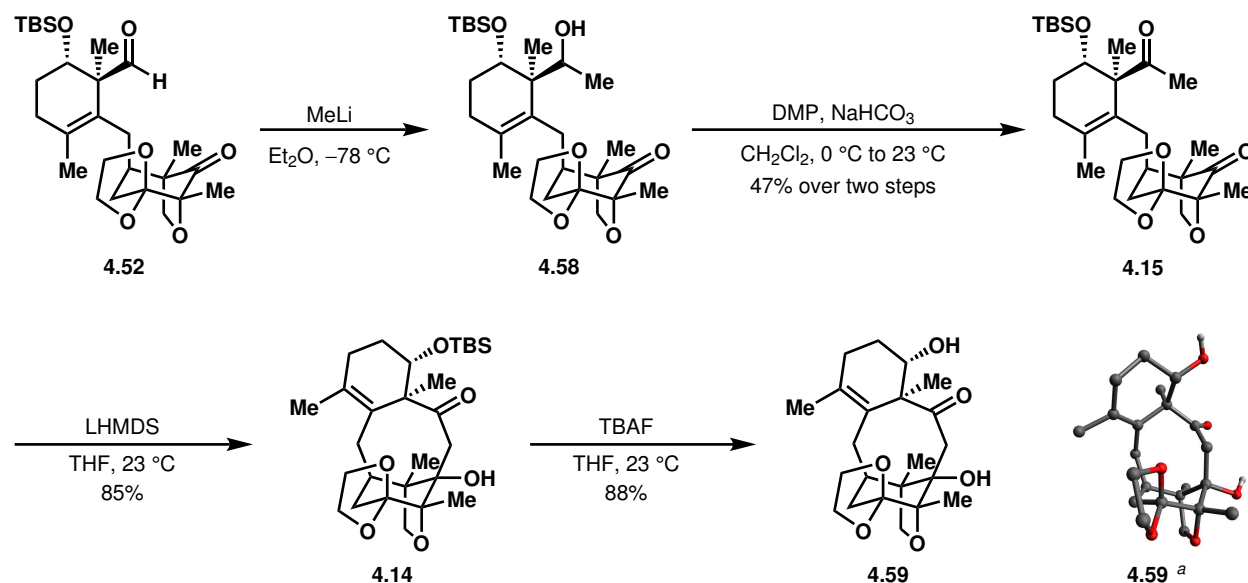
**Table 4.2:** Optimization of the cross-coupling of northern coupling partner **4.33** with more oxidized southern coupling partner **4.17**. <sup>a</sup><sup>1</sup>H NMR yield with mesitylene as an internal standard, based on the limiting coupling partner (**4.17**). <sup>b</sup>ND = not determined. <sup>c</sup>On 1.5 g scale, with respect to **4.33**. <sup>d</sup>Isolated yield.



Entry	Catalyst (mol %)	Ligand (mol %)	Additive (mol %)	dr ( <b>4.52</b> : <b>4.53</b> )	<sup>1</sup> H NMR yield ( <b>4.52</b> ) <sup>a</sup>
1	Pd(OAc) <sub>2</sub> (10%)	SPhos (20%)	—	0 : 100	0%
2	Pd(OAc) <sub>2</sub> (10%)	AsPh <sub>3</sub> (20%)	—	28 : 72	8%
3	Pd(OAc) <sub>2</sub> (20%)	AsPh <sub>3</sub> (50%)	—	30 : 70	19%
4	Pd(OAc) <sub>2</sub> (20%)	AsPh <sub>3</sub> (50%)	1,4-benzoquinone (20%)	85 : 15	57%
5	Pd(OAc) <sub>2</sub> (20%)	AsPh <sub>3</sub> (50%)	tetrafluorobenzoquinone (20%)	95 : 5	48%
6	Pd(OAc) <sub>2</sub> (20%)	AsPh <sub>3</sub> (50%)	chloranil (20%)	96 : 4	47%
7	Pd(OAc) <sub>2</sub> (20%)	AsPh <sub>3</sub> (50%)	bromanil (20%)	94 : 6	40%
8	Pd(OAc) <sub>2</sub> (20%)	AsPh <sub>3</sub> (50%)	DDQ (20%)	96 : 4	49%
9	Pd(OAc) <sub>2</sub> (20%)	AsPh <sub>3</sub> (50%)	2,6-dimethylbenzoquinone (20%)	96 : 4	54%
10	Pd(OAc) <sub>2</sub> (20%)	AsPh <sub>3</sub> (50%)	2,6-di- <i>t</i> -butylbenzoquinone (20%)	ND <sup>b</sup>	15%
11 <sup>c</sup>	Pd(OAc) <sub>2</sub> (20%)	AsPh <sub>3</sub> (50%)	1,4-benzoquinone (20%)	>95 : 5	68% <sup>d</sup>

With the desired cross-coupling product in hand, we then investigated the addition of a one-carbon unit selectively to the aldehyde. While this task proved challenging on the model system, we were gratified to find that MeLi could be added selectively to the aldehyde of **4.52**, with typical selectivities of ~7–8.5:1 of aldehyde-selective addition to ketone-selective and double addition products (Scheme 4.17). As with the addition of TMSCH<sub>2</sub>Li to model

system **4.41**, diethyl ether was preferable to THF as a solvent, and controlling the rate of addition was important to maximize conversion while limiting non-selective addition. We attribute the added ease with which chemoselectivity could be achieved in this system to the presence of the C13 ketal, the axial oxygen of which would engender a 1,3-diaxial interaction with nucleophiles approaching the A-ring ketone from the  $\beta$ -face. Dess–Martin oxidation of the secondary alcohol provided methyl ketone **4.15**, after which treatment with LHMDS effected the aldol cyclization to yield **4.14**, completing the synthesis of a highly oxidized tetracyclic core of the taxagifine-like natural products. Remarkably, this aldol cyclization proceeds despite the sterically demanding environment on the A-ring, characterized by the four consecutive tetrasubstituted carbons in the aldol product. The structure of **4.14** was confirmed by X-ray crystallographic analysis following cleavage of the TBS ether.



**Scheme 4.17:** Synthesis of tetracyclic core **4.14**. <sup>a</sup>X-ray crystal structure of **4.59**.

## 4.4 Alternative Strategies for B-Ring Closure

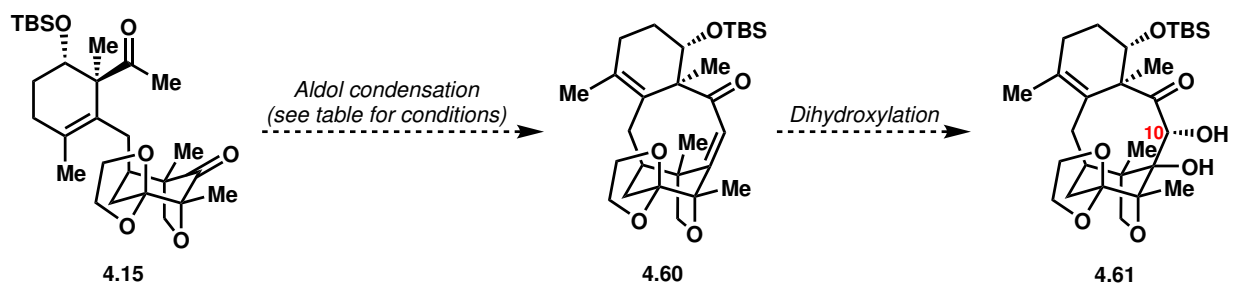
While the described synthetic route to **4.14** provided expedient access to the tetracyclic core of the taxagifine-like natural products, we imagined that alternative modes of B-ring closure might facilitate the installation of oxidation at C10 (see **4.61** in Table 4.3 for numbering) required for the natural product. These alternative modes of B-ring closure became especially attractive to us in light of the challenges encountered in oxidizing at C10 after aldol cyclization (see Section 5.1).

### 4.4.1 Aldol Condensation

We first investigated an aldol condensation toward **4.60**, which, after dihydroxylation, would yield C10-oxidized compound **4.61**. As a result of the highly caged nature of the tetracyclic enone, we expected that the dihydroxylation step would exclusively provide the desired

stereoisomer (**4.61**), which would be formed by approach of the dihydroxylation reagent from the convex face. However, we were unable to effect aldol condensation with *t*-BuOK or Triton B as bases at elevated temperatures (entries 1 and 2, Table 4.3). Suspecting that the lithium counteraction was important for successful cyclization—as had been demonstrated in the synthesis of model tetracyclic core **4.51**, and as had been noted by Weber et al. in the synthesis of model tetracyclic core **4.4**<sup>3</sup>—we attempted the aldol condensation with LiOMe as the base, achieving similar results (entry 3). Finally, we attempted aldol cyclization with LHMDS, followed by addition of Burgess reagent or MsCl in the same pot; these conditions yielded multiple products with only minor quantities of the desired enone (entries 4 and 5).

**Table 4.3:** Attempted aldol condensations from methyl ketone **4.15**.



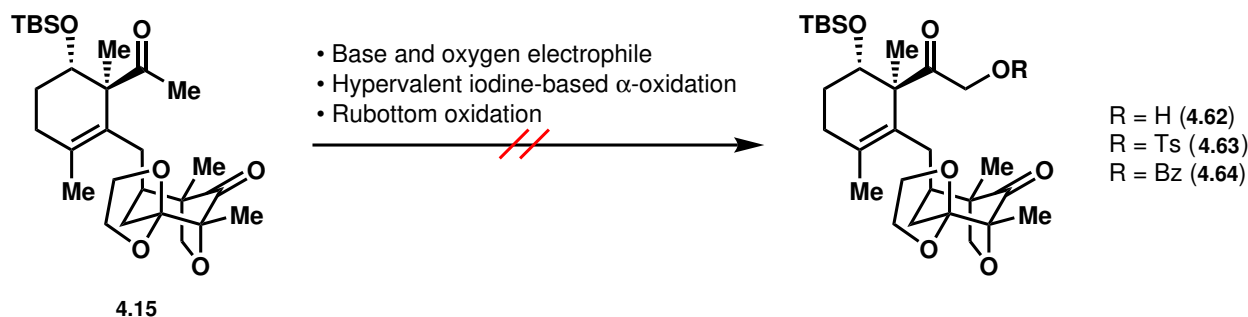
Entry	Conditions	Results
1	<i>t</i> -BuOK, <i>t</i> -BuOH, 80 °C, 17 h	No conversion
2	Triton B, MeOH, 65 °C, 16 h	No conversion
3	LiOMe, MeOH, 65 °C, 10 h	No conversion
4	LHMDS, THF, 23 °C, 4 h; then, Burgess reagent, 65 °C, 1.5 h	Multiple products, low yields of <b>4.60</b>
5	LHMDS, THF, 23 °C, 15 h; then, MsCl, 6 h	Multiple products, low yields of <b>4.60</b>

#### 4.4.2 Cyclization of $\alpha$ -Functionalized Methyl Ketones

We next considered whether an  $\alpha$ -functionalized methyl ketone, such as  $\alpha$ -hydroxy ketone **4.62** (Scheme 4.18), could be synthesized and subjected to the aldol cyclization to deliver a tetracyclic compound that already possessed functionalization at C10. Formation of the enolate of **4.15** at temperatures low enough to avoid aldol cyclization, followed by addition of an oxygen electrophile (e.g., Davis oxaziridine,<sup>19</sup> MoOPD,<sup>20</sup> O<sub>2</sub> and P(OEt)<sub>3</sub>), typically resulted in either recovery of starting material or in decomposition.  $\alpha$ -Oxidation with hypervalent iodine reagents (e.g., PIDA in methanolic KOH,<sup>21</sup> or Koser's reagent<sup>22</sup>) and  $\alpha$ -oxybenzoylation with *N*-methyl-*O*-benzoylhydroxylamine<sup>23</sup> were similarly unsuccessful. Finally, formation of the silyl enol ether and attempted Rubottom oxidation<sup>24</sup> resulted in the epoxidation only of the tetrasubstituted alkene.

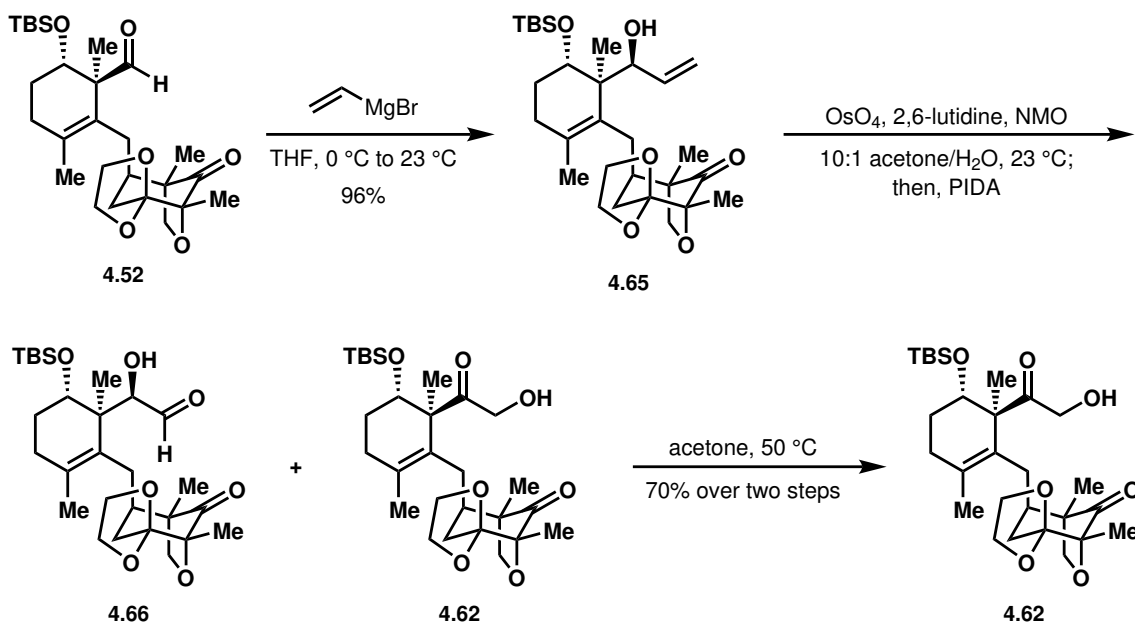
Given challenges with direct  $\alpha$ -oxidation of methyl ketone **4.15**, we considered whether oxygenation could be introduced through nucleophilic addition to aldehyde **4.52**. Attempted addition of hydroxymethyl anion surrogates, such as Bu<sub>3</sub>SnCH<sub>2</sub>OMOM<sup>25</sup> and (*O*-*i*Pr)Me<sub>2</sub>SiCH<sub>2</sub>MgCl,<sup>26</sup>





**Scheme 4.18:** Attempted  $\alpha$ -oxidation of methyl ketone **4.15**.

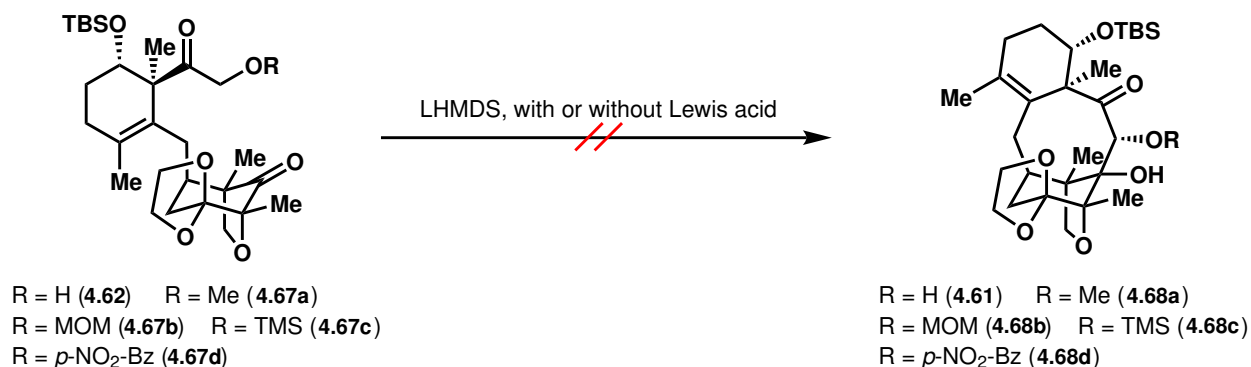
resulted in no conversion; however, the nucleophilic addition of vinylmagnesium bromide successfully yielded allylic alcohol **4.65** (Scheme 4.19). Upjohn dihydroxylation of the terminal alkene, followed by PIDA-induced cleavage of the 1,2-diol,<sup>27</sup> yielded both  $\alpha$ -hydroxy aldehyde **4.66** and  $\alpha$ -hydroxy ketone **4.62**, the latter presumably arising from a Lobry De Bruyn–Alberda–van Ekenstein transformation.<sup>28</sup> We speculate that the steric hindrance provided in part by the neighboring quaternary center prevents further oxidative cleavage of the  $\alpha$ -hydroxy aldehyde by PIDA. While there was run-to-run variability in the ratio of aldehyde **4.66** to ketone **4.62** isolated, the former could be fully converted to the latter by stirring the mixture in acetone at 50 °C. Overall, this sequence provided to us ready access to  $\alpha$ -hydroxy ketone **4.62**.



**Scheme 4.19:** Synthesis of  $\alpha$ -hydroxy ketone **4.62**.

With **4.62** in hand, we began exploring conditions for aldol cyclization. Direct treatment of **4.62** with strong base typically led to decomposition (Scheme 4.20). A series of *O*-protected compounds were then prepared (**4.67a–4.67d**) and subjected to LHMDS, with or without added Lewis acid. In each case, either no conversion or decomposition was observed.

Consistent with these experimental results, preliminary calculations suggested that the aldol reaction was not thermodynamically favorable for any of the  $\alpha$ -oxy methyl ketones, but was favorable with methyl ketone **4.15** (Table 4.4).

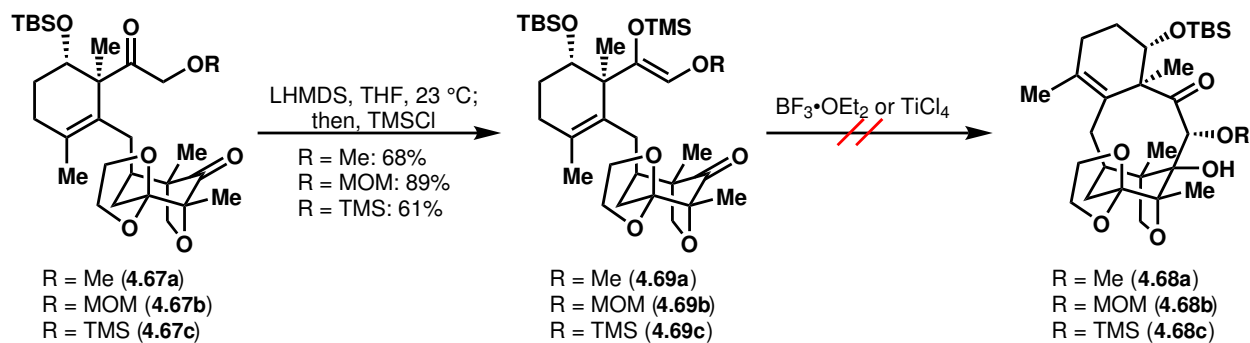


**Scheme 4.20:** Attempted aldol reaction of compounds **4.62** and **4.67a–4.67d**.

**Table 4.4:** DFT calculations indicating the thermodynamic unfavorability of the aldol reaction for  $\alpha$ -functionalized ketones. Calculations were carried out in THF using the IEFPCM solvent model at the B3LYP/6-31G\* level of theory.

Entry	R	$\Delta G$ (kcal/mol)	Entry	R	$\Delta G$ (kcal/mol)
1	H	-3.2	10	OMs	+14.0
2	OMe	+34.0	11	OTs	+14.0
3	<i>O</i> -allyl	+11.8	12	OPiv	+7.0
4	OBn	+8.8	13	O(COOMe)	+10.5
5	OTMS	+18.9	14	OAc	+9.1
6	OTBDPS	+21.2	15	OTFA	+6.6
7	OMEM	+9.9	16	OBz	+4.3
8	OSEM	+10.2	17	OBz-F <sub>5</sub>	+6.0
9	OCF <sub>3</sub>	+10.7	18	OBz- <i>p</i> -NO <sub>2</sub>	+2.3

Treatment of compounds **4.67a** to **4.67c** with LHMDS, followed by trapping with TM-SCl, yielded silyl enol ethers **4.69a** to **4.69c**, confirming that enolate formation was taking place and providing test material that could be subjected to Mukaiyama aldol conditions

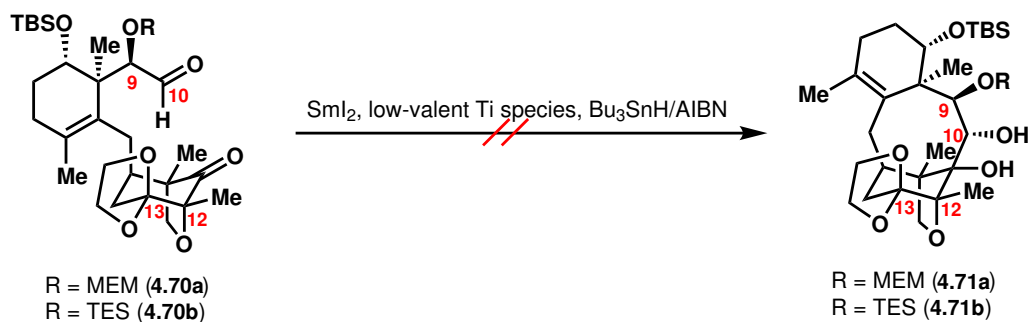


**Scheme 4.21:** Attempted Mukaiyama aldol reactions of compounds **4.62** and **4.67a–4.67d**.

(Scheme 4.21). Unfortunately, under all conditions attempted to induce a Mukaiyama aldol, only the silyl-cleaved  $\alpha$ -oxy compounds were recovered.

### 4.4.3 Pinacol Coupling

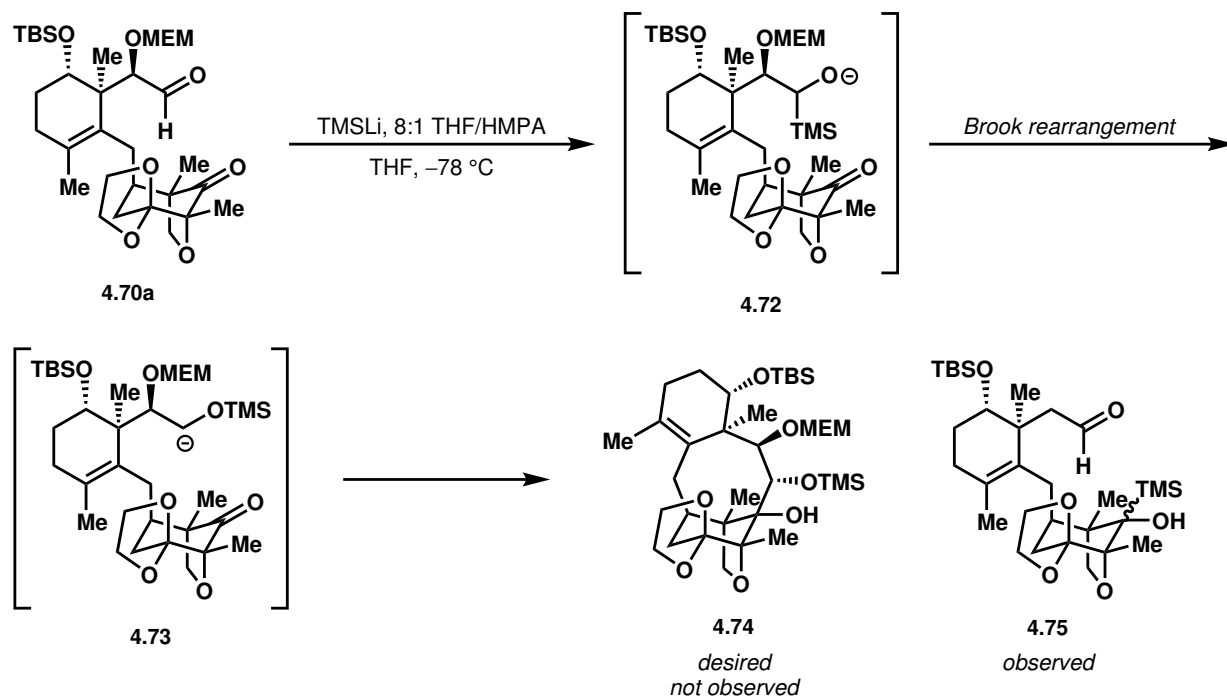
Realizing that our synthetic route towards  $\alpha$ -hydroxy ketone **4.62** could be adapted for the synthesis of possible pinacol coupling precursors, we synthesized aldehydes **4.70a** and **4.70b** (in an analogous fashion to the synthesis of  $\alpha$ -hydroxy aldehyde **4.66**; see experimental methods and procedures for details). These keto-aldehydes were subjected to pinacol coupling conditions (Scheme 4.22). We were especially intrigued by the possibility that the pinacol coupling products (**4.71a** and **4.71b**) would harbor the desired *trans*-disposed oxygen atoms at the C9 and C10 carbons; this was especially attractive given our difficulties with setting the C9 stereocenter after cyclization (see Section 5.1). However, upon treatment of aldehydes **4.70a** and **4.70b** with various pinacol coupling conditions (e.g., SmI<sub>2</sub>, low-valent Ti species, Bu<sub>3</sub>SnH/AIBN<sup>29</sup>) we observed either no conversion, decomposition, or mixtures of products that had been deoxygenated at C9, C12, and/or C13, which suggested that the deoxygenation pathways outcompeted the slow cyclization.



**Scheme 4.22:** Attempted pinacol coupling of aldehydes **4.70a** and **4.70b**.

#### 4.4.4 Brook Rearrangement

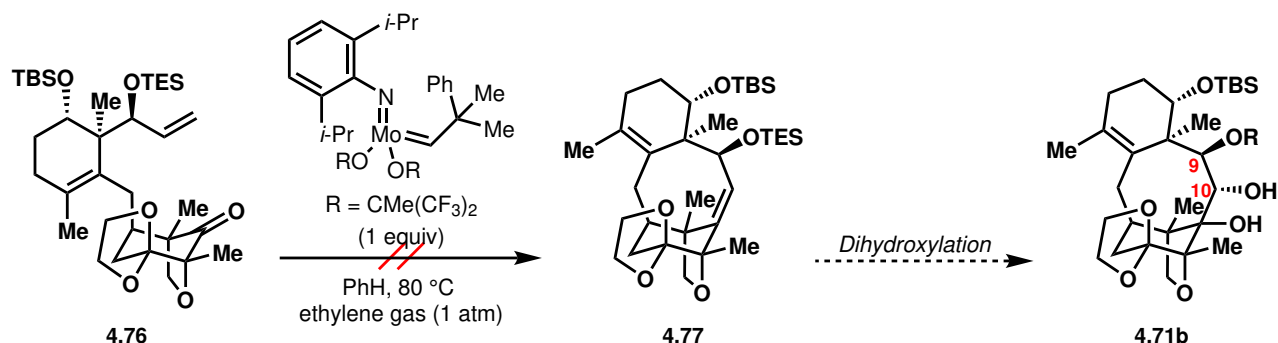
We imagined that addition of TMSLi into aldehyde **4.70a** might yield  $\alpha$ -silyl alkoxide **4.72**; subsequent Brook rearrangement to yield intermediate **4.73**, followed by carbanion nucleophilic addition to the A-ring ketone, would yield compound **4.74** (Scheme 4.23). However, upon treatment of aldehyde **4.70a** with TMSLi, we observed only compound **4.75** as a mixture of diastereomers, suggesting that both  $\alpha$ -deoxygenation from the intermediate carbanion and competitive silyllithium addition to the A-ring ketone would be major obstacles to the success of this route.



Scheme 4.23: Attempted synthesis of **4.75**.

#### 4.4.5 Carbonyl–Olefin Metathesis

Finally, we investigated the carbonyl–olefin metathesis of tricycle **4.76** to yield tetracyclic compound **4.77**, which, upon dihydroxylation, would give diol **4.71b** (Scheme 4.24). Similarly to the Brook rearrangement and pinacol coupling strategies, the prospect of setting both the C9 and C10 stereocenters diastereoselectively was attractive to us. Unfortunately, no conversion of alkene **4.76** was observed under the action of a molybdenum alkylidene complex<sup>30</sup> at elevated temperatures.



Scheme 4.24: Attempted carbonyl-olefin metathesis of alkene **4.76**.

## 4.5 Conclusion

Building on lessons learned from the sequential preparation of model tetracyclic cores of the taxagifine-like natural products, a highly oxidized tetracyclic core (**4.14**) of these natural products has been synthesized. This core can be accessed in 14 steps in the longest linear sequence from the readily available chiral pool compound (*S*)-carvone, and is constructed in a convergent manner through the C–C cleavage/cross-coupling of a northern and southern coupling partner derived from diastereomeric cyclobutanols. Notably, the rational choice of ligand and additive greatly enhanced the efficiency of the cross-coupling reaction. While alternative cyclization strategies that would have facilitated installation of oxidation at C10—and, in some cases, the setting of the C9 stereocenter—proved unfruitful, the synthesis of **4.14** via an aldol reaction established a molecular platform upon which sequential C–H functionalizations could be innovated and implemented. Progress on these late-stage functionalizations is the focus of Chapter 5.

## 4.6 Experimental Contributors

Dr. Kyle Owens, Dr. Manuel Weber, Dr. Ahmad Masarwa, and Carolin Gerleve were responsible for all experimental work discussed in section 4.1. Yuto Kimura was responsible for the optimization of the one-pot procedure for the synthesis of the northern coupling partner **4.33** from diol **4.32** under the supervision of Brian Wang. Characterization of all compounds was conducted in concert with Melecio Perea and Dr. Benjamin Wyler. All other experimental work was developed and conducted by Brian Wang, with the aid of Dr. Benjamin Wyler.

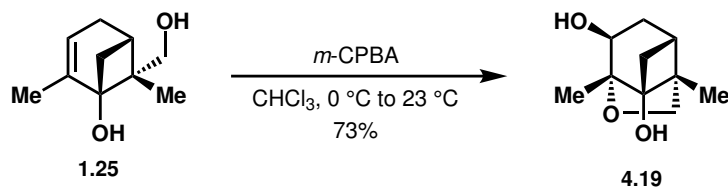
## 4.7 Experimental Methods and Procedures

### 4.7.1 General Methods

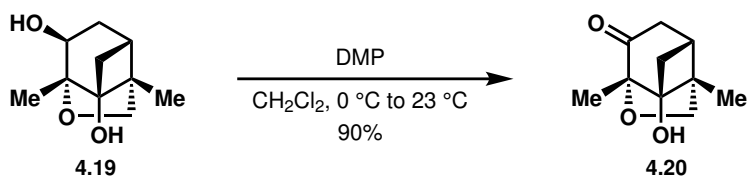
Unless otherwise stated, all reactions were stirred with Teflon<sup>TM</sup>-coated magnetic stir bars and were conducted in flame- or oven-dried glassware under an N<sub>2</sub> atmosphere following standard Schlenk technique. Anhydrous THF, Et<sub>2</sub>O, PhMe, PhH, MeCN, Et<sub>3</sub>N, and MeOH

were obtained by sparging with Ar followed by passage through a column of activated alumina, and were kept under an Ar atmosphere. Anhydrous  $\text{CH}_2\text{Cl}_2$  was obtained by distilling over  $\text{CaH}_2$  under an  $\text{N}_2$  atmosphere. All other solvents and reagents were purchased from commercial suppliers and used without further purification, unless otherwise stated. All reactions were monitored by thin layer chromatography on Silicycle Siliaplate<sup>TM</sup> 250  $\mu\text{m}$  silica gel (indicator F-254), with visualization by UV irradiation (254 nm) and staining by *p*-anisaldehyde. Reaction mixture temperatures above 23 °C were controlled by an IKA<sup>®</sup> temperature modulator. When stated, non-standard reaction mixture temperatures were obtained using a Thermo Scientific<sup>TM</sup> EK45/90 Immersion Cooler. Evaporation of solvents under reduced pressure was carried out on rotary evaporators. Purification by manual flash chromatography was conducted with Sorbent Technologies 60 Å silica gel of particle size 40–63  $\mu\text{m}$ . Automated flash column chromatography was performed on a Yamazen<sup>®</sup> Smart Flash EPCLC W-Prep 2XY automated flash chromatography system, with Universal Columns (60 Å silica gel of particle size 40  $\mu\text{m}$ ) or Universal Column Premiums (60 Å silica gel of particle size 30  $\mu\text{m}$ ). NMR spectra were acquired in deuterated solvents purchased from Cambridge Isotope Laboratories, Inc. NMR spectra were recorded on Bruker spectrometers at the UC Berkeley College of Chemistry NMR Facility, operating at 300, 400, 500, 600, or 700 MHz for  $^1\text{H}$  NMR, and at 75, 100, 125, 150, or 175 MHz for  $^{13}\text{C}$  NMR.  $^1\text{H}$  NMR spectra are calibrated to the residual solvent peak  $\text{CDCl}_3$  ( $\delta = 7.260$  ppm) or  $\text{C}_6\text{D}_6$  ( $\delta = 7.160$  ppm), and  $^{13}\text{C}$  NMR spectra are calibrated to the residual solvent peak  $\text{CDCl}_3$  ( $\delta = 77.16$  ppm).  $^1\text{H}$  NMR data are reported as follows: chemical shift (multiplicity, coupling constant, number of protons). Abbreviations of multiplicity patterns are as follows: d = doublet, t = triplet, br s = broad singlet, s = singlet, q = quartet, m = multiplet, dd = doublet of doublets, dt = doublet of triplets, dq = doublet of quartets, dp = doublet of pentets, ddd = doublet of doublet of doublets, dtd = doublet of triplet of doublets, tt = triplet of triplets. IR spectra were acquired on a Bruker ALPHA Platinum ATR spectrometer (neat), and select IR peaks are reported as frequency of absorption in  $\text{cm}^{-1}$ . High resolution mass spectrometry data was obtained from the Mass Spectral Facility at the University of California, Berkeley on a Finnigan/Thermo LTQ-FT instrument (ESI or EI) or from the Catalysis Facility of Lawrence Berkeley National Laboratory on a PerkinElmer AxION 2 UHPLC-TOF system (ESI or APCI). Data acquisition and processing were performed using Xcalibur<sup>TM</sup> software. Optical rotations were measured with a PerkinElmer 241 polarimeter with a Na D-line lamp (path length 1 dm, cell volume 1 mL, *c* in g/100 mL). X-ray data was collected on a Bruker APEX-II CCD diffractometer with Mo-K $\alpha$  radiation ( $\lambda = 0.71073$  Å) or a MicroStar-H X8 APEX-II diffractometer with Cu-K $\alpha$  radiation ( $\lambda = 1.54178$  Å). Avogadro was used for graphic rendering.

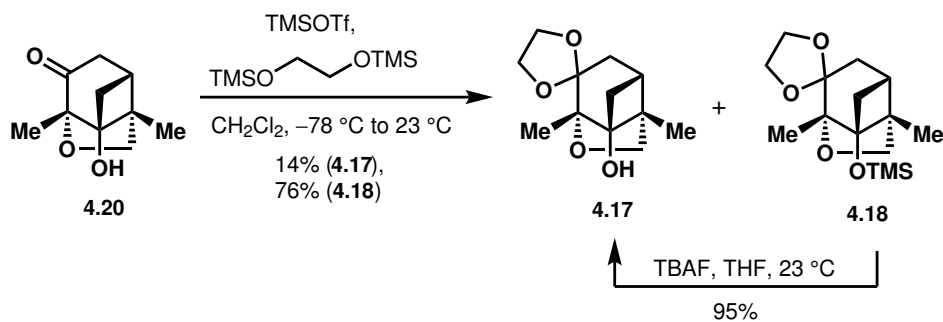
## 4.7.2 Experimental Procedures



To a solution of **1.25** (3.69 g, 21.9 mmol, 1 equiv) in  $\text{CHCl}_3$  (82 mL, 0.27 M) at  $0\text{ }^\circ\text{C}$  was added *m*-CPBA (70%, 11.9 g, 48.2 mmol, 2.2 equiv) in one portion. The resulting mixture was then warmed to  $23\text{ }^\circ\text{C}$  and stirred for 3 h. No special precautions were taken to exclude air or moisture. The reaction was then quenched by the addition of sat. aq.  $\text{Na}_2\text{S}_2\text{O}_3$  (50 mL), and the organic and aqueous layers were separated. The aqueous phase was extracted with EtOAc (3 x 30 mL), and the combined organic layers were washed with sat. aq.  $\text{NaHCO}_3$  (2 x 50 mL). The organic layer was then washed with brine (30 mL), dried over  $\text{Na}_2\text{SO}_4$ , filtered, and concentrated *in vacuo*. Purification by flash column chromatography (50% EtOAc/hexanes to 60% EtOAc/hexanes) afforded **4.19** (2.94 g, 73% yield) as a white powder. The spectral data is consistent with that reported in the literature.<sup>5</sup>

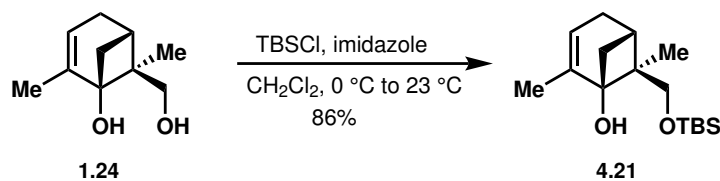


To a solution of **4.19** (3.70 g, 20.1 mmol, 1 equiv) in Fisher HPLC grade  $\text{CH}_2\text{Cl}_2$  (201 mL, 0.1 M) at  $0\text{ }^\circ\text{C}$  was added Dess-Martin periodinane (10.2 g, 24.1 mmol, 1.2 equiv) in one portion. The resulting mixture was then warmed to  $23\text{ }^\circ\text{C}$  and stirred for 3 h. No special precautions were taken to exclude air or moisture. The reaction was quenched by the addition of sat. aq.  $\text{Na}_2\text{S}_2\text{O}_3$  (75 mL) followed by sat. aq.  $\text{NaHCO}_3$  (75 mL). The organic and aqueous layers were separated, and the aqueous phase was extracted with  $\text{CH}_2\text{Cl}_2$  (5 x 90 mL). The combined organic layers were dried over  $\text{Na}_2\text{S}_2\text{O}_4$ , filtered, and concentrated *in vacuo*. Purification by Yamazen automated flash column chromatography (25 % EtOAc/hexanes to 75 % EtOAc/hexanes) afforded **4.20** (3.31 g, 90% yield) as a white powder. **TLC** (100% EtOAc):  $R_f = 0.8$  (*p*-anisaldehyde).  **$^1\text{H NMR}$**  (600 MHz,  $\text{CDCl}_3$ )  $\delta$  3.92 (d,  $J = 9.4$  Hz, 1H), 3.76 (d,  $J = 9.4$  Hz, 1H), 2.73 (s, 1H), 2.61 (d,  $J = 17.6$  Hz, 1H), 2.38 (dd,  $J = 17.6, 3.9$  Hz, 1H), 2.25–2.19 (m, 1H), 2.11–2.06 (m, 1H), 1.54 (d,  $J = 10.7$  Hz, 1H), 1.30 (s, 3H), 1.26 (s, 3H).  **$^{13}\text{C NMR}$**  (151 MHz,  $\text{CDCl}_3$ )  $\delta$  203.3, 93.1, 80.2, 73.2, 55.5, 39.0, 32.6, 30.3, 14.3, 12.1. **IR** (ATR, thin film):  $\nu$  3419, 2940, 2876, 1729, 1263  $\text{cm}^{-1}$ . **HRMS** (EI+)  $m/z$  calc'd for  $\text{C}_{10}\text{H}_{14}\text{O}_3$   $[\text{M}]^+$ : 182.0937, found: 182.0940.  $[\alpha]_{\text{D}}^{20} = +258.8^\circ$  ( $c = 0.71, \text{CHCl}_3$ ).

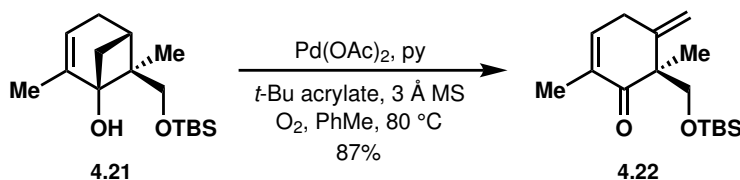


To a solution of **4.20** (3.71 g, 20.4 mmol, 1 equiv) and 1,2-bis(trimethylsilyloxy)ethane (20 mL, 81 mmol, 4 equiv) in  $\text{CH}_2\text{Cl}_2$  (203 mL, 0.1 M) at  $-78\text{ }^\circ\text{C}$  was added TMSOTf (370  $\mu\text{L}$ , 2.04 mmol, 0.1 equiv). The resulting mixture was then warmed to  $23\text{ }^\circ\text{C}$  and stirred for 4 h. The reaction was quenched by the addition of pyridine (42 mL) and  $\text{H}_2\text{O}$  (170 mL), and the organic and aqueous layers were separated. The aqueous phase was extracted with EtOAc (3 x 75 mL), and the combined organic layers were washed with sat. aq.  $\text{NaHCO}_3$  (200 mL). The organic layer was then washed with 10%  $\text{CuSO}_4$  (9 x 100 mL), brine (200 mL), dried over  $\text{Na}_2\text{SO}_4$ , filtered, and concentrated *in vacuo*. Purification by flash column chromatography (10% EtOAc in hexanes to 50% EtOAc in hexanes) afforded **4.17** (651 mg, 14% yield) as a white powder and **4.18** (4.59 g, 76% yield), also as a white powder. **4.18** was then converted to **4.17** using the following procedure: to a solution of **4.18** in THF at  $23\text{ }^\circ\text{C}$  was added TBAF (1.0 M in THF, 22.6 mL, 22.6 mmol, 2 equiv), and the resulting mixture was stirred at  $23\text{ }^\circ\text{C}$  for 50 min. No special precautions were taken to exclude air or moisture. The reaction was then quenched by the addition of sat. aq.  $\text{NaHCO}_3$  (100 mL), and the organic and aqueous layers were separated. The aqueous phase was extracted with EtOAc (6 x 70 mL), and the combined organic layers were dried over  $\text{Na}_2\text{SO}_4$ , filtered, and concentrated *in vacuo*. Purification by flash column chromatography (60% EtOAc/hexanes to 80% EtOAc/hexanes) afforded **4.17** (2.43 g, 95% yield). For **4.17**: **TLC** (50% EtOAc/hexanes):  $R_f = 0.2$  (*p*-anisaldehyde).  **$^1\text{H NMR}$**  (700 MHz,  $\text{CDCl}_3$ )  $\delta$  4.06–4.02 (m, 1H), 4.00–3.94 (m, 2H), 3.93–3.89 (m, 1H), 3.86 (d,  $J = 9.2$  Hz, 1H), 3.62 (d,  $J = 9.3$  Hz, 1H), 2.41 (d,  $J = 9.7$  Hz, 1H) 1.98–1.93 (m, 2H), 1.92–1.87 (m, 1H), 1.87–1.84 (m, 1H), 1.24 (s, 3H), 1.20 (s, 3H).  **$^{13}\text{C NMR}$**  (151 MHz,  $\text{CDCl}_3$ )  $\delta$  110.1, 93.5, 80.5, 72.1, 65.2, 64.9, 54.7, 35.6, 31.4, 30.3, 14.5, 13.3. **IR** (ATR, thin film):  $\nu$  3410, 2940, 2871, 1295  $\text{cm}^{-1}$ . **HRMS** (ESI+)  $m/z$  calc'd for  $\text{C}_{12}\text{H}_{18}\text{O}_4\text{Na}$   $[\text{M}+\text{Na}]^+$ : 249.1097, found: 249.1109.  $[\alpha]_{\text{D}}^{20} = +60.5^\circ$  ( $c = 0.62$ ,  $\text{CHCl}_3$ ). For **4.18**: **TLC** (50% EtOAc/hexanes):  $R_f = 0.6$  (*p*-anisaldehyde).  **$^1\text{H NMR}$**  (600 MHz,  $\text{CDCl}_3$ )  $\delta$  4.04–3.99 (m, 1H), 3.97–3.90 (m, 2H), 3.89–3.84 (m, 1H), 3.80 (d,  $J = 9.0$  Hz, 1H), 3.59 (d,  $J = 9.1$  Hz, 1H), 2.43 (d,  $J = 9.4$  Hz, 1H), 2.11–2.06 (m, 1H), 1.94–1.89 (m, 1H), 1.86–1.79 (m, 2H), 1.16 (s, 3H), 1.12 (s, 3H), 0.13 (s, 9H).  **$^{13}\text{C NMR}$**  (151 MHz,  $\text{CDCl}_3$ )  $\delta$  110.5, 94.5, 82.3, 72.3, 65.2, 64.9, 55.4, 35.5, 32.1, 31.2, 15.0, 14.2, 2.0. **IR** (ATR, thin film):  $\nu$  2954, 2868, 1261, 1252  $\text{cm}^{-1}$ . **HRMS** (ESI+)  $m/z$  calc'd for  $\text{C}_{15}\text{H}_{26}\text{O}_4\text{SiNa}$   $[\text{M}+\text{Na}]^+$ : 321.1493, found: 321.1490.  $[\alpha]_{\text{D}}^{20} = +57.2^\circ$  ( $c = 0.58$ ,  $\text{CHCl}_3$ ).



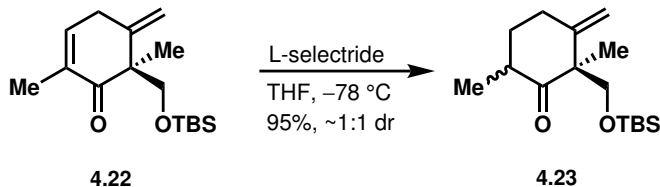


To a solution of **1.24** (6.59 g, 39.2 mmol, 1 equiv) in  $\text{CH}_2\text{Cl}_2$  (196 mL, 0.2 M) at 0 °C was added imidazole (6.67 g, 98.0 mmol, 2.5 equiv) and TBSCl (7.09 g, 47.0 mmol, 1.2 equiv), and the resulting mixture was then warmed to 23 °C and stirred for 3 h. The reaction was quenched with sat. aq.  $\text{NaHCO}_3$  (150 mL) and the organic and aqueous layers were separated. The aqueous phase was extracted with DCM (3 x 100 mL). The combined organic layers were dried over  $\text{Na}_2\text{SO}_4$ , filtered, and concentrated *in vacuo*. Purification by Yamazen automated flash column chromatography (5% EtOAc/hexanes) afforded **4.21** (9.56 g, 86% yield) as a colorless oil. **TLC** (50% EtOAc/hexanes):  $R_f = 0.9$  (*p*-anisaldehyde).  **$^1\text{H NMR}$**  (500 MHz,  $\text{CDCl}_3$ )  $\delta$  5.19–5.15 (m, 1H), 4.28 (d,  $J = 10.1$  Hz, 1H), 3.72 (d,  $J = 10.1$  Hz, 1H), 2.36 (dd,  $J = 8.6, 7.0$  Hz, 1H), 2.18–2.01 (m, 2H), 1.93–1.88 (m, 1H), 1.78–1.73 (m, 3H), 1.67 (d,  $J = 8.6$  Hz, 1H), 1.00 (s, 3H), 0.91 (s, 9H), 0.10 (s, 3H), 0.10 (s, 3H).  **$^{13}\text{C NMR}$**  (151 MHz,  $\text{CDCl}_3$ )  $\delta$  147.6, 116.6, 78.7, 70.9, 46.5, 40.8, 31.5, 30.6, 26.0, 18.3, 17.5, 14.9, –5.5, –5.5. **IR** (ATR, thin film):  $\nu$  3504, 2955, 2928, 2857, 1471  $\text{cm}^{-1}$ . **HRMS** (ESI+)  $m/z$  calc'd for  $\text{C}_{16}\text{H}_{31}\text{O}_2\text{Si}$   $[\text{M}+\text{H}]^+$ : 283.2088, found: 283.2087.  $[\alpha]_D^{20} = -42.4^\circ$  ( $c = 0.75$ ,  $\text{CHCl}_3$ ).

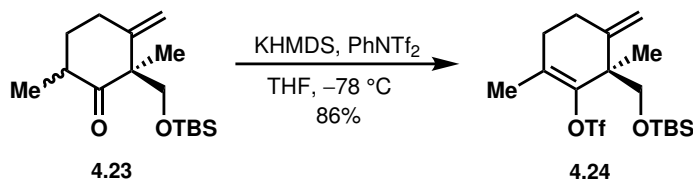


A 1L round-bottomed flask was charged with 3 Å molecular sieves (34 g, crushed into a powder with mortar and pestle) and flame-dried for 10 min under high vacuum. In a separate flask, a solution of **4.21** (9.56 g, 33.8 mmol, 1 equiv), anhydrous pyridine (5.45 mL, 67.7 mmol, 2.0 equiv), and *t*-Bu acrylate (12.4 mL, 84.6 mmol, 2.5 equiv) in toluene (338 mL, 0.1 M) was prepared under  $\text{N}_2$ , and after being thoroughly mixed, the solution was uncapped and added to the reaction flask.  $\text{Pd}(\text{OAc})_2$  (760 mg, 3.38 mmol, 0.1 equiv) was added and the flask was equipped with a reflux condenser sealed with a septum. The flask was evacuated and backfilled with  $\text{O}_2$  (5x) using an  $\text{O}_2$  balloon, and the reaction mixture was stirred at 80 °C for 18 h. The solution was then allowed to cool to 23 °C and the beige suspension was filtered over a plug of silica, washed with EtOAc, and concentrated *in vacuo*. The filtrate was purified by Yamazen automated flash chromatography (3% EtOAc/hexanes) to afford **4.22** (8.23 g, 87% yield) as a light yellow oil. **TLC** (5% EtOAc/hexanes):  $R_f = 0.3$  (UV/*p*-anisaldehyde).  **$^1\text{H NMR}$**  (600 MHz,  $\text{CDCl}_3$ )  $\delta$  6.70–6.66 (m, 1H), 4.97–4.91 (m, 2H), 3.74 (d,  $J = 9.2$  Hz, 1H), 3.59 (d,  $J = 9.2$  Hz, 1H), 3.35–3.25 (m, 1H), 3.07–2.98 (m, 1H), 1.78–1.76 (m, 3H), 1.25 (s, 3H), 0.83 (s, 9H), –0.01 (s, 3H), –0.02 (s, 3H).  **$^{13}\text{C NMR}$**  (151 MHz,  $\text{CDCl}_3$ )  $\delta$  201.3, 146.6, 142.2, 134.4, 111.1, 69.5, 55.6, 34.1, 25.9, 18.3, 17.3, 16.6, –5.5, –5.5. **IR** (ATR, thin film):  $\nu$  2954, 2928, 2857, 2884, 1673, 1650  $\text{cm}^{-1}$ .

**HRMS** (ESI+)  $m/z$  calc'd for  $C_{16}H_{28}O_2SiNa$   $[M+Na]^+$ : 303.1751, found: 303.1756.  $[\alpha]^{20}_D = +54.9^\circ$  ( $c = 0.79$ ,  $CHCl_3$ ).

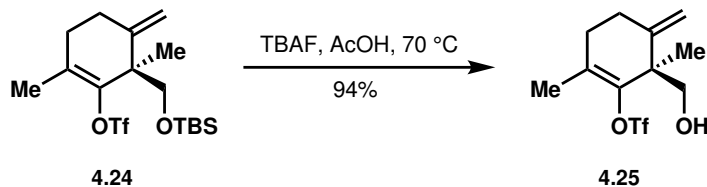


To a solution of **4.22** (12.89 g, 46.0 mmol, 1 equiv) in THF (328 mL, 0.14 M) at  $-78^\circ\text{C}$  was added L-Selectride (1.0 M in THF, 69 mL, 68.9 mmol, 1.5 equiv) over 5 min. The reaction mixture was stirred at  $-78^\circ\text{C}$  for 50 min. The solution was warmed to  $0^\circ\text{C}$ , and  $H_2O_2$  (35 wt% in  $H_2O$ , 67.0 mL) was added slowly followed by the addition of NaOH (15 wt% in  $H_2O$ , 67.0 mL). After stirring the mixture for an additional 4 h at  $0^\circ\text{C}$ , the solution was diluted with  $H_2O$  (250 mL) and  $Et_2O$  (250 mL), and the organic and aqueous layers were separated. The aqueous phase was extracted with  $Et_2O$  (3 x 250 mL), and the combined organic layers were washed with brine (500 mL), dried over  $Na_2SO_4$ , filtered, and concentrated *in vacuo*. The crude product was purified by Yamazen automated flash column chromatography (hexanes to 2%  $Et_2O$ /hexanes) to afford **4.23** (12.37 g, 95% yield, 1.25:1 dr) as a light yellow oil. **TLC** (5%  $EtOAc$ /hexanes):  $R_f = 0.6$  (*p*-anisaldehyde).  **$^1H$  NMR** (400 MHz,  $CDCl_3$ ) *Major diastereomer*:  $\delta$  4.88 (s, 1H), 4.83 (s, 1H), 4.00 (d,  $J = 9.3$  Hz, 1H), 3.47 (d,  $J = 9.5$  Hz, 1H), 1.22 (s, 3H), 1.04 (s, 3H), 0.84 (s, 9H), 0.00 (s, 6H). *Minor diastereomer*:  $\delta$  4.95 (s, 1H), 4.90 (s, 1H), 3.91 (d,  $J = 9.7$  Hz, 1H), 1.19 (s, 3H), 1.02 (s, 3H), 0.85 (s, 9H), 0.02 (d,  $J = 3.1$  Hz, 6H). *Major + minor diastereomers*:  $\delta$  2.70–2.65 (m, 2H), 2.59–2.44 (m, 2H), 2.44–2.35 (m, 1H), 2.08–1.96 (m, 2H), 1.48–1.37 (m, 1H), 1.37–1.24 (m, 2H).  **$^{13}C$  NMR** (151 MHz,  $CDCl_3$ )  $\delta$  215.4, 212.6, 150.6, 150.2, 110.6, 110.5, 70.6, 67.8, 58.7, 56.6, 42.3, 41.6, 34.0, 32.6, 31.6, 31.2, 26.0, 25.9, 21.8, 18.4, 18.3, 17.8, 15.1, 15.1,  $-5.4$ ,  $-5.5$ ,  $-5.5$ . **IR** (ATR, thin film):  $\nu$  2955, 2930, 2857, 1712, 1472  $cm^{-1}$ . **HRMS** (EI+)  $m/z$  calc'd for  $C_{16}H_{30}O_2Si$   $[M]^+$ : 282.2010, found: 282.2006.  $[\alpha]^{20}_D = +3.3^\circ$  ( $c = 0.36$ ,  $CHCl_3$ ).

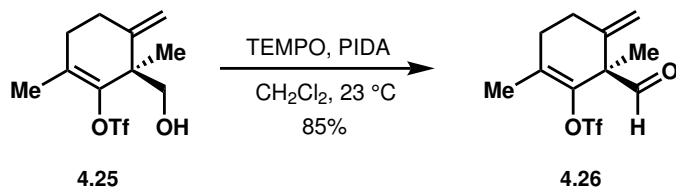


To a solution of **4.23** (5.55 g, 19.6 mmol, 1 equiv) and  $PhNTf_2$  (21.0 g, 58.9 mmol, 3 equiv) in THF (196 mL, 0.1 M) at  $-78^\circ\text{C}$  was added KHMDS (0.7 M in toluene, 56.0 mL, 39.2 mmol, 2 equiv) rapidly over 15 s. The reaction mixture was stirred at  $-78^\circ\text{C}$  for 1 h 15 min. The reaction was then quenched by the addition of sat.  $NH_4Cl$  (24 mL). The resulting solution was diluted with  $Et_2O$  (64 mL) and  $H_2O$  (64 mL), and the organic and aqueous layers were separated. The aqueous phase was extracted with  $Et_2O$  (3 x 80 mL), and the combined organic layers were dried over  $Na_2SO_4$ , filtered, and concentrated *in vacuo*. The crude product was purified by Yamazen automated flash column chromatography (100%

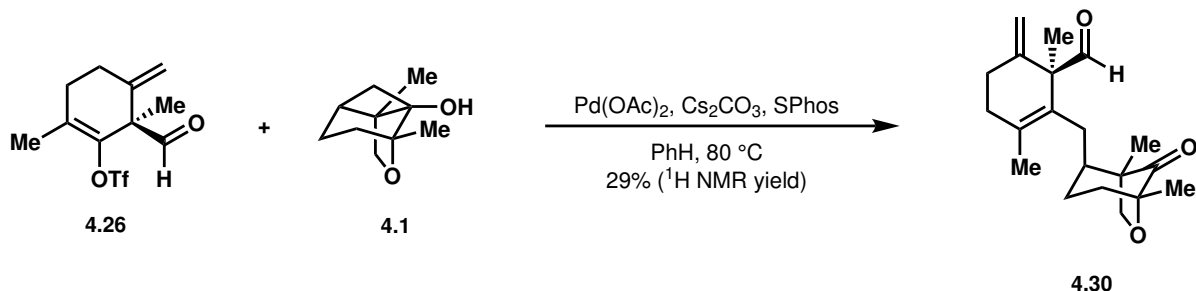
hexanes) to afford **4.24** (7.0 g, 86% yield) as a light yellow oil. **TLC** (5% EtOAc/hexanes):  $R_f = 0.75$  (UV/*p*-anisaldehyde).  **$^1\text{H NMR}$**  (600 MHz,  $\text{CDCl}_3$ )  $\delta$  4.91 (s, 1H), 4.84 (s, 1H), 3.69 (d,  $J = 9.9$  Hz, 1H), 3.56 (d,  $J = 9.9$  Hz, 1H), 2.49–2.43 (m, 1H), 2.34–2.29 (m, 1H), 2.18 (t,  $J = 6.4$  Hz, 2H), 1.80 (s, 3H), 1.19 (s, 3H), 0.84 (s, 9H), 0.00 (s, 3H),  $-0.01$  (s, 3H).  **$^{13}\text{C NMR}$**  (151 MHz,  $\text{CDCl}_3$ )  $\delta$  149.3, 145.4, 130.1, 118.9 (q,  $J = 319.7$  Hz), 109.1, 67.2, 47.5, 32.4, 30.6, 25.9, 20.4, 18.3, 18.2,  $-5.6$ ,  $-5.6$ . **IR** (ATR, thin film):  $\nu$  2954, 2923, 2886, 2858, 1402, 1206  $\text{cm}^{-1}$ . **HRMS** (APCI+)  $m/z$  calc'd for  $\text{C}_{16}\text{H}_{29}\text{O}_2\text{Si}$   $[\text{M}-\text{Tf}]^+$ : 281.1931, found: 281.1926.  $[\alpha]_D^{20} = +45.8^\circ$  ( $c = 0.23$ ,  $\text{CHCl}_3$ ).



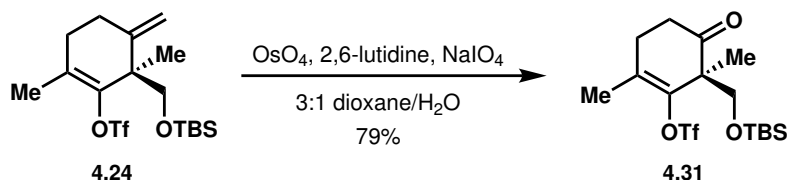
To a solution of **4.24** (34.8 mg, 0.084 mmol, 1 equiv) in THF (1 mL, 0.08 M) at 0 °C, AcOH (0.12 mL, 2.10 mmol, 25 equiv) and TBAF (1.0 M in THF, 0.42 mL, 0.42 mmol, 5 equiv) were added. The reaction mixture was then warmed to 70 °C and stirred for 24 h. No special precautions were taken to exclude air or moisture. The reaction was quenched with sat. aq.  $\text{NaHCO}_3$  (1 mL) and was stirred until no more gas evolution was observed. EtOAc (1 mL) was added, and the organic and aqueous layers were separated. The aqueous phase was extracted with EtOAc (3 x 1 mL), and the combined organic layers were dried over  $\text{Na}_2\text{SO}_4$ , filtered, and concentrated *in vacuo*. Purification by Yamazen automated flash column chromatography afforded **4.25** (23.8 mg, 94% yield) as a white crystalline solid.  **$^1\text{H NMR}$**  (600 MHz,  $\text{CDCl}_3$ )  $\delta$  5.02 (s, 1H), 4.92 (s, 1H), 3.73 (dd,  $J = 11.6, 5.7$  Hz, 1H), 3.57 (dd,  $J = 11.6, 8.4$  Hz, 1H), 2.57–2.49 (m, 1H), 2.42–2.33 (m, 1H), 2.31–2.17 (m, 2H), 1.85 (s, 3H), 1.76 (dd,  $J = 8.4, 5.8$  Hz, 1H), 1.22 (s, 3H).



To a solution of **4.25** (52.6 mg, 0.175 mmol, 1 equiv) in  $\text{CH}_2\text{Cl}_2$  (3.5 mL, 0.05 M), TEMPO (5.5 mg, 0.035 mmol, 0.2 equiv) and PIDA (67.7 mg, 0.210 mmol, 1.2 equiv) were added. The reaction mixture was stirred at 23 °C in the dark for 27 h. No special precautions were taken to exclude air or moisture. The reaction mixture was quenched with EtOH (2 mL) and stirred for 10 min, after which sat.  $\text{NaHCO}_3$  (3 mL) and EtOAc (4 mL) were added. The organic and aqueous layers were separated, and the aqueous layer was extracted with EtOAc (3 x 4 mL). The combined organic layers were dried over  $\text{Na}_2\text{SO}_4$ , filtered, and concentrated *in vacuo*. Purification by Yamazen automated flash column chromatography (5% EtOAc/hexanes) afforded **4.26** (44.3 mg, 85% yield).  **$^1\text{H NMR}$**  (500 MHz,  $\text{C}_6\text{D}_6$ )  $\delta$  9.13 (s, 1H), 4.60 (s, 1H), 4.48 (s, 1H), 1.89–1.73 (m, 1H), 1.72–1.61 (m, 1H), 1.55 (s, 3H), 1.53–1.41 (m, 2H), 1.33 (s, 3H).

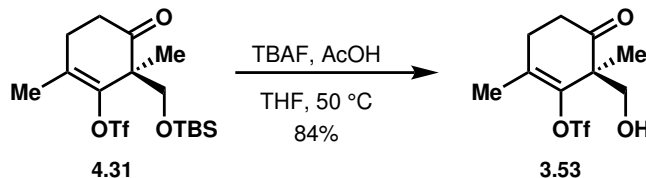


To a 1-dram vial was added **4.26** (7.8 mg, 0.026 mmol, 1.25 equiv), **4.1** (3.5 mg, 0.021 mmol, 1 equiv),  $\text{Pd(OAc)}_2$  (0.5 mg, 0.002 mmol, 0.1 equiv),  $\text{Cs}_2\text{CO}_3$  (13.6 mg, 0.042 mmol, 2 equiv), and SPhos (1.7 mg, 0.004 mmol, 0.2 equiv). The vial was brought into a glovebox. Deuterated benzene (degassed with three cycles of freeze/pump/thaw; 0.21 mL) was added. The reaction mixture was stirred at 23 °C for 10 min, after which the reaction mixture was warmed to 80 °C. After 24 h, the reaction mixture was cooled to 23 °C and filtered through Celite with the aid of EtOAc. The filtrate was concentrated *in vacuo*. Purification by flash column chromatography (5% EtOAc/hexanes to 10% EtOAc/hexanes) afforded **4.30**.  $^1\text{H}$  NMR (600 MHz,  $\text{CDCl}_3$ )  $\delta$  9.03 (s, 1H), 4.96 (s, 1H), 4.52 (s, 1H), 4.24 (d,  $J = 8.3$  Hz, 1H), 3.84 (d,  $J = 8.3$  Hz, 1H), 2.41–2.31 (m, 1H), 2.29–2.22 (m, 1H), 2.20–2.12 (m, 3H), 2.07–1.98 (m, 1H), 1.92–1.87 (m, 2H), 1.83 (dd,  $J = 13.3, 5.2$  Hz, 1H), 1.74 (d,  $J = 14.7$  Hz, 1H), 1.71 (s, 3H), 1.43 (dd,  $J = 14.5, 5.3$  Hz, 1H), 1.28 (s, 3H), 1.21 (s, 3H).

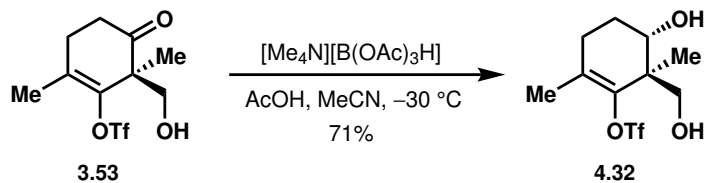


To a solution of **4.24** (7.0 g, 17 mmol, 1 equiv) in  $\text{H}_2\text{O}/1,4\text{-dioxane}$  (1:3, 168 mL, 0.1 M) was added 2,6-lutidine (3.9 mL, 34 mmol, 2 equiv) followed by the addition of  $\text{OsO}_4$  (4 wt% in  $\text{H}_2\text{O}$ , 2.2 mL, 0.34 mmol, 0.02 equiv) while the reaction mixture was stirred vigorously open to air. After 5 min  $\text{NaIO}_4$  (14.0 g, 67.6 mmol, 4 equiv) was added in one portion, and the solution was stirred vigorously at 23 °C for 2 d open to air. The reaction was then quenched by the addition of sat. aq.  $\text{Na}_2\text{S}_2\text{O}_3$  (168 mL), and the resulting solution was stirred for an additional 45 min. The solution was diluted with  $\text{Et}_2\text{O}$  (100 mL), and the organic and aqueous layers were separated. The aqueous phase was extracted with  $\text{Et}_2\text{O}$  (3 x 200 mL), and the combined organic layers were washed with brine (200 mL), dried over  $\text{Na}_2\text{SO}_4$ , filtered, and concentrated *in vacuo*. The crude product was purified by Yamazen automated flash column chromatography (3% EtOAc/hexanes) to afford **4.31** (5.56 g, 79% yield) as a light yellow oil. TLC (5% EtOAc/hexanes):  $R_f = 0.25$  (*p*-anisaldehyde)  $^1\text{H}$  NMR (600 MHz,  $\text{CDCl}_3$ )  $\delta$  3.78 (d,  $J = 9.5$  Hz, 1H), 3.61 (d,  $J = 9.5$  Hz, 1H), 2.65–2.50 (m, 2H), 2.47–2.32 (m, 2H), 1.93 (s, 3H), 1.15 (s, 3H), 0.82 (s, 9H), 0.00 (s, 3H),  $-0.01$  (s, 3H).  $^{13}\text{C}$  NMR (151 MHz,  $\text{CDCl}_3$ )  $\delta$  209.4, 143.2, 129.9, 118.8 (q,  $J = 319.7$  Hz), 66.8, 54.9, 37.4, 27.3, 25.8, 18.3, 18.20, 18.2,  $-5.70, -5.72$ . IR (ATR, thin film):  $\nu$  2955, 2931, 2885, 2859, 1727, 1404, 1209  $\text{cm}^{-1}$ . HRMS (APCI+)  $m/z$  calc'd for  $\text{C}_{15}\text{H}_{27}\text{O}_2\text{Si}$  [ $\text{M}-\text{OTf}$ ] $^+$ :

267.1775, found: 267.1784.  $[\alpha]_D^{20} = +18.5^\circ$  ( $c = 0.58$ ,  $\text{CHCl}_3$ ).

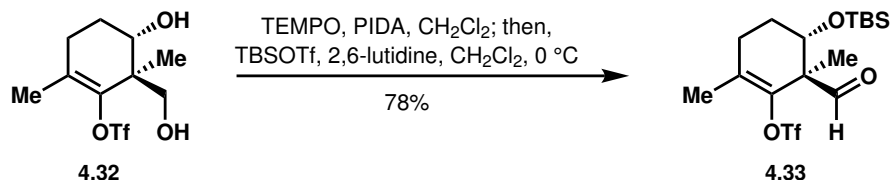


To a solution of **4.31** (1.75 g, 4.20 mmol, 1 equiv) and glacial AcOH (6.03 mL, 105 mmol, 25 equiv) in THF (42 mL, 0.1 M) at 0 °C was added TBAF (1.0 M in THF, 21 mL, 21 mmol, 5 equiv). After stirring at 0 °C for 10 min, the reaction mixture was warmed to 50 °C and stirred for an additional 15 h. No special precautions were taken to exclude air or moisture. The solution was cooled to 23 °C and diluted with H<sub>2</sub>O (35 mL) and EtOAc (35 mL), and the organic and aqueous layers were separated. The aqueous phase was extracted with EtOAc (3 x 30 mL), and the combined organic layers were washed with brine (30 mL), dried over Na<sub>2</sub>SO<sub>4</sub>, filtered, and concentrated *in vacuo*. The crude product was purified by Yamazen flash column chromatography (10% EtOAc/hexanes to 30% EtOAc/hexanes) to afford **3.53** (1.07 g, 84% yield) as a pale yellow oil. **TLC** (50% EtOAc/hexanes):  $R_f = 0.7$  (*p*-anisaldehyde) **<sup>1</sup>H NMR** (400 MHz, CDCl<sub>3</sub>)  $\delta$  3.76 (d,  $J = 11.6$  Hz, 1H), 3.68 (d,  $J = 11.6$  Hz, 1H), 2.73–2.59 (m, 2H), 2.56–2.35 (m, 2H), 1.97 (s, 3H), 1.18 (s, 3H). **<sup>13</sup>C NMR** (126 MHz, CDCl<sub>3</sub>)  $\delta$  209.6, 142.1, 131.4, 118.8 (q,  $J = 320.1$  Hz), 65.7, 55.0, 37.1, 27.5, 18.5, 18.3. **IR** (ATR, thin film):  $\nu$  3466, 2944, 1723, 1402, 1209 cm<sup>-1</sup>. **HRMS** (EI+)  $m/z$  calc'd for C<sub>10</sub>H<sub>13</sub>O<sub>5</sub>F<sub>3</sub>S [M]<sup>+</sup>: 302.0430, found: 302.0432.  $[\alpha]_D^{20} = +11.1^\circ$  ( $c = 0.47$ ,  $\text{CHCl}_3$ ).

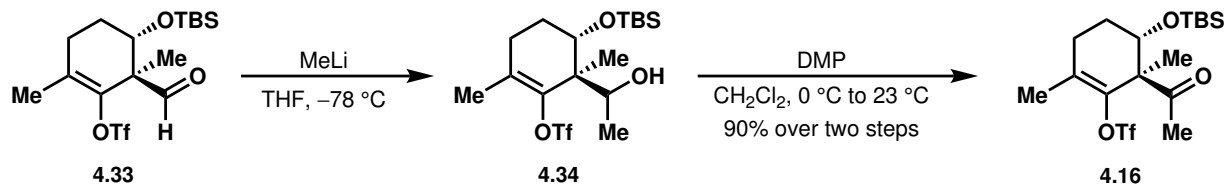


To a solution of Me<sub>4</sub>NB(OAc)<sub>3</sub>H (6.20 g, 23.5 mmol, 5 equiv) in glacial AcOH (31 mL, 0.15 M) and MeCN (31 mL, 0.15 M) at -30 °C was added a solution of **3.53** (1.42 g, 4.70 mmol, 1 equiv) in MeCN (31 mL, 0.15 M). [Note: The **3.53**/MeCN solution was added immediately after cooling the reaction flask to prevent the Me<sub>4</sub>NB(OAc)<sub>3</sub>H/AcOH/MeCN mixture from freezing.] The resulting mixture was stirred at -30 °C for 1.5 h. The reaction was then quenched by the addition of sat. aq. potassium sodium tartrate (25 mL), and the resulting solution was stirred for an additional 10 min. The mixture was diluted with sat. aq. NaHCO<sub>3</sub> (50 mL) and EtOAc (25 mL), and the organic and aqueous phases were separated. The aqueous phase was extracted with EtOAc (3 x 50 mL), and the combined organic layers were washed with brine (50 mL), dried over Na<sub>2</sub>SO<sub>4</sub>, filtered, and concentrated *in vacuo*. The crude product was purified by Yamazen automated flash column chromatography (50% EtOAc/hexanes) to afford **4.32** (1.01 g, 71% yield) as a white powder. **TLC** (50% EtOAc/hexanes):  $R_f = 0.4$  (*p*-anisaldehyde) **<sup>1</sup>H NMR** (600 MHz, CDCl<sub>3</sub>)  $\delta$  4.03 (dd,  $J = 11.1, 3.5$  Hz, 1H), 3.69 (s, 2H), 2.29–2.16 (m, 2H), 1.91–1.85 (m, 1H), 1.78 (s, 3H), 1.77–1.72 (m, 1H), 1.12 (s, 3H). **<sup>13</sup>C NMR** (126 MHz, CDCl<sub>3</sub>)  $\delta$  144.8, 129.5, 118.8 (q,  $J = 319.7$  Hz), 71.6, 66.1, 46.1, 28.7, 25.9, 17.8, 14.7. **IR** (ATR, thin film):  $\nu$  3272, 2957, 2886, 1400,

1203  $\text{cm}^{-1}$ . **HRMS** (EI+)  $m/z$  calc'd for  $\text{C}_{10}\text{H}_{15}\text{O}_5\text{F}_3\text{S}$   $[\text{M}]^+$ : 304.0587, found: 304.0591.  $[\alpha]_{\text{D}}^{20} = -15.5^\circ$  ( $c = 0.46$ ,  $\text{CHCl}_3$ ).



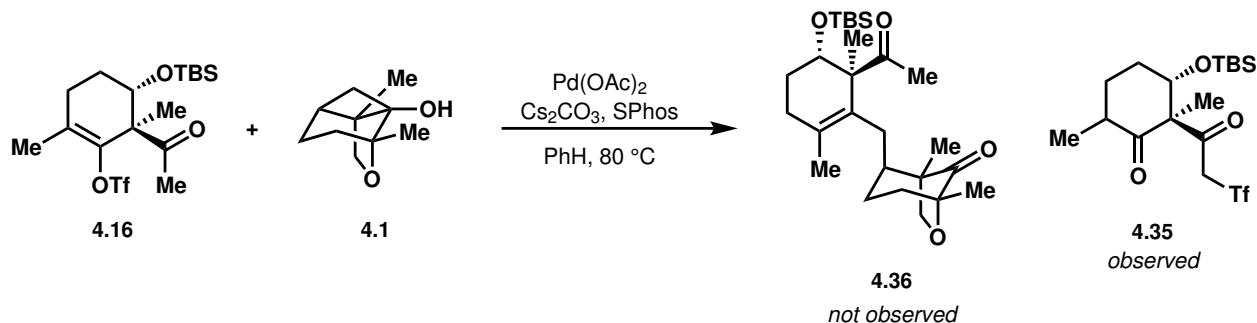
To a solution of **4.32** (1.00 g, 3.29 mmol, 1 equiv) in HPLC grade  $\text{CH}_2\text{Cl}_2$  (non-dried, 33 mL, 0.1 M) at 23 °C was added TEMPO (103 mg, 0.658 mmol, 0.2 equiv) followed by PIDA (1.27 g, 3.95 mmol, 1.2 equiv), and the mixture was stirred at 23 °C under air for 4 h. The reaction mixture was then cooled to 0 °C and under  $\text{N}_2$  was added 2,6-lutidine (1.90 mL, 16.4 mmol, 5 equiv) followed by the addition of TBSOTf (3.02 mL, 13.2 mmol, 4 equiv) over 1 min, and the mixture was stirred at 0 °C for 30 min. The reaction was then quenched by the addition of sat. aq.  $\text{Na}_2\text{S}_2\text{O}_3$  (100 mL), and the mixture was stirred at 23 °C for 10 min. The organic and aqueous layers were then separated, and the aqueous phase was extracted with  $\text{CH}_2\text{Cl}_2$  (4 x 50 mL). The combined organic layers were dried over  $\text{Na}_2\text{SO}_4$ , filtered, and concentrated *in vacuo*. The crude product was purified by Yamazen automated flash column chromatography (3%  $\text{CH}_2\text{Cl}_2$ /hexanes to 40%  $\text{CH}_2\text{Cl}_2$ /hexanes) to afford **4.33** (1.08 g, 78% yield) as a pale yellow oil. **TLC** (10% EtOAc/hexanes):  $R_f = 0.5$  (*p*-anisaldehyde)  **$^1\text{H}$  NMR** (500 MHz,  $\text{CDCl}_3$ )  $\delta$  9.55 (s, 1H), 4.03 (dd,  $J = 7.4, 3.2$  Hz, 1H), 2.39–2.31 (m, 1H), 2.29–2.21 (m, 1H), 1.87 (s, 3H), 1.80–1.70 (m, 2H), 1.32 (s, 3H), 0.86 (s, 9H), 0.06 (s, 3H), 0.04 (s, 3H).  **$^{13}\text{C}$  NMR** (126 MHz,  $\text{CDCl}_3$ )  $\delta$  200.6, 140.8, 131.3, 118.6 (q,  $J = 319.7$  Hz), 71.0, 57.8, 28.2, 26.8, 25.8, 18.1, 17.8, 13.9, -4.26, -4.91. **IR** (ATR, thin film):  $\nu$  2958, 2930, 2858, 1735, 1407, 1211  $\text{cm}^{-1}$ . **HRMS** (EI+)  $m/z$  calc'd for  $\text{C}_{15}\text{H}_{24}\text{O}_5\text{F}_3\text{SSi}$   $[\text{M}-\text{CH}_3]^+$ : 401.1060, found: 401.1064.  $[\alpha]_{\text{D}}^{20} = +38.2^\circ$  ( $c = 1.13$ ,  $\text{CHCl}_3$ ).



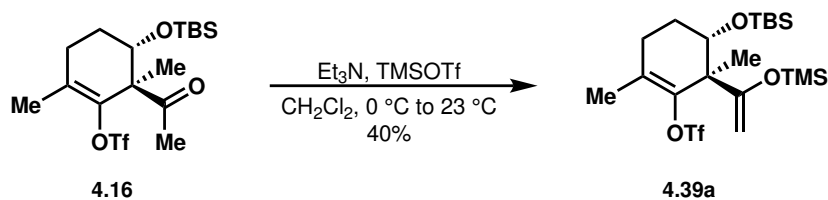
Trace water was removed from **4.33** (114 mg, 0.275 mmol, 1 equiv) via azeotropic distillation with benzene (1 x 5 mL). Then, to a solution of **4.33** in THF (5.5 mL, 0.05 M) at -78 °C, MeLi (1.0 M in  $\text{Et}_2\text{O}$ , 330  $\mu\text{L}$ , 0.330 mmol, 1.2 equiv) was added over 20 s. The reaction mixture was stirred at -78 °C for 40 min, after which the reaction was quenched with sat. aq.  $\text{NH}_4\text{Cl}$  (5.5 mL) and warmed to 23 °C. The organic and aqueous layers were separated, and the aqueous layer was extracted with EtOAc (3 x 3 mL). The combined organic layers were dried over  $\text{Na}_2\text{SO}_4$ , filtered, and concentrated *in vacuo* to yield crude **4.34** as a ~1:1 mixture of diastereomers, which was taken onto the next reaction without purification.

To a solution of crude **4.34** in  $\text{CH}_2\text{Cl}_2$  (5.5 mL) at 0 °C, Dess–Martin periodinane (233 mg, 0.549 mmol) was added, and the reaction mixture was warmed to 23 °C. No special precautions were taken to exclude air or moisture. After 1 h, the reaction was quenched

with sat. aq.  $\text{Na}_2\text{S}_2\text{O}_3$  (4 mL),  $\text{NaHCO}_3$  (4 mL), and  $\text{Et}_2\text{O}$  (5 mL), and the mixture was stirred vigorously for 15 min. The organic and aqueous layers were separated. The aqueous layer was extracted with  $\text{Et}_2\text{O}$  (3 x 4 mL), and the combined organic layers were dried over  $\text{Na}_2\text{SO}_4$ , filtered, and concentrated *in vacuo*. The crude material was taken up in  $\text{Et}_2\text{O}$ , filtered through Celite, and concentrated *in vacuo* to yield **4.16** as a white powder (107 mg, 90% yield over two steps).  $^1\text{H NMR}$  (400 MHz,  $\text{CDCl}_3$ )  $\delta$  4.10 (dd,  $J = 8.9, 4.2$  Hz, 1H), 2.29–2.23 (m, 2H), 2.18 (s, 3H), 1.82 (s, 3H), 1.77–1.65 (m, 2H), 1.41 (s, 3H), 0.86 (s, 9H), 0.05 (s, 3H), 0.01 (s, 3H).

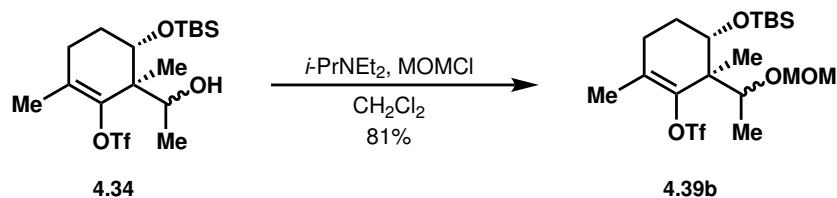


To a 1-dram vial was added **4.16** (15.6 mg, 0.036 mmol, 1.25 equiv), **4.1** (4.9 mg, 0.029 mmol, 1 equiv),  $\text{Pd}(\text{OAc})_2$  (0.7 mg, 0.003 mmol, 0.1 equiv),  $\text{Cs}_2\text{CO}_3$  (18.9 mg, 0.058 mmol, 2 equiv), and SPhos (1.2 mg, 0.003 mmol, 0.1 equiv). The vial was brought into a glovebox. Deuterated benzene (degassed with three cycles of freeze/pump/thaw; 0.21 mL) was added. The reaction mixture was stirred at 23 °C for 10 min, after which the reaction mixture was warmed to 80 °C. After 21 h, the reaction mixture was cooled to 23 °C and filtered through Celite with the aid of  $\text{EtOAc}$ . The filtrate was concentrated *in vacuo*. Purification by flash column chromatography (10%  $\text{EtOAc}$ /hexanes to 30%  $\text{EtOAc}$ /hexanes) afforded **4.35**.  $^1\text{H NMR}$  (500 MHz,  $\text{CDCl}_3$ )  $\delta$  4.50 (dd,  $J = 15.8, 0.8$  Hz, 1H), 4.45 (dd,  $J = 6.2, 4.9$  Hz, 1H), 4.42 (dd,  $J = 15.7, 0.6$  Hz, 1H), 2.58 (dp,  $J = 12.8, 6.4$  Hz, 1H), 2.05–1.93 (m, 2H), 1.92–1.81 (m, 1H), 1.52 (s, 3H), 1.23 (dd,  $J = 13.5, 3.6$  Hz, 1H), 1.00 (d,  $J = 6.4$  Hz, 3H), 0.84 (s, 9H), 0.11 (s, 3H), 0.06 (s, 3H).

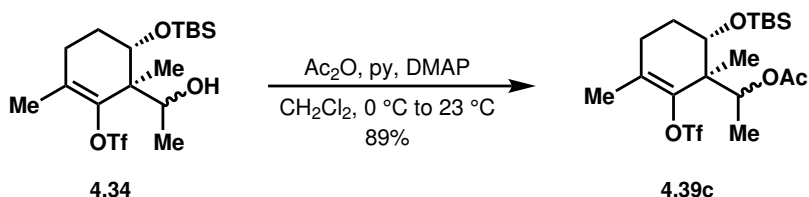


To a solution of **4.16** (9.6 mg, 0.022 mmol, 1 equiv) in  $\text{CH}_2\text{Cl}_2$  (0.25 mL, 0.09 M) at 0 °C,  $\text{Et}_3\text{N}$  (12.4  $\mu\text{L}$ , 0.089 mmol, 4 equiv) and TMSOTf (8.1  $\mu\text{L}$ , 0.045 mmol, 2 equiv) were added, and the reaction mixture was warmed to 23 °C. After 1 h, the reaction was diluted with  $\text{Et}_2\text{O}$  (1 mL) and quenched with sat. aq.  $\text{NaHCO}_3$  (1 mL). The organic and aqueous layers were separated, and the aqueous layer was extracted with  $\text{Et}_2\text{O}$  (3 x 1 mL). The combined organic layers were dried over  $\text{Na}_2\text{SO}_4$ , filtered, and concentrated *in vacuo* to afford **4.39a** (4.5 mg, 40% yield) as a white solid.  $^1\text{H NMR}$  (400 MHz,  $\text{CDCl}_3$ )  $\delta$  4.29 (d,

$J = 2.0$  Hz, 1H), 4.21 (d,  $J = 2.1$  Hz, 1H), 4.05 (dd,  $J = 9.1, 3.0$  Hz, 1H), 2.36–2.05 (m, 2H), 1.77 (s, 3H), 1.84–1.72 (m, 1H), 1.72–1.60 (m, 1H), 1.22 (s, 3H), 0.87 (s, 9H), 0.18 (s, 9H), 0.03 (s, 3H), 0.02 (s, 3H).

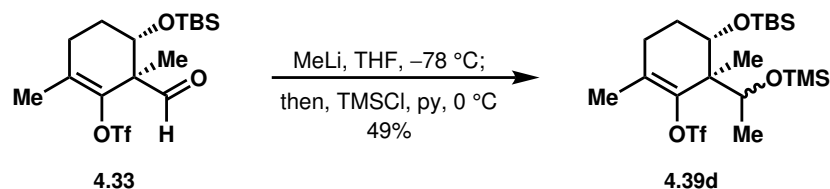


To a solution of **4.34** (17.4 mg, 0.040 mmol, 1 equiv) in  $\text{CH}_2\text{Cl}_2$  (0.80 mL, 0.05 M) at 23 °C,  $i\text{-PrNEt}_2$  (14.7  $\mu\text{L}$ , 0.084 mmol, 2.1 equiv) and MOMCl (6.1  $\mu\text{L}$ , 0.080 mmol, 2 equiv) were added. After 18 h,  $i\text{-PrNEt}_2$  (21.0  $\mu\text{L}$ , 0.12 mmol, 3 equiv) and MOMCl (9.2  $\mu\text{L}$ , 0.12 mmol, 3 equiv) were added. After another 24 h,  $i\text{-PrNEt}_2$  (21.0  $\mu\text{L}$ , 0.12 mmol, 3 equiv) and MOMCl (9.2  $\mu\text{L}$ , 0.12 mmol, 3 equiv) were added. After another 24 h, the reaction was diluted with  $\text{Et}_2\text{O}$  (1 mL) and quenched with sat. aq.  $\text{NH}_4\text{Cl}$  (1 mL), and the organic and aqueous layers were separated. The aqueous layer was extracted with  $\text{Et}_2\text{O}$  (3 x 1 mL), and the combined organic layers were dried over  $\text{Na}_2\text{SO}_4$ , filtered, and concentrated *in vacuo*. Purification by flash column chromatography (4% EtOAc/hexanes) afforded **4.39b** (15.5 mg, 81% yield) as a clear oil as a ~1:1 mixture of diastereomers.  $^1\text{H NMR}$  (600 MHz,  $\text{CDCl}_3$ )  $\delta$  4.67 (d,  $J = 6.9$  Hz, 1H), 4.65 (d,  $J = 6.9$  Hz, 1H), 4.58 (d,  $J = 6.9$  Hz, 1H), 4.53 (d,  $J = 6.9$  Hz, 1H), 4.00–3.94 (m, 2H), 3.75 (dq,  $J = 12.8, 6.4$  Hz, 2H), 3.35 (s, 3H), 3.33 (s, 3H), 2.31–2.17 (m, 2H), 2.16–2.03 (m, 2H), 1.88–1.81 (m, 1H), 1.79 (s, 3H), 1.78 (s, 3H), 1.76–1.64 (m, 3H), 1.19 (d,  $J = 5.3$  Hz, 3H), 1.18 (d,  $J = 5.1$  Hz, 3H), 1.16 (s, 3H), 1.15 (s, 3H), 0.89 (s, 9H), 0.88 (s, 9H), 0.09–0.05 (m, 12H).

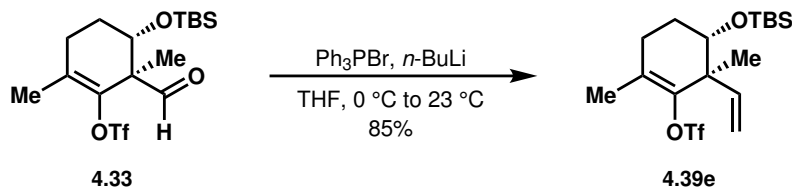


To a solution of **4.34** (17.2 mg, 0.040 mmol, 1 equiv) and DMAP (0.5 mg, 0.004 mmol, 0.1 equiv) in  $\text{CH}_2\text{Cl}_2$  (0.8 mL, 0.05 M) at 0 °C, anhydrous pyridine (9.6  $\mu\text{L}$ , 0.119 mmol, 3 equiv) and  $\text{Ac}_2\text{O}$  (11.3  $\mu\text{L}$ , 0.119 mmol, 3 equiv) were added, and the reaction mixture was warmed to 23 °C. After 19 h, the reaction was diluted with  $\text{Et}_2\text{O}$  (1 mL) and quenched with sat. aq.  $\text{NH}_4\text{Cl}$  (1 mL), and the aqueous and organic layers were separated. The aqueous layer was extracted with  $\text{Et}_2\text{O}$  (3 x 1 mL), and the combined organic layers were dried over  $\text{Na}_2\text{SO}_4$ , filtered, and concentrated *in vacuo*. Purification by flash column chromatography (5% EtOAc/hexanes) afforded **4.39c** (16.9 mg, 89% yield) as a clear oil as a ~1:1 mixture of diastereomers.  $^1\text{H NMR}$  (500 MHz,  $\text{CDCl}_3$ )  $\delta$  5.13–5.00 (m, 2H), 3.83 (dd,  $J = 7.1, 2.7$  Hz, 1H), 3.74 (dd,  $J = 9.4, 3.6$  Hz, 1H), 2.30 (dt,  $J = 17.7, 6.8$  Hz, 1H), 2.21 (dt,  $J = 17.8, 5.2$  Hz, 1H), 2.17–2.06 (m, 1H), 2.03 (s, 3H), 2.03 (s, 3H), 1.79 (s, 3H), 1.78 (s, 3H), 1.78–1.71 (m, 3H), 1.71–1.64 (m, 1H), 1.21 (d,  $J = 6.6$  Hz, 3H), 1.18 (d,  $J = 6.4$  Hz, 3H), 1.17 (s, 3H), 1.15 (s, 3H), 0.90 (s, 9H), 0.89 (s, 9H), 0.10 (s, 3H), 0.08 (s, 3H), 0.07 (s, 6H).

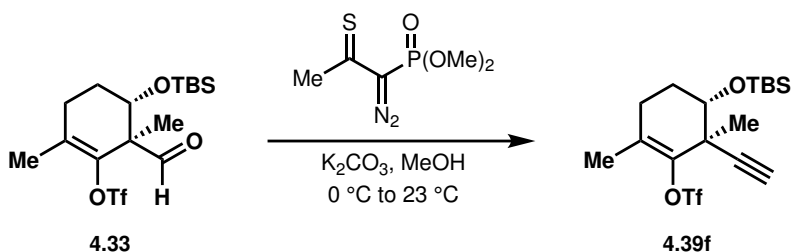




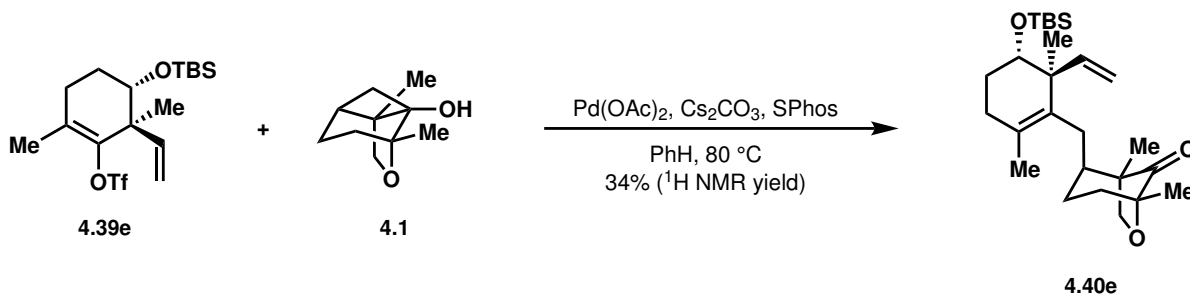
To a solution of **4.33** (21.8 mg, 0.052 mmol, 1 equiv) in THF (1.0 mL, 0.05 M) at  $-78\text{ }^\circ\text{C}$ , MeLi (1.0 M in  $\text{Et}_2\text{O}$ , 62.8  $\mu\text{L}$ , 0.063 mmol, 1.2 equiv) was added over 20 s. After 50 min, anhydrous pyridine (5.1  $\mu\text{L}$ , 0.063 mmol, 1.2 equiv) and TMSCl (8.0  $\mu\text{L}$ , 0.063 mmol, 1.2 equiv) were added, and the reaction mixture was warmed to  $0\text{ }^\circ\text{C}$ . After 1 h, the reaction was quenched with sat. aq.  $\text{NH}_4\text{Cl}$  (1 mL) and  $\text{Et}_2\text{O}$  (1 mL), and the aqueous and organic layers were separated. The aqueous layer was extracted with  $\text{Et}_2\text{O}$  (3 x 1 mL), and the combined organic layers were dried over  $\text{Na}_2\text{SO}_4$ , filtered, and concentrated *in vacuo*. Purification by flash column chromatography (1%  $\text{Et}_2\text{O}$ /hexanes) afforded **4.39d** (13.0 mg, 49% yield) as a ~1:1 mixture of diastereomers.  $^1\text{H NMR}$  (600 MHz,  $\text{CDCl}_3$ )  $\delta$  4.06 (dd,  $J = 5.5, 2.3$  Hz, 1H), 3.97 (dd,  $J = 8.9, 2.8$  Hz, 1H), 3.92 (q,  $J = 6.7$  Hz, 1H), 3.89 (q,  $J = 6.4$  Hz, 1H), 2.43–2.30 (m, 1H), 2.21 (dt,  $J = 17.6, 5.8$  Hz, 1H), 2.08–1.96 (m, 2H), 1.89–1.81 (m, 1H), 1.79 (s, 3H), 1.76 (s, 3H), 1.76–1.71 (m, 1H), 1.69–1.60 (m, 2H), 1.13 (d,  $J = 6.7$  Hz, 6H), 1.11 (s, 3H), 1.10 (s, 3H), 0.89 (s, 9H), 0.88 (s, 9H), 0.08 (s, 9H), 0.07–0.05 (m, 12H), 0.05 (s, 9H).



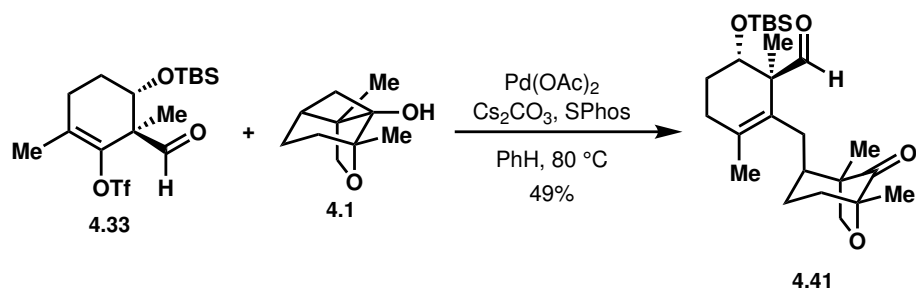
To a solution of  $\text{PPh}_3\text{Br}$  (305 mg, 0.853 mmol, 3 equiv) at  $0\text{ }^\circ\text{C}$  in THF (2.5 mL),  $n\text{-BuLi}$  (1.6 M in hexanes, 0.50 mL, 0.80 mmol, 2.8 equiv) was added over 20 s. After 1 h, a solution of **4.33** (119 mg, 0.284 mmol, 1 equiv) in THF (2.5 mL) was added and the reaction mixture was warmed to  $23\text{ }^\circ\text{C}$ . After 1 h, the reaction was quenched with sat. aq.  $\text{NH}_4\text{Cl}$  (5 mL) and  $\text{Et}_2\text{O}$  (5 mL), and the aqueous and organic layers were separated. The aqueous layer was extracted with  $\text{Et}_2\text{O}$  (3 x 3 mL), and the combined organic layers were dried over  $\text{Na}_2\text{SO}_4$ , filtered, and concentrated *in vacuo*. Purification by flash column chromatography (1%  $\text{EtOAc}$ /hexanes) afforded **4.39g** (100 mg, 85% yield) as a clear liquid.  $^1\text{H NMR}$  (400 MHz,  $\text{CDCl}_3$ )  $\delta$  5.69 (dd,  $J = 17.4, 10.7$  Hz, 1H), 5.21 (dd,  $J = 10.7, 0.8$  Hz, 1H), 5.15 (dd,  $J = 17.4, 0.8$  Hz, 1H), 3.63 (dd,  $J = 7.1, 2.3$  Hz, 1H), 2.31 (dt,  $J = 17.7, 7.1$  Hz, 1H), 2.12 (dt,  $J = 17.6, 5.7$  Hz, 1H), 1.91–1.81 (m, 1H), 1.80 (s, 3H), 1.62 (dq,  $J = 13.1, 6.2$  Hz, 1H), 1.22 (s, 3H), 0.88 (s, 9H), 0.04 (s, 3H), 0.04 (s, 3H).



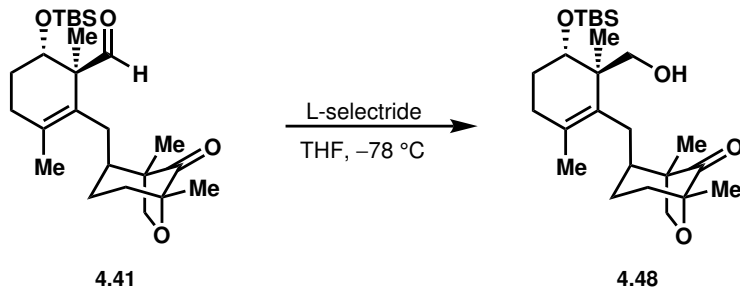
To a solution of **4.33** (22.4 mg, 0.054 mmol, 1 equiv) and  $\text{K}_2\text{CO}_3$  in MeOH at 0 °C, the Ohira–Bestmann reagent (24.2  $\mu\text{L}$ , 0.161 mmol, 3 equiv) was added, and the reaction mixture was warmed to 23 °. After 1 h, the reaction was quenched with sat. aq.  $\text{NH}_4\text{Cl}$  (1 mL) and  $\text{Et}_2\text{O}$  (1 mL), and the aqueous and organic layers were separated. The aqueous layer was extracted with  $\text{Et}_2\text{O}$  (3 x 1 mL), and the combined organic layers were dried over  $\text{Na}_2\text{SO}_4$ , filtered, and concentrated *in vacuo*. Purification by flash column chromatography (1% EtOAc/hexanes) afforded **4.39f** as a clear oil.  $^1\text{H NMR}$  (500 MHz,  $\text{CDCl}_3$ )  $\delta$  3.98 (dd,  $J = 6.2, 1.7$  Hz, 1H), 2.34 (tt,  $J = 12.0, 5.8$  Hz, 1H), 2.29 (s, 1H), 2.16–2.13 (m, 1H), 2.12–2.08 (m, 1H), 1.79 (s, 3H), 1.70 (dtd,  $J = 12.6, 6.2, 2.8$  Hz, 1H), 1.38 (s, 3H), 0.89 (s, 9H), 0.10 (s, 3H), 0.09 (s, 3H).



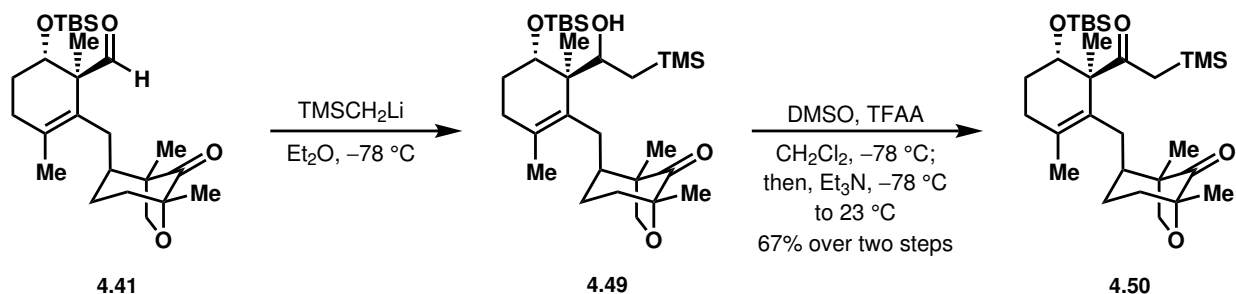
To a 1-dram vial was added **4.39e** (96.4 mg, 0.232 mmol, 1.25 equiv), **4.1** (31.3 mg, 0.186 mmol, 1 equiv),  $\text{Pd(OAc)}_2$  (4.2 mg, 0.019 mmol, 0.1 equiv),  $\text{Cs}_2\text{CO}_3$  (121 mg, 0.372 mmol, 2 equiv), and SPhos (15.3 mg, 0.037 mmol, 0.2 equiv). The vial was brought into a glovebox. Deuterated benzene (degassed with three cycles of freeze/pump/thaw; 1.9 mL) was added. The reaction mixture was stirred at 23 °C for 10 min, after which the reaction mixture was warmed to 80 °C. After 21 h, the reaction mixture was cooled to 23 °C and filtered through Celite with the aid of EtOAc. The filtrate was concentrated *in vacuo*. Purification by Yamazen automated flash column chromatography (3% EtOAc/hexanes) afforded **4.40e** as an orange oil.  $^1\text{H NMR}$  (500 MHz,  $\text{CDCl}_3$ )  $\delta$  5.57 (dd,  $J = 17.4, 10.6$  Hz, 1H), 5.07 (dd,  $J = 10.6, 1.4$  Hz, 1H), 4.95 (dd,  $J = 17.4, 1.4$  Hz, 1H), 4.24 (d,  $J = 8.1$  Hz, 1H), 3.82 (d,  $J = 8.1$  Hz, 1H), 2.21 (s, 1H), 2.16–2.08 (m, 1H), 2.05–1.58 (m, 8H), 1.55 (s, 3H), 1.46 (m, 1H), 1.20 (s, 3H), 1.08 (s, 3H), 1.04 (s, 3H), 0.84 (s, 9H), 0.00 (s, 3H),  $-0.03$  (s, 3H).



To a 1-dram vial was added **4.33** (138 mg, 0.332 mmol, 1.25 equiv), **4.1** (44.7 mg, 0.266 mmol, 1 equiv), Pd(OAc)<sub>2</sub> (6.0 mg, 0.027 mmol, 0.1 equiv), Cs<sub>2</sub>CO<sub>3</sub> (173 mg, 0.532 mmol, 2 equiv), and SPhos (21.8 mg, 0.053 mmol, 0.2 equiv). The vial was brought into a glovebox. Deuterated benzene (degassed with three cycles of freeze/pump/thaw; 2.7 mL) was added. The reaction mixture was stirred at 23 °C for 10 min, after which the reaction mixture was warmed to 80 °C. After 14 h, the reaction mixture was cooled to 23 °C and filtered through Celite with the aid of EtOAc. The filtrate was concentrated *in vacuo*. Purification by Yamazen automated flash column chromatography (7% EtOAc/hexanes) afforded **4.40e** (71.3 mg, 49%) as a white solid. <sup>1</sup>H NMR (500 MHz, CDCl<sub>3</sub>) δ 9.36 (s, 1H), 4.25 (d, *J* = 8.2 Hz, 1H), 4.07 (dd, *J* = 9.1, 6.4 Hz, 1H), 3.82 (d, *J* = 8.2 Hz, 1H), 2.18 (d, *J* = 7.8 Hz, 3H), 2.05–1.92 (m, 2H), 1.92–1.85 (m, 1H), 1.80–1.69 (m, 4H), 1.59 (s, 3H), 1.35 (dd, *J* = 14.4, 5.4 Hz, 1H), 1.20 (s, 3H), 1.16 (s, 3H), 0.99 (s, 3H), 0.82 (s, 9H), 0.04 (s, 3H), –0.01 (s, 3H).

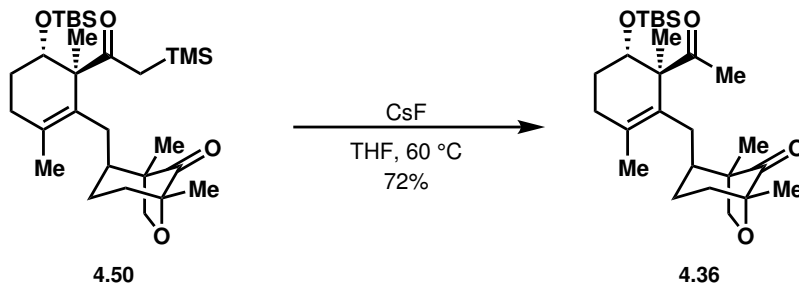


To a solution of **4.41** (2.4 mg, 0.006 mmol, 1 equiv) in THF (0.15 mL, 0.04 M) at –78 °C, L-selectride (1 M in THF, 6.6 μL, 0.007 mmol, 1.2 equiv) was added. The reaction mixture was stirred at –78 °C for 30 min, after which the reaction was quenched with sat. aq. NH<sub>4</sub>Cl (1 mL) and Et<sub>2</sub>O (1 mL). The organic and aqueous layers were separated, and the aqueous layer was extracted with Et<sub>2</sub>O (3 x 1 mL). The combined organic layers concentrated *in vacuo*. Purification by flash column chromatography (10% EtOAc/hexanes) afforded **4.41** as a white solid. <sup>1</sup>H NMR (600 MHz, CDCl<sub>3</sub> with two drops of D<sub>2</sub>O) δ 4.27 (d, *J* = 8.2 Hz, 1H), 3.86 (d, *J* = 8.2 Hz, 1H), 3.83 (dd, *J* = 8.8, 5.7 Hz, 1H), 3.57 (d, *J* = 10.7 Hz, 1H), 3.48 (d, *J* = 10.7 Hz, 1H), 2.32–2.24 (m, 1H), 2.14–2.05 (m, 3H), 2.03–1.95 (m, 2H), 1.95–1.88 (m, 1H), 1.85 (dd, *J* = 13.5, 5.4 Hz, 1H), 1.74–1.67 (m, 2H), 1.56 (s, 3H), 1.50 (dd, *J* = 14.4, 5.4 Hz, 1H), 1.22 (s, 3H), 1.14 (s, 3H), 0.92 (s, 3H), 0.89 (s, 9H), 0.07 (s, 6H).



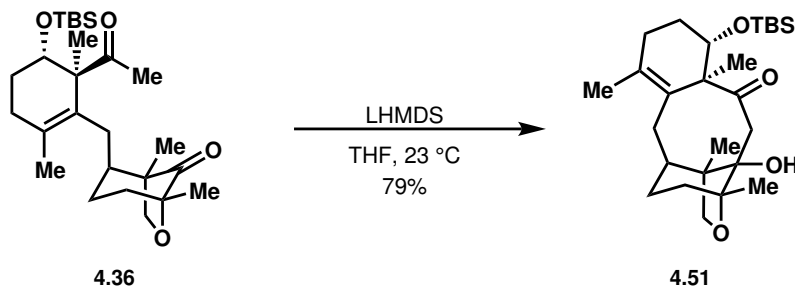
Two reactions were set up side by side. To a solution of **4.41** (30.4 mg, 0.070 mmol, 1 equiv; 30.9 mg, 0.071 mmol, 1 equiv) in Et<sub>2</sub>O (1.4 mL, 0.05 M; 1.4 mL, 0.05 M) at  $-78\text{ }^\circ\text{C}$ , TMSCH<sub>2</sub>Li (1 M in pentane, 105  $\mu\text{L}$ , 0.105 mmol, 1.5 equiv; 1 M in pentane, 107  $\mu\text{L}$ , 0.107 mmol, 1.5 equiv) was added over 3 s. The reaction mixture was stirred at  $-78\text{ }^\circ\text{C}$  for 20 min, after which the reaction was quenched with sat. aq. NH<sub>2</sub>Cl (1 mL; 1 mL). The aqueous and organic layers were separated, and the aqueous layer was extracted with Et<sub>2</sub>O (3 x 1.5 mL; 3 x 1.5 mL). The combined organic layers were dried over Na<sub>2</sub>SO<sub>4</sub>, filtered, and concentrated *in vacuo* to reveal crude **4.49**. The crude products were combined and taken on to the next reaction without purification.

To anhydrous DMSO (93.3  $\mu\text{L}$ , 1.31 mmol) in CH<sub>2</sub>Cl<sub>2</sub> (0.9 mL) at  $-78\text{ }^\circ\text{C}$ , TFAA (124  $\mu\text{L}$ , 0.88 mmol) was added dropwise over 1 min. After 15 min, a solution of crude **4.49** in CH<sub>2</sub>Cl<sub>2</sub> (0.9 mL) was added dropwise over 4 min. The reaction mixture was stirred for 2 h. Et<sub>3</sub>N (244  $\mu\text{L}$ , 1.75 mmol) was then added, and the reaction mixture was warmed to  $23\text{ }^\circ\text{C}$ . After 3 h, the reaction was quenched with sat. aq. NaHCO<sub>3</sub> (2 mL) and the aqueous and organic layers were separated. The aqueous layer was extracted with CH<sub>2</sub>Cl<sub>2</sub> (3 x 1 mL). The combined organic layers were dried over Na<sub>2</sub>SO<sub>4</sub>, filtered, and concentrated *in vacuo*. Purification by Yamazen automated flash column chromatography (6% EtOAc/hexanes) afforded **4.50** (49 mg, 67% yield over two steps). <sup>1</sup>H NMR (600 MHz, CDCl<sub>3</sub>)  $\delta$  4.24 (d,  $J = 8.2$  Hz, 1H), 4.13 (dd,  $J = 9.3, 3.4$  Hz, 1H), 3.83 (d,  $J = 8.2$  Hz, 1H), 2.27–2.21 (m, 1H), 2.19–2.11 (m, 1H), 2.06 (d,  $J = 15.1$  Hz, 1H), 1.97 (d,  $J = 15.1$  Hz, 1H), 2.10–1.94 (m, 3H), 1.93–1.87 (m, 1H), 1.84 (dd,  $J = 13.4, 5.2$  Hz, 1H), 1.61 (s, 3H), 1.74–1.57 (m, 3H), 1.47 (dd,  $J = 14.5, 5.2$  Hz, 1H), 1.21 (s, 3H), 1.18 (s, 3H), 1.05 (s, 3H), 0.84 (s, 9H), 0.10 (s, 9H), 0.05 (s, 3H), 0.03 (s, 3H).

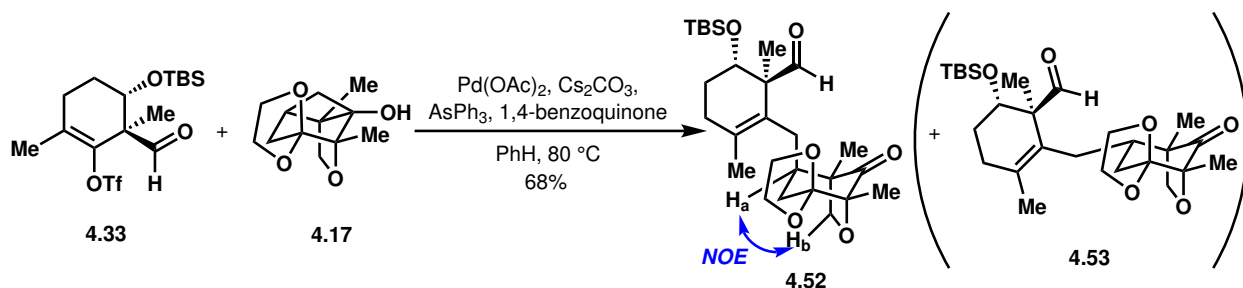


CsF (41.8 mg, 0.275 mmol, 2.5 equiv) was heated under high vacuum at  $100\text{ }^\circ\text{C}$  for 1 h. Then, the CsF was cooled to  $60\text{ }^\circ\text{C}$  and a solution of **4.50** (57.3 mg, 0.110 mmol, 1 equiv) in THF (2.2 mL, 0.05 M) was added. The reaction mixture was stirred at  $60\text{ }^\circ\text{C}$  for 13 h, after which it was quenched with sat. aq. NH<sub>4</sub>Cl (2 mL) and Et<sub>2</sub>O (2 mL). The aqueous and

organic layers were separated, and the aqueous layer was extracted with Et<sub>2</sub>O (3 x 2 mL). The combined organic layers were dried over Na<sub>2</sub>SO<sub>4</sub>, filtered, and concentrated *in vacuo*. Purification by Yamazen automated flash column chromatography (7% EtOAc/hexanes) afforded **4.36** (35.7 mg, 72%) as a white solid. <sup>1</sup>H NMR (500 MHz, CDCl<sub>3</sub>) δ 4.22 (d, *J* = 8.2 Hz, 1H), 4.13 (dd, *J* = 10.6, 5.2 Hz, 1H), 3.80 (d, *J* = 8.2 Hz, 1H), 2.21–2.13 (m, 3H), 2.07 (s, 3H), 2.03–1.92 (m, 2H), 1.90–1.81 (m, 2H), 1.76 (dd, *J* = 13.5, 5.5 Hz, 1H), 1.73–1.65 (m, 2H), 1.55 (s, 3H), 1.18 (s, 3H), 1.17 (s, 3H), 0.95 (s, 3H), 0.79 (s, 9H), 0.03 (s, 3H), -0.01 (s, 3H).

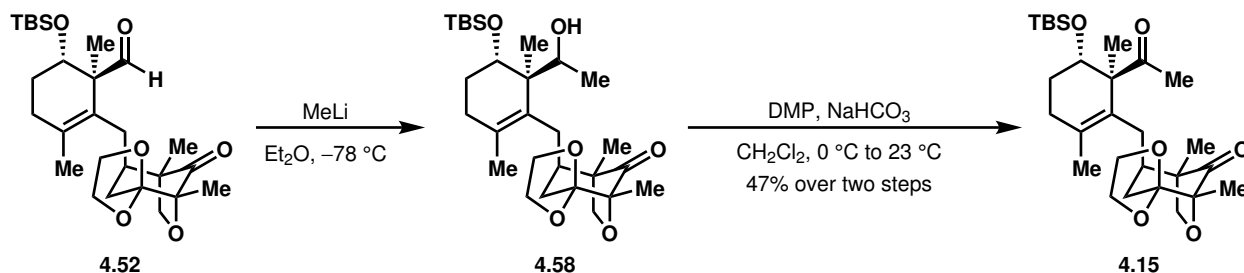


To a solution of **4.36** (35.7 mg, 0.080 mmol, 1 equiv) in THF (1.6 mL, 0.05 M) at 23 °C, LHMDS (1 M in THF, 398 μL, 5 equiv) was added dropwise over 15 s. After 30 min, the reaction was quenched with sat. aq. NH<sub>4</sub>Cl (2 mL) and Et<sub>2</sub>O (2 mL). The aqueous and organic layers were separated, and the aqueous layer was extracted with Et<sub>2</sub>O (3 x 2 mL). The combined organic layers were dried over Na<sub>2</sub>SO<sub>4</sub>, filtered, and concentrated *in vacuo*. Purification by Yamazen automated flash column chromatography afforded **4.51** (28.3 mg, 79% yield). <sup>1</sup>H NMR (600 MHz, CDCl<sub>3</sub>) δ 3.79 (d, *J* = 7.4 Hz, 1H), 3.79 (dd, *J*, 7.4 Hz, 3.9 Hz, 1H) 3.62 (d, *J* = 7.7 Hz, 1H), 3.32 (d, *J* = 13.4 Hz, 1H), 3.19 (s, 1H), 2.60 (dd, *J* = 15.8, 5.8 Hz, 1H), 2.39–2.26 (m, 1H), 2.26–2.15 (m, 1H), 2.10 (d, *J* = 13.4 Hz, 1H), 1.82 (s, 3H), 1.77–1.66 (m, 3H), 1.61 (dd, *J* = 13.6, 8.8 Hz, 1H), 1.22 (s, 3H), 1.19 (s, 3H), 0.93 (s, 3H), 0.86 (s, 9H), 0.02 (s, 3H), -0.04 (s, 3H). <sup>13</sup>C NMR (151 MHz, CDCl<sub>3</sub>) δ 213.9, 132.4, 132.1, 86.9, 80.4, 79.6, 77.4, 77.2, 77.0, 71.0, 61.5, 50.1, 47.5, 41.0, 35.9, 32.2, 30.5, 27.6, 25.8, 21.6, 21.0, 19.4, 18.1, 17.2, 14.1, -3.8, -4.8.



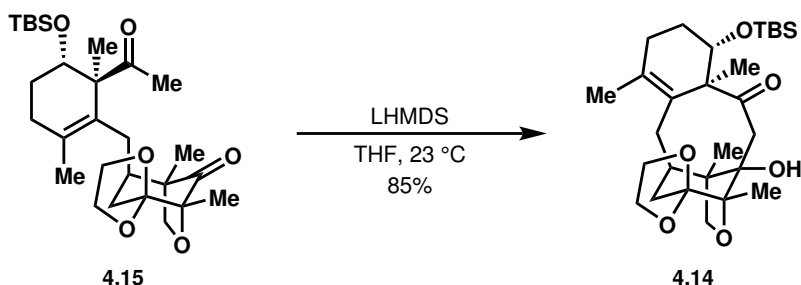
To a 100 mL Schlenk flask was added **4.33** (1.51 g, 3.63 mmol, 1.25 equiv), **4.17** (656 mg, 2.90 mmol, 1.0 equiv), AsPh<sub>3</sub> (444 mg, 1.45 mmol, 0.5 equiv), 1,4-benzoquinone (62.7 mg, 0.580 mmol, 0.2 equiv), and Pd(OAc)<sub>2</sub> (130 mg, 0.580 mmol, 0.2 equiv). The Schlenk was evacuated and backfilled with N<sub>2</sub>, sealed, and taken into a N<sub>2</sub>-filled glovebox where Cs<sub>2</sub>CO<sub>3</sub> (1.90 g, 5.80 mmol, 2 equiv) and benzene (29 mL, 0.10 M) were added. The vial was

sealed again, taken out of the glovebox and the mixture was stirred at 23 °C for 10 min and then warmed to 80 °C and stirred for 27 h. The reaction mixture was then filtered through Celite with EtOAc and concentrated *in vacuo*. Purification by flash column chromatography (5% EtOAc/hexanes to 25% EtOAc/hexanes) afforded **4.52** (970 mg, 68% yield) as a light yellow waxy solid. NOE analysis of **4.52** confirmed its relative stereochemistry. Undesired diastereomer **4.53** was observed in substantial yields under unoptimized conditions. For **4.52**: **TLC** (25% EtOAc/hexanes):  $R_f = 0.5$  (*p*-anisaldehyde) **<sup>1</sup>H NMR** (600 MHz, CDCl<sub>3</sub>)  $\delta$  9.39 (s, 1H), 4.13 (d,  $J = 8.4$  Hz, 1H), 4.09–4.02 (m, 2H), 4.01–3.96 (m, 1H), 3.83 (d,  $J = 8.4$  Hz, 1H), 3.82–3.73 (m, 2H), 2.36–2.29 (m, 1H), 2.25–2.12 (m, 3H), 2.11–2.05 (m, 1H), 1.79–1.71 (m, 2H), 1.70–1.63 (m, 4H), 1.58 (d,  $J = 14.7$  Hz, 1H), 1.19 (s, 3H), 1.17 (s, 3H), 1.01 (s, 3H), 0.81 (s, 9H), 0.03 (s, 3H), –0.02 (s, 3H). **<sup>13</sup>C NMR** (151 MHz, CDCl<sub>3</sub>)  $\delta$  210.1, 205.1, 133.3, 126.9, 115.0, 83.4, 75.8, 71.2, 65.7, 65.7, 57.0, 49.5, 41.3, 32.0, 31.6, 29.8, 26.4, 25.7, 19.5, 18.0, 15.4, 13.1, 11.8, –3.7, –4.9. **IR** (ATR, thin film):  $\nu$  2930, 2882, 1762, 1729, 1253 cm<sup>–1</sup>. **HRMS** (EI+)  $m/z$  calc'd for C<sub>27</sub>H<sub>44</sub>O<sub>6</sub>Si [M]<sup>+</sup>: 492.2902, found: 492.2905.  $[\alpha]_D^{20} = +42.4^\circ$  ( $c = 1.10$ , CHCl<sub>3</sub>). For **4.53**: **<sup>1</sup>H NMR** (700 MHz, CDCl<sub>3</sub>)  $\delta$  9.50 (s, 1H), 4.08 (d,  $J = 8.4$  Hz, 1H), 4.07–4.04 (m, 1H), 4.01–3.97 (m, 1H), 3.91 (dd,  $J = 8.4, 3.4$  Hz, 1H), 3.87–3.83 (m, 2H), 3.83 (d,  $J = 8.4$  Hz, 1H), 2.24–2.09 (m, 4H), 1.94 (d,  $J = 14.7$  Hz, 1H), 1.73 (s, 3H), 1.77–1.65 (m, 5H), 1.18 (s, 3H), 1.17 (s, 3H), 1.10 (s, 3H), 0.84 (s, 9H), 0.04 (s, 3H), 0.02 (s, 3H).

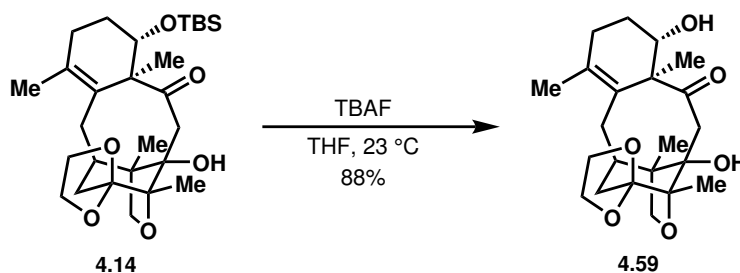


To a solution of **4.52** (1.28 g, 2.60 mmol, 1 equiv) in Et<sub>2</sub>O (52 mL, 0.05 M) at –78 °C was added MeLi (1.6 M in Et<sub>2</sub>O, 2.10 mL, 3.38 mmol, 1.3 equiv) via syringe pump (over 2 min) directly into the reaction mixture (not down the sides of the flask). [Note: Prior to reaction setup, **4.52** was dried via azeotropic distillation with benzene (3 x 10 mL) and concentrated *in vacuo* overnight.] The resulting mixture was then stirred at –78 °C for 24 min. The reaction was quenched by the addition of sat. aq. NH<sub>4</sub>Cl (30 mL). The reaction was repeated two additional times, once on 2.58 mmol scale and once on 2.82 mmol scale (based on mmol of **4.52**) following the same procedure. After quenching the last batch, all three reaction mixtures were combined, and the organic and aqueous layers were separated. The aqueous phase was extracted with Et<sub>2</sub>O (3 x 40 mL), and the combined organic layers were dried over Na<sub>2</sub>SO<sub>4</sub>, filtered, and concentrated *in vacuo*. The crude product was used without purification and was reconstituted in HPLC grade CH<sub>2</sub>Cl<sub>2</sub> (non-dried, 80 mL, 0.1 M) in a non-flame dried flask and cooled to 0 °C. NaHCO<sub>3</sub> (3.4 g, 40 mmol, 5 equiv) was added followed by the addition of Dess–Martin periodinane (6.8 g, 16 mmol, 2 equiv) in one portion and the reaction mixture was warmed to 23 °C. After stirring for 3.5 h, the reaction was quenched by the addition of sat. aq. Na<sub>2</sub>S<sub>2</sub>O<sub>3</sub> (80 mL), and the organic and aqueous layers were separated. The aqueous phase was extracted with CH<sub>2</sub>Cl<sub>2</sub> (3 x 50 mL), and the

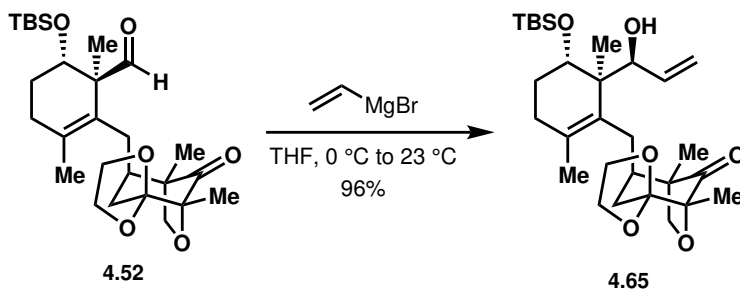
combined organic layers were washed with brine (150 mL), dried over Na<sub>2</sub>SO<sub>4</sub>, filtered, and concentrated *in vacuo*. The crude product was purified by Yamazen automated flash column chromatography (1% EtOAc/CH<sub>2</sub>Cl<sub>2</sub> to 3% EtOAc/CH<sub>2</sub>Cl<sub>2</sub>) to afford **4.15** (1.9 g, 47% yield over two steps) as a white powder. **TLC** (2% EtOAc/CH<sub>2</sub>Cl<sub>2</sub>): R<sub>f</sub> = 0.4 (*p*-anisaldehyde) **<sup>1</sup>H NMR** (600 MHz, CDCl<sub>3</sub>) δ 4.17–4.12 (m, 2H), 4.07–4.03 (m, 1H), 4.01–3.97 (m, 1H), 3.83 (d, *J* = 8.5 Hz, 1H), 3.82–3.74 (m, 2H), 2.37–2.31 (m, 1H), 2.26–2.12 (m, 3H), 2.11–2.07 (m, 4H), 1.76–1.71 (m, 2H), 1.65 (s, 3H), 1.60 (d, *J* = 14.7 Hz, 1H), 1.58–1.53 (m, 1H), 1.22 (s, 3H), 1.17 (s, 3H), 1.02 (s, 3H), 0.81 (s, 9H), 0.05 (s, 3H), 0.02 (s, 3H). **<sup>13</sup>C NMR** (151 MHz, CDCl<sub>3</sub>) δ 211.7, 210.3, 131.8, 129.0, 115.1, 83.4, 75.9, 73.8, 65.7, 65.7, 59.2, 49.5, 42.1, 32.1, 31.8, 29.7, 27.1, 26.6, 25.7, 19.6, 18.1, 17.5, 13.0, 11.8, −3.13, −4.92. **IR** (ATR, thin film): ν 2927, 2855, 1763, 1734, 1709, 1462, 1371, 1252, 1118, 1065, 1005, 837, 774 cm<sup>−1</sup>. **HRMS** (EI+) *m/z* calc'd for C<sub>28</sub>H<sub>46</sub>O<sub>6</sub>Si [M]<sup>+</sup>: 506.3058, found: 506.3061. [α]<sub>D</sub><sup>20</sup> = +16.7° (*c* = 0.06, CHCl<sub>3</sub>).



To a solution of **4.15** (1.9 g, 3.75 mmol, 1 equiv) in THF (75 mL, 0.05M) at 23 °C was added LHMDS (1M in THF, 18.8 mL, 18.8 mmol, 5 equiv) rapidly dropwise, and the resulting mixture was stirred at 23 °C for 9.5 h. The reaction was then quenched by the addition of sat. aq. NH<sub>4</sub>Cl (50 mL), and the organic and aqueous layers were separated. The aqueous phase was extracted with EtOAc (3 x 50 mL), and the combined organic layers were washed with brine (150 mL), dried over Na<sub>2</sub>SO<sub>4</sub>, filtered, and concentrated *in vacuo*. The crude product was purified by Yamazen automated flash column chromatography (10% EtOAc/hexanes to 50% EtOAc/hexanes) to afford **4.14** (1.62 g, 85% yield) as a white foam. **TLC** (50% EtOAc/hexanes): R<sub>f</sub> = 0.3 (*p*-anisaldehyde) **<sup>1</sup>H NMR** (600 MHz, CDCl<sub>3</sub>) δ 4.08–4.03 (m, 2H), 3.96–3.92 (m, 1H), 3.90–3.85 (m, 1H), 3.84 (d, *J* = 7.9 Hz, 1H), 3.79–3.73 (m, 2H), 3.60 (d, *J* = 7.9 Hz, 1H), 3.39 (br s, 1H), 2.58 (dd, *J* = 15.9, 7.0 Hz, 1H), 2.30–2.22 (m, 2H), 2.17–2.12 (m, 1H), 2.11–2.00 (m, 3H), 1.93 (d, *J* = 14.2 Hz, 1H), 1.80 (s, 3H), 1.74–1.67 (m, 2H), 1.19 (s, 3H), 1.16 (s, 3H), 0.94 (s, 3H), 0.85 (s, 9H), 0.02 (s, 3H), −0.04 (s, 3H). **<sup>13</sup>C NMR** (151 MHz, CDCl<sub>3</sub>) δ 215.1, 132.0, 131.6, 111.4, 90.9, 80.8, 79.2, 70.9, 65.6, 64.4, 61.4, 49.3, 44.9, 39.8, 34.8, 32.1, 30.1, 27.6, 25.8, 21.6, 18.0, 17.3, 14.1, 11.7, −3.8, −4.83. **IR** (ATR, thin film): ν 3534, 2927, 2856, 1702 cm<sup>−1</sup>. **HRMS** (EI+) *m/z* calc'd for C<sub>28</sub>H<sub>46</sub>O<sub>6</sub>Si [M]<sup>+</sup>: 506.3058, found: 506.3064. [α]<sub>D</sub><sup>20</sup> = +4.63° (*c* = 1.75, CHCl<sub>3</sub>).



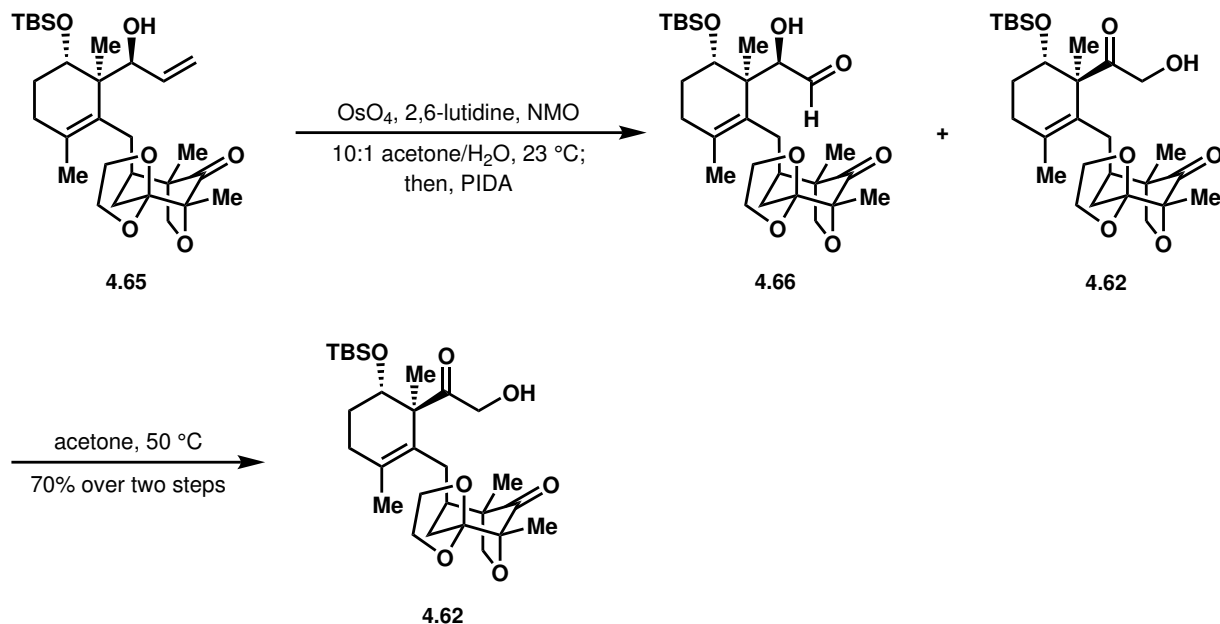
To a solution of **4.14** (10 mg, 0.020 mmol, 1 equiv) in THF (1.0 mL, 0.020 M) at 23 °C was added TBAF (1M in THF, 0.1 mL, 0.10 mmol, 5 equiv) dropwise. The resulting mixture was then stirred at 23 °C for 18 h. The reaction was diluted with H<sub>2</sub>O (2 mL) and EtOAc (2 mL) and the organic and aqueous layers were separated. The aqueous phase was extracted with EtOAc (2 x 1 mL), and the combined organic layers were washed with brine (3 mL), dried over MgSO<sub>4</sub>, filtered, and concentrated *in vacuo*. The crude product was purified by Yamazen automated flash column chromatography (40% acetone/hexanes) to afford **4.59** (6.9 mg, 88% yield) as a white crystalline solid. **TLC** (50% acetone/hexanes): R<sub>f</sub> = 0.5 (*p*-anisaldehyde) **<sup>1</sup>H NMR** (600 MHz, CDCl<sub>3</sub>) δ 4.13 (d, *J* = 13.9 Hz, 1H), 4.05–4.00 (m, 1H), 3.97–3.93 (m, 1H), 3.90–3.84 (m, 2H), 3.78–3.72 (m, 2H), 3.63 (d, *J* = 8.0 Hz, 1H), 3.18 (s, 1H), 2.64 (dd, *J* = 15.9, 6.6 Hz, 1H), 2.35–2.27 (m, 2H), 2.23–2.18 (m, 1H), 2.16–2.11 (m, 1H), 2.11–2.04 (m, 3H), 1.90–1.85 (m, 1H), 1.83 (s, 3H), 1.71–1.65 (m, 2H), 1.22 (s, 3H), 1.16 (s, 3H), 0.95 (s, 3H). **<sup>13</sup>C NMR** (151 MHz, CDCl<sub>3</sub>) δ 217.5, 132.8, 130.8, 111.4, 91.0, 80.7, 79.5, 70.1, 65.6, 64.5, 61.0, 49.3, 44.9, 40.1, 35.1, 32.0, 30.4, 25.9, 21.6, 17.2, 13.6, 11.6. **IR** (ATR, thin film): ν 3476, 2935, 2878, 1703 cm<sup>-1</sup>. **HRMS** (ESI+) *m/z* calc'd for C<sub>22</sub>H<sub>32</sub>O<sub>6</sub>Na [M+Na]<sup>+</sup>: 415.2091, found: 415.2086. [α]<sub>D</sub><sup>20</sup> = -30.4° (*c* = 0.8, CHCl<sub>3</sub>).



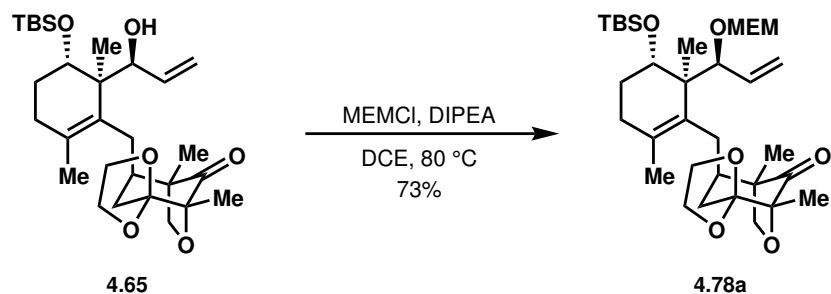
To a solution of **4.52** (165 mg, 0.336 mmol, 1 equiv) in THF (6.7 mL, 0.05 M) at -78 °C, vinylmagnesium bromide (1.0 M in THF, 0.50 mL, 0.50 mmol, 1.5 equiv) was added dropwise over 1 min. The reaction mixture was warmed to 23 °C and stirred for 20 min, after which the reaction was quenched with sat. aq. NH<sub>4</sub>Cl (7 mL). The organic and aqueous layers were separated, and the aqueous layer was extracted with EtOAc (3 x 6 mL). The combined organic layers were dried over Na<sub>2</sub>SO<sub>4</sub>, filtered, and concentrated to reveal **4.65** (167 mg, 96% yield) as a light brown solid. **<sup>1</sup>H NMR** (500 MHz, CDCl<sub>3</sub>) δ 5.83 (ddd, *J* = 17.2, 10.7, 2.7 Hz, 1H), 5.52 (dt, *J* = 17.1, 2.3 Hz, 1H), 5.24 (dt, *J* = 10.7, 2.2 Hz, 1H), 4.31–4.25 (m, 1H), 4.15 (d, *J* = 8.4 Hz, 1H), 4.10–4.03 (m, 1H), 3.98 (d, *J* = 9.3 Hz, 1H), 4.02–3.94 (m, 2H), 3.88 (d, *J* = 8.4 Hz, 1H), 3.85–3.72 (m, 2H), 2.39–2.27 (m, 2H), 2.22 (m, 1H), 2.13–1.98 (m, 2H), 1.92 (d, *J* = 13.2 Hz, 1H), 1.72 (d, *J* = 14.9 Hz, 1H), 1.80–1.68 (m,



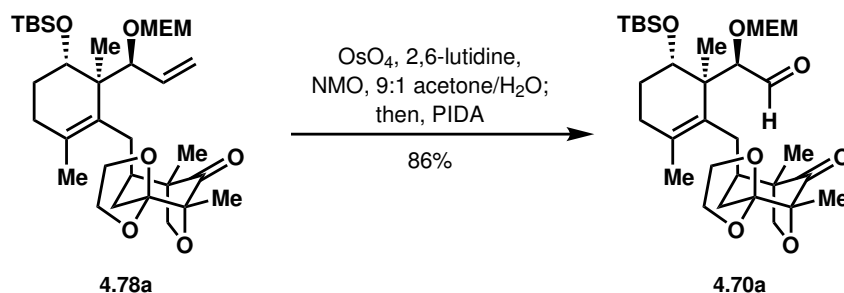
1H), 1.68–1.62 (m, 1H), 1.62 (s, 3H), 1.30 (s, 3H), 1.20 (s, 3H), 1.15 (s, 3H), 0.90 (s, 9H), 0.10 (s, 3H), 0.08 (s, 3H).



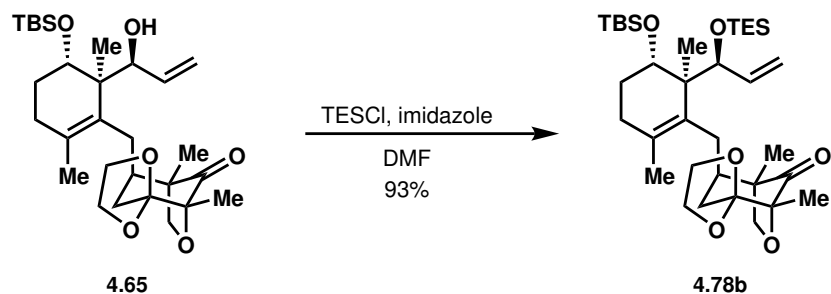
To a solution of **4.65** (167 mg, 0.321 mmol, 1 equiv) in a 10:1 mixture of HPLC grade acetone and water (11.7 mL and 1.2 mL; 0.025 M), 2,6-lutidine (74.7  $\mu\text{L}$ , 0.64 mmol, 2 equiv), NMO (113 mg, 0.96 mmol, 3 equiv), and  $\text{OsO}_4$  (4 wt% in  $\text{H}_2\text{O}$ , 0.25 mL, 0.03 mmol, 0.1 equiv) were added. The resulting reaction mixture was stirred vigorously for 13 h. PIDA (103 mg, 0.32 mmol, 1 equiv) was then added, and the reaction was stirred for 7 min. The reaction was then quenched by pouring the reaction mixture into sat. aq.  $\text{Na}_2\text{S}_2\text{O}_3$  (10 mL), and the aqueous and organic layers were separated. The aqueous layer was extracted with EtOAc (3 x 10 mL), and the combined organic layers were washed with brine (2 x 10 mL). The combined organic layers were then dried over  $\text{Na}_2\text{SO}_4$ , filtered, and concentrated *in vacuo*. Purification by Yamazen automated flash chromatography afforded a mixture of **4.66** and **4.62**. This mixture was then taken up in HPLC grade acetone (12 mL), warmed to 50  $^\circ\text{C}$ , and stirred for 16 h, after which the reaction mixture was cooled to 23  $^\circ\text{C}$  and concentrated *in vacuo* to afford **4.62** (117 mg, 70% over two steps).  $^1\text{H NMR}$  (700 MHz,  $\text{CDCl}_3$ )  $\delta$  4.33–4.28 (m, 2H), 4.12 (d,  $J = 8.4$  Hz, 1H), 4.05 (ddd,  $J = 7.7, 5.8, 3.8$  Hz, 1H), 4.00 (dd,  $J = 6.8, 4.6$  Hz, 1H), 4.00–3.97 (ddd,  $J = 7.7, 5.8, 3.8$  Hz, 1H), 3.85 (d,  $J = 8.4$  Hz, 1H), 3.81 (td,  $J = 7.8, 5.9$  Hz, 1H), 3.76 (td,  $J = 7.9, 6.1$  Hz, 1H), 3.19 (t,  $J = 4.7$  Hz, 1H), 2.30 (dd,  $J = 15.0, 13.2$  Hz, 1H), 2.25–2.12 (m, 2H), 1.98–1.90 (m, 1H), 1.80–1.69 (m, 2H), 1.64 (s, 3H), 1.65–1.61 (m, 1H), 1.59 (d,  $J = 14.7$  Hz, 1H), 1.33 (s, 3H), 1.17 (s, 3H), 0.99 (s, 3H), 0.81 (s, 9H), 0.04 (s, 3H),  $-0.03$  (s, 3H).



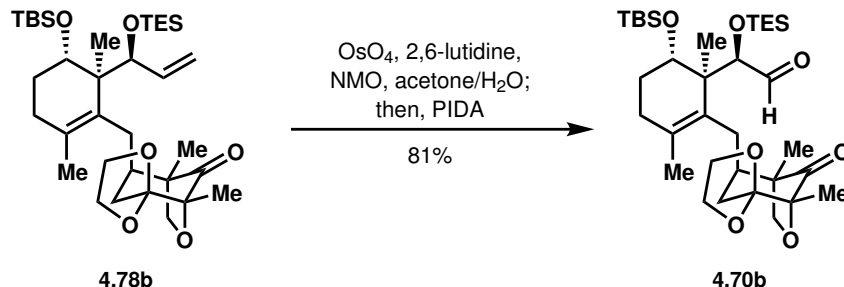
To a solution of **4.65** (99.8 mg, 0.192 mmol, 1 equiv) in anhydrous 1,2-DCE (1.9 mL) at 23 °C, MEMCl (109  $\mu\text{L}$ , 0.958 mmol, 5 equiv) and DIPEA (167  $\mu\text{L}$ , 0.958 mmol, 5 equiv) were added, and the resulting reaction mixture was warmed to 80 °C. The reaction was stirred at 80 °C for 8 h, after which it was quenched with sat. aq.  $\text{NaHCO}_3$  (2 mL) and  $\text{Et}_2\text{O}$  (2 mL). The aqueous and organic layers were separated, and the aqueous layer was extracted with  $\text{Et}_2\text{O}$  (3 x 2 mL). The combined organic layers were dried over  $\text{Na}_2\text{SO}_4$ , filtered, and concentrated *in vacuo*. Purification by Yamazen automated column chromatography (25%  $\text{EtOAc}$ /hexanes) afforded **4.78a** (85.3 mg, 73% yield) as a white solid.



To a solution of **4.78a** (75.4 mg, 0.124 mmol, 1 equiv) in a 9:1 mixture of acetone and  $\text{H}_2\text{O}$  (4.5 mL and 0.5 mL; 0.025 M), 2,6-lutidine (26.5  $\mu\text{L}$ , 0.248 mmol, 2 equiv), NMO (29.0 mg, 0.248 mmol, 2 equiv), and  $\text{OsO}_4$  (4 wt% in  $\text{H}_2\text{O}$ , 97.0  $\mu\text{L}$ , 0.012 mmol, 0.1 equiv) were added. The reaction mixture was stirred at 23 °C for 71 h. PIDA (59.8 mg, 0.186 mmol, 1.5 equiv) was then added, and the reaction mixture was stirred for 1 h. The reaction was then quenched with sat. aq.  $\text{Na}_2\text{S}_2\text{O}_3$  (5 mL) and  $\text{EtOAc}$  (5 mL), and the aqueous and organic layers were separated. The aqueous layer was extracted with  $\text{EtOAc}$  (3 x 3 mL), and the combined organic layers were dried over  $\text{Na}_2\text{SO}_4$ , filtered, and concentrated *in vacuo*. Purification by Yamazen automated column chromatography (30%  $\text{EtOAc}$ /hexanes) afforded **4.70a** (64.9 mg, 86% yield) as a waxy part-white solid.  $^1\text{H NMR}$  (700 MHz,  $\text{CDCl}_3$ )  $\delta$  9.68 (d,  $J = 2.1$  Hz, 1H), 4.74 ( $J, J = 7.1$  Hz, 1H), 4.65 ( $J, J = 7.1$  Hz, 1H), 4.09 ( $J, J = 8.4$  Hz, 1H), 4.06–4.01 (m, 1H), 3.98 (d,  $J = 2.0$  Hz, 1H), 3.98–3.95 (m, 1H), 3.88 (d,  $J = 8.4$  Hz, 1H), 3.88–3.80 (m, 2H), 3.77 (dd,  $J = 5.0, 2.6$  Hz, 1H), 3.73 (dt,  $J = 10.9, 4.4$  Hz, 1H), 3.65 (dt,  $J = 11.0, 4.6$  Hz, 1H), 3.49 (t,  $J = 4.6$  Hz, 2H), 3.36 (s, 3H), 2.34 (dd,  $J = 14.4, 12.1$  Hz, 1H), 2.23–2.08 (m, 4H), 2.01–1.93 (m, 1H), 1.93–1.85 (m, 1H), 1.82 (d,  $J = 14.8$  Hz, 1H), 1.69 (s, 3H), 1.69–1.63 (m, 1H), 1.21 (s, 3H), 1.20 (s, 3H), 1.19 (s, 3H), 0.86 (s, 9H), 0.05 (s, 3H), 0.02 (s, 3H).



To a solution of **4.65** (4.5 mg, 0.009 mmol, 1 equiv) and imidazole (1.8 mg, 0.026 mmol, 3 equiv) in anhydrous DMF (0.2 mL, 0.05 M), TESCl (2.2  $\mu$ L, 0.013 mmol, 1.5 equiv) was added, and the reaction mixture was stirred at 23 °C. After 4 h, imidazole (1.8 mg, 0.026 mmol, 3 equiv) and TESCl (2.2  $\mu$ L, 0.013 mmol, 1.5 equiv) was added. After another 4 h, the reaction was quenched with sat. aq. NaHCO<sub>3</sub> (0.5 mL) and Et<sub>2</sub>O (0.5 mL), and the aqueous and organic layers were separated. The aqueous layer was extracted with Et<sub>2</sub>O (3 x 0.5 mL), and the combined organic layers were concentrated *in vacuo*. Purification by flash column chromatography (10% EtOAc/hexanes) afforded **4.78b** (5.1 mg, 93% yield) as an oil. <sup>1</sup>H NMR (700 MHz, CDCl<sub>3</sub>)  $\delta$  5.74 (ddd,  $J = 17.2, 10.5, 7.5$  Hz, 1H), 5.15–5.07 (m, 2H), 4.07 (d,  $J = 8.2$  Hz, 1H), 4.08–4.02 (m, 1H), 4.00–3.94 (m, 2H), 3.87 (d,  $J = 8.2$  Hz, 1H), 3.86–3.83 (m, 2H), 3.44–3.41 (m, 1H), 2.29 (d,  $J = 13.9$  Hz, 1H), 2.26–2.20 (m, 1H), 2.20–2.13 (m, 1H), 2.11–2.06 (m, 2H), 1.95–1.81 (m, 3H), 1.68 (s, 3H), 1.54–1.48 (m, 1H), 1.30–1.22 (m, 1H), 1.20 (s, 3H), 1.19 (s, 3H), 1.05 (s, 3H), 0.90 (t,  $J = 8.0$  Hz, 9H), 0.84 (s, 9H), 0.51 (q,  $J = 8.0$  Hz, 6H), 0.00 (s, 3H), –0.01 (s, 3H).

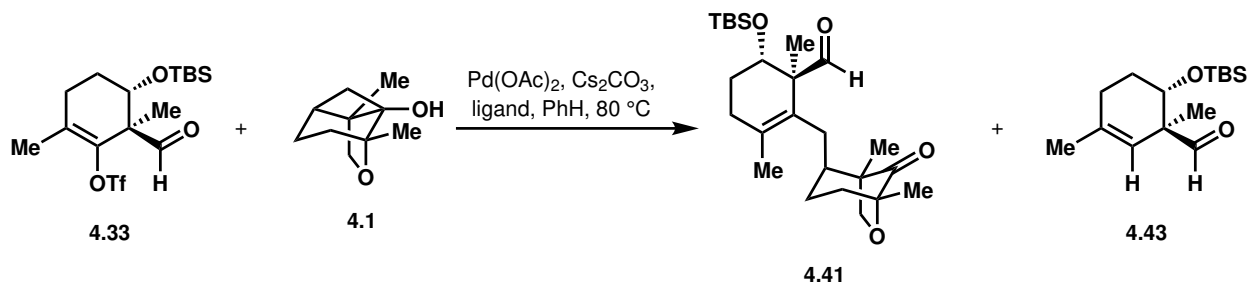


To a solution of **4.78b** (50.3 mg, 0.079 mmol, 1 equiv) in a mixture of acetone and water (2.9 mL, 0.23 mL; 0.025 M), 2,6-lutidine (18.4  $\mu$ L, 0.158 mmol, 2 equiv), NMO (27.8 mg, 0.24 mmol, 3 equiv), and OsO<sub>4</sub> (4 wt% in H<sub>2</sub>O, 62  $\mu$ L, 0.008 mmol, 0.1 equiv) were added, and the reaction mixture was stirred vigorously at 23 °C for 7.5 d. PIDA (38.3 mg, 0.12 mmol, 1.5 equiv) was then added and the reaction mixture was stirred for 40 min. The reaction was then quenched with sat. aq. Na<sub>2</sub>S<sub>2</sub>O<sub>3</sub> (3 mL) and EtOAc (1.5 mL), and the organic and aqueous layers were separated. The aqueous layer was extracted with EtOAc (3 x 1.5 mL), and the combined organic layers were concentrated *in vacuo*. Purification by Yamazen flash automated column chromatography (10% EtOAc/hexanes) afforded **4.70b** (40.6 mg, 81% yield). <sup>1</sup>H NMR (500 MHz, CDCl<sub>3</sub>)  $\delta$  9.59 (d,  $J = 2.9$  Hz, 1H), 4.09 (d,  $J = 8.4$  Hz, 1H), 4.07–4.02 (m, 1H), 4.01–3.95 (m, 1H), 3.92–3.81 (m, 4H), 3.71–3.68 (m, 1H), 2.30 (dd,  $J = 14.2, 11.7$  Hz, 1H), 2.24–2.06 (m, 4H), 1.98–1.86 (m, 2H), 1.83 (d,  $J = 14.4$  Hz, 1H),

1.69 (s, 3H), 1.66–1.60 (m, 1H), 1.21 (s, 3H), 1.21 (s, 3H), 1.20 (s, 3H), 0.93 (t,  $J = 8.0$  Hz, 9H), 0.86 (s, 9H), 0.56 (q,  $J = 8.0$  Hz, 6H), 0.04 (s, 3H), 0.01 (s, 3H).

### 4.7.3 Supplementary Figures

**Table S4.1:** Ligand screening for cross-coupling of model southern coupling partner **4.1** with northern coupling partner **4.33**.  $^1\text{H}$  NMR yield with mesitylene as an internal standard.



Entry	Ligand (mol %)	% yield <b>4.41</b> <sup>a</sup>	<b>4.41</b> : <b>4.43</b>	Entry	Ligand (mol %)	% yield <b>4.41</b> <sup>a</sup>	<b>4.41</b> : <b>4.43</b>
1	SPhos (20%)	45	65 : 35	11	<i>t</i> -BuDavePhos (20%)	1	3 : 97
2	SIMes-HBF <sub>4</sub> (20%)	1	2 : 98	12	( <i>S,S</i> )-DIOP (10%)	5	9 : 91
3	Mor-DalPhos (20%)	1	8 : 92	13	PhDavePhos (20%)	10	17 : 83
4	Josiphos SL-J009-1 (10%)	0	0 : 100	14	JohnPhos (20%)	1	6 : 94
5	dppf (10%)	12	27 : 73	15	CyJohnPhos (20%)	3	6 : 94
6	Xantphos (10%)	1	12 : 88	16	RuPhos (20%)	35	52 : 48
7	PCy <sub>3</sub> (20%)	13	22 : 78	17	CPhos (20%)	7	17 : 83
8	( <i>S</i> )-BINAP	29	62 : 38	18	P(2-furyl) <sub>3</sub> (20%)	22	31 : 69
9	XPhos (20%)	4	12 : 88	19	P(C <sub>6</sub> F <sub>5</sub> ) <sub>3</sub> (20%)	0	N/A
10	DavePhos (20%)	15	21 : 79	20	P(OPh) <sub>3</sub> (20%)	0	0 : 100

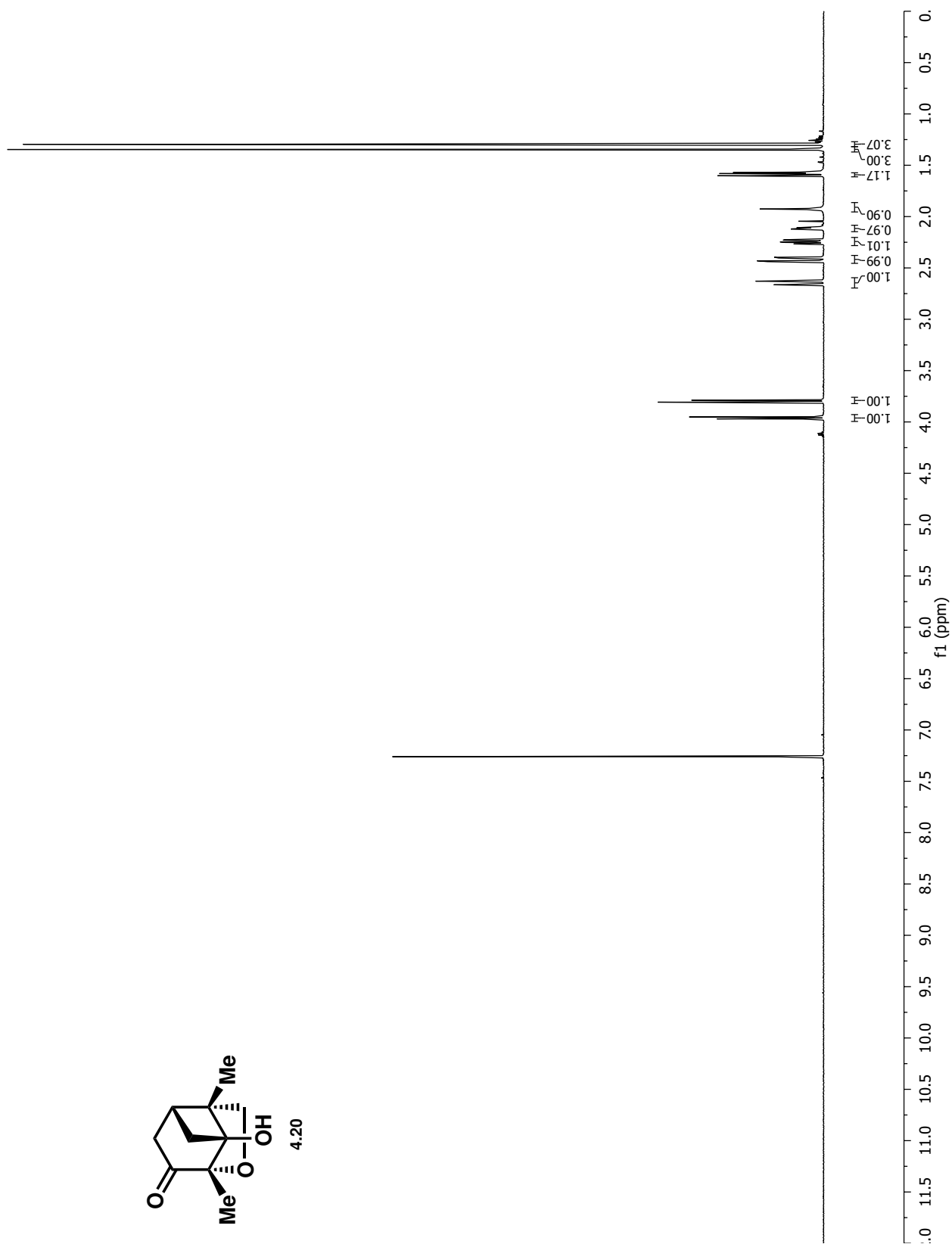
## 4.8 References

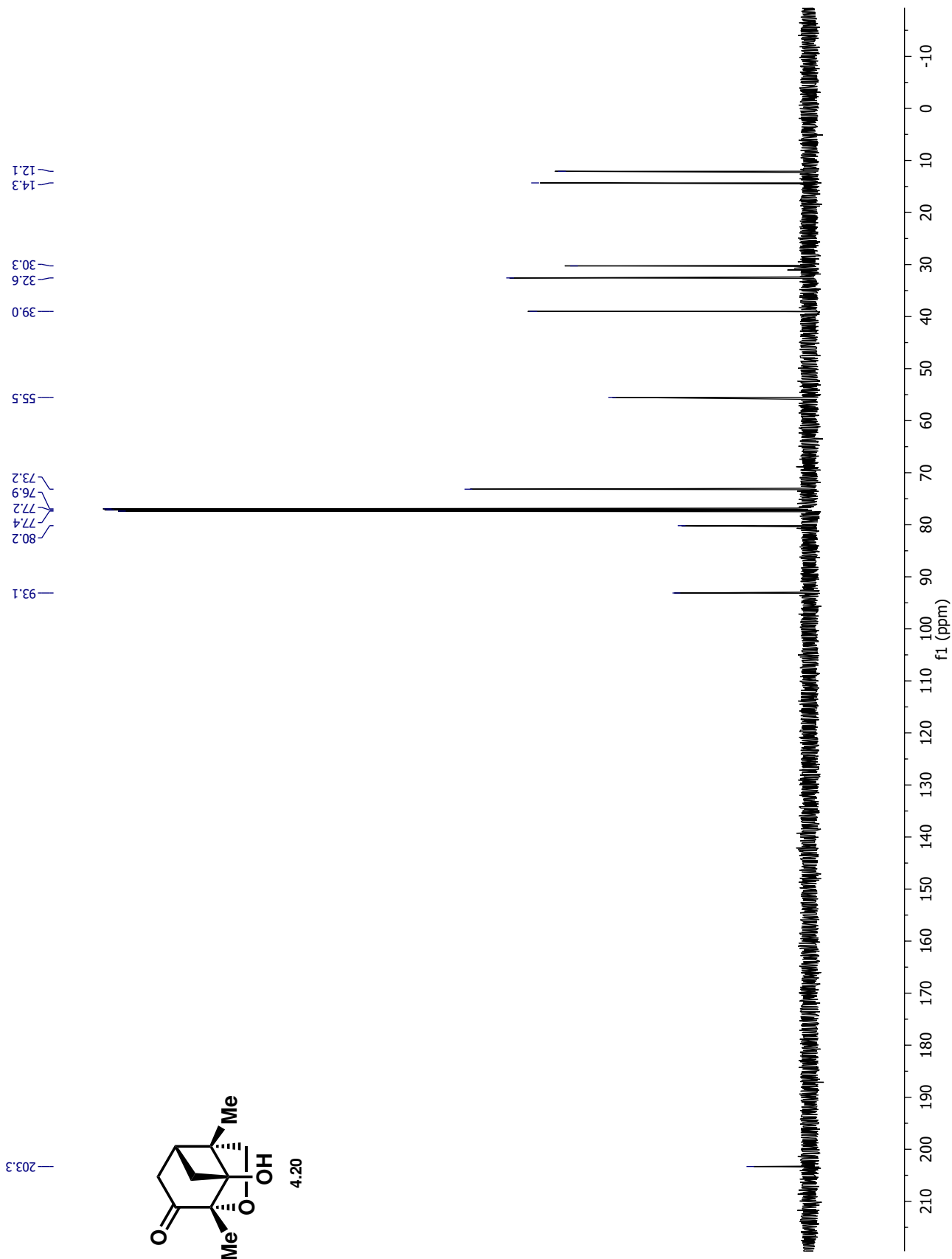
- (1) (a) Matsumura, S.; Maeda, Y.; Nishimura, T.; Uemura, S. *J. Am. Chem. Soc.* **2003**, *125*, 8862–8869; (b) Nishimura, T.; Uemura, S. *J. Am. Chem. Soc.* **1999**, *121*, 11010–11011; (c) Nishimura, T.; Ohe, K.; Uemura, S. *J. Am. Chem. Soc.* **1999**, *121*, 2645–2646.
- (2) (a) Bermejo, F. A.; Fernández Mateos, A.; Marcos Escribano, A.; Martín Lago, R.; Mateos Burón, L.; Rodríguez López, M.; Rubio González, R. *Tetrahedron* **2006**, *62*, 8933–8942; (b) Martín-Rodríguez, M.; Galán-Fernández, R.; Marcos-Escribano, A.; Bermejo, F. A. *J. Org. Chem.* **2009**, *74*, 1798–1801.
- (3) Weber, M.; Owens, K.; Masarwa, A.; Sarpong, R. *Org. Lett.* **2015**, *17*, 5432–5435.

- (4) For exposition on the difficulty of using intramolecular C–C bond-forming reactions to construct 8-membered rings, see: Petasis, N. A.; Patane, M. A. *Tetrahedron* **1992**, *48*, 5757–5821.
- (5) Masarwa, A.; Weber, M.; Sarpong, R. *J. Am. Chem. Soc.* **2015**, *137*, 6327–6334.
- (6) Dess, D. B.; Martin, J. C. *J. Org. Chem.* **1983**, *48*, 4155–4156.
- (7) Tsunoda, T.; Suzuki, M.; Noyori, R. *Tetrahedron Lett.* **1980**, *21*, 1357–1358.
- (8) De Mico, A.; Margarita, R.; Parlanti, L.; Vescovi, A.; Piancatelli, G. *J. Org. Chem.* **1997**, *62*, 6974–6977.
- (9) Tanino, K.; Aoyagi, K.; Kirihara, Y.; Ito, Y.; Miyashita, M. *Tetrahedron Lett.* **2005**, *46*, 1169–1172.
- (10) Pappo, R.; Allen D. S., J.; Lemieux, R. U.; Johnson, W. S. *J. Org. Chem.* **1956**, *21*, 478–479.
- (11) Yu, W.; Mei, Y.; Kang, Y.; Hua, Z.; Jin, Z. *Org. Lett.* **2004**, *6*, 3217–3219.
- (12) (a) Saksena, A. K.; Mangiaracina, P. *Tetrahedron Lett.* **1983**, *24*, 273–276; (b) Evans, D. A.; Chapman, K. T.; Carreira, E. M. *J. Am. Chem. Soc.* **1988**, *110*, 3560–3578.
- (13) Jacobsen, E. N.; Marko, I.; Mungall, W. S.; Schroeder, G.; Sharpless, K. B. *J. Am. Chem. Soc.* **1988**, *110*, 1968–1970.
- (14) Aoyama, T.; Shioiri, T. *Synthesis* **1988**, *1988*, 228–229.
- (15) (a) Omura, K.; Sharma, A. K.; Swern, D. *J. Org. Chem.* **1976**, *41*, 957–962; (b) Omura, K.; Swern, D. *Tetrahedron* **1978**, *34*, 1651–1660.
- (16) Hartwig, J. F., *Organotransition Metal Chemistry: From Bonding to Catalysis*; University Science Books: Sausalito, CA, 2010.
- (17) (a) Farina, V.; Krishnan, B. *J. Am. Chem. Soc.* **1991**, *113*, 9585–9595; (b) Otto, S.; Roodt, A. *Inorganica Chim. Acta* **2004**, *357*, 1–10; (c) Levason, W.; Reid, G. In *Comprehensive Coordination Chemistry II: From Biology to Nanotechnology*, McClverty, J. A., Meyer, T. J., Eds.; Elsevier Science: Amsterdam, 2003.
- (18) (a) Chen, X.; Li, J.-J.; Hao, X.-S.; Goodhue, C. E.; Yu, J.-Q. *J. Am. Chem. Soc.* **2006**, *128*, 78–79; (b) Hull, K. L.; Sanford, M. S. *J. Am. Chem. Soc.* **2009**, *131*, 9651–9653; (c) Sköld, C.; Kleimark, J.; Trejos, A.; Odell, L. R.; Nilsson Lill, S. O.; Norrby, P.-O.; Larhed, M. *Chem. Eur. J.* **2012**, *18*, 4714–4722.
- (19) Davis, F. A.; Vishwakarma, L. C.; Billmers, J. G.; Finn, J. *J. Org. Chem.* **1984**, *49*, 3241–3243.
- (20) Anderson, J. C.; Smith, S. C. *Synlett* **1990**, *1990*, 107–108.
- (21) Moriarty, R. M.; Hu, H.; Gupta, S. C. *Tetrahedron Lett.* **1981**, *22*, 1283–1286.
- (22) Koser, G. F.; Relenyyi, A. G.; Kalos, A. N.; Rebrovic, L.; Wettach, R. H. *J. Org. Chem.* **1982**, *47*, 2487–2489.
- (23) Beshara, C. S.; Hall, A.; Jenkins, R. L.; Jones, K. L.; Jones, T. C.; Killeen, N. M.; Taylor, P. H.; Thomas, S. P.; Tomkinson, N. C. O. *Org. Lett.* **2005**, *7*, 5729–5732.

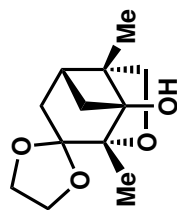
- (24) (a) Rubottom, G. M.; Vazquez, M. A.; Pelegrina, D. R. *Tetrahedron Lett.* **1974**, *15*, 4319–4322; (b) Brook, A. G.; Macrae, D. M. *J. Organomet. Chem.* **1974**, *77*, C19–C21.
- (25) Johnson, C. R.; Medich, J. R. *J. Org. Chem.* **1988**, *53*, 4131–4133.
- (26) Tamao, K.; Ishida, N. *Tetrahedron Lett.* **1984**, *25*, 4245–4248.
- (27) Nicolaou, K. C.; Adsool, V. A.; Hale, C. R. H. *Org. Lett.* **2010**, *12*, 1552–1555.
- (28) Speck, J. C. In *Advances in Carbohydrate Chemistry*, Wolfrom, M. L., Ed.; Academic Press: 1958; Vol. 13, pp 63–103.
- (29) Hays, D. S.; Fu, G. C. *J. Am. Chem. Soc.* **1995**, *117*, 7283–7284.
- (30) Fu, G. C.; Grubbs, R. H. *J. Am. Chem. Soc.* **1993**, *115*, 3800–3801.

# Appendix 4a: NMR Spectra Relevant to Chapter 4

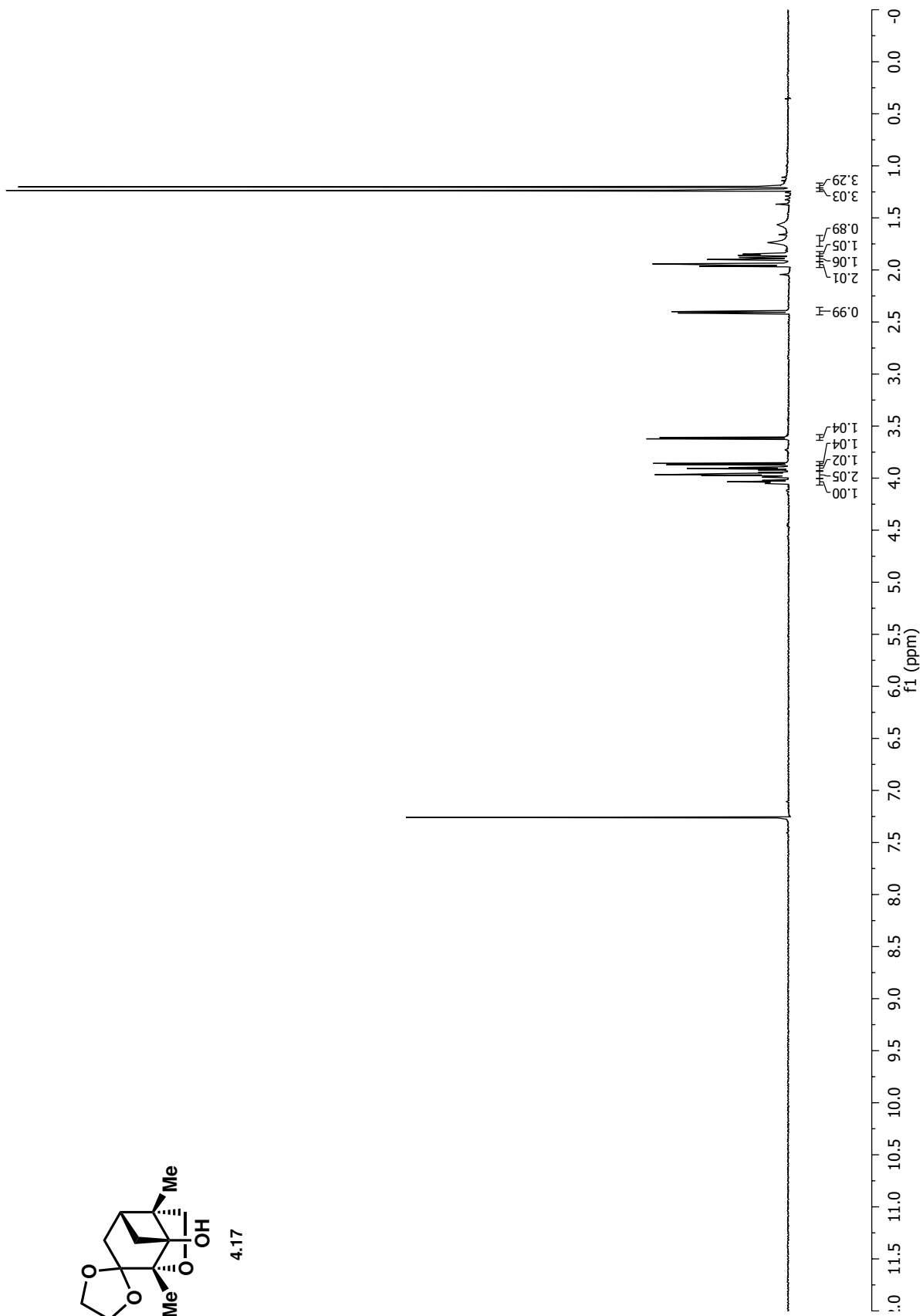


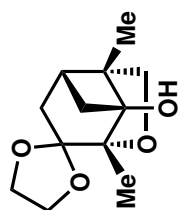




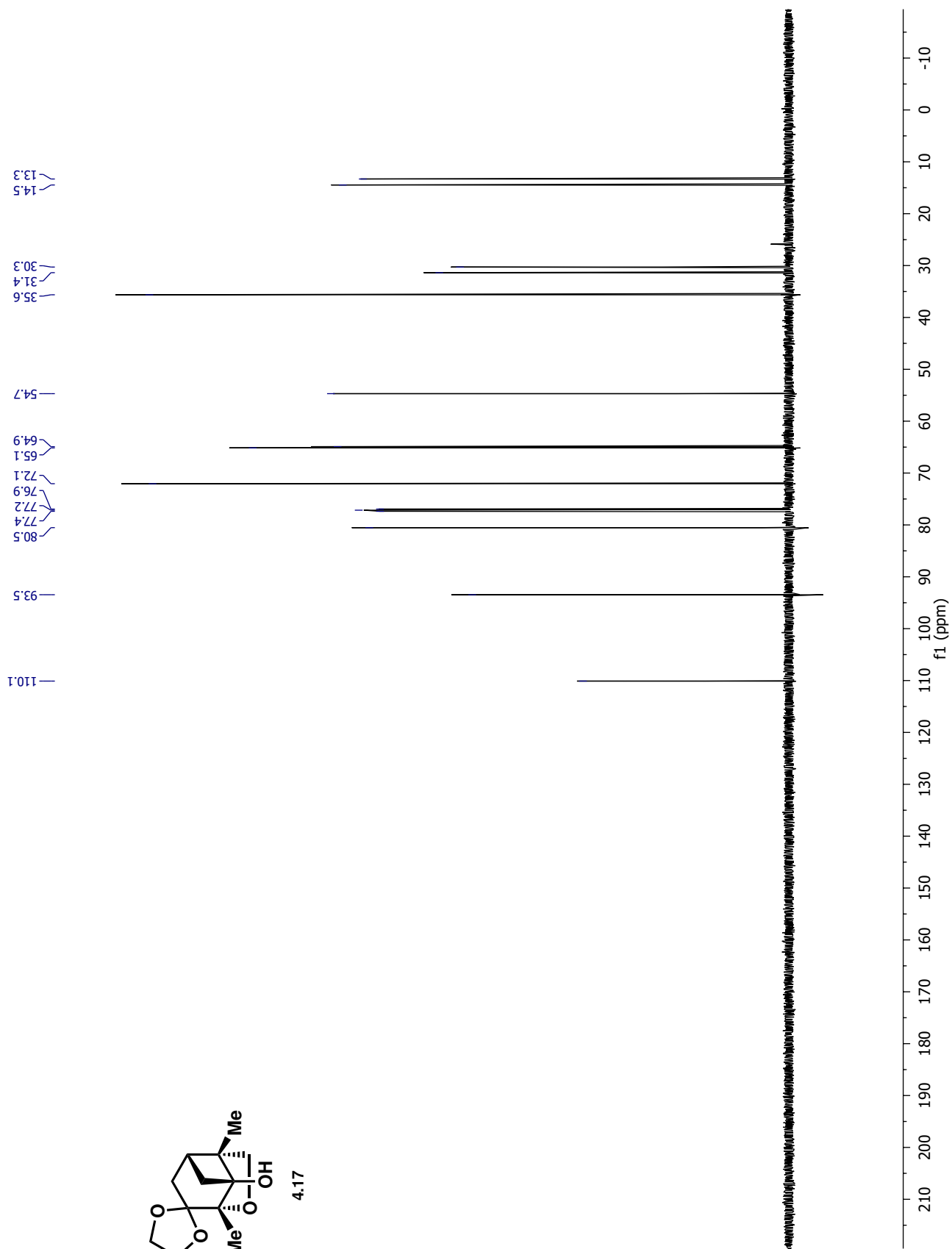


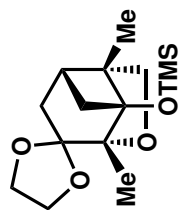
4.17



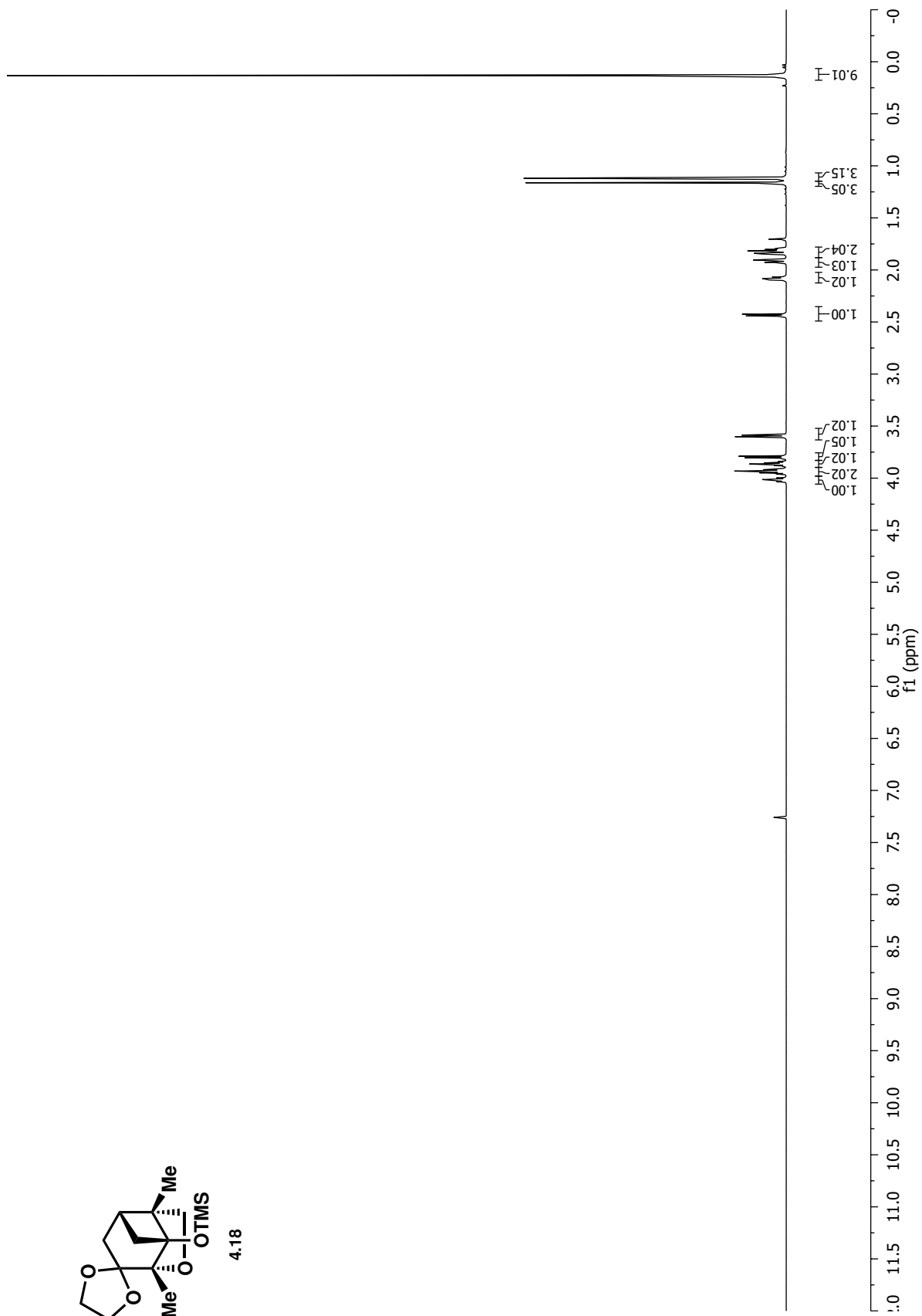


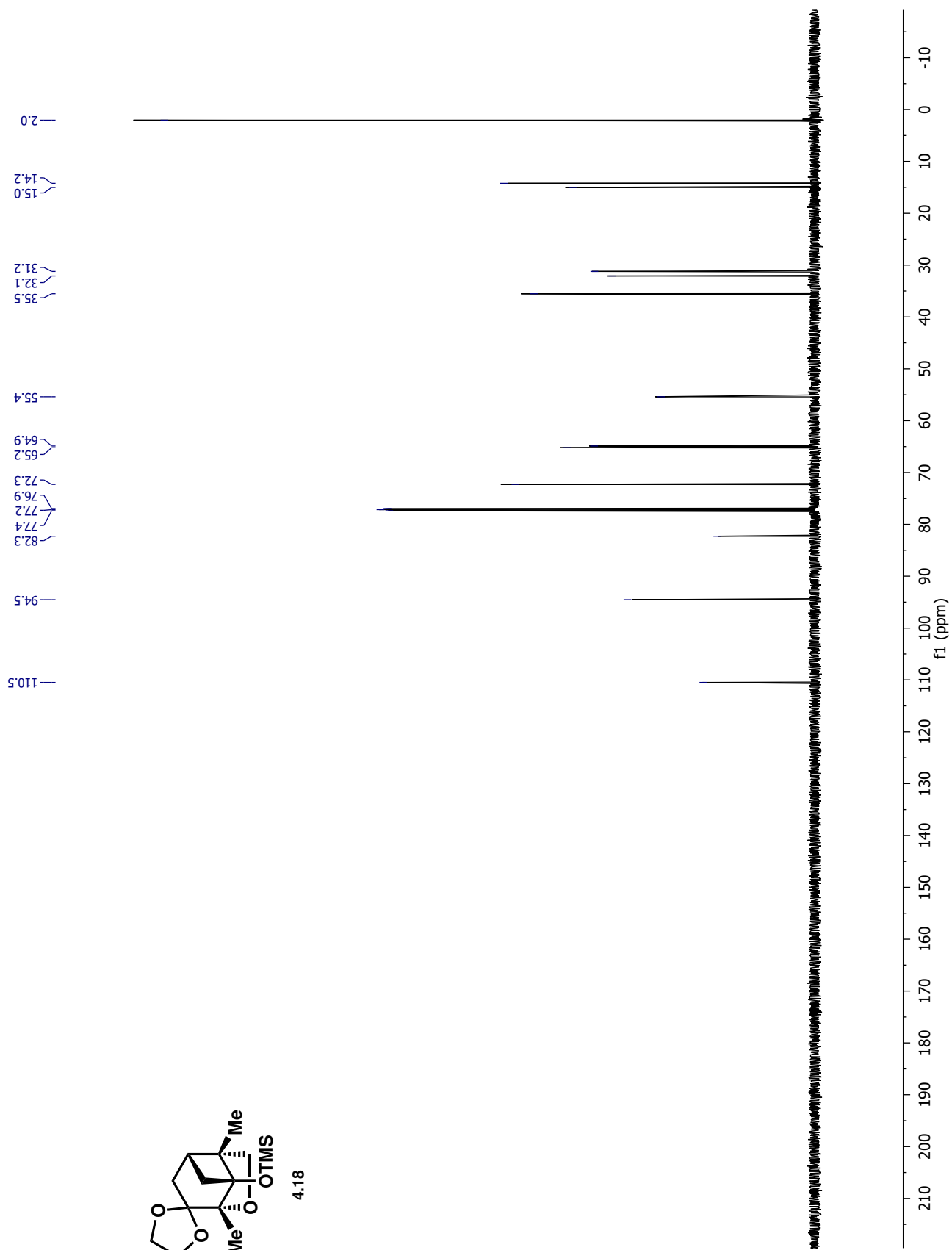
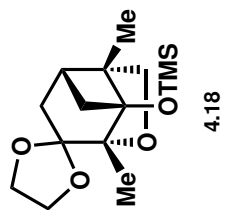
4.17

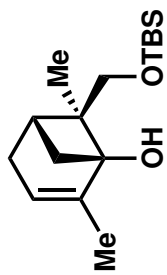




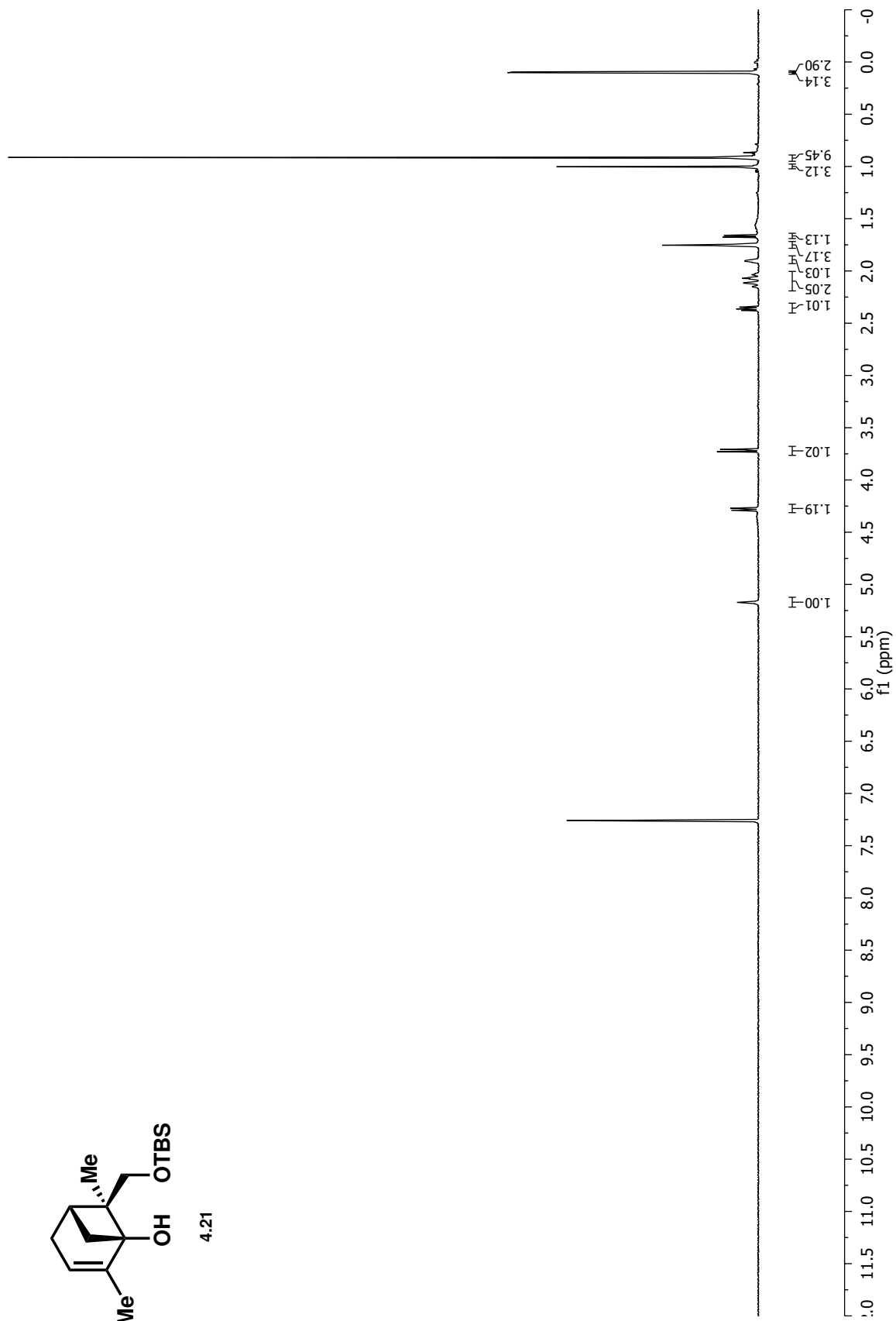
4.18

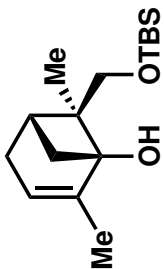




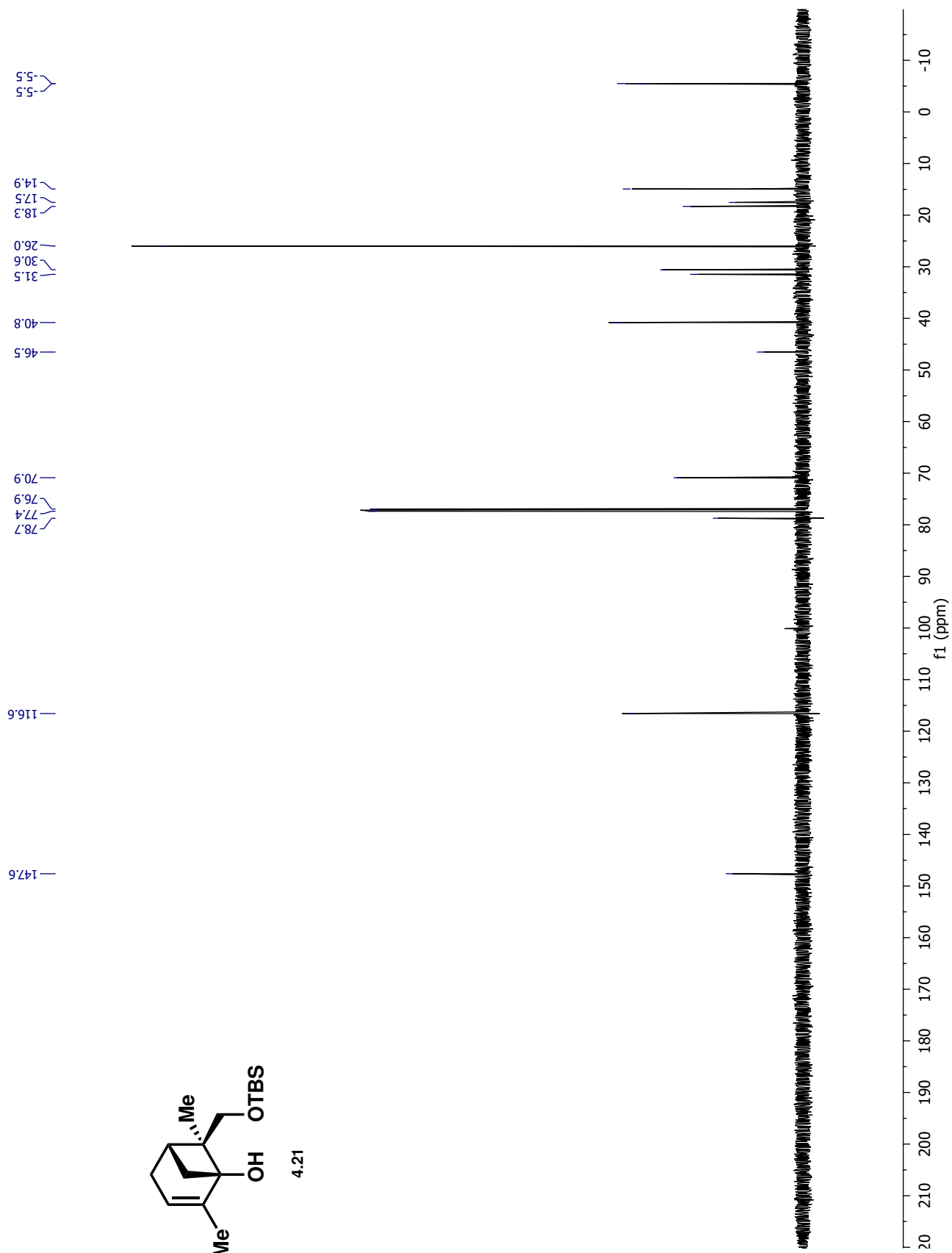


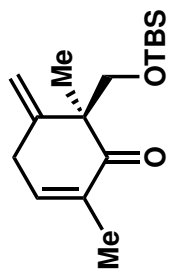
4.21



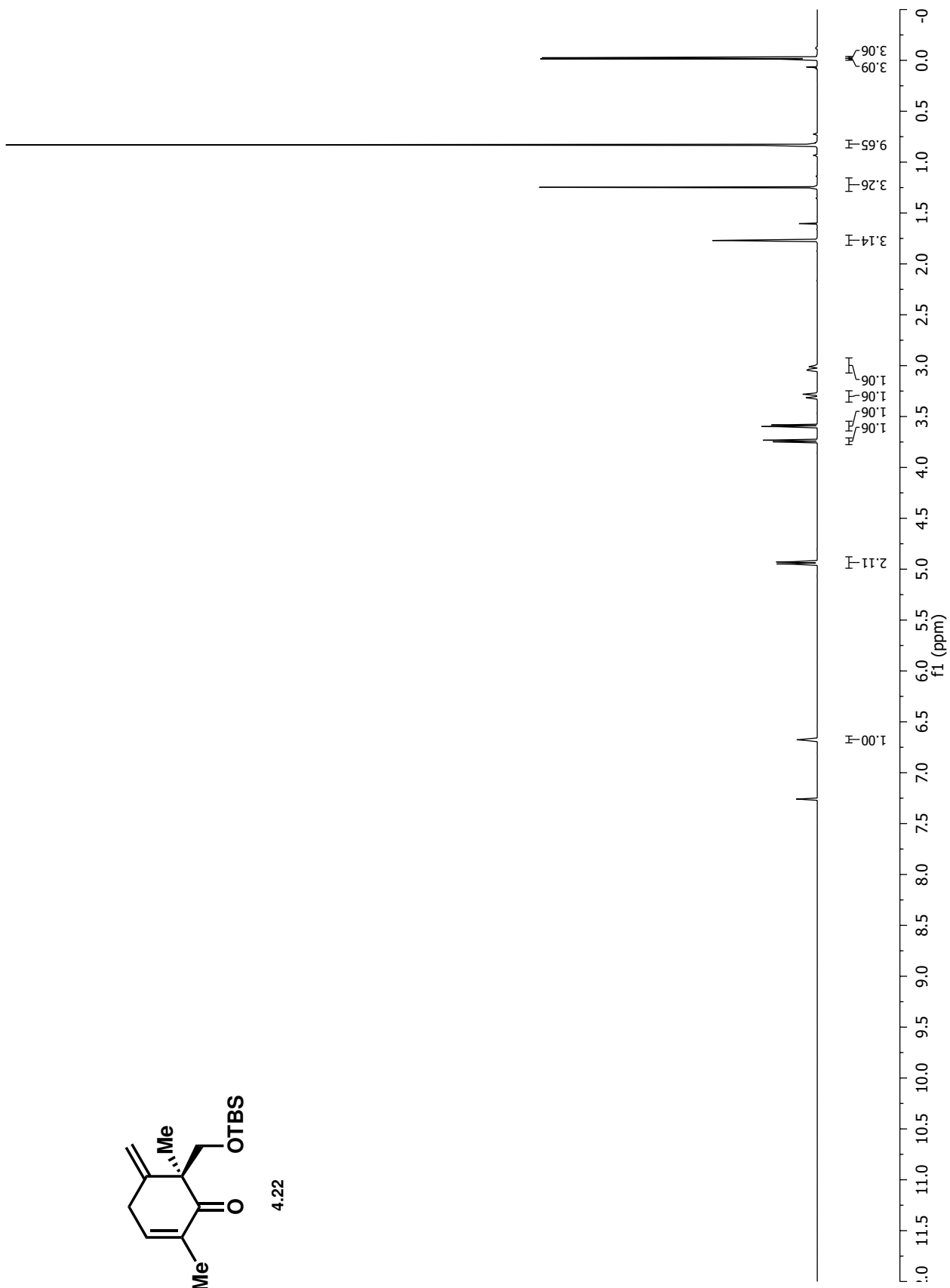


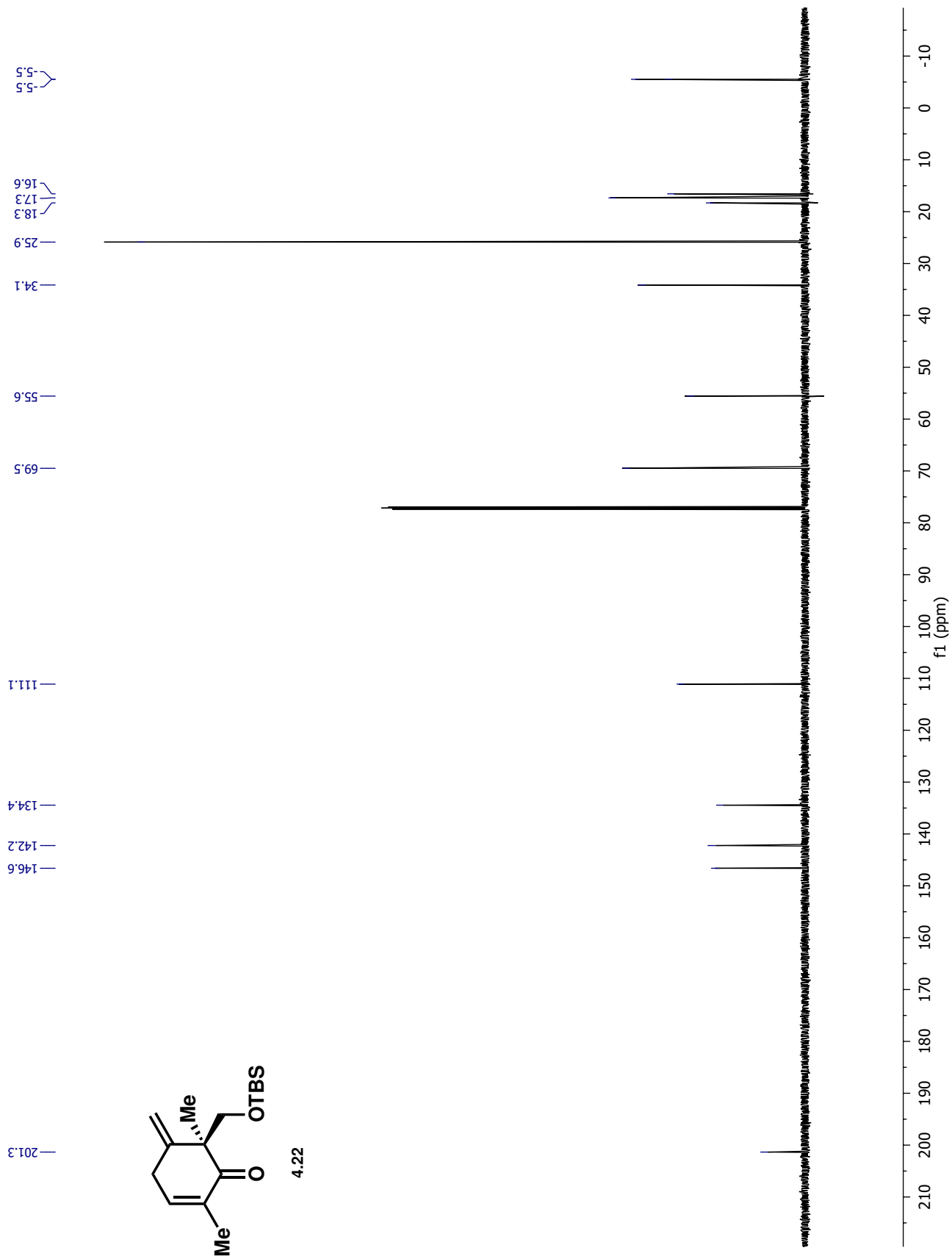
4.21



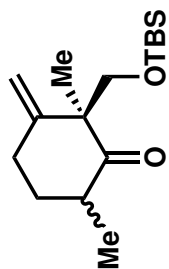


4.22

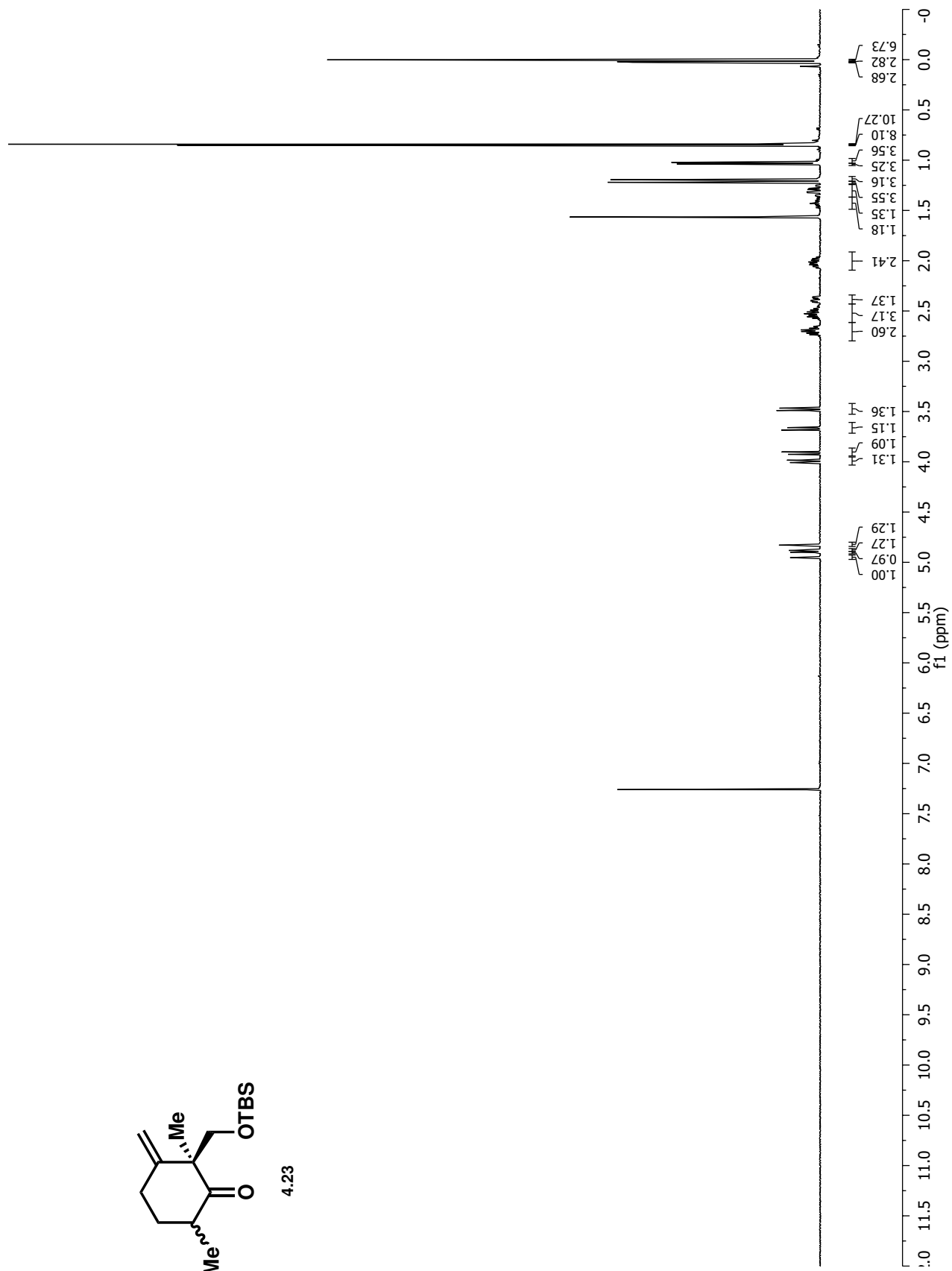


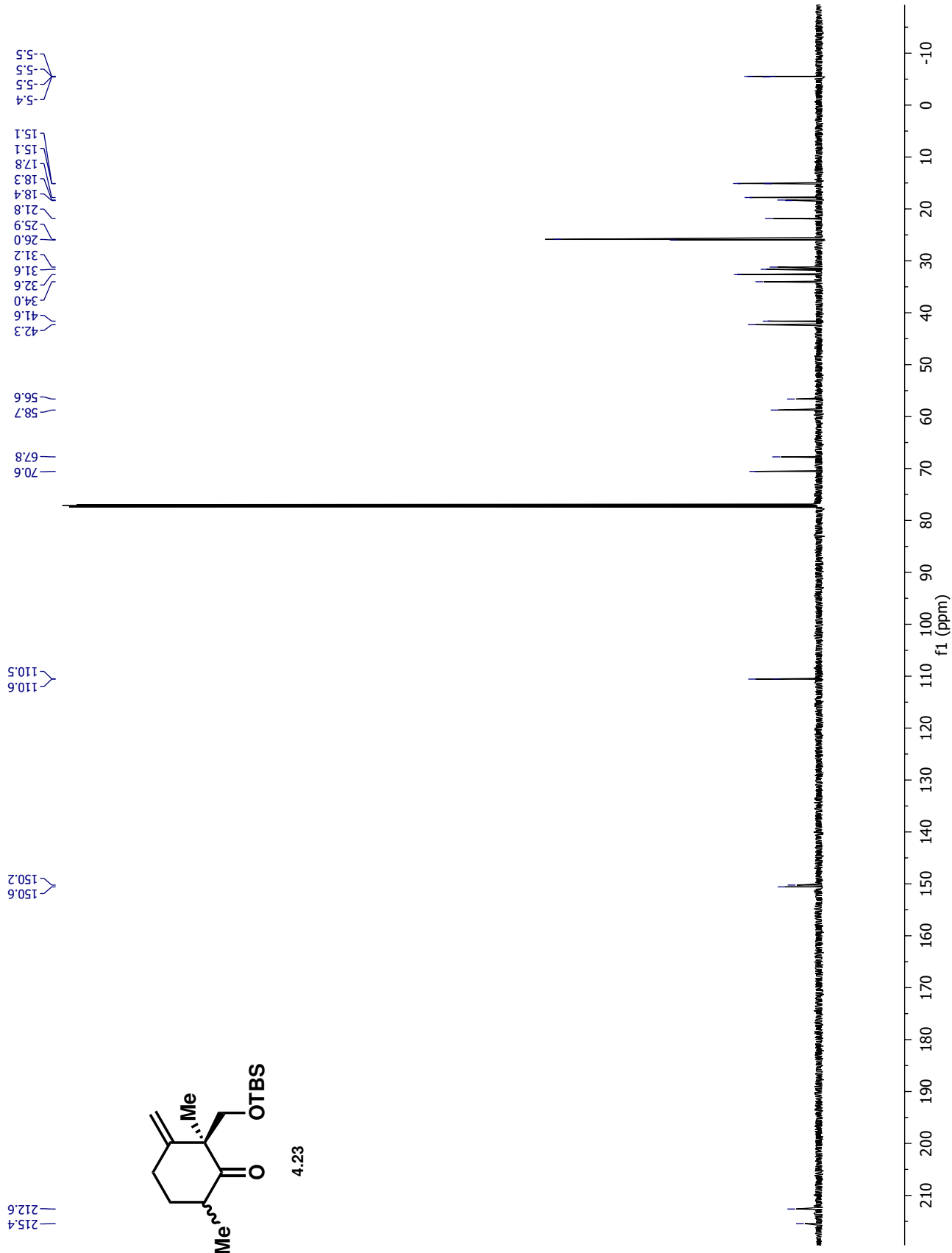


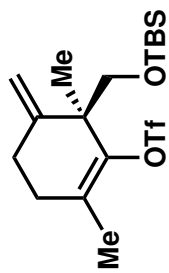




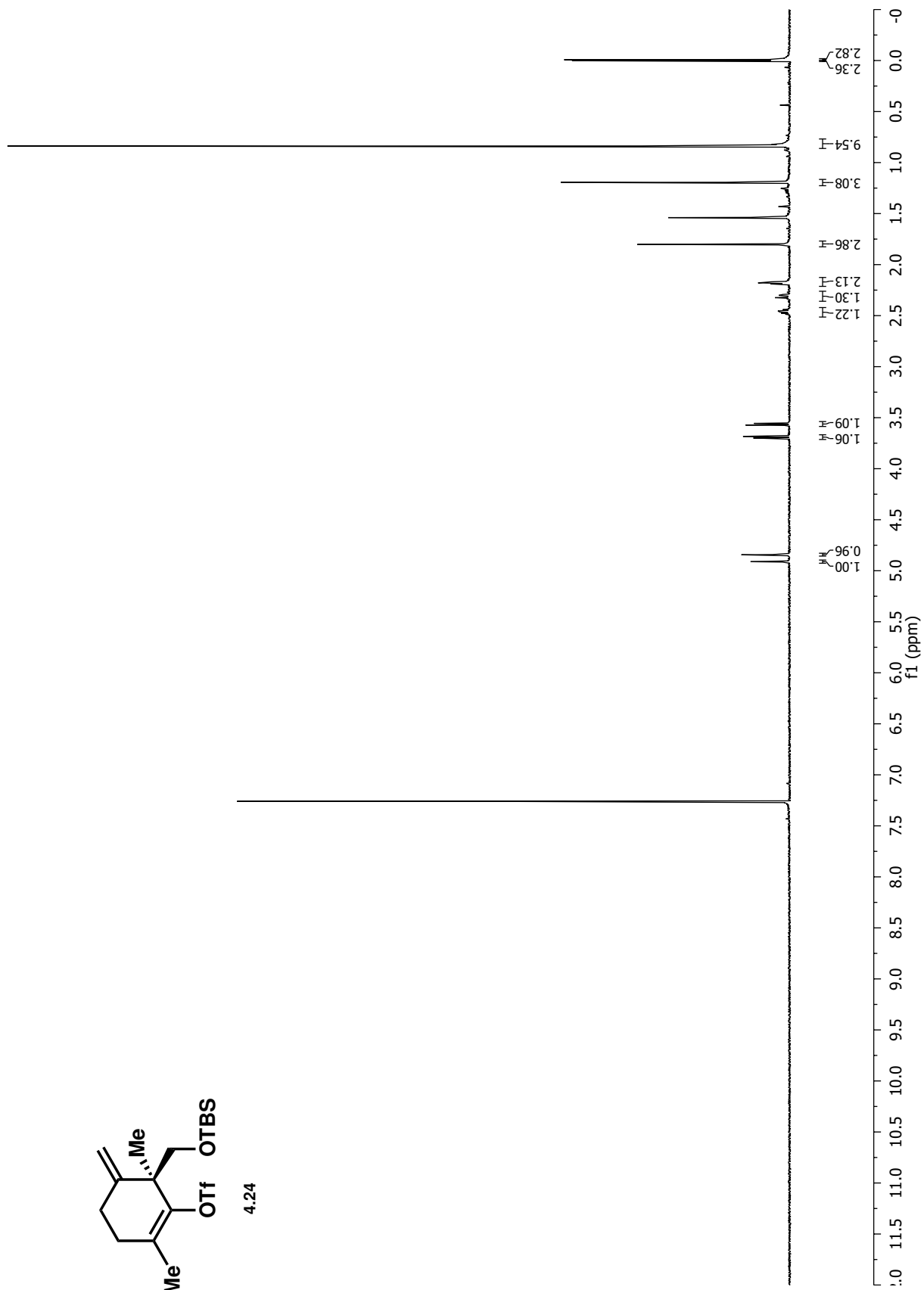
4.23

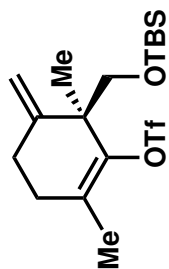




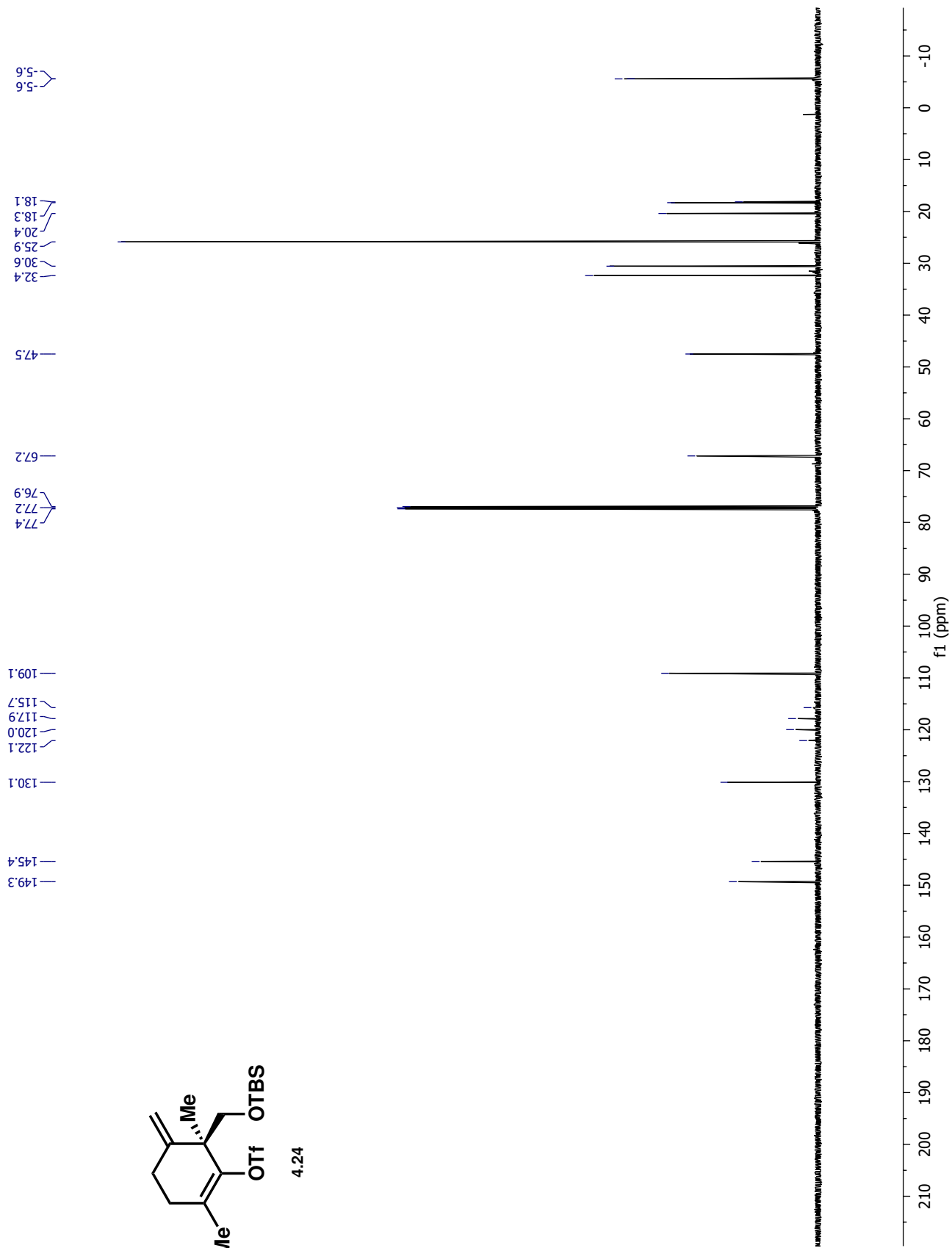


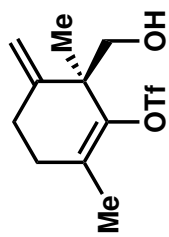
4.24



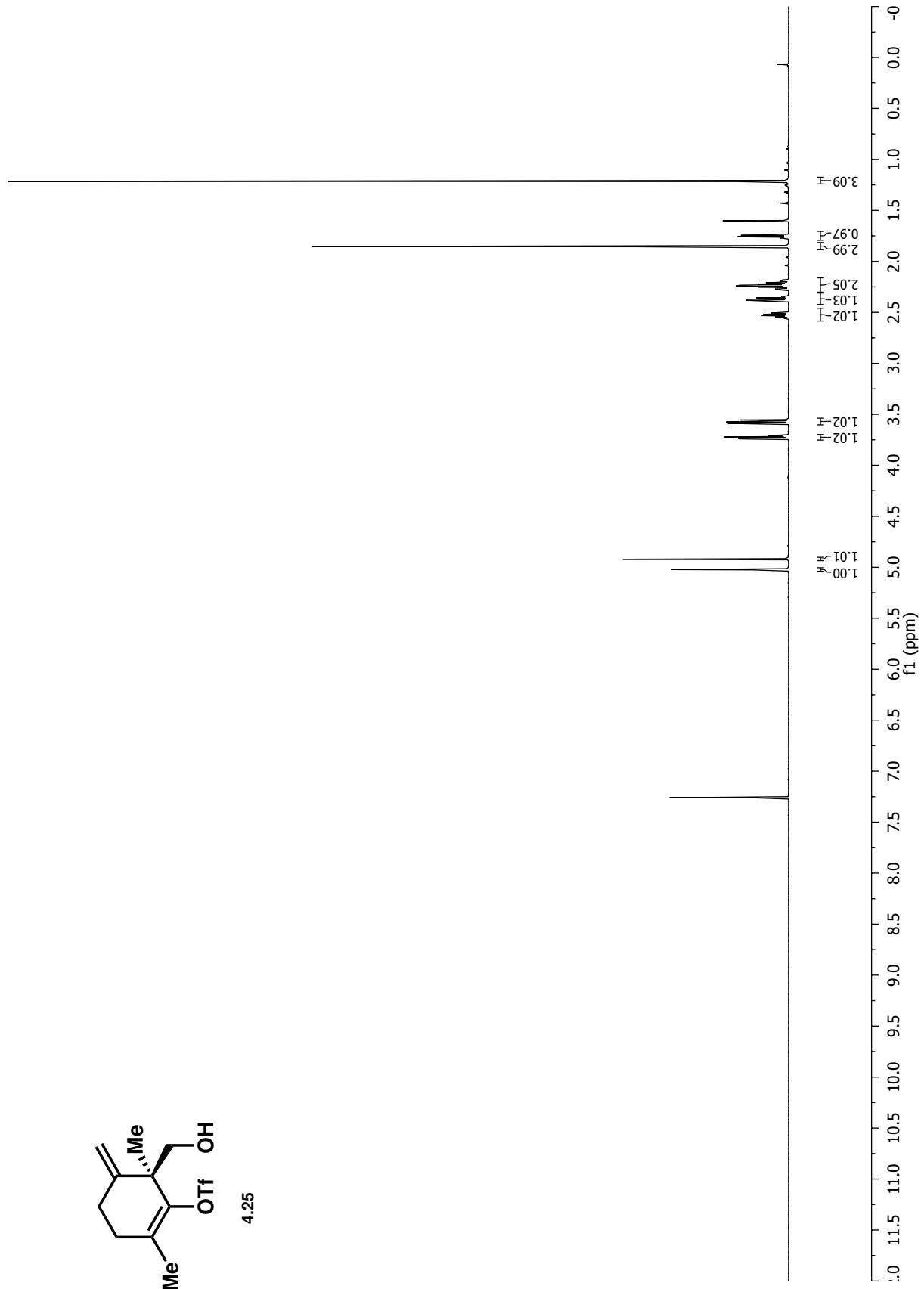


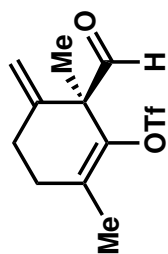
4.24



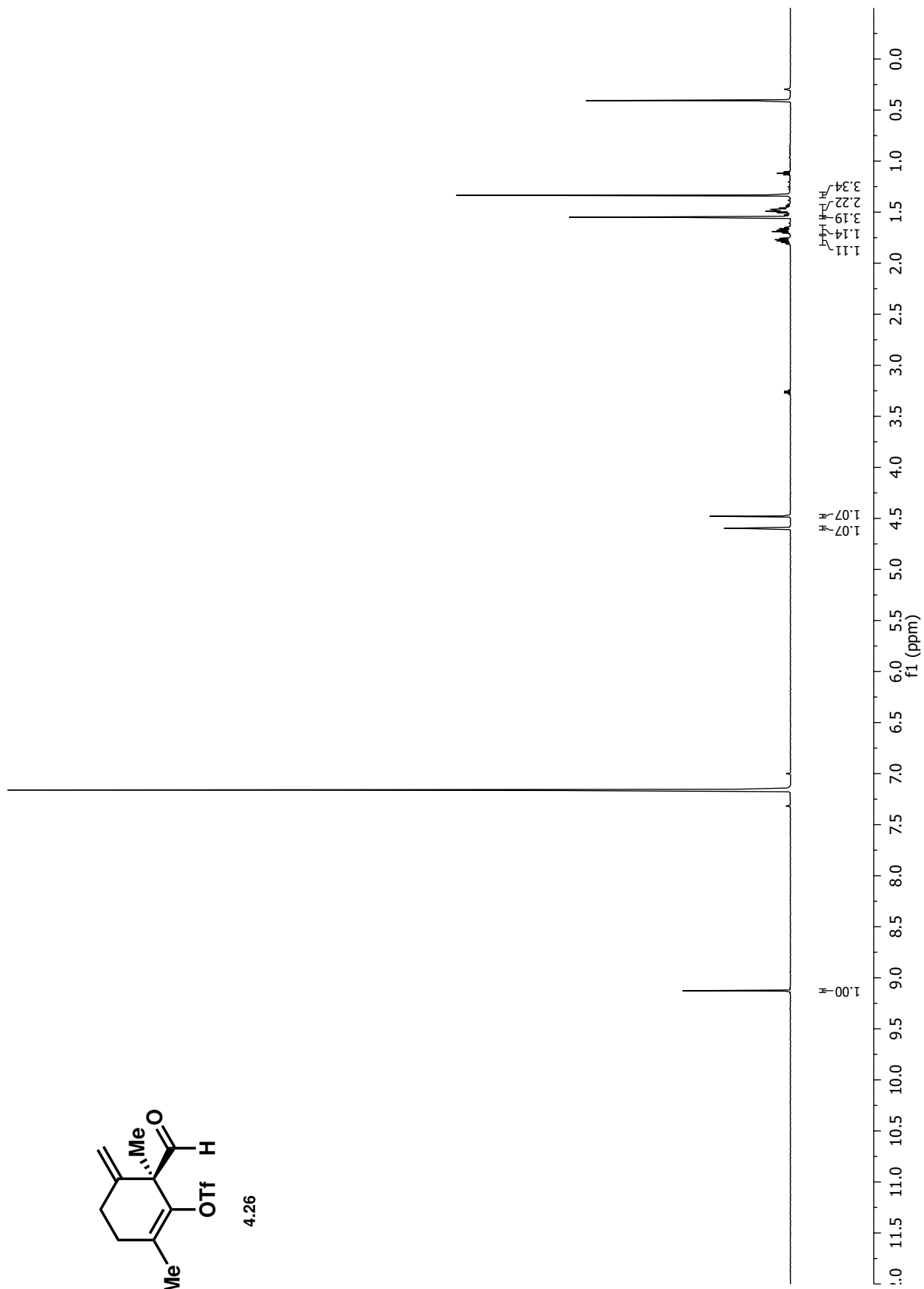


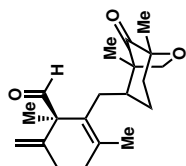
4.25



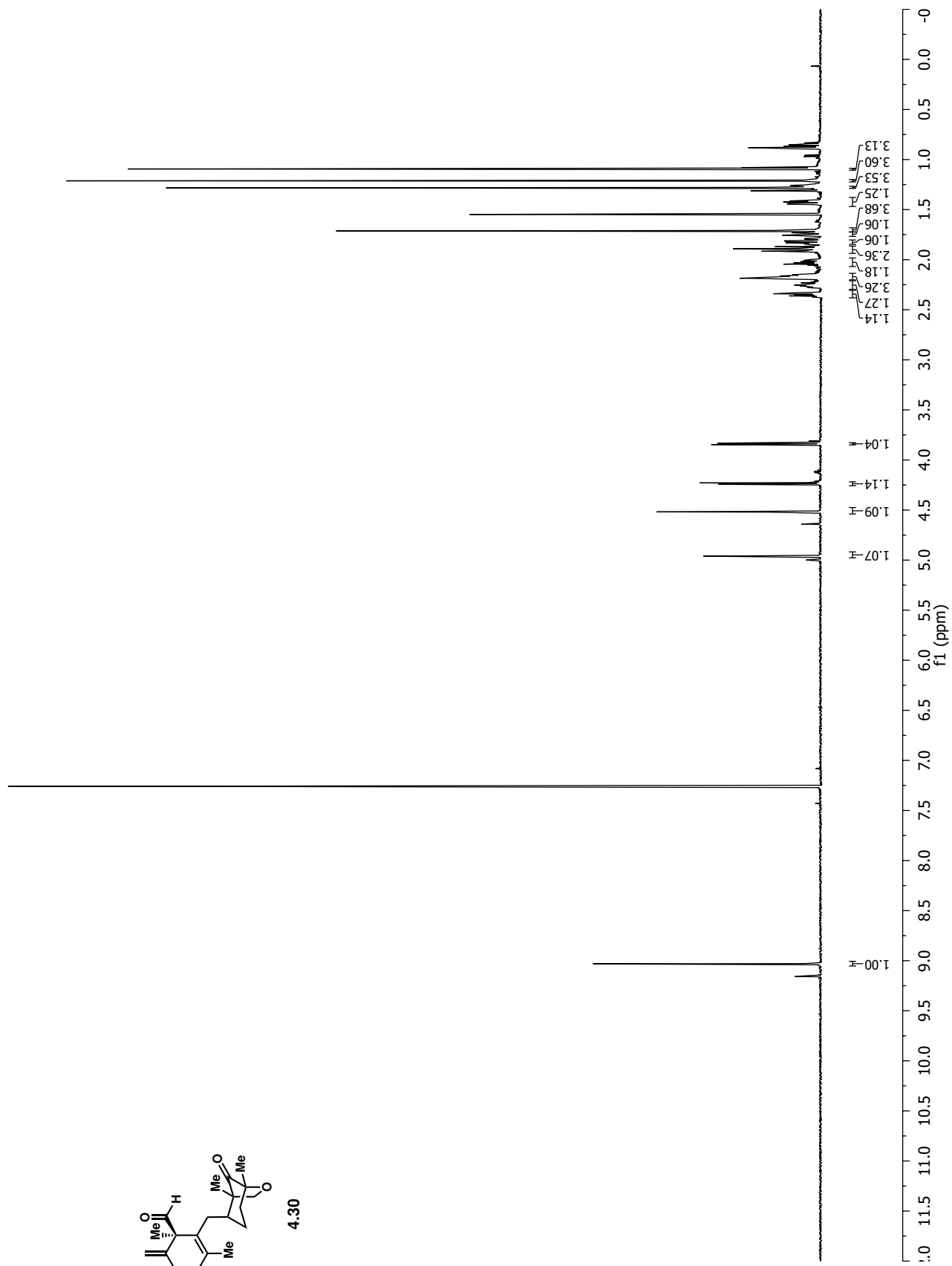


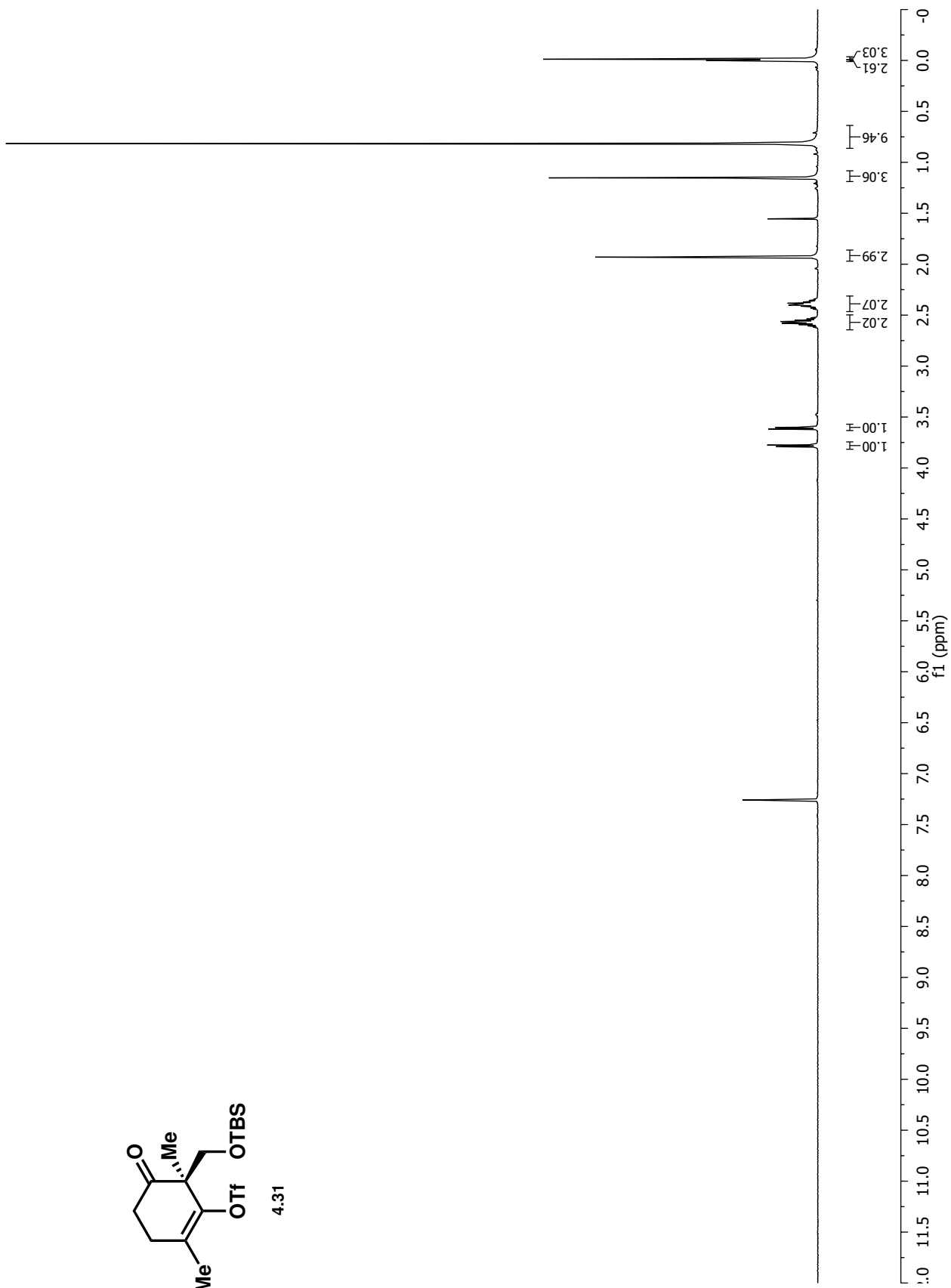
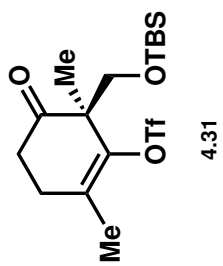
4.26



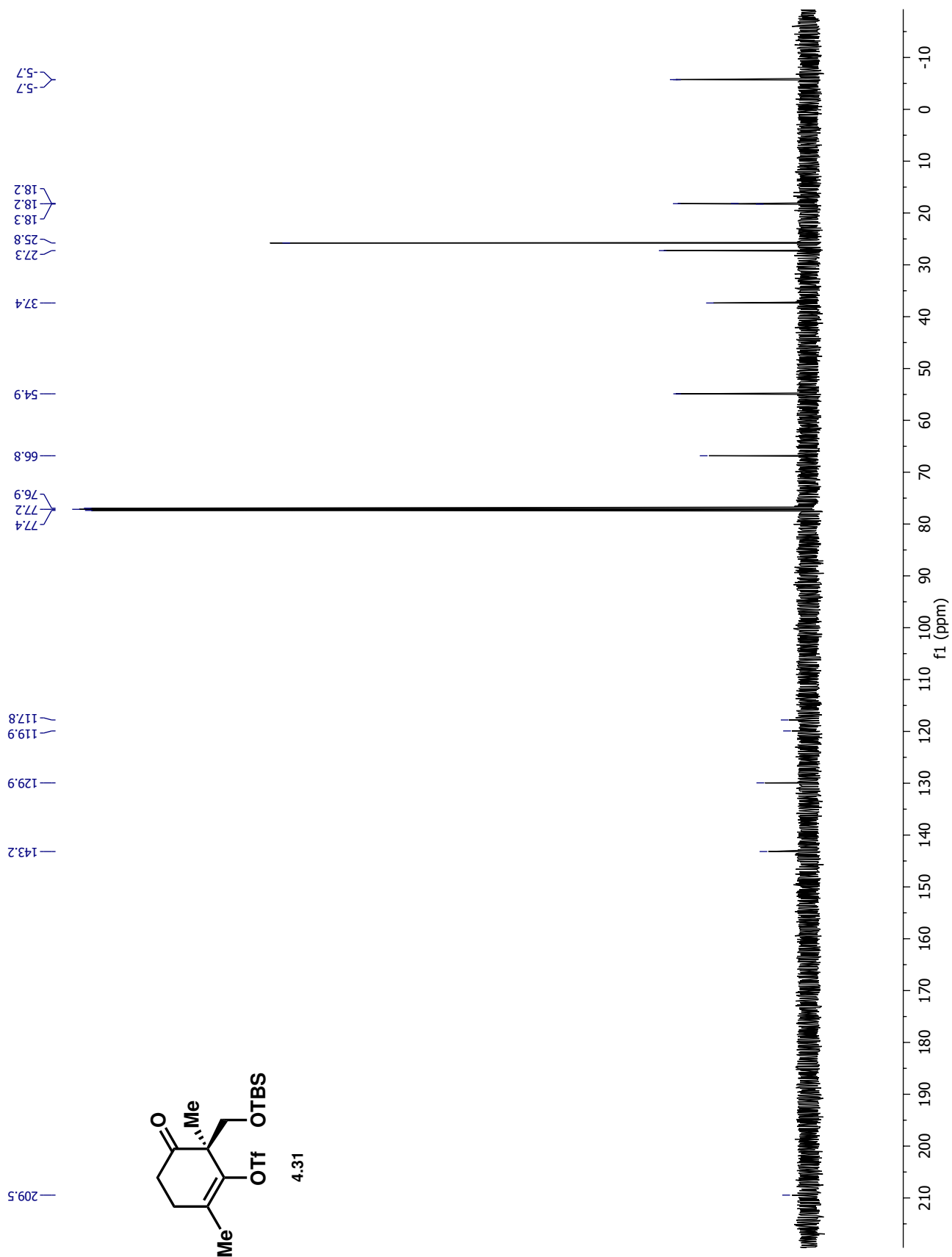


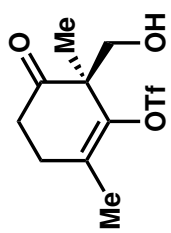
4.30



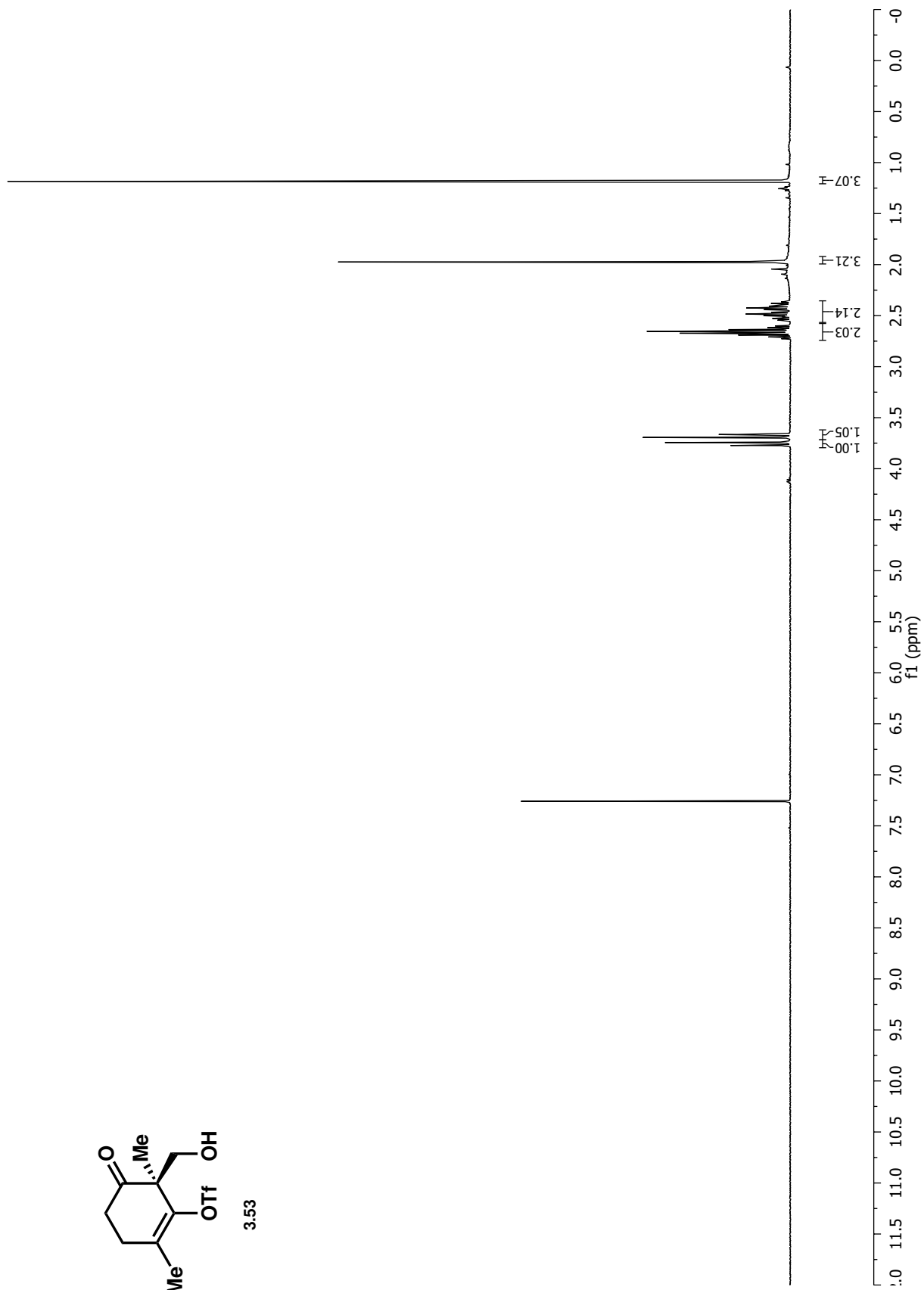


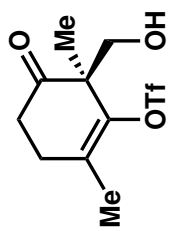




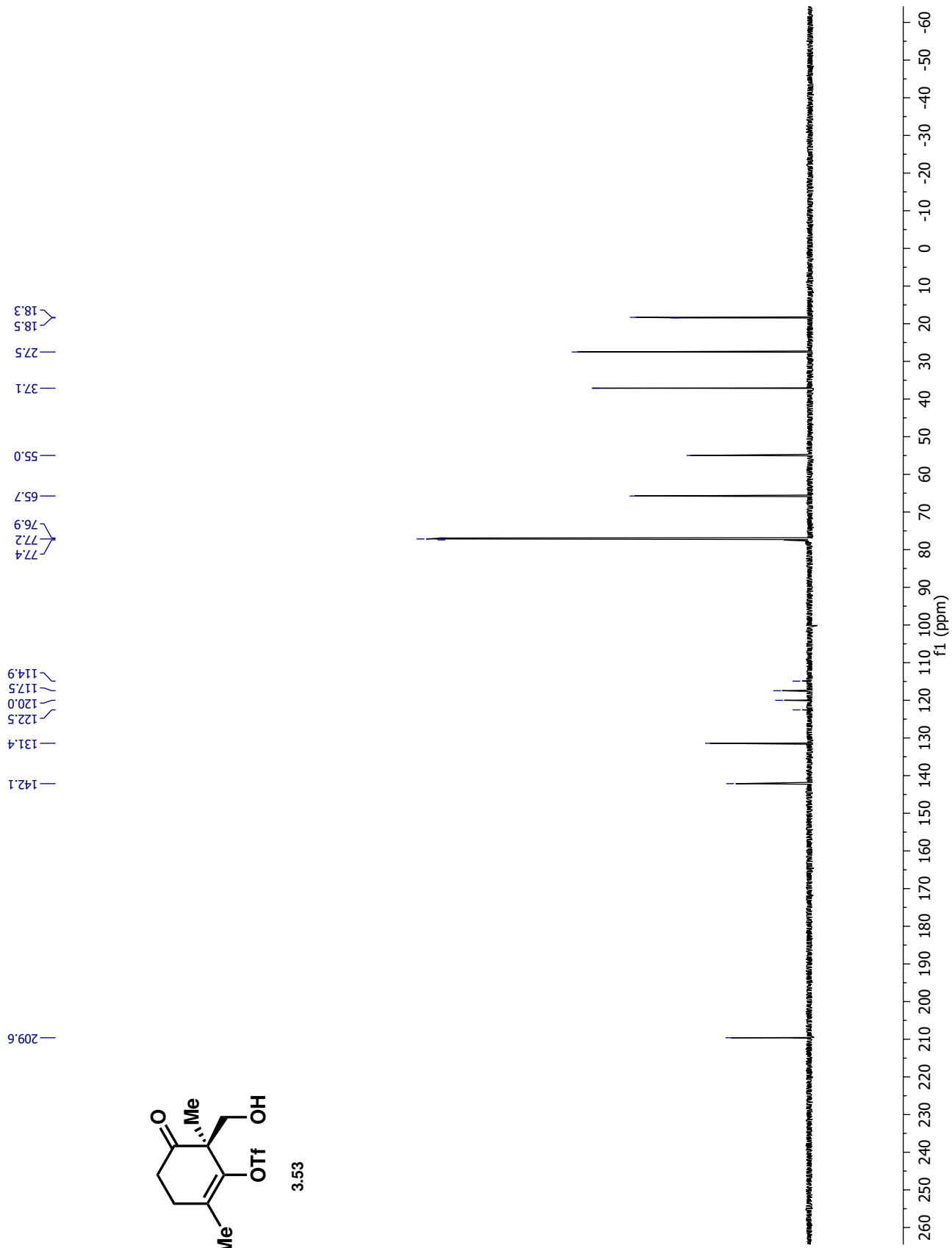


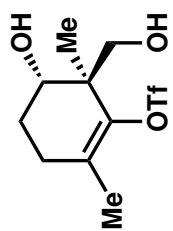
3.53



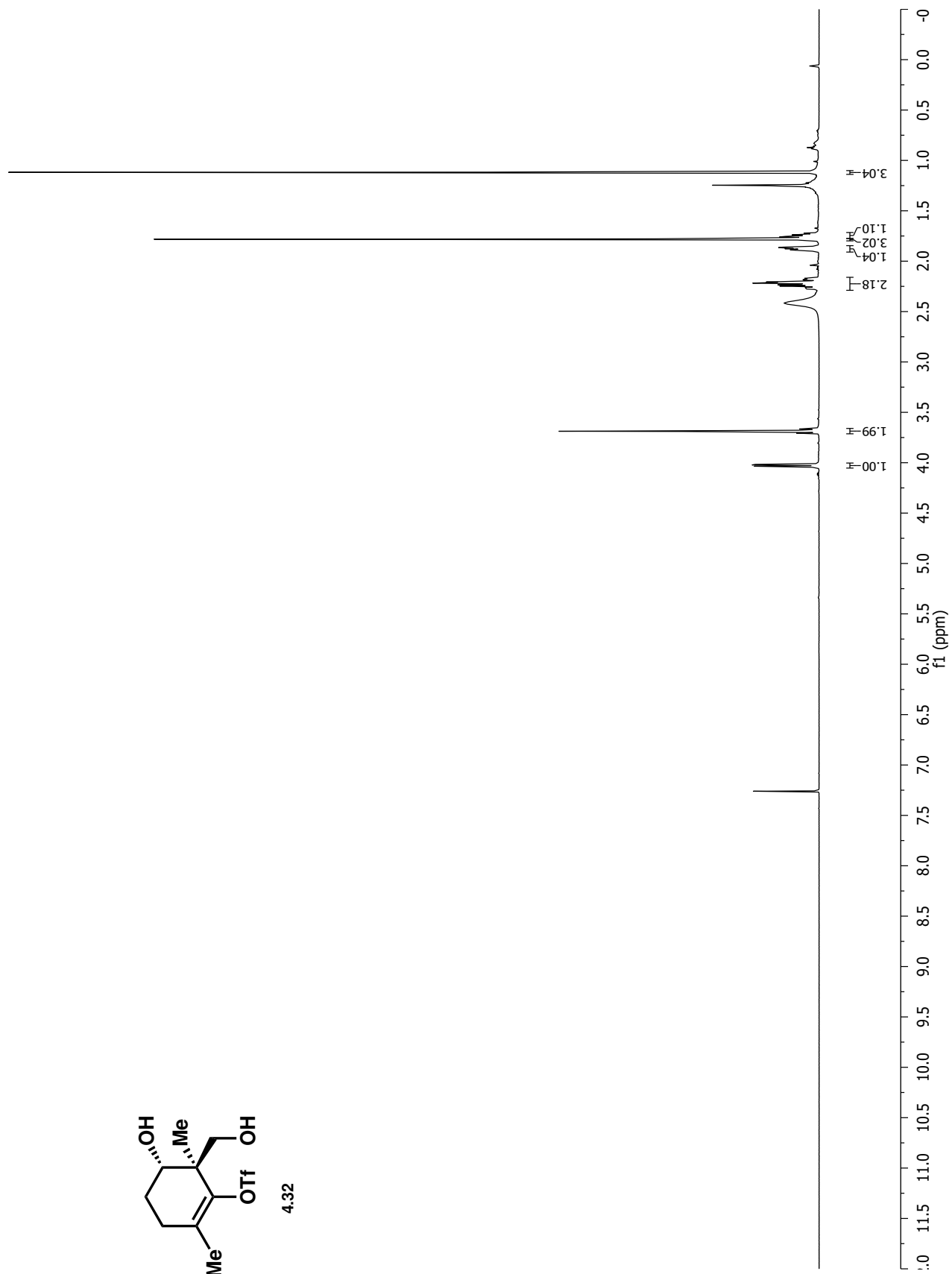


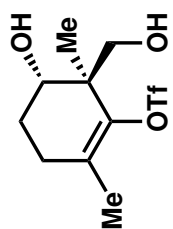
3.53



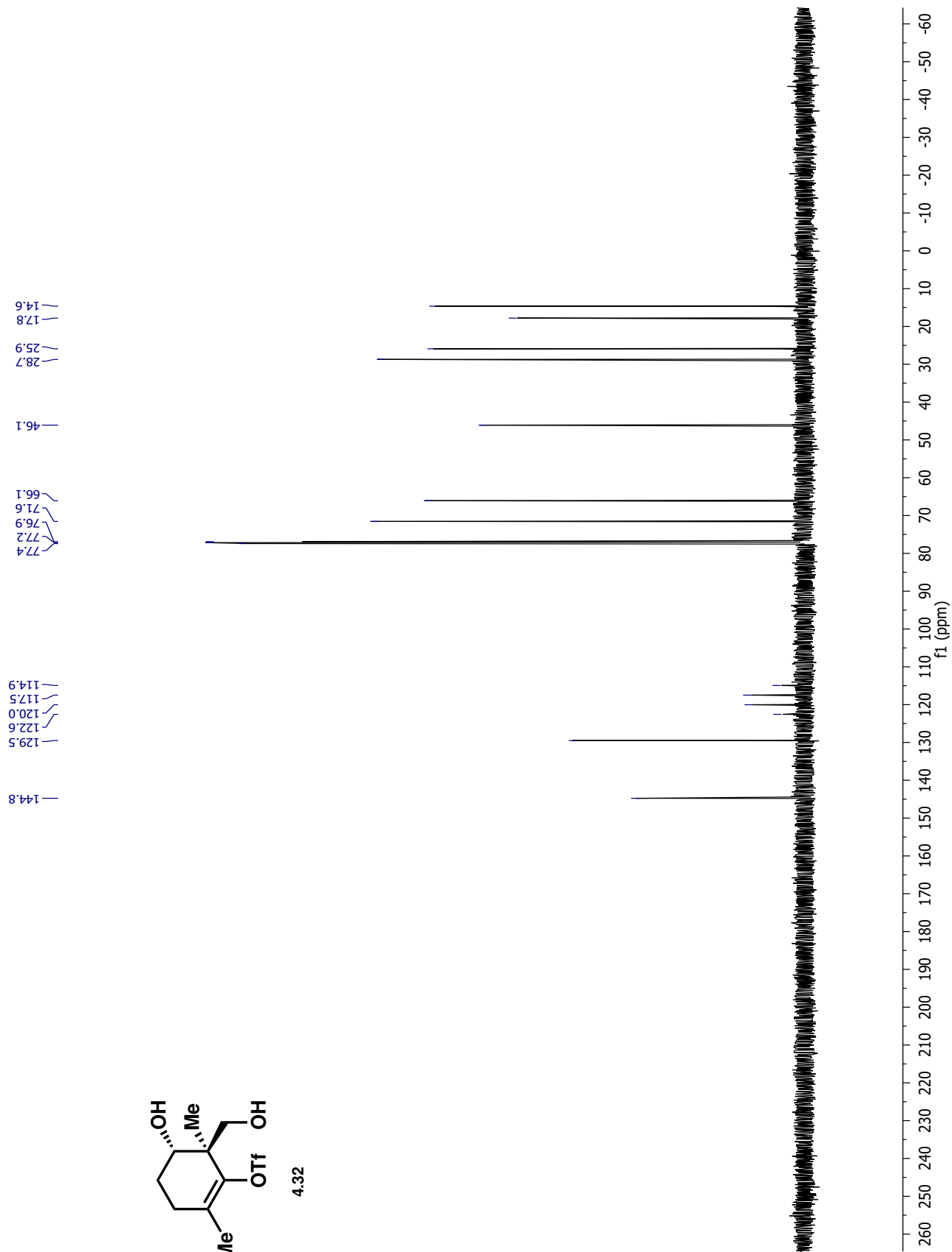


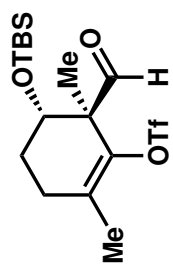
4.32



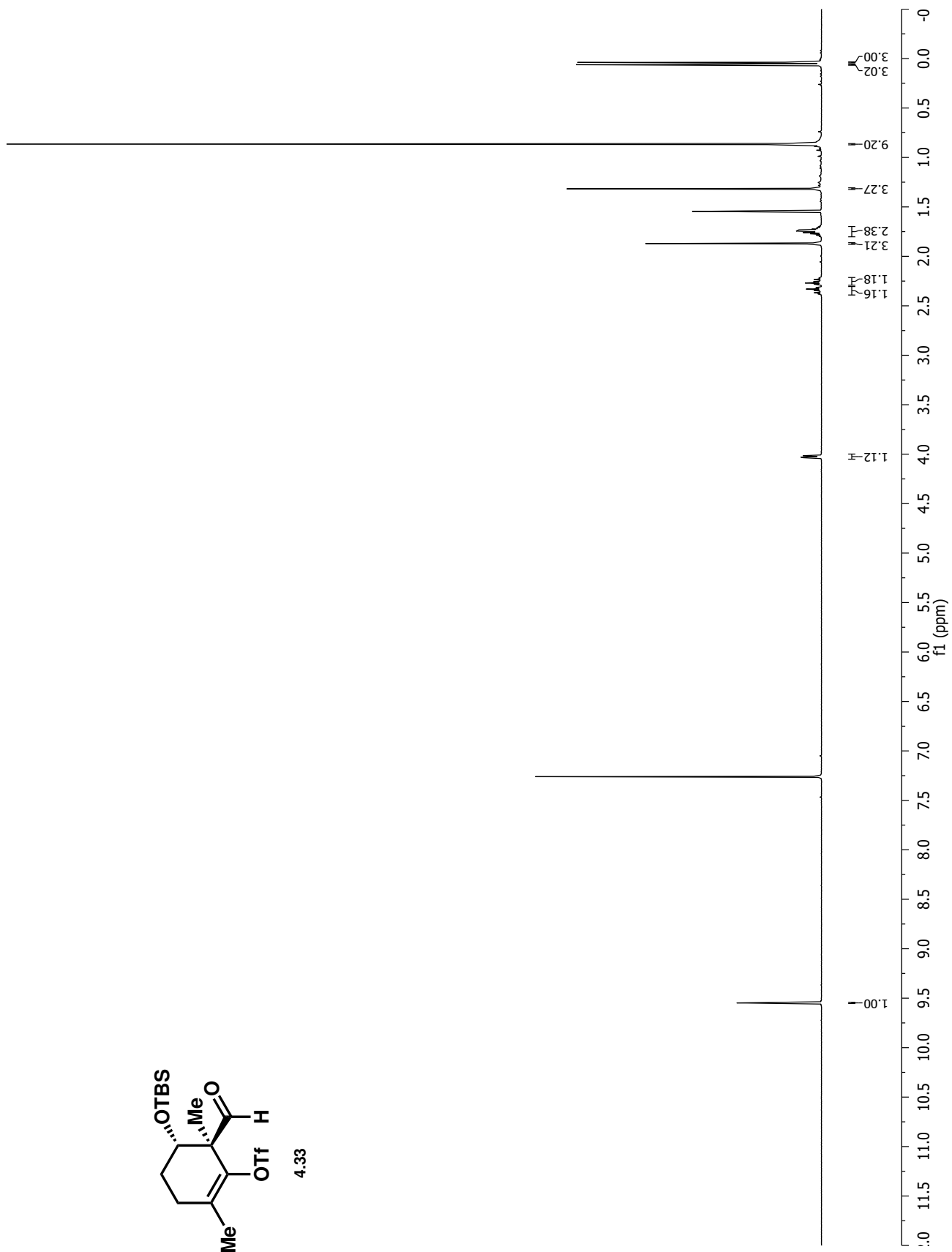


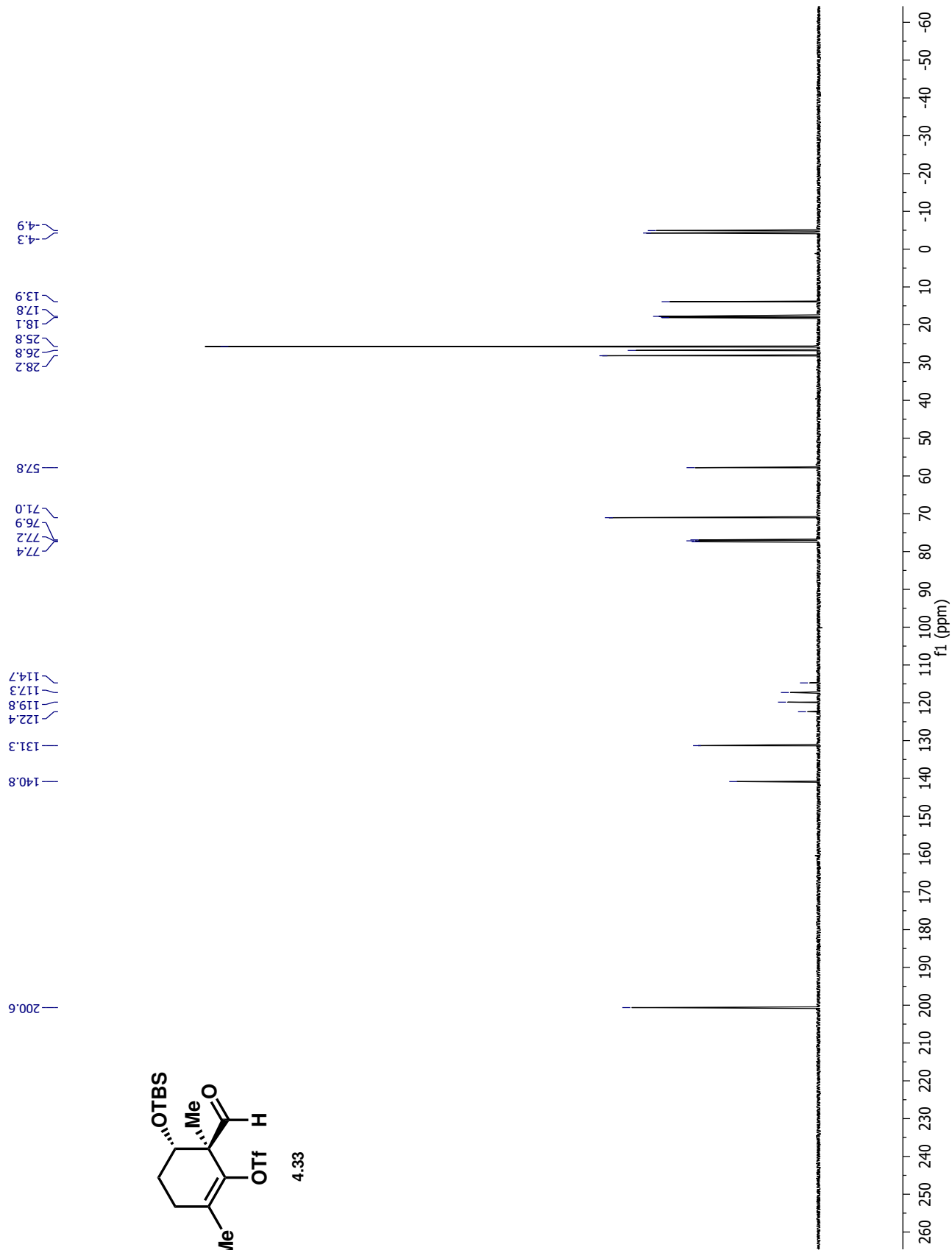
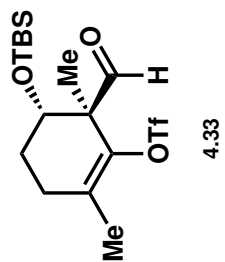
4.32

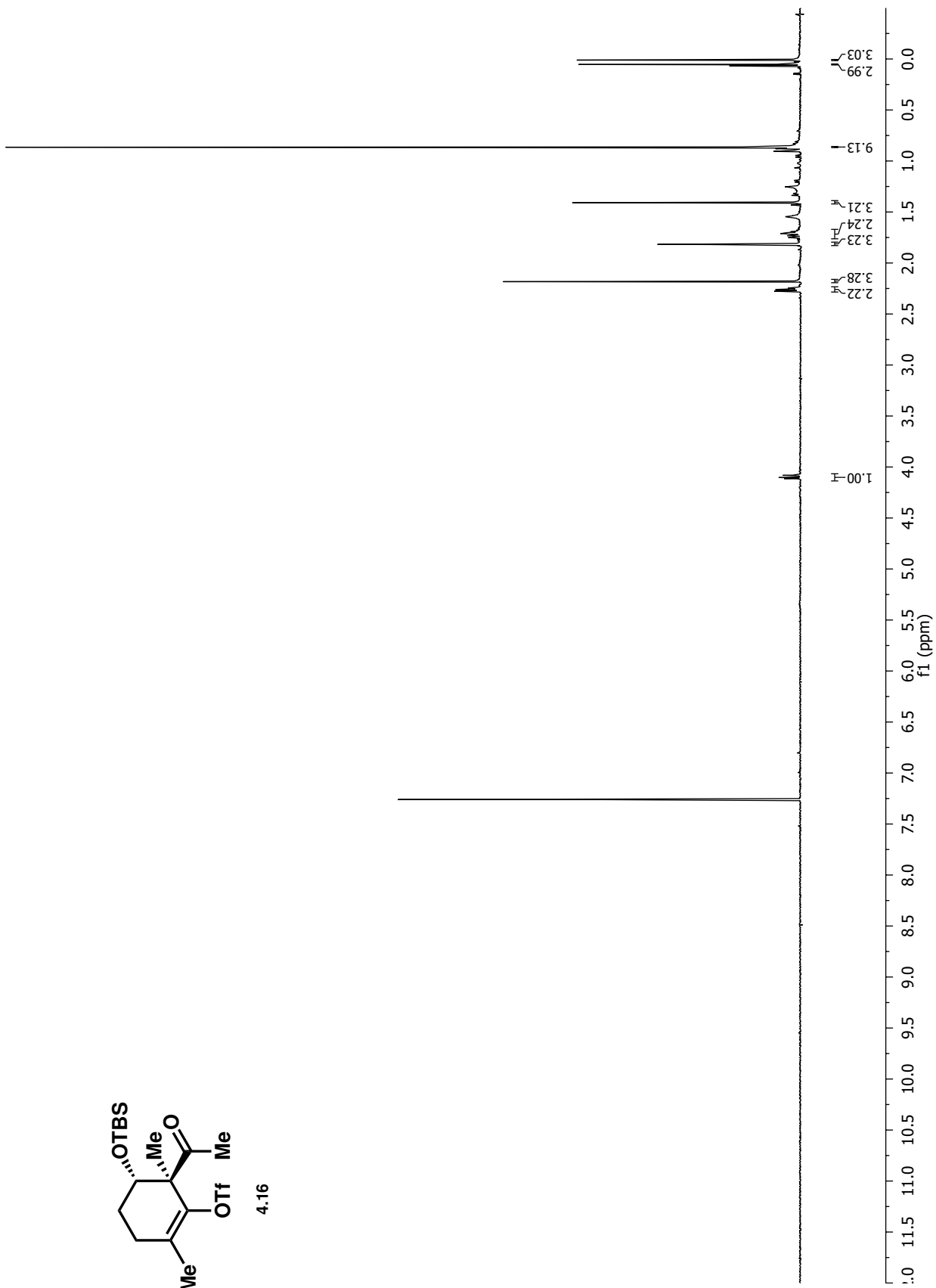
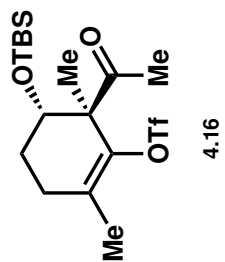




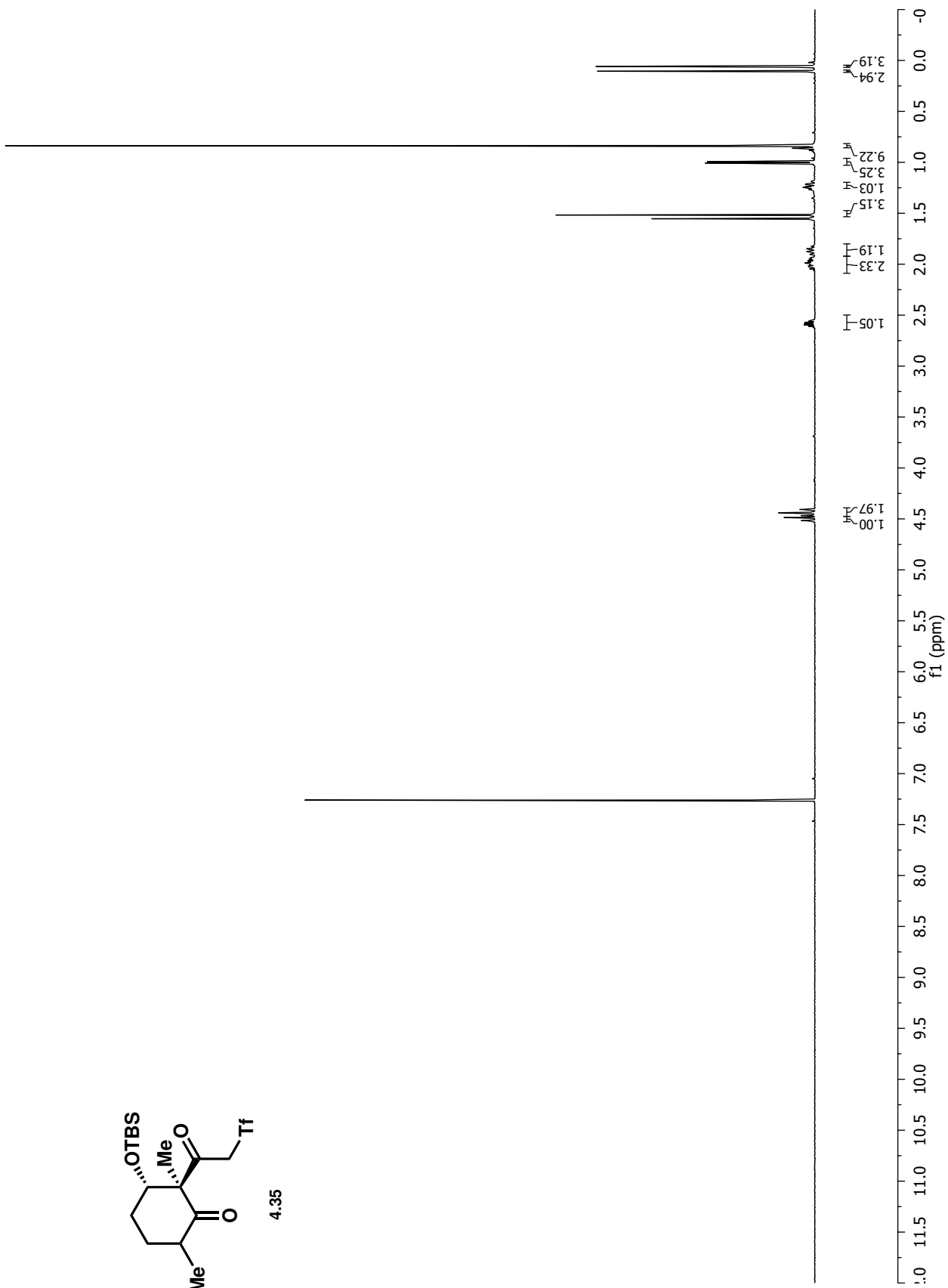
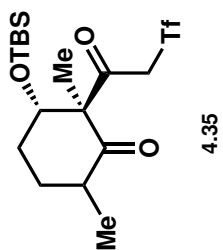
4.33

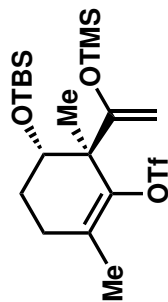




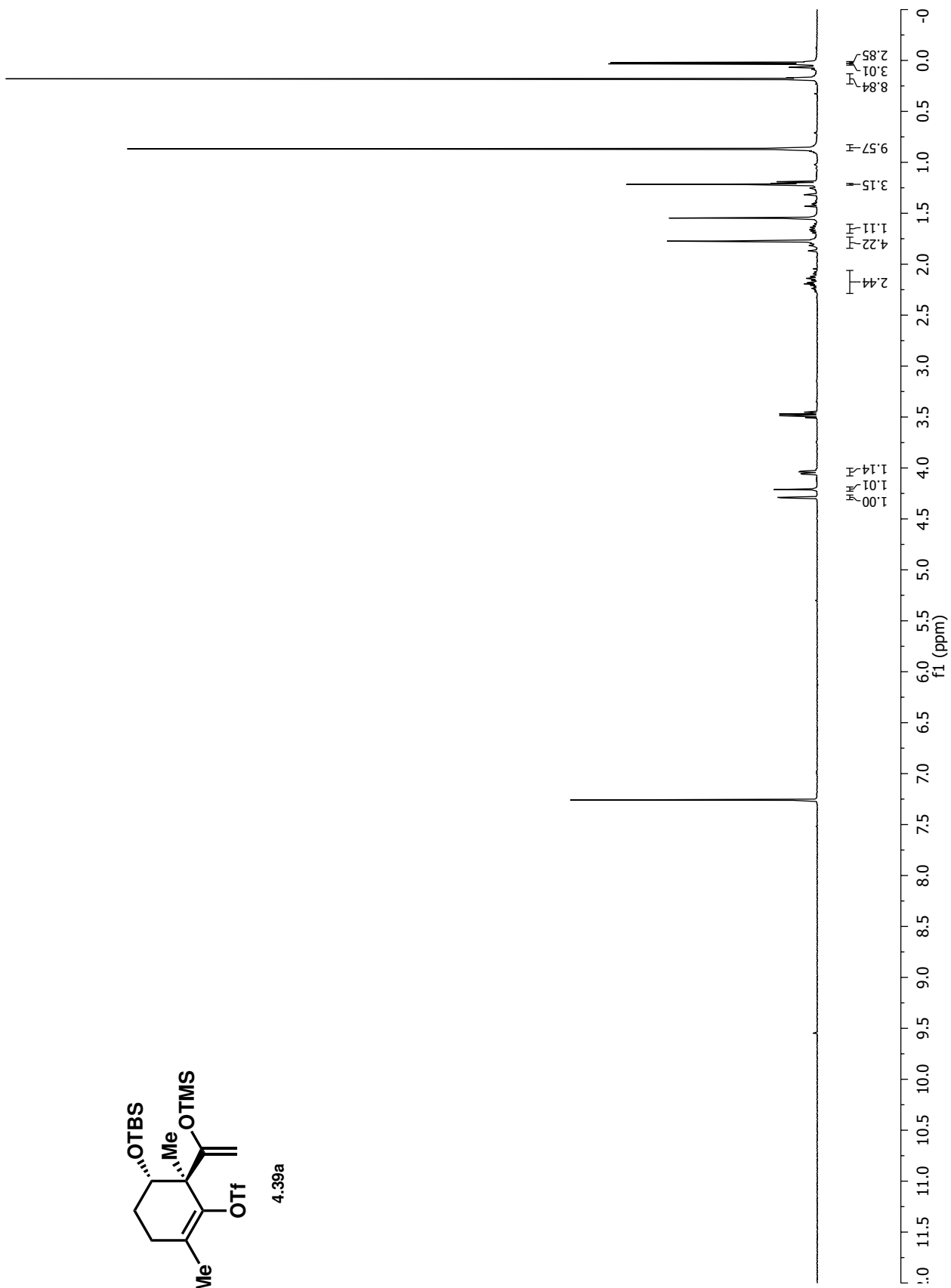


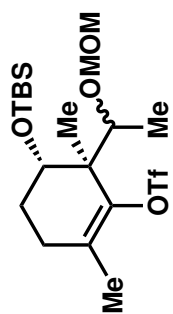




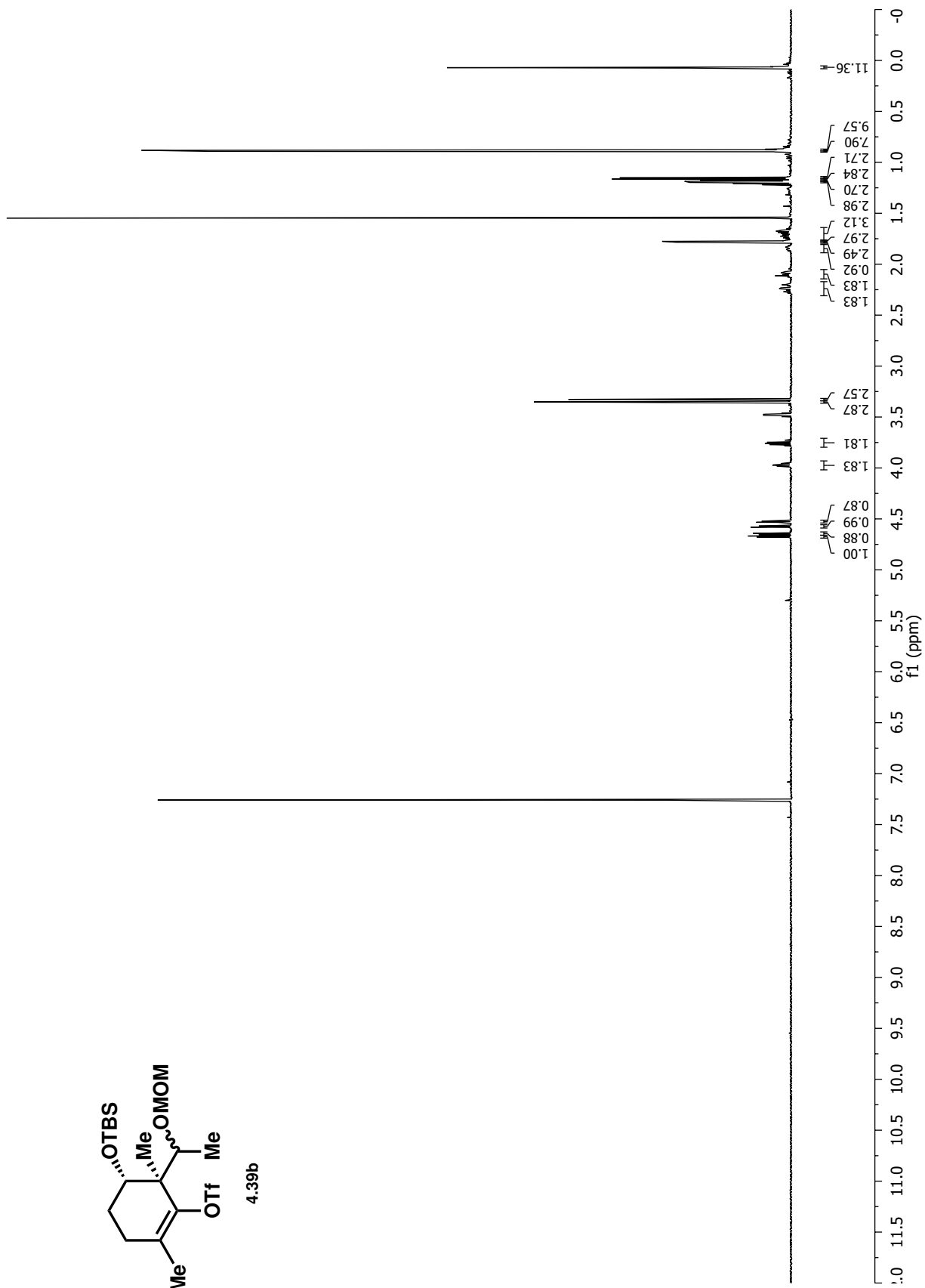


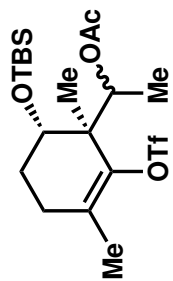
4.39a



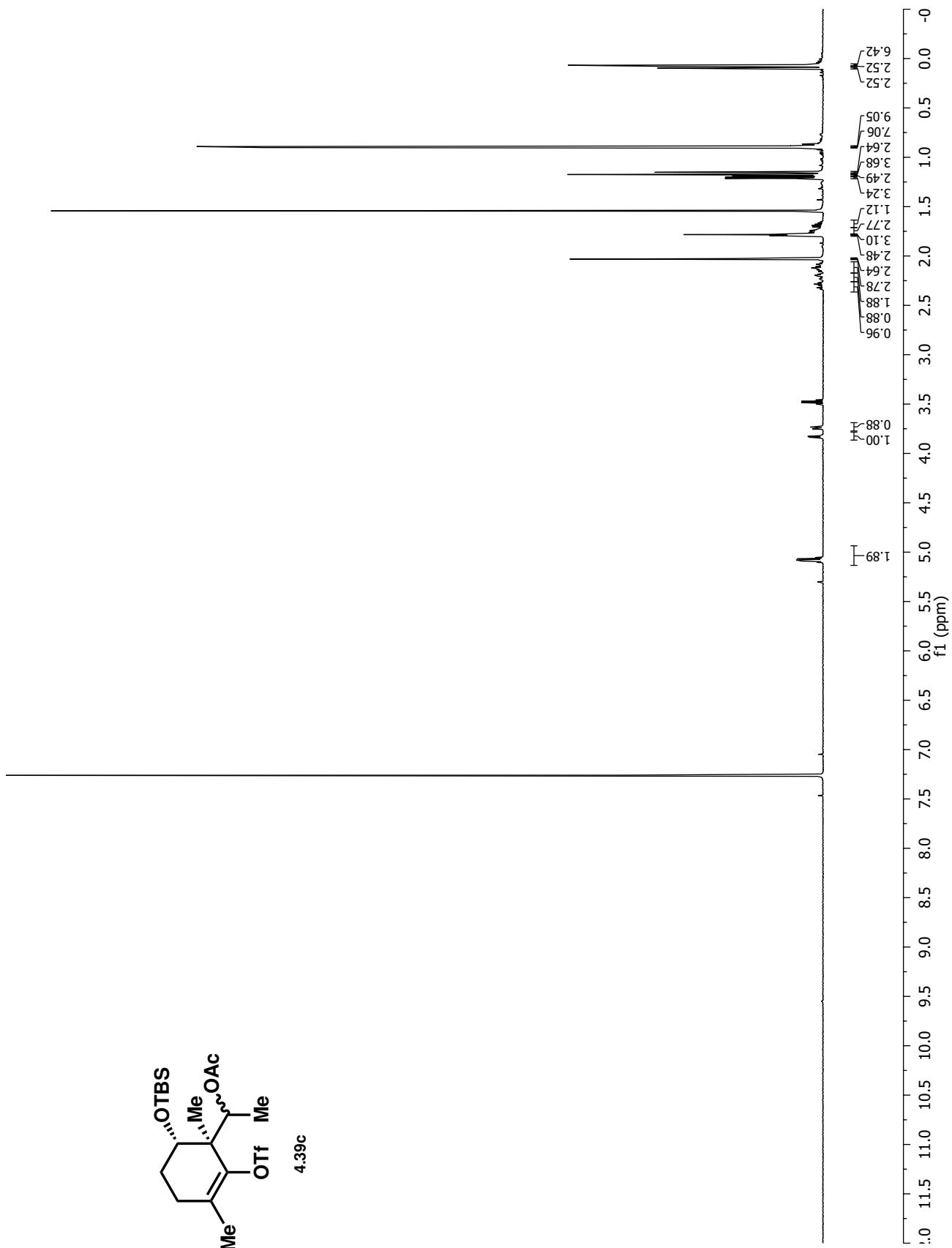


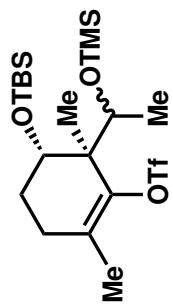
4.39b



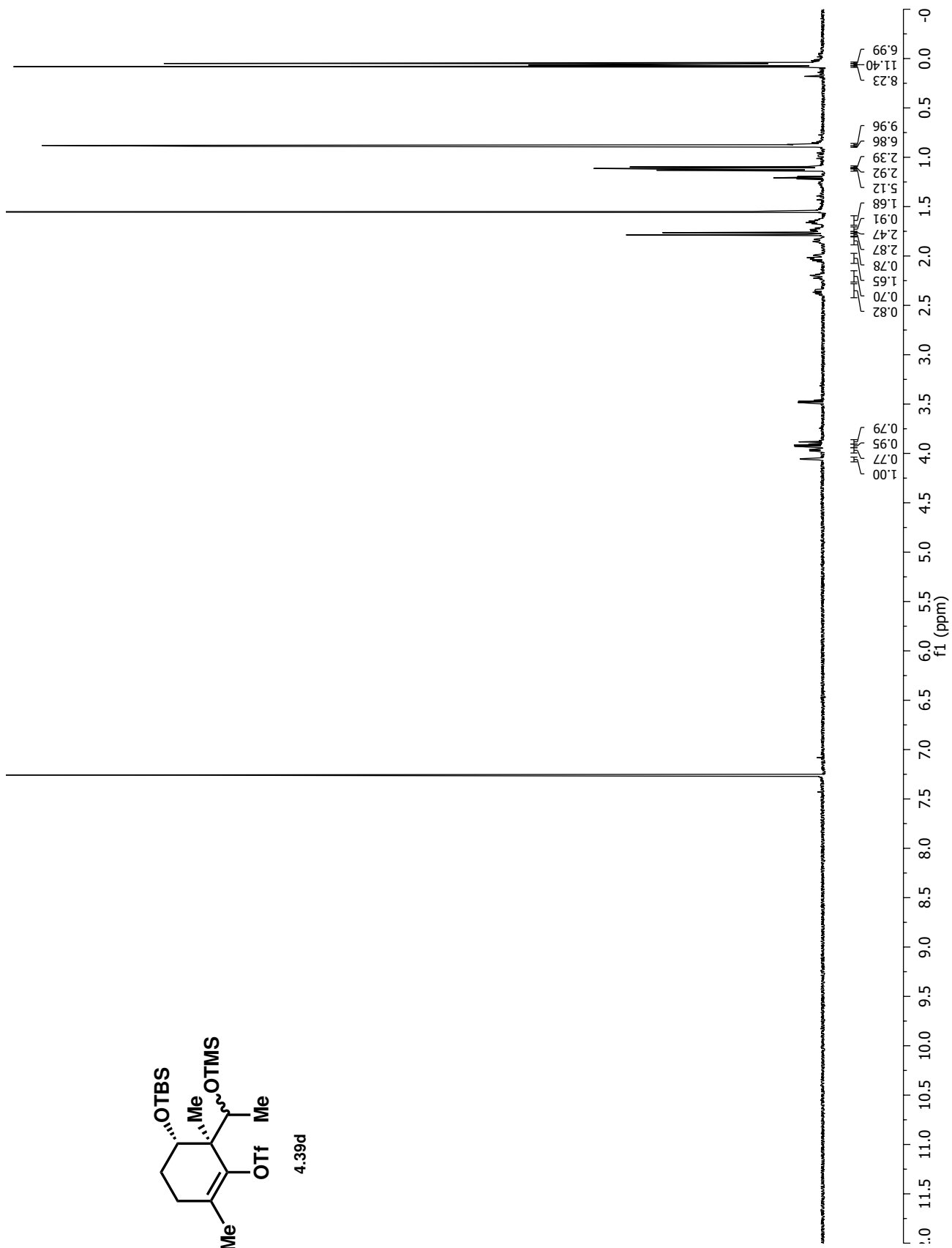


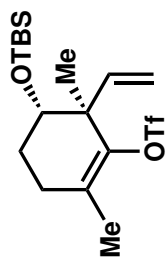
4.39c



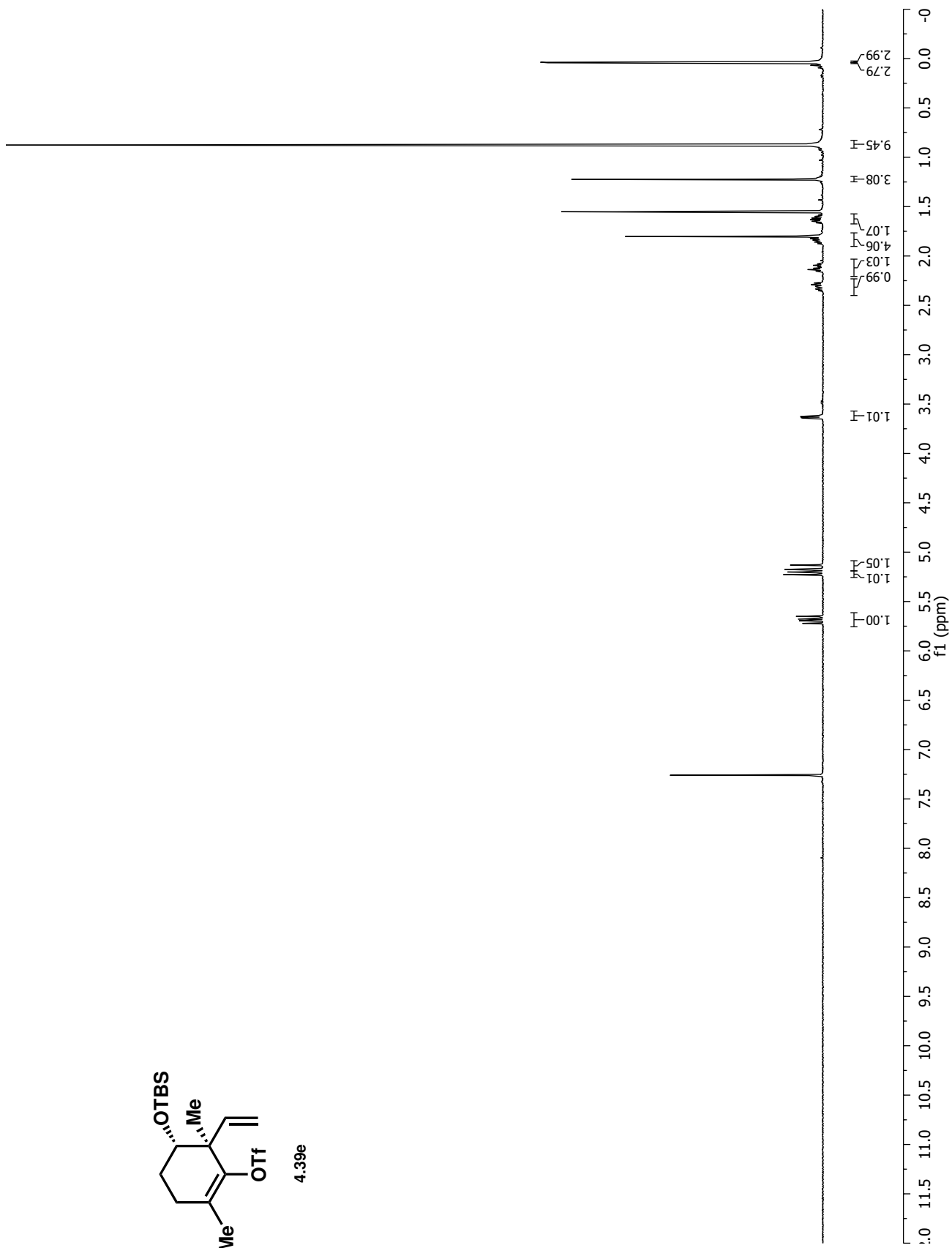


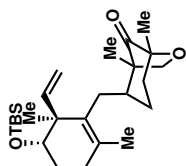
4.39d



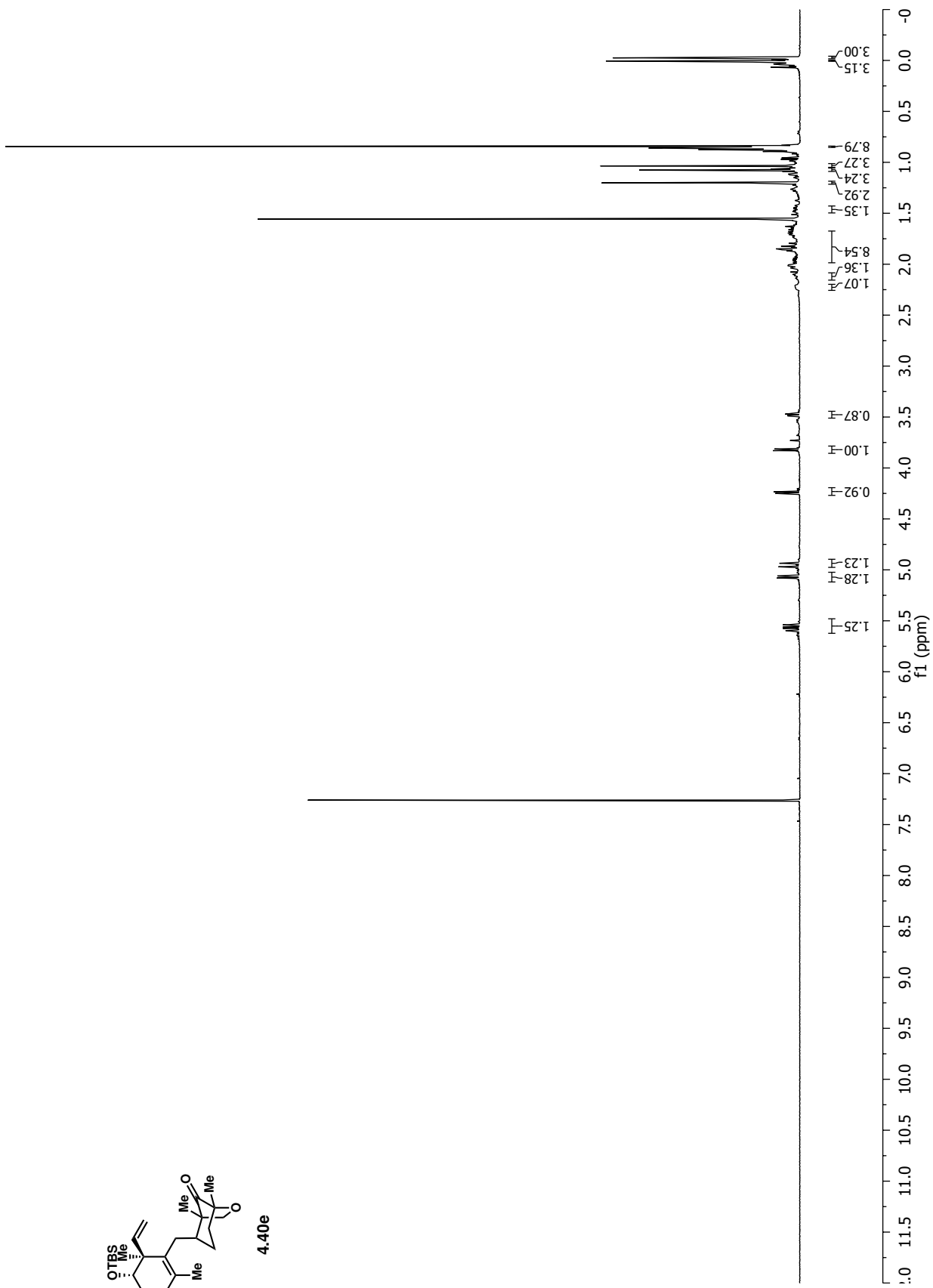


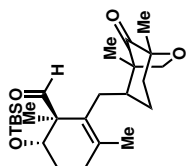
4.39e



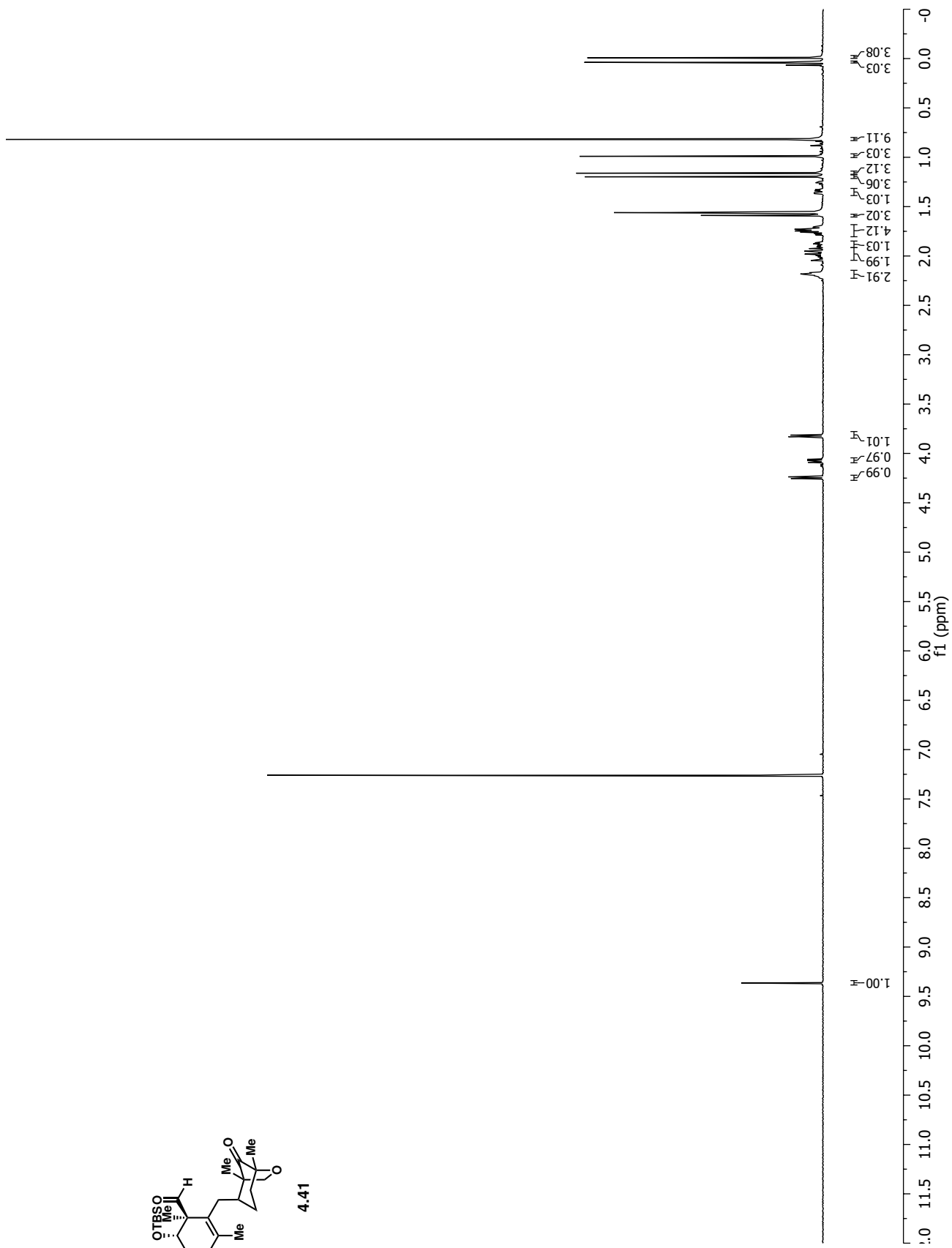


4.40e

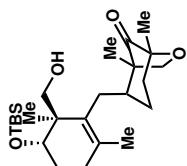




4.41

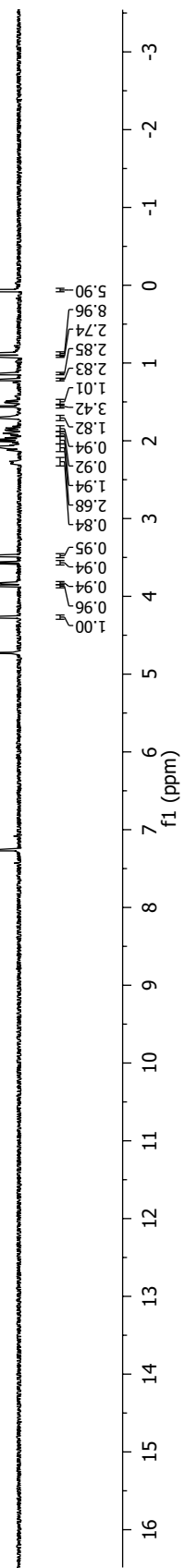


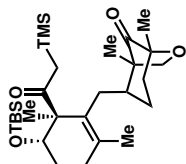




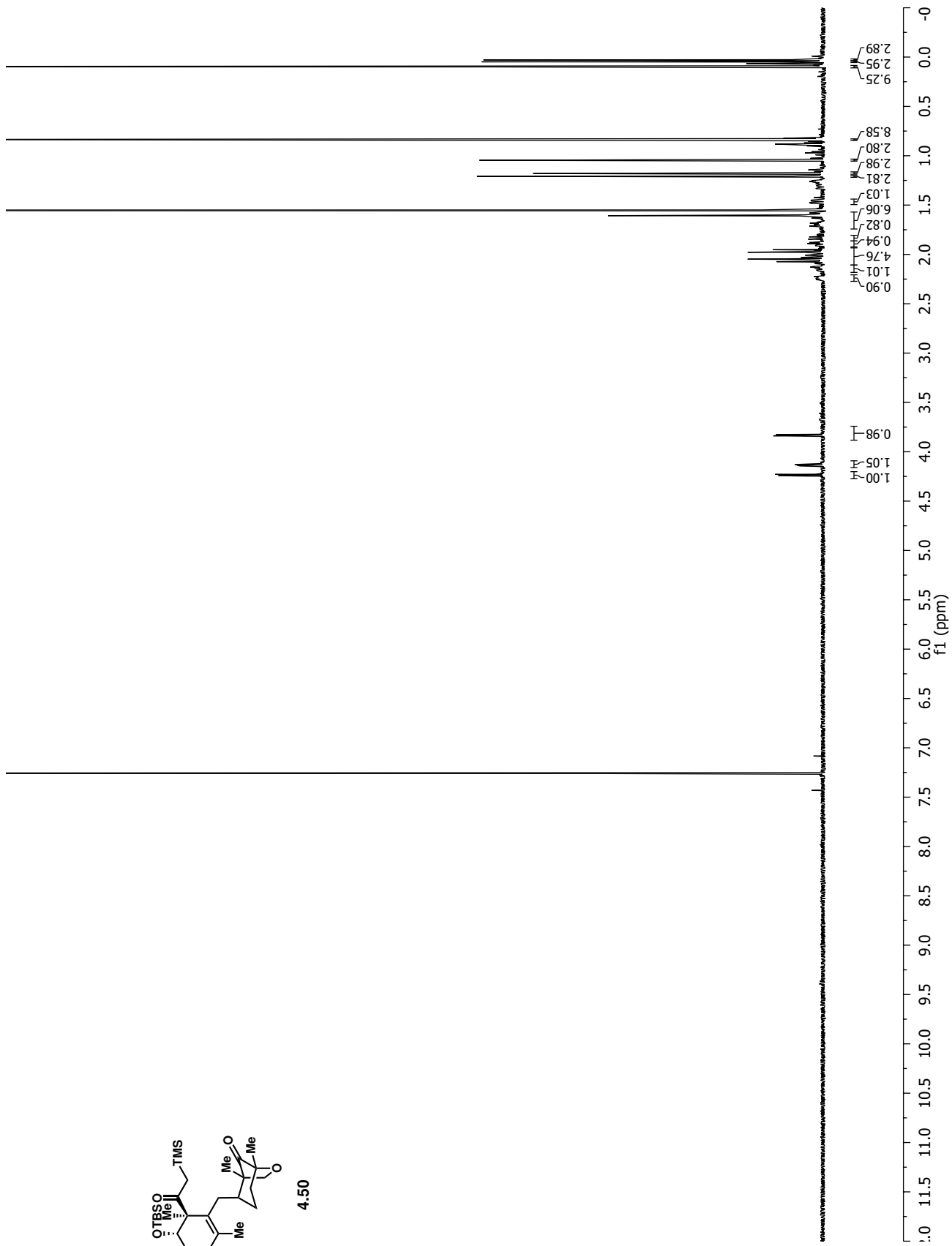
4.48

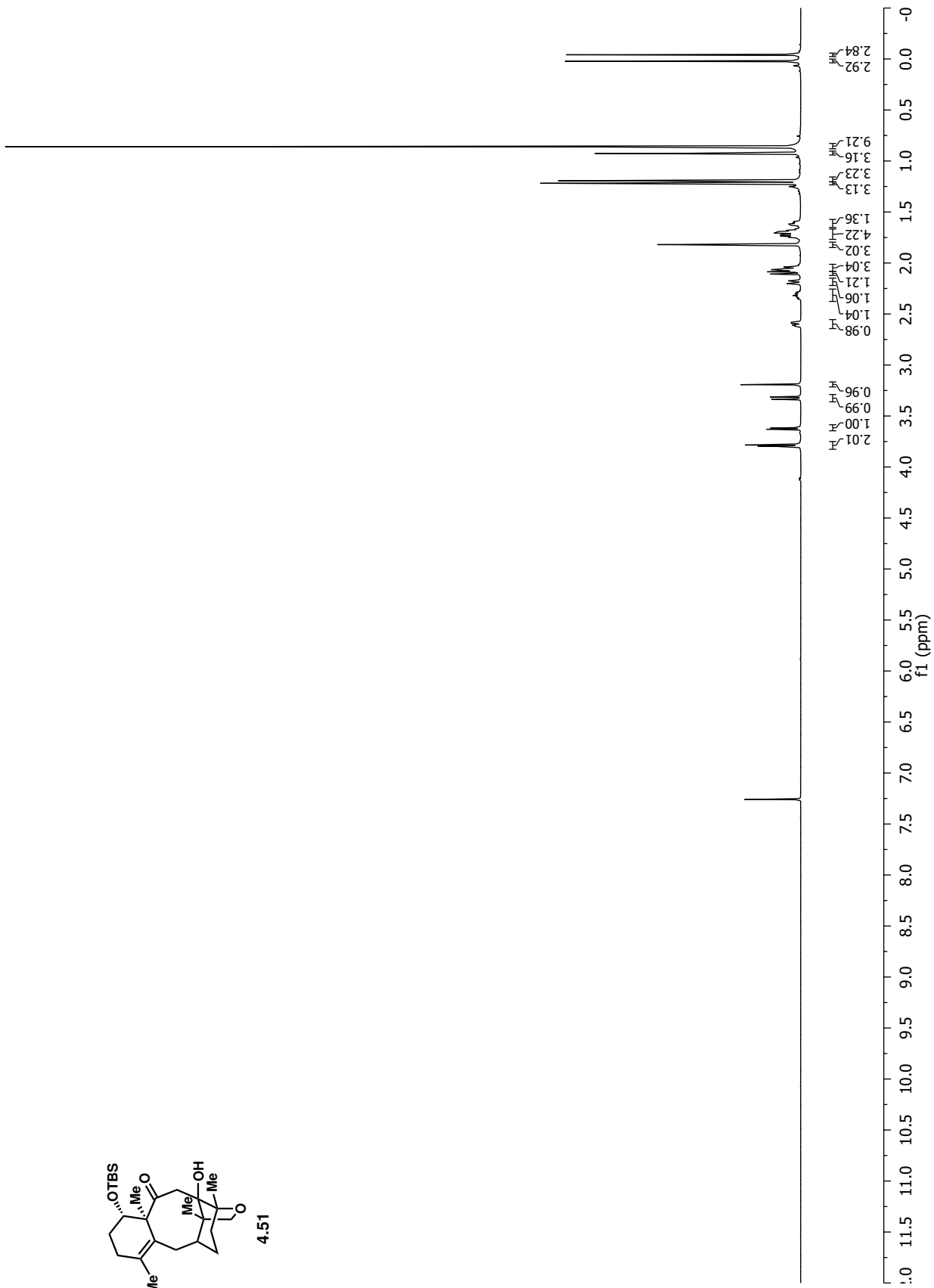
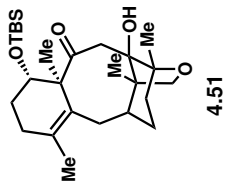
200

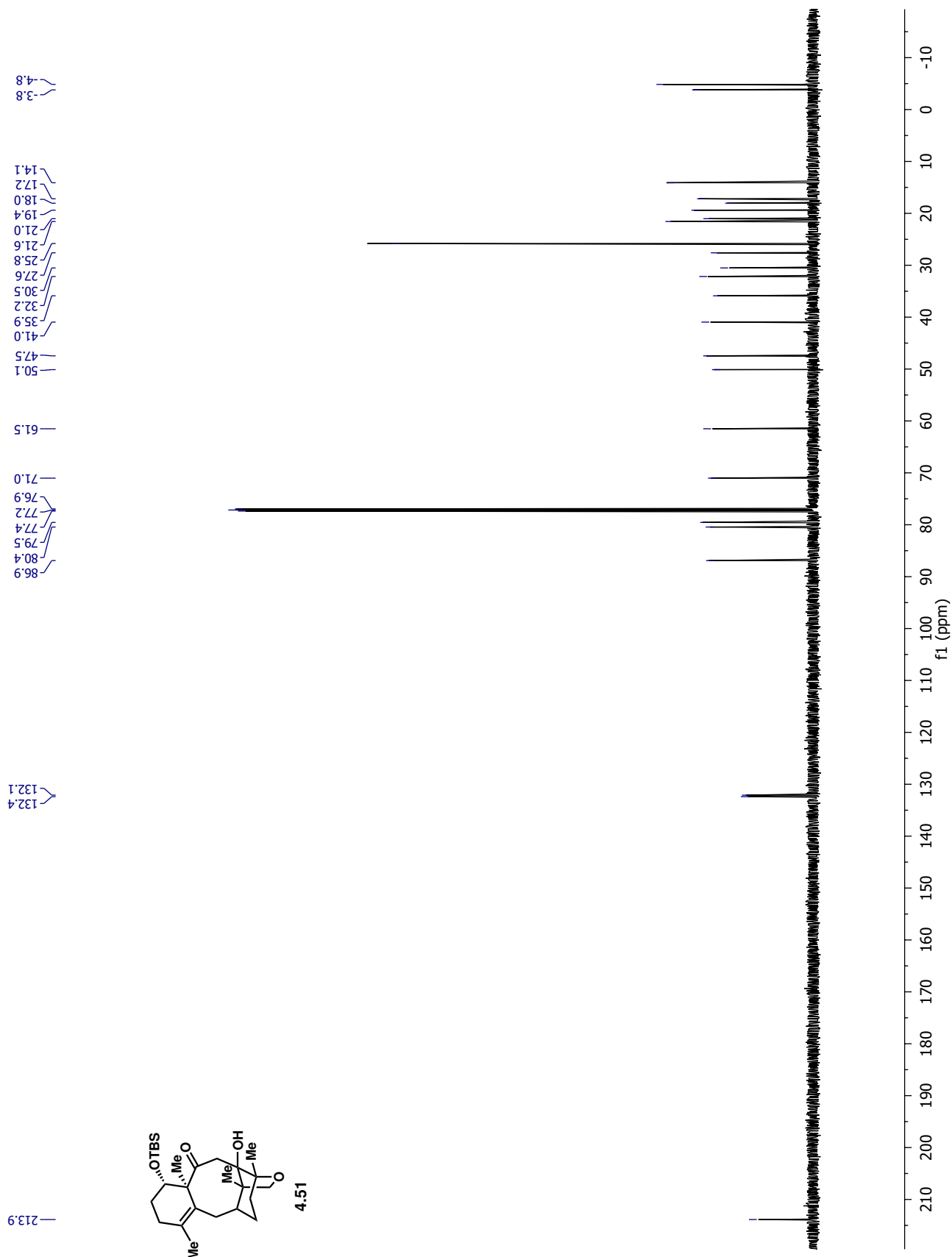


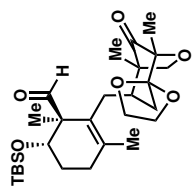


4.50

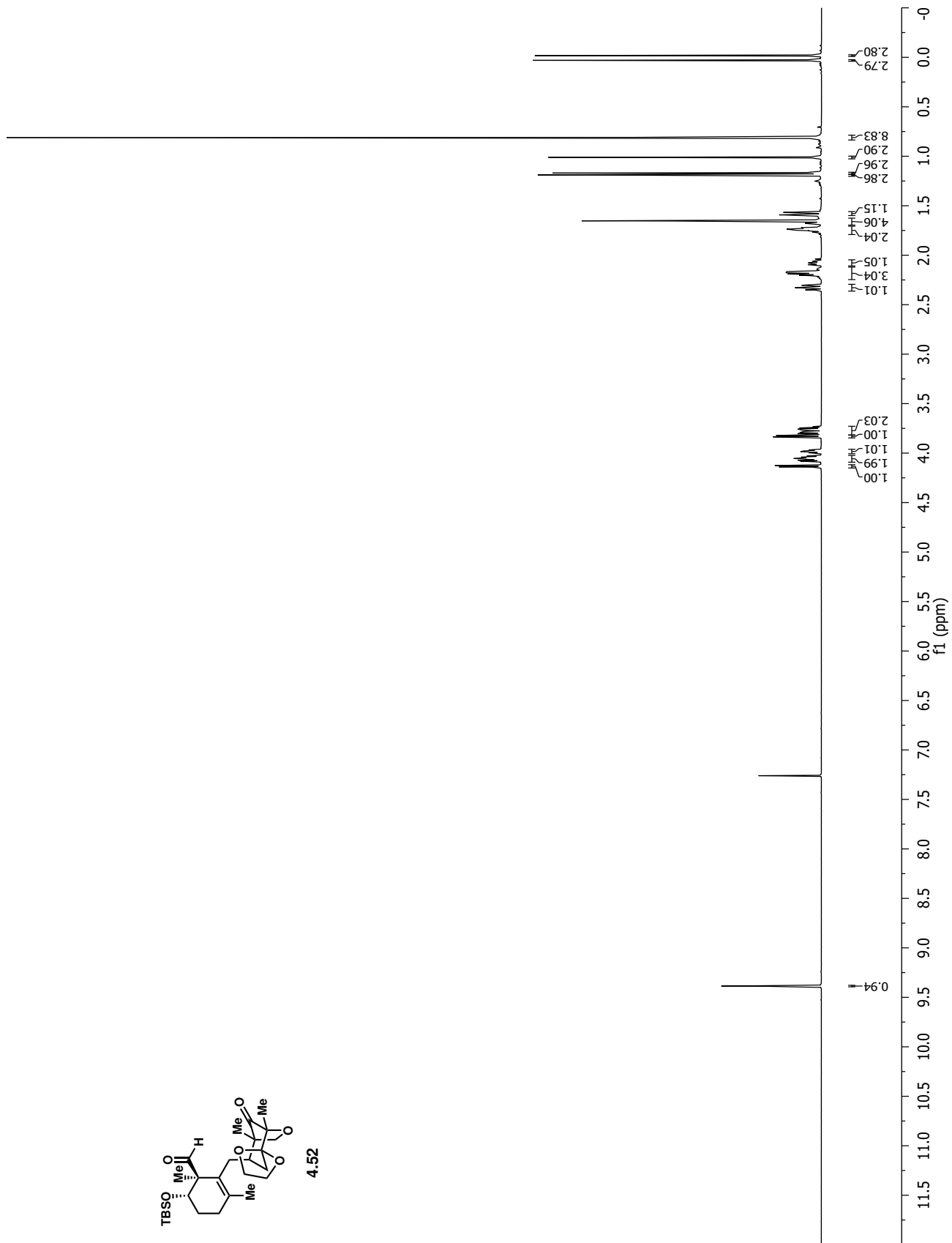


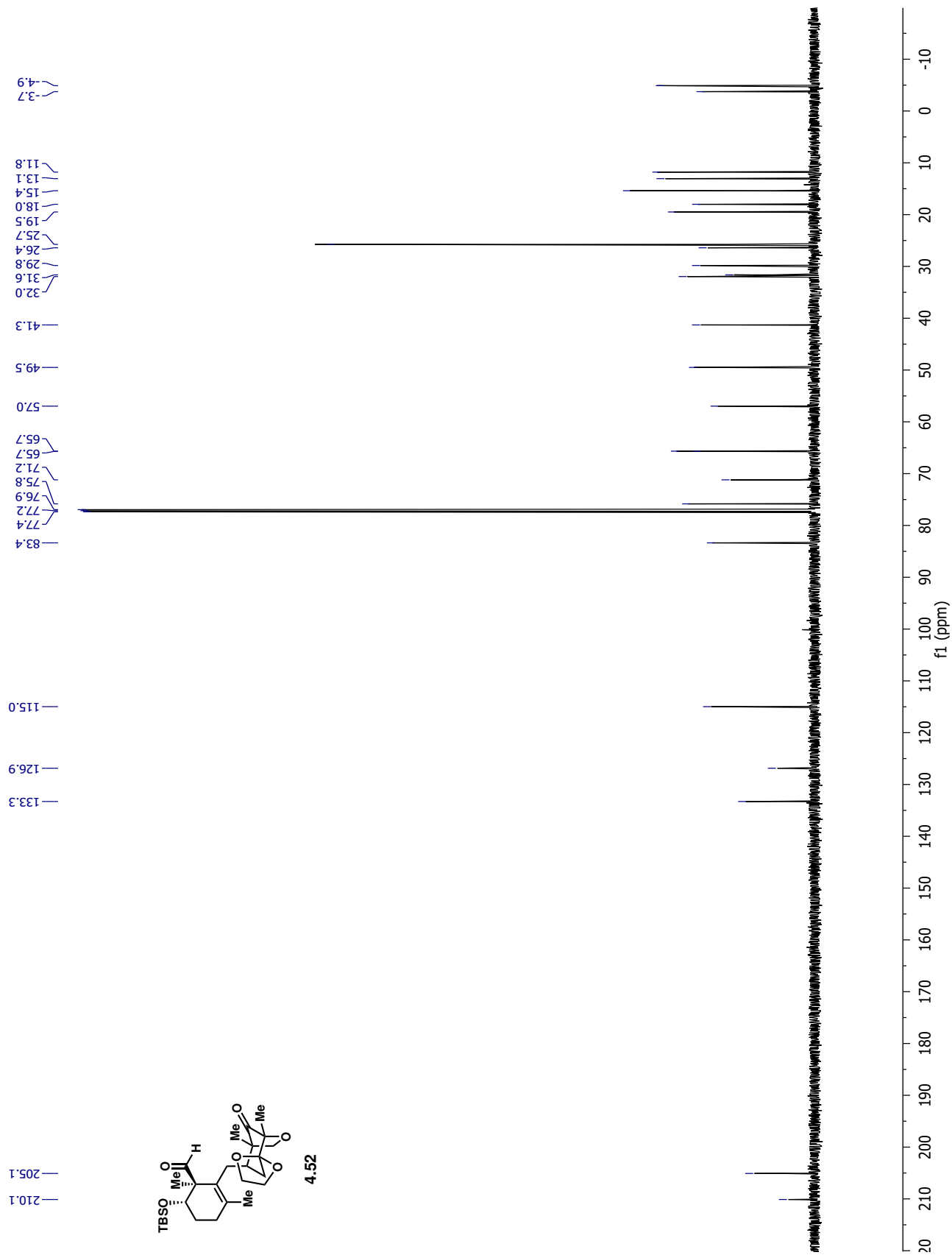


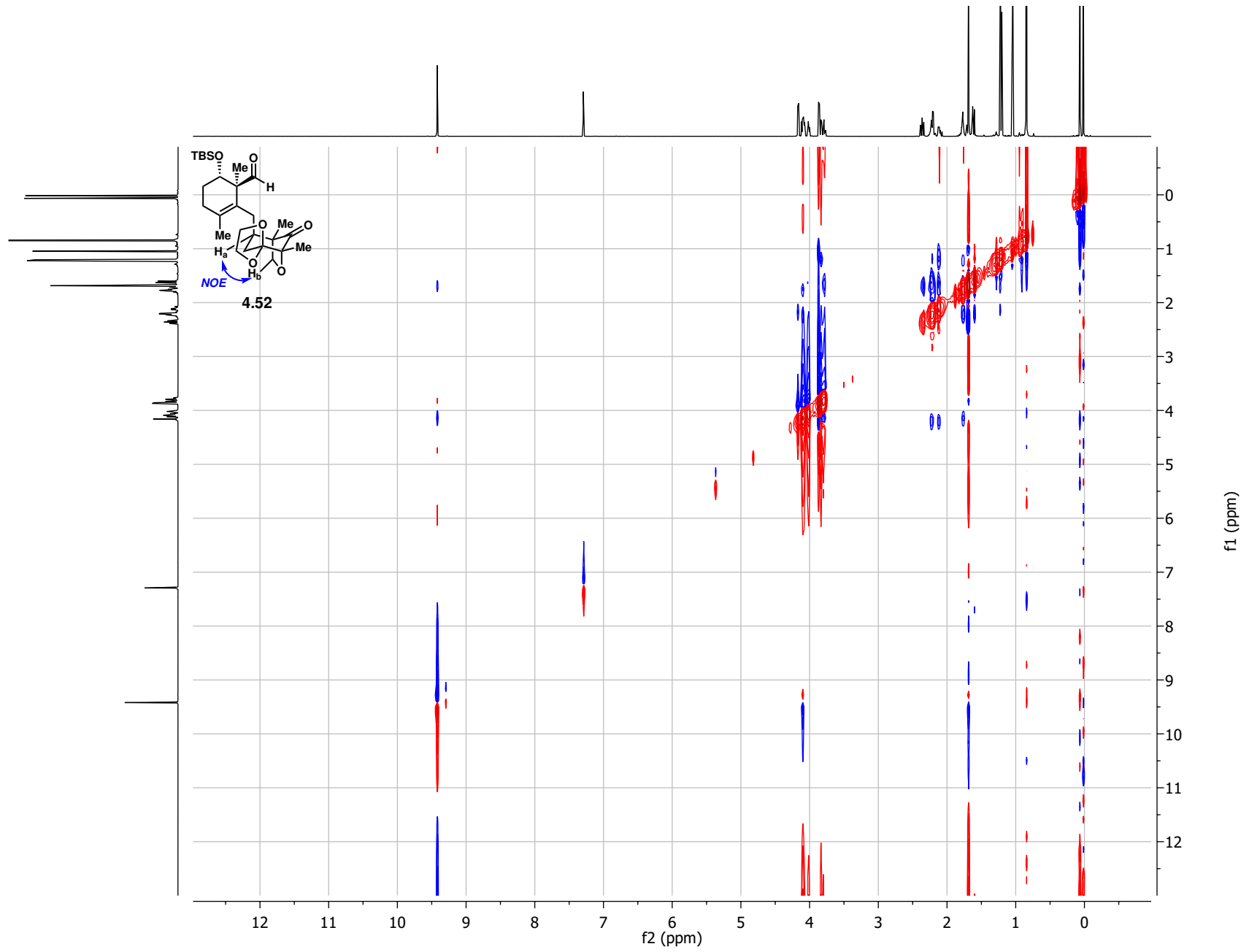


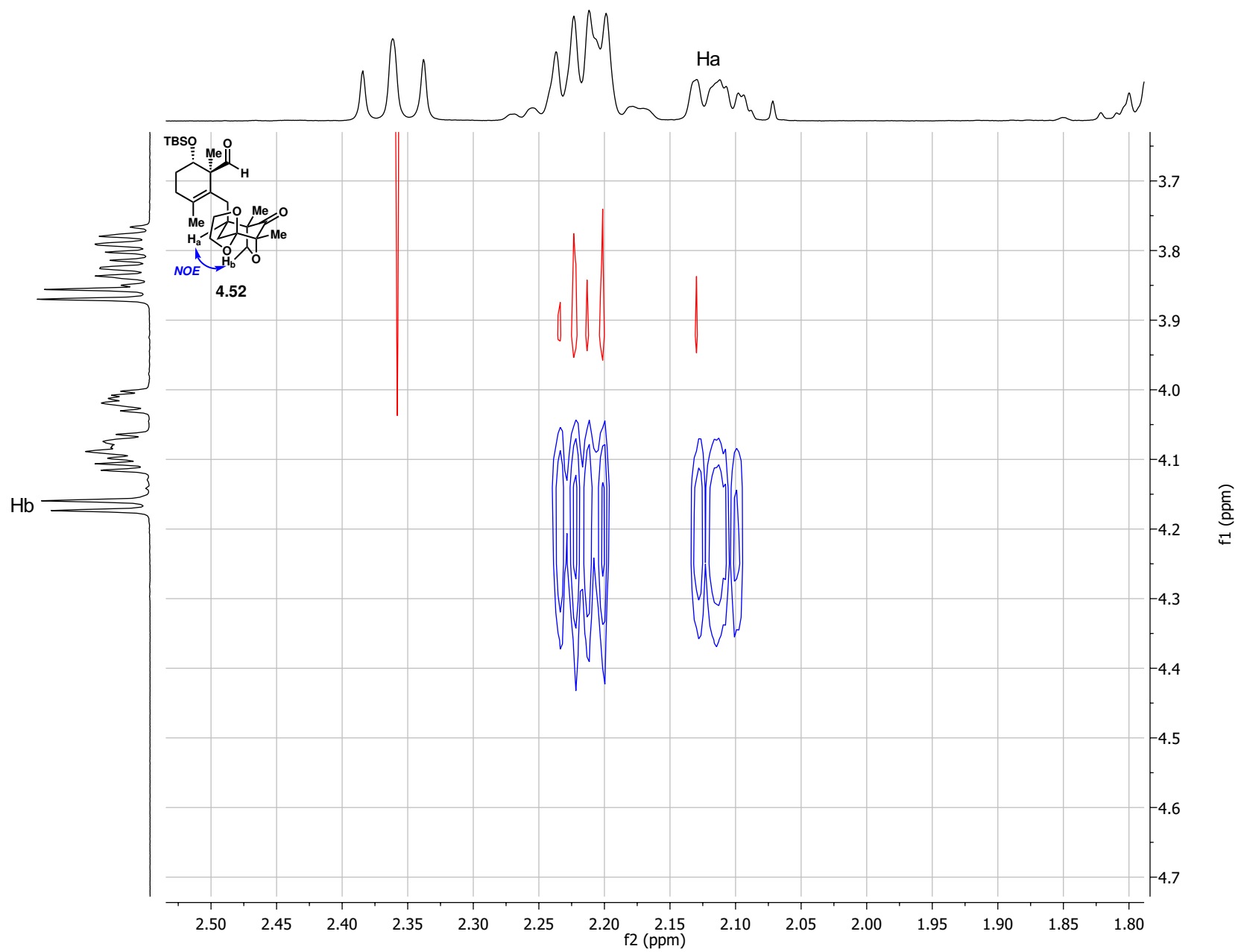


4.52

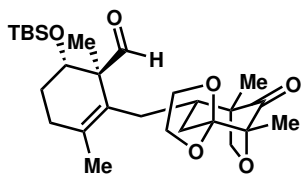




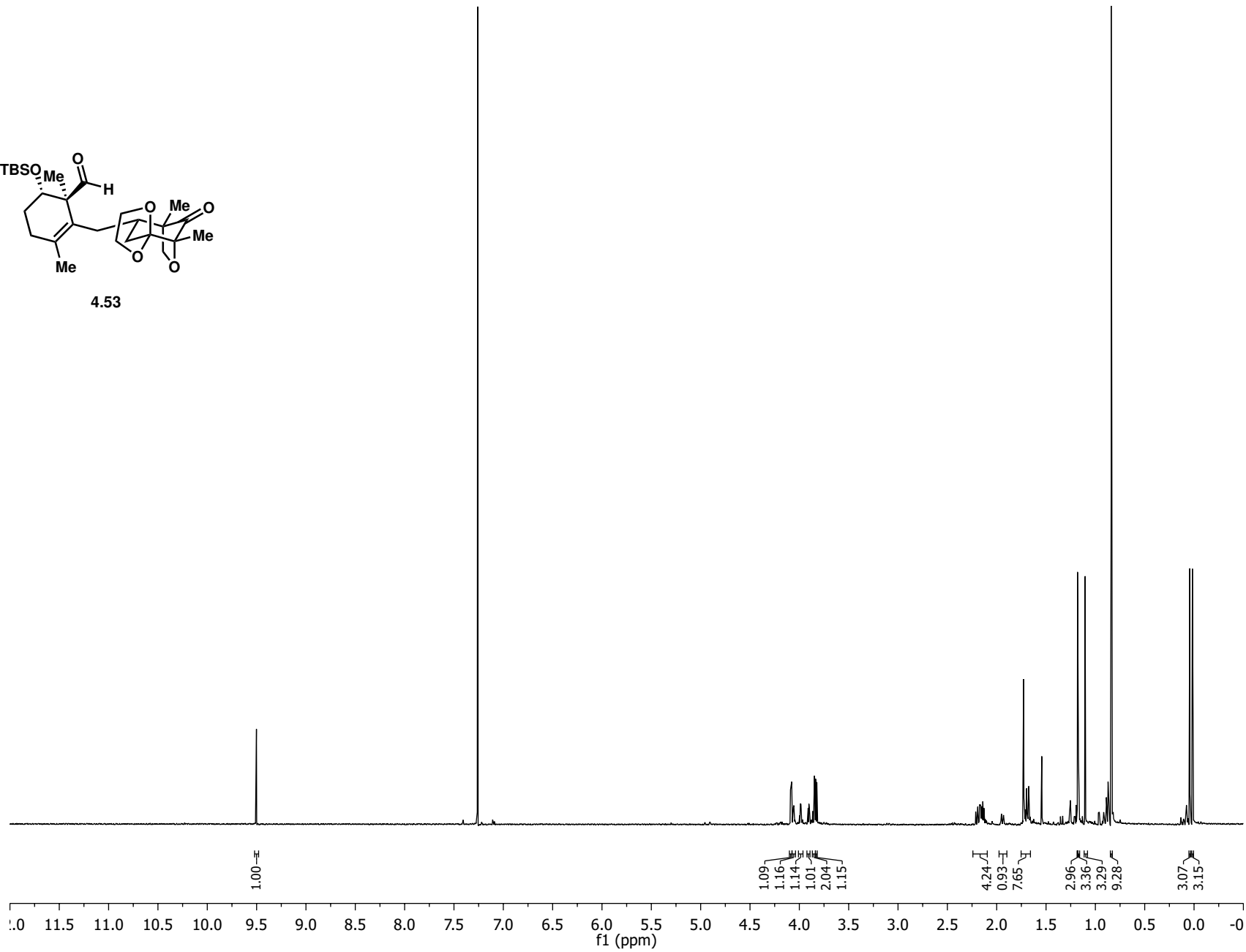


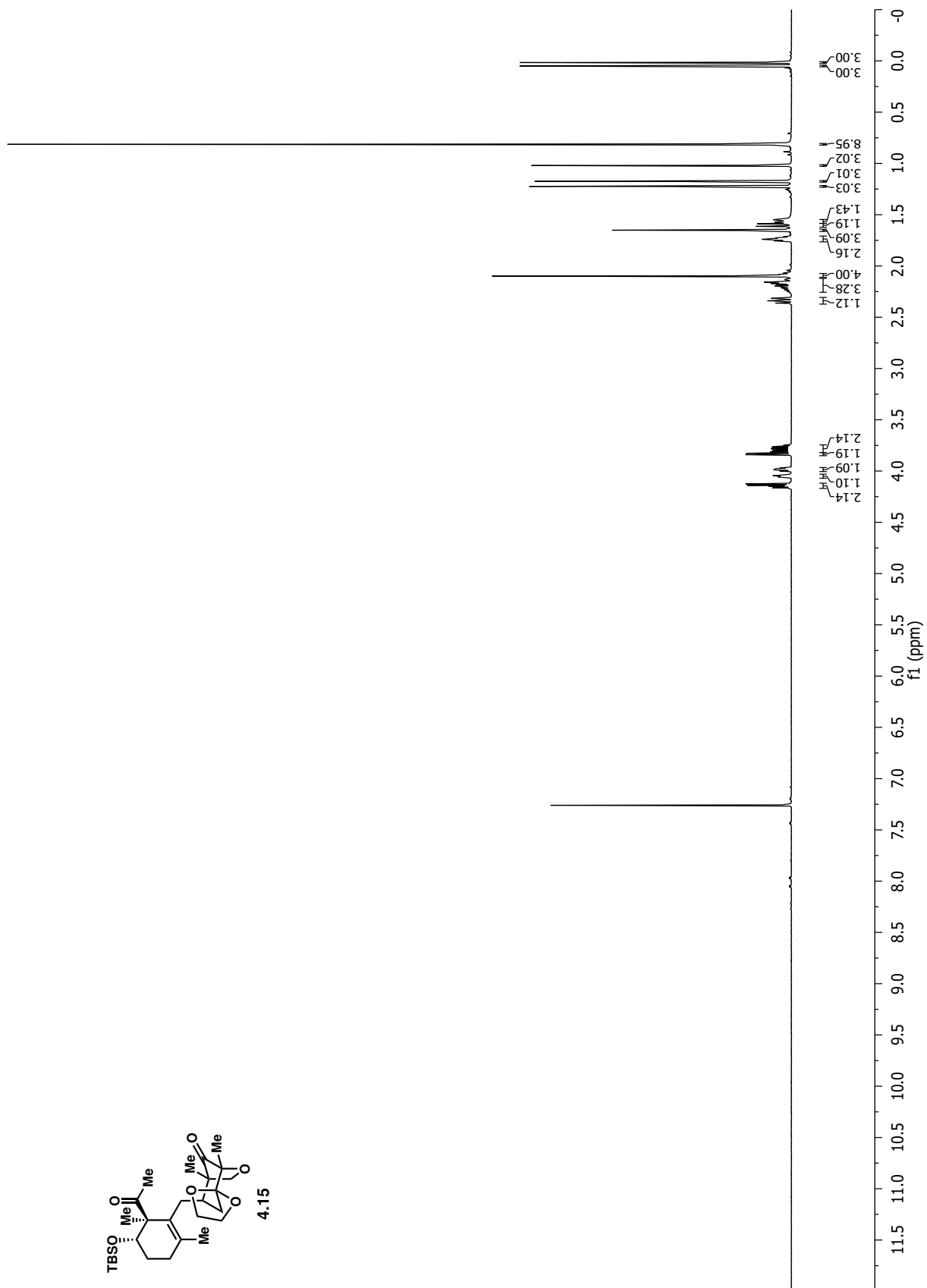
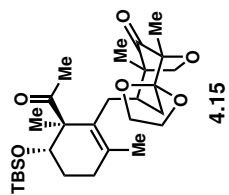




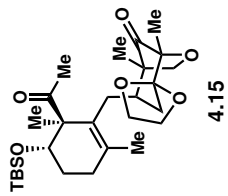
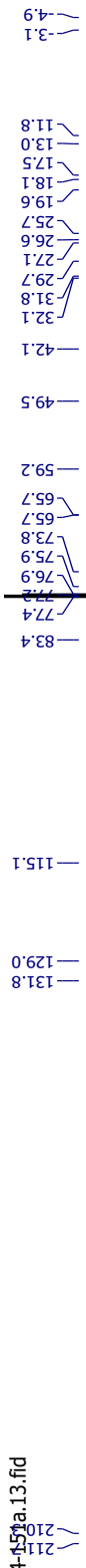


4.53

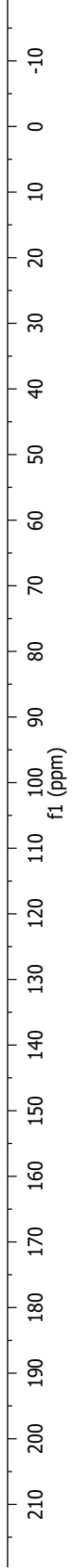


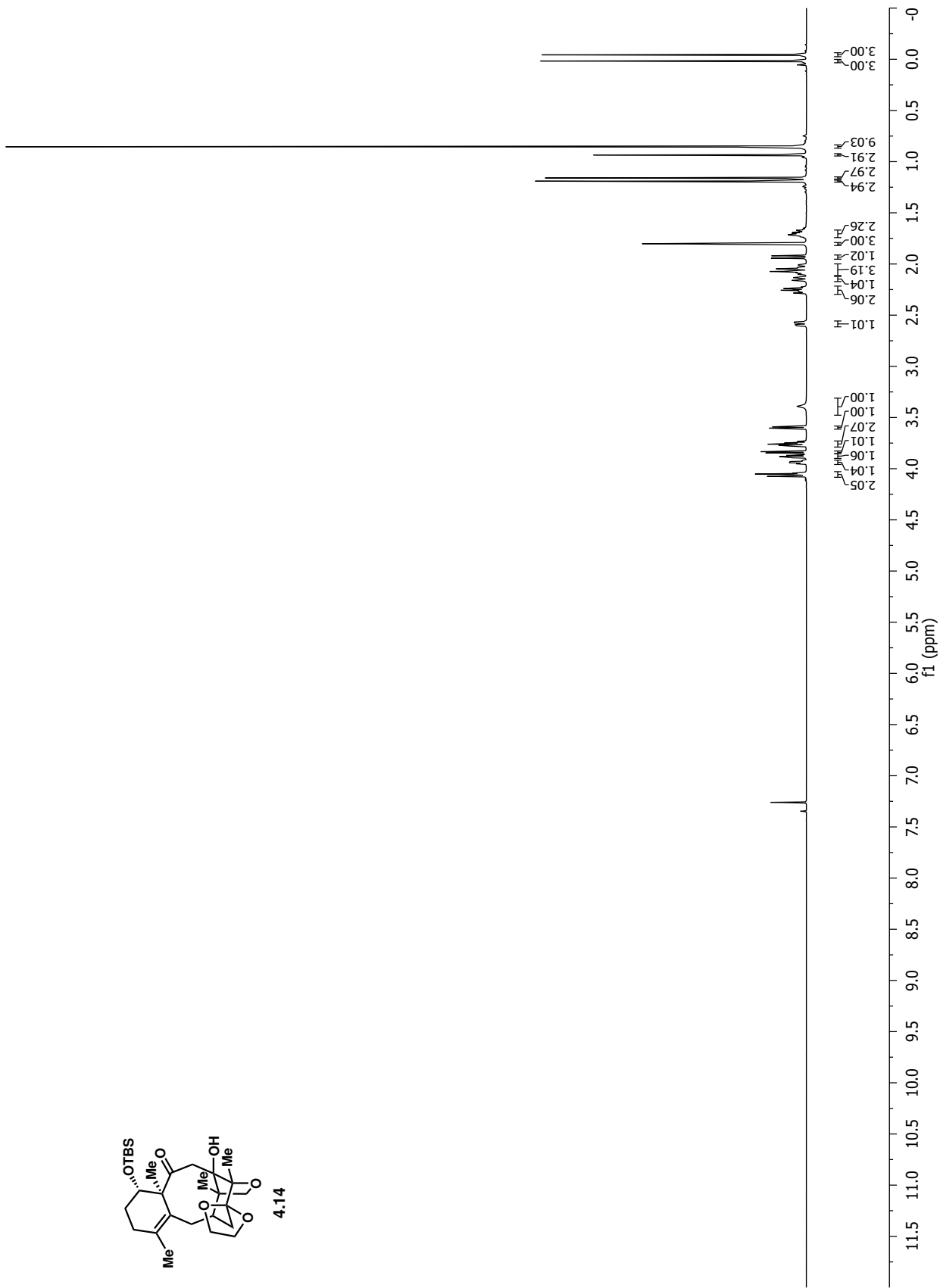
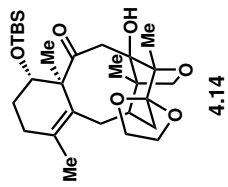


bw4-157a.13.fid

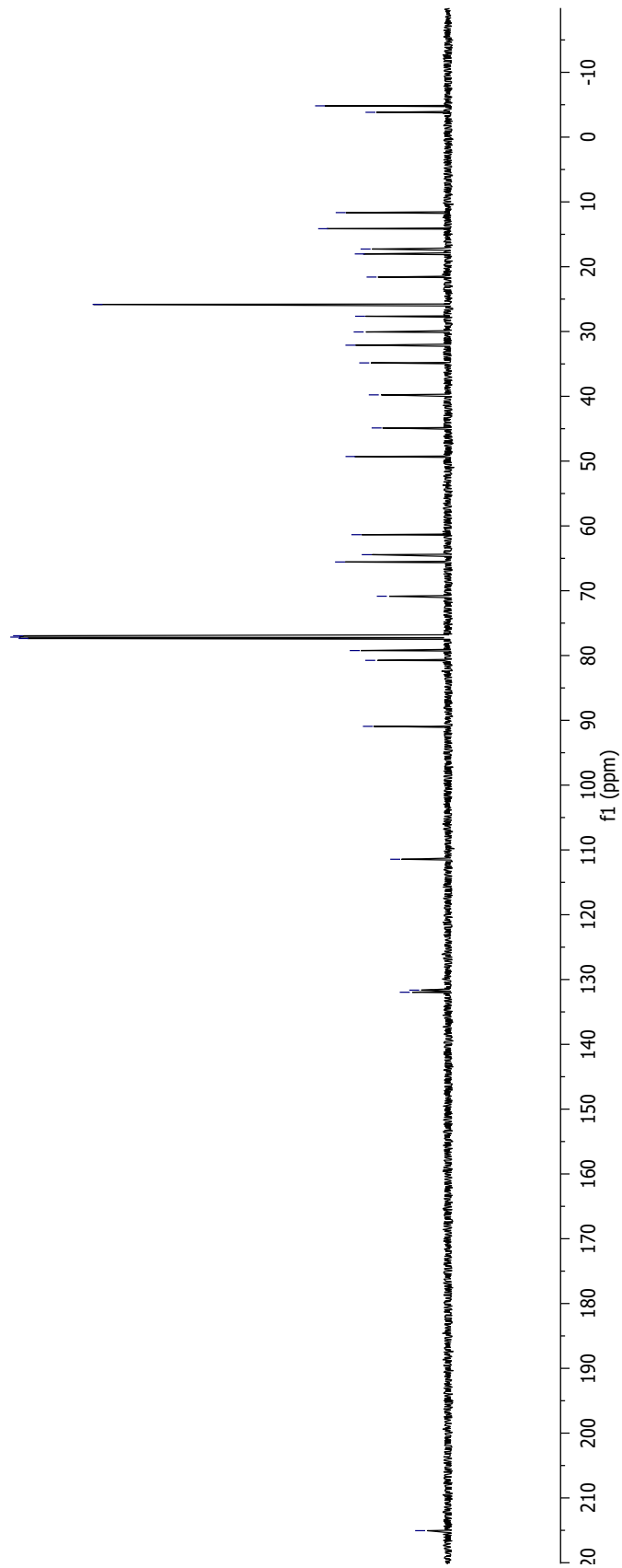
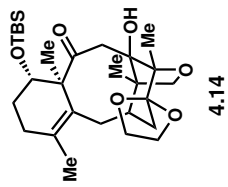


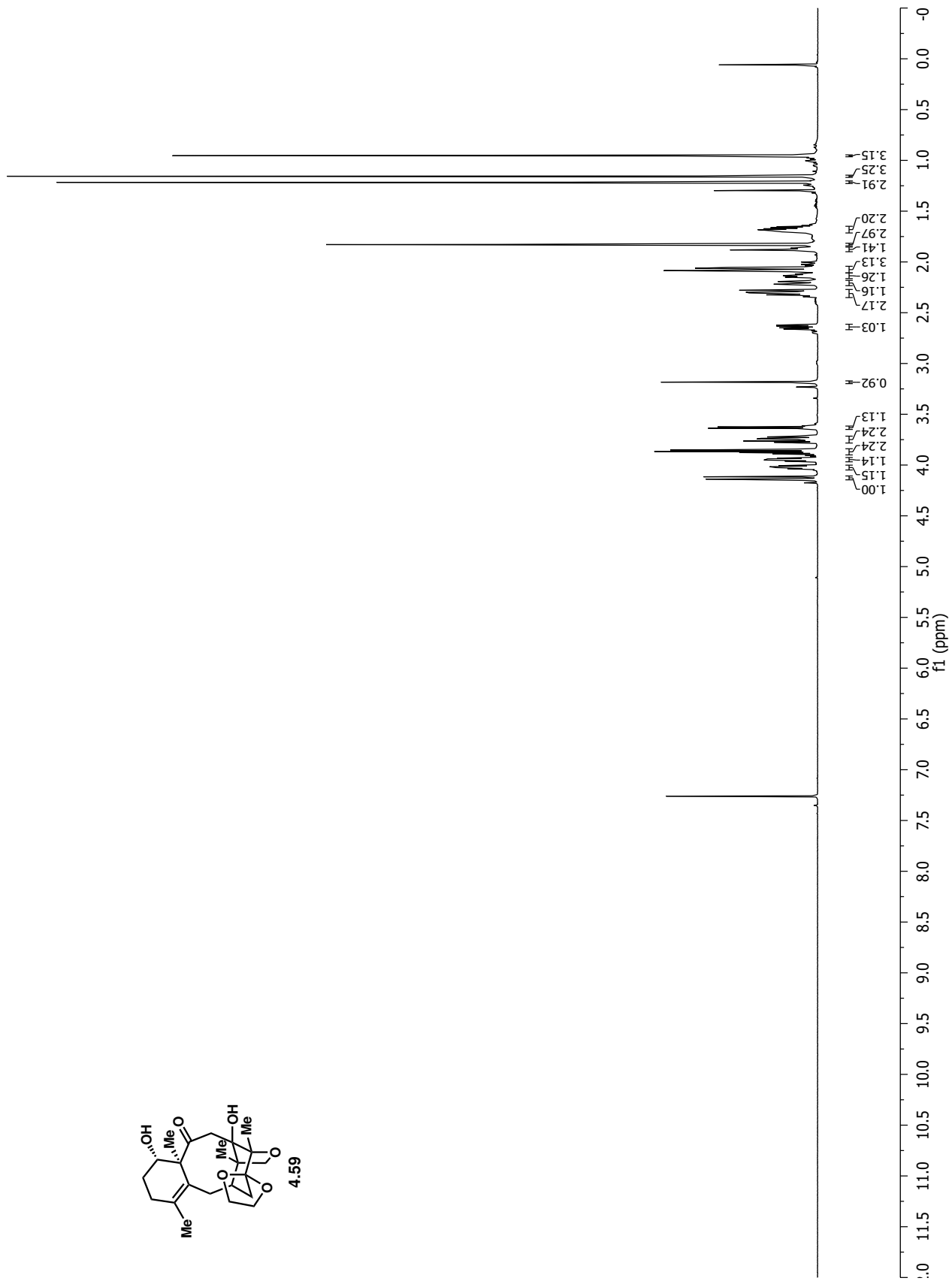
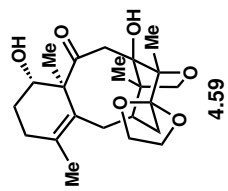
4.15

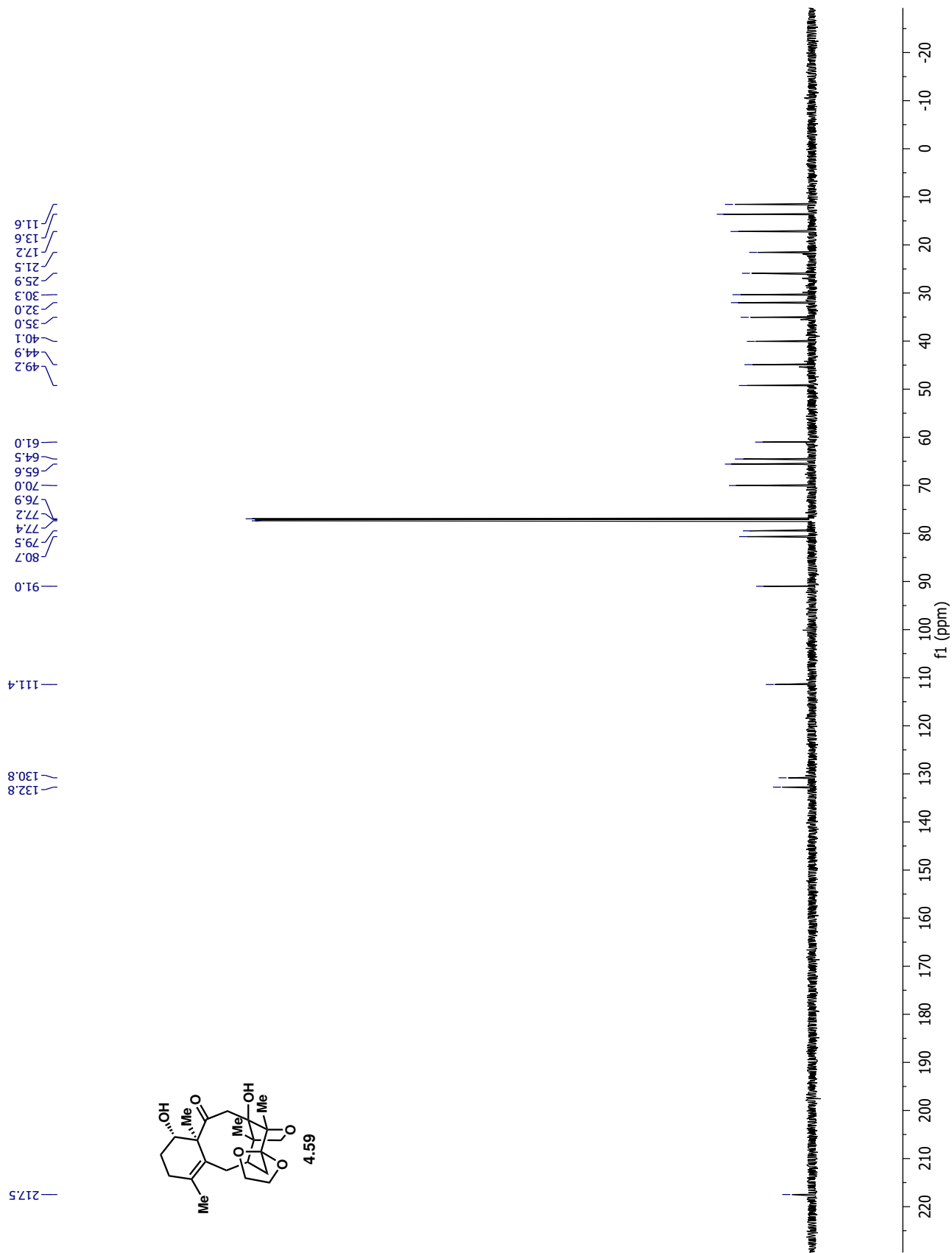


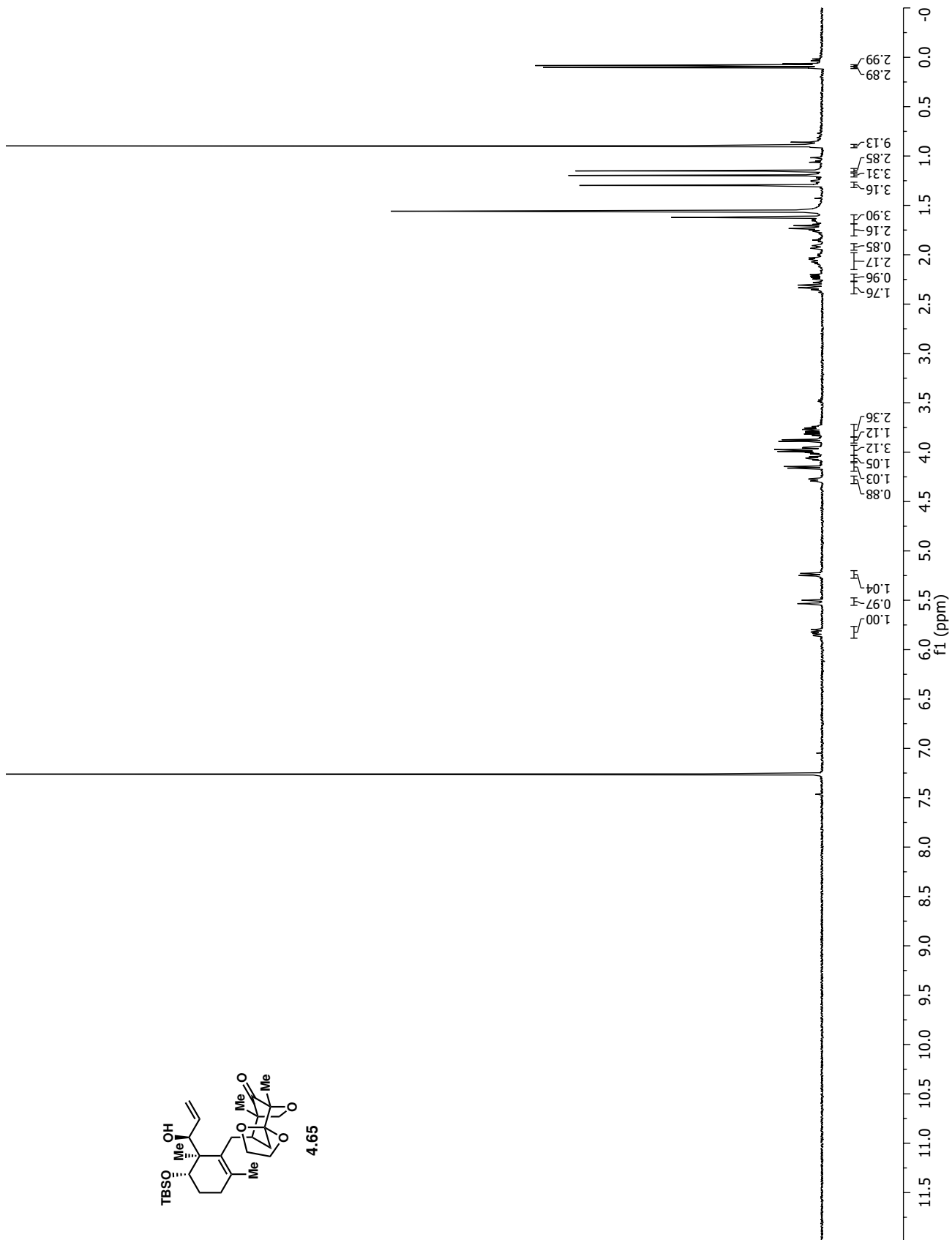
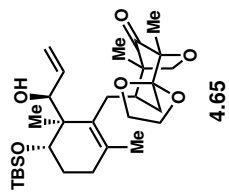


215.1  
 132.0  
 131.6  
 111.4  
 90.9  
 80.7  
 79.2  
 77.4  
 77.2  
 76.9  
 70.8  
 65.6  
 64.4  
 61.4  
 49.3  
 44.9  
 39.8  
 34.8  
 32.1  
 30.1  
 27.6  
 25.8  
 21.6  
 18.0  
 17.3  
 14.1  
 11.6  
 3.8  
 -4.8

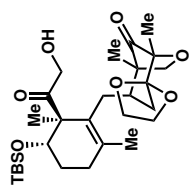




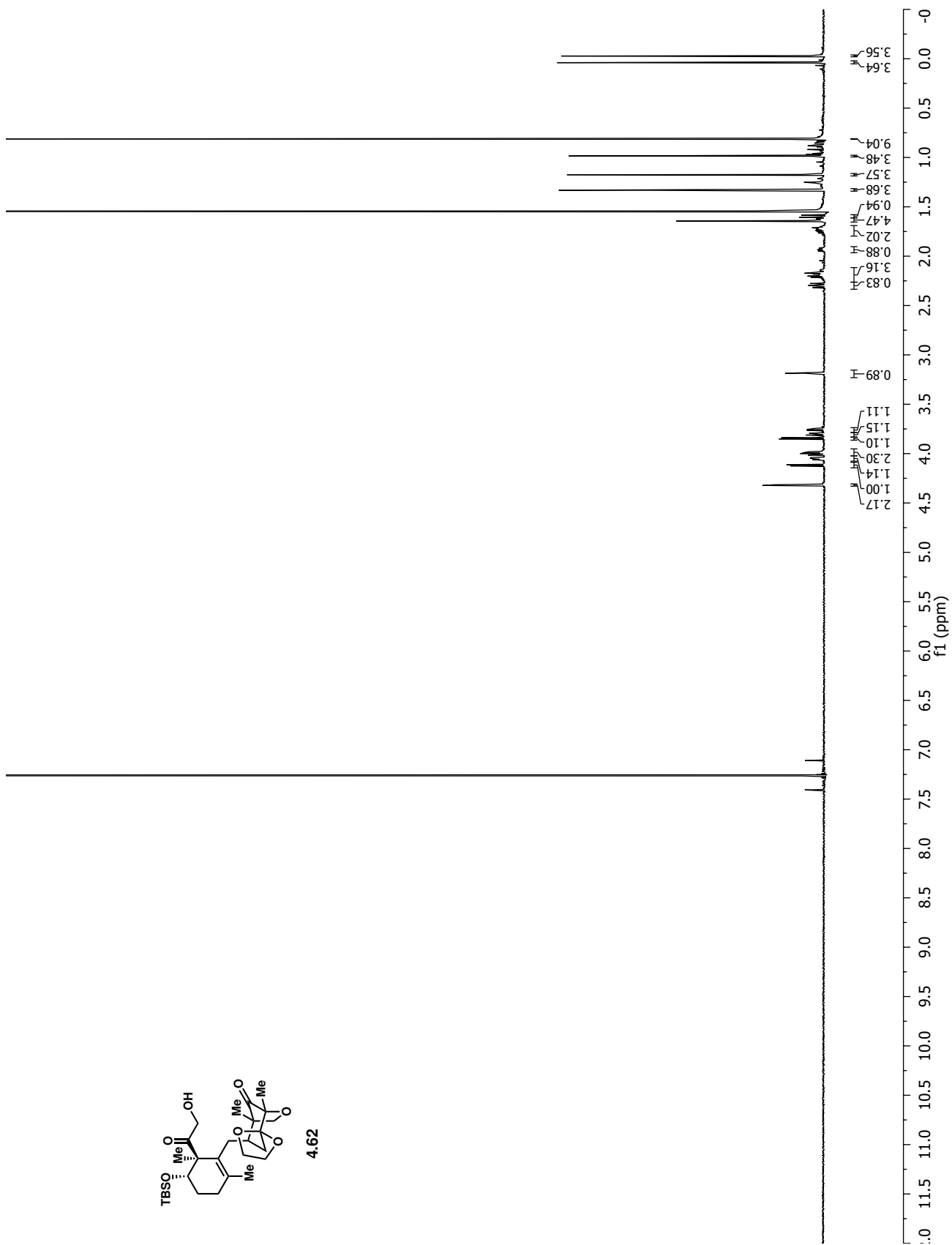


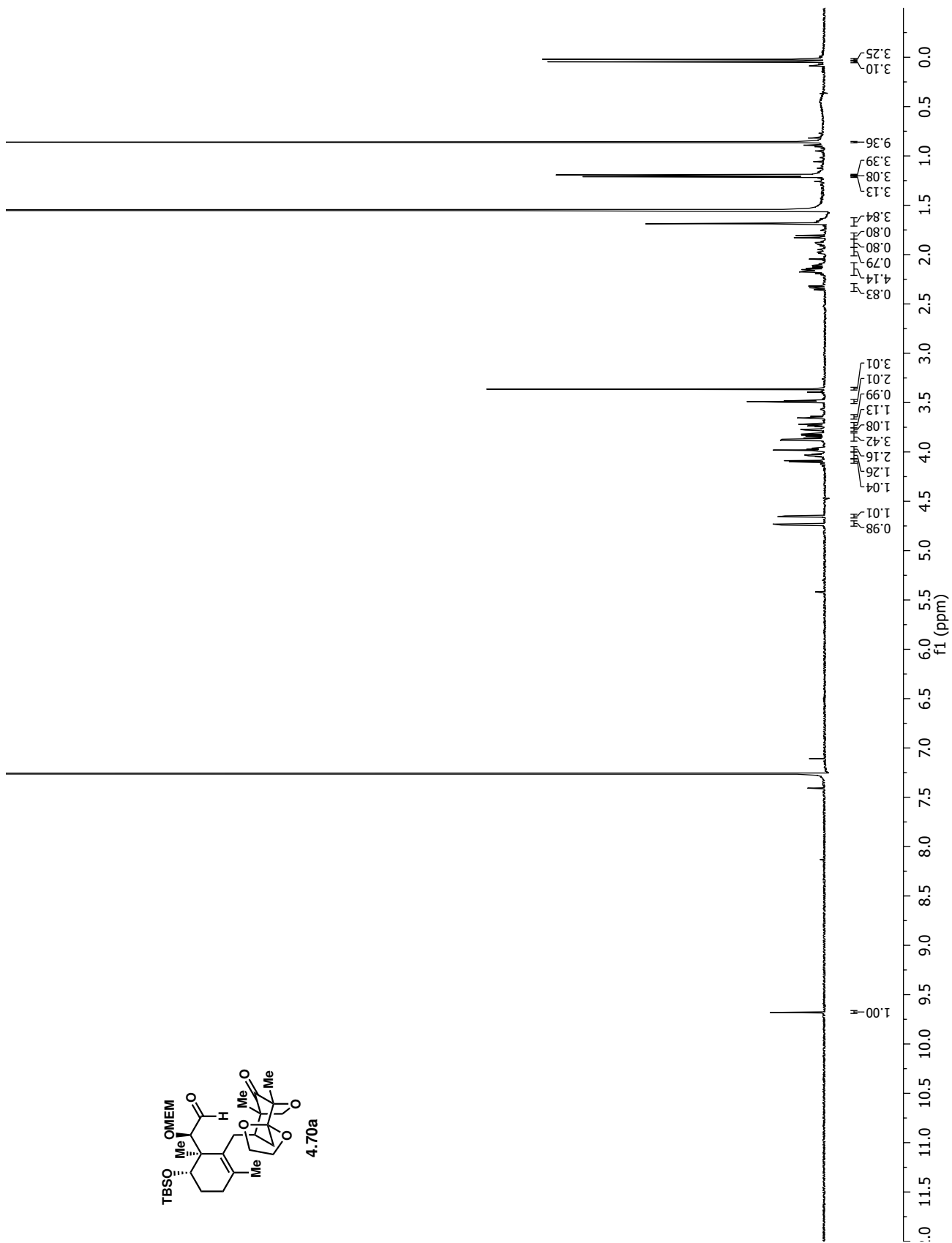
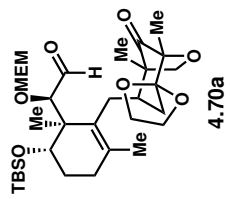


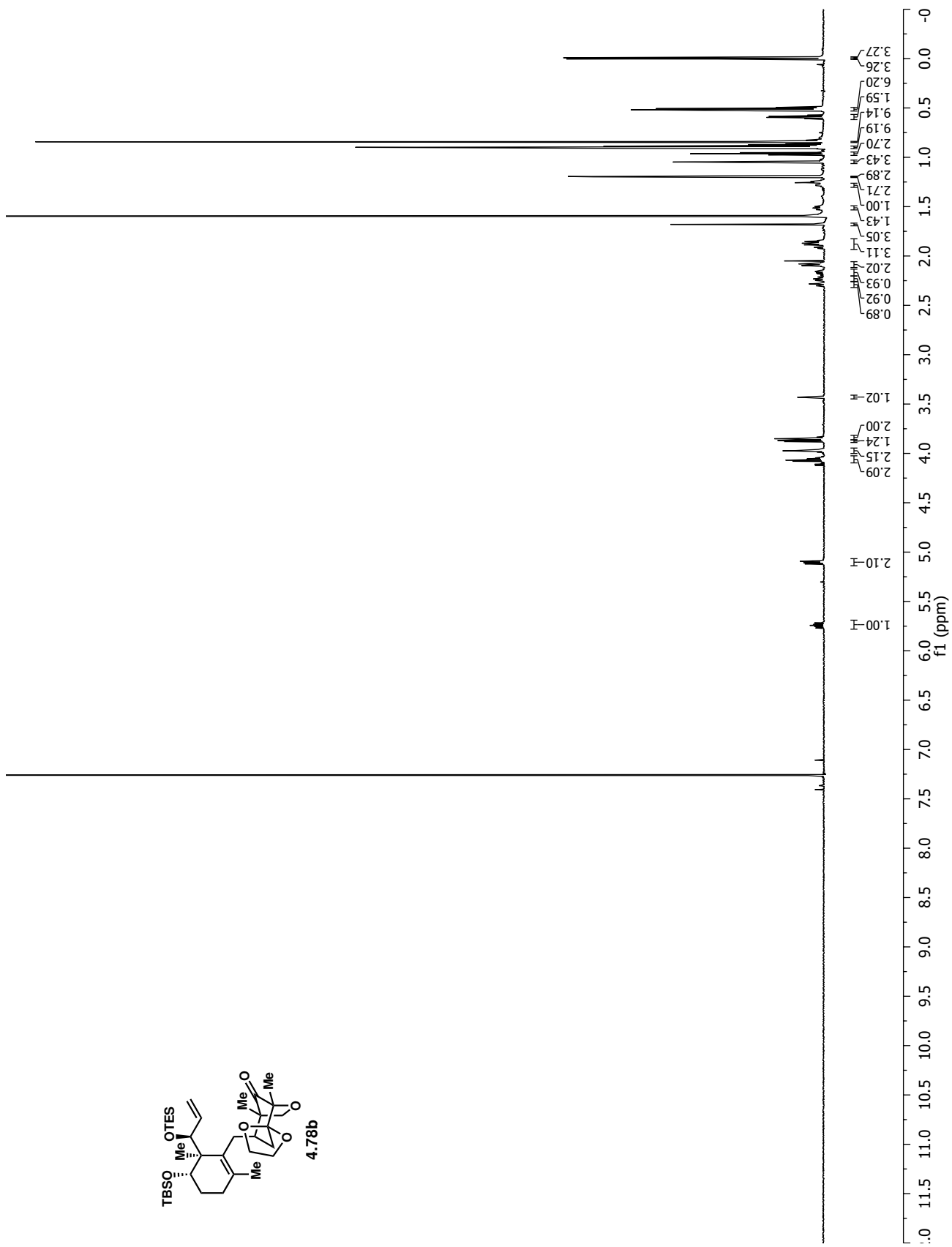
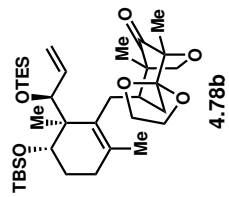


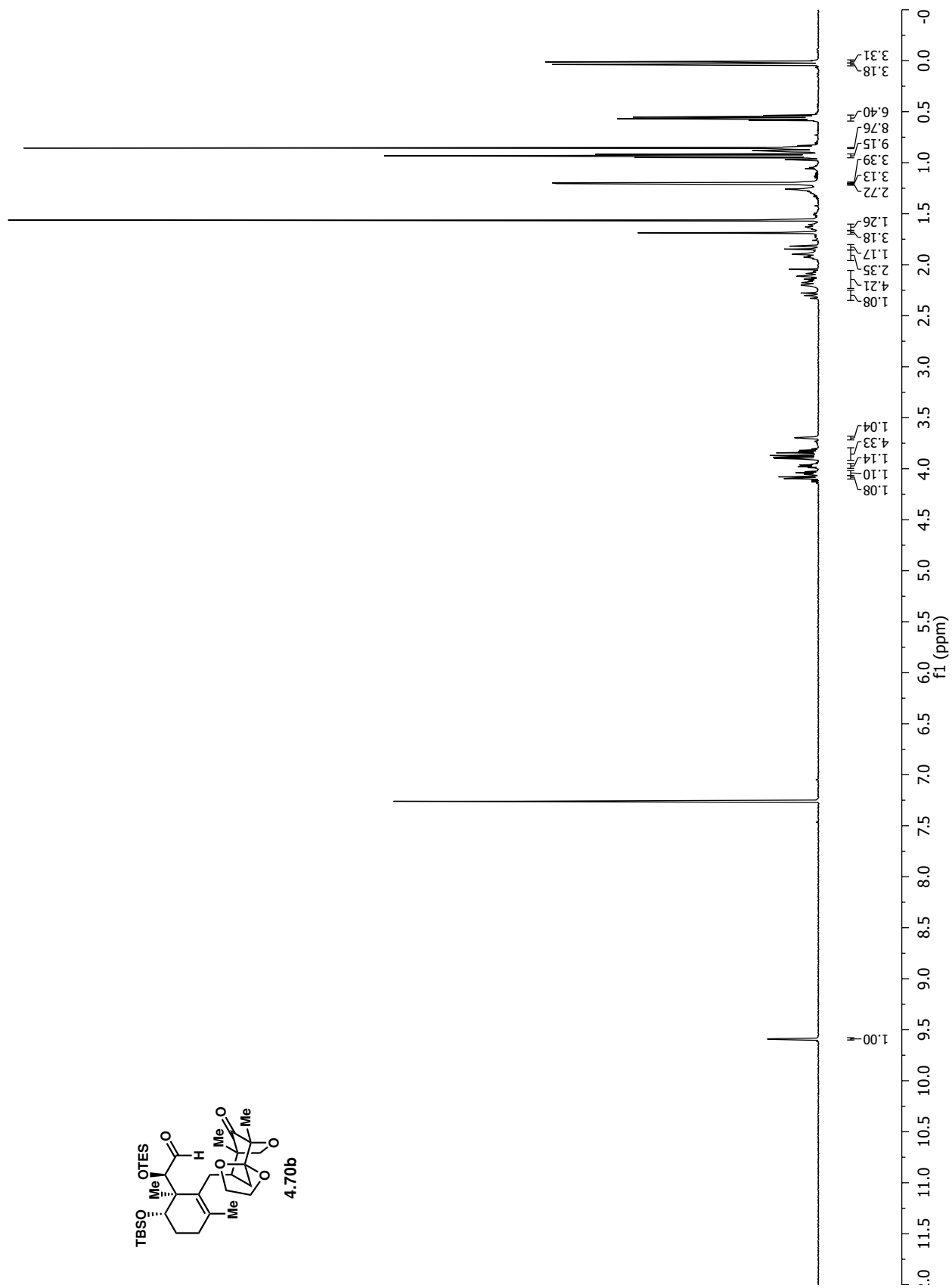
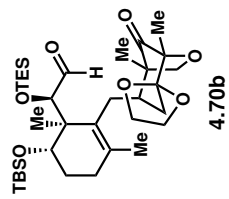


4.62









## Appendix 4b: X-Ray Crystallographic Data Relevant to Chapter 4

X-ray crystallographic analysis of tetracycline 4.59

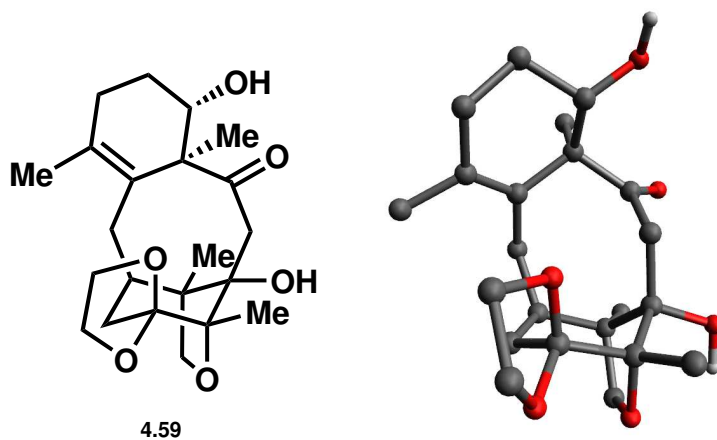


Table 1. Crystal data and structure refinement for bcwii\_011.

Identification code	BCWII_011	
Empirical formula	C <sub>22</sub> H <sub>32</sub> O <sub>6</sub>	
Formula weight	392.47	
Temperature	100(2) K	
Wavelength	1.54178 Å	
Crystal system	Orthorhombic	
Space group	P 21 21 21	
Unit cell dimensions	a = 10.0940(10) Å	= 90°.
	b = 13.0229(13) Å	= 90°.
	c = 14.4302(14) Å	= 90°.
Volume	1896.9(3) Å <sup>3</sup>	
Z	4	
Density (calculated)	1.374 Mg/m <sup>3</sup>	
Absorption coefficient	0.806 mm <sup>-1</sup>	
F(000)	848	
Crystal size	0.180 x 0.110 x 0.060 mm <sup>3</sup>	
Theta range for data collection	4.573 to 68.358°.	
Index ranges	-12<=h<=11, -14<=k<=15, -17<=l<=17	
Reflections collected	44101	
Independent reflections	3479 [R(int) = 0.0305]	
Completeness to theta = 67.000°	100.0 %	
Absorption correction	Semi-empirical from equivalents	
Max. and min. transmission	0.753 and 0.687	
Refinement method	Full-matrix least-squares on F <sup>2</sup>	
Data / restraints / parameters	3479 / 0 / 273	
Goodness-of-fit on F <sup>2</sup>	1.047	
Final R indices [I>2sigma(I)]	R1 = 0.0283, wR2 = 0.0735	
R indices (all data)	R1 = 0.0284, wR2 = 0.0736	
Absolute structure parameter	0.04(3)	
Extinction coefficient	n/a	
Largest diff. peak and hole	0.249 and -0.197 e.Å <sup>-3</sup>	

Table 2. Atomic coordinates ( $\times 10^4$ ) and equivalent isotropic displacement parameters ( $\text{\AA}^2 \times 10^3$ ) for bcwii\_011.  $U(\text{eq})$  is defined as one third of the trace of the orthogonalized  $U^{\text{ij}}$  tensor.

	x	y	z	$U(\text{eq})$
C(1)	5228(2)	2477(2)	5590(1)	23(1)
C(2)	6399(2)	2360(2)	4956(2)	25(1)
C(3)	6978(2)	3300(2)	6268(1)	18(1)
C(4)	8548(2)	1879(2)	6771(1)	22(1)
C(5)	8174(2)	2995(2)	6891(1)	18(1)
C(6)	9248(2)	4566(2)	7119(2)	24(1)
C(7)	8004(2)	3328(2)	7919(1)	17(1)
C(8)	8066(2)	4514(2)	7798(1)	19(1)
C(9)	8422(2)	5140(2)	8660(2)	25(1)
C(10)	6833(2)	4962(2)	7292(1)	19(1)
C(11)	6667(2)	4448(1)	6329(1)	19(1)
C(12)	5536(2)	5132(2)	7864(1)	21(1)
C(13)	4516(2)	4286(2)	7987(1)	18(1)
C(14)	3510(2)	4126(2)	7399(1)	21(1)
C(15)	3229(2)	4773(2)	6556(2)	26(1)
C(16)	2535(2)	3249(2)	7507(1)	24(1)
C(17)	2462(2)	2819(2)	8481(2)	24(1)
C(18)	3860(2)	2652(2)	8826(2)	22(1)
C(19)	4607(2)	3697(2)	8912(1)	19(1)
C(20)	4056(2)	4351(2)	9703(2)	25(1)
C(21)	6054(2)	3438(1)	9107(1)	16(1)
C(22)	6776(2)	2830(1)	8369(1)	17(1)
O(1)	5861(1)	2664(1)	6462(1)	19(1)
O(2)	7320(1)	3091(1)	5319(1)	21(1)
O(3)	9250(1)	3633(1)	6579(1)	22(1)
O(4)	9199(1)	2996(1)	8364(1)	24(1)
O(5)	6582(1)	3694(1)	9832(1)	21(1)
O(6)	3950(2)	2121(1)	9684(1)	26(1)

Table 3. Bond lengths [Å] and angles [°] for bcwii\_011.

---

C(1)-O(1)	1.431(2)
C(1)-C(2)	1.502(3)
C(1)-H(1A)	0.9900
C(1)-H(1B)	0.9900
C(2)-O(2)	1.429(3)
C(2)-H(2A)	0.9900
C(2)-H(2B)	0.9900
C(3)-O(1)	1.427(2)
C(3)-O(2)	1.439(2)
C(3)-C(11)	1.531(3)
C(3)-C(5)	1.556(3)
C(4)-C(5)	1.512(3)
C(4)-H(4A)	0.9800
C(4)-H(4B)	0.9800
C(4)-H(4C)	0.9800
C(5)-O(3)	1.440(2)
C(5)-C(7)	1.555(3)
C(6)-O(3)	1.442(3)
C(6)-C(8)	1.545(3)
C(6)-H(6A)	0.9900
C(6)-H(6B)	0.9900
C(7)-O(4)	1.433(2)
C(7)-C(22)	1.542(3)
C(7)-C(8)	1.555(3)
C(8)-C(9)	1.530(3)
C(8)-C(10)	1.557(3)
C(9)-H(9A)	0.9800
C(9)-H(9B)	0.9800
C(9)-H(9C)	0.9800
C(10)-C(11)	1.552(3)
C(10)-C(12)	1.564(3)
C(10)-H(10)	0.99(2)
C(11)-H(11A)	0.9900
C(11)-H(11B)	0.9900



C(12)-C(13)	1.518(3)
C(12)-H(12A)	0.9900
C(12)-H(12B)	0.9900
C(13)-C(14)	1.340(3)
C(13)-C(19)	1.542(3)
C(14)-C(15)	1.507(3)
C(14)-C(16)	1.515(3)
C(15)-H(15A)	0.9800
C(15)-H(15B)	0.9800
C(15)-H(15C)	0.9800
C(16)-C(17)	1.515(3)
C(16)-H(16A)	0.9900
C(16)-H(16B)	0.9900
C(17)-C(18)	1.512(3)
C(17)-H(17A)	0.9900
C(17)-H(17B)	0.9900
C(18)-O(6)	1.421(2)
C(18)-C(19)	1.561(3)
C(18)-H(18)	1.09(2)
C(19)-C(21)	1.525(3)
C(19)-C(20)	1.528(3)
C(20)-H(20A)	0.9800
C(20)-H(20B)	0.9800
C(20)-H(20C)	0.9800
C(21)-O(5)	1.220(2)
C(21)-C(22)	1.515(3)
C(22)-H(22A)	0.9900
C(22)-H(22B)	0.9900
O(4)-H(4)	0.85(3)
O(6)-H(6)	0.84(4)
O(1)-C(1)-C(2)	101.64(17)
O(1)-C(1)-H(1A)	111.4
C(2)-C(1)-H(1A)	111.4
O(1)-C(1)-H(1B)	111.4
C(2)-C(1)-H(1B)	111.4

H(1A)-C(1)-H(1B)	109.3
O(2)-C(2)-C(1)	102.81(16)
O(2)-C(2)-H(2A)	111.2
C(1)-C(2)-H(2A)	111.2
O(2)-C(2)-H(2B)	111.2
C(1)-C(2)-H(2B)	111.2
H(2A)-C(2)-H(2B)	109.1
O(1)-C(3)-O(2)	105.44(14)
O(1)-C(3)-C(11)	113.21(16)
O(2)-C(3)-C(11)	106.81(15)
O(1)-C(3)-C(5)	110.59(15)
O(2)-C(3)-C(5)	108.34(15)
C(11)-C(3)-C(5)	112.04(16)
C(5)-C(4)-H(4A)	109.5
C(5)-C(4)-H(4B)	109.5
H(4A)-C(4)-H(4B)	109.5
C(5)-C(4)-H(4C)	109.5
H(4A)-C(4)-H(4C)	109.5
H(4B)-C(4)-H(4C)	109.5
O(3)-C(5)-C(4)	109.33(15)
O(3)-C(5)-C(7)	102.69(15)
C(4)-C(5)-C(7)	113.87(15)
O(3)-C(5)-C(3)	104.95(14)
C(4)-C(5)-C(3)	111.91(16)
C(7)-C(5)-C(3)	113.20(15)
O(3)-C(6)-C(8)	107.82(15)
O(3)-C(6)-H(6A)	110.1
C(8)-C(6)-H(6A)	110.1
O(3)-C(6)-H(6B)	110.1
C(8)-C(6)-H(6B)	110.1
H(6A)-C(6)-H(6B)	108.5
O(4)-C(7)-C(22)	111.11(15)
O(4)-C(7)-C(8)	108.44(16)
C(22)-C(7)-C(8)	119.83(16)
O(4)-C(7)-C(5)	104.50(15)
C(22)-C(7)-C(5)	111.90(15)

C(8)-C(7)-C(5)	99.54(15)
C(9)-C(8)-C(6)	108.12(16)
C(9)-C(8)-C(7)	116.62(17)
C(6)-C(8)-C(7)	98.40(15)
C(9)-C(8)-C(10)	111.60(16)
C(6)-C(8)-C(10)	107.68(16)
C(7)-C(8)-C(10)	113.12(16)
C(8)-C(9)-H(9A)	109.5
C(8)-C(9)-H(9B)	109.5
H(9A)-C(9)-H(9B)	109.5
C(8)-C(9)-H(9C)	109.5
H(9A)-C(9)-H(9C)	109.5
H(9B)-C(9)-H(9C)	109.5
C(11)-C(10)-C(8)	110.16(15)
C(11)-C(10)-C(12)	116.28(16)
C(8)-C(10)-C(12)	118.41(16)
C(11)-C(10)-H(10)	106.6(13)
C(8)-C(10)-H(10)	103.6(14)
C(12)-C(10)-H(10)	99.6(13)
C(3)-C(11)-C(10)	116.77(16)
C(3)-C(11)-H(11A)	108.1
C(10)-C(11)-H(11A)	108.1
C(3)-C(11)-H(11B)	108.1
C(10)-C(11)-H(11B)	108.1
H(11A)-C(11)-H(11B)	107.3
C(13)-C(12)-C(10)	121.79(16)
C(13)-C(12)-H(12A)	106.9
C(10)-C(12)-H(12A)	106.9
C(13)-C(12)-H(12B)	106.9
C(10)-C(12)-H(12B)	106.9
H(12A)-C(12)-H(12B)	106.7
C(14)-C(13)-C(12)	123.57(18)
C(14)-C(13)-C(19)	121.03(18)
C(12)-C(13)-C(19)	114.96(16)
C(13)-C(14)-C(15)	124.50(19)
C(13)-C(14)-C(16)	122.99(18)

C(15)-C(14)-C(16)	112.50(18)
C(14)-C(15)-H(15A)	109.5
C(14)-C(15)-H(15B)	109.5
H(15A)-C(15)-H(15B)	109.5
C(14)-C(15)-H(15C)	109.5
H(15A)-C(15)-H(15C)	109.5
H(15B)-C(15)-H(15C)	109.5
C(17)-C(16)-C(14)	113.94(17)
C(17)-C(16)-H(16A)	108.8
C(14)-C(16)-H(16A)	108.8
C(17)-C(16)-H(16B)	108.8
C(14)-C(16)-H(16B)	108.8
H(16A)-C(16)-H(16B)	107.7
C(18)-C(17)-C(16)	108.24(17)
C(18)-C(17)-H(17A)	110.1
C(16)-C(17)-H(17A)	110.1
C(18)-C(17)-H(17B)	110.1
C(16)-C(17)-H(17B)	110.1
H(17A)-C(17)-H(17B)	108.4
O(6)-C(18)-C(17)	114.62(17)
O(6)-C(18)-C(19)	108.91(16)
C(17)-C(18)-C(19)	110.59(17)
O(6)-C(18)-H(18)	108.4(11)
C(17)-C(18)-H(18)	106.6(12)
C(19)-C(18)-H(18)	107.4(12)
C(21)-C(19)-C(20)	109.52(16)
C(21)-C(19)-C(13)	109.05(15)
C(20)-C(19)-C(13)	110.36(16)
C(21)-C(19)-C(18)	106.53(15)
C(20)-C(19)-C(18)	111.65(16)
C(13)-C(19)-C(18)	109.63(16)
C(19)-C(20)-H(20A)	109.5
C(19)-C(20)-H(20B)	109.5
H(20A)-C(20)-H(20B)	109.5
C(19)-C(20)-H(20C)	109.5
H(20A)-C(20)-H(20C)	109.5

H(20B)-C(20)-H(20C)	109.5
O(5)-C(21)-C(22)	122.40(17)
O(5)-C(21)-C(19)	121.04(17)
C(22)-C(21)-C(19)	116.54(16)
C(21)-C(22)-C(7)	117.59(16)
C(21)-C(22)-H(22A)	107.9
C(7)-C(22)-H(22A)	107.9
C(21)-C(22)-H(22B)	107.9
C(7)-C(22)-H(22B)	107.9
H(22A)-C(22)-H(22B)	107.2
C(3)-O(1)-C(1)	106.19(14)
C(2)-O(2)-C(3)	108.55(15)
C(5)-O(3)-C(6)	108.46(14)
C(7)-O(4)-H(4)	108(2)
C(18)-O(6)-H(6)	106(2)

---

Symmetry transformations used to generate equivalent atoms:

Table 4. Anisotropic displacement parameters ( $\text{\AA}^2 \times 10^3$ ) for bcwii\_011. The anisotropic displacement factor exponent takes the form:  $-2^2 [h^2 a^{*2} U^{11} + \dots + 2 h k a^* b^* U^{12}]$

	U <sup>11</sup>	U <sup>22</sup>	U <sup>33</sup>	U <sup>23</sup>	U <sup>13</sup>	U <sup>12</sup>
C(1)	26(1)	26(1)	18(1)	-2(1)	-4(1)	-1(1)
C(2)	31(1)	24(1)	19(1)	-2(1)	-1(1)	-1(1)
C(3)	18(1)	21(1)	14(1)	1(1)	2(1)	0(1)
C(4)	24(1)	23(1)	19(1)	0(1)	3(1)	7(1)
C(5)	16(1)	21(1)	17(1)	1(1)	3(1)	2(1)
C(6)	18(1)	25(1)	28(1)	-3(1)	5(1)	-4(1)
C(7)	14(1)	22(1)	16(1)	-2(1)	-1(1)	3(1)
C(8)	17(1)	22(1)	20(1)	-3(1)	4(1)	-4(1)
C(9)	23(1)	27(1)	26(1)	-7(1)	2(1)	-8(1)
C(10)	21(1)	15(1)	21(1)	1(1)	5(1)	0(1)
C(11)	21(1)	20(1)	17(1)	3(1)	3(1)	3(1)
C(12)	23(1)	18(1)	21(1)	0(1)	5(1)	4(1)
C(13)	16(1)	19(1)	19(1)	1(1)	4(1)	5(1)
C(14)	18(1)	25(1)	21(1)	2(1)	2(1)	7(1)
C(15)	23(1)	31(1)	24(1)	5(1)	-2(1)	7(1)
C(16)	17(1)	32(1)	25(1)	1(1)	-4(1)	2(1)
C(17)	21(1)	26(1)	28(1)	-1(1)	0(1)	-2(1)
C(18)	20(1)	26(1)	21(1)	5(1)	0(1)	-3(1)
C(19)	16(1)	23(1)	18(1)	1(1)	2(1)	2(1)
C(20)	23(1)	31(1)	22(1)	-2(1)	6(1)	7(1)
C(21)	18(1)	15(1)	16(1)	3(1)	1(1)	-2(1)
C(22)	17(1)	19(1)	16(1)	1(1)	0(1)	-1(1)
O(1)	18(1)	23(1)	16(1)	1(1)	0(1)	-3(1)
O(2)	24(1)	24(1)	14(1)	-1(1)	3(1)	0(1)
O(3)	17(1)	27(1)	22(1)	-2(1)	6(1)	-1(1)
O(4)	17(1)	37(1)	18(1)	0(1)	-1(1)	6(1)
O(5)	20(1)	25(1)	17(1)	-2(1)	-2(1)	0(1)
O(6)	23(1)	31(1)	23(1)	7(1)	-1(1)	-4(1)

Table 5. Hydrogen coordinates ( $\times 10^4$ ) and isotropic displacement parameters ( $\text{\AA}^2 \times 10^3$ ) for bcwii\_011.

	x	y	z	U(eq)
H(1A)	4663	3062	5403	28
H(1B)	4687	1843	5608	28
H(2A)	6763	1655	4983	29
H(2B)	6159	2524	4308	29
H(4A)	8785	1751	6123	33
H(4B)	7795	1444	6943	33
H(4C)	9306	1718	7169	33
H(6A)	9157	5169	6707	29
H(6B)	10089	4630	7467	29
H(9A)	7662	5156	9082	38
H(9B)	8650	5843	8476	38
H(9C)	9180	4824	8973	38
H(11A)	5740	4553	6124	23
H(11B)	7245	4813	5883	23
H(12A)	5809	5351	8493	25
H(12B)	5070	5723	7581	25
H(15A)	3861	5343	6529	39
H(15B)	2326	5047	6594	39
H(15C)	3316	4351	5997	39
H(16A)	1643	3492	7324	29
H(16B)	2789	2690	7078	29
H(17A)	1991	3306	8892	29
H(17B)	1971	2161	8480	29
H(20A)	4074	3953	10279	38
H(20B)	3141	4548	9561	38
H(20C)	4599	4969	9775	38
H(22A)	6136	2670	7870	21
H(22B)	7055	2169	8645	21
H(4)	9060(30)	2990(20)	8940(20)	35(7)
H(6)	3220(40)	1820(30)	9760(30)	69(11)

H(10)	7080(20)	5686(18)	7176(16)	18(5)
H(18)	4370(20)	2199(17)	8296(15)	14(5)

---

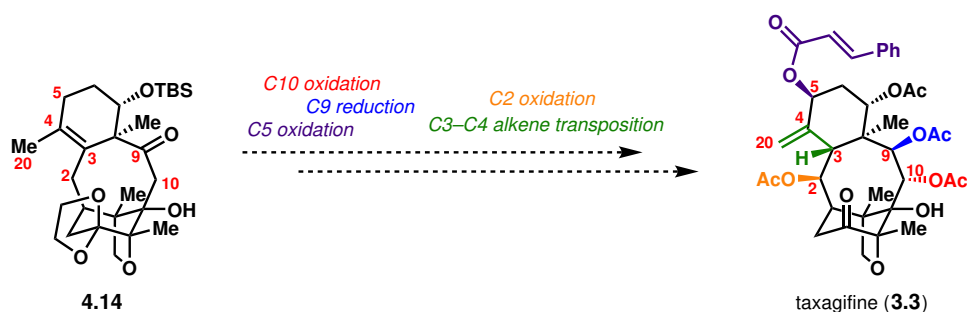


## Chapter 5

# Late-Stage Progress Toward the Total Syntheses of Taxagifine-Like Natural Products

## 5.1 Installation of C10 Oxygenation

### 5.1.1 Initial Attempts at Enolate C10-Oxidation

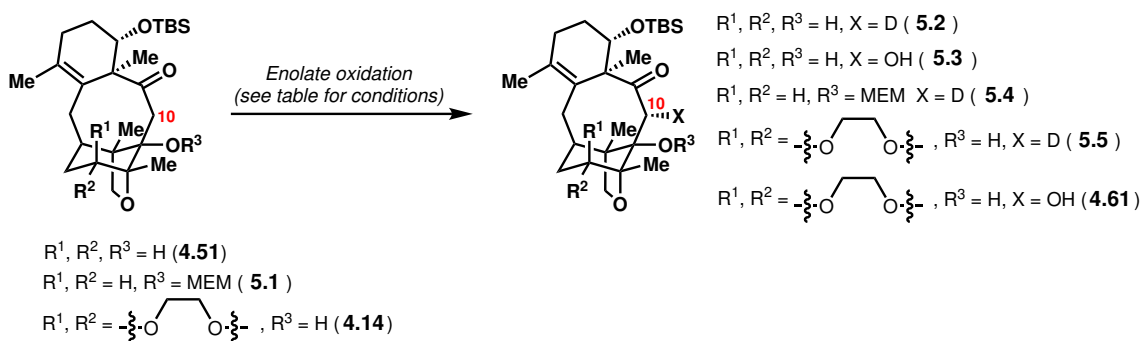


**Scheme 5.1:** Remaining transformations required to synthesize taxagifine from tetracyclic core **4.14**.

From tetracyclic core **4.14**, a number of transformations are needed to complete the total synthesis of taxagifine—specifically: 1) diastereoselective oxygenation at C10, 2) diastereoselective reduction at C9, 3) diastereoselective oxygenation at C5, 4) diastereoselective oxygenation at C2, and 5) transposition of the C3–C4 double bond to a C4–C20 double bond, with concomitant stereoselective placement of a hydrogen atom at C3 (Scheme 5.1). Given the harsh conditions we imagined would be required for C10 oxidation and C9 reduction that may not be tolerant of additional oxygenation placed on the molecule, we chose to pursue C10 oxidation and C9 reduction first. We initially envisioned that C10 oxidation could be accomplished by formation of an enolate followed by trapping with an oxygen electrophile; the oxygen electrophile was expected to approach from the convex face, yielding the C10- $\alpha$ -OH epimer. Given material constraints, we began with C10-oxidation

attempts on model tetracyclic compound **4.51** (Table 5.1). Treatment of **4.51** with either  $\text{KO}t\text{-Bu}$  or  $\text{KHMDS}$  followed by addition of Davis oxaziridine resulted in only recovery of starting material (entries 1 and 2). When **4.51** was treated with  $\text{LHMDS}$  with subsequent quenching with  $\text{CD}_3\text{OD}$ , only O-deutero, C10-protio compound was observed, suggesting that  $\text{LHMDS}$  was either too sterically hindered or too weak a base for deprotonation of the tertiary hydroxy group and C10-deprotonation (entry 3). Under the assumption that protection of the C11-hydroxy group would facilitate C10-deprotonation by requiring only the formation of a monoanionic species rather than a dianionic species, we attempted to prepare C11-hydroxy-protected compounds. While the extreme steric hindrance of the C11 hydroxy group—being attached to a tetrasubstituted carbon and flanked by two other tetrasubstituted carbons—prohibited the installation of many protecting groups, we were able to install a MEM group under extended reaction times (see Section 5.10 for details). Treatment of MEM-protected compound **5.1** with either  $\text{LHMDS}$  or  $\text{LDA}$ , however, did not result in C10-deprotonation and only starting material was recovered in these cases (entries 4 and 5). We continued attempts at enolate oxidation on C13-oxidized tetracyclic core **4.14**. Treatment of **4.14** with  $\text{LDA}$  followed by bubbling of  $\text{O}_2$  through the reaction mixture did not result

**Table 5.1:** Initially attempted enolate oxidations of tetracyclic cores.



Entry	Substrate	Conditions	Results
1	<b>4.51</b>	$\text{KO}t\text{-Bu}$ (5 equiv), THF/DMPU, $-65^\circ\text{C}$ ; then, Davis oxaziridine (5 equiv), $-55^\circ\text{C}$ to $23^\circ\text{C}$	No conversion
2	<b>4.51</b>	$\text{KHMDS}$ (2 equiv), THF, $-78^\circ\text{C}$ ; then, Davis oxaziridine (2 equiv), $-78^\circ\text{C}$ to $23^\circ\text{C}$	No conversion
3	<b>4.51</b>	$\text{LHMDS}$ (5 equiv), THF, $23^\circ\text{C}$ ; then, $\text{CD}_3\text{OD}$	Only O-deuteration
4	<b>5.1</b>	$\text{LHMDS}$ (2 equiv), THF, $23^\circ\text{C}$ ; then, $\text{CD}_3\text{OD}$	No conversion
5	<b>5.1</b>	$\text{LDA}$ (3.4 equiv), THF, $-78^\circ\text{C}$ ; then, $\text{CD}_3\text{OD}$	No conversion
6	<b>4.14</b>	$\text{LDA}$ (7 equiv), THF, $-78^\circ\text{C}$ to $-35^\circ\text{C}$ ; then, $\text{P}(\text{OEt})_3$ , $\text{O}_2$ , $-78^\circ\text{C}$ to $23^\circ\text{C}$	No conversion
7	<b>4.14</b>	$\text{DIPEA}$ ( $\text{PhSeO}$ ) $_2\text{O}$ (1.2 equiv), PhMe, $23^\circ\text{C}$ to $130^\circ\text{C}$	No conversion
8	<b>4.14</b>	$\text{NaH}$ (3 equiv), ( $\text{PhSeO}$ ) $_2\text{O}$ (2 equiv), PhCl, $130^\circ\text{C}$	No conversion
9	<b>4.14</b>	$\text{LTMP}$ (5 equiv), THF, $0^\circ\text{C}$ to $23^\circ\text{C}$ ; then, $\text{CD}_3\text{OD}$	Only O-deuteration
10	<b>4.14</b>	$\text{LiNEt}_2$ (4 equiv), THF, $23^\circ\text{C}$ ; then, MoOPH (10 equiv), $-20^\circ\text{C}$	6% conversion
11	<b>4.14</b>	$\text{LiNEt}_2$ (4 equiv), THF, $23^\circ\text{C}$ ; then, Davis oxaziridine (10 equiv), $-78^\circ\text{C}$	19% conversion

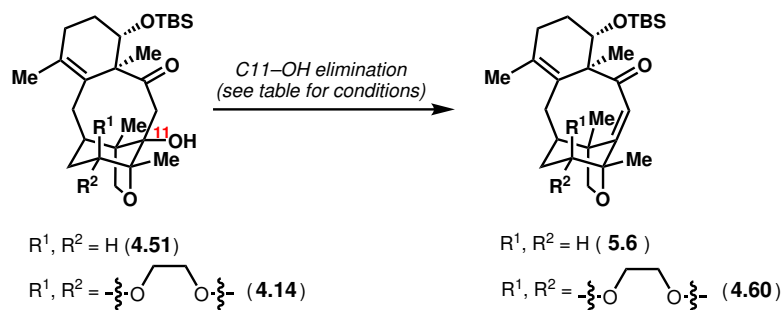
in conversion of the starting material, consistent with a lack of deprotonation at C10 (entry 6). Further attempts at oxidation with benzeneseleninic acid anhydride as electrophile and with DIPEA or NaH as base were similarly unsuccessful (entries 7 and 8). LTMP did not effect C10-deprotonation either (entry 9). Finally, LiNEt<sub>2</sub> was found to be competent for the C10-deprotonation of **4.14** (entries 10 and 11), in accordance with the unique success of this base for the deprotonation of C9 in Baran and coworkers' synthesis of decinnamoyltaxinine E and taxabaccatin III.<sup>1</sup> The success of LiNEt<sub>2</sub> at C10-deprotonation in contrast with other, generally more sterically hindered bases suggests that steric factors are important for this deprotonation. However, only low conversions were observed, yielding non-synthetically useful quantities of the desired product; in addition, when Davis oxaziridine was used as the electrophile, the desired product was chromatographically inseparable from large quantities of the byproduct benzenesulfonamide, presumably generated from undesired reactivity between LiNEt<sub>2</sub> and Davis oxaziridine. Difficulty in separating C10-oxidized product **4.61** from remaining starting material **4.14** contributed further to the practical unviability of these reaction conditions.

### 5.1.2 Initial Attempts at C11–OH Elimination

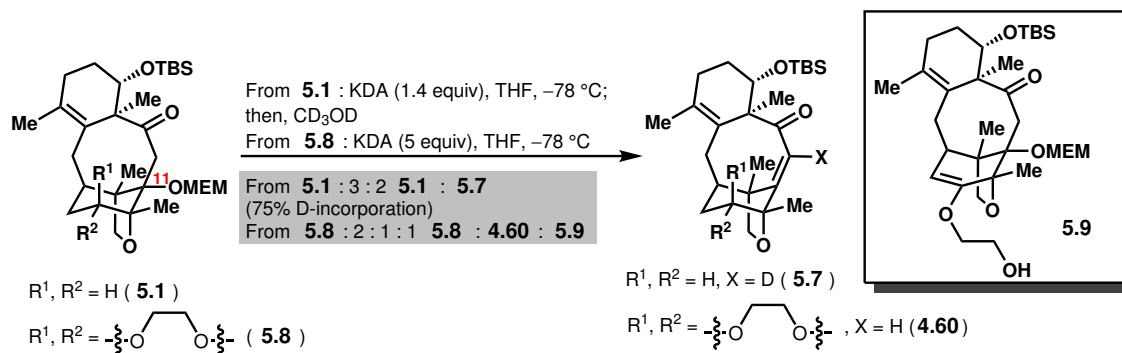
Given our difficulties in effecting a direct C10-hydroxylation via enolate oxidation, we turned to alternative methods of introducing the C10 hydroxy group, including exploiting elimination of the C11 hydroxy group (see **5.6**, Table 5.2) followed by dihydroxylation. On model tetracyclic compound **4.51**, we were able to synthesize enone **5.6** in moderate yields by treatment with the Burgess reagent (entry 1); however, similar conditions on C13-oxidized tetracyclic compound **4.14** only yielded 14% of desired product **4.60** (entry 2). Treatment of **4.14** with SOCl<sub>2</sub> did not provide synthetically useful yields of **4.60** either (entry 3), and **4.14** did not react with Martin sulfurane (entry 4). Swern-type conditions for tertiary alcohol elimination<sup>2</sup> applied to **4.14** yielded only messy reaction mixtures which did not contain desired product, while attempts at one-pot Chugaev elimination or oxyphosphonium formation and elimination yielded no conversion (entries 6 and 7).

We then turned to a two-step procedure for C11–OH elimination, in which the first step would involve conversion of the tertiary hydroxy group to a leaving group. While attempted conversion of the tertiary hydroxy group to a mesylate from model system **4.51** did not proceed, similarly to attempted transformations of **4.14** to a tosylate, *N,N*-dimethyl carbamate, benzoate, trifluoroacetate, triflate, methyl xanthate (for subsequent Chugaev elimination), MOM ether, or trifluoroethyl alcohol, we were able to synthesize MEM-protected compounds **5.1** and **5.8** (Scheme 5.2). Although treatment of **5.1** with LHMDS or LDA did not effect alkoxide elimination (*vide supra*), we found that upon addition of KDA (formed *in situ* from *KOt*-Bu and LDA) to **4.51**, we isolated some quantity of desired product **5.7** after quenching with CD<sub>3</sub>OD, albeit with incomplete conversion. However, when KDA was added to C13-oxidized compound **5.8**, equimolar quantities of two inseparable products were isolated, the structures of which we assigned to **4.60** and (more tentatively) **5.9**, along with recovered starting material. The lengthy reaction procedure associated with the preparation of **5.8** and the presence of side product **5.9** upon KDA-induced elimination dissuaded us from pursuing the MEM-alkoxide elimination route any further.

**Table 5.2:** Initially attempted C11–OH eliminations on tetracyclic compounds. <sup>41</sup>H NMR yield with mesitylene as an internal standard.



Entry	Substrate	Conditions	Results
1	<b>4.51</b>	Burgess reagent, PhMe, 100 °C	41% <sup>a</sup> <b>5.6</b>
2	<b>4.14</b>	Burgess reagent, PhMe, 60 °C	14% <sup>a</sup> <b>4.60</b>
3	<b>4.14</b>	SOCl <sub>2</sub> , pyridine, CH <sub>2</sub> Cl <sub>2</sub> , 23 °C	18% <sup>a</sup> <b>4.60</b>
4	<b>4.14</b>	Martin sulfurane, CH <sub>2</sub> Cl <sub>2</sub> , 23 °C	No conversion
5	<b>4.14</b>	DMSO, TFAA, CH <sub>2</sub> Cl <sub>2</sub> , –78 °C; then, Et <sub>3</sub> N, –78 °C to 23 °C	Multiple products, <b>4.60</b> not observed
6	<b>4.14</b>	Phenyl chlorodithioformate, DIPEA, PhMe, μW, 150 °C	No conversion
7	<b>4.14</b>	PPh <sub>3</sub> , DIAD, PhMe, 60 °C	No conversion



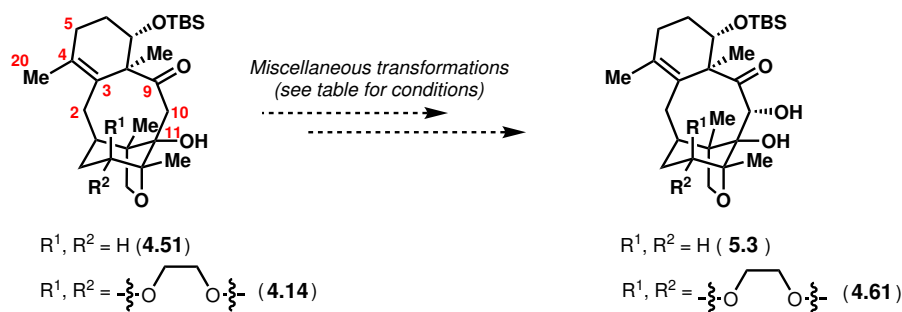
**Scheme 5.2:** Eliminations of MEM-alkoxides **5.1** and **5.8**.

### 5.1.3 Miscellaneous C10 Oxidation Attempts

None of our miscellaneous attempts at C10 oxidation were ultimately successful, but each provided insight into the nature of the tetracyclic core. Attempted Riley oxidation, which we hoped would also oxidize allylic positions C5 and/or C2, returned mostly starting material, even under forcing conditions (entry 1, Table 5.3); this result speaks to the extremely sterically hindered environment around the C3–C4 tetrasubstituted alkene, particularly at C3, which is adjacent to a quaternary center. In addition, the minor products that were isolated seemed to suggest that SeO<sub>2</sub>-mediated conditions would preferentially oxidize C20 if higher conversion could be attained. Attempted formation of a silyl enol ether from the C9 carbonyl—which could be subjected to subsequent Rubottom oxidation conditions—resulted

only in silylation of the tertiary hydroxy group, illustrating the steric hindrance surrounding the quaternary center-adjacent C9 position (entry 2). In accordance with this result, we were unable to effect condensation between Tomkinson's reagent<sup>3</sup> (entry 3) or hydrazine (entry 4) and the C9 carbonyl, either for  $\alpha$ -oxybenzoylation<sup>4</sup> or to leverage for C9–C10 alkene formation (e.g., via Shapiro reaction of the resulting hydrazone).

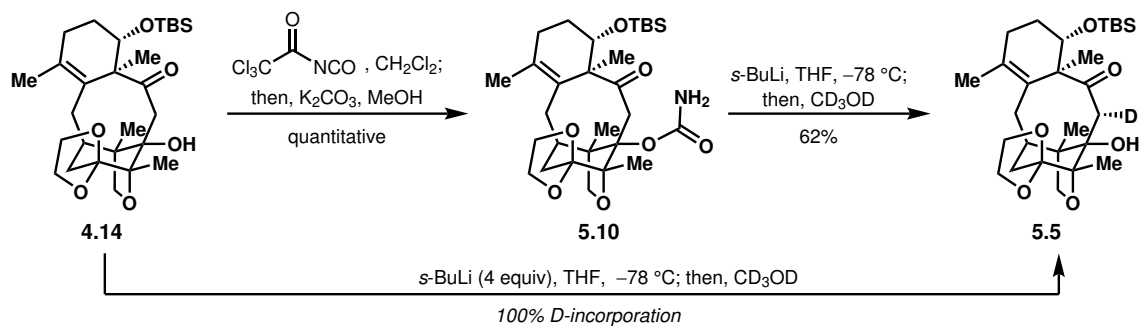
**Table 5.3:** Miscellaneous reactions toward C10 oxidation.



Entry	Substrate	Conditions	Results
1	<b>4.51</b>	SeO <sub>2</sub> (10 equiv), dioxane, 85 °C to 110 °C	Mostly <b>4.51</b> ; products contained a mixture of C5 oxidation, C20 oxidation, and C11–OH elimination
2	<b>4.51</b>	TMSOTf (6 equiv), Et <sub>3</sub> N, CH <sub>2</sub> Cl <sub>2</sub> , 0 °C to 23 °C	Only O-silylation, no silyl enol ether formation
3	<b>4.14</b>	• HCl, DMSO, 23 °C	Ketal opening
4	<b>4.14</b>	H <sub>2</sub> NNH <sub>2</sub> , Et <sub>3</sub> N, EtOH, 50 °C to 120 °C	No conversion

### 5.1.4 *s*-BuLi-based C10 Oxidation

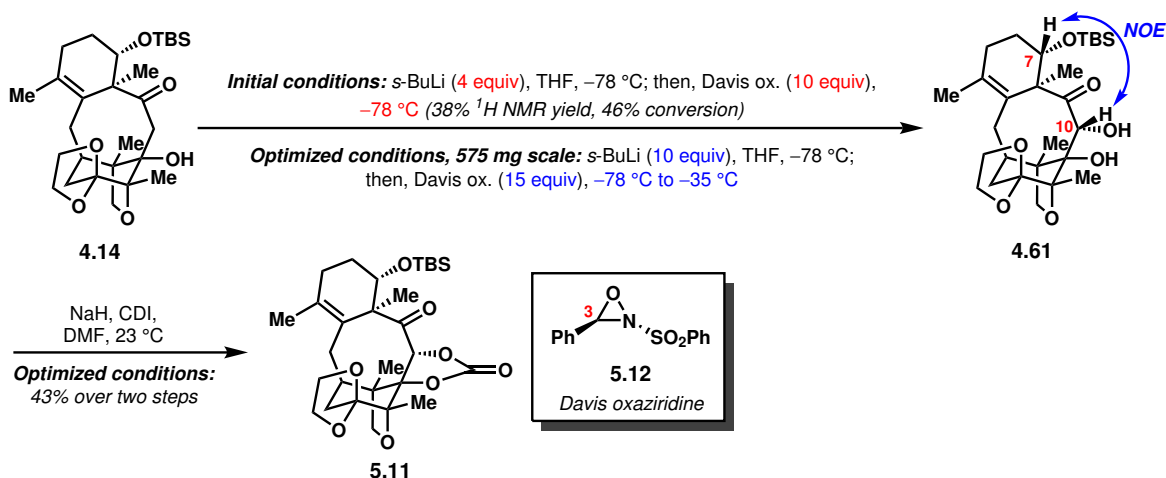
Inspired by the recent total synthesis of (–)-virosaine A,<sup>5</sup> which employed a carbamate-directed C–H lithiation with *s*-BuLi, we prepared carbamate **5.10** (Scheme 5.3). To our delight, after subjection of **5.10** to *s*-BuLi and quenching with CD<sub>3</sub>OD, we observed **5.5**, the result of C10 deprotonation and concomitant cleavage of the carbamate. We then discovered that subjection of free alcohol **4.14** to *s*-BuLi followed by a CD<sub>3</sub>OD quench also resulted



**Scheme 5.3:** Successful C10-deuteration.

in full deuterium incorporation at C10, suggesting that C10 deprotonation by *s*-BuLi did not require an amide directing group and was made possible by the particular properties of *s*-BuLi as a strong, relatively sterically unhindered base. Subsequent studies revealed that *n*-BuLi was also adequate for C10-deprotonation, while *t*-BuLi was not. It is hypothesized that steric factors preclude the nucleophilic addition of *s*-BuLi to the C9 carbonyl.

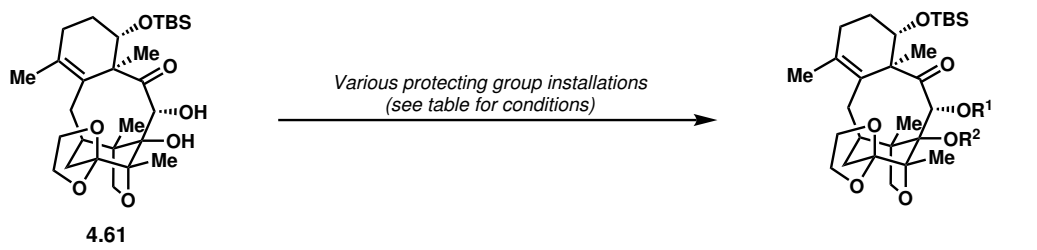
With our deuteration studies pointing to *s*-BuLi as a competent base for the full C10-deprotonation of **4.14**, we then attempted to install C10-oxygenation by trapping the thus generated enolate with an oxygen electrophile. Extensive screening and optimization studies were conducted in tandem with graduate student Mel Perea and postdoctoral researcher Dr. Nicholas O'Connor. Initial studies suggested Davis oxaziridine (**5.12**) as the most suitable oxygen electrophile; other oxygen electrophiles returned either starting material (MoOPH, dialkyl peroxides, triisopropyl borate) or led to decomposition ( $O_2/P(OEt)_3$ ) (Scheme 5.4). Oxidation by Davis oxaziridine occurred on the convex face of the intermediate enolate, as confirmed by an observed NOE correlation between protons at C7 and C10 on the product **4.61**. Our small-scale studies with Davis oxaziridine consistently yielded only ~40–50% conversion, even at extended reaction times; since our deuteration studies indicated that full deprotonation was taking place, we assumed that the enolate was being quenched prematurely, perhaps by solvent or by the benzylic proton of Davis oxaziridine. However, use of alternative solvents (THF- $d_8$ , MTBE, dimethoxymethane, 10% HMPA/THF) did not yield increases in conversion, nor did the use of other oxaziridines (e.g., 3,3-dimethyl-Davis oxaziridine, 3-deutero-Davis oxaziridine, 3-(*p*-NO<sub>2</sub>-phenyl)-2-(benzenesulfonyl) oxaziridine, camphorsulfonyl oxaziridine). The addition of Lewis acid additives (e.g., ZnCl<sub>2</sub>, CeCl<sub>3</sub>, La(OTf)<sub>3</sub>, LaCl<sub>3</sub>·2LiCl) did not raise the conversion. Finally, we discovered that 1) increasing the reaction temperature after Davis oxaziridine addition to  $-35\text{ }^\circ\text{C}$  and 2) raising the amount of *s*-BuLi (10 equiv) and Davis oxaziridine (15 equiv) were important for attaining conversions of >70%, particularly on larger scale. With the large excesses of Davis oxaziridine used, purification of **4.61** away from Davis oxaziridine byproducts was not possible on large scale; in addition, for runs where conversion was lower, separation of **4.61** from starting material **4.14** was difficult and could only be achieved by preparatory TLC if needed. As a

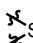
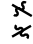
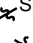




**Scheme 5.4:** Optimization of C10 oxidation and preparation of carbonate **5.11**.

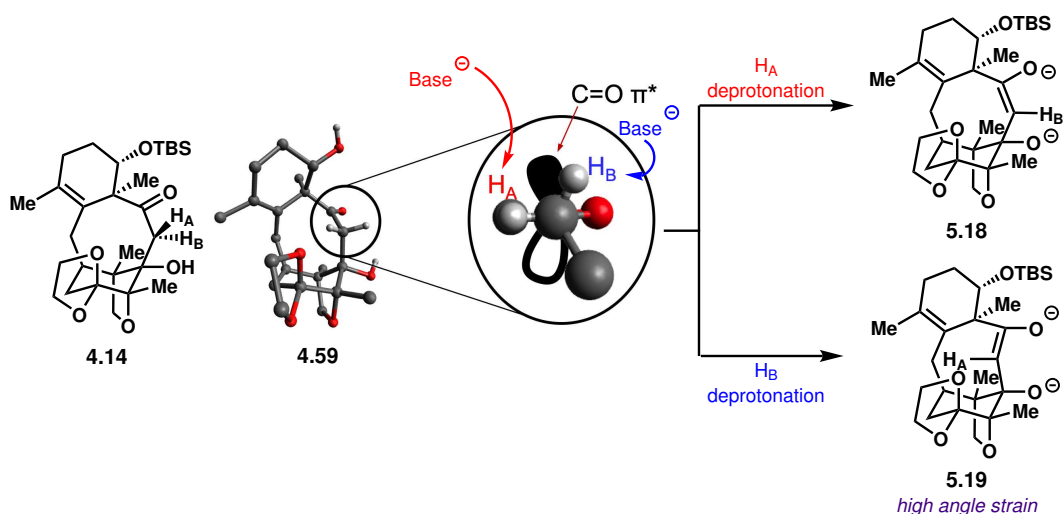
result, on large scale, we subjected the mixture of **4.61**, Davis oxaziridine byproducts, and any recovered **4.14** obtained after one chromatographic purification to a subsequent diol protection step, at which point carbonate **5.11** could be separated cleanly. On small scale, several other diol-protected compounds could also be prepared (Table 5.4) to be used for further studies.

**Table 5.4:** Preparation of protected diol compounds.  $^1\text{H}$  NMR yield with mesitylene as internal standard.



Entry	R <sup>1</sup> , R <sup>2</sup>	Conditions	Results
1	TMS, H <b>4.68c</b>	Et <sub>3</sub> N, TMSCl, CH <sub>2</sub> Cl <sub>2</sub> , 23 °C	77% yield
2	 <b>(5.13)</b>	Me <sub>2</sub> SiCl <sub>2</sub> , Et <sub>3</sub> N, DMAP, CH <sub>2</sub> Cl <sub>2</sub> , 23 °C	83% yield
3	 <b>(5.14)</b>	Et <sub>2</sub> SiCl <sub>2</sub> , Et <sub>3</sub> N, DMAP, CH <sub>2</sub> Cl <sub>2</sub> , 23 °C	70% yield
4	 <b>(5.15)</b>	<i>i</i> Pr <sub>2</sub> Si(OTf) <sub>2</sub> , Et <sub>3</sub> N, DMAP, CH <sub>2</sub> Cl <sub>2</sub> , 0 °C to 23 °C	50% yield <sup>a</sup>
5	 <b>(5.16)</b>	PhB(OH) <sub>2</sub> , PhMe, 80 °C	quantitative yield
6	 <b>5.17</b>	<i>p</i> -TsOH, 2,2-dimethoxypropane, CH <sub>2</sub> Cl <sub>2</sub> , 23 °C	ketal cleavage; no diol protection

At this point, it is worth reflecting on the unique characteristics of tetracyclic core **4.14** that may contribute to its especially difficult deprotonation at C10. Each C10 proton (*endo*-



**Scheme 5.5:** Deprotonation of either H<sub>A</sub> or H<sub>B</sub> of **4.14**. X-ray crystal structure of **4.59** is provided for conformational insight.

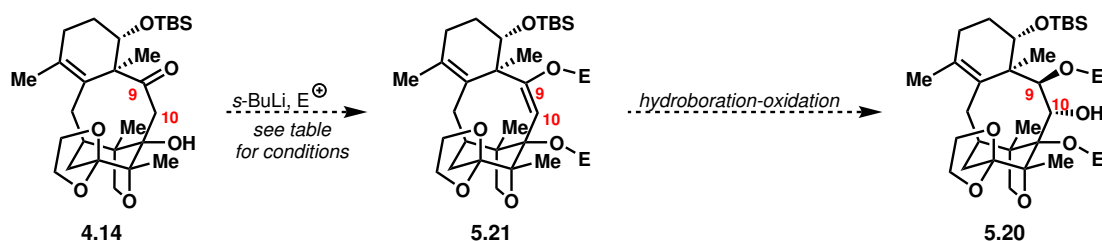
proton H<sub>A</sub> and *exo*-proton H<sub>B</sub>) will be considered separately, with the X-ray crystal structure of desilylated compound **4.59** providing conformational insight (Scheme 5.5). First, the deprotonation of H<sub>A</sub>—which results in *E*-enolate **5.18**—may be challenging, as the C–H<sub>A</sub> bond is placed nearly orthogonal to the C9 carbonyl π\*, increasing the kinetic barrier to deprotonation. In addition, its position in the concave face of the molecule may preclude its deprotonation by more sterically hindered bases. Alternatively, the more sterically accessible H<sub>B</sub> may be deprotonated, facilitated by the reasonable alignment of C–H<sub>B</sub> with the C9 carbonyl π\*. However, the resulting *Z*-enolate (**5.19**) would harbor a *trans*-alkene in the central eight-membered ring, which may be associated with considerable angle strain. At this stage, it is unclear whether H<sub>A</sub> or H<sub>B</sub> is deprotonated by *s*-BuLi.

## 5.2 Strategies for Accessing C9,C10-*trans*-Diol Motifs

### 5.2.1 Hydroboration of Enol Ethers

In addition to C10-oxidation, the C9 carbonyl had to be stereoselectively converted to a β-hydroxy group to yield the C9,C10-*trans*-diol motif found in taxagifine. One strategy for accessing these *trans*-diols (e.g., **5.20**) involved the formation of enol ethers (**5.21**) with subsequent hydroboration-oxidation from the convex face—a strategy that could now be attempted given the discovery of *s*-BuLi as a competent base for C10-deprotonation (Table 5.5). It should be noted that the desired C9,C10-*trans* configuration would only be attained if the formation of (*E*)-enol ethers **5.21** was favored over the stereoisomeric *Z*-enol ethers, which was not a given (*vide supra*). When we attempted to form the TMS enol ether by treatment of **4.14** with *s*-BuLi and TMSCl, we instead isolated enone compound **4.60**

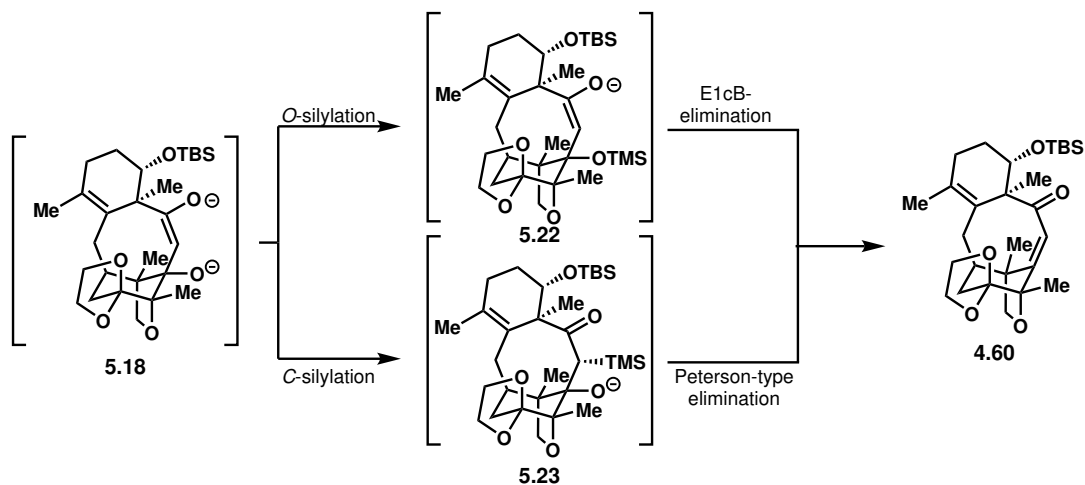
**Table 5.5:** Attempts at implementing an enol ether formation/hydroboration-oxidation strategy for the formation of *trans*-diols **5.20**.



Entry	Conditions (enol ether formation)	Results
1	<i>s</i> -BuLi (5 equiv), THF, –78 °C; then, TMSCl (15 equiv), –78 °C to 23 °C	68% of C10–C11 alkene (enone compound <b>4.60</b> )
2	<i>s</i> -BuLi, THF, –78 °C; then, TBSOTf	Mostly <b>4.14</b> ; messy otherwise
3	<i>s</i> -BuLi, THF, –78 °C, TMEDA; then, methyl chloroformate	Two unknown products
4	<i>s</i> -BuLi, THF, –78 °C; then, TFAA, –78 °C to 23 °C	C10–C11 alkene observed, otherwise messy
5	<i>s</i> -BuLi, THF, –78 °C; then, Ac <sub>2</sub> O, –78 °C to 23 °C	Unknown product, which when subjected to hydroboration yielded no conversion



(entry 1). Mechanistically, this could occur either by *O*-silylation of dianion **5.18** followed by E1cB-type elimination, or by an unusual *C*-silylation at C10—driven by the sterically hindered environment surrounding both the C9 and C11 oxyanions—followed by an elimination similar to what occurs in the Peterson olefination (Scheme 5.6). Attempted formation of the TBS silyl enol ether resulted in no conversion (entry 2). Attempted conversion to the enol carbonate, enol trifluoroacetate, or enol acetate were similarly unsuccessful (entries 3–5).



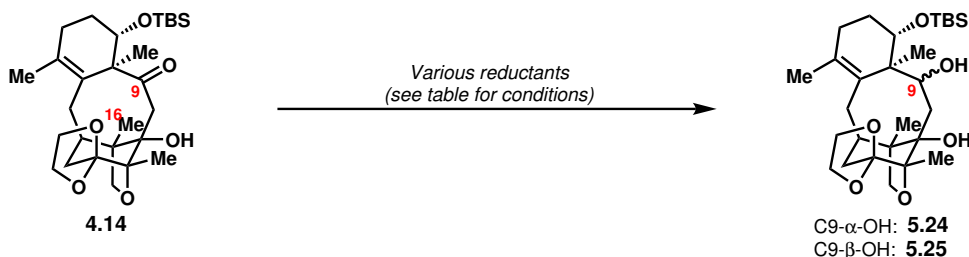
**Scheme 5.6:** Possible mechanisms for the formation of enone **4.60** by trapping of dianion **5.18** with TMSCl.

## 5.2.2 Direct Reduction of C10-Oxidized Compounds

A second strategy for accessing the C9,C10-*trans*-diol motif involved the direct reduction of C10-oxidized compound **4.61** or its diol-protected derivatives. In order to gain insight into how various hydride or single-electron reductants would react with **4.61**, we first conducted model reduction studies on **4.14**, which lacks the C10-hydroxy group (Table 5.6). LiAlH<sub>4</sub> reduction of **4.14** and Red-Al reduction gave only undesired diastereomer **5.24**, suggesting a preference for nucleophile approach from the concave β-face, presumably to avoid steric interactions with the C16 methyl group on the α-face. Directed hydride reductions (e.g., Narasaka-Prasad, Evans-Saksena, Evans-Tishchenko) yielded no conversion (entries 3–5), in accordance with the steric hindrance around the C9 carbonyl precluding the formation of organized transition states. Samarium iodide as a single electron reductant returned mostly starting material, and the reduced products observed favored the undesired diastereomer (**5.24**, entry 6); meanwhile, more speculative conditions in which we hoped reduction of the C9 carbonyl would occur via PCET-mediated one-electron reduction followed by HAT only gave starting material (entry 7).<sup>6</sup> Finally, harsher one-electron dissolving metal conditions afforded mainly the desired diastereomer **5.25** (entry 8), presumably via a C9-radical/anion intermediate with a configuration such that the C9-hydroxy group was placed in the pseudo-equatorial β-position, which would be more stable than its C9-epimer. Notably, the stereoselectivity of this reduction was sensitive to the stirring speed of the reaction. The opposite

diastereoselectivity was observed in cases where the reaction mixture did not turn the deep blue color associated with dissolved electrons, as a result of the stirring speed being insufficient for the stir bar to break up larger pieces of lithium wire. Attempted epimerization of **5.24** to **5.25** via hydrogen atom abstraction<sup>7</sup> yielded only starting material and oxidation to the ketone (entry 9).

**Table 5.6:** C9 reductions of **4.14**.

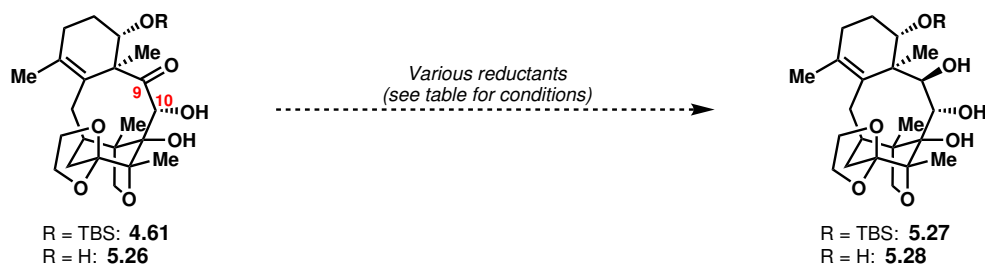


Entry	Conditions	Results
1	LiAlH <sub>4</sub> , THF, 0 °C to 65 °C	69% <b>5.24</b>
2	Red-Al, PhMe, 23 °C	<b>5.24</b>
3	Et <sub>2</sub> BOMe, THF/MeOH, -78 °C; then, NaBH <sub>4</sub>	No conversion
4	[Me <sub>4</sub> N][B(OAc) <sub>3</sub> H], AcOH, 23 °C	No conversion
5	Sml <sub>2</sub> (cat.), propanal, THF, -20 °C to 23 °C	No conversion
6	Sml <sub>2</sub> , THF/H <sub>2</sub> O, 23°C	77:15:8 ratio of <b>4.14</b> : <b>5.24</b> : <b>5.25</b>
7	Ru(bpy) <sub>3</sub> (PF <sub>6</sub> ) <sub>2</sub> , (PhO) <sub>2</sub> PO <sub>2</sub> H, Hantzsch ester, PhSH, blue LED, THF	No conversion
8	Li, NH <sub>3</sub> , THF/IPA, -78 °C	77%, 6:1 <b>5.25</b> : <b>5.24</b>
9	<i>For conversion of 5.24 to 5.25 :</i> Ir[dF(CF <sub>3</sub> )ppy] <sub>2</sub> (dtbbpy)PF <sub>6</sub> , [ <i>n</i> -Bu <sub>4</sub> N][H <sub>2</sub> PO <sub>4</sub> ], quinuclidine, PhSH, blue LED, MeCN, 23 °C	<b>5.24</b> and <b>4.14</b>

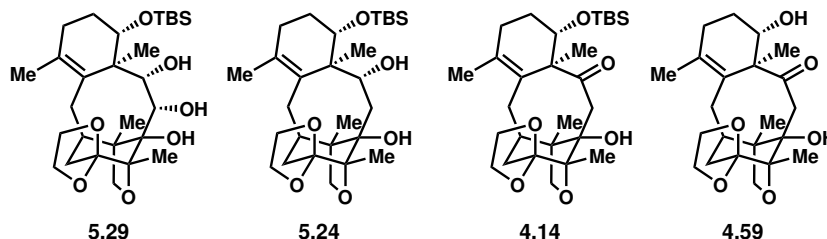
We then turned to C9 reductions on the C10-oxidized compound **4.61**. In accordance with our studies on C10-unoxidized compound **4.14**, treatment of **4.61** with LiAlH<sub>4</sub> yielded solely undesired diastereomer **5.29** (entry 1, Table 5.7). DIBALH reduction afforded unknown products, with neither **5.27** nor **5.29** observed by <sup>1</sup>H NMR in the crude reaction mixture (entry 2). An attempt to invert the C9 stereochemical configuration of undesired diastereomer **5.29** via Mitsunobu provided only undesired products whose instability on silica gel precluded thorough characterization (entry 3). Treatment with Li/NH<sub>3</sub>, which straightforwardly delivered the C9- $\beta$ -hydroxy epimer from C10-unoxidized compound **4.14**, gave C10-reduced compound **5.24**, the result of C9 carbonyl  $\alpha$ -deoxygenation and further C9 reduction (entry 4). Subjection to Na in IPA similarly resulted in mostly over-reduced products (entry 5). Motivated by Baran and coworkers' syntheses of decinnamoyltaxinine E and taxabaccatin III,<sup>1</sup> in which C9 reduction in the presence of a C10 hydroxy group could only be accomplished with 5% Na/Hg amalgam, we treated **4.61** with 20% Na/Hg amalgam; however, we observed C10-deoxygenated **4.14** as the sole product (entry 6). Although in-house-prepared 2.7% Na/Hg amalgam exhibited a slower rate of reduction, **4.14** remained the sole product (entry 7). We hypothesized that, as C10-deoxygenation was presumably

occurring via the generation of a C9 anion and subsequent  $\beta$ -elimination, C10-deoxygenation could be decreased if an intermediate C9 radical could be trapped by a hydrogen atom donor before further reduction to the anion. To this end, we treated **4.14** with  $\text{SmI}_2$  as reductant and PhSH as hydrogen atom donor<sup>8,9</sup>; however, C10-reduction was still observed, along with other unknown, undesired products (entry 8). Using  $\text{SmI}_2$  as reductant and AcOH as proton source, a set of conditions previously shown to reduce the C9 carbonyl of taxol-derived compounds with a C10 hydroxy group,<sup>10</sup> afforded only over-reduction products (entry 9). Use of the same conditions on TBS-cleaved compound **5.26**—the C7 hydroxy group of which might have bound  $\text{SmI}_2$ , preventing chelation to the C10 hydroxy group and its activation as a leaving group<sup>10</sup>—provided only C10-deoxygenated compound **4.59** (entry 10).

**Table 5.7:** Attempted C9 reductions of C10-oxidized compound **4.61**. SM = starting material.

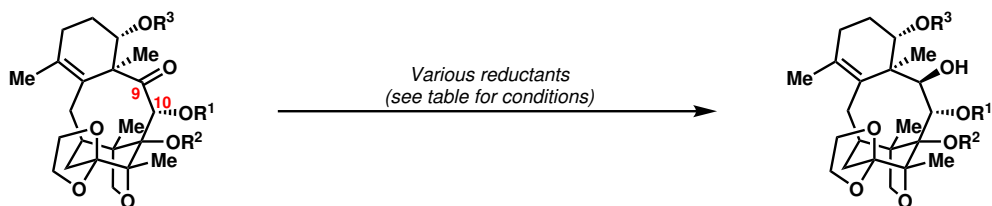


Entry	R	Conditions	Results
1	TBS	$\text{LiAlH}_4$ , THF, 0 °C to 65 °C	<b>5.29</b>
2	TBS	DIBALH, PhMe, 0 °C to 23 °C	Messy, unknown products
3	TBS	<i>For conversion of 5.29 to 9-O-acetyl- 5.27 :</i> $\text{PPh}_3$ , DEAD, AcOH, THF, 0 °C to 23 °C	Two unknown products
4	TBS	Li, $\text{NH}_3$ , THF/IPA, -78 °C	Mostly <b>5.24</b>
5	TBS	Na, IPA, 80 °C	Messy, over-reduction
6	TBS	20% Na/Hg, MeOH, 23 °C	1:1 SM: <b>4.14</b>
7	TBS	2.7% Na/Hg, MeOH, 23 °C	6:1 SM: <b>4.14</b>
8	TBS	$\text{SmI}_2$ , PhSH, THF, -10 °C	Some C10 reduction, and unknown products
9	TBS	$\text{SmI}_2$ , AcOH, THF, -10 °C	Over-reduction products
10	H	$\text{SmI}_2$ , AcOH, THF, -10 °C	1:1 SM: <b>4.59</b>

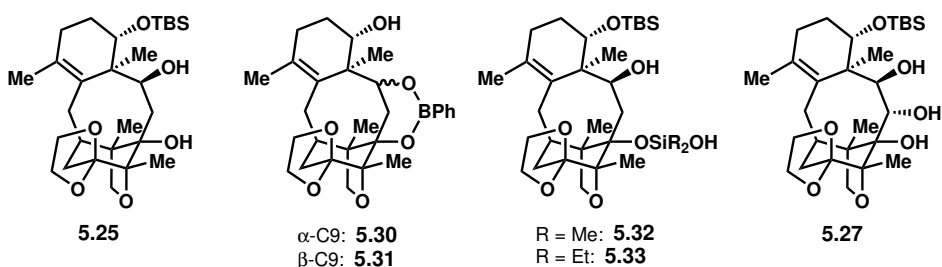


We hypothesized that protecting the C10 hydroxy group could reduce its chelation to metals, therefore reducing its viability as a leaving group. Therefore, we treated several C10-protected compounds to single-electron reduction conditions (Table 5.8). C10-TMS ether and C10,C11-phenylboronate compounds afforded only C10-deoxygenated products upon

**Table 5.8:** Attempted C9 reductions of C10-hydroxy-protected compounds. SM = starting material.



Entry	R <sup>1</sup> , R <sup>2</sup> , R <sup>3</sup>	Conditions	Results
1	TMS, H, TBS	Sml <sub>2</sub> , AcOH, THF, -10 °C	C10 reduction products
2	TMS, H, TBS	Li, NH <sub>3</sub> , THF/IPA, -78 °C	<b>5.25</b>
3	<del>BPh</del> , TBS	Li, NH <sub>3</sub> , THF/IPA, -78 °C	Mostly C10 reduction
4	<del>BPh</del> , H	Sml <sub>2</sub> , AcOH, THF, -78 °C	<b>5.30</b>
5	<del>BPh</del> , H	Li, NH <sub>3</sub> , THF/IPA, -78 °C	<b>5.31</b>
6	<del>SiMe<sub>2</sub></del> , TBS	Li, NH <sub>3</sub> , THF/IPA, -78 °C	32:50:18 <b>5.32</b> : <b>5.25</b> : <b>5.27</b>
7	<del>SiMe<sub>2</sub></del> , TBS	Sml <sub>2</sub> , AcOH, THF, -10 °C	No conversion
8	<del>SiMe<sub>2</sub></del> , TBS	Na, NH <sub>3</sub> , THF/IPA, -78 °C	50:45:5 <b>5.32</b> : <b>5.25</b> : <b>5.27</b>
9	<del>SiMe<sub>2</sub></del> , TBS	2.7% Na/Hg, MeOH, 23 °C	Mostly desilylation, traces of C10 reduction
10	<del>SiMe<sub>2</sub></del> , TBS	Li, NH <sub>3</sub> , THF/HFIP, -78 °C	Only C10 reduction
11	<del>SiMe<sub>2</sub></del> , TBS	Li, NH <sub>3</sub> , THF/MeOH, -78 °C	Mostly C10 reduction
12	<del>SiMe<sub>2</sub></del> , TBS	Li, NH <sub>3</sub> , THF/H <sub>2</sub> O, -78 °C	SM and C10 reduction
13	<del>SiMe<sub>2</sub></del> , TBS	Li, NH <sub>3</sub> , THF/NH <sub>4</sub> Cl, -78 °C	Only C10 reduction
14	<del>SiEt<sub>2</sub></del> , TBS	Li, NH <sub>3</sub> , THF/IPA, -78 °C	<b>5.33</b>
15	<del>SiMe<sub>2</sub></del> , TBS	[Ru <sub>2</sub> (PEt <sub>3</sub> ) <sub>6</sub> (OTf) <sub>3</sub> ](OTf), NMM, IPA, TFE, 110 °C	No conversion
16	<del>SiMe<sub>2</sub></del> , TBS	Al(O <i>i</i> -Pr) <sub>3</sub> , IPA, 80 °C	No conversion



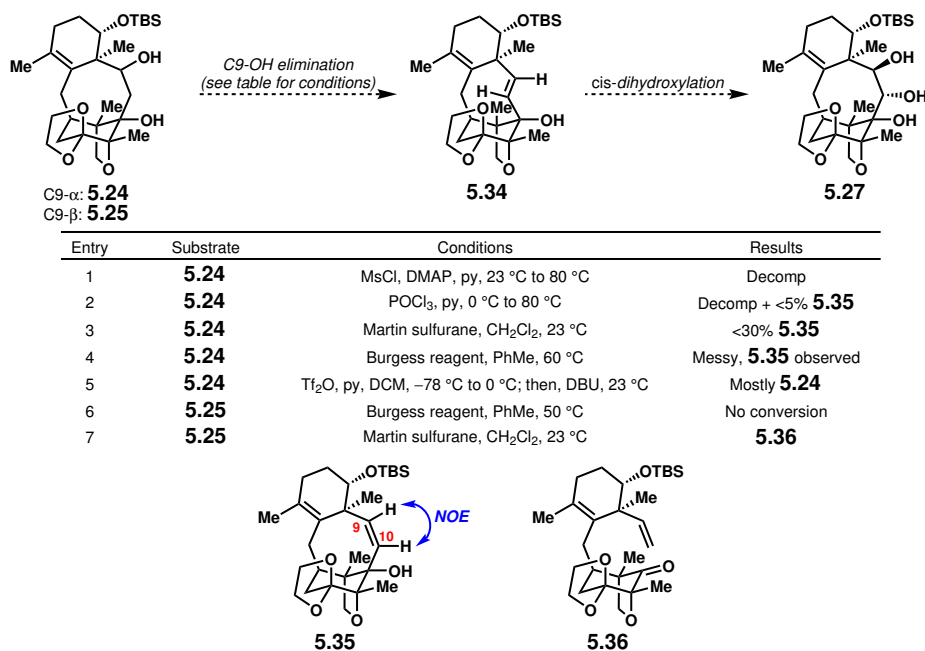
single electron reduction (entries 1–5). For the first time, we observed desired product **5.27** after treatment of C10,C11-dimethylsilyl-protected compound **5.13** with Li/NH<sub>3</sub> with IPA as proton source, albeit in <18% yield (entry 6). Unfortunately, subjecting of **5.13** to other

dissolving metal conditions (entries 7–9) or to the same conditions with varied proton sources (entries 10–13) did not improve the yield of **5.27**. C10,C11-diethylsilyl-protected compound **5.14** provided only C10-deoxygenated silanol **5.33** upon dissolving metal reduction (entry 14). Finally, we attempted transfer hydrogenation<sup>11</sup> (entry 15) and Meerwein–Ponndorf–Verley reductions (entry 16) of C10,C11-carbonate **5.11**, with no conversion observed in either case.

### 5.2.3 Attempted C9,C10-*trans*-Diol Synthesis via Alkene Dihydroxylations

With hydride reductions of C10-oxidized compounds providing the undesired C9 epimer and single-electron reductions failing to retain oxidation at C10, we turned to another strategy for introducing the C9,C10-*trans*-diol motif. This strategy involved elimination of the C9-hydroxy group of diols **5.24** or **5.25** to yield *trans*-alkene **5.34**, which upon *cis*-dihydroxylation from the convex face would afford triol **5.27** with the desired C9,C10-stereoconfiguration (Table 5.9). To this end, dehydration of C9- $\alpha$ -OH epimer **5.24** was attempted with MsCl, POCl<sub>3</sub>, Martin sulfurane, Burgess reagent, or Tf<sub>2</sub>O; in all cases, the only identifiable alkene product observed was *cis*-alkene **5.35**, whose stereochemical configuration was confirmed by an observed NOE correlation between protons at C9 and C10 (entries 1–5). In addition, treatment of C9- $\beta$ -OH epimer **5.25** with Burgess reagent resulted in no conversion (entry 6), while treatment with Martin sulfurane afforded only Grob fragmentation product **5.36** (entry 7).

**Table 5.9:** Attempted dehydrations for the formation of *trans*-alkene **5.34**.

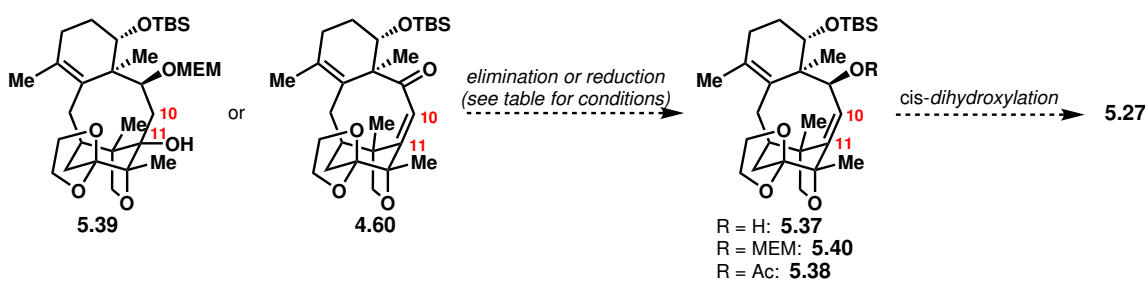


Entry	Substrate	Conditions	Results
1	<b>5.24</b>	MsCl, DMAP, py, 23 °C to 80 °C	Decomp
2	<b>5.24</b>	POCl <sub>3</sub> , py, 0 °C to 80 °C	Decomp + <5% <b>5.35</b>
3	<b>5.24</b>	Martin sulfurane, CH <sub>2</sub> Cl <sub>2</sub> , 23 °C	<30% <b>5.35</b>
4	<b>5.24</b>	Burgess reagent, PhMe, 60 °C	Messy, <b>5.35</b> observed
5	<b>5.24</b>	Tf <sub>2</sub> O, py, DCM, -78 °C to 0 °C; then, DBU, 23 °C	Mostly <b>5.24</b>
6	<b>5.25</b>	Burgess reagent, PhMe, 50 °C	No conversion
7	<b>5.25</b>	Martin sulfurane, CH <sub>2</sub> Cl <sub>2</sub> , 23 °C	<b>5.36</b>

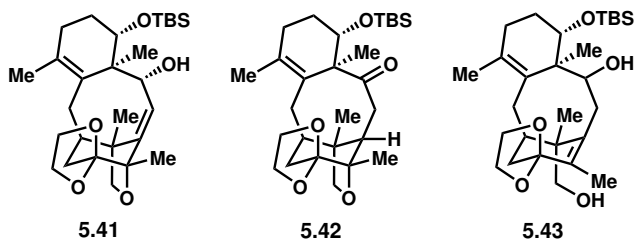
Alternatively, we envisioned that C9- $\beta$ -allylic alcohol **5.37** or its C9-OH-protected derivatives (**5.40** and **5.38**) could undergo *cis*-dihydroxylation to yield triol **5.27** or the analogous

C9-OH-protected compounds (Table 5.10). However, access to allylic alcohol **5.37** was non-trivial. Attempted elimination of the tertiary hydroxy group of C9-OMEM compound **5.39** with Martin sulfurane, Burgess reagent, or  $\text{SOCl}_2/\text{py}$  resulted in no conversion (entry 1), as did attempted reductions of enone **4.60** with  $\text{LiAlH}_4$  or under Luche conditions<sup>12</sup> (entry 2). Reduction of enone **4.60** with DIBALH afforded undesired diastereomer **5.41** (entry 3), which could not be converted into  $\beta$ -acetoxy compound **5.38** under Mitsunobu conditions (entry 4). Attempted reduction with  $\text{SmI}_2$  or 20%  $\text{Na}/\text{Hg}$  only yielded 1,4-reduction compound **5.42** (entry 5). Finally, under dissolving metal conditions ( $\text{Li}/\text{NH}_3$ ), some allylic alcohol **5.37** could be obtained, albeit with an equimolar quantity of a compound tentatively assigned as ether ring-opened isomer **5.43**; in addition, these results were not reproducible, with subsequent attempts yielding mainly over-reduced products (entry 6). The allylic alcohol **5.37** that could be isolated was subjected to hydroxy-directed dihydroxylation,<sup>13</sup> but only starting material was recovered (entry 7).

**Table 5.10:** Attempted synthesis and subsequent dihydroxylation of allylic alcohols **5.37**–**5.38**.

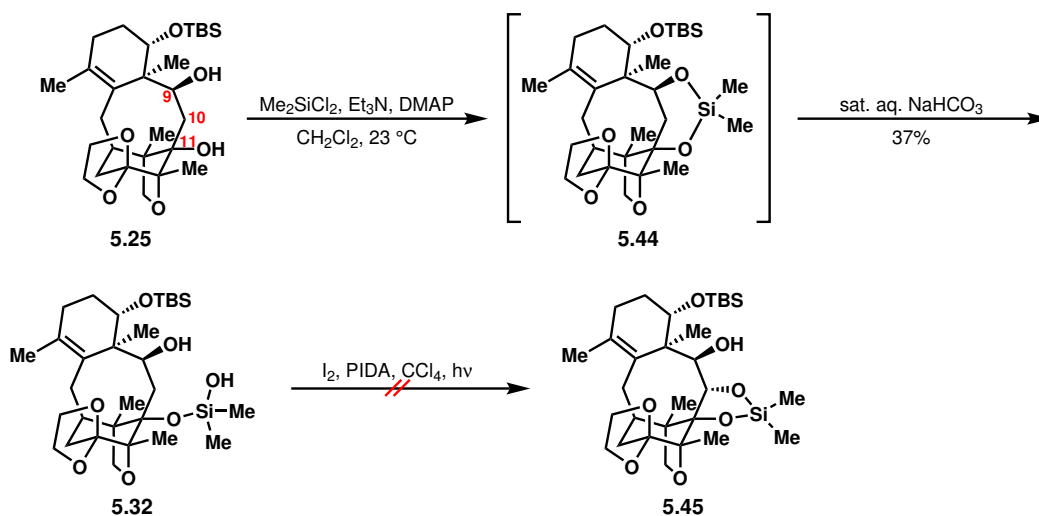


Entry	Substrate	Conditions	Results
1	<b>5.39</b>	Martin sulfurane, $\text{CH}_2\text{Cl}_2$ , 23 °C or Burgess reagent, PhMe, 60 °C or $\text{SOCl}_2$ , py, 23 °C	No conversion
2	<b>4.60</b>	$\text{LiAlH}_4$ , THF, 65 °C or $\text{NaBH}_4$ , $\text{CeCl}_3$ , MeOH, 23 °C to 65 °C	No conversion
3	<b>4.60</b>	DIBALH, PhMe, 0 °C to 23 °C	72% of <b>5.41</b>
4	<b>5.41</b>	<i>For conversion of <b>5.41</b> to <b>5.38</b>:</i> $\text{PPh}_3$ , DEAD, AcOH, THF, 23 °C	No conversion
5	<b>4.60</b>	$\text{SmI}_2$ , THF, AcOH, -10 °C or 20% $\text{Na}/\text{Hg}$ , MeOH, 23 °C	<b>5.42</b>
6	<b>4.60</b>	Li, $\text{NH}_3$ , THF/IPA, -78 °C	1:1 <b>5.37</b> : <b>5.43</b> (not reproducible)
7	<b>5.37</b>	<i>For conversion of <b>5.37</b> to <b>5.27</b>:</i> $\text{OsO}_4$ , TMEDA, $\text{CH}_2\text{Cl}_2$ , 0 °C to 23 °C	No conversion



## 5.2.4 Attempted C9- or C11-Hydroxy-Directed C10-Oxidations

We next attempted strategies for accessing the C9,C10-*trans* diol from easily accessible C9- $\beta$ -hydroxy compound **5.25**; we hypothesized that we could install a directing group on either the C9 or C11 hydroxy groups to direct stereoselective C10 oxidation. Examination of the conformation of **5.25** suggests that directing groups installed on either the C9 or C11 hydroxy groups would be well-positioned to oxidize C10 from the convex  $\alpha$ -face, despite the  $\beta$ -configuration at C9. We first installed a silanol directing group on the C11 hydroxy group by treating **5.25** with  $\text{Me}_2\text{SiCl}_2$ ; presumably, silane diether **5.44** was initially formed, which upon basic aqueous workup hydrolyzed to silanol **5.32** (Scheme 5.7). We postulate that the steric hindrance associated with C11 may impede the subsequent hydrolysis of **5.32** to the free diol; however, we should note that this reaction was not entirely reproducible, with the relative formations of silanol **5.32**, silane diether **5.44**, and starting material **5.25** varying from run to run. We imagined that the dimethylhydroxysilyl group could serve as a two-atom “extension” of the C11 hydroxy group, preparing substrate **5.32** for Suárez-type oxidation.<sup>14</sup> However, upon treatment of **5.32** with  $\text{I}_2$ /PIDA with sunlamp irradiation, we recovered mostly starting material, with an isolated minor product determined not to be desired product **5.45**.

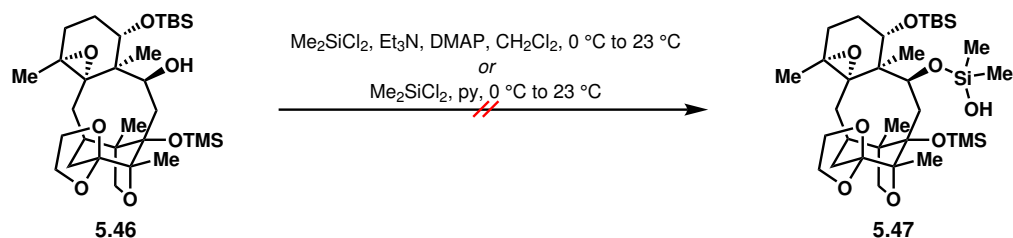


**Scheme 5.7:** Attempted preparation and use of silanol **5.45** for directed C10-oxidation.

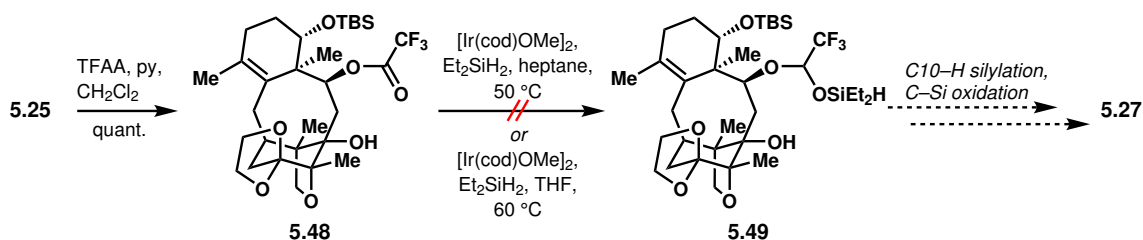
We next prepared secondary alcohol **5.46**, where the tetrasubstituted alkene and tertiary hydroxy group have been protected in order to avoid undesired reactivity (Scheme 5.8). However, attempted formation of a silanol from the C9-hydroxy group only returned starting material; presumably, silanol **5.47** is formed, but is too unstable to hydrolysis to isolate.

We turned next to the Hartwig method for the formation of 1,2-diols.<sup>15</sup> While we were able to synthesize trifluoroacetate **5.48** from diol **5.25**, attempted hydrosilylation to prepare **5.49**—the substrate for further directed C10-H silylation and Tamao-Fleming oxidation to yield triol **5.27**—did not result in any observable conversion (Scheme 5.9).

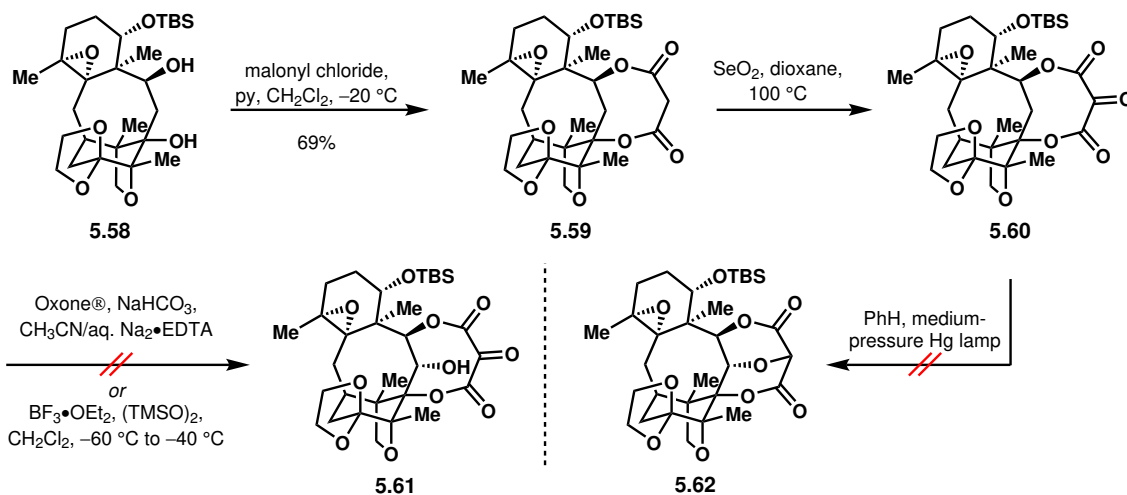
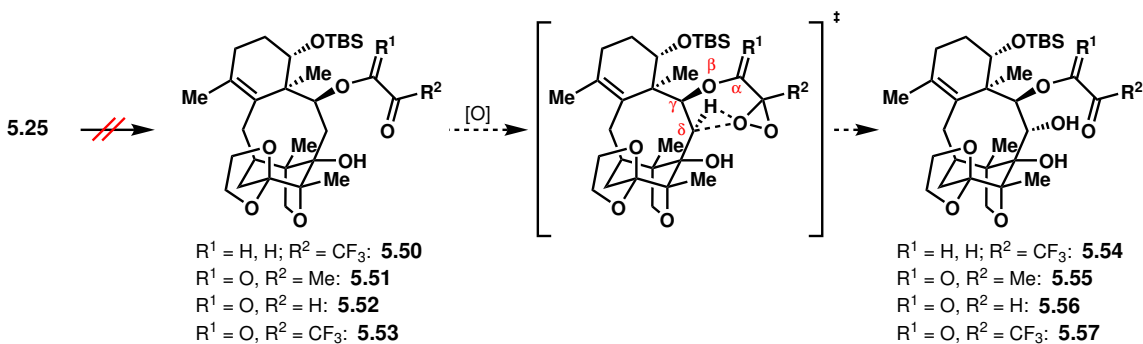
Finally, drawing from the work of Yang and coworkers,<sup>16</sup> we attempted to tether a carbonyl group to the C9 hydroxy group as a precursor for dioxirane formation, after which



Scheme 5.8: Attempted preparation of silanol 5.46 for directed C10-oxidation.



Scheme 5.9: Attempted Hartwig hydroxy-directed synthesis of 1,2-diols.



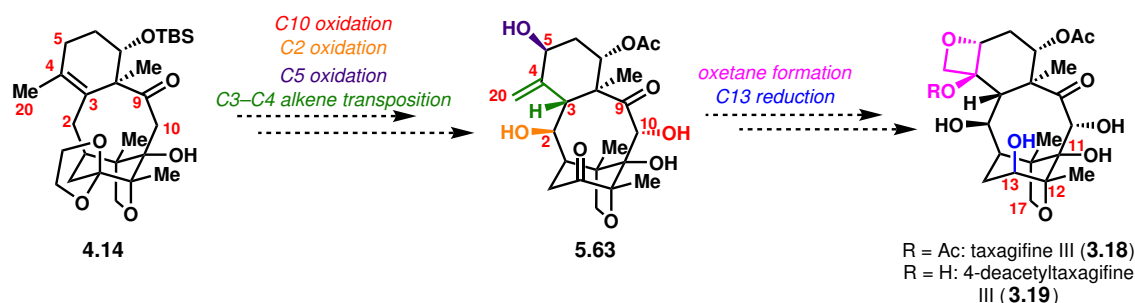
Scheme 5.10: Attempted intramolecular C10-H oxidation via dioxirane intermediates.



intramolecular C–H oxidation via  $\gamma$  C–H insertion would take place (Scheme 5.10). While we were unable to form substrates **5.50–5.53** from diol **5.25**, we were able to transform diol **5.58**—whose tetrasubstituted alkene has been epoxidized to preclude its interference with further chemistry—to malonic ester **5.59**, which could be oxidized with  $\text{SeO}_2$  to a compound tentatively assigned as tricarbonyl compound **5.60**. This highly polar compound was unstable to silica gel column chromatography with MeOH as a co-eluent. Impure **5.60**, when subjected to Oxone<sup>®</sup><sup>16a</sup> or  $\text{BF}_3 \cdot \text{Et}_2\text{O} / (\text{TMSO})_2$ ,<sup>17</sup> did not yield C10–H oxidation product **5.61** via a dioxirane intermediate, only ester hydrolysis products without oxidation at C10. In addition, attempted C10–O bond formation to yield **5.62** via a Norrish type II-like process resulted only in decomposition.

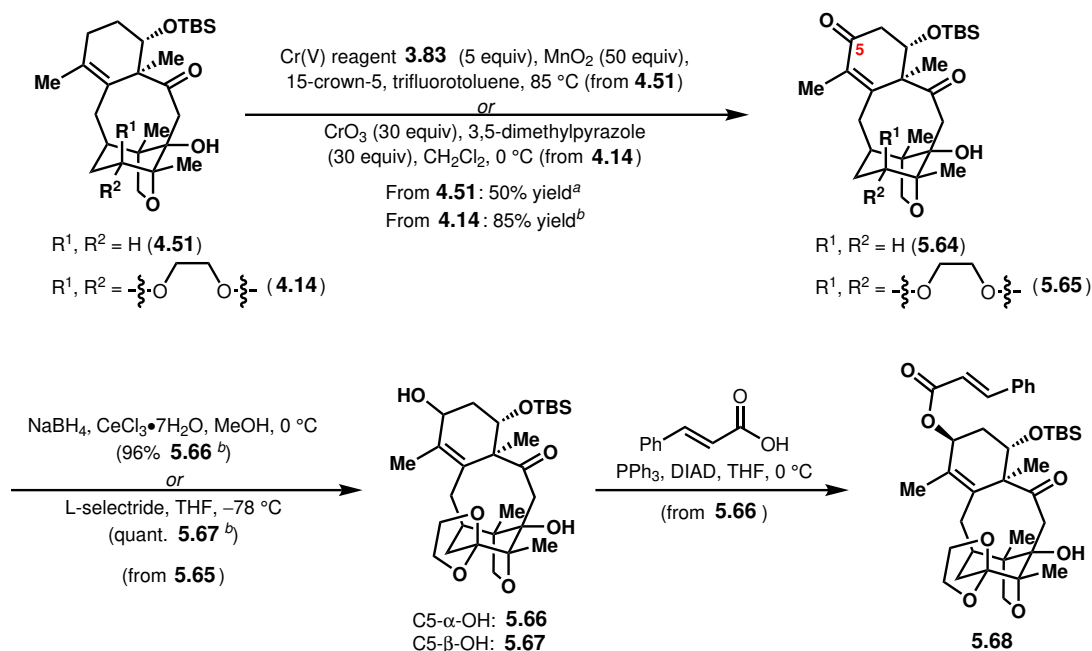
### 5.3 Installation of C5 Oxygenation

Given our challenges accessing the C9,C10 *trans*-diol motif found in taxagifine, we turned our sights to taxagifine III (**3.18**) and 4-deacetyltaxagifine III (**3.19**), taxagifine-like natural products possessing a carbonyl group at C9 (Scheme 5.11). Neither taxagifine III nor 4-deacetyltaxagifine III have been subjected to bioactivity studies; however, their biological activity is of potential interest as they possess structural features found in both taxagifine (e.g., a C11 hydroxy group, an ether bridge between C12 and C17) and taxol (e.g., alcohol oxidation state at C13, carbonyl at C9, oxetane ring). Given that “hybrid” natural products often possess strong bioactivity—which, in some cases, exceeds that of the “parent” natural products<sup>18</sup>—taxagifine III and 4-deacetyltaxagifine III represent attractive synthetic targets. The transformations required for the syntheses of **3.18** and **3.19** resemble those required for the synthesis of taxagifine; however, C9 carbonyl reduction is no longer needed, while C13 carbonyl reduction and oxetane formation are now necessary.



**Scheme 5.11:** Remaining transformations required to synthesize taxagifine III and 4-deacetyltaxagifine III from tetracyclic core **4.14**.

With C10 oxidation accomplished and C9 carbonyl reduction no longer necessary, we turned our attention to oxidation of the allylic C5 position. Our studies on both model tetracyclic system **4.51** and C13-oxidized system **4.14** quickly revealed the use of Salmond and coworkers’ conditions ( $\text{CrO}_3$  and 3,5-dimethylpyrazole)<sup>19</sup> to be optimal for allylic oxidation to the C5 carbonyl compound, albeit requiring large excesses of both reagents (Scheme 5.12). In contrast, Baran’s Cr(V) reagent-mediated oxidation<sup>20</sup> provided lower yields and required

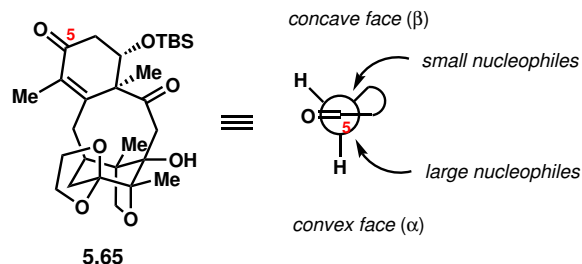


**Scheme 5.12:** C5 oxidation and further transformations. <sup>a</sup><sup>1</sup>H NMR yield with mesitylene as internal standard. <sup>b</sup>Isolated yield.

elevated temperatures and prolonged reaction times (24 h vs. 15 min with Salmond's conditions). From C13-oxidized C5 carbonyl compound **5.65**, both diastereomers of the C5 allylic alcohol could be accessed stereoselectively, with Luche reduction conditions<sup>12</sup> affording the C5- $\alpha$  allylic alcohol (**5.66**) and L-selectride affording the C5- $\beta$  allylic alcohol (**5.67**); meanwhile, Li(*o*-Bu)<sub>3</sub>AlH did not react with **5.65**, whereas DIBALH gave only a complex mixture. In accordance with our previous studies on C9 reduction, we found that the C9 carbonyl was inert to less forcing hydride reduction conditions. We were able to convert C5- $\alpha$  allylic alcohol **5.66** to **5.68** via a Mitsunobu reaction with cinnamic acid, incorporating the C5- $\beta$  cinnamoyl ester present in taxagifine.

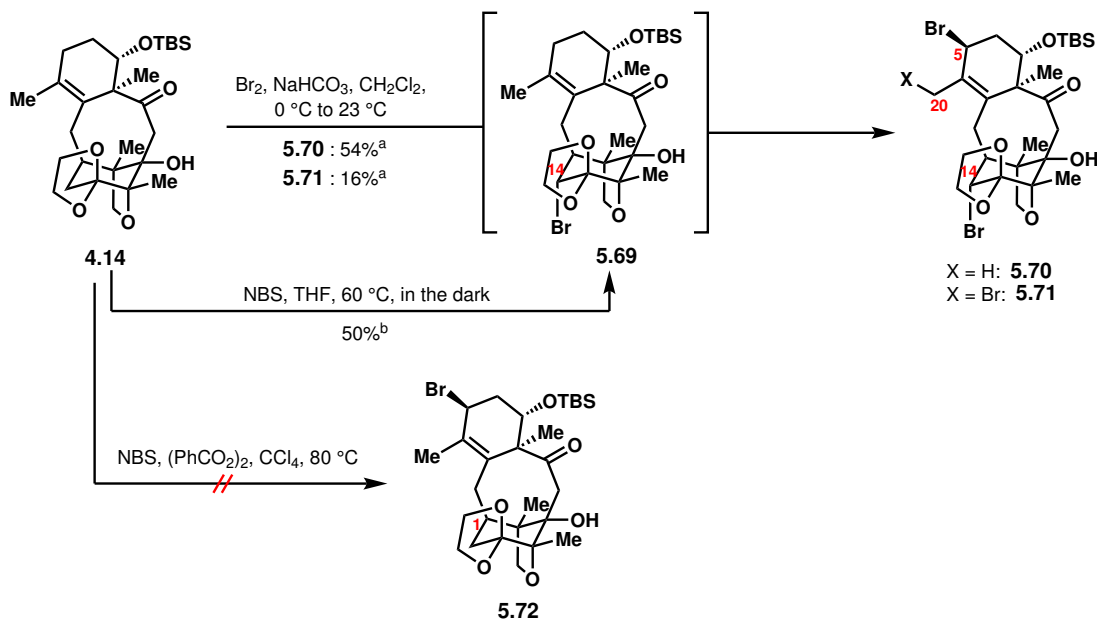
The divergent diastereoselectivities observed with NaBH<sub>4</sub>/CeCl<sub>3</sub> and L-Selectride with respect to C5 carbonyl reduction are consistent with the influence of torsional strain.<sup>21</sup> Nucleophilic addition of small hydride reagents such as NaBH<sub>4</sub> occurs preferentially from the concave  $\beta$ -face in order to avoid torsional strain in the transition state, whereas nucleophilic addition of large hydride reagents such as L-Selectride occurs preferentially from the sterically less hindered  $\alpha$ -face (Scheme 5.13).

In addition to transition metal-mediated SET, we discovered that C5 functionalization could be accomplished via radical C–H abstraction as well. Treatment of **4.14** with Br<sub>2</sub> yielded dibrominated compound **5.70** in 54% yield and tribrominated compound **5.71** in 18% yield (Scheme 5.14). Presumably, these brominated products arise via the intermediacy of C14 bromide **5.69**, which itself might be generated via a polar mechanism, with Br<sub>2</sub> as an electrophile. Subsequent sequential radical C–H abstraction/bromination events—first at the more activated C5 position and second at C20—would then afford the two observed products, with bromine radicals generated from the homolysis of Br<sub>2</sub> under ambient light. Notably, C14 bromide **5.69** can be isolated when **4.14** is treated with NBS without a radical



**Scheme 5.13:** Influence of torsional strain on the diastereoselectivity of C5 carbonyl reductions.

initiator, supporting the mechanistic proposal whereby **5.69** is produced via a polar mechanism. In contrast, when **4.14** is subjected to NBS in the presence of a radical initiator, a complex mixture, rather than the desired C5 monobrominated product **5.72**, is formed. Presumably, the presence of a bromine atom at C14 on compound **5.69** sterically and electronically deactivates the C1 position that is otherwise prone to radical C–H abstraction, which has previously been observed in taxane scaffolds; the thus generated C1 radical may be susceptible to decomposition pathways.<sup>22,23</sup> This explanation is consistent with radical C–H abstraction yielding two major products from intermediate **5.69** yet affording only a complex mixture from **4.14**. Overall, these studies suggest that radical C–H abstraction and subsequent functionalization could occur site- and stereoselectively at C5, but only after the deactivation of C1.



**Scheme 5.14:** Synthesis of brominated products **5.69–5.71**. <sup>a</sup><sup>1</sup>H NMR yield with mesitylene as internal standard. <sup>b</sup>Isolated yield.

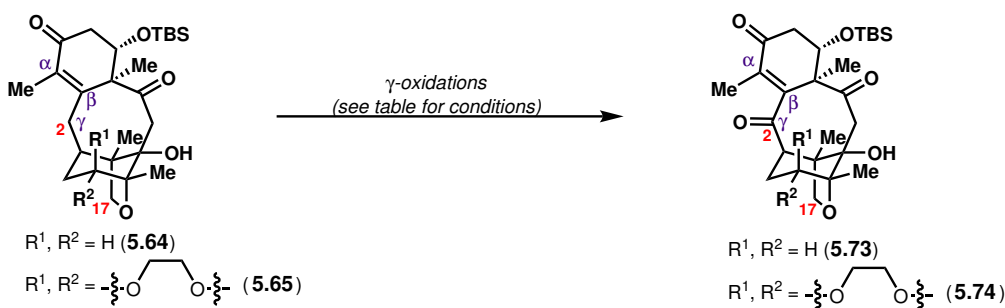
## 5.4 Installation of C2 Oxygenation

### 5.4.1 Attempts at Radical C2–H Abstraction

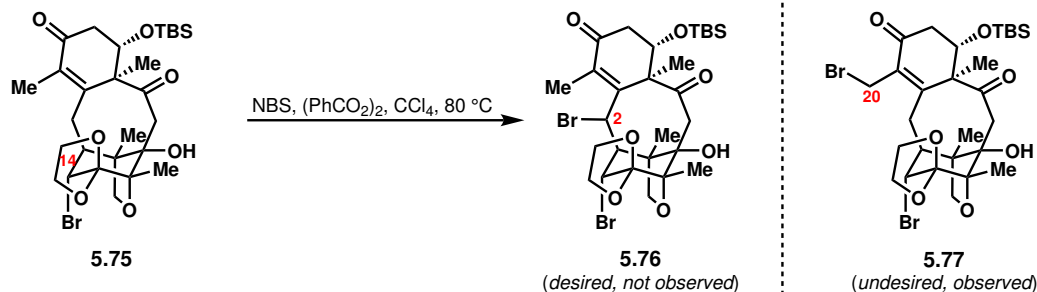
With solutions to C10 and C5 oxidation identified, we turned next to the oxidation of C2. While our studies on the allylic bromination of tetracyclic compound **4.14** revealed that C5 and C20—and potentially C1—are the most activated for radical C–H abstraction, we hoped that the introduction of C5 oxidation would further activate the  $\gamma$  position at C2, which would be consistent with observations made in the course of Baran and coworkers' synthesis of taxuyunnanine D.<sup>20</sup> To this end, we subjected C5-oxidized compounds **5.64** and **5.65** to a variety of transition metal-mediated radical C–H abstraction/oxidation conditions<sup>24–28</sup>; however, in all cases, no C2 oxidation products were observed (Table 5.11). The only identifiable product in any run was that of C17 oxidation on C13-unoxidized substrate **5.64** (entry 2). Furthermore, treatment of substrate **5.75** to radical allylic bromination conditions yielded not desired C2-brominated product **5.76**, but rather C20-brominated product **5.77**, suggesting that C2 was not the most activated position even after the deactivation of C1 by the presence of the C14 bromine (Scheme 5.15).

The unreactivity at C2 to radical C–H abstraction can be explained on the basis of its rigid conformation. C2–H abstraction from **5.65** would afford a radical intermediate that cannot be stabilized by the vicinal enone conjugated  $\pi$  system as a result of its configuration (Scheme 5.16). As a result, C–H abstraction occurs preferentially at other positions where the resultant radical would be more stabilized (e.g., the methine C–H at C1, or at the C20 methyl group whose free rotation ensures that the radical could be stabilized by the adjacent  $\pi$  system).

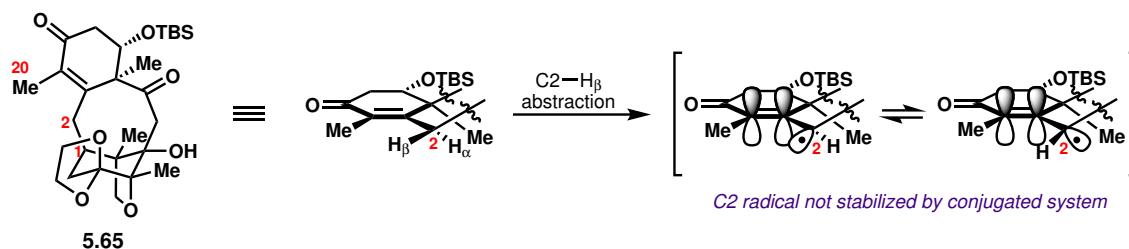
**Table 5.11:** Attempted C2 oxidation of C5-oxidized compounds **5.64** and **5.65**.



Entry	Substrate	Conditions	Results
1	<b>5.64</b>	Pd(OH) <sub>2</sub> /C, TBHP, K <sub>2</sub> CO <sub>3</sub> , CH <sub>2</sub> Cl <sub>2</sub> , 0 °C to 23 °C	Messy
2	<b>5.64</b>	Mn <sub>3</sub> (OAc) <sub>3</sub> O, TBHP, 3 Å MS, O <sub>2</sub> , EtOAc, 23 °C	Recovered <b>5.64</b> + C17 oxidation
3	<b>5.65</b>	CuBr, TBHP, PhH, 65 °C	Decomposition
4	<b>5.65</b>	Co(acac) <sub>2</sub> , NHPI, MeCN, O <sub>2</sub> , 70 °C	No conversion
5	<b>5.65</b>	Rh <sub>2</sub> (cap) <sub>4</sub> , K <sub>2</sub> CO <sub>3</sub> , TBHP, CH <sub>2</sub> Cl <sub>2</sub> , 23 °C to 40 °C	No conversion



**Scheme 5.15:** Attempted C2 bromination of **5.75**.

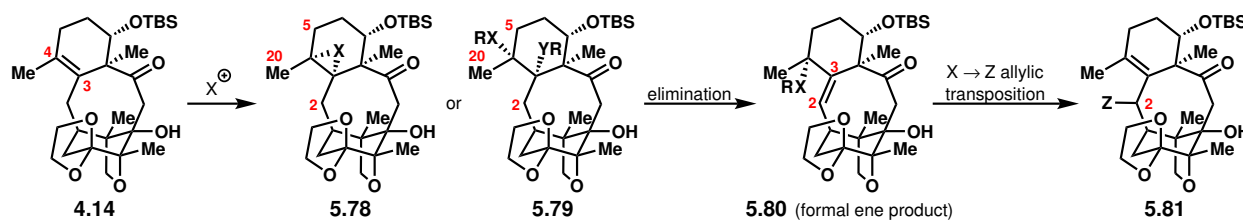


**Scheme 5.16:** Conformation of radical intermediate after C2-H abstraction.

## 5.4.2 Attempts at C2 Functionalization via Formal Ene/Allylic Transposition

We next turned to two-electron chemistry to functionalize C2. We envisioned that difunctionalization of the C3–C4 alkene of **4.14** via electrophilic addition would yield compounds of the types **5.78** or **5.79** (Scheme 5.17). Elimination would then generate formal ene products of the type **5.80**, after which X → Z allylic transposition would yield C2-functionalized compounds of the type **5.81**. C2 selectivity for the elimination process would be necessary for this mechanistic proposal to be viable for the installation of C2 functionalization; at the outset, we had no particular reason to believe that elimination from C2 would be favorable over that from C5 or C20.

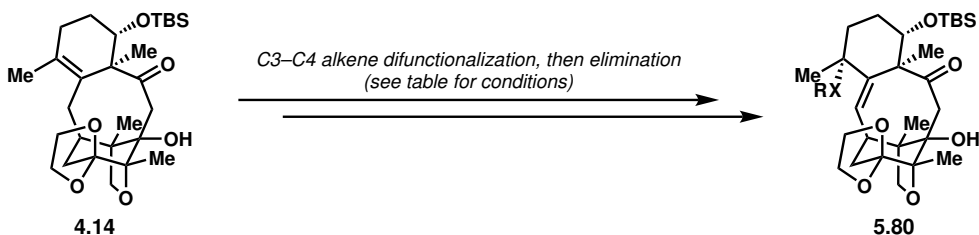
We began with an attempted Schenck ene reaction with singlet oxygen; however, only a messy reaction mixture resulted (entry 1, Table 5.12). Attempted Upjohn dihydroxylation of the C3–C4 alkene resulted in no conversion (entry 2). Epoxidation of the C3–C4 alkene proceeded in quantitative yield; however, several attempts to open the epoxide un-



**Scheme 5.17:** General scheme for the formal ene/allylic transposition strategy for C2 functionalization.

der acidic or basic conditions gave only messy reaction mixtures (entry 3). Subjection to Prévost reaction conditions returned only starting material (entry 4). A formal iodinative ene reaction with NIS yielded no conversion (entry 5), as did attempted iodohydroxylation with *in situ*-generated “I–OH”<sup>29</sup> (entry 6). Treatment with PhSeCl and NCS<sup>30</sup> for allylic chlorination afforded only a C14-chlorinated product, as could be expected based on our bromination studies (*vide supra*) (entry 7). Attempted formation of an allylic selenide, which could theoretically be converted to a C2 alcohol after selenoxide formation and subsequent [2,3]-sigmatropic rearrangement, did not proceed upon treatment of phenylselenyl electrophiles PhSe-*N*-succinimide<sup>30b</sup> or *in situ*-generated PhSeOTf (entries 8 and 9). Attempted phenylselenylhydroxylation<sup>31</sup> returned only starting material (entry 10), as did attempted sulfenylation of the alkene with *in situ*-generated PhSCl and subsequent elimination (entry 11). Finally, attempted ene reaction with enophile 4-phenyl-1,2,4-triazoline-3,5-dione (PTAD) did not proceed (entry 12).

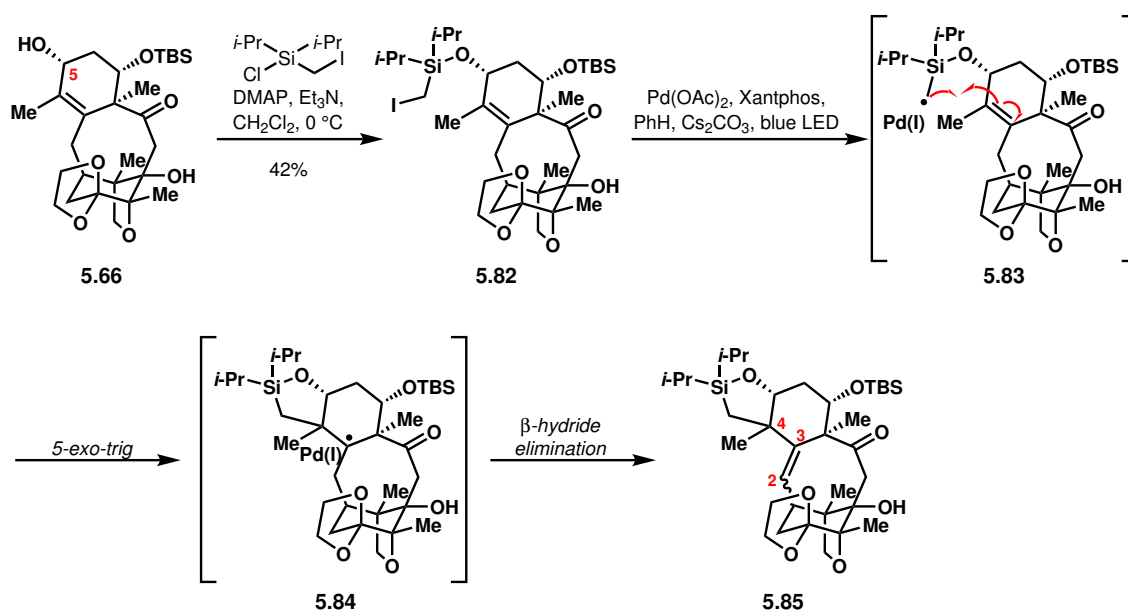
**Table 5.12:** Attempted formal ene conditions on **4.14**.



Entry	XR	Conditions	Results
1	OH	O <sub>2</sub> , tetraphenylporphyrin, 1,2-DCE, sunlamp, 0 °C; then, P(OEt) <sub>3</sub>	Messy
2	OH	OsO <sub>4</sub> , NMO, acetone/H <sub>2</sub> O, 50 °C (followed by hypothetical tertiary alcohol elimination)	dihydroxylation yielded no conversion
3	OH	<i>m</i> -CPBA, CH <sub>2</sub> Cl <sub>2</sub> , 23 °C; then, LDA, THF, –78 °C to 0 °C or 15% HCl, THF, 23 °C or LiNEt <sub>2</sub> , HMPA, Et <sub>2</sub> O, –40 °C to 23 °C or TMSOTf, Et <sub>3</sub> N, 1,2-DCE, 84 °C or Al(O- <i>i</i> -Pr) <sub>3</sub> , PhMe, 110 °C	quant. formation of epoxide (single dias.); eliminations messy
4	OBz	I <sub>2</sub> , AgOBz, PhH, 80 °C	No conversion
5	I	NIS, CH <sub>2</sub> Cl <sub>2</sub> , 50 °C	No conversion
6	I	IBX, I <sub>2</sub> , DMSO (followed by hypothetical tertiary alcohol elimination)	No conversion
7	Cl	PhSeCl, NCS, CH <sub>2</sub> Cl <sub>2</sub> , 23 °C	C14 chlorination (80%)
8	SePh	PhSe- <i>N</i> -succinimide, PhMe, 110 °C	No conversion
9	SePh	PhSeCl/AgOTf, py, CH <sub>2</sub> Cl <sub>2</sub> , 0 °C to 23 °C	No conversion
10	SePh	PhSeSePh, DDQ, MeCN/H <sub>2</sub> O, 30 °C (followed by hypothetical tertiary alcohol elimination)	No conversion
11	SPh	PhSH, NCS, Na <sub>2</sub> CO <sub>3</sub> , CH <sub>2</sub> Cl <sub>2</sub> , 50 °C	No conversion
12	PTAD	PTAD  , 1,2-DCE, 85 °C	Mostly <b>4.14</b>

### 5.4.3 C5-Tether-Assisted C2 Functionalization

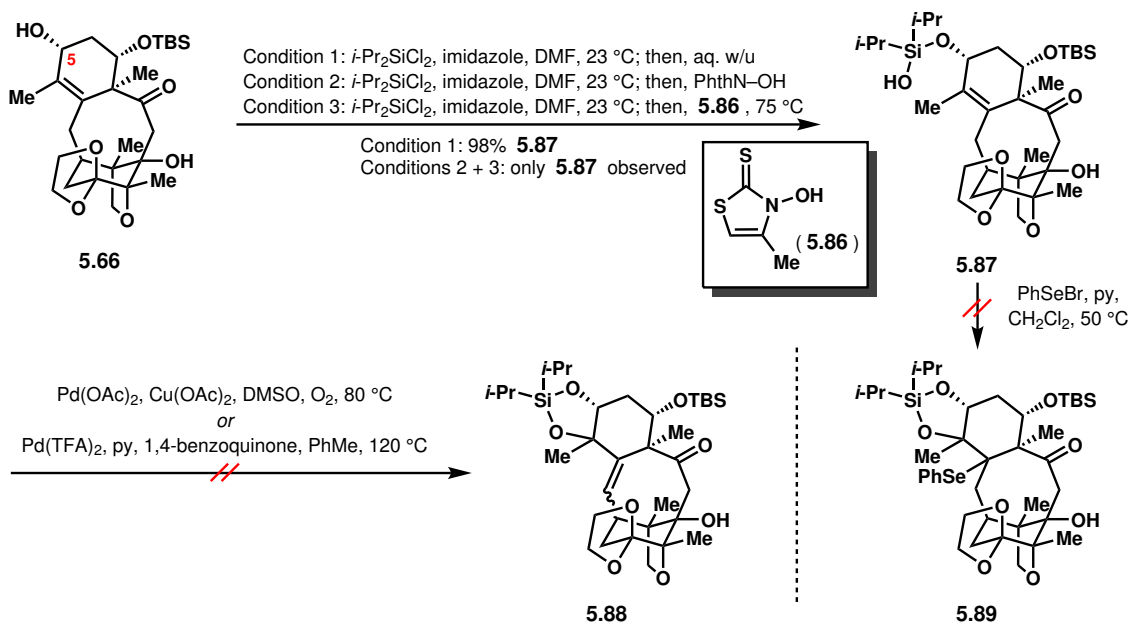
It became clear from our studies that the sterically hindered environment around the C3–C4 alkene generally impeded attempts at its difunctionalization. Therefore, we considered tethering a reactive species to the C5 position via an easily installable C5 hydroxy group; this reactive species would react with the C3–C4 alkene, ultimately yielding ene-type products with a C2–C3 alkene after elimination, similar to the strategy in the previous section. Proof-of-concept was provided by subjecting substrate **5.82** to Pd(OAc)<sub>2</sub> under blue LED irradiation; silyl methyl Heck reaction<sup>32</sup> proceeded via hybrid Pd-radical species **5.83** and **5.84** to provide C2–C3 alkene-containing product **5.85** (Scheme 5.18). The stereochemistry with respect to the C2–C3 alkene and the C4 stereocenter was left undetermined. Compound **5.85** was the first we had synthesized containing any sort of functionalization at C2; however, the extra C–C bond formed at C4 would preclude this reaction as a viable way forward in the synthesis. As a result, we began investigating methods of recreating similar reactivity while forming a C4–heteroatom bond.



**Scheme 5.18:** C2 functionalization via intramolecular silyl methyl Heck reaction.

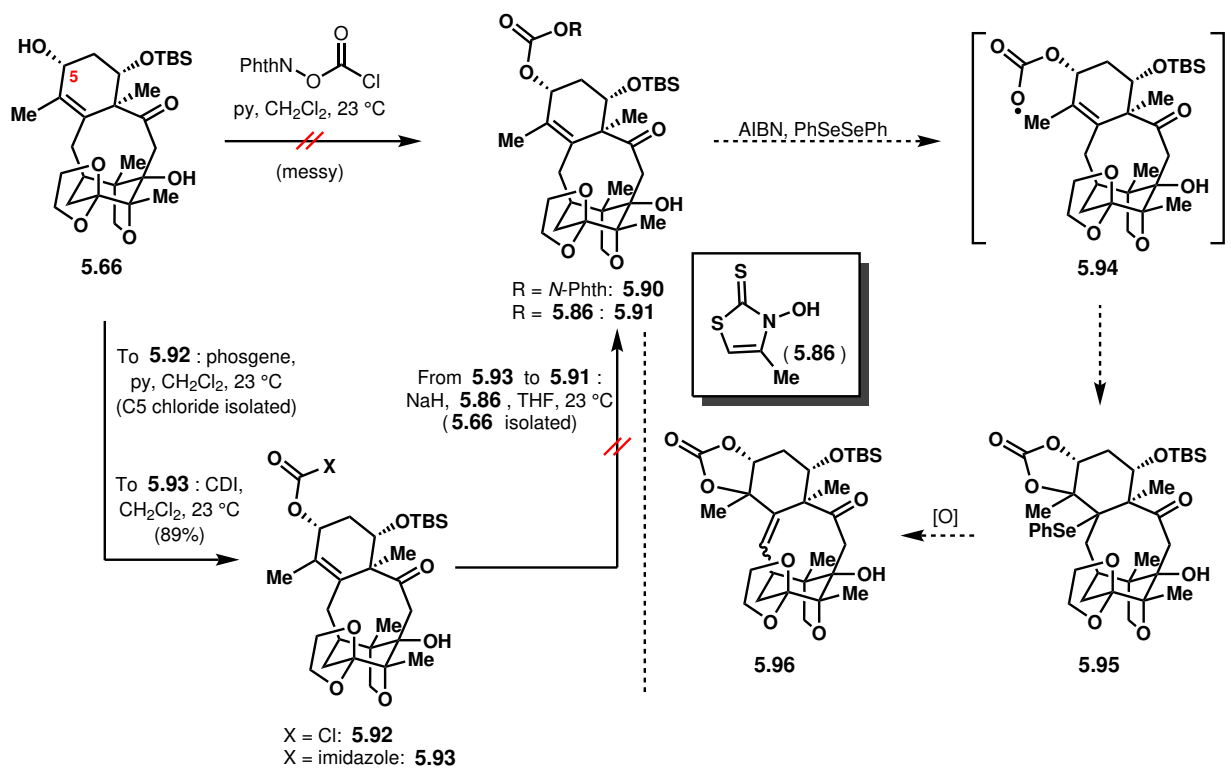
We began by preparing a C5-OH-tethered silanol; ultimately, only diisopropyl variant compound **5.87** could be synthesized, with the diethyl variant too susceptible to hydrolysis to be isolated (Scheme 5.19). Notably, attempts to prepare mixed silyl diethers—which could serve as oxy radical precursors—by trapping the putative silyl chloride intermediate with nucleophiles such as PhthN–OH and *N*-hydroxythiazolinthione **5.86**<sup>33</sup> gave only silanol **5.87**. Attempts to effect an unprecedented silanol oxa-Heck reaction under the conditions reported by Andersson<sup>34</sup> or Stoltz<sup>35</sup> for alcohol cyclizations returned only starting material or C5 carbonyl compound **5.65**, the product of silyl ether cleavage and further oxidation. In addition, attempted intramolecular phenylselenoetherification<sup>36</sup> to provide product **5.89** returned only allylic alcohol **5.66**.

We next turned to the preparation of C5-carbonates; we hypothesized that C5-carbonates



**Scheme 5.19:** Attempted reactions of silanol **5.87** towards C2 functionalization.

such as **5.90** and **5.91** could be converted to alkoxy-carbonyloxy radical **5.94**, which upon



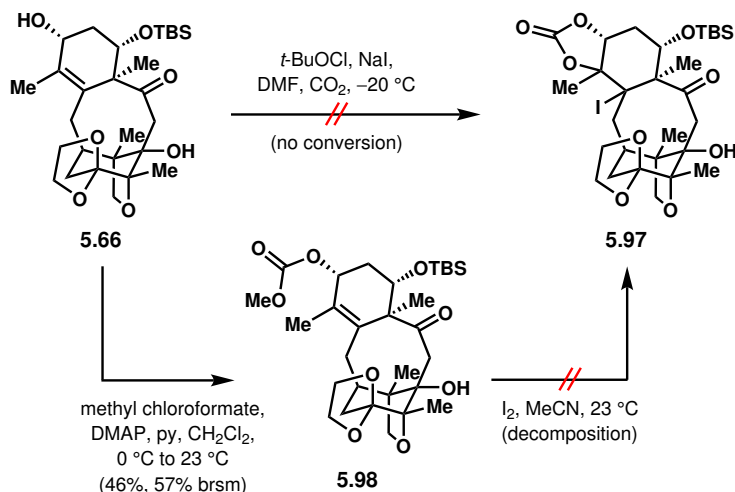
**Scheme 5.20:** Attempted preparation of carbonates **5.90** and **5.91** as alkoxy-carbonyloxy radical precursors.



5-*exo-trig* cyclization would yield a C3 radical that could be trapped with a radicalophile such as diphenyl diselenide, affording **5.95** (Scheme 5.20). It should be noted that alkoxy-carbonyloxy radicals exhibit slow rates of decarboxylation,<sup>37</sup> allowing for their addition to alkenes.<sup>38</sup> From **5.95**, oxidation of the selenide to the selenoxide and subsequent elimination to give **5.96** would then result in C2 functionalization in the form of a C2–C3 alkene.

First, we attempted to prepare *N*-oxycarbonyloxyphthalimide **5.90** from C5 allylic alcohol **5.66** via its reaction with *N*-chlorocarbonyloxyphthalimide<sup>39</sup>; however, only a complex reaction mixture resulted, presumably as a result of the instability of the desired product. Attempted preparation of chloroformate **5.92** by reaction of **5.66** with phosgene returned a compound tentatively assigned as the C5-chloride, possibly as a result of nucleophilic displacement of a chloroformate intermediate. In contrast, we were able to prepare **5.93** by reaction of **5.66** with CDI; however, attempted transformation of **5.93** to mixed carbonate **5.91** was unsuccessful, returning only the free alcohol **5.66**.

Finally, we attempted iodo(alkoxycarbonyloxy)lation of the C3–C4 alkene using the methods of Minakata<sup>40</sup> (direct formation of **5.97** from C5 allylic alcohol **5.66**) and Cardillo<sup>41</sup> (formation of **5.97** via methyl carbonate **5.98**) (Scheme 5.21). However, treatment of **5.66** with CO<sub>2</sub> and *in situ*-generated *t*-BuOI resulted in no conversion, whereas treatment of methyl carbonate **5.98** with I<sub>2</sub> led to decomposition.

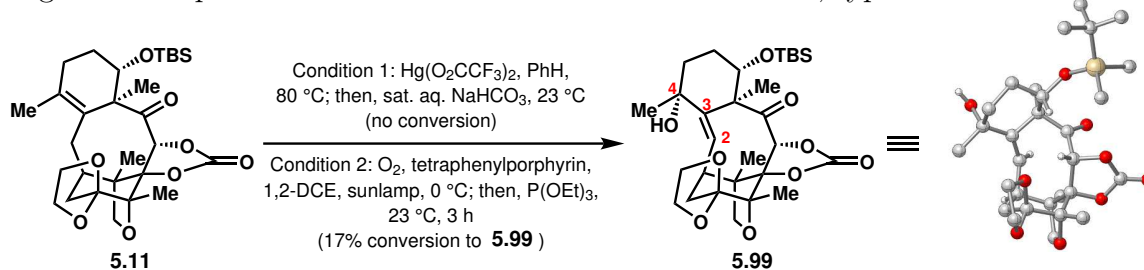


**Scheme 5.21:** Attempted iodo(alkoxycarbonyloxy)lation of the C3–C4 alkene of **5.66**.

#### 5.4.4 Successful C2 Functionalization via Formal Ene/Allylic Transposition

At this stage, we returned to attempted functionalization via an intermolecular formal ene/allylic transposition, except with C10-oxidized compound **5.11** as substrate rather than C10-unoxidized compound **4.14**. While Treibs oxidation<sup>42</sup> with concomitant alkene migration<sup>43</sup> to yield C4 allylic alcohol **5.99** did not proceed (condition 1, Scheme 5.22), we were gratified to see that **5.99** could be generated by Schenck ene reaction with singlet O<sub>2</sub>, albeit at low levels of conversion (condition 2). The structure of **5.99** was confirmed by X-ray

crystallographic analysis, in particular establishing the stereochemistry at C4 and the *trans*-configuration of the C2–C3 alkene with respect to the eight-membered ring. The dihedral angle with respect to the *trans*-C2–C3 alkene was about 40°, typical of *trans*-cyclooctenes.<sup>44</sup>



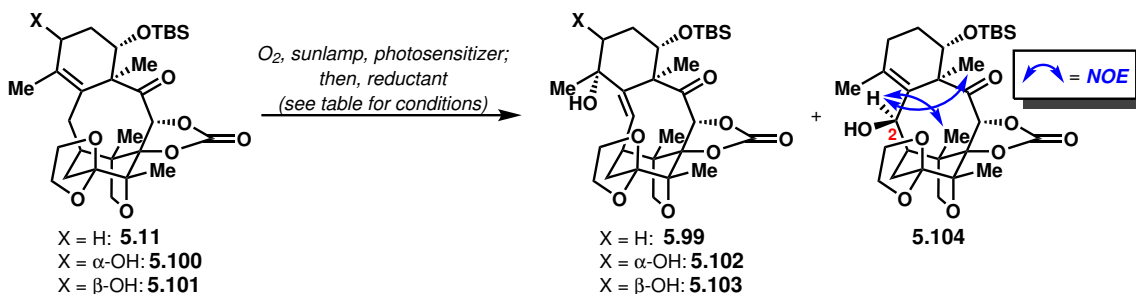
**Scheme 5.22:** Synthesis of the allylic alcohol **5.99**.

As described in Section 5.4.2, attempted Schenck ene reaction with C10-unoxidized tetracyclic compound **4.14** yielded only a complex reaction mixture; this raises the question of why C10-oxidized but otherwise identical compound **5.11** was a suitable substrate for this reaction. Modeling indicated that the conformations of compounds **4.14** and **5.11** were nearly identical. While **5.11** is theoretically less susceptible to decomposition by retro-aldol and Grob fragmentation pathways, we had previously observed the retro-aldol of **4.14** only at elevated temperatures under basic conditions, and we had never observed Grob fragmentation; it would therefore be unusual for these pathways to be responsible for the decomposition of **4.14** under the relatively mild Schenck ene conditions. To date, the difference in behavior of substrates **5.11** and **4.14** under Schenck ene conditions remains a puzzle, and highlights the danger in relying on even highly similar model systems to predict the reactivities of synthetic intermediates in complex natural product synthesis.

We next turned to the optimization of the Schenck ene reaction of substrate **5.11**. Carrying out the Schenck ene reaction on C5-oxidized substrates **5.100** and **5.101** resulted in low conversions, similarly to **5.11** (entries 1–3, Table 5.13). The use of different photosensitizers (methylene blue, Rose Bengal) did not result in increased conversion (entries 4 and 5). We found that lowering the amount of tetraphenylporphyrin and increasing the reaction temperature to 23 °C resulted in greatly increased conversions; under these conditions, we were also able to observe the formation of C2-oxidized compound **5.104** (entry 6). We speculate that higher concentrations of photosensitizer result in higher rates of singlet oxygen quenching, ultimately lowering singlet oxygen lifetimes<sup>45,46</sup>; this would explain our higher observed rates of conversion at lower stoichiometries of photosensitizer. At 15 °C, we observed higher yields than at 23 °C, perhaps as a result of decreased rates of decomposition of peroxide intermediates (entry 7). Use of a C10,C11-diisopropylsilyl protected diol substrate (**5.15**) rather than C10,C11-carbonate protected diol **5.11** gave much lower yields, reinforcing the uniqueness of **5.11** as a substrate for this reaction (entry 8). A brief solvent screen showed that use of CCl<sub>4</sub> afforded products in lower yields (entry 9), whereas use of pyridine gave a cleaner reaction where only C4 alcohol **5.99** was formed (entry 10), albeit at lower conversion than in 1,2-DCE. Greatly extended reaction times in pyridine successfully resulted in complete consumption of starting material; in addition, we found that the use of polymer-bound triphenylphosphine simplified purification, as triphenylphosphine oxide is difficult to chromatographically separate from C4 alcohol **5.99** (entry 11). Upon increasing the scale,

we observed lower rates of conversion, perhaps as a result of decreased light penetration into the reaction vessel (entries 12 and 13). Future engineering efforts will be undertaken in order to optimize the reaction on larger scales.

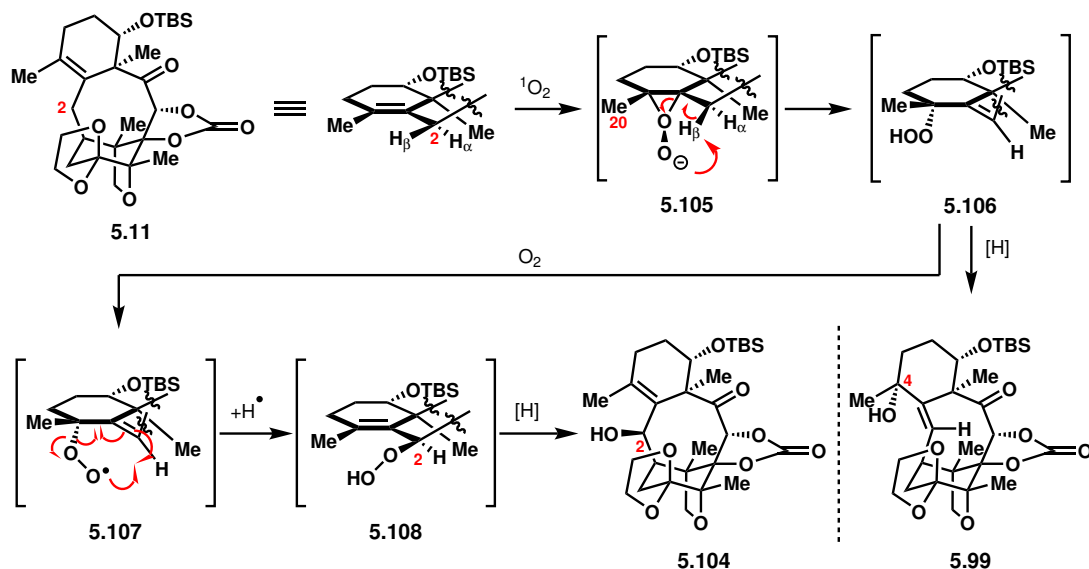
**Table 5.13:** Optimization of Schenck ene reaction for C2 functionalization. TPP = tetraphenylporphyrin. <sup>a</sup>All reactions carried out on 0.005 mmol scale and at 0.026 M unless otherwise indicated. <sup>b</sup><sup>1</sup>H NMR yields with mesitylene as internal standard, provided as **5.99/5.104/5.11**. <sup>c</sup>C10,C11-diisopropylsilyl protected diol **5.15** used as substrate. <sup>d</sup>0.062 mmol scale. <sup>e</sup> 0.104 mmol scale.



Entry <sup>a</sup>	X	Photosensitizer (equiv.), reductant (equiv.)	Temperature	Solvent	Time	Results
1	H	TPP (0.2), P(OEt) <sub>3</sub> (5)	0 °C	1,2-DCE	3 h	17% conversion
2	α-OH	TPP (0.2), P(OEt) <sub>3</sub> (5)	0 °C	1,2-DCE	7 h	11% conversion
3	β-OH	TPP (0.2), P(OEt) <sub>3</sub> (5)	0 °C	1,2-DCE	7 h	5% conversion
4	H	methylene blue (0.2), P(OEt) <sub>3</sub> (5)	23 °C	MeOH	10 h	3% conversion
5	H	Rose Bengal (0.02), PPh <sub>3</sub> (5)	15 °C	MeOH	9.5 h	Very little conversion
6	H	TPP (0.02), P(OEt) <sub>3</sub> (5)	23 °C	1,2-DCE	9.5 h	28/5/37 <sup>b</sup>
7	H	TPP (0.02), P(OEt) <sub>3</sub> (5)	15 °C	1,2-DCE	9.5 h	38/10/32 <sup>b</sup>
8 <sup>c</sup>	H	TPP (0.02), P(OEt) <sub>3</sub> (5)	15 °C	1,2-DCE	9.5 h	18/10/26 <sup>b</sup>
9	H	TPP (0.02), P(OEt) <sub>3</sub> (5)	15 °C	CCl <sub>4</sub>	9.5 h	5/11/13 <sup>b</sup>
10	H	TPP (0.02), PPh <sub>3</sub> (5)	15 °C	py	9.5 h	25/0/52 <sup>b</sup>
11	H	TPP (0.02), PPh <sub>3</sub> (poly-bound) (5)	15 °C	py	48 h	62/0/0 <sup>b</sup>
12 <sup>d</sup>	H	TPP (0.02), PPh <sub>3</sub> (poly-bound) (5)	15 °C	py	48 h	61/0/17 <sup>b</sup>
13 <sup>e</sup>	H	TPP (0.02), PPh <sub>3</sub> (poly-bound) (5)	15 °C	py	48 h	37/0/25 <sup>b</sup>

At this stage, it is worth providing a mechanistic rationale for the observed Schenck ene products **5.99** and **5.104**. Reaction of substrate **5.11** with singlet oxygen on the convex face first generates peroxide intermediate **5.105** (Scheme 5.23). We propose that the illustrated stereoisomer (with respect to the neutral oxygen of the peroxide) is preferentially generated in order to avoid steric interactions between the terminal oxide of the peroxide and axial substituents in the six-membered ring. At this point, proton abstraction could theoretically occur at C20 or at C2; given that C20–H abstraction would generate two adjacent tetrasubstituted centers, C2–H abstraction is favored.<sup>47</sup> Only C2–H<sub>β</sub> is available for abstraction; as a result, *trans*-alkene-containing hydroperoxide **5.106** is formed rather than the *cis*-isomer. Reduction of this hydroperoxide intermediate affords C4 allylic alcohol product **5.99**; alternatively, in the presence of oxygen, an allylic hydroperoxide rearrangement via peroxy radical intermediate **5.107** occurs to generate C2 hydroperoxide **5.108**. Upon reduction, C2 allylic alcohol product **5.104** is produced. It is unclear at this point why carrying out the reaction in pyridine prevents production of C2 allylic alcohol product **5.99**, although

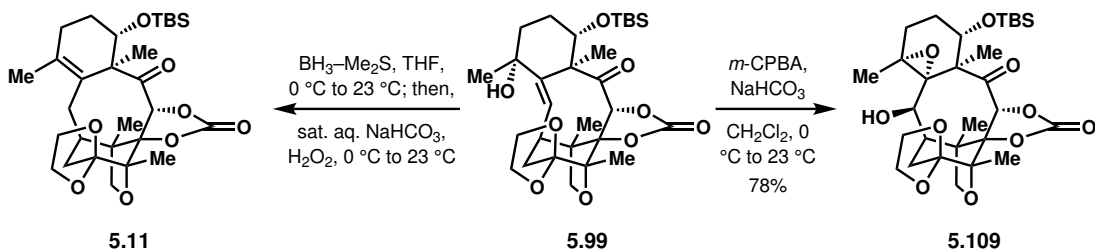
we speculate that hydrogen bonding between pyridine and hydroperoxide intermediate **5.106** stabilizes it against hydrogen atom abstraction.



**Scheme 5.23:** Mechanism of the Schenck ene reaction on substrate **5.11**.

Presumably, high angle strain is associated with the formation of the *trans*-alkene<sup>48</sup>; we hypothesized that this strain could be leveraged to carry out an allylic transposition of the C4 hydroxy group in **5.99** to the C2 hydroxy group in **5.104**, as has already been observed with their corresponding peroxy radicals. The tendency for alkene migration in **5.99** was manifested in its reaction with *m*-CPBA (yielding epoxyalcohol **5.109**) and with borane-THF (yielding reductive transposition product **5.11**) (Scheme 5.24).

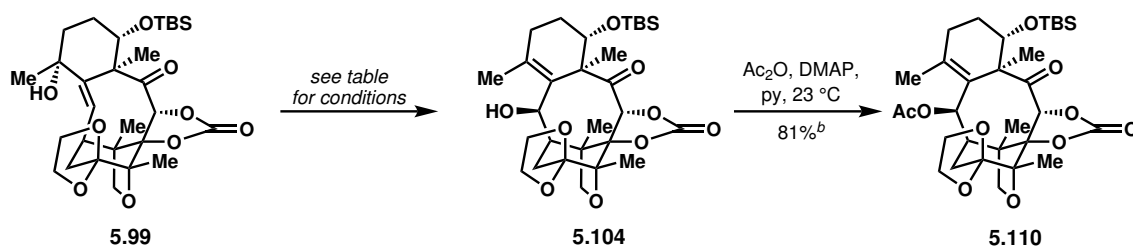
Our efforts began with attempted rhenium-catalyzed allylic alcohol transposition<sup>49</sup> of **5.99**; under these conditions, we observed desired C2 allylic alcohol **5.104**, albeit in 32% yield (entry 1, Table 5.14). Stirring in  $H_2O$ /dioxane<sup>50</sup> at elevated temperatures did not effect allylic transposition (entry 2). MsOH-mediated transposition<sup>51</sup> gave desired product **5.104** in 57% yield but also gave 12% of the C2 mesylate (entry 3). Other sulfonic acids ( $H_2SO_4$  and *p*-TsOH· $H_2O$ ) gave increased yields, although the use of *p*-TsOH· $H_2O$  still afforded an undesired C2 tosylate product in 11% yield (entries 4 and 5). Finally, by modifying the stoichiometry of the *p*-TsOH· $H_2O$  and the composition of the solvent, we were able to produce desired C2 alcohol **5.104** in 87% yield with only negligible quantities of the



**Scheme 5.24:** Observed migration of the C2–C3 alkene of **5.99**.

C2 tosylate. The C2 alcohol could then be protected as the acetate **5.110** in 81% yield, with acetylation proceeding more readily than attempted protections of **5.110** as MOM or TIPS ethers. Alternatively, we imagined possible ways of converting C4 alcohol **5.99** to C2 acetate **5.110** in one pot. To this end, we treated **5.99** with AcOH at elevated temperatures; however, only a complex reaction mixture resulted (entry 7). We were initially successful in synthesizing **5.110** from **5.99** in 55% yield and with a qualitatively clean crude  $^1\text{H}$  NMR by treatment with  $\text{Ac}_2\text{O}$ , DMAP, and pyridine at elevated temperatures, perhaps via [3,3] sigmatropic rearrangement of an intermediate C4-OAc compound; however, this reaction proved to be irreproducible, with subsequent attempts returning yields of  $\sim 20\%$  and with qualitatively much messier crude  $^1\text{H}$  NMRs (entry 8). As a result, we opted to continue with the two-step protocol for the synthesis of **5.110**.

**Table 5.14:** Optimization of C4 to C2 allylic alcohol transposition. <sup>a</sup>All yields are  $^1\text{H}$  NMR yields with mesitylene as internal standard. <sup>b</sup>Isolated yield.



Entry	Conditions	Results <sup>a</sup>
1	$\text{O}_3\text{ReOSiPh}_3$ , $\text{Et}_2\text{O}$ , $-10\text{ }^\circ\text{C}$	32% <b>5.104</b>
2	$\text{H}_2\text{O}/\text{dioxane}$ , $80\text{ }^\circ\text{C}$	No conversion
3	$\text{MsOH}$ (2 equiv), $\text{THF}/\text{H}_2\text{O}$ (4:1), $23\text{ }^\circ\text{C}$	57% <b>5.104</b> , 12% C2-OMs
4	$\text{H}_2\text{SO}_4$ (2 equiv), $\text{THF}/\text{H}_2\text{O}$ (4:1), $23\text{ }^\circ\text{C}$	72% <b>5.104</b> , 6% <b>5.99</b>
5	$p\text{-TsOH}\cdot\text{H}_2\text{O}$ (2 equiv), $\text{acetone}/\text{H}_2\text{O}$ (4:1), $23\text{ }^\circ\text{C}$	74% <b>5.104</b> , 8% <b>5.99</b> , 11% C2-OTs
6	$p\text{-TsOH}\cdot\text{H}_2\text{O}$ (1 equiv), $\text{acetone}/\text{H}_2\text{O}$ (1:1), $23\text{ }^\circ\text{C}$	87% <b>5.104</b> , 2% C2-OTs
7	AcOH, THF, $23\text{ }^\circ\text{C}$ to $60\text{ }^\circ\text{C}$	Messy
8	$\text{Ac}_2\text{O}$ , DMAP, py, $110\text{ }^\circ\text{C}$	55% <b>5.110</b> (not reproducible)

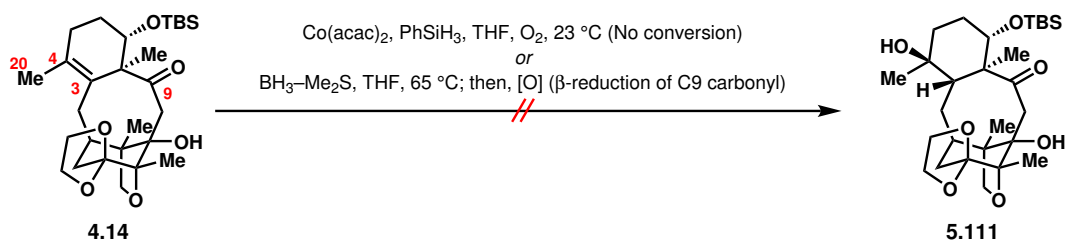
While optimization of C4 to C2 allylic alcohol transposition was conducted on small scale with pure starting material, on large scale we found that C4 alcohol **5.99** was unstable to extended residence times on silica gel. As a result, in practice, we simply filter and conduct an aqueous workup on **5.99** after the Schenck ene reaction, after which we subject the resulting material directly to  $p\text{-TsOH}\cdot\text{H}_2\text{O}$ . With this protocol, we have obtained the C2 alcohol (**5.104**) in 48% yield over two steps from C2-unfunctionalized compound **5.11**.

## 5.5 Transposition of the C3–C4 Alkene and Setting of the C3 Stereocenter

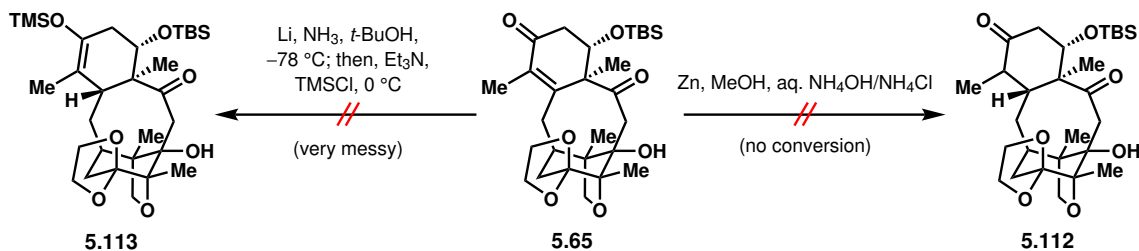
### 5.5.1 Non-Directed C3–C4 Alkene Functionalization

With solutions to C10, C5, and C2 oxidation, one of the few remaining challenges was the transposition of the C3–C4 tetrasubstituted alkene to the C4–C20 *exo*-methylene required for eventual oxetane formation, with concomitant setting of the C3 stereocenter. We anticipated that this task would be challenging for at least three reasons: 1) the fact that the C3–C4 alkene was tetrasubstituted and adjacent to a quaternary center suggested that it was relatively thermodynamically stable and sterically inaccessible, and therefore likely fairly unreactive, 2) additions to the tetrasubstituted alkene may not be regioselective, and 3) the hydrogen atom at C3 needed to be installed from the concave face of the incredibly caged tetracycle; in fact, C3 could be said to reside at the deepest point in the “cave.” In general, our studies toward C3–C4 alkene transposition would be conducted on model systems lacking C10 or C2 oxidation; we hoped these studies would provide insights on how to carry out later alkene transposition on a more highly functionalized system possessing oxidation at these sites.

We decided first to probe the reactivity of the C3–C4 double bond. In accordance with our initial assessment of its low reactivity, neither Mukaiyama hydration or hydroboration-oxidation of the C3–C4 alkene of **4.14** proceeded, with the latter conditions only reducing the C9 carbonyl from the  $\beta$ -face (Scheme 5.25). Furthermore, attempted single electron reductions of the enone of **5.65** were unsuccessful (Scheme 5.26).



**Scheme 5.25:** Attempted Mukaiyama hydration and hydroboration of the C3–C4 alkene of **4.14**.



**Scheme 5.26:** Attempted single electron reductions of the enone of **5.65**.

Given that epoxidation was one of the few methods that successfully functionalized the

C3–C4 alkene, we next investigated reductive epoxide ring-openings. From C2 alcohol substrate **5.109**, neither Ti(III)-mediated reductive epoxide opening conditions nor hydrogenation conditions gave desired product **5.115** (entries 1 and 2, Table 5.15). In addition, single-electron  $\alpha$ -deoxygenation of C2 ketone **5.114** yielded only a messy reaction mixture (entry 3).

**Table 5.15:** Attempted reductive C3–C4 epoxide openings.

Entry	Substrate	Conditions	Results
1	<b>5.109</b>	Cp <sub>2</sub> TiCl <sub>2</sub> , Zn, 1,4-CHD, THF, 23 °C	No conversion
2	<b>5.109</b>	H <sub>2</sub> (1 atm), Pd/C, EtOH, 23 °C	No conversion
3	<b>5.114</b>	Sml <sub>2</sub> , THF, MeOH, –78 °C	Very messy

<p>X = <math>\beta</math>-OH, <math>\alpha</math>-H: <b>5.109</b> X = O: <b>5.114</b></p> <p>X = <math>\beta</math>-OH, <math>\alpha</math>-H: <b>5.115</b> X = O: <b>5.116</b></p>

## 5.5.2 Pd-Catalyzed C3–C4 Alkene Reductive Transposition

Given our uncertainties regarding the stereoselective, non-directed installation of a C3 H atom from the concave face of the molecule, we next undertook a directed approach to C3–C4 alkene transposition and concomitant stereoselective placement of the C3 H atom. Specifically, given that we could access both C5- $\alpha$ - and C5- $\beta$ -functionalized substrates (see Section 5.3), we anticipated that we could leverage the stereochemical information at C5 to facilitate stereoselective C3 H placement. As one instance of this strategy, we investigated the Pd-catalyzed invertive reductive allylic transposition<sup>52</sup> of C5- $\alpha$ -carbonate **5.98** and C5- $\alpha$ -formate **5.117** (Table 5.16). The C4–C5 alkene of the desired product would then be transformed to the desired motif, with a  $\beta$ -disposed C5 hydroxy group and a C4–C20 *exo*-methylene. Under most conditions attempted, no reaction was observed (entries 1–3, 5); only at temperatures of 145 °C did we observe conversion of the starting material to a messy reaction mixture without the desired product (entry 4). Presumably, the observed lack of reactivity results from the steric demands associated with the nucleophilic displacement of the equatorially oriented C5 carbonate/formate from the concave face by the bulky Pd catalyst.

**Table 5.16:** Attempted Pd-catalyzed reductive transposition of **5.98** and **5.117**.

Entry	Substrate	Conditions	Results
1	<b>5.98</b>	Pd(OAc) <sub>2</sub> , PBu <sub>3</sub> , NH <sub>4</sub> CO <sub>2</sub> H, PhH, 23 °C	No conversion
2	<b>5.98</b>	Pd(acac) <sub>2</sub> , PBu <sub>3</sub> , NH <sub>4</sub> CO <sub>2</sub> H, THF, 65 °C	No conversion
3	<b>5.98</b>	Pd(dba) <sub>3</sub> •CHCl <sub>3</sub> , PPh <sub>3</sub> , NH <sub>4</sub> CO <sub>2</sub> H, PhMe, 105 °C	No conversion
4	<b>5.98</b>	[allylPdCl] <sub>2</sub> , HCO <sub>2</sub> H, Et <sub>3</sub> N, PPh <sub>3</sub> , DMF, 145 °C	Very messy
5	<b>5.117</b>	Pd(OAc) <sub>2</sub> , PBu <sub>3</sub> , NH <sub>4</sub> CO <sub>2</sub> H, THF, 65 °C	No conversion

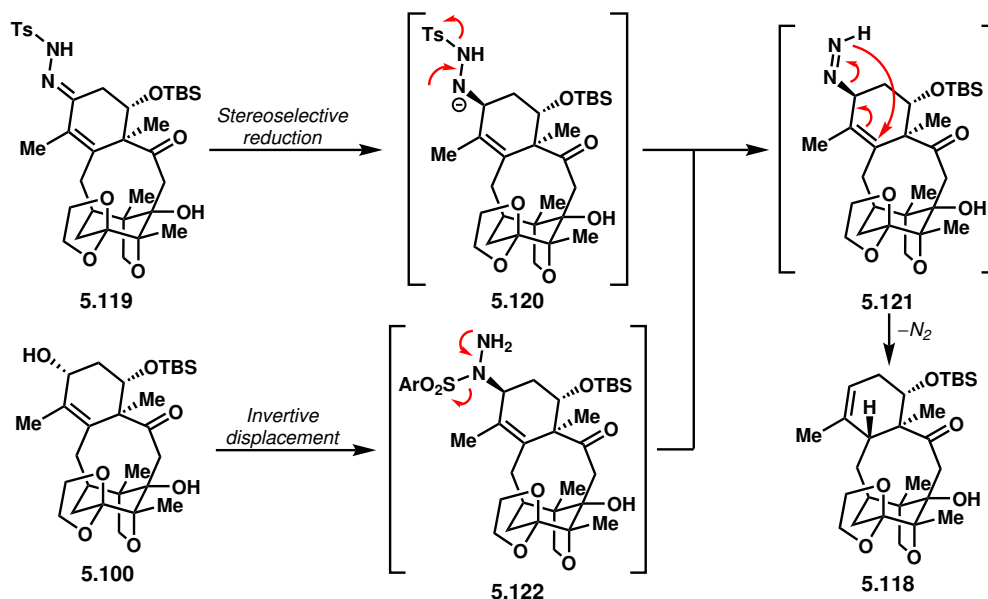
  

<p>X = OCO<sub>2</sub>Me: <b>5.98</b> X = OCHO: <b>5.117</b></p> <p><b>5.118</b></p>



### 5.5.3 Allylic Diazene Rearrangement

We next considered whether we could effect an allylic diazene rearrangement from  $\beta$ -disposed diazene **5.121** to **5.118** (Scheme 5.27). We proposed accessing diazene intermediate **5.121** via either the stereoselective reduction of C5-tosylhydrazone<sup>53</sup> **5.119** or via the invertive displacement (e.g, Mitsunobu reaction)<sup>54</sup> of C5- $\alpha$ -allylic alcohol **5.100**.



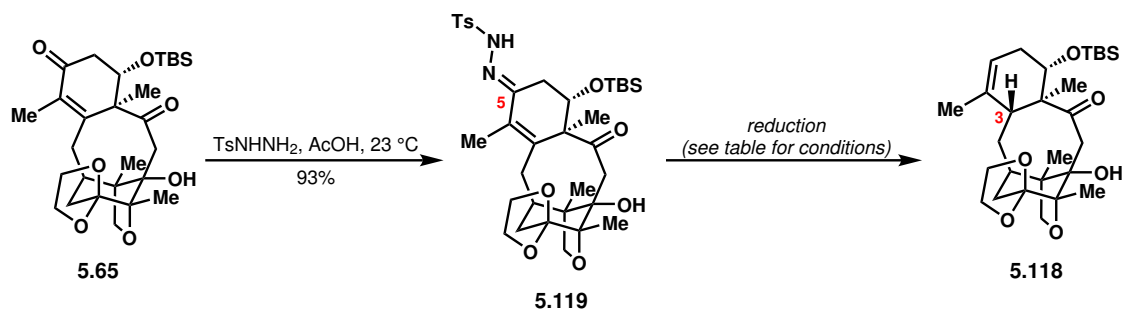
**Scheme 5.27:** Mechanism of allylic diazene rearrangement and preparation of precursor substrates.

We began by investigating the stereoselective reduction of tosylhydrazone **5.119**, which could be readily accessed from C5 ketone **5.65** in 93% yield (Table 5.17). Reduction with catecholborane as originally reported by Kabalka<sup>53a</sup> gave only the undesired epimer at C3, suggesting initial stereoselective reduction of the tosylhydrazone from the undesired  $\beta$ -face (entry 1), whereas attempted reduction with bis(benzoyloxy)borane<sup>53b</sup> yielded no conversion (entry 2). While attempted reductions with sodium borohydride<sup>55</sup> (entry 3) and STAB-H<sup>56</sup> (entry 4) were unfruitful, and use of  $NaCNBH_3$ <sup>57</sup> with  $BF_3 \cdot OEt_2$  in THF at 0 °C gave only the undesired C3 epimer (entry 5), we found that reduction with  $NaCNBH_3$  with HCl in DMF at 80 °C gave the desired product selectively over the undesired C3 epimer, albeit with moderate diastereoselectivity and amidst an otherwise complex reaction mixture (entry 6). Entries 5 and 6 together indicate that the diastereoselectivity of the reduction is sensitive not only to the structure of the reductant, but also to the choice of acid and/or solvent. Given our previous results with C5 carbonyl reduction (see Section 5.3), we hypothesized that use of larger reducing agents would improve the diastereoselectivity by favoring reduction of the tosylhydrazone from the desired, sterically less hindered  $\alpha$ -face. However, attempted reductions with bulky borane reagents (entries 7 and 8), borohydride reagents with or without Lewis acid at a variety of temperatures (entries 9–12), aluminum-based reductants (entries 14–16), and silane reductants under acidic conditions (17 and 18) failed to afford synthetically



useful quantities of the desired product **5.118**. In addition, we speculated that the acidity of the tosylhydrazone *N*-proton may have interfered with reduction by L-selectride, which might act as a base; however, treatment of an *N*-TBS protected<sup>58</sup> derivative of **5.119** with L-selectride only returned *N*-TBS cleaved product with no reduction (entry 13).

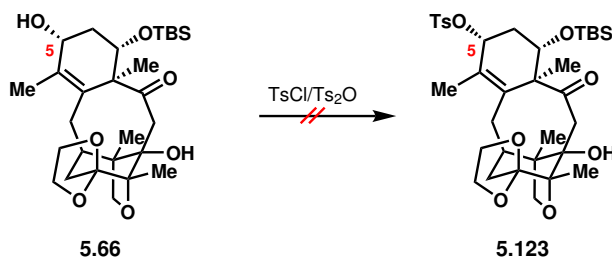
**Table 5.17:** Attempts at stereoselective C5 tosylhydrazone reduction/allylic diazene rearrangement. <sup>a</sup>*N*-TBS protected tosylhydrazone used as substrate.



Entry	Conditions	Results
1	catecholborane, $\text{CHCl}_3$ , 0 °C; then, $\text{NaOAc}\cdot 3\text{H}_2\text{O}$ , 0 °C to 60 °C	C3-epimer of <b>5.118</b>
2	$\text{BzOH}$ , $\text{BH}_3\cdot\text{THF}$ , $\text{CHCl}_3$ , 0 °C; then, $\text{NaOAc}\cdot 3\text{H}_2\text{O}$ , 23 °C	No conversion
3	$\text{NaBH}_4$ , $\text{AcOH}$ , 70 °C	Messy
4	STAB-H, $\text{AcOH}$ , $\text{THF}$ 23 °C to 60 °C	No conversion
5	$\text{NaCNBH}_3$ , $\text{BF}_3\cdot\text{OEt}_2$ , $\text{THF}$ , 0 °C	C3-epimer of <b>5.118</b>
6	$\text{NaCNBH}_3$ , $\text{HCl}$ , $\text{DMF}$ , 23 °C to 80 °C	1.5:1 <b>5.118</b> to C3-epimer of <b>5.118</b>
7	9-BBN, $\text{THF}$ , 0 °C to 75 °C; then, $\text{NaOAc}\cdot 3\text{H}_2\text{O}$	No conversion
8	pinacolborane, $\text{THF}$ , 23 °C; then, $\text{NaOAc}\cdot 3\text{H}_2\text{O}$ , 23 °C	Messy
9	L-selectride, $\text{THF}$ , -78 °C to 0 °C	No conversion
10	L-selectride, $\text{BF}_3\cdot\text{OEt}_2$ , $\text{THF}$ , 0 °C to 23 °C	Messy
11	L-selectride, $\text{THF}$ , 65 °C	Messy
12	L-selectride, $\text{CeCl}_3$ , $\text{THF}$ , -78 °C to 60 °C	Messy
13 <sup>a</sup>	L-selectride, $\text{THF}$ , 0 °C; then, $\text{AcOH}$ , $\text{TFE}$ , $\text{H}_2\text{O}$ , 23 °C	<b>5.119</b>
14	DIBALH, $\text{CH}_2\text{Cl}_2$ , 0 °C	1:1 <b>5.119</b> to C3-epimer of <b>5.118</b>
15	$\text{Al}(\textit{i}\text{-Bu})_3$ , $\text{PhH}$ , 23 °C	Messy
16	$\text{LiAl}(\text{O}\textit{t}\text{-Bu})_3\text{H}$ , $\text{THF}$ , 23 °C to 60 °C	No conversion
17	$\text{Et}_3\text{SiH}$ , $\text{TFA}$ , 0 °C	Decomp
18	$\text{BF}_3\cdot\text{OEt}_2$ , $\text{Et}_3\text{SiH}$ , $\text{CH}_2\text{Cl}_2$ , 23 °C; then, $\text{NaOAc}\cdot 3\text{H}_2\text{O}$ , 40 °C	Messy, some loss of ketal

With our attempts to stereoselectively reduce tosylhydrazone **5.119** failing to provide good yields of desired product **5.118**, we next turned to invertive displacement of C5- $\alpha$ -allylic alcohol **5.66**, anticipating that this strategy would grant us greater stereocontrol. Attempted synthesis of C5- $\alpha$ -tosylate **5.123** in preparation for invertive nucleophilic displacement was unsuccessful, yielding only a C5 chloride product when  $\text{TsCl}$  was used as the tosylating agent and a complex reaction mixture when  $\text{Ts}_2\text{O}$  was used (Scheme 5.28). As a result, and encouraged by our previous success at conversion of **5.66** to the  $\beta$ -disposed cinnamoyl ester via Mitsunobu reaction (see Scheme 5.12, Section 5.3), we turned to Mitsunobu displacements of the C5 allylic hydroxy group. Mitsunobu reaction with an arylsulfonyl hydrazide nucleophile

proved more difficult than Mitsunobu reaction with a carboxylate nucleophile, in part due to the increased steric bulk and decreased acidity of the arylsulfonyl hydrazine reagent.

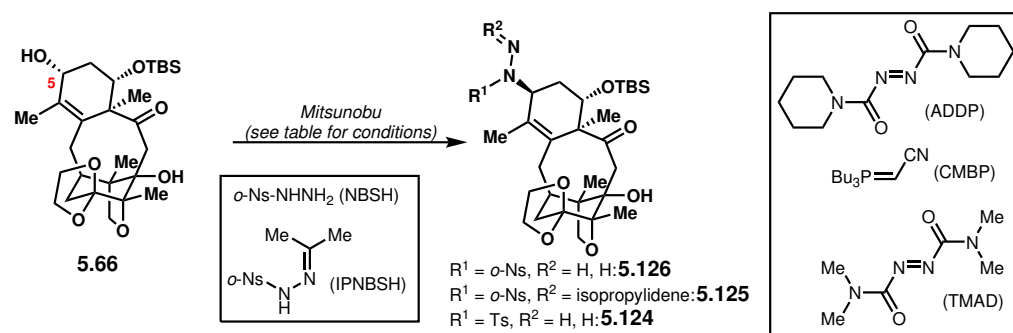


**Scheme 5.28:** Attempted preparation of C5-tosylate **5.123**.

Our studies began with the attempted Mitsunobu displacement of the allylic hydroxy group with *o*-nitrobenzenesulfonyl hydrazine (NBSH),<sup>54a</sup> with no conversion observed (entry 1, Table 5.18). *p*-Ts-hydrazine was not a competent nucleophile to displace the unactivated allylic hydroxy group<sup>59</sup> (entry 2), but was competent under Mitsunobu conditions, albeit delivering product **5.124** in only 21% yield (entry 3). Use of the more stable *N*-isopropylidene-*N'*-*o*-nitrobenzenesulfonyl hydrazine (IPNBSH) reagent provided desired product **5.125** in an improved 39% yield (48% based on recovered starting material) (entry 4); interestingly, the *p*-nitrobenzene derivative of IPNBSH was not as suitable for the reaction (entry 5). Alternative phosphine/diazo reagent combinations<sup>60–62</sup> did not improve the yield over the use of PPh<sub>3</sub>/DIAD (entries 6–11). When a substrate with an acetate rather than a TBS ether at C7 was used, the yield drops considerably, with more elimination products observed (entry 12). Presumably, given the higher electron-withdrawing ability and less demanding steric profile of an acetate group, E2 elimination of the C5 oxyphosphonium intermediate becomes more favorable. The order of addition of reagents, which has been observed to be an important variable for Mitsunobu reactions,<sup>63</sup> in our case did not significantly affect the outcome (entries 13 and 14), nor did running the reaction at 23 °C (entry 15). At 50 °C or 0 °C, however, the reaction yield suffered (entries 16 and 17). A solvent screen identified toluene as the only solvent comparable to THF (entries 18–22). Increasing the reaction concentration did not improve the reaction yield (entry 23), nor did the addition of excess neopentyl alcohol (entry 24), which has been previously observed to improve reaction yields.<sup>63</sup> The addition of triethylamine seemed to facilitate the reaction, presumably to assist in the deprotonation of the IPNBSH nucleophile, whose acidity is lower than that of traditionally used carboxylic acids (entry 25). From the Mitsunobu product **5.125**, while we were unable to effect hydrazone exchange with phenylhydrazine<sup>54b</sup> or hydrolyze the hydrazone under neutral aqueous conditions to trigger the allylic diazene rearrangement, we found that the use of slightly acidic aqueous conditions with extended reaction times was sufficient for hydrolysis. However, when the sulfonohydrazide product **5.125** was subjected to these hydrolysis/allylic diazene rearrangement conditions in the same pot after Mitsunobu inversion, the yield of the final trisubstituted alkene product **5.118** was fairly low (entry 26).

Notably, under most reaction conditions affording desired invertive products at C5 from C10,C2-unoxidized compound **5.66**, we also observed the stereoretentive displacement product as a minor diastereomer (e.g., 5.6:1 d.r. under the conditions in entry 4, Table 5.18). When we attempted to carry out Mitsunobu displacement on substrates with additional C10

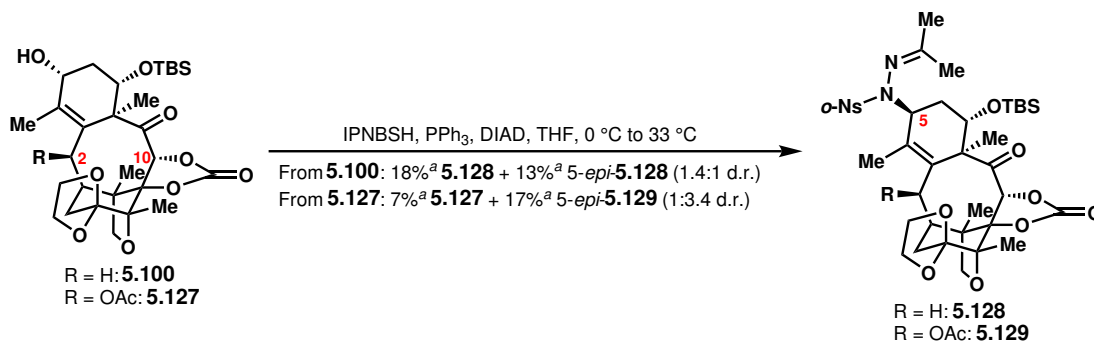
**Table 5.18:** Attempts at invertive displacement of C5 allylic alcohol. <sup>a</sup>All yields are <sup>1</sup>H NMR yields with mesitylene as an internal standard. <sup>b</sup>Conditions provided are deviations from those used in entry 4. brsm = based on recovered starting material. Order of addition **A** = add diazo reagent to phosphine and substrate in solvent, stir for 10 min at 0 °C; then, add sulfonohydrazide in solvent, warm to reaction temperature. Order of addition **B** = pre-mix phosphine and diazo reagent at 0 °C, then add substrate and sulfonohydrazide in solvent, warm to reaction temperature. Order of addition **C** = pre-mix phosphine, substrate, and sulfonohydrazide in solvent, then add diazo reagent slowly over 1 min.



Entry	Conditions	Results <sup>a</sup>
1	NBSH, PPh <sub>3</sub> , DEAD, <i>N</i> -methylmorpholine, -15 °C to 23 °C	No conversion
2	<i>p</i> -TsNHNH <sub>2</sub> , MeNO <sub>2</sub> , 65 °C, o/n	No conversion
3	TsNHNH <sub>2</sub> , PPh <sub>3</sub> , DIAD, THF, 0 °C to 23 °C	21%
4	IPNBSH (3 equiv), PPh <sub>3</sub> (3 equiv), DIAD (3 equiv), THF (0.02 M), 0 °C to 33 °C, 14 h, order of addition <b>A</b>	39% (48% brsm)
5	<i>p</i> -IPNBSH instead of <i>o</i> -IPNBSH <sup>b</sup>	13% (26% brsm)
6	IPNBSH, PBu <sub>3</sub> , ADDP, THF, 0 °C to 33 °C	No conversion
7	IPNBSH, PBu <sub>3</sub> , TMAD, THF/PhMe (1:1), 0 °C to 33 °C	No conversion
8	IPNBSH, CMBP, PhMe, 80 °C	No conversion
9	DEAD instead of DIAD <sup>b</sup>	41% (46% brsm)
10	Di- <i>t</i> -butyl azodicarboxylate instead of DIAD <sup>b</sup>	23% (47% brsm)
11	Dibenzyl azodicarboxylate instead of DIAD <sup>b</sup>	No conversion
12	C7-OAc as substrate instead of <b>5.66</b> <sup>b</sup>	18%, observed elimination products
13	Order of addition <b>B</b> <sup>b</sup>	41% (43% brsm)
14	Order of addition <b>C</b> <sup>b</sup>	36% (44% brsm)
15	23 °C for 24 h instead of 33 °C for 14 h <sup>b</sup>	32% (43% brsm)
16	50 °C instead of 33 °C <sup>b</sup>	8% (24% brsm)
17	0 °C instead of 33 °C <sup>b</sup>	6% (14% brsm)
18	PhMe instead of THF, order of addition <b>C</b> <sup>b</sup>	37% (43% brsm)
19	Et <sub>2</sub> O instead of THF, order of addition <b>C</b> <sup>b</sup>	No conversion
20	CH <sub>2</sub> Cl <sub>2</sub> instead of THF <sup>b</sup>	6% (15% brsm)
21	MeCN instead of THF <sup>b</sup>	No conversion
22	<i>N</i> -methylmorpholine instead of THF <sup>b</sup>	No conversion
23	0.09 M instead of 0.02 M, order of addition <b>C</b> <sup>b</sup>	29% (39% brsm)
24	2 equiv additional neopentyl alcohol <sup>b</sup>	No conversion
25	Additional 3 equiv Et <sub>3</sub> N <sup>b</sup>	42/8/29; 59
26	After Mitsunobu: add AcOH, TFE, H <sub>2</sub> O, 23 °C, 54 h <sup>b</sup>	16% <b>5.118</b> (26% brsm)

and/or C2 oxidation, we found that the diastereoselectivity of the reaction decreased; with C10-oxidized substrate **5.100**, the diastereoselectivity was 1.4:1, and with C2-OAc substrate **5.127**, the stereoretentive product was the major diastereomer (d.r. 1:3.4), with the desired

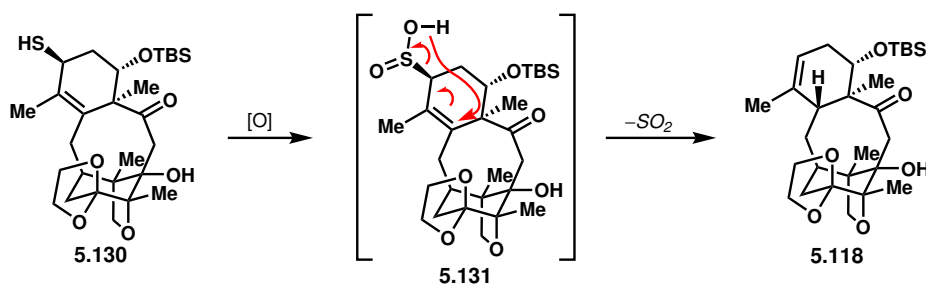
product afforded in only 7% yield (Scheme 5.29). Presumably, the electron-withdrawing oxygenation at C10 and C2 increased the electron deficiency at C5, which lowered the kinetic barrier to displacement of the initially formed sulfonohydrazide by a second molecule of IPNBSH. This stereoretentive, C5- $\alpha$  double displacement product would be the more thermodynamically stable product, with the bulky sulfonohydrazide substituent oriented in the equatorial position of the C ring.



**Scheme 5.29:** Mitsunobu reaction on C10 and/or C2-oxidized substrates **5.100** and **5.127**. <sup>a</sup>1H NMR yield with mesitylene as internal standard.

### 5.5.4 Allylsulfinic Acid Rearrangement

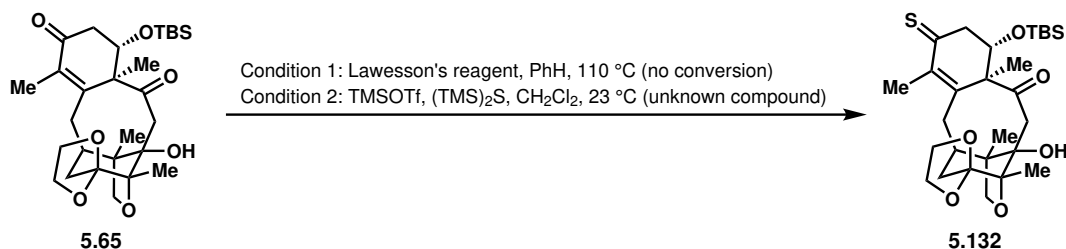
Given the low yield of the Mitsunobu reaction with IPNBSH as nucleophile on the C10,C2-oxidized substrate **5.127**, and lacking a strategy to restore favorable diastereoselectivity, we suspended our investigations of an allylic diazene rearrangement strategy for C3–C4 alkene transposition in favor of a similar allylsulfinic acid rearrangement<sup>64,65</sup> strategy. We envisioned that, if we could access C5-allylic thiol **5.130** as a single diastereomer, oxidation to the sulfinic acid (**5.131**) would trigger a sulfinyl retro-ene reaction, transposing the C3–C4 alkene with concomitant loss of SO<sub>2</sub> to stereoselectively introduce a hydrogen atom at C3 from the  $\beta$ -face (Scheme 5.30).



**Scheme 5.30:** Mechanism of allylsulfinic acid rearrangement for C3–C4 alkene transposition.

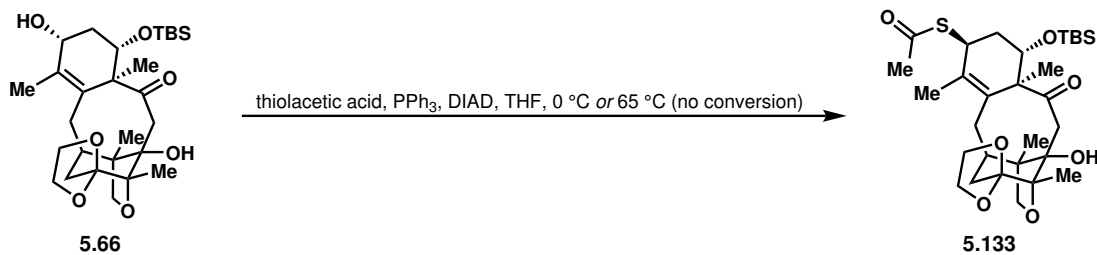
We briefly investigated introduction of the allylic C5- $\beta$ -sulfhydryl group by stereoselective reduction of the corresponding C5 thione. However, the C5 thione **5.132** proved difficult to synthesize from enone **5.65** with Lawesson's reagent or under TMSOTf-promoted

conditions<sup>66</sup> (Scheme 5.31). The inaccessibility of thione **5.132** was partially expected, as  $\alpha,\beta$ -unsaturated thiocarbonyl compounds are tricky to handle and not particularly stable, with their synthesis complicated by facile tautomerization to the enethiol.<sup>67</sup>



**Scheme 5.31:** Attempted synthesis of C5 thione **5.132**.

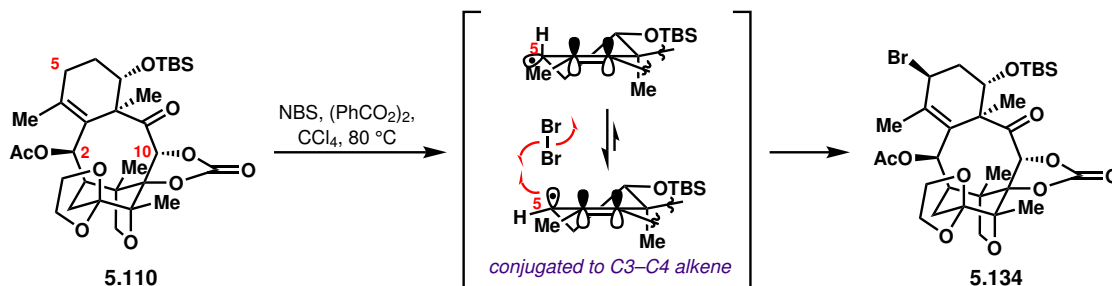
We also briefly investigated the Mitsunobu reaction of allylic alcohol **5.66** with thiolacetic acid as a nucleophile. We had expected this Mitsunobu reaction to proceed more readily than when IPNBSH was used as a nucleophile given the lower  $pK_a$  of thiolacetic acid. In addition, we hoped that the smaller size of thiolacetic acid would both make initial nucleophilic displacement more favorable, as well as lower the energy difference between the axial C5- $\beta$  and the equatorial C5- $\alpha$  isomers, making double displacement less favorable. To our surprise, when allylic alcohol **5.66** was subjected to Mitsunobu conditions, we observed no conversion to thioester product **5.133** (Scheme 5.32). It should be noted that our Mitsunobu reactions with IPNBSH were generally plagued by reproducibility issues, with reaction conditions that had once afforded desired product often yielding no conversion upon repetition. This phenomenon might also be responsible for the lack of observed conversion of **5.66** to **5.133**, although this reaction was repeated multiple times without success.



**Scheme 5.32:** Attempted synthesis of C5 thioester **5.133**.

Given our challenges installing a sulfhydryl group via the C5 thione or C5 allylic alcohol, and given that each of these approaches would require multiple steps, at this stage we began investigating a potentially more efficient strategy for the synthesis of thiol **5.130**. Our previous studies on C5 functionalization suggested that the C5 position was one of the most activated towards radical C–H abstraction (see Section 5.3), and that radical trapping would occur on the  $\beta$ -face. Therefore, a radical allylic thiolation could potentially provide access to thiol **5.130** site- and stereoselectively from the C5-unfunctionalized compound in one step. While the clean C5 bromination of C10,C2-unfunctionalized tetracycle **4.14** seemed to require the initial installation of a C14 bromide to inactivate the C1 position, we hypothesized that a C2-OAc group could serve the same purpose. Therefore, as a proof of concept, we

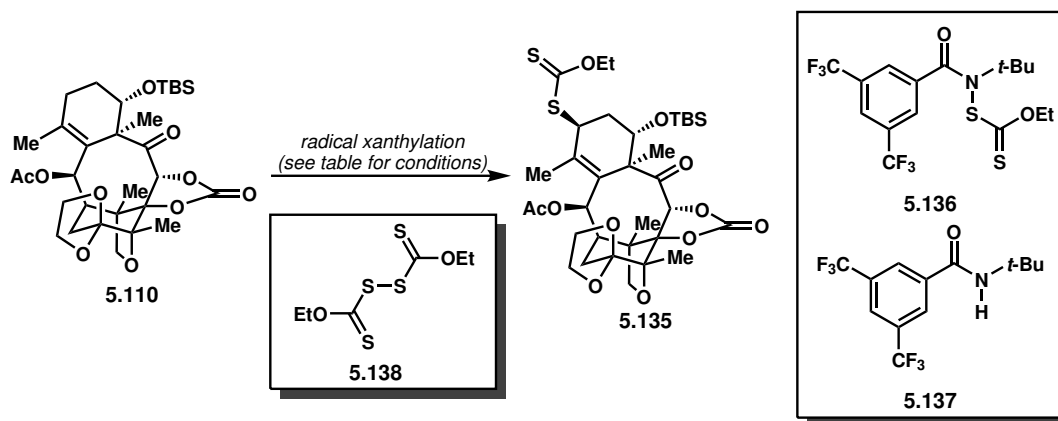
subjected C10,C2-oxidized compound **5.110** to radical bromination conditions; gratifyingly, the only identifiable product was C5- $\beta$ -bromide **5.134** (Scheme 5.33). We hypothesize that the stereoselectivity arises from the conjugative stabilization of the  $\beta$ -epimer of the C5 radical resulting from hydrogen atom abstraction, and thus preferential radical trapping from the concave  $\beta$ -face.<sup>68</sup>



**Scheme 5.33:** Site- and stereoselective radical bromination of **5.110**.

We then began to examine radical C5-H xanthylation to afford **5.135** (Table 5.19). With the xanthylamide reagent developed by Alexanian (**5.136**),<sup>69</sup> we did not observe any conversion of starting material (entries 1 and 2); however, we did observe amide **5.137** and **5.138**, suggesting that homolysis of the reagent was taking place. It is possible that the *t*-butyl substituent of the amidyl radical of **5.136** renders it too sterically hindered to approach the concave face of substrate **5.110** for C-H abstraction. Attempted radical xanthylation using diethylxanthogen disulfide (**5.138**) directly under radical initiation conditions also did not yield conversion of the starting material (entries 3–5). The S-H bond formed from

**Table 5.19:** Attempted site- and stereoselective radical xanthylation of **5.110**.

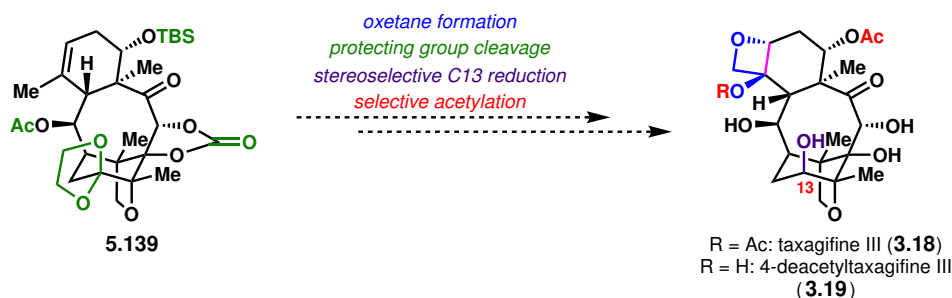


Entry	Conditions	Results
1	<b>5.136</b> , PhCF <sub>3</sub> , blue LED, 23 °C	No conversion; <b>5.137</b> and <b>5.138</b> observed
2	<b>5.136</b> , C <sub>6</sub> F <sub>6</sub> , blue LED, 80 °C	No conversion; <b>5.137</b> and <b>5.138</b> observed
3	<b>5.138</b> , AIBN, PhH, 80 °C	No conversion
4	<b>5.138</b> , (PhCO <sub>2</sub> ) <sub>2</sub> , CCl <sub>4</sub> , 80 °C	No conversion
5	<b>5.138</b> , PhH, blue LED, 23 °C	No conversion

xanthyl radical C–H abstraction may not be strong enough for the abstraction event to be thermodynamically favorable. The development and synthesis of less hindered xanthylamide reagents may be required for the successful C5 xanthylation of **5.110**.

## 5.6 Model System Studies of Future Transformations

After successful transposition of the C3–C4 double bond to the C4–C5 double bond, several transformations would be needed to complete the syntheses of taxagifine III or 4-deacetyltaxagifine III: 1) oxetane formation, 2) protecting group cleavages, 3) stereoselective C13 carbonyl reduction, and 4) selective acetylation of the C7 and/or C4 hydroxy groups (Scheme 5.34). In order to streamline endgame investigations, we decided to examine each of these transformations on a model system.

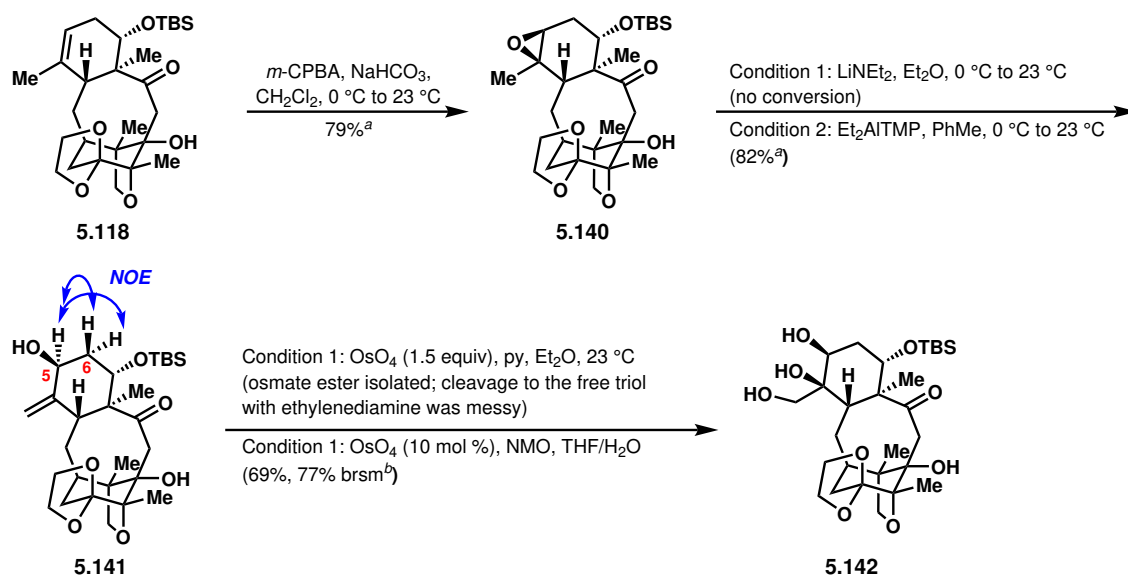


**Scheme 5.34:** Transformations required to convert **5.139** to taxagifine III and 4-deacetyltaxagifine III.

### 5.6.1 Oxetane Formation

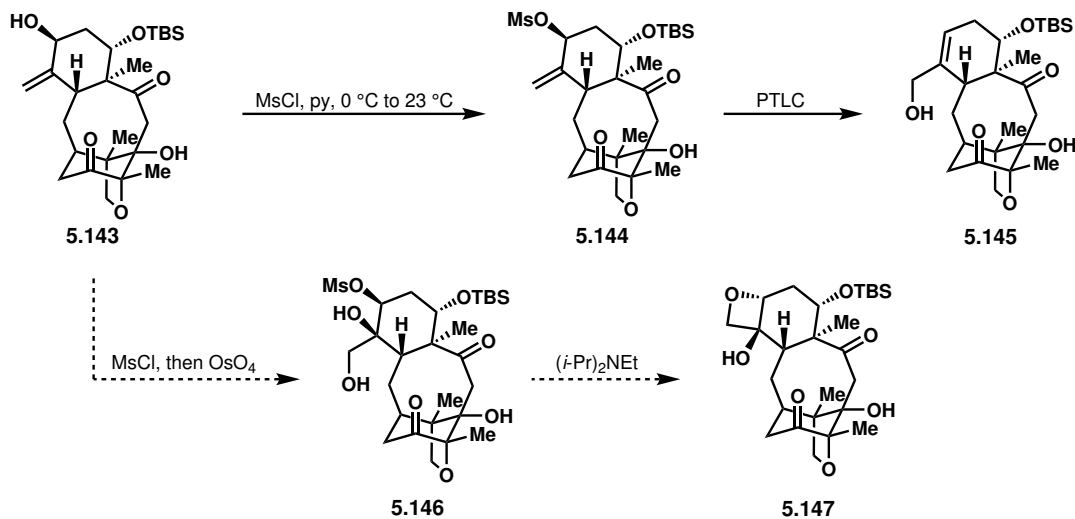
On the basis of previous syntheses of taxol and simpler taxoid natural products, we envisioned that the trisubstituted C4–C5 double bond in **5.118** could be readily transformed to the oxetane. First, **5.118** was epoxidized to deliver **5.140** as a single diastereomer (Scheme 5.35). While attempted epoxide ring-opening with  $\text{LiNEt}_2$  yielded no conversion, treatment with *in situ*-generated  $\text{Et}_2\text{AlTMP}$  effectively generated *exo*-methylene-containing compound **5.141**, whose stereochemistry was determined by observed NOE correlations between the equatorial C5- $\beta$  proton and the two methylene protons at C6. Upon extended reaction times, ketal cleavage could also be observed. Dihydroxylation of **5.141** with stoichiometric osmium tetroxide afforded an osmate ester product, whose cleavage to the free triol (**5.142**) with ethylenediamine was qualitatively not high-yielding. As a result, we turned to Upjohn dihydroxylation conditions instead, which afforded the triol product in 69% yield. The diastereoselectivity of the dihydroxylation was not determined experimentally, but is tentatively assumed based on observations from previous syntheses of taxol.

Triol **5.142** could presumably be transformed to the oxetane with protocols established in previous syntheses of taxol; however, these protocols typically require extra protecting group manipulations. As a result, we also investigated initial mesylation of allylic alcohol **5.143** prior to dihydroxylation (Scheme 5.36); however, we found that upon attempted purification



**Scheme 5.35:** Towards the oxetane on a model system. <sup>a</sup>Isolated yield. <sup>b</sup><sup>1</sup>H NMR yield with mesitylene as internal standard.

of mesylate **5.144**, primary allylic alcohol **5.145** was generated via S<sub>N</sub>2'. Future efforts will examine one-pot mesylation/dihydroxylation as established in the Sato/Chida synthesis of taxol,<sup>70</sup> whose product diol **5.146** could be transformed in one step to the oxetane **5.147**.

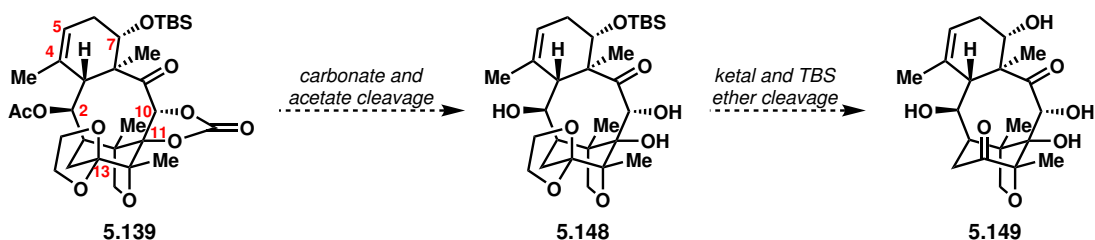


**Scheme 5.36:** Toward a two-step construction of the oxetane from model system **5.143**.

## 5.6.2 Protecting Group Cleavages

From C4–C5 trisubstituted alkene **5.139**, we envision that the immediate subsequent steps would involve, first, the concomitant cleavage of the C2-acetate and C10,C11-carbonate, and second, the concomitant cleavage of the C13-ketal and C7-TBS ether (Scheme 5.37).

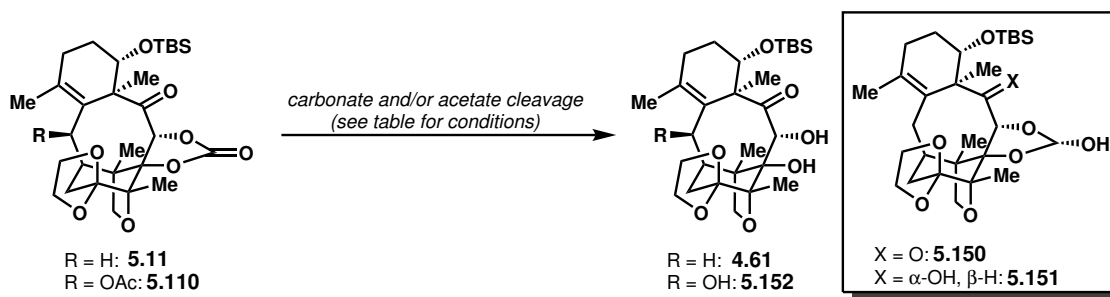




**Scheme 5.37:** Proposed sequence of protecting group cleavages from **5.139**.

We began investigating each of these protecting group cleavage events on model systems. From **5.11** lacking a C2-OAc group, milder carbonate cleavage conditions were ineffective (entries 1 and 2, Table 5.20), and hydride reagents tended to give incomplete carbonate cleavage and/or C9 carbonyl reduction products (e.g., **5.150** and **5.151**) (entry 3). We eventually found that carbonate cleavage occurred readily under  $\text{K}_2\text{CO}_3/\text{MeOH}$  conditions at elevated temperatures (entry 4). However, when we subjected allylic C2-OAc compound **5.110** to these conditions, we isolated an undesired product whose identity could not be established. This compound's lack of a TBS group and putative possession of a C2–C3 *trans*-alkene suggested that it was the result of undesired reactivity, and may involve the  $\text{S}_{\text{N}}2'$  displacement of the C2-acetoxy group. As a result, we suspect that this undesired reactivity may not be replicated on the real system, which will bear a C4–C5 alkene, where the C2-acetoxy group is not allylic.

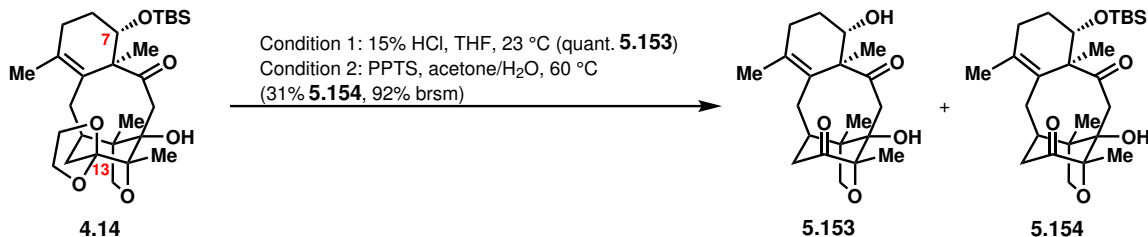
**Table 5.20:** Carbonate and/or acetate cleavages on model systems.  $^1\text{H}$  NMR yield with mesitylene as internal standard.



Entry	Substrate	Conditions	Results
1	<b>5.11</b>	$\text{LiOH}$ , THF/ $\text{H}_2\text{O}$	No conversion
2	<b>5.11</b>	py/ $\text{H}_2\text{O}$ , reflux	No conversion
3	<b>5.11</b>	DIBALH, $\text{CH}_2\text{Cl}_2$ , $-78^\circ\text{C}$	2:1 <b>5.150</b> : <b>5.151</b>
4	<b>5.11</b>	$\text{K}_2\text{CO}_3$ , MeOH, reflux	69% <sup>a</sup> <b>4.61</b>
5	<b>5.110</b>	$\text{K}_2\text{CO}_3$ , MeOH, reflux	Unknown compound; no TBS group; C2–C3 <i>trans</i> -alkene?

We next examined the concomitant cleavage of the C13 ketal and C7 TBS ether. We quickly identified that treatment of **4.14** with aqueous HCl readily delivered desired product **5.153** (Scheme 5.38). We also found that treatment with PPTS afforded selective ketal cleavage product **5.154** if the reaction was worked up prematurely, which could be desired

for certain variations of the endgame.



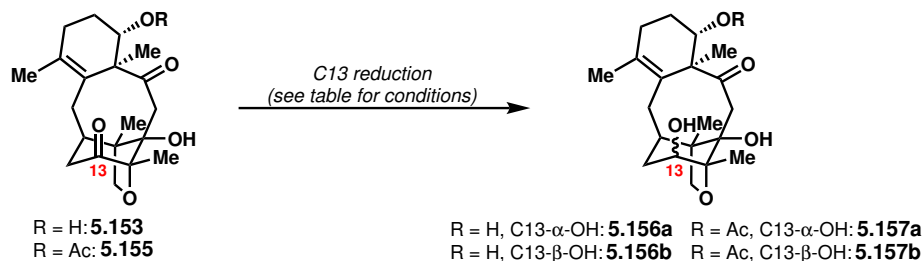
**Scheme 5.38:** Ketal and/or TBS ether cleavages on model system.

### 5.6.3 Stereoselective C13 Carbonyl Reduction

Once the C13 carbonyl has been unveiled, stereoselective carbonyl reduction would be required to afford the C13- $\beta$ -hydroxy group found in the natural products taxagifine III and 4-deacetyltaxagifine III. The presence of the ether bridge renders the stereoselectivity of the carbonyl reduction less predictable, as both faces of the carbonyl could be said to be concave. In addition, the ether bridge is not present in taxol, and so the stereoselectivity of C13 carbonyl reduction conditions used in previous syntheses in taxol could not be expected to directly translate to taxagifine-like systems. As a result, we decided to study the stereoselectivity of C13 carbonyl reduction experimentally on model taxagifine-like compounds.

We first tried C13 carbonyl reduction on **5.153** with a free C7-hydroxy group. Under Luche reduction conditions, only undesired C13- $\alpha$ -OH epimer **5.156a** was obtained (entry 1, Table 5.21). When sodium borohydride or K-selectride were used, we only observed complex reaction mixtures (entries 2 and 3). Hypothesizing that retro-aldol pathways initiating from the free C7-OH were responsible for the observed undesired reactivity, we next attempted

**Table 5.21:** Attempted stereoselective C13 carbonyl reductions on model systems.

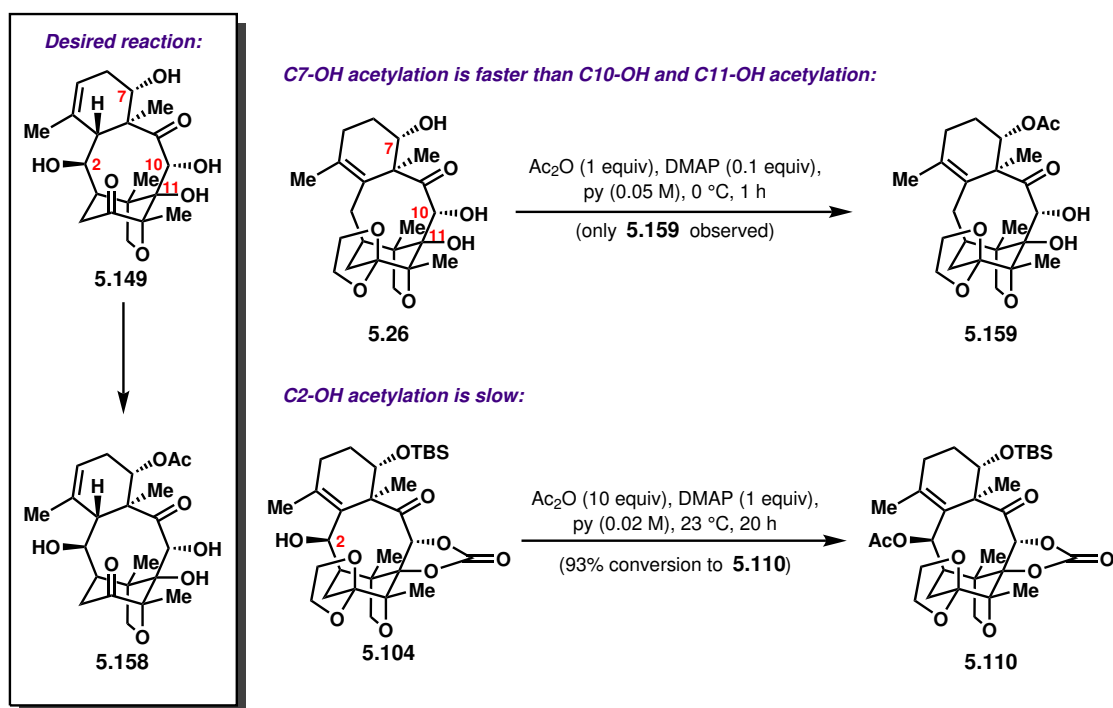


Entry	Substrate	Conditions	Results
1	<b>5.153</b>	NaBH <sub>4</sub> (2 equiv), CeCl <sub>3</sub> •7H <sub>2</sub> O (2 equiv), MeOH, 0 °C	82% <b>5.156a</b>
2	<b>5.153</b>	NaBH <sub>4</sub> , MeOH, 0 °C	Messy
3	<b>5.153</b>	K-selectride, THF, -78 °C	Messy
4	<b>5.155</b>	NaBH <sub>4</sub> (60 equiv), CeCl <sub>3</sub> •7H <sub>2</sub> O (3 equiv), MeOH, 20 °C	1:1.2 <b>5.157b</b> : <b>5.157a</b>
5	<b>5.155</b>	NaBH <sub>4</sub> , MeOH, -10 °C	2.5:1 <b>5.157b</b> : <b>5.157a</b>
6	<b>5.155</b>	K-selectride, THF, -23 °C	Messy

C13 carbonyl reduction on C7-OAc compound **5.155**. When we used Luche reduction conditions that were reported to yield only the C13- $\beta$ -hydroxy isomer when carried out on taxagifine,<sup>71</sup> we observed an approximately equimolar mixture of diastereomers **5.157a** and **5.157b** (entry 4). In contrast, treatment with sodium borohydride at  $-10\text{ }^{\circ}\text{C}$  afforded the desired compound **5.157b** as the major diastereomer, albeit with modest diastereoselectivity (entry 5). It should be noted that the inclusion of  $\text{CeCl}_3$  has previously been shown to invert the diastereoselectivity of sodium borohydride reductions.<sup>72</sup> Finally, conditions with K-selectride, which had been used for C13 carbonyl reduction in Mukayama's total synthesis of taxol,<sup>73</sup> gave only a complex reaction mixture.

#### 5.6.4 Selective C7-OH and/or C4-OH Acetylations

Lastly, we investigated the acetylations of the C7- and C4-hydroxy groups, as hydroxy groups at these positions are the only that ones are acetylated in the natural products. From intermediate **5.149**, we envisioned that selective acetylation of the C7-hydroxy group would need to be carried out in the presence of the C10-, C11-, and C2-hydroxy groups (Scheme 5.39). We therefore decided to investigate the propensity for acetylation at each of these positions on model systems. On **5.26** bearing free hydroxy groups at C7, C10, and C11, acetylation with  $\text{Ac}_2\text{O}$ /DMAP in pyridine proceeded to deliver solely C7-OH-acetylated product **5.159** in 1 h at  $0\text{ }^{\circ}\text{C}$ , indicating that the C7-OH group could be acetylated faster than the C10- and C11-OH groups. In addition, acetylation of the C2-OH in compound **5.104** was sluggish, with full conversion not yet reached after 20 h with large excesses of reagents at  $23\text{ }^{\circ}\text{C}$ . Together, these acetylation studies suggest that selective C7-OH acetylation of **5.149**



**Scheme 5.39:** Studies indicating that selective C7-OH acetylation of **5.149** is plausible.

is plausible, although the model systems used presumably have slightly different steric and electronic profiles than **5.149**.

While we lacked access to oxetane-bearing compounds to experimentally probe the rate of C4-OH acetylation, we can make some tentative statements given the rate of C4-OH acetylations in previous syntheses of taxol. Surveying these syntheses, late-stage C4-OH acetylation with an Ac<sub>2</sub>O/DMAP/pyridine system typically required reaction times of 13–25 hours at 23 °C, and was always carried out in the absence of other free hydroxy groups.<sup>73–75</sup> Therefore, it is likely that selective C4-OH acetylation would not be possible in the presence of a free C2-hydroxy group, with free hydroxy groups at C10 and C13 potentially interfering as well. As a result, it may be best for acetylation of the C4-OH to be attempted when these other hydroxy groups have been protected.

## 5.7 Studies Toward Other Taxoid Cores and Other Oxidation Patterns

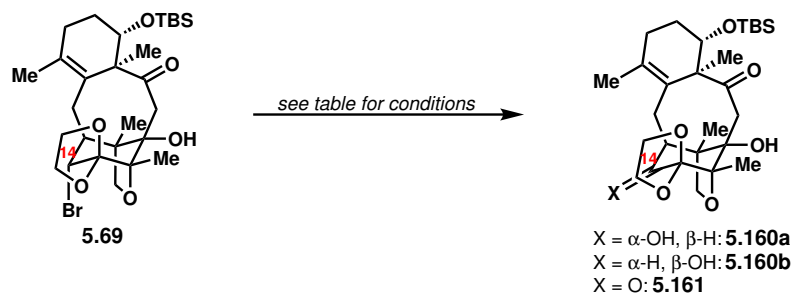
While we were pursuing total syntheses of taxagifine III and 4-deacetyltaxagifine III, we were also exploring oxidations at positions not oxidized in these particular natural products, either for the eventual synthesis of non-natural taxagifine-like derivatives or to enable access to other taxoid natural products with oxidation at these positions; in particular, we explored oxidations at C14 and C19. In addition, we found that we were able to translate the tetracyclic core of the taxagifine-like natural products to both unnatural and other natural taxoid cores.

### 5.7.1 C14 and C19 Oxidation

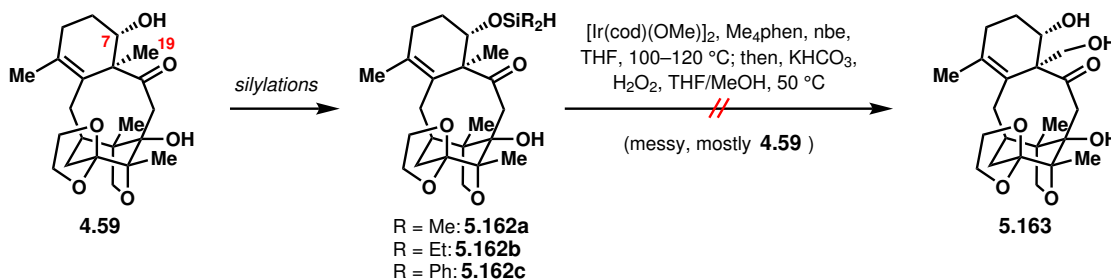
Given that we already had access to C14-brominated product **5.69** (see Section 5.3), we took the opportunity to attempt installation of C14-oxygenation, which is found in many taxoid natural products, typically at the alcohol oxidation state as the  $\alpha$ -isomer (Table 5.22).<sup>76</sup> With silver-mediated substitution conditions,<sup>20</sup> we were unable to install oxygenation at C14 (entries 1 and 2). Attempted Kornblum and Ganem oxidations did not proceed (entries 3 and 4), and attempted oxygenation via a C14 radical<sup>77</sup> led to decomposition (entry 5). Finally, we discovered that hybrid Pd-radical generation followed by trapping with TEMPO<sup>78</sup> generated the C14- $\alpha$  TEMPO adduct; the N–O bond could then be cleaved under reductive Zn/AcOH conditions to give compound **5.160a**, albeit in low yields (entry 6). Alternatively, after TEMPO adduct generation, *N*-oxidation and Cope elimination could be effected in the same pot to generate C14 carbonyl compound **5.161** (entry 7). The Pd(I)-mediated process used here represents a new strategy for transforming alkyl bromides to hydroxy or carbonyl groups on substrates where steric hindrance may impede more traditional methods.

We also briefly investigated the possibility of using the C7 hydroxy group to direct oxidation at C19; this would enable access to several C19-oxidized taxagifine-like natural products. Thus, we prepared (hydrido)silyl ethers **5.162a–5.162c** and subjected them to directed C–H silylation/Tamao-Fleming oxidation as reported by Hartwig (Scheme 5.40).<sup>79</sup> However, for each (hydrido)silyl ether, we never observed synthetically useful yields of the desired product **5.163**, with reaction mixtures often being complex and with the major component being recovered **4.59**, indicating unsuccessful C–H silylation.

**Table 5.22:** Installation of C14 oxygenation from C14 bromide **5.69**.



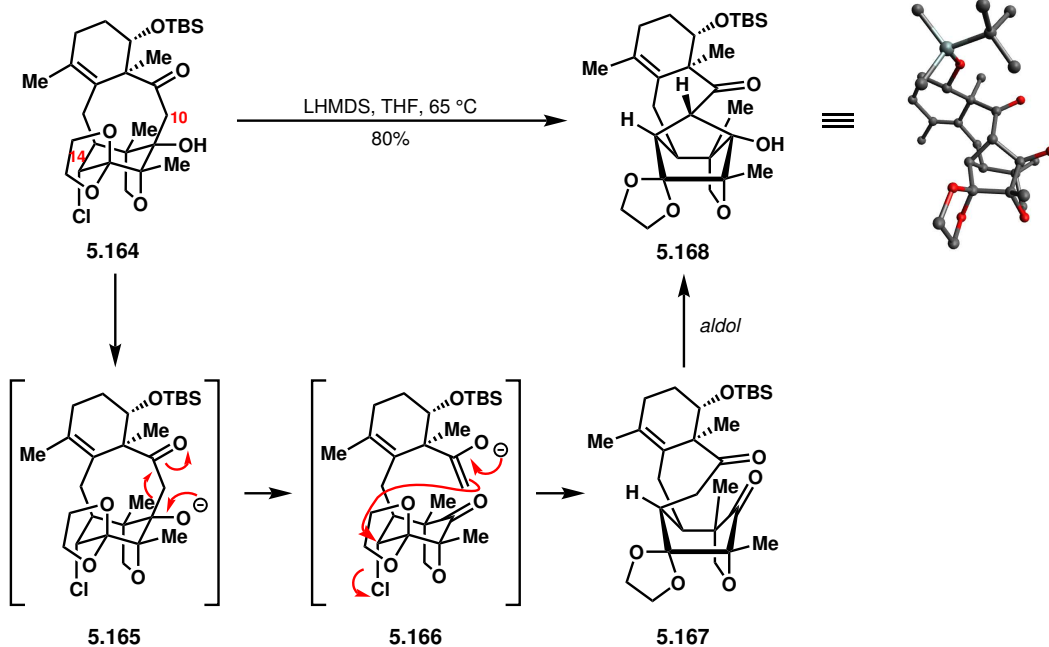
Entry	Conditions	Results
1	AgOTf, 2,6-dtbpy, TMSOH, 4 Å MS, PhMe, 110 °C	No conversion
2	AgNO <sub>3</sub> , acetone/H <sub>2</sub> O (1:1), 80 °C	Decomp
3	AgBF <sub>4</sub> , DMSO, 65 °C; then, Et <sub>3</sub> N, 23 °C	No conversion
4	Ag <sub>2</sub> O, pyridine <i>N</i> -oxide, MeCN, 60 °C	No conversion
5	Bu <sub>3</sub> SnH, AIBN, O <sub>2</sub> , PhMe, 80 °C	Messy
6	1. Pd(OAc) <sub>2</sub> , Xantphos, Cs <sub>2</sub> CO <sub>3</sub> , TEMPO, blue LED, PhH, 23 °C; 2. Zn, AcOH/THF	After 1: 85% C14- $\alpha$ TEMPO adduct; after 2: <b>5.160a</b> observed, messy
7	Pd(OAc) <sub>2</sub> , Xantphos, Cs <sub>2</sub> CO <sub>3</sub> , TEMPO, blue LED, PhH, 23 °C; then, <i>m</i> -CPBA, CH <sub>2</sub> Cl <sub>2</sub> , 23 °C	83% <b>5.161</b>



**Scheme 5.40:** Attempted C19 oxidation by C7-directed C19-H silylation/Tamao-Fleming oxidation.

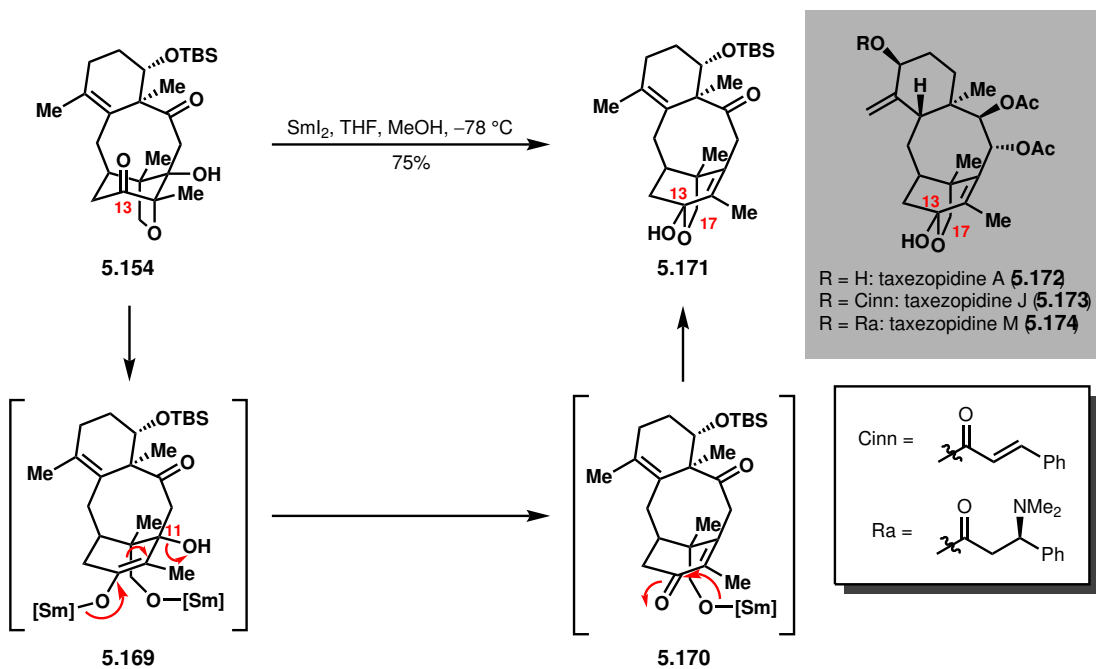
## 5.7.2 Access to Unnatural and Other Natural Taxoid Cores

While investigating the reactivity of C14 chloride compound **5.164**, we discovered that treatment with LHMDS afforded unusual pentacyclic compound **5.168**, whose structure was unambiguously confirmed by X-ray crystallographic analysis (Scheme 5.41). This pentacycle contains an additional bond formed between C10 and C14, not found in any taxoid natural product. In light of our previous difficulties deprotonating at C10 with LHMDS (see Section 5.1.1), we hypothesize that direct deprotonation and cyclization at C10 does not take place; rather, retro-aldol reaction from alkoxide **5.165** generates C10-enolate **5.166**, which displaces the C14 chloride to yield compound **5.167**. A final aldol reaction would afford pentacycle **5.168**. Notably, **5.167** can be isolated as a minor compound when the reaction does not reach completion; when resubjected to the reaction conditions, pentacycle **5.168** is generated.



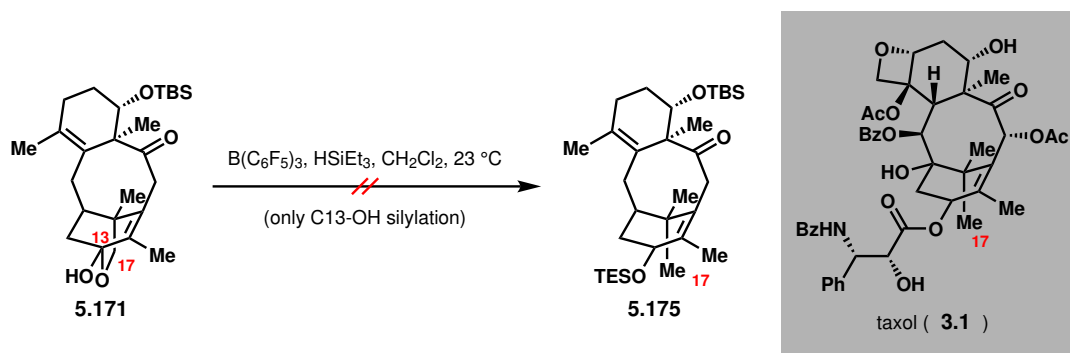
**Scheme 5.41:** Synthesis of pentacycle **5.168**. X-ray crystal structure of **5.168** is shown at right.

The synthesis of pentacycle **5.168** could enable access to a set of molecules containing this unnatural taxoid scaffold whose bioactivity profiles might be quite different from those of natural taxoids.



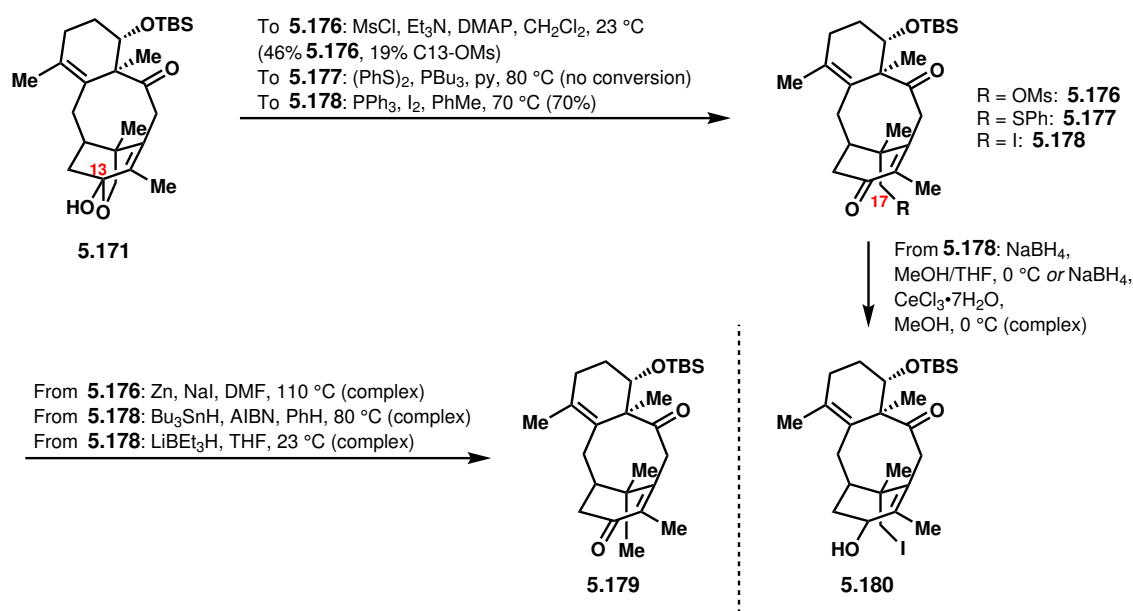
**Scheme 5.42:** Synthesis of the core of the natural products taxezopidines A, J, and M.

We also considered whether taxanes without a C12,C17-ether bridge could be accessed from the tetracyclic core of the taxagifine-like natural products. To this end, we subjected C13 carbonyl compound **5.154** to  $\text{SmI}_2$  (Scheme 5.42). While we had expected only  $\alpha$ -deoxygenation, we isolated C13,17-ether-bridged compound **5.171** as the sole product. Presumably, after  $\alpha$ -oxy reduction, elimination of the C11 hydroxy group from enolate **5.169** occurs; hemiketalization from **5.170** then affords **5.171**. Notably, the newly formed C13,C17-ether bridge can be found in taxezopidines A, J, and M (**5.172–5.174**); as a result, this  $\text{SmI}_2$ -mediated reductive process represents a one-step transformation from the core of one group of natural products to the core of another.



**Scheme 5.43:** Attempted direct C17 reduction of **5.171**.

We then attempted to reduce C17 further to a methyl group in order to access the core of the majority of taxoid natural products (i.e., the taxol core). From **5.164**, we first attempted direct C17 ether reduction with  $\text{B}(\text{C}_6\text{F}_5)_3/\text{Et}_3\text{SiH}^{80}$ ; however, only silylation of the C13 hydroxy group could be observed (Scheme 5.43). We next attempted to synthesize and reduce C17-functionalized compounds **5.176–5.178** (Scheme 5.44). Mesylation of **5.171** provided **5.176** as the major product, with a minor amount of C13-OMs product isolated as well; attempted reduction with Zn and NaI gave only a complex reaction mixture. While attempted phenylsulfide synthesis yielded no conversion, we were able to cleanly synthesize primary iodide **5.177**. However, under both reductive radical and hydride conditions, only complex reaction mixtures could be obtained. We assumed that the reactive enone could be susceptible to undesired intramolecular and/or intermolecular reactivity under reductive conditions. As a result, we next attempted to reduce the C13 carbonyl of **5.178** to attenuate reactivity. However, attempted sodium borohydride reduction with or without  $\text{CeCl}_3$  gave only unknown products. It is possible that the steric bulk of the neopentyl iodide impedes reduction of the C13 carbonyl from the  $\alpha$ -face; future efforts should focus on reduction at C13 of hemiketal **5.71** before C17-reduction.



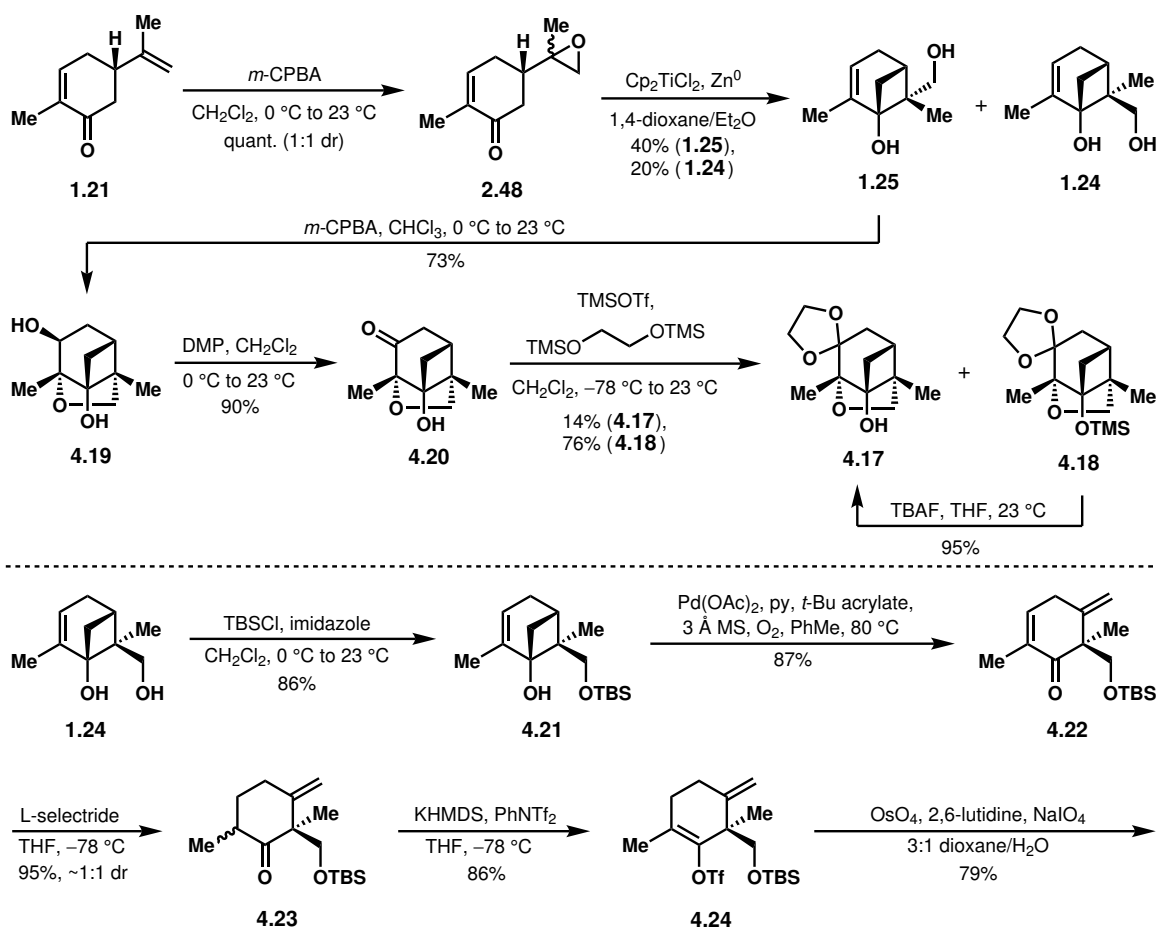
Scheme 5.44: Attempted C17 reductions of **5.171**.

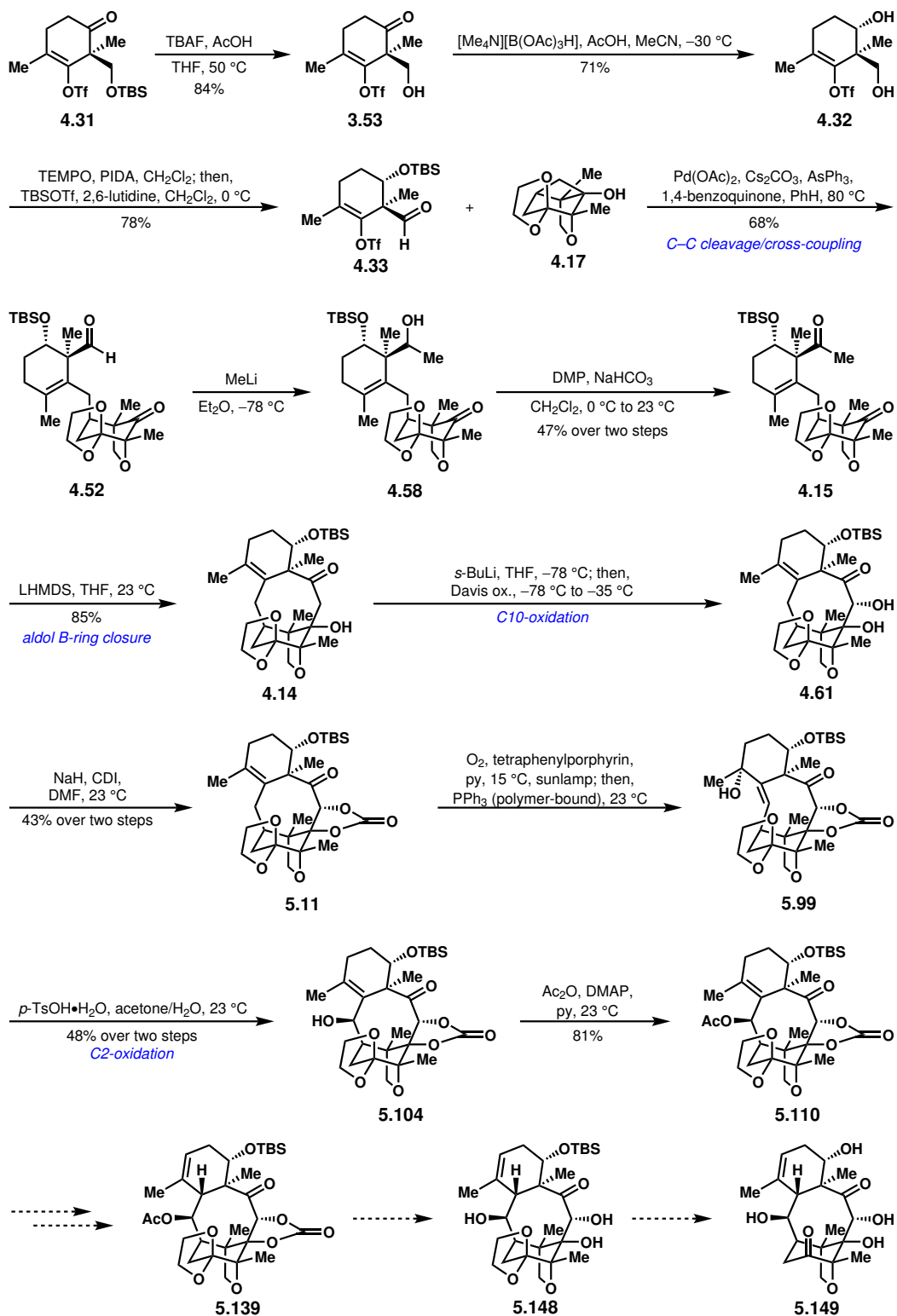
## 5.8 Conclusion and Outlook

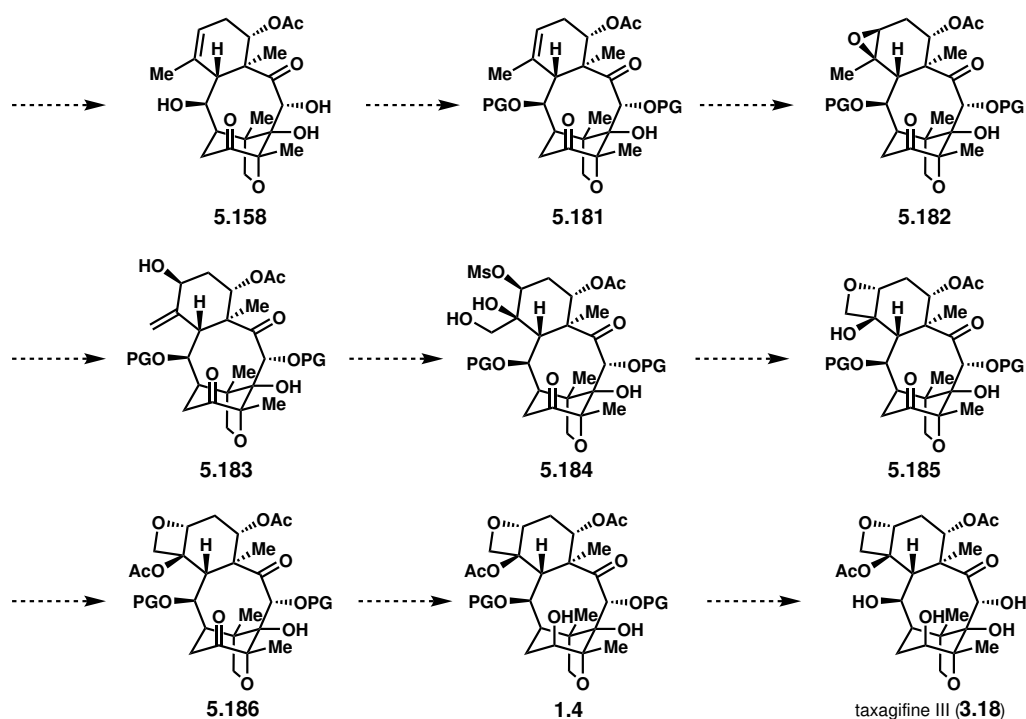
From the tetracyclic core of the taxagifine-like natural products, a number of studies were conducted on late-stage oxidations required for the first total syntheses of these natural products. Investigation of C10 oxidation revealed that deprotonation at C10 was particularly challenging, illustrating the idiosyncratic reactivity of the tetracyclic core produced by its conformation. In the end, *s*-BuLi/Davis oxaziridine sufficed to effect C10 oxidation. The C9,C10-*trans*-diol motif found in taxagifine proved to be inaccessible by C9 carbonyl reduction or by other methods; future developments in mild single-electron reductions of dialkyl ketones may aid future efforts toward C9 carbonyl reduction. If desired, C5 oxygenation could be straightforwardly installed by allylic oxidation. C2 oxygenation was installed via a Schenck ene/allylic alcohol transposition sequence via an unusual *trans*-cyclooctene intermediate. Studies have been carried out on the transposition of the C3–C4 alkene with concomitant stereoselective placement of a hydrogen atom at C3; immediate next efforts will be focused on overcoming this challenge. A number of studies on model systems have been carried out to facilitate the last steps in the synthesis. In particular, formation of the oxetane, protecting group cleavages, stereoselective C13 carbonyl reduction, and selective C7 and/or C4 acetylations have been investigated. Finally, in the course of our studies, we examined additional oxidations at C14 and C19 and conducted studies to access alternative taxane scaffolds.

Our synthetic studies so far have culminated in the synthesis of C10,C2-oxidized compound **5.110** (Scheme 5.45). The complete synthetic route to-date and anticipated final steps are illustrated below. The completion of the first total synthesis of taxagifine III would help provide entry to the taxagifine-like natural products at large, and would aid in the biological investigations of this largely unstudied class of complex molecules.









**Scheme 5.45:** Synthetic route toward the first total synthesis of taxagifine III.

## 5.9 Experimental Contributors

Experimental work was developed and conducted primarily by Brian Wang, with assistance from Dr. Shota Nagasawa, Dr. Nicholas O'Connor, and Melecio Perea. Characterization of all compounds was conducted by Brian Wang, Melecio Perea, and Dr. Nicholas O'Connor.

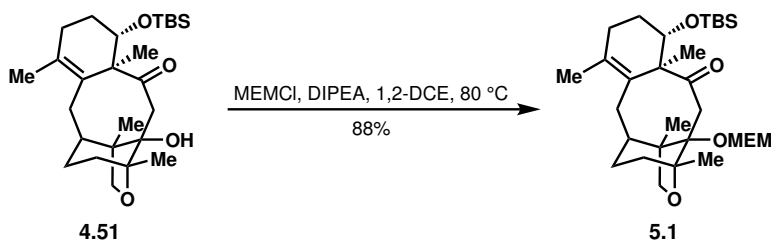
## 5.10 Experimental Methods and Procedures

### 5.10.1 General Methods

Unless otherwise stated, all reactions were stirred with Teflon<sup>TM</sup>-coated magnetic stir bars and were conducted in flame- or oven-dried glassware under an N<sub>2</sub> atmosphere following standard Schlenk technique. Anhydrous THF, Et<sub>2</sub>O, PhMe, PhH, MeCN, Et<sub>3</sub>N, and MeOH were obtained by sparging with Ar followed by passage through a column of activated alumina, and were kept under an Ar atmosphere. Anhydrous CH<sub>2</sub>Cl<sub>2</sub> was obtained by distilling over CaH<sub>2</sub> under an N<sub>2</sub> atmosphere. All other solvents and reagents were purchased from commercial suppliers and used without further purification, unless otherwise stated. All reactions were monitored by thin layer chromatography on Silicycle Siliaplate<sup>TM</sup> 250 μm silica gel (indicator F-254), with visualization by UV irradiation (254 nm) and staining by *p*-anisaldehyde. Reaction mixture temperatures above 23 °C were controlled by an IKA<sup>®</sup> temperature modulator. When stated, non-standard reaction mixture temperatures were obtained using a Thermo Scientific<sup>TM</sup> EK45/90 Immersion Cooler. “Blue LED” signifies a 40 W Kessil A160WE Tuna Blue LED, while “sunlamp” signifies a 90W halogen floodlight

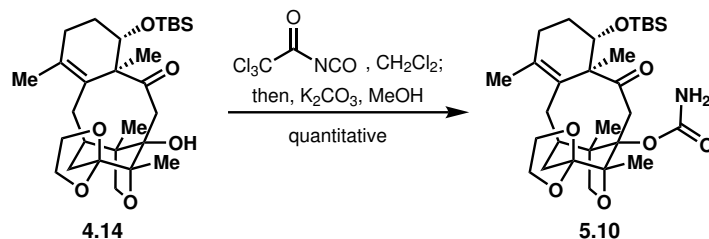
(GE Lighting 62716). Evaporation of solvents under reduced pressure was carried out on rotary evaporators. Purification by manual flash chromatography was conducted with Sorbent Technologies 60 Å silica gel of particle size 40–63 μm. Automated flash column chromatography was performed on a Yamazen<sup>®</sup> Smart Flash EPCLC W-Prep 2XY automated flash chromatography system, with Universal Columns (60 Å silica gel of particle size 40 μm) or Universal Column Premiums (60 Å silica gel of particle size 30 μm). NMR spectra were acquired in deuterated solvents purchased from Cambridge Isotope Laboratories, Inc. NMR spectra were recorded on Bruker spectrometers at the UC Berkeley College of Chemistry NMR Facility, operating at 300, 400, 500, 600, or 700 MHz for <sup>1</sup>H NMR, and at 75, 100, 125, 150, or 175 MHz for <sup>13</sup>C NMR. <sup>1</sup>H NMR spectra are calibrated to the residual solvent peak CDCl<sub>3</sub> (δ = 7.260 ppm) or C<sub>6</sub>D<sub>6</sub> (δ = 7.160 ppm), and <sup>13</sup>C NMR spectra are calibrated to the residual solvent peak CDCl<sub>3</sub> (δ = 77.16 ppm). <sup>1</sup>H NMR data are reported as follows: chemical shift (multiplicity, coupling constant, number of protons). Abbreviations of multiplicity patterns are as follows: d = doublet, t = triplet, br s = broad singlet, s = singlet, q = quartet, m = multiplet, dd = doublet of doublets, dt = doublet of triplets, dq = doublet of quartets, dp = doublet of pentets, ddd = doublet of doublet of doublets, dtd = doublet of triplet of doublets, tt = triplet of triplets. IR spectra were acquired on a Bruker ALPHA Platinum ATR spectrometer (neat), and select IR peaks are reported as frequency of absorption in cm<sup>-1</sup>. High resolution mass spectrometry data was obtained from the Mass Spectral Facility at the University of California, Berkeley on a Finnigan/Thermo LTQ-FT instrument (ESI or EI) or from the Catalysis Facility of Lawrence Berkeley National Laboratory on a PerkinElmer AxION 2 UHPLC-TOF system (ESI or APCI). Data acquisition and processing were performed using Xcalibur<sup>™</sup> software. Optical rotations were measured with a Perkin-Elmer 241 polarimeter with a Na D-line lamp (path length 1 dm, cell volume 1 mL, c in g/100 mL). X-ray data was collected on a Bruker APEX-II CCD diffractometer with Mo-Kα radiation (λ = 0.71073 Å) or a MicroStar-H X8 APEX-II diffractometer with Cu-Kα radiation (λ = 1.54178 Å). CYLview and Avogadro were used for graphic rendering.

### 5.10.2 Experimental Procedures

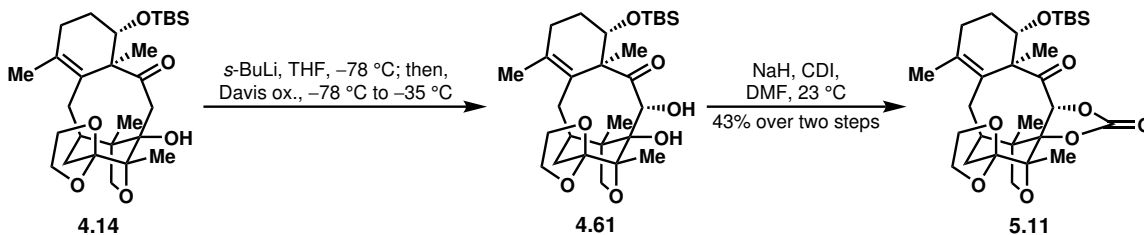


To **4.51** (10.1 mg, 0.023 mmol, 1 equiv) in anhydrous 1,2-dichloroethane (0.45 mL, 0.05 M), DIPEA (19.6 μL, 0.113 mmol, 5 equiv) was added, followed by MEMCl (12.9 μL, 0.113 mmol, 5 equiv). The reaction mixture was warmed to 80 °C and stirred for 25 h, after which DIPEA (19.6 μL, 0.113 mmol, 5 equiv) and MEMCl (12.9 μL, 0.113 mmol, 5 equiv) were added. After another 23 h, the reaction mixture was quenched with sat. aq. NaHCO<sub>3</sub> (1 mL) and CH<sub>2</sub>Cl<sub>2</sub> (1 mL), and the aqueous and organic layers were separated. The aqueous layer was extracted with CH<sub>2</sub>Cl<sub>2</sub> (3 x 1 mL). The combined organic layers were dried over

Na<sub>2</sub>SO<sub>4</sub>, filtered, and concentrated *in vacuo*. Purification by flash column chromatography (20% EtOAc/hexanes) afforded **5.1** (10.6 mg, 88%) as a white solid. <sup>1</sup>H NMR (500 MHz, CDCl<sub>3</sub>) δ 5.94 (d, *J* = 7.4 Hz, 1H), 4.93 (d, *J* = 7.4 Hz, 1H), 4.06 (dd, *J* = 10.3, 5.8 Hz, 1H), 3.94 (ddd, *J* = 10.7, 5.6, 3.9 Hz, 1H), 3.73 (d, *J* = 7.3 Hz, 1H), 3.64 (ddd, *J* = 10.5, 6.3, 3.8 Hz, 1H), 3.55–3.46 (m, 2H), 3.54 (d, *J* = 7.3 Hz, 1H), 3.35 (s, 3H), 3.26 (d, *J* = 15.3 Hz, 1H), 2.96 (d, *J* = 15.2 Hz, 1H), 2.54 (dd, *J* = 15.5, 7.5 Hz, 1H), 2.43–2.28 (m, 1H), 2.13–1.88 (m, 4H), 1.81 (s, 3H), 1.79–1.64 (m, 4H), 1.58–1.54 (m, 1H), 1.21 (s, 3H), 1.17 (s, 3H), 0.89 (s, 3H), 0.84 (s, 9H), 0.04 (s, 3H), –0.01 (s, 3H).



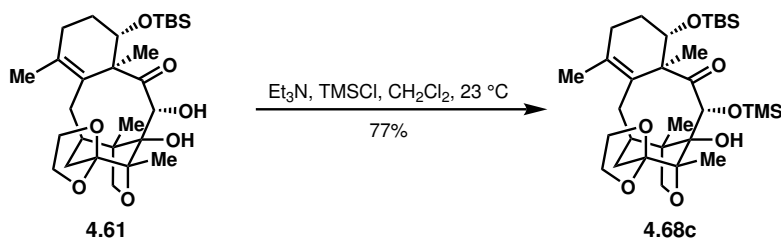
Trace water was removed from **4.14** (5.1 mg, 0.01 mmol, 1 equiv) via azeotropic distillation with anhydrous benzene (1 x 0.4 mL). Then, to **4.14** in anhydrous CH<sub>2</sub>Cl<sub>2</sub> (0.25 mL, 0.04 M) at 0 °C, trichloroacetyl isocyanate (3.6 μL, 0.03 mmol, 3 equiv) was added, and the reaction mixture was warmed to 23 °C. After 6 h, the reaction solvent was evaporated under N<sub>2</sub>; then, K<sub>2</sub>CO<sub>3</sub> (13.9 mg, 0.10 mmol, 10 equiv) and anhydrous MeOH (0.25 mL, 0.04 M) were added. The reaction mixture was stirred for 1 h, after which it was quenched with brine (0.5 mL) and EtOAc (0.5 mL). The aqueous and organic layers were separated, and the aqueous layer was extracted with EtOAc (3 x 0.5 mL). The combined organic layers were concentrated *in vacuo*. Purification by flash column chromatography (80% EtOAc/hexanes) afforded **5.10** (7.0 mg, quant.). <sup>1</sup>H NMR (700 MHz, CDCl<sub>3</sub>) δ 4.57 (br s, 2H), 4.20 (d, *J* = 15.9 Hz, 1H), 4.09 (ddd, *J* = 7.7, 6.1, 3.9 Hz, 1H), 3.96 (ddd, *J* = 7.5, 6.3, 3.9 Hz, 1H), 3.92 (d, *J* = 15.9 Hz, 1H), 3.89 (d, *J* = 7.9 Hz, 1H), 3.90–3.87 (m, 1H), 3.87–3.83 (m, 1H), 3.79–3.73 (m, 1H), 3.64 (d, *J* = 7.9 Hz, 1H), 2.61 (dd, *J* = 15.9, 7.2 Hz, 1H), 2.31–2.23 (m, 2H), 2.15 (d, *J* = 16.0 Hz, 1H), 2.11–2.07 (m, 2H), 2.06–2.02 (m, 1H), 1.81 (s, 3H), 1.74–1.69 (m, 2H), 1.23 (s, 3H), 1.18 (s, 3H), 1.00 (s, 3H), 0.85 (s, 9H), 0.03 (s, 3H), 0.00 (s, 3H).



Trace water was removed from **4.14** (575 mg, 1.14 mmol, 1 equiv) via azeotropic distillation with anhydrous benzene. Then, to a solution of **4.14** in anhydrous THF (19 mL) at –78 °C, *s*-BuLi (1.4 M in cyclohexane, 8.1 mL, 11.4 mmol, 10 equiv) was added rapidly dropwise while stirring vigorously. After 30 min, a solution of Davis oxaziridine (4.5 g, 17.1 mmol, 15 equiv) in anhydrous THF (38 mL) was added rapidly dropwise, and the reaction mixture was warmed to –35 °C. After 1 h, the reaction mixture was quenched with sat.

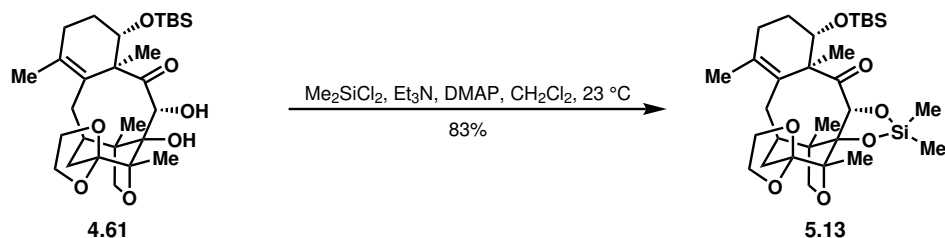
aq.  $\text{NH}_4\text{Cl}$ , and the organic and aqueous layers were separated. The aqueous layer was extracted 3x with EtOAc, and the combined organic layers washed with brine, dried over  $\text{Na}_2\text{SO}_4$ , filtered, and concentrated *in vacuo*. The crude product was purified by Yamazen automated flash column chromatography (25% EtOAc/hexanes to 75% EtOAc/hexanes) to afford **4.61** contaminated with Davis oxaziridine-related byproducts. On smaller scale, pure **4.61** could be isolated for characterization.  $^1\text{H NMR}$  (400 MHz,  $\text{CDCl}_3$ )  $\delta$  5.44 (d,  $J = 10.7$  Hz, 1H), 4.18 (ddd,  $J = 7.7, 6.0, 3.2$  Hz, 1H), 4.01 (dd,  $J = 11.4, 3.9$  Hz, 1H), 3.98–3.94 (m, 1H), 3.92 (d,  $J = 7.9$  Hz, 1H), 3.93–3.84 (m, 1H), 3.78–3.70 (m, 1H), 3.66 (d,  $J = 7.9$  Hz, 1H), 3.22 (d,  $J = 10.6$  Hz, 1H), 2.81 (s, 1H), 2.62 (dd,  $J = 15.9, 6.4$  Hz, 1H), 2.32 (dd,  $J = 16.0, 11.6$  Hz, 1H), 2.31–2.21 (m, 1H), 2.19–1.98 (m, 4H), 1.85 (s, 3H), 1.81–1.72 (m, 1H), 1.67 (td,  $J = 12.1, 5.4$  Hz, 1H), 1.28 (s, 3H), 1.23 (s, 3H), 0.88 (s, 3H), 0.87 (s, 9H), 0.05 (s, 3H), 0.01 (s, 3H).

To this mixture, CDI (555 mg, 3.42 mmol) and anhydrous DMF (34.2 mL) were added; NaH (90 wt% in mineral oil, 82 mg) was then added portionwise over 2 min. The reaction was stirred at 23 °C for 1.5 h, after which the reaction mixture was cooled to 0 °C and quenched with sat. aq.  $\text{NH}_4\text{Cl}$ . The organic and aqueous layers were separated, and the aqueous layer was extracted 3x with EtOAc. The combined organic layers were washed with brine, dried over  $\text{Na}_2\text{SO}_4$ , filtered, and concentrated *in vacuo*. Purification by Yamazen automated flash column chromatograph (5% EtOAc/ $\text{CH}_2\text{Cl}_2$ ) afforded pure **5.11** (271 mg, 43%) as a white solid. TLC (10% EtOAc/hexanes):  $R_f = 0.70$  (*p*-anisaldehyde)  $^1\text{H NMR}$  (700 MHz,  $\text{CDCl}_3$ )  $\delta$  6.16 (s, 1H), 4.17 (ddd,  $J = 7.6, 6.0, 3.7$  Hz, 1H), 4.02–3.97 (m, 2H), 3.91 (d,  $J = 8.0$  Hz, 1H), 3.90–3.86 (m, 1H), 3.81–3.77 (m, 1H), 3.73 (d,  $J = 8.1$  Hz, 1H), 2.64 (dd,  $J = 16.1, 6.8$  Hz, 1H), 2.29–2.22 (m, 2H), 2.16–2.05 (m, 4H), 1.85 (s, 3H), 1.84–1.79 (m, 1H), 1.71 (qd,  $J = 12.3, 5.7$  Hz, 1H), 1.27 (s, 3H), 1.24 (s, 3H), 0.96 (s, 3H), 0.85 (s, 9H), 0.05 (s, 3H), 0.03 (s, 3H).  $^{13}\text{C NMR}$  (176 MHz,  $\text{CDCl}_3$ )  $\delta$  205.4, 154.0, 135.0, 127.4, 111.2, 91.0, 89.4, 81.0, 72.4, 70.9, 66.7, 64.8, 60.0, 45.4, 44.2, 33.8, 32.1, 29.8, 27.6, 25.8, 22.3, 18.1, 15.9, 14.9, 11.3, –3.6, –5.0. HRMS (ESI+)  $m/z$  calc'd for  $\text{C}_{29}\text{H}_{44}\text{NaO}_8\text{Si}$   $[\text{M}+\text{Na}]^+$ : 571.2697, found: 571.2693.

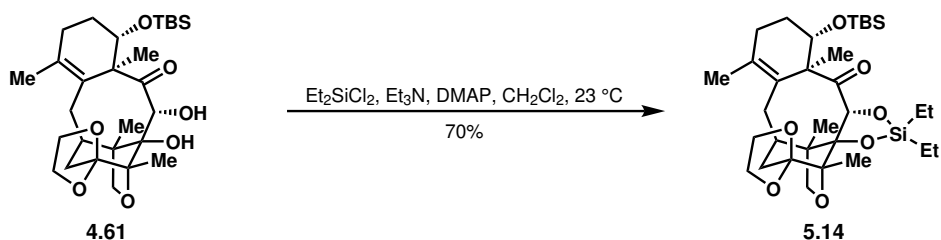


To **4.61** (2.4 mg, 0.005 mmol, 1 equiv) in anhydrous  $\text{CH}_2\text{Cl}_2$  (0.2 mL, 0.023 M), anhydrous triethylamine (12.8  $\mu\text{L}$ , 0.092 mmol, 20 equiv) was added, followed by TMSCl (5.8  $\mu\text{L}$ , 0.046 mmol, 10 equiv). The reaction mixture was stirred at 23 °C for 24 h, after which it was quenched with sat. aq.  $\text{NaHCO}_3$  (0.5 mL) and EtOAc (0.5 mL). The aqueous and organic layers were separated, and the aqueous layer was extracted with EtOAc (3 x 0.5 mL). The combined organic layers were concentrated *in vacuo*. Purification by flash column chromatography (30% EtOAc/hexanes to 40% EtOAc/hexanes) afforded **4.68c** (2.1 mg, 77%).  $^1\text{H NMR}$  (500 MHz,  $\text{CDCl}_3$ )  $\delta$  5.89 (s, 1H), 4.25 (s, 1H), 4.07–4.01 (m, 1H), 4.00–3.91 (m, 2H), 3.94 (d,  $J = 7.5$  Hz, 1H), 3.78–3.72 (m, 2H), 3.62 (d,  $J = 7.4$  Hz, 1H),

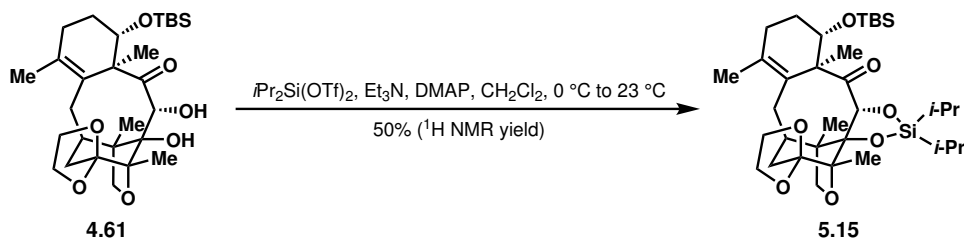
2.68–2.58 (m, 1H), 2.34 (dd,  $J = 15.6, 10.9$  Hz, 1H), 2.30–2.20 (m, 2H), 2.14–2.00 (m, 3H), 1.90 (s, 3H), 1.79–1.68 (m, 2H), 1.31 (s, 3H), 1.13 (s, 3H), 0.95 (s, 3H), 0.89 (s, 9H), 0.15 (s, 9H), 0.09 (s, 3H), 0.08 (s, 3H).



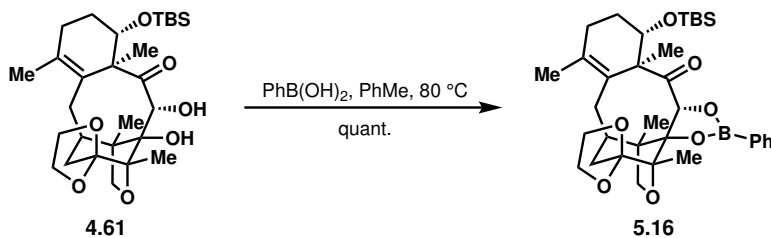
To **4.61** (5.0 mg, 0.010 mmol, 1 equiv) and DMAP (spatula tip) in anhydrous  $\text{CH}_2\text{Cl}_2$  (0.3 mL, 0.03 M), added anhydrous  $\text{Et}_3\text{N}$  (8.0  $\mu\text{L}$ , 0.057 mmol, 6 equiv) and  $\text{Me}_2\text{SiCl}_2$  (1.9  $\mu\text{L}$ , 0.019 mmol, 2 equiv). The reaction mixture was stirred at 23  $^\circ\text{C}$  for 3 h, after which it was quenched with  $\text{H}_2\text{O}$  (0.5 mL) and  $\text{EtOAc}$  (0.5 mL). The aqueous and organic layers were separated, and the aqueous layer was extracted with  $\text{EtOAc}$  (3 x 0.5 mL). The combined organic layers were concentrated *in vacuo*. Purification by flash column chromatography (30%  $\text{EtOAc}$ /hexanes with 1%  $\text{Et}_3\text{N}$ ) afforded **5.13** (4.6 mg, 83%).  $^1\text{H NMR}$  (700 MHz,  $\text{CDCl}_3$ )  $\delta$  5.78 (s, 1H), 4.29 (dd,  $J = 11.8, 4.3$  Hz, 1H), 4.15–4.08 (m, 1H), 4.00–3.93 (m, 1H), 3.90 (d,  $J = 7.5$  Hz, 1H), 3.84 (q,  $J = 7.5$  Hz, 1H), 3.78–3.71 (m, 1H), 3.60 (d,  $J = 7.5$  Hz, 1H), 2.54 (dd,  $J = 16.0, 7.9$  Hz, 1H), 2.30–2.22 (m, 1H), 2.23 (dd,  $J = 15.5, 10.2$  Hz, 1H), 2.09–1.97 (m, 4H), 1.83 (s, 3H), 1.83–1.78 (m, 1H), 1.70 (qd,  $J = 12.4, 5.9$  Hz, 1H), 1.19 (s, 6H), 0.87 (s, 3H), 0.84 (s, 9H), 0.51 (s, 3H), 0.33 (s, 3H), 0.06 (s, 3H), 0.05 (s, 3H).



To **4.61** (30.4 mg, 0.058 mmol, 1 equiv) and DMAP (0.7 mg, 0.006 mmol, 0.1 equiv) in anhydrous  $\text{CH}_2\text{Cl}_2$  (0.97 mL, 0.06 M), added anhydrous  $\text{Et}_3\text{N}$  (48.6  $\mu\text{L}$ , 0.349 mmol, 6 equiv) and  $\text{Et}_2\text{SiCl}_2$  (17.4  $\mu\text{L}$ , 0.116 mmol, 2 equiv). The reaction mixture was stirred at 23  $^\circ\text{C}$  for 14 h, after which brine (1 mL) was added. The aqueous and organic layers were separated, and the aqueous layer was extracted with  $\text{EtOAc}$  (3 x 1 mL). The combined organic layers were concentrated *in vacuo*. Purification by flash column chromatography (25%  $\text{EtOAc}$ /hexanes) afforded **5.14** (24.8 mg, 70%) as a yellow oil.  $^1\text{H NMR}$  (500 MHz,  $\text{CDCl}_3$ )  $\delta$  5.77 (s, 1H), 4.35 (dd,  $J = 11.8, 4.4$  Hz, 1H), 4.13 (ddd,  $J = 7.6, 6.0, 3.5$  Hz, 1H), 3.96 (ddd,  $J = 7.4, 6.0, 3.5$  Hz, 1H), 3.91 (d,  $J = 7.4$  Hz, 1H), 3.82 (td,  $J = 8.0, 6.0$  Hz, 1H), 3.75–3.69 (m, 1H), 3.58 (d,  $J = 7.4$  Hz, 1H), 2.52 (dd,  $J = 15.5, 7.6$  Hz, 1H), 2.31–2.22 (m, 1H), 2.21 (dd,  $J = 15.2, 10.2$  Hz, 1H), 2.09–1.95 (m, 4H), 1.85–1.79 (m, 1H), 1.82 (s, 3H), 1.71 (qd,  $J = 12.3, 6.1$  Hz, 1H), 1.18 (s, 3H), 1.18 (s, 3H), 1.09–0.94 (m, 10H), 0.88 (s, 3H), 0.83 (s, 9H), 0.06 (s, 3H), 0.05 (s, 3H).

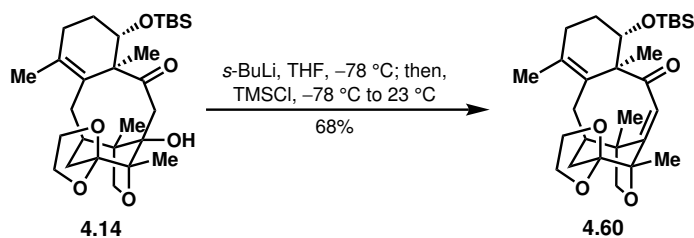


To **4.61** (5.0 mg, 0.010 mmol, 1 equiv) and DMAP (spatula tip) in anhydrous  $\text{CH}_2\text{Cl}_2$  (0.3 mL, 0.03 M) at 0 °C, anhydrous  $\text{Et}_3\text{N}$  (8  $\mu\text{L}$ , 0.0576 mmol, 6 equiv) and  $i\text{-Pr}_2\text{Si(OTf)}_2$  (5.7  $\mu\text{L}$ , 0.0192 mmol, 2 equiv) were added. The reaction mixture was warmed to 23 °C and stirred for 2 h, after which  $\text{H}_2\text{O}$  and  $\text{EtOAc}$  were added. The aqueous and organic layers were separated, and the aqueous layer was extracted 3x with  $\text{EtOAc}$ . The combined organic layers were washed 1x with brine, then dried over  $\text{Na}_2\text{SO}_4$ , filtered, and concentrated *in vacuo*. Crude  $^1\text{H NMR}$  analysis revealed a 50% yield of **5.15**. Purification by preparatory TLC (50%  $\text{EtOAc}$ /hexanes) afforded pure **5.15**.  $^1\text{H NMR}$  (700 MHz,  $\text{CDCl}_3$ )  $\delta$  5.77 (s, 1H), 4.50 (dd,  $J = 11.9, 4.4$  Hz, 1H), 4.16–4.09 (m, 1H), 3.99–3.90 (m, 2H), 3.77 (q,  $J = 7.5$  Hz, 1H), 3.70 (q,  $J = 7.3$  Hz, 1H), 3.56 (d,  $J = 7.2$  Hz, 1H), 2.49 (dd,  $J = 15.7, 8.5$  Hz, 1H), 2.31–2.23 (m, 1H), 2.17 (dd,  $J = 15.3, 10.4$  Hz, 1H), 2.10–1.99 (m, 2H), 1.93 (dd,  $J = 15.4, 7.8$  Hz, 2H), 1.90–1.84 (m, 1H), 1.82–1.71 (m, 2H), 1.79 (s, 3H), 1.23–1.11 (m, 19H), 0.90 (s, 3H), 0.86–0.82 (m, 9H), 0.09 (s, 3H), 0.07 (s, 3H).

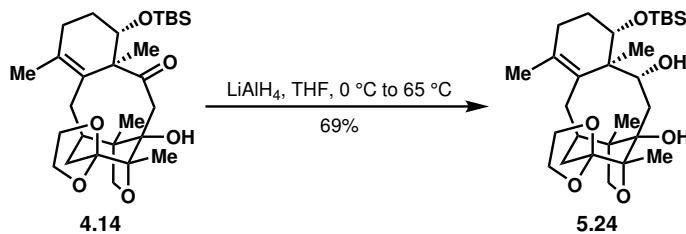


To **4.61** (1.9 mg, 0.004 mmol, 1 equiv) and  $\text{PhB(OH)}_2$  (0.7 mg, 0.005 mmol, 1.5 equiv), anhydrous  $\text{PhMe}$  (0.2 mL 0.02 M) was added. The reaction mixture was stirred at 80 °C for 5 h, after which it was cooled to 23 °C and concentrated *in vacuo*. Purification by flash column chromatography (20%  $\text{EtOAc}$ /hexanes to 40%  $\text{EtOAc}$ /hexanes) afforded **5.16** (2.3 mg, quant.).  $^1\text{H NMR}$  (700 MHz,  $\text{CDCl}_3$ )  $\delta$  7.90–7.83 (m, 2H), 7.49–7.44 (m, 1H), 7.39–7.33 (m, 2H), 4.20 (dd,  $J = 11.8, 4.1$  Hz, 1H), 4.17–4.13 (m, 1H), 4.07 (d,  $J = 7.7$  Hz, 1H), 3.98 (ddd,  $J = 7.6, 6.2, 3.8$  Hz, 1H), 3.88 (td,  $J = 8.0, 6.2$  Hz, 1H), 3.76 (td,  $J = 7.9, 6.1$  Hz, 1H), 3.71 (d,  $J = 7.6$  Hz, 1H), 2.65–2.58 (m, 1H), 2.33–2.26 (m, 1H), 2.30 (dd,  $J = 15.6, 10.5$  Hz, 1H), 2.16 (d,  $J = 15.9$  Hz, 1H), 2.12–2.04 (m, 2H), 2.09 (d,  $J = 15.5$  Hz, 1H), 1.87 (s, 3H), 1.86–1.80 (m, 1H), 1.72 (qd,  $J = 12.3, 5.7$  Hz, 1H), 1.24 (s, 3H), 1.13 (s, 3H), 0.95 (s, 3H), 0.87 (s, 9H), 0.13 (s, 3H), 0.11 (s, 3H).

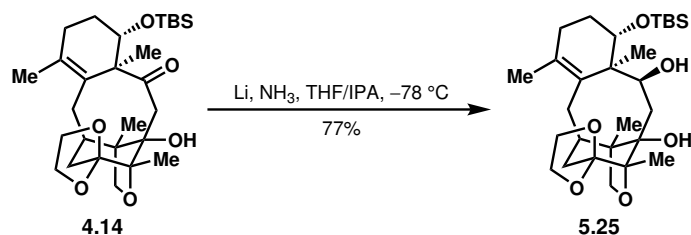




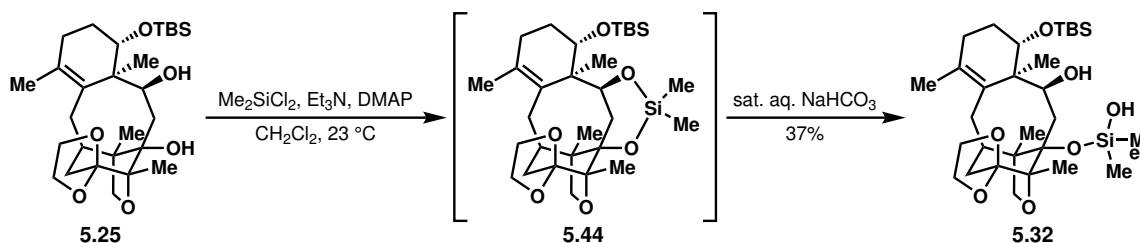
Trace water was removed from **4.14** (10.0 mg, 0.020 mmol, 1 equiv) via azeotropic distillation with anhydrous benzene. Then, to a solution of **4.14** in anhydrous THF (0.5 mL, 0.039 M) at  $-78\text{ }^\circ\text{C}$ , *s*-BuLi (1.4 M in cyclohexane, 70.5  $\mu\text{L}$ , 0.10 mmol, 5 equiv) was added over 15 s. After 1 h, TMSCl (37.6  $\mu\text{L}$ , 0.30 mmol, 15 equiv) was added; after 2 min, the reaction mixture was warmed to  $23\text{ }^\circ\text{C}$ . After 30 min, the reaction mixture was quenched with sat. aq.  $\text{NaHCO}_3$  (0.5 mL) and EtOAc (0.5 mL), and the aqueous and organic layers were separated. The aqueous layer was extracted with EtOAc (3 x 0.5 mL), and the combined organic layers were concentrated *in vacuo*. Purification by flash column chromatography (20% EtOAc/hexanes to 60% EtOAc/hexanes) afforded **4.60** (6.6 mg, 68%) and **4.14** (1.4 mg, 14%).  $^1\text{H NMR}$  (700 MHz,  $\text{CDCl}_3$ )  $\delta$  6.26 (s, 1H), 4.09 (dd,  $J = 10.2, 5.1$  Hz, 1H), 4.04–3.99 (m, 2H), 3.84–3.77 (m, 3H), 3.75 (d,  $J = 8.1$  Hz, 1H), 2.61 (dd,  $J = 15.8, 5.9$  Hz, 1H), 2.23–2.13 (m, 3H), 2.06–1.97 (m, 3H), 1.75 (s, 3H), 1.73–1.69 (m, 2H), 1.22 (s, 6H), 1.16 (s, 3H), 0.87 (s, 9H), 0.06 (s, 3H), 0.04 (s, 3H).



To  $\text{LiAlH}_4$  (7.9 mg, 0.207 mmol, 3 equiv) at  $0\text{ }^\circ\text{C}$  in anhydrous THF (0.7 mL), **4.14** (35.0 mg, 0.069 mmol, 1 equiv) was added as a solution in anhydrous THF (0.7 mL), and the reaction mixture was warmed to  $65\text{ }^\circ\text{C}$ . After 70 min, the reaction mixture was cooled to  $0\text{ }^\circ\text{C}$  and was quenched dropwise with  $\text{H}_2\text{O}$  (1 mL) and EtOAc (1 mL). The organic and aqueous layers were separated, and the aqueous layer was extracted with EtOAc (3 x 1 mL). The combined organic layers were dried over  $\text{Na}_2\text{SO}_4$ , filtered, and concentrated *in vacuo*. Purification by flash column chromatography (60% EtOAc/hexanes) afforded **5.24** (24.2 mg, 69%) as a white solid.  $^1\text{H NMR}$  (500 MHz,  $\text{CDCl}_3$ )  $\delta$  4.21–4.16 (m, 1H), 3.99 (ddd,  $J = 7.5, 6.1, 4.1$  Hz, 1H), 3.91 (ddd,  $J = 7.1, 6.1, 4.1$  Hz, 1H), 3.82 (d,  $J = 8.4$  Hz, 1H), 3.87–3.80 (m, 1H), 3.78–3.73 (m, 1H), 3.71 (d,  $J = 8.5$  Hz, 1H), 3.38 (dd,  $J = 9.7, 3.3$  Hz, 1H), 2.70 (s, 1H), 2.58 (d,  $J = 16.5$  Hz, 1H), 2.51–2.40 (m, 2H), 2.21–2.03 (m, 3H), 2.01–1.90 (m, 4H), 1.74–1.65 (m, 1H), 1.71 (s, 3H), 1.64–1.58 (m, 1H), 1.31 (s, 3H), 1.14 (s, 3H), 1.09 (s, 3H), 0.88 (s, 9H), 0.06 (s, 3H), 0.05 (s, 3H).

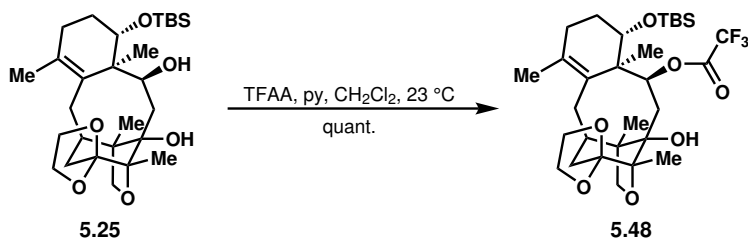


To a flame-dried Schlenk flask under Ar at  $-78\text{ }^\circ\text{C}$ ,  $\text{NH}_3$  ( $\sim 0.4\text{ mL}$ ) was condensed. Then, **4.14** (20 mg, 0.039 mmol, 1 equiv) was added as a solution in anhydrous THF (0.2 mL) and anhydrous isopropyl alcohol (0.2 mL). A small piece of Li wire in paraffin oil was washed with hexanes (5.4 mg after wash, 0.778 mmol, 20 equiv) and placed in the arm of the Schlenk flask, which was then quickly placed back under Ar. The piece of Li wire was then allowed to fall into the Schlenk flask. After 1 h, the reaction mixture was quenched with sat. aq.  $\text{NH}_4\text{Cl}$  (0.5 mL) and EtOAc (0.5 mL) and warmed to  $23\text{ }^\circ\text{C}$ . The aqueous and organic layers were separated, and the aqueous layer was extracted with EtOAc (3 x 0.5 mL). The combined organic layers were concentrated *in vacuo*. Purification by flash column chromatography (85% EtOAc/hexanes) afforded **5.25** (15.4 mg, 77%) as a colorless oil.  $^1\text{H NMR}$  (600 MHz,  $\text{CDCl}_3$ )  $\delta$  4.77 (d,  $J = 7.8\text{ Hz}$ , 1H), 4.30–4.23 (m, 2H), 4.05 – 4.00 (m, 1H), 3.94 – 3.89 (m, 1H), 3.84–3.79 (m, 1H), 3.78 (d,  $J = 8.5\text{ Hz}$ , 1H), 3.75–3.69 (m, 1H), 3.66 (d,  $J = 8.4\text{ Hz}$ , 1H), 2.98 (dd,  $J = 16.7, 3.0\text{ Hz}$ , 1H), 2.51 (dd,  $J = 15.8, 7.6\text{ Hz}$ , 1H), 2.24–2.07 (m, 4H), 2.03 (d,  $J = 15.3\text{ Hz}$ , 1H), 2.00–1.94 (m, 2H), 1.88–1.81 (m, 1H), 1.81–1.75 (m, 1H), 1.74 (s, 3H), 1.47 (dd,  $J = 16.7, 4.0\text{ Hz}$ , 1H), 1.32 (s, 3H), 1.21 (s, 3H), 1.13 (s, 3H), 0.91 (s, 9H), 0.18 (s, 3H), 0.16 (s, 3H).

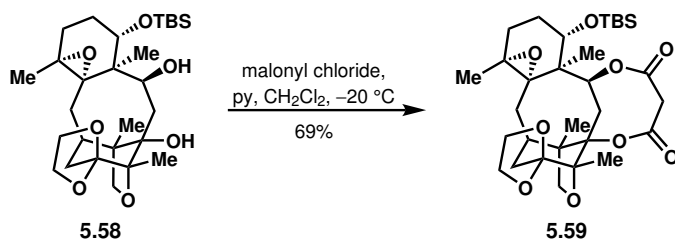


Trace water was removed from **5.25** (1.9 mg, 0.004 mmol, 1 equiv) via azeotropic distillation with anhydrous benzene (3 x 1 mL). Then, to **5.25** and DMAP (0.1 mg, 0.0007 mmol, 0.2 equiv) under Ar, anhydrous  $\text{CH}_2\text{Cl}_2$  (0.15 mL, 0.025 M) was added, followed by anhydrous  $\text{Et}_3\text{N}$  (1.6  $\mu\text{L}$ , 0.011 mmol, 3 equiv) and  $\text{Me}_2\text{SiCl}_2$  (0.5  $\mu\text{L}$ , 0.006 mmol, 1.5 equiv). The reaction mixture was stirred at  $23\text{ }^\circ\text{C}$  for 1.5 h, after which the reaction mixture was quenched with sat. aq.  $\text{NaHCO}_3$  (0.5 mL) and EtOAc (0.5 mL). The mixture was stirred vigorously for 30 min. The aqueous and organic layers were separated, and the aqueous layer was extracted with EtOAc (2 x 0.5 mL). The combined organic layers were concentrated *in vacuo*. Purification by flash column chromatography (40% EtOAc/hexanes) afforded **5.32** (0.8 mg, 37%).  $^1\text{H NMR}$  (700 MHz,  $\text{CDCl}_3$ )  $\delta$  6.43 (s, 1H), 5.63 (d,  $J = 7.6\text{ Hz}$ , 1H), 4.41–4.36 (m, 1H), 4.29 (dd,  $J = 12.1, 4.2\text{ Hz}$ , 1H), 4.02 (ddd,  $J = 7.7, 6.1, 3.6\text{ Hz}$ , 1H), 3.90 (ddd,  $J = 7.4, 6.2, 3.6\text{ Hz}$ , 1H), 3.81 (d,  $J = 7.5\text{ Hz}$ , 1H), 3.80–3.73 (m, 1H), 3.72–3.65 (m, 1H), 3.54 (d,  $J = 7.5\text{ Hz}$ , 1H), 3.14 (dd,  $J = 17.4, 3.1\text{ Hz}$ , 1H), 2.50 (dd,  $J = 15.8, 7.7\text{ Hz}$ , 1H), 2.21–2.09 (m, 4H), 1.99 (dd,  $J = 17.6, 6.4\text{ Hz}$ , 1H), 1.95 (d,  $J = 14.8\text{ Hz}$ , 1H), 1.85

(qd,  $J = 12.1, 6.4$  Hz, 1H), 1.80–1.75 (m, 1H), 1.74 (s, 3H), 1.69 (dd,  $J = 17.4, 4.1$  Hz, 1H), 1.30 (s, 3H), 1.19 (s, 3H), 1.09 (s, 3H), 0.90 (s, 9H), 0.22 (s, 3H), 0.18 (s, 3H), 0.16 (s, 3H), 0.16 (s, 3H).

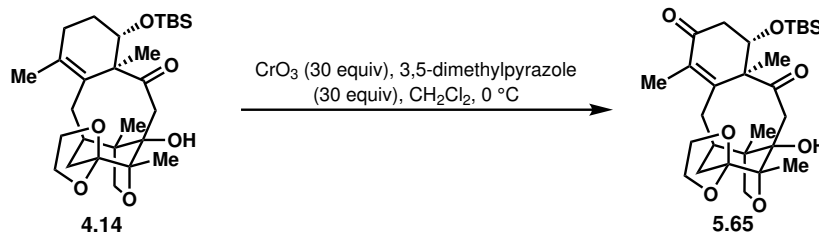


Trace water was removed from **5.25** (3.4 mg, 0.007 mmol, 1 equiv) via azeotropic distillation with anhydrous benzene (2 x 1 mL). Then, to **5.25** in anhydrous  $\text{CH}_2\text{Cl}_2$  (0.3 mL, 0.02 M) at 0 °C, anhydrous pyridine (1.3  $\mu\text{L}$ , 0.017 mmol, 2.5 equiv) and trifluoroacetic anhydride (1.4  $\mu\text{L}$ , 0.010 mmol, 1.5 equiv) were added. The reaction mixture was warmed to 23 °C and stirred for 80 min, after which it was quenched with sat. aq.  $\text{NaHCO}_3$  (0.5 mL) and EtOAc (0.5 mL). The aqueous and organic layers were separated, and the aqueous layer was extracted with EtOAc (3 x 0.5 mL). The combined organic layers were dried over  $\text{Na}_2\text{SO}_4$ , filtered, and concentrated *in vacuo* to afford **5.48** (4.1 mg, quant.) as a white solid.  $^1\text{H}$  NMR (500 MHz,  $\text{CDCl}_3$ )  $\delta$  5.56 (t,  $J = 3.8$  Hz, 1H), 4.20 (dd,  $J = 6.9, 3.3$  Hz, 1H), 4.03 (ddd,  $J = 7.6, 6.1, 3.8$  Hz, 1H), 3.94 (ddd,  $J = 7.3, 6.1, 3.8$  Hz, 1H), 3.86–3.80 (m, 1H), 3.82 (d,  $J = 8.3$  Hz, 1H), 3.77–3.69 (m, 1H), 3.65 (d,  $J = 8.3$  Hz, 1H), 3.47 (dd,  $J = 17.4, 4.2$  Hz, 1H), 2.66 (dd,  $J = 16.0, 6.8$  Hz, 1H), 2.27–2.14 (m, 4H), 2.05 (d,  $J = 14.4$  Hz, 1H), 1.94 (dt,  $J = 17.2, 6.1$  Hz, 1H), 1.82 (s, 3H), 1.78–1.66 (m, 2H), 1.47 (dd,  $J = 17.4, 3.3$  Hz, 1H), 1.38 (s, 3H), 1.11 (s, 3H), 1.08 (s, 3H), 0.88 (s, 9H), 0.08 (s, 3H), 0.05 (s, 3H).

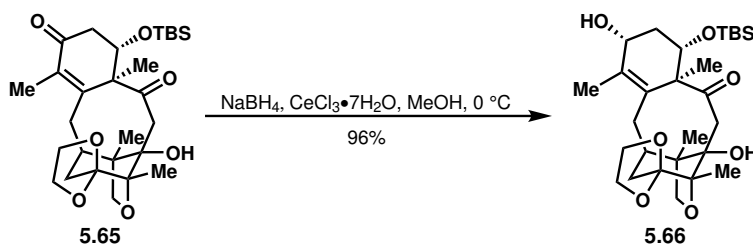


Trace water was removed from **5.58** (7.8 mg, 0.015 mmol, 1 equiv) via azeotropic distillation with anhydrous benzene (1 x 1 mL). Then, to **5.58** in anhydrous  $\text{CH}_2\text{Cl}_2$  (0.6 mL, 0.025 M) at –20 °C, anhydrous pyridine (6.0  $\mu\text{L}$ , 0.07 mmol, 5 equiv) was added, followed by malonyl chloride (1.6  $\mu\text{L}$ , 0.016 mmol, 1.1 equiv). The reaction mixture was stirred for 10 min, after which it was quenched with sat. aq.  $\text{NaHCO}_3$  (0.5 mL) and warmed to 23 °C. The aqueous and organic layers were separated, and the aqueous layer was extracted 5x with 3:1  $\text{CHCl}_3$ :IPA. The combined organic layers were concentrated *in vacuo*. Purification by flash column chromatography (5% MeOH/EtOAc) afforded **5.59** (6.1 mg, 69%).  $^1\text{H}$  NMR (700 MHz,  $\text{CDCl}_3$ )  $\delta$  5.48 (dd,  $J = 4.9, 2.4$  Hz, 1H), 4.10–4.06 (m, 1H), 4.00 (dt,  $J = 7.4, 6.3$  Hz, 1H), 3.95 (dt,  $J = 7.9, 5.9$  Hz, 1H), 3.91 (dt,  $J = 7.7, 6.3$  Hz, 1H), 3.84 (d,  $J = 8.3$  Hz, 1H), 3.81 (dd,  $J = 11.2, 3.8$  Hz, 1H), 3.61 (d,  $J = 8.3$  Hz, 1H), 3.49 (s, 1H), 3.25 (s, 1H), 3.21 (dd,  $J = 17.5, 2.4$  Hz, 1H), 2.54 (d,  $J = 16.5$  Hz, 1H), 2.28 (dd,  $J = 16.1, 10.5$

Hz, 1H), 2.18 (d,  $J = 16.0$  Hz, 1H), 2.05–2.01 (m, 1H), 1.84 (dt,  $J = 14.6, 4.0$  Hz, 1H), 1.78 (ddd,  $J = 14.4, 12.2, 4.3$  Hz, 1H), 1.65–1.57 (m, 2H), 1.49 (dd,  $J = 16.7, 7.7$  Hz, 1H), 1.44 (s, 3H), 1.43–1.39 (m, 1H), 1.37 (s, 3H), 1.18 (s, 3H), 1.07 (s, 3H), 0.87 (s, 9H), 0.07 (s, 3H), 0.04 (s, 3H).

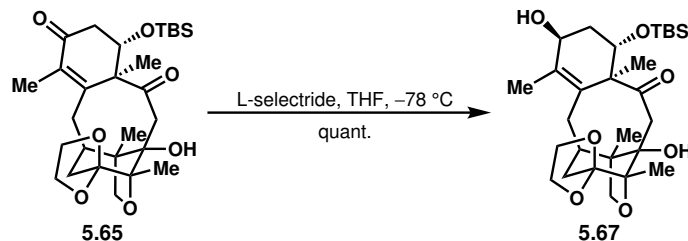


To **4.14** (100 mg, 0.197 mmol, 1 equiv) in anhydrous  $\text{CH}_2\text{Cl}_2$  (3.9 mL, 0.05 M) at 0 °C, 3,5-dimethylpyrazole (569 mg, 5.92 mmol, 30 equiv) was added in one portion, and then  $\text{CrO}_3$  (592 mg, 5.92 mmol, 30 equiv) was added in one portion. After 15 min, 5 M NaOH (4 mL) was added, and the reaction mixture was stirred vigorously for 1 h. The aqueous and organic layers were then separated, and the aqueous layer was extracted with  $\text{CHCl}_3$  (3 x 4 mL). The combined organic layers were washed with 1 M HCl (4 x 4 mL), sat. aq.  $\text{NaHCO}_3$  (1 x 4 mL), and brine (1 x 4 mL). The combined organic layers were then dried over  $\text{Na}_2\text{SO}_4$ , filtered, and concentrated *in vacuo*. Purification by automated Yamazen flash column chromatography (60% EtOAc/hexanes) afforded **5.65** (87.4 mg, 85%) as a clear oil.  $^1\text{H NMR}$  (400 MHz,  $\text{CDCl}_3$ )  $\delta$  4.18 (dd,  $J = 12.5, 5.2$  Hz, 1H), 4.05–4.00 (m, 1H), 4.04 (d,  $J = 14.9$  Hz, 1H), 3.95 (ddd,  $J = 7.3, 5.9, 4.0$  Hz, 1H), 3.89 (d,  $J = 8.2$  Hz, 1H), 3.88–3.81 (m, 1H), 3.80–3.73 (m, 1H), 3.66 (d,  $J = 8.2$  Hz, 1H), 2.84 (dd,  $J = 15.0, 6.8$  Hz, 1H), 2.72–2.51 (m, 2H), 2.48–2.30 (m, 3H), 2.09–2.03 (m, 2H), 1.98 (s, 3H), 1.34 (s, 3H), 1.17 (s, 3H), 1.01 (s, 3H), 0.86 (s, 9H), 0.06 (s, 3H), –0.01 (s, 3H).

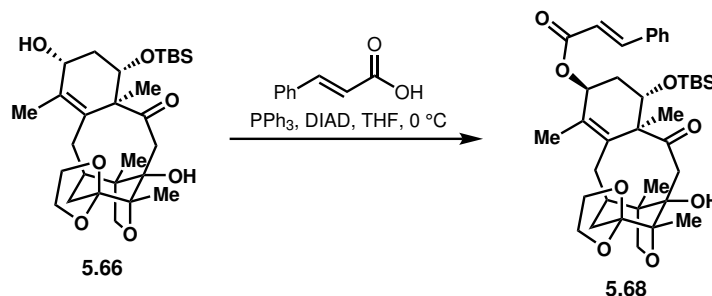


To **5.65** (19.9 mg, 0.038 mmol, 1 equiv) in anhydrous MeOH (1.9 mL, 0.02 M) at 0 °C,  $\text{CeCl}_3 \cdot 7\text{H}_2\text{O}$  (21.4 mg, 0.057 mmol, 1.5 equiv) was added, and the reaction mixture was stirred for 10 min. Then,  $\text{NaBH}_4$  (2.2 mg, 0.057 mmol, 1.5 equiv) was added, and the reaction mixture was stirred for 10 min. Then, brine (2 mL) and EtOAc (4 mL) were added, and the aqueous and organic layers were separated. The aqueous layer was extracted with EtOAc (3 x 2 mL). The combined organic layers were washed with brine (2 x 2 mL), and the aqueous layers were extracted with EtOAc (1 x 2 mL). The organic layers were dried over  $\text{Na}_2\text{SO}_4$ , filtered, and concentrated *in vacuo*. Purification by flash column chromatography (80% EtOAc/hexanes) afforded **5.66** (19.2 mg, 96%) as a clear oil.  $^1\text{H NMR}$  (700 MHz,  $\text{CDCl}_3$ )  $\delta$  4.24 (br s, 1H), 4.08–4.04 (m, 1H), 4.05 (d,  $J = 14.2$  Hz, 1H), 3.96 (ddd,  $J = 7.4, 6.2, 3.9$  Hz, 1H), 3.93–3.88 (m, 1H), 3.86 (d,  $J = 8.0$  Hz, 1H), 3.80 (dd,  $J = 11.7, 3.6$  Hz,

1H), 3.80–3.75 (m, 1H) 3.62 (d,  $J = 8.0$  Hz, 1H), 3.31 (s, 1H), 2.67 (dd,  $J = 15.9, 6.9$  Hz, 1H), 2.31 (dd,  $J = 15.9, 11.1$  Hz, 1H), 2.23–2.11 (m, 4H), 1.96 (s, 3H), 1.94 (d,  $J = 14.2$  Hz, 1H), 1.77 (td,  $J = 11.9, 9.7$  Hz, 1H), 1.63 (br s, 1H), 1.26 (s, 3H), 1.17 (s, 3H), 0.95 (s, 3H), 0.87 (s, 9H), 0.06 (s, 3H),  $-0.01$  (s, 3H).

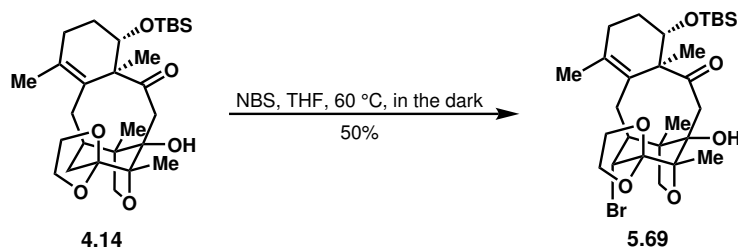


To **5.67** (2.5 mg, 0.005 mmol, 1 equiv) in anhydrous THF (0.3 mL, 0.02 M) at  $-78$  °C, L-selectride (1 drop from 1 mL syringe) was added. The reaction mixture was stirred for 1 h, after which the reaction mixture was warmed to  $0$  °C.  $\text{H}_2\text{O}_2$  (1 drop from 1 mL syringe) and 15 wt% aq. NaOH (1 drop from 1 mL syringe) were added and the reaction mixture was stirred for 30 min, after which EtOAc was added, and the aqueous and organic layers were separated. The aqueous layer was extracted with EtOAc, and the combined organic layers were dried over  $\text{Na}_2\text{SO}_4$ , filtered, and concentrated *in vacuo*. Purification by flash column chromatography (50% EtOAc/hexanes) afforded **5.67** (2.9 mg, quant.).  $^1\text{H NMR}$  (700 MHz,  $\text{CDCl}_3$ )  $\delta$  4.16 (dd,  $J = 12.4, 4.0$  Hz, 1H), 4.10–4.07 (m, 1H), 4.09 (d,  $J = 14.6$  Hz, 1H), 4.02 (br s, 1H), 3.99–3.92 (m, 2H), 3.87 (d,  $J = 8.0$  Hz, 1H), 3.81 (td,  $J = 7.3, 6.1$  Hz, 1H), 3.63 (d,  $J = 8.1$  Hz, 1H), 3.15 (s, 1H), 2.61 (dd,  $J = 15.7, 7.4$  Hz, 1H), 2.32 (dd,  $J = 16.0, 11.3$  Hz, 1H), 2.21–2.14 (m, 2H), 2.09 (d,  $J = 15.9$  Hz, 1H), 2.04 (d,  $J = 14.4$  Hz, 1H), 2.01 (s, 3H), 2.01–1.97 (m, 1H), 1.81–1.76 (m, 1H), 1.18 (s, 3H), 1.17 (s, 3H), 0.97 (s, 3H), 0.87 (s, 9H), 0.07 (s, 3H),  $-0.01$  (s, 3H).

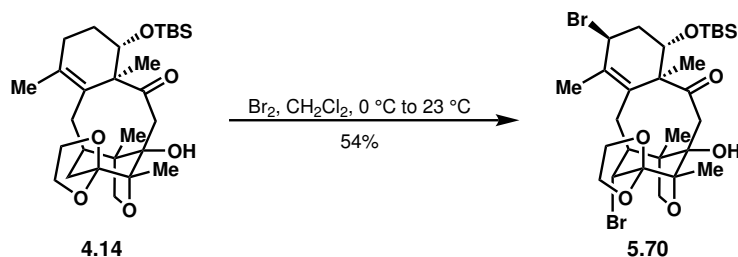


To  $\text{PPh}_3$  (3.1 mg, 0.012 mmol, 1.5 equiv) and cinnamic acid (1.8 mg, 0.012 mmol, 1.5 equiv), **5.66** (4.0 mg, 0.008 mmol, 1 equiv) in anhydrous THF (0.3 mL, 0.027 M) was added. The solution was cooled to  $0$  °C, and DIAD (1 drop from 1 mL syringe) was added. The reaction mixture was stirred for 25 min, after which the reaction mixture was concentrated *in vacuo*. Purification by preparatory TLC (75% EtOAc/hexanes) afforded **5.68**.  $^1\text{H NMR}$  (700 MHz,  $\text{CDCl}_3$ )  $\delta$  7.76 (d,  $J = 16.0$  Hz, 1H), 7.56–7.51 (m, 2H), 7.44–7.40 (m, 3H), 6.48 (d,  $J = 16.0$  Hz, 1H), 5.45–5.42 (m, 1H), 4.27 (d,  $J = 14.4$  Hz, 1H), 4.18 (dd,  $J = 11.2, 4.9$  Hz, 1H), 3.96 (ddd,  $J = 7.7, 6.2, 4.0$  Hz, 1H), 3.92–3.88 (m, 1H), 3.89 (d,  $J = 8.0$  Hz, 1H), 3.85 (td,  $J = 7.7, 6.2$  Hz, 1H), 3.73 (td,  $J = 7.6, 6.2$  Hz, 1H), 3.64 (d,  $J = 8.0$  Hz,

1H), 3.38 (s, 1H), 2.65 (dd,  $J = 15.7, 7.0$  Hz, 1H), 2.33–2.23 (m, 2H), 2.22–2.18 (m, 1H), 2.11–2.07 (m, 2H), 1.97–1.93 (m, 2H), 1.91 (s, 3H), 1.25 (s, 3H), 1.23 (s, 3H), 0.98 (s, 3H), 0.85 (s, 9H), –0.02 (s, 3H), –0.04 (s, 3H).

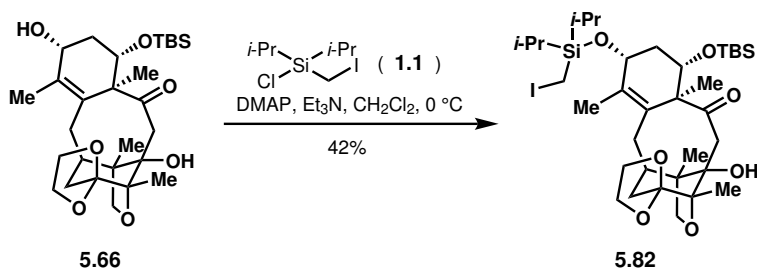


To NBS (4.9 mg, 0.028 mmol, 1.5 equiv) in a  $\mu\text{W}$  vial in the dark, a solution of **4.14** (9.3 mg, 0.018 mmol, 1 equiv) in anhydrous THF (0.37 mL, 0.05 M) was added. The reaction mixture was warmed to 60 °C and stirred for 1.5 h, after which NBS (4.9 mg, 0.028 mmol, 1.5 equiv) was added. The reaction mixture was stirred for another 30 min, after which it was quenched with sat. aq.  $\text{NaHCO}_3$  (0.5 mL) and sat. aq.  $\text{Na}_2\text{SO}_3$  (0.5 mL). EtOAc (0.5 mL) was also added, and the aqueous and organic layers were separated. The aqueous layer was extracted with EtOAc (3 x 0.5 mL), and the combined organic layers were concentrated *in vacuo*. Purification by preparatory TLC (40% EtOAc/hexanes) afforded **5.69** (5.4 mg, 50%).  $^1\text{H NMR}$  (700 MHz,  $\text{CDCl}_3$ )  $\delta$  4.30 (d,  $J = 4.3$  Hz, 1H), 4.23 (q,  $J = 6.7$  Hz, 1H), 4.11–3.99 (m, 3H), 3.92 (d,  $J = 8.3$  Hz, 1H), 3.87 (s, 1H), 3.87 (d,  $J = 8.3$  Hz, 1H), 3.80 (dd,  $J = 11.3, 4.5$  Hz, 1H), 3.21 (d,  $J = 14.3$  Hz, 1H), 2.95 (dd,  $J = 15.9, 7.8$  Hz, 1H), 2.69–2.64 (m, 1H), 2.42–2.34 (m, 1H), 2.17 (d,  $J = 17.6$  Hz, 1H), 2.13 (dd,  $J = 18.0$  Hz, 5.3 Hz, 1H), 2.15–2.11 (m, 1H), 2.05 (d,  $J = 14.3$  Hz, 1H), 1.92 (s, 3H), 1.80–1.74 (m, 2H), 1.27–1.24 (s, 6H), 0.98 (s, 3H), 0.89 (s, 9H), 0.06 (s, 3H), –0.01 (s, 3H).



Trace water was removed from **4.14** (10.4 mg, 0.021 mmol, 1 equiv) via azeotropic distillation with anhydrous benzene (1 x 0.4 mL). Then, to **4.14**, anhydrous  $\text{CH}_2\text{Cl}_2$  (0.4 mL, 0.05 M) was added. At 0 °C,  $\text{Br}_2$  (2.6  $\mu\text{L}$ , 0.057 mmol, 2.5 equiv) was added, and the reaction mixture was warmed to 23 °C and stirred for 1.5 h. The reaction mixture was then quenched with sat. aq.  $\text{NaHCO}_3$  (0.5 mL) and EtOAc (0.5 mL), and the aqueous and organic layers were separated. The aqueous layer was extracted with EtOAc (3 x 0.5 mL), and the combined organic layers were concentrated. Purification by flash column chromatography (25% EtOAc/hexanes) afforded **5.70** (7.4 mg, 54%).  $^1\text{H NMR}$  (700 MHz,  $\text{CDCl}_3$ )  $\delta$  4.71 (br s, 1H), 4.42 (dd,  $J = 11.6, 3.7$  Hz, 1H), 4.26 (d,  $J = 3.8$  Hz, 1H), 4.21–4.17 (m, 1H), 4.05–4.02 (m, 2H), 3.99–3.94 (m, 1H), 3.92 (d,  $J = 8.3$  Hz, 1H), 3.89 (d,  $J = 8.4$  Hz, 1H), 3.64 (s, 1H), 3.42 (d,  $J = 14.7$  Hz, 1H), 2.92 (dd,  $J = 15.7, 8.1$  Hz, 1H), 2.81–2.75 (m, 1H), 2.25 (ddd,  $J$

= 14.5, 3.7, 2.1 Hz, 1H), 2.20–2.13 (m, 3H), 2.09 (s, 3H), 1.26 (s, 3H), 1.22 (s, 3H), 0.95 (s, 3H), 0.87 (s, 9H), 0.08 (s, 3H), 0.01 (s, 3H).

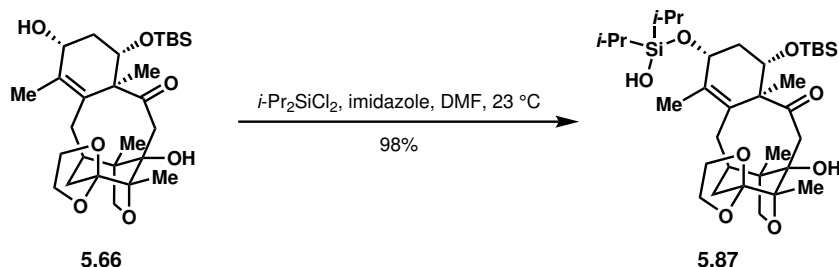


To **5.66** (6.5 mg, 0.0124 mmol, 1 equiv) and DMAP (1.0 mg, 0.008 mmol, 0.66 equiv) in anhydrous  $\text{CH}_2\text{Cl}_2$  (0.3 mL, 0.04 M), anhydrous  $\text{Et}_3\text{N}$  (1.7  $\mu\text{L}$ , 0.0124 mmol, 1 equiv) and silane reagent **1.1** (large excess, solution in hexanes) were added. The reaction mixture was stirred at 0 °C for 30 min, after which it was warmed to 23 °C. After 110 min, extra silane reagent **1.1** (large excess, solution in hexanes) was added. After another 1 h, the reaction was quenched with sat. aq.  $\text{NH}_4\text{Cl}$  and  $\text{EtOAc}$ , and the aqueous and organic layers were separated. The aqueous layer was extracted 3x with  $\text{EtOAc}$ , and the combined organic layers were washed 1x with brine, dried over  $\text{Na}_2\text{SO}_4$ , filtered, and concentrated *in vacuo*. Purification by preparatory TLC (50%  $\text{EtOAc}$ /hexanes) afforded **5.82** (4.0 mg, 42%).  $^1\text{H}$  NMR (700 MHz,  $\text{CDCl}_3$ )  $\delta$  4.59 (dd,  $J = 10.4, 6.1$  Hz, 1H), 4.10–4.06 (m, 1H), 4.04 (d,  $J = 14.4$  Hz, 1H), 3.99–3.94 (m, 1H), 3.93–3.89 (m, 1H), 3.86 (d,  $J = 8.0$  Hz, 1H), 3.79–3.74 (m, 2H), 3.62 (d,  $J = 8.0$  Hz, 1H), 3.32 (br s, 1H), 2.67 (dd,  $J = 15.9, 6.9$  Hz, 1H), 2.28 (dd,  $J = 16.0, 11.3$  Hz, 1H), 2.21–2.11 (m, 6H), 1.94 (d,  $J = 14.1$  Hz, 1H), 1.94 (s, 3H), 1.83 (q,  $J = 11.6$  Hz, 1H), 1.24 (s, 3H), 1.17 (s, 3H), 1.14–1.06 (m, 14H), 0.94 (s, 3H), 0.87 (s, 9H), 0.06 (s, 3H),  $-0.02$  (s, 3H).

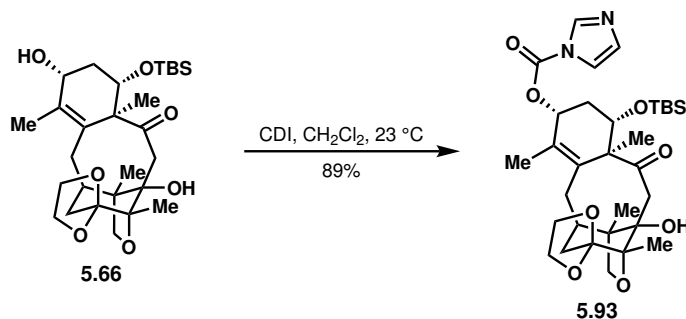


To **5.82** (4.0 mg, 0.0051 mmol, 1 equiv), Xantphos (3.0 mg, 0.0051 mmol, 1 equiv), and  $\text{Pd}(\text{OAc})_2$  (0.6 mg, 0.0026 mmol, 0.5 equiv) in a glovebox, added  $\text{Cs}_2\text{CO}_3$  (5.0 mg, 0.0153 mmol, 3 equiv) and anhydrous benzene (degassed with three cycles of freeze/pump/thaw; 0.1 mL, 0.05 M). The reaction mixture was brought out of the glovebox and stirred at 23 °C under irradiation with a blue LED for 13 h. The reaction mixture was filtered through a pad of Celite with the aid of  $\text{EtOAc}$  and concentrated *in vacuo*. Purification by preparatory TLC (50%  $\text{EtOAc}$ /hexanes) afforded **5.85**.  $^1\text{H}$  NMR (700 MHz,  $\text{CDCl}_3$ )  $\delta$  5.69 (d,  $J = 5.1$  Hz, 1H), 4.42 (s, 1H), 4.23 (d,  $J = 13.0$  Hz, 1H), 4.16–4.09 (m, 1H), 4.00–3.95 (m, 1H), 3.89 (q,  $J = 7.7$  Hz, 1H), 3.84 (dd,  $J = 10.8, 6.4$  Hz, 1H), 3.80 (d,  $J = 8.0$  Hz, 1H), 3.74 (q,  $J = 7.5$  Hz, 1H), 3.66 (dd,  $J = 11.6, 4.0$  Hz, 1H), 3.62 (d,  $J = 8.2$  Hz, 1H), 2.56 (dd,  $J =$

9.6, 5.0 Hz, 1H), 2.38 (dd,  $J = 14.9, 9.6$  Hz, 1H), 2.23–2.16 (m, 1H), 1.89 (d,  $J = 12.9$  Hz, 1H), 1.80–1.72 (m, 2H), 1.46 (s, 3H), 1.37 (s, 3H), 1.33 (d,  $J = 15.5$  Hz, 1H), 1.23 (s, 3H), 1.12–1.03 (m, 14H), 1.10 (s, 3H), 0.86 (s, 9H), 0.84 (s, 3H), 0.74 (d,  $J = 15.5$  Hz, 1H), 0.03 (s, 3H),  $-0.04$  (s, 3H). **HRMS** (ESI+)  $m/z$  calc'd for  $C_{35}H_{60}NaO_7Si_2$   $[M+Na]^+$ : 671.3762, found: 671.3770.



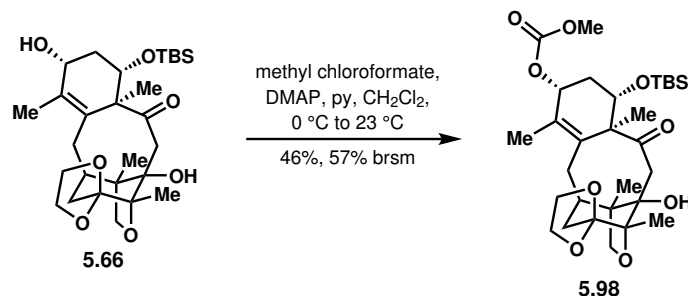
To **5.66** (4.9 mg, 0.009 mmol, 1 equiv) and imidazole (2.6 mg, 0.037 mmol, 4 equiv) at 0 °C, anhydrous DMF (0.2 mL, 0.05 M) was added, followed by  $i\text{-Pr}_2\text{SiCl}_2$  (3.4  $\mu\text{L}$ , 0.019 mmol, 2 equiv). The reaction mixture was warmed to 23 °C and stirred for 2 h, after which it was quenched with  $\text{H}_2\text{O}$  (0.5 mL) and EtOAc (0.5 mL). The aqueous and organic layers were separated, and the aqueous layer was extracted with EtOAc (3 x 0.5 mL). The combined organic layers were concentrated *in vacuo*. Purification by flash column chromatography (60% EtOAc/hexanes with 1%  $\text{Et}_3\text{N}$ ) afforded **5.87** (6.0 mg, 98%) as a colorless oil.  **$^1\text{H}$  NMR** (700 MHz,  $\text{CDCl}_3$ )  $\delta$  4.52 (dd,  $J = 10.4, 6.2$  Hz, 1H), 4.07 (ddd,  $J = 7.6, 6.2, 3.9$  Hz, 1H), 4.02 (d,  $J = 14.3$  Hz, 1H), 3.98–3.93 (m, 1H), 3.90 (td,  $J = 7.8, 6.3$  Hz, 1H), 3.86 (d,  $J = 8.0$  Hz, 1H), 3.81–3.73 (m, 2H), 3.62 (d,  $J = 8.0$  Hz, 1H), 3.34 (s, 1H), 2.67 (dd,  $J = 15.9, 7.0$  Hz, 1H), 2.28 (dd,  $J = 16.0, 11.2$  Hz, 1H), 2.22–2.17 (m, 2H), 2.15–2.10 (m, 2H), 1.94 (d,  $J = 14.3$  Hz, 1H), 1.92 (s, 3H), 1.88–1.79 (m, 1H), 1.25 (s, 3H), 1.17 (s, 3H), 1.11–1.02 (m, 14H), 0.95 (s, 3H), 0.87 (s, 9H), 0.04 (s, 3H),  $-0.03$  (s, 3H).



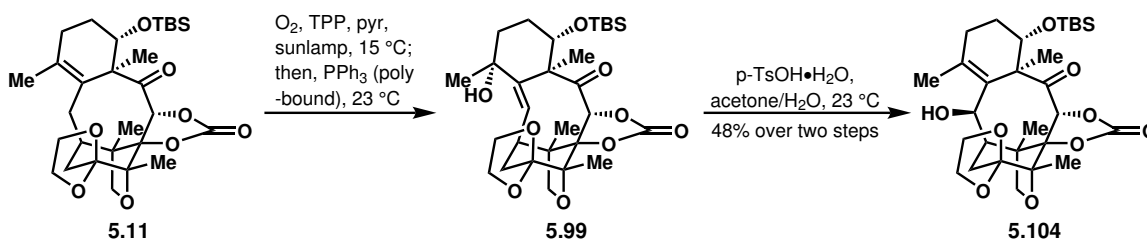
To **5.66** (2.1 mg, 0.004 mmol, 1 equiv) and CDI (1.0 mg, 0.006 mmol, 1.5 equiv), anhydrous  $\text{CH}_2\text{Cl}_2$  (0.1 mL, 0.04 M) was added. The reaction mixture was stirred at 23 °C for 20 h, after which  $\text{CH}_2\text{Cl}_2$  (0.5 mL) and  $\text{H}_2\text{O}$  (0.5 mL) were added. The aqueous and organic layers were separated, and the aqueous layer was extracted with  $\text{CH}_2\text{Cl}_2$  (3 x 0.5 mL). The combined organic layers were dried over  $\text{Na}_2\text{SO}_4$ , filtered, and concentrated *in vacuo*. Purification by flash column chromatography (100% EtOAc) afforded **5.93** (2.2 mg, 89%).  **$^1\text{H}$  NMR** (500 MHz,  $\text{CDCl}_3$ )  $\delta$  8.16 (s, 1H), 7.45 (s, 1H), 7.11 (s, 1H), 5.70 (dd,  $J = 10.3, 6.8$  Hz, 1H), 4.14 – 4.09 (m, 1H), 4.03 (d,  $J = 14.5$  Hz, 1H), 3.96 (ddd,  $J = 7.1, 6.1,$



3.9 Hz, 1H), 3.94–3.86 (m, 3H), 3.80 (td,  $J = 7.3, 6.1$  Hz, 1H), 3.63 (d,  $J = 8.1$  Hz, 1H), 3.28 (s, 1H), 2.71 (dd,  $J = 15.9, 7.0$  Hz, 1H), 2.41–2.30 (m, 2H), 2.27 (d,  $J = 15.7$  Hz, 1H), 2.23–2.16 (m, 1H), 2.09 (d,  $J = 15.9$  Hz, 1H), 2.00 (d,  $J = 14.4$  Hz, 1H), 2.00–1.91 (m, 1H), 1.88 (s, 3H), 1.31 (s, 3H), 1.19 (s, 3H), 0.97 (s, 3H), 0.87 (s, 9H), 0.07 (s, 3H), 0.00 (s, 3H).



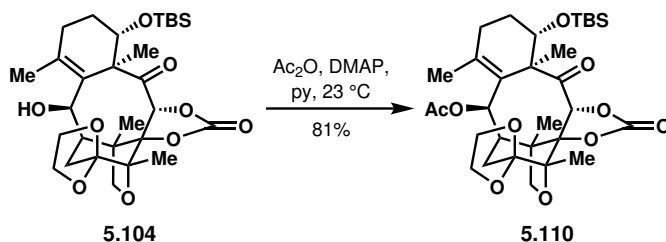
To a solution of **5.66** (3.7 mg, 0.007 mmol, 1 equiv) and DMAP (a small spatula tip) in  $\text{CH}_2\text{Cl}_2$  (0.15 mL, 0.05 M) at 0 °C, pyridine (2.9  $\mu\text{L}$ , 0.020 mmol, 5 equiv) and methyl chloroformate (0.8  $\mu\text{L}$ , 0.012 mmol, 1.5 equiv) were added. The reaction mixture was stirred at 0 ° for 30 min, after which it was warmed to 23 °C. After 80 min, pyridine (1 drop from 1 mL syringe) and methyl chloroformate (3  $\mu\text{L}$ , 0.039 mmol, 5.5 equiv) were added. After another 1.5 h, another spatula tip of DMAP was added. After another 3 h,  $\text{H}_2\text{O}$  (0.5 mL) and  $\text{EtOAc}$  (0.5 mL) were added to the reaction mixture, and the aqueous and organic layers were separated. The aqueous layer was extracted with  $\text{EtOAc}$  (3 x 0.5 mL), and the combined organic layers were concentrated. Purification by flash column chromatography (50%  $\text{EtOAc}$ /hexanes to 80%  $\text{EtOAc}$ /hexanes) afforded **5.98** (1.9 mg, 46%) and recovered **5.66** (0.7 mg, 19%).  $^1\text{H NMR}$  (700 MHz,  $\text{CDCl}_3$ )  $\delta$  5.35 (dd,  $J = 10.3, 6.8$  Hz, 1H), 4.10–4.07 (m, 1H), 4.02 (d,  $J = 14.5$  Hz, 1H), 3.98–3.93 (m, 1H), 3.92–3.88 (m, 1H), 3.88–3.84 (m, 2H), 3.83 (s, 3H), 3.80–3.75 (m, 1H), 3.62 (d,  $J = 8.1$  Hz, 1H), 3.30 (s, 1H), 2.67 (dd,  $J = 15.9, 7.0$  Hz, 1H), 2.31 (dd,  $J = 15.9, 11.1$  Hz, 1H), 2.28–2.25 (m, 1H), 2.21 (d,  $J = 15.8$  Hz, 1H), 2.19–2.12 (m, 1H), 2.09 (d,  $J = 15.7$  Hz, 1H), 1.97 (d,  $J = 14.0$  Hz, 1H), 1.84 (s, 3H), 1.25 (s, 3H), 1.17 (s, 3H), 0.95 (s, 3H), 0.86 (s, 9H), 0.06 (s, 3H),  $-0.02$  (s, 3H).



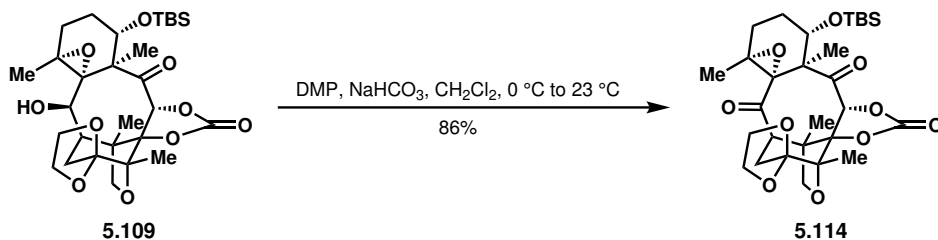
To **5.11** (33.5 mg, 0.061 mmol, 1 equiv), a solution of tetraphenylporphyrin (0.7 mg, 0.0012 mmol, 0.02 equiv) in anhydrous pyridine (0.61 mL, 0.1M) was added. The reaction mixture was irradiated with a sunlamp at 15 °C while  $\text{O}_2$  was allowed to bubble through. After 49.5 h, the sunlamp,  $\text{O}_2$  balloon, and cryobath were removed, and polymer-bound triphenylphosphine (3 mmol/g, 102 mg, 0.305 mmol, 5 equiv) was added. The reaction mixture was stirred at 23 °C for 1 h, after which it was filtered through Celite with the aid of  $\text{EtOAc}$  and concentrated *in vacuo*. To the resulting crude product was added 1M  $\text{HCl}$  and



1H), 4.19–4.15 (m, 2H), 4.13–4.06 (m, 2H), 4.04–3.99 (m, 1H), 3.95 (d,  $J = 8.4$  Hz, 1H), 3.82 (d,  $J = 8.3$  Hz, 1H), 3.79 (dd,  $J = 11.7, 4.0$  Hz, 1H), 2.97 (d,  $J = 1.1$  Hz, 1H), 2.46 (d,  $J = 10.1$  Hz, 1H), 2.27 (dd,  $J = 16.3, 51.4$  Hz, 1H), 2.27 (dd,  $J = 16.3, 61.6$  Hz), 2.00 (dt,  $J = 14.8, 3.5$  Hz, 1H), 1.94–1.87 (m, 1H), 1.76 (qd,  $J = 12.6, 4.1$  Hz, 1H), 1.69 (s, 3H), 1.53–1.49 (m, 1H), 1.32 (s, 3H), 1.31 (s, 3H), 1.03 (s, 3H), 0.83 (s, 9H), 0.02 (s, 3H), 0.00 (s, 3H).

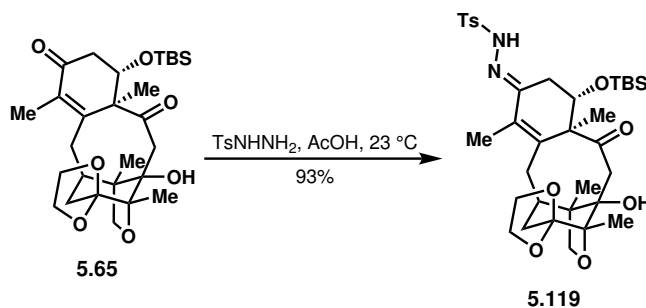


Trace water was removed from **5.104** (9.1 mg, 0.016 mmol, 1 equiv) was removed via azeotropic distillation with anhydrous benzene. To **5.104** and DMAP (0.4 mg, 0.003 mmol, 0.2 equiv), anhydrous pyridine (0.16 mL, 0.1 M) and  $\text{Ac}_2\text{O}$  (3.0  $\mu\text{L}$ , 0.032 mmol, 2 equiv) were added. The reaction mixture was stirred at 23  $^\circ\text{C}$  for 21.5 h, after which it was quenched with sat. aq.  $\text{NaHCO}_3$  (0.5 mL) and EtOAc (0.5 mL), and the aqueous and organic layers were separated. The aqueous layer was extracted with EtOAc (3 x 0.5 mL), and the combined organic layers were washed with brine (1 x 1 mL). The combined aqueous layers were extracted with EtOAc (1 x 0.5 mL). The combined organic layers were then concentrated *in vacuo*. Purification by flash column chromatography (50% EtOAc/hexanes) afforded **5.110** (7.9 mg, 81%).  $^1\text{H NMR}$  (400 MHz,  $\text{CDCl}_3$ )  $\delta$  6.16 (s, 1H), 5.44 (s, 1H), 4.19 (ddd,  $J = 7.6, 6.0, 4.0$  Hz, 1H), 4.06–4.01 (m, 1H), 3.99 (dd,  $J = 11.6, 4.2$  Hz, 1H), 3.95–3.90 (m, 1H), 3.93 (d,  $J = 8.3$  Hz, 1H), 3.88–3.80 (m, 1H), 3.77 (d,  $J = 8.4$  Hz, 1H), 2.44 (d,  $J = 15.8$  Hz, 1H), 2.34–2.19 (m, 2H), 2.20–2.08 (m, 2H), 2.05 (s, 3H), 2.04 (s, 3H), 1.85–1.75 (m, 1H), 1.70 (td,  $J = 12.2, 5.7$  Hz, 1H), 1.37 (s, 3H), 1.26 (s, 3H), 1.10 (s, 3H), 0.85 (s, 9H), 0.05 (s, 3H), 0.04 (s, 3H).

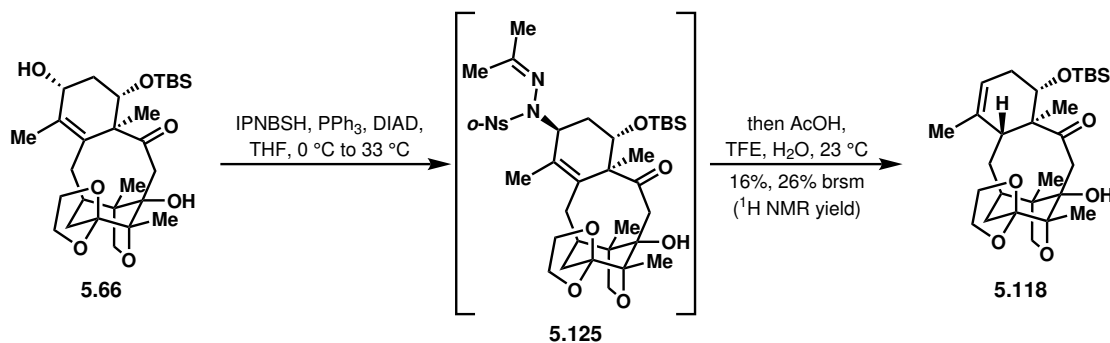


To **5.11** (1.4 mg, 0.002 mmol, 1 equiv) in  $\text{CH}_2\text{Cl}_2$  (0.1 mL, 0.02 M) at 0  $^\circ\text{C}$ ,  $\text{NaHCO}_3$  (1.0 mg, 0.012 mmol, 5 equiv) and DMP (3.1 mg, 0.007 mmol, 3 equiv) were added. The reaction mixture was warmed to 23  $^\circ\text{C}$  and stirred for 70 min, after which it was quenched with sat. aq.  $\text{NaHCO}_3$  (0.5 mL), sat. aq.  $\text{Na}_2\text{S}_2\text{O}_3$  (0.5 mL), and EtOAc (0.5 mL). The resulting mixture was stirred vigorously for 15 min; then, the aqueous and organic layers were separated. The aqueous layer was extracted with EtOAc (3 x 0.5 mL), and the combined organic layers were concentrated *in vacuo*. Purification by preparatory TLC (80% EtOAc/hexanes) afforded

**5.114** (1.2 mg, 86%) as a white solid.  $^1\text{H NMR}$  (500 MHz,  $\text{CDCl}_3$ )  $\delta$  6.64 (s, 1H), 4.34–4.26 (m, 1H), 4.20–4.14 (m, 1H), 4.11–4.06 (m, 2H), 3.98 (d,  $J = 8.6$  Hz, 1H), 3.90 (dd,  $J = 11.5, 4.0$  Hz, 1H), 3.74 (d,  $J = 8.6$  Hz, 1H), 3.18 (d,  $J = 10.1$  Hz, 1H), 2.40–2.21 (m, 2H), 2.12–1.94 (m, 2H), 1.92–1.79 (m, 1H), 1.60–1.55 (m, 1H), 1.38 (s, 3H), 1.37 (s, 3H), 1.29 (s, 3H), 0.84 (s, 3H), 0.83 (s, 9H), 0.03 (s, 3H), 0.01 (s, 3H).



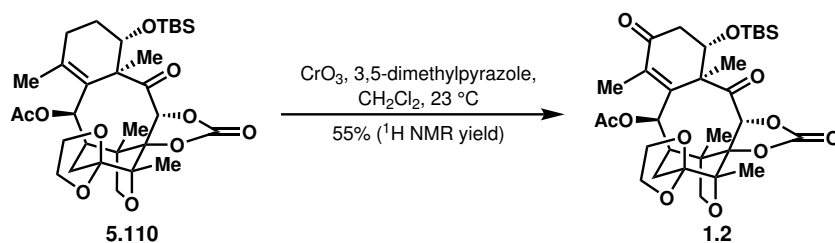
To **5.65** (30.0 mg, 0.0576 mmol, 1 equiv),  $\text{TsNHNH}_2$  (29.0 mg, 0.156 mmol, 2.7 equiv) and glacial  $\text{AcOH}$  (1.4 mL) were added. The reaction mixture was stirred at  $23\text{ }^\circ\text{C}$  for 14 h, after which acetophenone (5 equiv) was added. The mixture was stirred for 1 h, then concentrated *in vacuo*. Purification by preparatory TLC afforded **5.119** (36.8 mg, 93%).  $^1\text{H NMR}$  (700 MHz,  $\text{CDCl}_3$ )  $\delta$  7.89 (d,  $J = 8.3$  Hz, 2H), 7.33 (d,  $J = 8.4$  Hz, 2H), 4.03–3.97 (m, 2H), 3.95–3.91 (m, 1H), 3.93 (d,  $J = 14.7$  Hz, 1H), 3.88–3.84 (m, 2H), 3.77 (td,  $J = 7.6, 6.2$  Hz, 1H), 3.64 (d,  $J = 8.2$  Hz, 1H), 2.73 (dd,  $J = 15.5, 7.6$  Hz, 1H), 2.67 (dd,  $J = 15.9, 5.5$  Hz, 1H), 2.44 (s, 3H), 2.40–2.30 (m, 1H), 2.25 (d,  $J = 15.7$  Hz, 1H), 2.23–2.18 (m, 1H), 2.10–2.03 (m, 2H), 1.99 (d,  $J = 14.6$  Hz, 1H), 1.96 (s, 3H), 1.16 (s, 3H), 1.15 (s, 3H), 0.96 (s, 3H), 0.86 (s, 9H), 0.08 (s, 3H),  $-0.02$  (s, 3H).



To a solution of **5.66** (2.1 mg, 0.004 mmol, 1 equiv) and  $\text{PPh}_3$  (3.1 mg, 0.012 mmol, 3 equiv) in anhydrous  $\text{THF}$  (0.1 mL) at  $0\text{ }^\circ\text{C}$ ,  $\text{DIAD}$  (2.4  $\mu\text{L}$ , 0.012 mmol, 3 equiv) was added. The reaction mixture was stirred for 10 min; then, a solution of  $\text{IPNBSH}$  (3.1 mg, 0.012 mmol, 3 equiv) in anhydrous  $\text{THF}$  (0.1 mL) was added, and the reaction mixture was warmed to  $33\text{ }^\circ\text{C}$ . The reaction mixture was stirred for 14 h; if desired, at this point, an aqueous workup could be conducted followed by purification with preparatory TLC (two sequential preparatory TLC runs, first with 30%  $\text{EtOAc}/\text{CH}_2\text{Cl}_2$ , second with 60%  $\text{EtOAc}/\text{hexanes}$ ) to afford analytically pure **5.125**.  $^1\text{H NMR}$  (700 MHz,  $\text{CDCl}_3$ )  $\delta$  7.86 (d,  $J = 8.1$  Hz, 1H), 7.73 (t,  $J = 7.8$  Hz, 1H), 7.67 (t,  $J = 7.8$  Hz, 1H), 7.54 (d,  $J = 8.1$  Hz, 1H), 4.66 (d,  $J = 8.0$

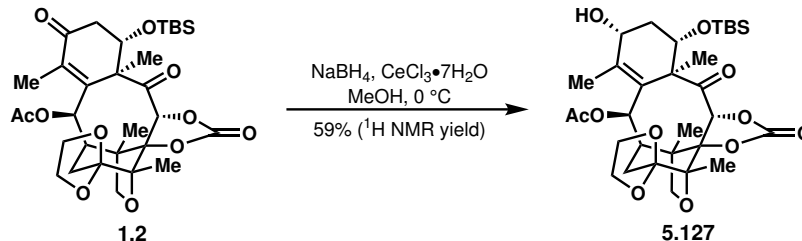
Hz, 1H), 4.10–4.06 (m, 1H), 4.04–4.00 (m, 1H), 3.97 (dd,  $J = 11.8, 4.6$  Hz, 1H), 3.90–3.84 (m, 2H), 3.83 (d,  $J = 8.2$  Hz, 1H), 3.59 (d,  $J = 8.2$  Hz, 1H), 2.99 (d,  $J = 13.8$  Hz, 1H), 2.56 (dd,  $J = 15.8, 7.9$  Hz, 1H), 2.30 (dd,  $J = 16.3, 11.8$  Hz, 1H), 2.25 (s, 3H), 2.24 (d,  $J = 16.1$  Hz, 1H), 2.23 (s, 3H), 2.18–2.10 (m, 1H), 2.04 (s, 1H), 1.90 (s, 3H), 1.83 (dd,  $J = 16.3, 4.9$  Hz, 1H), 1.74–1.67 (m, 1H), 1.46 (dd,  $J = 14.1, 4.5$  Hz, 1H), 1.18 (s, 3H), 1.13 (s, 3H), 0.95 (s, 3H), 0.72 (s, 9H),  $-0.16$  (s, 3H),  $-0.39$  (s, 3H).

Otherwise, the reaction mixture was cooled to 23 °C and glacial AcOH (0.1 mL), 2,2,2-trifluoroethanol (0.1 mL), and deionized H<sub>2</sub>O (0.1 mL) were added. The reaction mixture was stirred at 23 °C for 54 h, after which sat. aq. NaHCO<sub>3</sub> (0.5 mL) and EtOAc (0.5 mL) were added. The aqueous and organic layers were separated, and the aqueous layer was extracted with EtOAc (3 x 0.5 mL). The combined organic layers were washed with brine (2 x 1 mL) and concentrated *in vacuo*. <sup>1</sup>H NMR analysis with mesitylene as internal standard revealed 16% yield of **5.118** with 37% remaining **5.66** (26% **5.118** brsm). If desired, the crude mixture could be purified by preparatory TLC (50% EtOAc/hexanes) to afford analytically pure **5.118**. <sup>1</sup>H NMR (700 MHz, CDCl<sub>3</sub>) δ 5.36 (s, 1H), 4.36 (d,  $J = 14.2$  Hz, 1H), 4.20–4.16 (m, 1H), 4.03–3.96 (m, 2H), 3.94 (dd,  $J = 9.8, 6.3$  Hz, 1H), 3.86 (d,  $J = 7.7$  Hz, 1H), 3.80 (q,  $J = 6.8, 6.0$  Hz, 1H), 3.59 (d,  $J = 7.8$  Hz, 1H), 3.19–3.13 (m, 1H), 3.00 (s, 1H), 2.45 (dd,  $J = 16.1, 11.7$  Hz, 1H), 2.29–2.22 (m, 1H), 2.08–2.03 (m, 1H), 2.01–1.94 (m, 1H), 1.92 (d,  $J = 14.3$  Hz, 1H), 1.79–1.74 (m, 1H), 1.75 (d,  $J = 15.8$  Hz, 1H), 1.72 (s, 3H), 1.66 (ddd,  $J = 16.3, 9.4, 2.5$  Hz, 1H), 1.23 (s, 3H), 1.05 (s, 3H), 0.87 (s, 3H), 0.84 (s, 9H), 0.02 (s, 3H),  $-0.03$  (s, 3H).

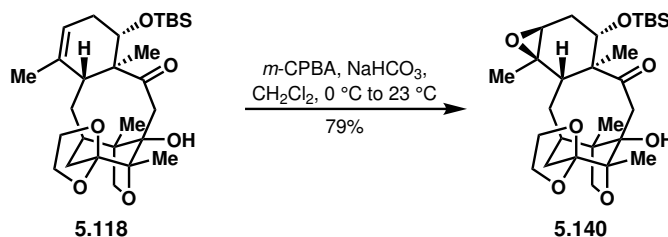


To **5.110** (10.0 mg, 0.016 mmol, 1 equiv) in anhydrous CH<sub>2</sub>Cl<sub>2</sub> at 23 °C, 3,5-dimethylpyrazole (15.8 mg, 0.165 mmol, 10 equiv) and CrO<sub>3</sub> (16.5 mg, 0.165 mmol, 10 equiv) were added. Every 12 h for the next 60 h, another 10 equiv 3,5-dimethylpyrazole and 10 equiv CrO<sub>3</sub> were added. After the last addition, the reaction mixture was stirred for another 12 h; then, the reaction mixture was filtered through a plug of silica gel with the aid of EtOAc and then concentrated *in vacuo*. EtOAc (2 mL) and 1 M HCl (2 mL) were added, and the aqueous and organic layers were separated. The organic layer was washed with 1 M HCl (2 x 2 mL), and the combined aqueous layers were extracted with EtOAc (3 x 2 mL). The combined organic layers were washed with sat. aq. NaHCO<sub>3</sub> (1 x 2 mL), with brine (1 x 2 mL), and then dried over Na<sub>2</sub>SO<sub>4</sub>, filtered, and concentrated *in vacuo*. Crude <sup>1</sup>H NMR analysis with mesitylene as internal standard revealed a 55% yield of **1.2**. Purification by flash column chromatography afforded **1.2**. <sup>1</sup>H NMR (700 MHz, CDCl<sub>3</sub>) δ 6.24 (s, 1H), 5.58 (s, 1H), 4.52 (dd,  $J = 13.0, 5.1$  Hz, 1H), 4.09–4.04 (m, 1H), 4.04–4.00 (m, 1H), 3.96 (d,  $J = 8.5$  Hz, 1H), 3.83–3.78 (m, 1H), 3.79 (d,  $J = 8.7$  Hz, 1H), 3.75 (q,  $J = 7.3$  Hz, 1H), 2.80 (dd,  $J = 16.4, 4.8$  Hz, 1H), 2.60 (dd,  $J = 16.0, 13.0$  Hz, 1H), 2.37–2.31 (m, 1H), 2.30–2.24 (m, 2H), 2.18 (s, 3H), 2.07–2.05 (m, 3H), 1.53 (s, 3H), 1.24 (s, 3H), 1.14 (s, 3H), 0.85 (s, 9H), 0.09 (s,

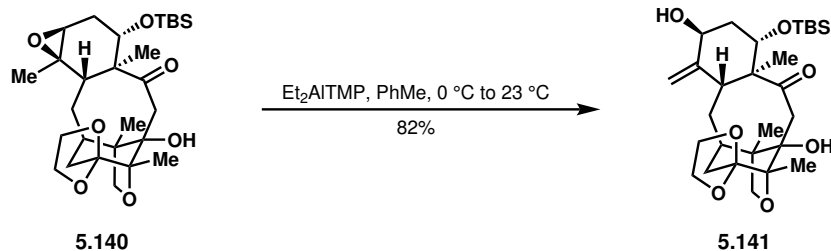
3H), 0.06 (s, 3H).



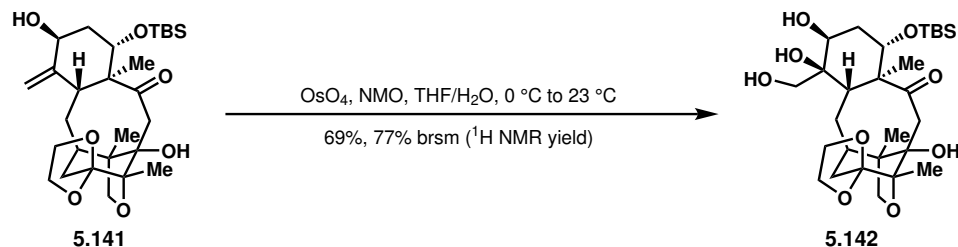
To **1.2** (1.6 mg, 0.003 mmol, 1 equiv) in anhydrous  $\text{MeOH}$  (0.13 mL, 0.02 M) at  $0\text{ }^\circ\text{C}$ ,  $\text{CeCl}_3 \cdot 7\text{H}_2\text{O}$  was added. The reaction mixture was stirred for 10 min, after which  $\text{NaBH}_4$  (spatula tip) was added. After 15 min, another spatula tip of  $\text{NaBH}_4$  was added. After another 15 min, the reaction was quenched with sat. aq.  $\text{NH}_4\text{Cl}$  (0.5 mL) and  $\text{EtOAc}$  (0.5 mL), and the aqueous and organic layers were separated. The aqueous layer was extracted with  $\text{EtOAc}$  (3 x 0.5 mL), and the combined organic layers were concentrated *in vacuo*. Crude  $^1\text{H}$  NMR analysis with mesitylene as internal standard revealed a 59% yield of **5.127**. Purification by preparatory TLC (70%  $\text{EtOAc}$ /hexanes) afforded pure **5.127**.  $^1\text{H}$  NMR (700 MHz,  $\text{CDCl}_3$ )  $\delta$  6.13 (s, 1H), 5.49 (d,  $J = 2.1$  Hz, 1H), 4.21 (dd,  $J = 10.1, 6.3$  Hz, 1H), 4.18 (ddd,  $J = 7.6, 6.0, 4.0$  Hz, 1H), 4.08–4.00 (m, 2H), 3.97–3.91 (m, 1H), 3.93 (d,  $J = 8.3$  Hz, 1H), 3.84 (td,  $J = 7.9, 6.0$  Hz, 1H), 3.78 (d,  $J = 8.3$  Hz, 1H), 2.49 (d,  $J = 16.0$  Hz, 1H), 2.27–2.21 (m, 2H), 2.18 (d,  $J = 0.9$  Hz, 3H), 2.15 (dd,  $J = 9.9, 2.2$  Hz, 1H), 2.06 (s, 3H), 1.79 (td,  $J = 12.0, 10.2$  Hz, 1H), 1.25 (s, 3H), 1.10 (s, 3H), 0.85 (s, 9H), 0.08 (s, 3H), 0.05 (s, 3H).



To **5.118** (2.2 mg, 0.004 mmol, 1 equiv) in anhydrous  $\text{CH}_2\text{Cl}_2$  (0.1 mL, 0.04 M) at  $0\text{ }^\circ\text{C}$ ,  $\text{NaHCO}_3$  (1.8 mg, 5 equiv) and  $m\text{-CPBA}$  (75 wt%, 1.5 mg, 0.007 mmol, 1.5 equiv) were added. The reaction mixture was warmed to  $23\text{ }^\circ\text{C}$  and stirred for 2 h, after which it was quenched with sat. aq.  $\text{Na}_2\text{S}_2\text{O}_3$  (0.5 mL), sat. aq.  $\text{NaHCO}_3$  (0.5 mL), and  $\text{Et}_2\text{O}$  (0.5 mL). The resulting mixture was stirred vigorously for 15 min, after which the aqueous and organic layers were separated. The aqueous layer was extracted with  $\text{Et}_2\text{O}$  (4 x 0.5 mL), and the combined organic layers were concentrated *in vacuo*. Purification by flash column chromatography (50%  $\text{EtOAc}$ /hexanes to 60%  $\text{EtOAc}$ /hexanes) afforded **5.140** (1.8 mg, 79%).  $^1\text{H}$  NMR (700 MHz,  $\text{CDCl}_3$ )  $\delta$  4.33 (d,  $J = 14.5$  Hz, 1H), 4.18 (ddd,  $J = 8.0, 6.3, 4.1$  Hz, 1H), 4.13–4.06 (m, 1H), 4.04–3.97 (m, 1H), 3.91 (dd,  $J = 9.7, 6.3$  Hz, 1H), 3.85 (d,  $J = 7.8$  Hz, 1H), 3.84–3.78 (m, 1H), 3.59 (d,  $J = 7.8$  Hz, 1H), 3.05 (d,  $J = 2.8$  Hz, 1H), 2.74 (d,  $J = 10.1$  Hz, 1H), 2.52–2.38 (m, 2H), 2.15–2.08 (m, 1H), 1.83 (t,  $J = 15.1$  Hz, 2H), 1.79–1.71 (m, 2H), 1.69–1.61 (m, 1H), 1.27 (s, 3H), 1.21 (s, 3H), 1.04 (s, 3H), 0.84 (s, 3H), 0.82 (s, 9H), 0.04 (s, 3H),  $-0.04$  (s, 3H).

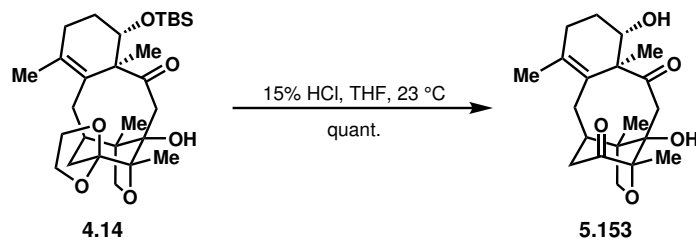


Trace water was removed from **5.141** (1.1 mg, 0.002 mmol, 1 equiv) via azeotropic distillation with anhydrous benzene (3 x 1 mL). To 2,2,6,6-tetramethylpiperidine (3.6  $\mu\text{L}$ , 0.021 mmol, 10 equiv, distilled over  $\text{CaH}_2$ ) in anhydrous PhMe (0.1 mL) at 0  $^\circ\text{C}$  under Ar, *n*-BuLi (1.6 M in hexanes, 11.8  $\mu\text{L}$ , 0.019 mmol, 9 equiv) was added. After 10 min,  $\text{Et}_2\text{AlCl}$  (0.9 M in PhMe, 21.0  $\mu\text{L}$ , 0.019 mmol, 9 equiv) was added. After another 30 min, a solution of **5.141** in anhydrous PhMe (0.1 mL) was added, and the reaction mixture was warmed to 23  $^\circ\text{C}$ . After stirring for 80 min, the reaction was quenched with sat. aq.  $\text{NaHCO}_3$  (0.5 mL) and EtOAc (0.5 mL), and the aqueous and organic layers were separated. The aqueous layer was extracted with EtOAc (3 x 0.5 mL), and the combined organic layers were concentrated *in vacuo*. Purification by flash column chromatography afforded **5.141** (0.9 mg, 82%) as a white solid.  $^1\text{H NMR}$  (700 MHz,  $\text{CDCl}_3$ )  $\delta$  5.12 (s, 1H), 4.78 (s, 1H), 4.63 (d,  $J = 14.4$  Hz, 1H), 4.39 (t,  $J = 3.0$  Hz, 1H), 4.35 (dd,  $J = 11.2, 4.9$  Hz, 1H), 4.21–4.16 (m, 1H), 4.00–3.92 (m, 2H), 3.87 (d,  $J = 7.8$  Hz, 1H), 3.84–3.78 (m, 1H), 3.60 (d,  $J = 8.9$  Hz), 3.59 (d,  $J = 7.6$  Hz, 2H), 3.06 (s, 1H), 2.41 (dd,  $J = 15.9, 11.7$  Hz, 1H), 2.15–2.09 (m, 1H), 2.08–2.03 (m, 1H), 1.98 (d,  $J = 14.4$  Hz, 1H), 1.78–1.70 (m, 1H), 1.67–1.61 (m, 2H), 1.66 (d,  $J = 15.5$  Hz, 1H), 1.25 (s, 3H), 0.91 (s, 3H), 0.85 (s, 3H), 0.83 (s, 9H), 0.04 (s, 3H),  $-0.01$  (s, 3H).

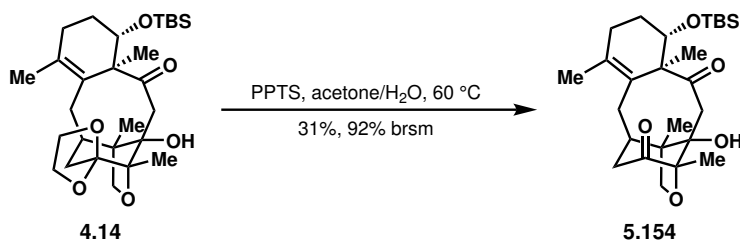


To **5.141** (0.9 mg, 0.002 mmol, 1 equiv) in anhydrous THF (0.1 mL) and deionized  $\text{H}_2\text{O}$  (50  $\mu\text{L}$ ) at 0  $^\circ\text{C}$ , NMO (50 wt% in  $\text{H}_2\text{O}$ , 2.0  $\mu\text{L}$ , 0.01 mmol, 5 equiv) was added, followed by  $\text{OsO}_4$  (4 wt% in  $\text{H}_2\text{O}$ , 1.1  $\mu\text{L}$ , 0.0002 mmol, 0.1 equiv). The reaction mixture was warmed to 23  $^\circ\text{C}$  and stirred vigorously. After 2 h, sat. aq.  $\text{Na}_2\text{S}_2\text{O}_3$  (0.5 mL) and EtOAc (0.5 mL) were added, and the mixture was stirred vigorously for 1 h. The aqueous and organic layers were separated, and the aqueous layer was extracted with EtOAc (3 x 0.5 mL). The combined organic layers were concentrated *in vacuo*. Crude  $^1\text{H NMR}$  analysis revealed a 69% yield of **5.142** (77% brsm). Purification by preparatory TLC (5% MeOH/EtOAc) afforded pure **5.142**.  $^1\text{H NMR}$  (700 MHz,  $\text{CDCl}_3$ )  $\delta$  4.68 (d,  $J = 14.4$  Hz, 1H), 4.29–4.21 (m, 2H), 4.08–4.01 (m, 2H), 4.00 (t,  $J = 2.9$  Hz, 1H), 3.86 (d,  $J = 7.7$  Hz, 1H), 3.82–3.78 (m, 1H), 3.74 (d,  $J = 10.9$  Hz, 1H), 3.63 (d,  $J = 7.8$  Hz, 1H), 3.58 (d,  $J = 10.9$  Hz, 1H), 3.35 (br s, 1H), 3.19 (d,  $J = 8.7$  Hz, 1H), 2.82 (br s, 1H), 2.67 (br s, 1H), 2.31 (dd,  $J = 15.8, 11.3$  Hz, 1H), 2.11–2.08 (m, 1H), 2.07 (d,  $J = 15.9$  Hz, 1H), 2.06–2.02 (m, 1H), 2.01 (d,  $J = 14.4$  Hz,

1H), 1.92 (br s, 1H), 1.83–1.73 (m, 2H), 1.56–1.52 (m, 1H), 1.27 (s, 3H), 1.05 (s, 3H), 0.86 (s, 9H), 0.84 (s, 3H), 0.06 (s, 3H), –0.02 (s, 3H).

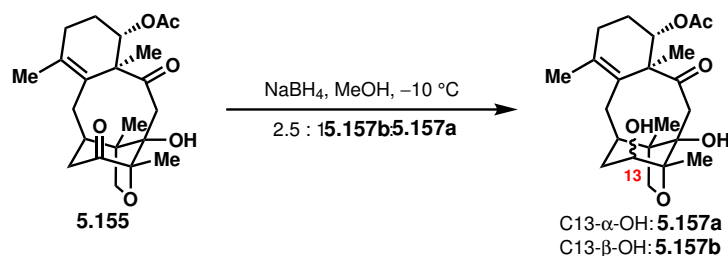


A solution of **5.10** (15.0 mg, 0.030 mmol, 1 equiv) was stirred in 15 wt% HCl (0.3 mL) and anhydrous THF (0.3 mL) at 23 °C for 13 h. Then, the reaction was quenched with sat. aq. NaHCO<sub>3</sub> (1.0 mL) and EtOAc (1.0 mL), and the aqueous and organic layers were separated. The aqueous layer was extracted with EtOAc (3 x 1 mL), and the combined organic layers were concentrated *in vacuo*. Purification by flash column chromatography (60% EtOAc/hexanes) afforded **5.153** (10.2 mg, quant.) as a white solid. <sup>1</sup>H NMR (400 MHz, CDCl<sub>3</sub>) δ 4.10 (d, *J* = 8.1 Hz, 1H), 3.77 (d, *J* = 8.0 Hz, 1H), 3.67 (dd, *J* = 11.9, 3.9 Hz, 1H), 3.54 (s, 1H), 3.02 (dd, *J* = 18.4, 11.9 Hz, 1H), 2.68 (dd, *J* = 16.4, 7.6 Hz, 1H), 2.66 (d, *J* = 13.8 Hz, 1H), 2.48 (dd, *J* = 18.4, 1.5 Hz, 1H), 2.42–2.29 (m, 2H), 2.25 (d, *J* = 16.6 Hz, 1H), 2.19 (d, *J* = 13.8 Hz, 1H), 2.08 (dd, *J* = 18.2, 6.2 Hz, 1H), 1.92–1.83 (m, 1H), 1.82 (s, 3H), 1.67 (qd, *J* = 12.2, 6.1 Hz, 1H), 1.26 (s, 3H), 1.22 (s, 3H), 1.05 (s, 3H).

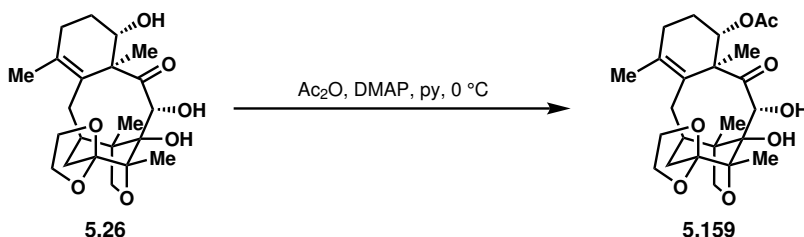


A solution of **4.14** (20.0 mg, 0.039 mmol, 1 equiv) and PPTS (10.0 mg, 0.039 mmol, 1 equiv) in acetone (HPLC grade, 1.5 mL) and deionized H<sub>2</sub>O (0.5 mL) was stirred at 60 °C. After 24 h, the reaction mixture was cooled to 23 °C and concentrated *in vacuo*. Purification by flash column chromatography (5% EtOAc/hexanes to 50% EtOAc/hexanes) afforded **5.154** (6.0 mg, 31%) and recovered **4.14** (13.0 mg, 65%). <sup>1</sup>H NMR (600 MHz, CDCl<sub>3</sub>) δ 4.10 (d, *J* = 8.1 Hz, 1H), 3.75 (d, *J* = 8.1 Hz, 1H), 3.71 (dd, *J* = 11.4, 4.4 Hz, 1H), 3.68 (br s, 1H), 2.99 (dd, *J* = 18.4, 11.9 Hz, 1H), 2.67–2.61 (m, 1H), 2.62 (d, *J* = 14.0 Hz, 1H), 2.48 (d, *J* = 19.1 Hz, 1H), 2.39–2.33 (m, 1H), 2.33–2.24 (m, 1H), 2.21 (d, *J* = 16.0 Hz, 1H), 2.07–2.01 (m, 1H), 2.03 (d, *J* = 14.4 Hz, 1H), 1.80 (s, 3H), 1.76–1.65 (m, 2H), 1.27 (s, 3H), 1.21 (s, 3H), 1.04 (s, 3H), 0.84 (s, 9H), 0.00 (s, 3H), –0.08 (s, 3H).

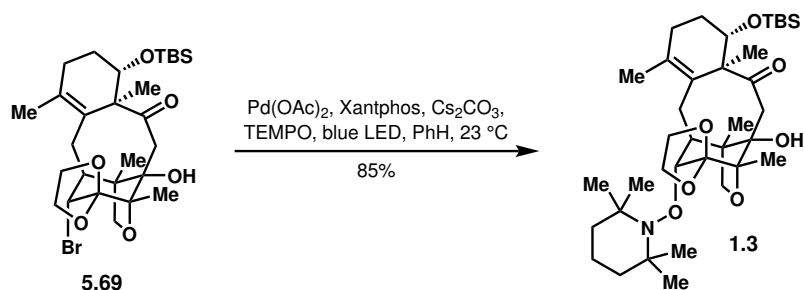




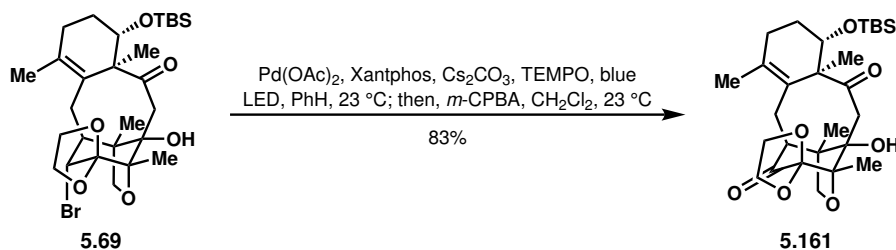
To **5.155** (1.4 mg, 0.004 mmol, 1 equiv) in anhydrous MeOH (0.2 mL, 0.02 M) at  $-10\text{ }^\circ C$ ,  $NaBH_4$  (0.7 mg, 0.018 mmol, 5 equiv) was added. The reaction mixture was stirred for 30 min, after which it was quenched with sat. aq.  $NH_4Cl$  (0.5 mL) and EtOAc (0.5 mL). The resulting mixture was stirred vigorously for 15 min, and the aqueous and organic layers were separated. The aqueous layer was extracted with EtOAc (3 x 0.5 mL), and the combined organic layers were concentrated *in vacuo*. Crude  $^1H$  NMR analysis revealed a 2.5 : 1 ratio of **5.157b** (desired) to **5.157a** (undesired). If desired, the crude reaction mixture could be purified by preparatory TLC (80% EtOAc/hexanes) to afford pure **5.157a** and **5.157b**. *Minor diastereomer (5.157a)*:  $^1H$  NMR (700 MHz,  $CDCl_3$ )  $\delta$  5.13–5.06 (m, 1H), 3.86 (d,  $J = 8.0$  Hz, 1H), 3.60–3.55 (m, 1H), 3.55 (d,  $J = 8.0$  Hz, 1H), 3.19 (s, 1H), 3.06 (d,  $J = 13.9$  Hz, 1H), 2.64 (dd,  $J = 15.8, 7.2$  Hz, 1H), 2.48–2.38 (m, 1H), 2.32 (d,  $J = 13.9$  Hz, 1H), 2.28 (dd,  $J = 15.4, 7.7$  Hz, 1H), 2.19–2.09 (m, 3H), 2.01 (s, 3H), 1.88 (s, 3H), 1.85–1.79 (m, 3H), 1.72–1.62 (m, 1H), 1.27 (s, 3H), 1.27 (s, 3H), 0.92 (s, 3H). *Major diastereomer (5.157b)*:  $^1H$  NMR (700 MHz,  $CDCl_3$ )  $\delta$  5.17–5.13 (m, 1H), 3.94 (d,  $J = 14.5$  Hz, 1H), 3.85–3.81 (m, 1H), 3.79 (d,  $J = 8.0$  Hz, 1H), 3.55 (d,  $J = 7.9$  Hz, 1H), 3.26 (s, 1H), 2.65–2.56 (m, 1H), 2.49 (ddd,  $J = 16.2, 11.1, 8.7$  Hz, 1H), 2.46–2.39 (m, 1H), 2.22–2.07 (m, 4H), 2.00 (s, 3H), 1.84–1.79 (m, 2H), 1.81 (s, 3H), 1.73–1.66 (m, 2H), 1.29 (s, 3H), 1.28 (s, 3H), 0.93 (s, 3H).



To **5.26** (2.0 mg, 0.005 mmol, 1 equiv) and DMAP (spatula tip) in anhydrous pyridine (0.1 mL, 0.05 M) at  $0\text{ }^\circ C$ ,  $Ac_2O$  (0.5  $\mu L$ , 0.005 mmol, 1 equiv) was added. The reaction mixture was stirred for 1 h, after which it was quenched with sat. aq.  $NaHCO_3$  and EtOAc, and the aqueous and organic layers were separated. The aqueous layer was extracted 3x with EtOAc, and the combined organic layers were dried over  $Na_2SO_4$ , filtered, and concentrated *in vacuo*. Crude  $^1H$  NMR analysis revealed **5.159** as the only significant product. Purification by preparatory TLC (60% EtOAc/hexanes) afforded pure **5.159**.  $^1H$  NMR (600 MHz,  $CDCl_3$ )  $\delta$  5.60 (d,  $J = 2.6$  Hz, 1H), 5.19 (dd,  $J = 12.1, 4.1$  Hz, 1H), 4.14 (ddd,  $J = 7.4, 5.8, 3.3$  Hz, 1H), 3.99–3.94 (m, 2H), 3.97 (s, 1H), 3.93 (d,  $J = 2.6$  Hz, 1H), 3.87 (td,  $J = 8.1, 6.2$  Hz, 1H), 3.75 (td,  $J = 8.0, 6.1$  Hz, 1H), 3.64 (d,  $J = 7.7$  Hz, 1H), 2.62 (dd,  $J = 15.8, 6.4$  Hz, 1H), 2.43–2.35 (m, 1H), 2.32 (dd,  $J = 15.6, 10.9$  Hz, 1H), 2.17–2.08 (m, 3H), 2.06 (d,  $J = 15.5$  Hz, 1H), 2.06 (s, 3H), 1.88 (s, 3H), 1.87–1.82 (m, 1H), 1.82–1.76 (m, 1H), 1.29 (s, 3H), 1.24 (s, 3H), 0.87 (s, 3H).

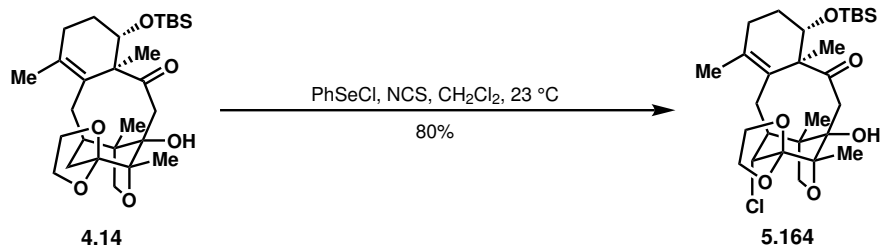


To **5.69** (2.9 mg, 0.005 mmol, 1 equiv), Pd(OAc)<sub>2</sub> (0.3 mg, 0.001 mmol, 0.3 equiv), Xantphos (1.7 mg, 0.002 mmol, 0.6 equiv), and TEMPO (0.9 mg, 0.006 mmol, 1.2 equiv) in a glovebox, Cs<sub>2</sub>CO<sub>3</sub> (9.7 mg, 0.030 mmol, 6 equiv) and anhydrous benzene (degassed with three cycles of freeze/pump/thaw; 0.25 mL, 0.02 M) were added. The reaction mixture was removed from the glovebox and stirred at 23 °C under irradiation with a blue LED. After 14 h, the reaction mixture was filtered through Celite with the aid of EtOAc and then concentrated *in vacuo*. Purification by flash column chromatography (25% EtOAc/hexanes) afforded **1.3** (2.8 mg, 85%) as a white solid. <sup>1</sup>H NMR (500 MHz, CDCl<sub>3</sub>) δ 4.24 (d, *J* = 7.3 Hz, 1H), 4.21–4.14 (m, 3H), 4.12 (d, *J* = 14.1 Hz, 1H), 4.06–3.92 (m, 2H), 3.74–3.69 (m, 1H), 3.71 (d, *J* = 7.3 Hz, 1H), 3.37 (s, 1H), 3.04–2.94 (m, 1H), 2.83 (dd, *J* = 15.8, 6.1 Hz, 1H), 2.26 (d, *J* = 16.4 Hz, 1H), 2.24–2.17 (m, 1H), 2.05–1.98 (m, 1H), 1.89 (d, *J* = 14.1 Hz, 1H), 1.84 (s, 3H), 1.74–1.68 (m, 2H), 1.62–1.57 (m, 1H), 1.51–1.40 (m, 4H), 1.33 (s, 3H), 1.29–1.25 (m, 1H), 1.24 (s, 3H), 1.20 (s, 3H), 1.19 (s, 3H), 1.17 (s, 3H), 1.15 (s, 3H), 0.91 (s, 3H), 0.87 (s, 9H), 0.02 (s, 3H), –0.03 (s, 3H).

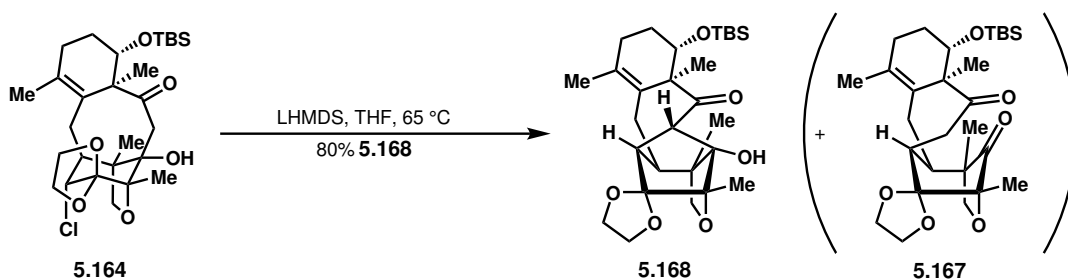


To **5.161** (5.4 mg, 0.009 mmol, 1 equiv), Pd(OAc)<sub>2</sub> (1.0 mg, 0.005 mmol, 0.5 equiv), and Xantphos (5.3 mg, 0.009 mmol, 1.0 equiv) in a glovebox, TEMPO (2.2 mg, 0.014 mmol, 1.5 equiv) and Cs<sub>2</sub>CO<sub>3</sub> (9.0 mg, 0.028 mmol, 3 equiv) were added, followed by anhydrous benzene (degassed with three cycles of freeze/pump/thaw; 90 μL, 0.1 M). The reaction mixture was brought out of the glovebox and was stirred at 23 °C under irradiation by a blue LED. After 12 h, *m*-CPBA (10.3 mg, 0.046 mmol, 5 equiv) and CH<sub>2</sub>Cl<sub>2</sub> (0.1 mL) were added, and the reaction mixture was stirred at 23 °C. After 40 min, the reaction mixture was filtered through Celite with the aid of EtOAc; then, sat. aq. NaHCO<sub>3</sub> (0.5 mL) and sat. aq. Na<sub>2</sub>S<sub>2</sub>O<sub>3</sub> (0.5 mL) were added, and the aqueous and organic layers were separated. The aqueous layer was extracted with EtOAc (3 x 0.5 mL), and the combined organic layers were concentrated *in vacuo*. Purification by flash column chromatography (30% EtOAc/hexanes to 40% EtOAc/hexanes) afforded **5.161** (4.0 mg, 83%). <sup>1</sup>H NMR (700 MHz, CDCl<sub>3</sub>) δ 4.40 (td, *J* = 7.1, 4.8 Hz, 1H), 4.16 (td, *J* = 7.1, 4.8 Hz, 1H), 4.10 (q, *J* = 7.2 Hz, 1H), 4.03 (q, *J* = 6.9 Hz, 1H), 3.98 (d, *J* = 8.4 Hz, 1H), 3.88 (d, *J* = 14.3 Hz, 1H), 3.80 (s, 1H), 3.72

(dd,  $J = 11.5, 4.2$  Hz, 1H), 3.49 (d,  $J = 8.4$  Hz, 1H), 3.26 (dd,  $J = 15.8, 6.7$  Hz, 1H), 2.60 (dd,  $J = 6.8, 3.1$  Hz, 1H), 2.23–2.15 (m, 2H), 2.08 (d,  $J = 14.4$  Hz, 1H), 2.01 (dd,  $J = 18.0, 5.5$  Hz, 1H), 1.74–1.62 (m, 2H), 1.65 (s, 3H), 1.25 (s, 3H), 1.22 (s, 3H), 0.98 (s, 3H), 0.87 (s, 9H), 0.03 (s, 3H),  $-0.03$  (s, 3H).

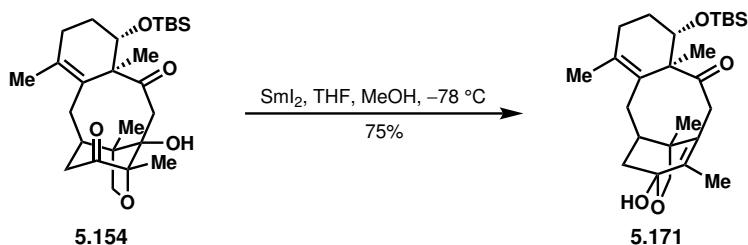


Trace water was removed from **4.14** (8.0 mg, 0.016 mmol, 1 equiv) via azeotropic distillation with anhydrous benzene (1 x 1 mL). Then, to **4.14**, PhSeCl (4.5 mg, 0.024 mmol, 1.5 equiv), and NCS (6.3 mg, 0.047 mmol, 3 equiv), CH<sub>2</sub>Cl<sub>2</sub> (0.4 mL, 0.04 M) was added. The reaction mixture was stirred at 23 °C for 3 h, after which it was quenched with sat. aq. NaHCO<sub>3</sub> (0.3 mL) and sat. aq. Na<sub>2</sub>S<sub>2</sub>O<sub>3</sub> (0.3 mL). The aqueous and organic layers were separated, and the aqueous layer was extracted with CH<sub>2</sub>Cl<sub>2</sub> (3 x 0.5 mL). The combined organic layers were concentrated *in vacuo*. Purification by column chromatography (30% EtOAc/hexanes) afforded **5.164** (6.8 mg, 80%) as an oil. <sup>1</sup>H NMR (700 MHz, CDCl<sub>3</sub>)  $\delta$  4.18–4.13 (m, 2H), 4.10–4.02 (m, 2H), 3.97 (td,  $J = 7.6, 7.2, 6.3$  Hz, 1H), 3.88 (d,  $J = 8.3$  Hz, 1H), 3.85 (s, 1H), 3.79–3.75 (m, 1H), 3.76 (d,  $J = 8.1$  Hz, 1H), 3.12 (d,  $J = 14.2$  Hz, 1H), 2.90 (dd,  $J = 15.9, 7.9$  Hz, 1H), 2.42–2.30 (m, 2H), 2.18 (d,  $J = 16.0$  Hz, 1H), 2.10 (dd,  $J = 18.1, 5.7$  Hz, 1H), 2.02 (d,  $J = 14.2$  Hz, 1H), 1.85 (s, 3H), 1.79–1.69 (m, 2H), 1.23 (s, 3H), 1.22 (s, 3H), 0.96 (s, 3H), 0.86 (s, 9H), 0.03 (s, 3H),  $-0.04$  (s, 3H).

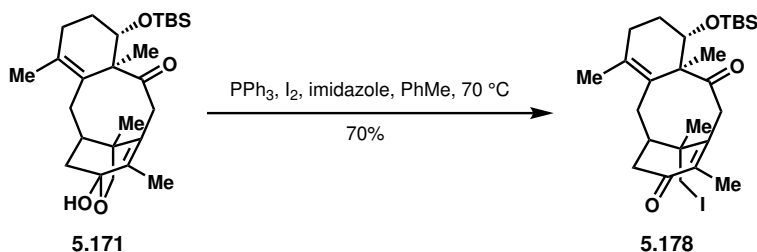


Trace water was removed from **5.164** (63.7 mg, 0.118 mmol, 1 equiv) via azeotropic distillation with anhydrous benzene (3 x 1.5 mL). Then, to **5.164** in anhydrous THF (2.4 mL, 0.05 M), LHMDS (1.0 M in THF, 388  $\mu$ L, 0.388 mmol, 3.3 equiv) was added. The reaction mixture was warmed to 65 °C and stirred for 18 h, after which it was quenched with sat. aq. NH<sub>4</sub>Cl (2.4 mL). The aqueous and organic layers were separated, and the aqueous layer was extracted with EtOAc (3 x 2 mL), and the combined organic layers were dried over Na<sub>2</sub>SO<sub>4</sub>, filtered, and concentrated *in vacuo*. Purification by Yamazen automated flash column chromatography (30% EtOAc/hexanes) afforded **5.168** (47.7 mg, 80%) as a white solid. *Pentacyclic compound 5.168*: <sup>1</sup>H NMR (500 MHz, CDCl<sub>3</sub>)  $\delta$  4.69 (s, 1H), 4.13–4.06 (m, 2H), 4.02–3.95 (m, 3H), 3.89 (d,  $J = 8.1$  Hz, 1H), 3.81 (d,  $J = 8.1$  Hz, 1H), 2.76 (dd,

$J = 15.6, 12.2$  Hz, 1H), 2.46 (t,  $J = 2.1$  Hz, 1H), 2.39–2.27 (m, 3H), 2.26–2.17 (m, 1H), 2.04 (d,  $J = 15.4$  Hz, 1H), 1.89–1.79 (m, 2H), 1.66 (s, 3H), 1.25 (s, 3H), 1.18 (s, 3H), 1.04 (s, 3H), 0.89 (s, 9H), 0.09 (s, 3H), 0.03 (s, 3H). *Intermediate 5.167*, which can be isolated at shorter reaction times:  $^1\text{H NMR}$  (500 MHz,  $\text{CDCl}_3$ )  $\delta$  4.32–4.24 (m, 1H), 4.10–4.04 (m, 1H), 4.08 (d,  $J = 8.5$  Hz, 1H), 3.99 (td,  $J = 7.4, 3.3$  Hz, 1H), 3.90–3.84 (m, 1H), 3.84 (d,  $J = 8.5$  Hz, 1H), 3.66 (dd,  $J = 9.8, 3.3$  Hz, 1H), 2.91–2.84 (m, 1H), 2.77 (dd,  $J = 12.3, 4.3$  Hz, 1H), 2.47–2.30 (m, 2H), 2.13–2.06 (m, 2H), 1.92 (dd,  $J = 11.9, 6.6$  Hz, 1H), 1.78 (d,  $J = 13.2$  Hz, 1H), 1.73–1.66 (m, 1H), 1.66 (s, 3H), 1.63–1.57 (m, 1H), 1.27 (s, 3H), 1.17 (s, 3H), 1.05 (s, 3H), 0.86 (s, 9H),  $-0.02$  (s, 3H),  $-0.04$  (s, 3H).



Trace water was removed from **5.154** (18.8 mg, 0.04 mmol, 1 equiv) via azeotropic distillation with anhydrous benzene (3 x 2 mL). Then, to **5.154** under Ar, anhydrous THF (0.82 mL) and anhydrous MeOH (8.2  $\mu\text{L}$ , 0.20 mmol, 5 equiv) were added; at  $-78\text{ }^\circ\text{C}$ ,  $\text{SmI}_2$  (0.1 M in THF, 2.0 mL, 0.2 mmol, 5 equiv) was added dropwise over 3 min. After 1.5 h, the reaction was quenched with sat. aq.  $\text{NH}_4\text{Cl}$  (2 mL) and EtOAc (2 mL), and the aqueous and organic layers were separated. The aqueous layer was extracted with EtOAc (3 x 2 mL), and the combined organic layers were dried over  $\text{Na}_2\text{SO}_4$ , filtered, and concentrated *in vacuo*. Purification by preparatory TLC (40% EtOAc/hexanes) afforded **5.171** (13.7 mg, 75%).  $^1\text{H NMR}$  (700 MHz,  $\text{CDCl}_3$ )  $\delta$  4.37 (dd,  $J = 11.8, 4.7$  Hz, 1H), 3.73 (d,  $J = 14.0$  Hz, 1H), 3.46 (d,  $J = 7.9$  Hz, 1H), 3.13 (d,  $J = 7.9$  Hz, 1H), 3.09 (d,  $J = 14.1$  Hz, 1H), 2.82 (s, 1H), 2.34 (dd,  $J = 15.4, 6.3$  Hz, 1H), 2.28 (dt,  $J = 19.0, 9.7$  Hz, 1H), 2.02 (dd,  $J = 18.1, 7.7$  Hz, 1H), 1.98–1.93 (m, 1H), 1.91–1.81 (m, 2H), 1.86 (s, 3H), 1.81 (d,  $J = 15.3$  Hz, 1H), 1.78–1.70 (m, 1H), 1.59–1.57 (m, 1H), 1.57 (s, 3H), 1.09 (s, 3H), 1.01 (s, 3H), 0.83 (s, 9H), 0.11 (s, 3H), 0.08 (s, 3H).  $^{13}\text{C NMR}$  (176 MHz,  $\text{CDCl}_3$ )  $\delta$  212.4, 135.9, 131.7, 130.2, 127.8, 96.9, 73.9, 71.9, 60.2, 43.1, 42.3, 40.9, 35.0, 30.9, 28.7, 27.7, 25.7, 22.3, 19.9, 18.1, 16.3, 12.1,  $-2.8, -4.7$ .



To **5.171** (2.3 mg, 0.005 mmol, 1 equiv),  $\text{PPh}_3$  (4.1 mg, 0.015 mmol, 3 equiv), imidazole (2.1 mg, 0.031 mmol, 6 equiv), and iodine (3.9 mg, 0.015 mmol, 3 equiv), PhMe (0.2 mL, 0.026 M) was added. The reaction mixture was stirred at  $70\text{ }^\circ\text{C}$  for 3 h; then, it was

quenched with sat. aq.  $\text{Na}_2\text{S}_2\text{O}_3$  (0.5 mL) and EtOAc (0.5 mL), and the aqueous and organic layers were separated. The aqueous layer was extracted with EtOAc (3 x 0.5 mL), and the combined organic layers were concentrated *in vacuo*. Purification by preparatory TLC (15% EtOAc/hexanes) afforded **5.178** (2.0 mg, 70%) as a white solid.  $^1\text{H NMR}$  (700 MHz,  $\text{CDCl}_3$ )  $\delta$  4.35 (dd,  $J = 11.6, 4.3$  Hz, 1H), 3.94 (d,  $J = 14.0$  Hz, 1H), 3.38 (d,  $J = 14.0$  Hz, 1H), 3.30 (d,  $J = 10.2$  Hz, 1H), 3.09 (d,  $J = 10.2$  Hz, 1H), 2.94 (dd,  $J = 19.9, 5.8$  Hz, 1H), 2.75–2.70 (m, 1H), 2.70 (d,  $J = 20.0$  Hz, 1H), 2.43–2.39 (m, 1H), 2.26–2.19 (m, 1H), 2.14–2.09 (m, 1H), 1.98 (s, 3H), 1.92 (dd,  $J = 18.0, 6.9$  Hz, 1H), 1.83–1.77 (m, 1H), 1.71 (qd,  $J = 12.0, 7.0$  Hz, 1H), 1.64 (s, 3H), 1.34 (s, 3H), 1.12 (s, 3H), 0.84 (s, 9H), 0.08 (s, 3H), 0.07 (s, 3H).

## 5.11 References

- (1) Yuan, C.; Jin, Y.; Wilde, N. C.; Baran, P. S. *Angew. Chem. Int. Ed.* **2016**, *55*, 8280–8284.
- (2) Gleiter, R.; Herb, T.; Hofmann, J. *Synlett* **1996**, *1996*, 987–989.
- (3) Tomkinson, N. C. O. In *Encyclopedia of Reagents for Organic Synthesis*; American Cancer Society: 2009.
- (4) Beshara, C. S.; Hall, A.; Jenkins, R. L.; Jones, K. L.; Jones, T. C.; Killeen, N. M.; Taylor, P. H.; Thomas, S. P.; Tomkinson, N. C. O. *Org. Lett.* **2005**, *7*, 5729–5732.
- (5) Hughes, J. M. E.; Gleason, J. L. *Angew. Chem. Int. Ed.* **2017**, *56*, 10830–10834.
- (6) Rono, L. J.; Yayla, H. G.; Wang, D. Y.; Armstrong, M. F.; Knowles, R. R. *J. Am. Chem. Soc.* **2013**, *135*, 17735–17738.
- (7) Jeffrey, J. L.; Terrett, J. A.; MacMillan, D. W. C. *Science* **2015**, *349*, 1532–1536.
- (8) Banwell, M. G.; Hockless, D. C. R.; McLeod, M. D. *New J. Chem.* **2003**, *27*, 50–59.
- (9) Molander, G. A.; Czakó, B.; Rheam, M. *J. Org. Chem.* **2007**, *72*, 9406–9406.
- (10) Georg, G. I.; Harriman, G. C. B.; Datta, A.; Ali, S.; Cheruvallath, Z.; Dutta, D.; Vander Velde, D. G.; Himes, R. H. *J. Org. Chem.* **1998**, *63*, 8926–8934.
- (11) Hill, C. K.; Hartwig, J. F. *Nat. Chem.* **2017**, *9*, 1213–1221.
- (12) Luche, J. L. *J. Am. Chem. Soc.* **1978**, *100*, 2226–2227.
- (13) Donohoe, T. J.; Blades, K.; Moore, P. R.; Waring, M. J.; Winter, J. J. G.; Helliwell, M.; Newcombe, N. J.; Stemp, G. *J. Org. Chem.* **2002**, *67*, 7946–7956.
- (14) Concepción, J. I.; Francisco, C. G.; Hernández, R.; Salazar, J. A.; Suárez, E. *Tetrahedron Lett.* **1984**, *25*, 1953–1956.
- (15) Bunescu, A.; Butcher, T. W.; Hartwig, J. F. *J. Am. Chem. Soc.* **2018**, *140*, 1502–1507.
- (16) (a) Yang, D.; Wong, M.-K.; Wang, X.-C.; Tang, Y.-C. *J. Am. Chem. Soc.* **1998**, *120*, 6611–6612; (b) Wong, M.-K.; Chung, N.-W.; He, L.; Wang, X.-C.; Yan, Z.; Tang, Y.-C.; Yang, D. *J. Org. Chem.* **2003**, *68*, 6321–6328.
- (17) Zinzalla, G.; Milroy, L.-G.; Ley, S. V. *Org. Biomol. Chem.* **2006**, *4*, 1977–2002.

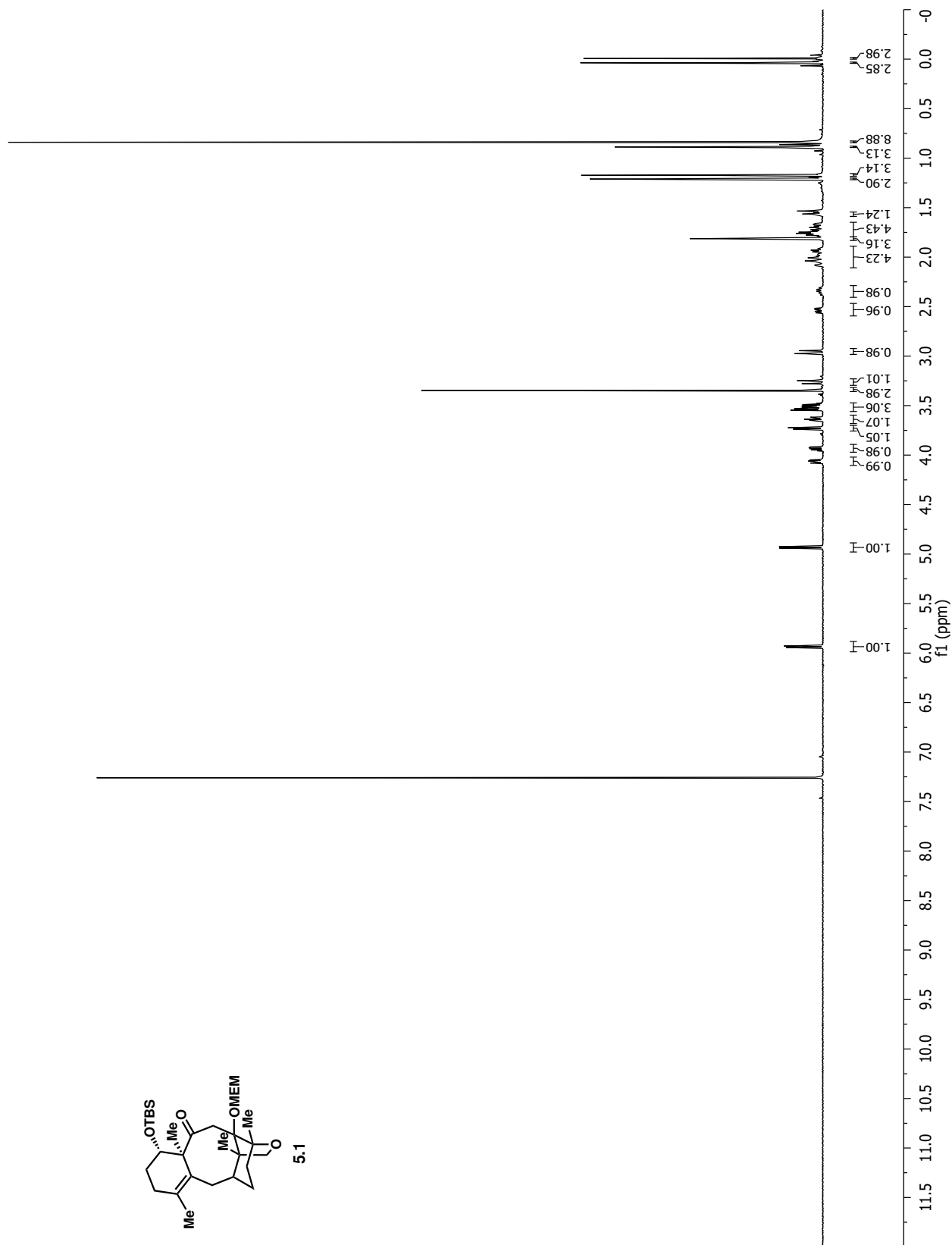
- (18) Tietze, L. F.; Bell, H. P.; Chandrasekhar, S. *Angew. Chem. Int. Ed.* **2003**, *42*, 3996–4028.
- (19) Salmond, W. G.; Barta, M. A.; Havens, J. L. *J. Org. Chem.* **1978**, *43*, 2057–2059.
- (20) Wilde, N. C.; Isomura, M.; Mendoza, A.; Baran, P. S. *J. Am. Chem. Soc.* **2014**, *136*, 4909–4912.
- (21) Chérest, M.; Felkin, H. *Tetrahedron Lett.* **1968**, *9*, 2205–2208.
- (22) (a) Bigi, M. A.; Reed, S. A.; White, M. C. *Nat. Chem.* **2011**, *3*, 216–222; (b) Bigi, M. A.; Reed, S. A.; White, M. C. *J. Am. Chem. Soc.* **2012**, *134*, 9721–9726.
- (23) Chen, S.-H.; Huang, S.; Gao, Q.; Golik, J.; Farina, V. *J. Org. Chem.* **1994**, *59*, 1475–1484.
- (24) Yu, J.-Q.; Corey, E. J. *J. Am. Chem. Soc.* **2003**, *125*, 3232–3233.
- (25) Shing, T. K. M.; Yeung; Su, P. L. *Org. Lett.* **2006**, *8*, 3149–3151.
- (26) Ishii, Y.; Iwahama, T.; Sakaguchi, S.; Nakayama, K.; Nishiyama, Y. *J. Org. Chem.* **1996**, *61*, 4520–4526.
- (27) Zhao, Q.; Qian, C.; Chen, X.-Z. *Steroids* **2015**, *94*, 1–6.
- (28) Catino, A. J.; Forslund, R. E.; Doyle, M. P. *J. Am. Chem. Soc.* **2004**, *126*, 13622–13623.
- (29) Moorthy, J. N.; Senapati, K.; Kumar, S. *J. Org. Chem.* **2009**, *74*, 6287–6290.
- (30) (a) Hori, T.; Sharpless, K. B. *J. Org. Chem.* **1979**, *44*, 4204–4208; (b) Hori, T.; Sharpless, K. B. *J. Org. Chem.* **1979**, *44*, 4208–4210; (c) Tunge, J. A.; Mellegaard, S. R. *Org. Lett.* **2004**, *6*, 1205–1207.
- (31) Tiecco, M.; Testaferri, L.; Temperini, A.; Bagnoli, L.; Marini, F.; Santi, C. *Synlett* **2001**, *2001*, 1767–1771.
- (32) Parasram, M.; Iaroshenko, V. O.; Gevorgyan, V. *J. Am. Chem. Soc.* **2014**, *136*, 17926–17929.
- (33) Barton, D. H. R.; Crich, D.; Kretzschmar, G. *J. Chem. Soc., Perkin Trans. 1* **1986**, 39–53.
- (34) Rönn, M.; Bäckvall, J.-E.; Andersson, P. G. *Tetrahedron Lett.* **1995**, *36*, 7749–7752.
- (35) (a) Trend, R. M.; Ramtohl, Y. K.; Ferreira, E. M.; Stoltz, B. M. *Angew. Chem. Int. Ed.* **2003**, *42*, 2892–2895; (b) Trend, R. M.; Ramtohl, Y. K.; Stoltz, B. M. *J. Am. Chem. Soc.* **2005**, *127*, 17778–17788.
- (36) Mojsilovic, B. M.; Bugarcic, Z. M. *Heteroatom Chem.* **2001**, *12*, 475–479.
- (37) Chateaufneuf, J.; Luszyk, J.; Maillard, B.; Ingold, K. U. *J. Am. Chem. Soc.* **1988**, *110*, 6727–6731.
- (38) Newcomb, M.; Dhanabalasingam, B. *Tetrahedron Lett.* **1994**, *35*, 5193–5196.
- (39) Imajo, H.; Kurita, K.; Iwakura, Y. *J. Poly. Sci.: Poly. Sci. Ed.* **1981**, *19*, 1855–1861.
- (40) Minakata, S.; Sasaki, I.; Ide, T. *Angew. Chem. Int. Ed.* **2010**, *49*, 1309–1311.

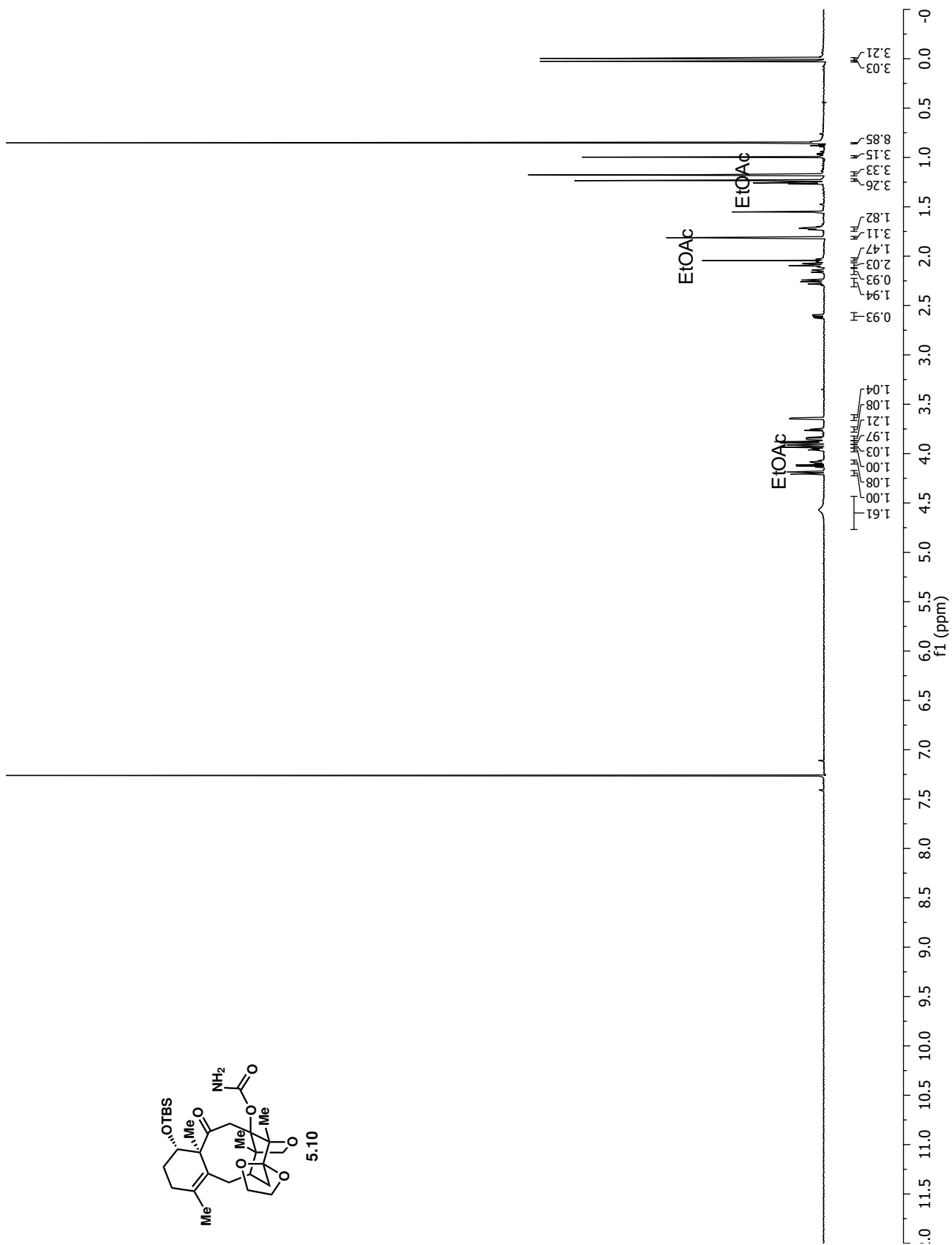
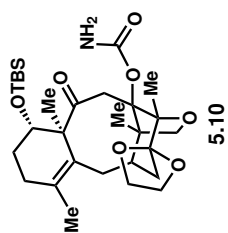
- (41) Bongini, A.; Cardillo, G.; Orena, M.; Porzi, G.; Sandri, S. *J. Org. Chem.* **1982**, *47*, 4626–4633.
- (42) Treibs, W. *Naturwissenschaften* **1948**, *35*, 125–125.
- (43) Yang, J.; Long, Y. O.; Paquette, L. A. *J. Am. Chem. Soc.* **2003**, *125*, 1567–1574.
- (44) Allinger, N. L.; Sprague, J. T. *J. Am. Chem. Soc.* **1972**, *94*, 5734–5747.
- (45) Schweitzer, C.; Schmidt, R. *Chem. Rev.* **2003**, *103*, 1685–1758.
- (46) Kořinek, M.; Dëdic, R.; Svoboda, A.; Hála, J. *J. Fluoresc.* **2004**, *14*, 71–74.
- (47) Orfanopoulos, M.; Stratakis, M.; Elemes, Y. *J. Am. Chem. Soc.* **1990**, *112*, 6417–6419.
- (48) Wiberg, K. B. *Angew. Chem. Int. Ed.* **1986**, *25*, 312–322.
- (49) (a) Morrill, C.; Grubbs, R. H. *J. Am. Chem. Soc.* **2005**, *127*, 2842–2843; (b) Morrill, C.; Beutner, G. L.; Grubbs, R. H. *J. Org. Chem.* **2006**, *71*, 7813–7825.
- (50) Li, P.-F.; Wang, H.-L.; Qu, J. *J. Org. Chem.* **2014**, *79*, 3955–3962.
- (51) Leleti, R. R.; Hu, B.; Prashad, M.; Repič, O. *Tetrahedron Lett.* **2007**, *48*, 8505–8507.
- (52) (a) Mandai, T.; Matsumoto, T.; Kawada, M.; Tsuji, J. *J. Org. Chem.* **1992**, *57*, 1326–1327; (b) Mandai, T.; Matsumoto, T.; Kawada, M.; Tsuji, J. *Tetrahedron* **1993**, *49*, 5483–5493.
- (53) (a) Kabalka, G. W.; Yang, D. T. C.; Baker, J. D. *J. Org. Chem.* **1976**, *41*, 574–575; (b) Kabalka, G. W.; Summers, S. T. *J. Org. Chem.* **1981**, *46*, 1217–1218.
- (54) (a) Myers, A. G.; Zheng, B. *Tetrahedron Lett.* **1996**, *37*, 4841–4844; (b) Movassaghi, M.; Ahmad, O. K. *J. Org. Chem.* **2007**, *72*, 1838–1841.
- (55) Caglioti, L. *Tetrahedron* **1966**, *22*, 487–493.
- (56) Abdel-Magid, A. F.; Carson, K. G.; Harris, B. D.; Maryanoff, C. A.; Shah, R. D. *J. Org. Chem.* **1996**, *61*, 3849–3862.
- (57) Hutchins, R. O.; Kacher, M.; Rua, L. *J. Org. Chem.* **1975**, *40*, 923–926.
- (58) Myers, A. G.; Kukkola, P. J. *J. Am. Chem. Soc.* **1990**, *112*, 8208–8210.
- (59) Corey, E. J.; Virgil, S. C. *J. Am. Chem. Soc.* **1990**, *112*, 6429–6431.
- (60) Tsunoda, T.; Yamamiya, Y.; Itô, S. *Tetrahedron Lett.* **1993**, *34*, 1639–1642.
- (61) Tsunoda, T.; Otsuka, J.; Yamamiya, Y.; Itô, S. *Chem. Lett.* **1994**, *23*, 539–542.
- (62) Tsunoda, T.; Ozaki, F.; Itô, S. *Tetrahedron Lett.* **1994**, *35*, 5081–5082.
- (63) Walker, M. A. *J. Org. Chem.* **1995**, *60*, 5352–5355.
- (64) Corey, E. J.; Engler, T. A. *Tetrahedron Lett.* **1984**, *25*, 149–152.
- (65) Chochrek, P.; Wicha, J. *Eur. J. Org. Chem.* **2007**, *2007*, 2534–2542.
- (66) Degl’Innocenti, A.; Capperucci, A.; Mordini, A.; Reginato, G.; Ricci, A.; Cerreta, F. *Tetrahedron Lett.* **1993**, *34*, 873–876.
- (67) Metzner, P. In *Organosulfur Chemistry I*, Page, P. C. B., Ed.; Topics in Current Chemistry; Springer: Berlin, Heidelberg, 1999, pp 127–181.

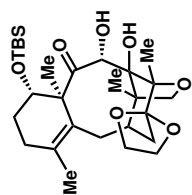
- (68) Nerinckx, W.; De Clercq, P. J.; Couwenhoven, C.; Overbeek, W. R. M.; Halkes, S. J. *Tetrahedron* **1991**, *47*, 9419–9430.
- (69) Czaplowski, W. L.; Na, C. G.; Alexanian, E. J. *J. Am. Chem. Soc.* **2016**, *138*, 13854–13857.
- (70) (a) Fukaya, K. et al. *Org. Lett.* **2015**, *17*, 2570–2573; (b) Fukaya, K.; Kodama, K.; Tanaka, Y.; Yamazaki, H.; Sugai, T.; Yamaguchi, Y.; Watanabe, A.; Oishi, T.; Sato, T.; Chida, N. *Org. Lett.* **2015**, *17*, 2574–2577.
- (71) Denis, J.-N.; Greene, A. E. *Nat. Prod. Lett.* **1996**, *8*, 27–32.
- (72) Krief, A.; Surleraux, D. *Synlett* **1991**, *1991*, 273–275.
- (73) Mukaiyama, T.; Shiina, I.; Iwadare, H.; Saitoh, M.; Nishimura, T.; Ohkawa, N.; Sakoh, H.; Nishimura, K.; Tani, Y.-i.; Hasegawa, M.; Yamada, K.; Saitoh, K. *Chem. Eur. J.* **1999**, *5*, 121–161.
- (74) (a) Holton, R. A.; Somoza, C.; Kim, H. B.; Liang, F.; Biediger, R. J.; Boatman, P. D.; Shindo, M.; Smith, C. C.; Kim, S. *J. Am. Chem. Soc.* **1994**, *116*, 1597–1598; (b) Holton, R. A.; Kim, H. B.; Somoza, C.; Liang, F.; Biediger, R. J.; Boatman, P. D.; Shindo, M.; Smith, C. C.; Kim, S. *J. Am. Chem. Soc.* **1994**, *116*, 1599–1600.
- (75) Danishefsky, S. J.; Masters, J. J.; Young, W. B.; Link, J. T.; Snyder, L. B.; Magee, T. V.; Jung, D. K.; Isaacs, R. C. A.; Bornmann, W. G.; Alaimo, C. A.; Coburn, C. A.; Di Grandi, M. J. *J. Am. Chem. Soc.* **1996**, *118*, 2843–2859.
- (76) Wang, Y.-F.; Shi, Q.-W.; Dong, M.; Kiyota, H.; Gu, Y.-C.; Cong, B. *Chem. Rev.* **2011**, *111*, 7652–7709.
- (77) Nakamura, E.; Inubushi, T.; Aoki, S.; Machii, D. *J. Am. Chem. Soc.* **1991**, *113*, 8980–8982.
- (78) Parasram, M.; Chuentragool, P.; Wang, Y.; Shi, Y.; Gevorgyan, V. *J. Am. Chem. Soc.* **2017**, *139*, 14857–14860.
- (79) Simmons, E. M.; Hartwig, J. F. *Nature* **2012**, *483*, 70–73.
- (80) Gevorgyan, V.; Rubin, M.; Benson, S.; Liu, J.-X.; Yamamoto, Y. *J. Org. Chem.* **2000**, *65*, 6179–6186.



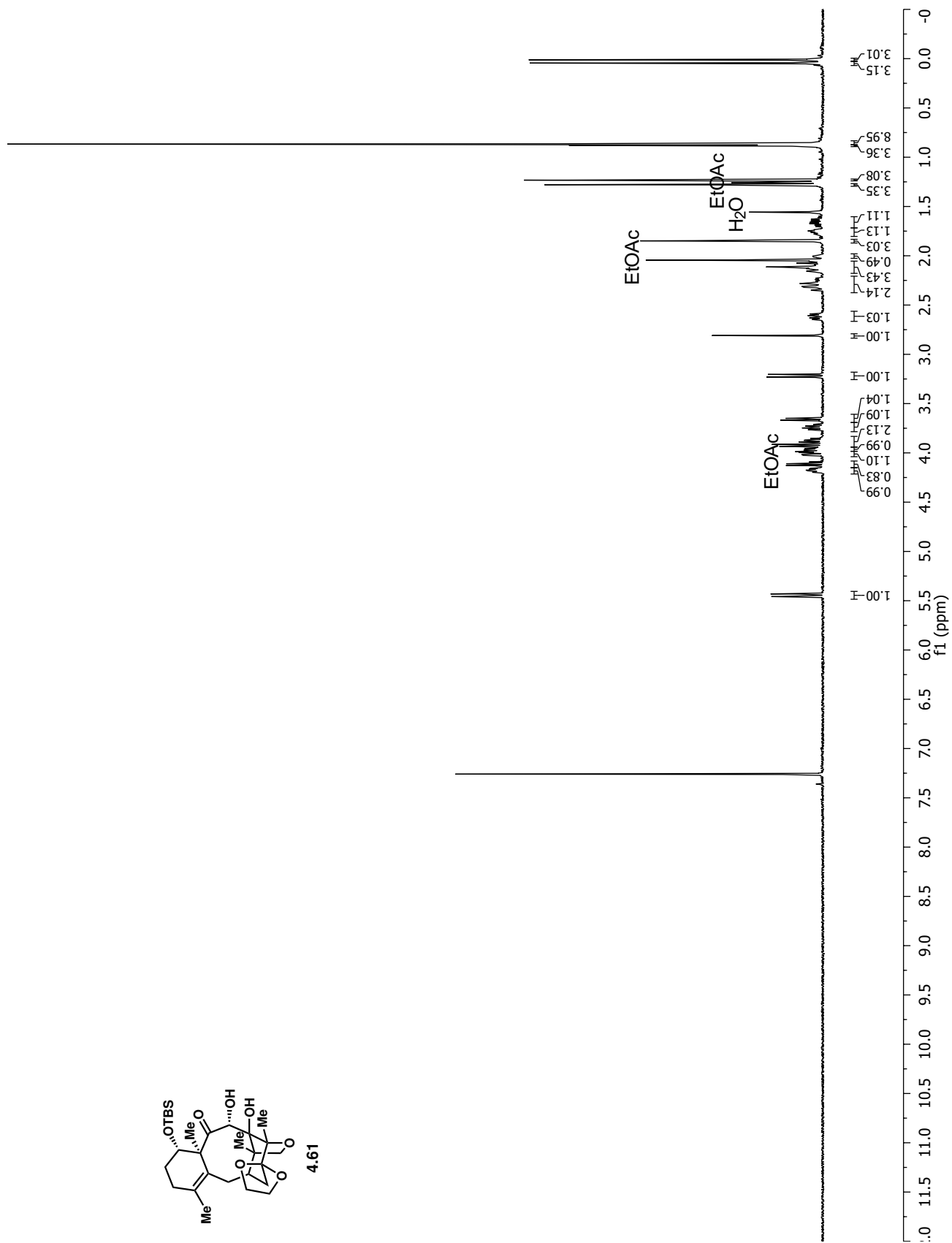
# Appendix 5a: NMR Spectra Relevant to Chapter 5

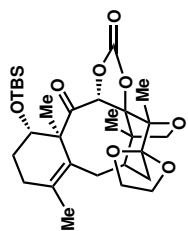




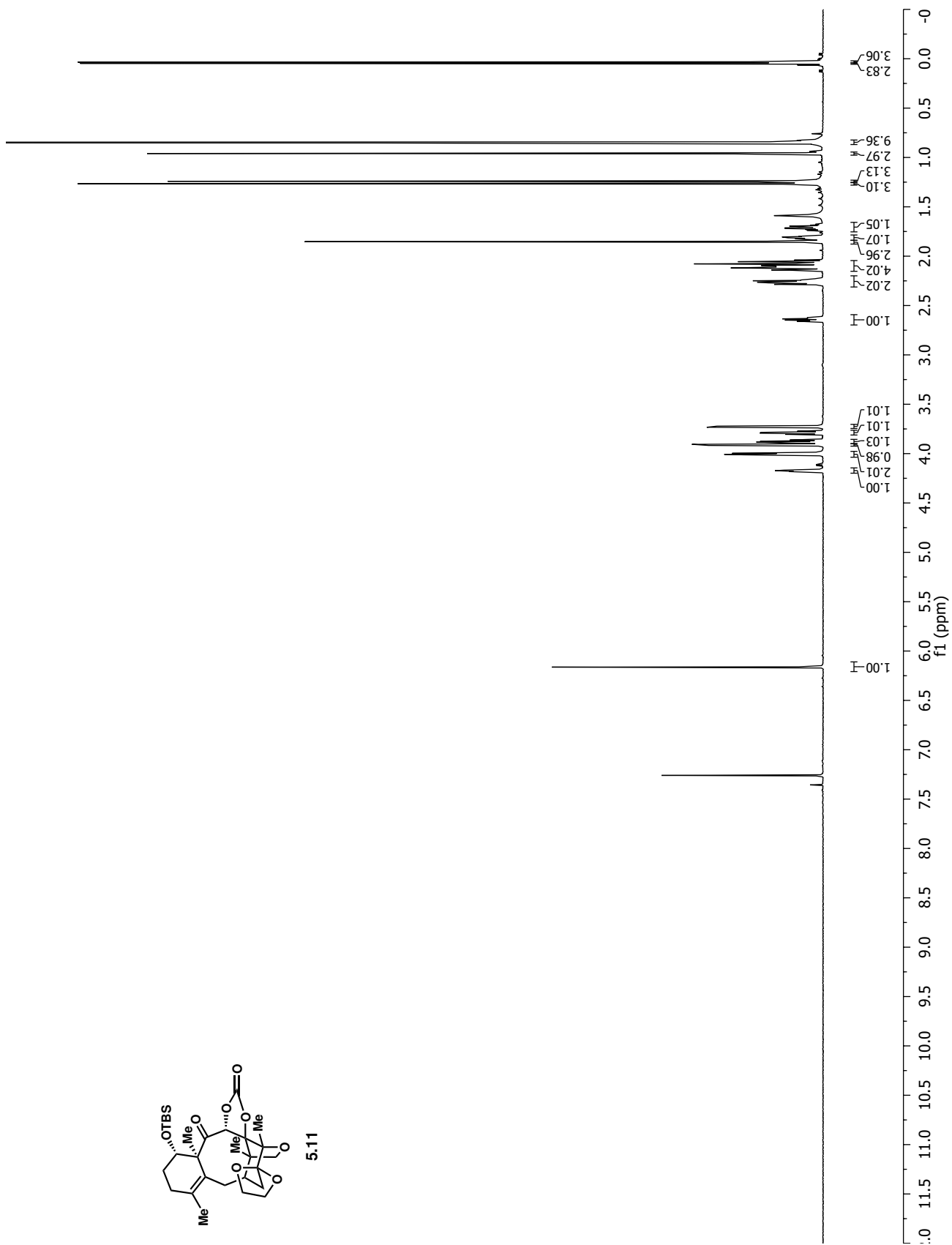


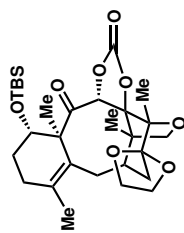
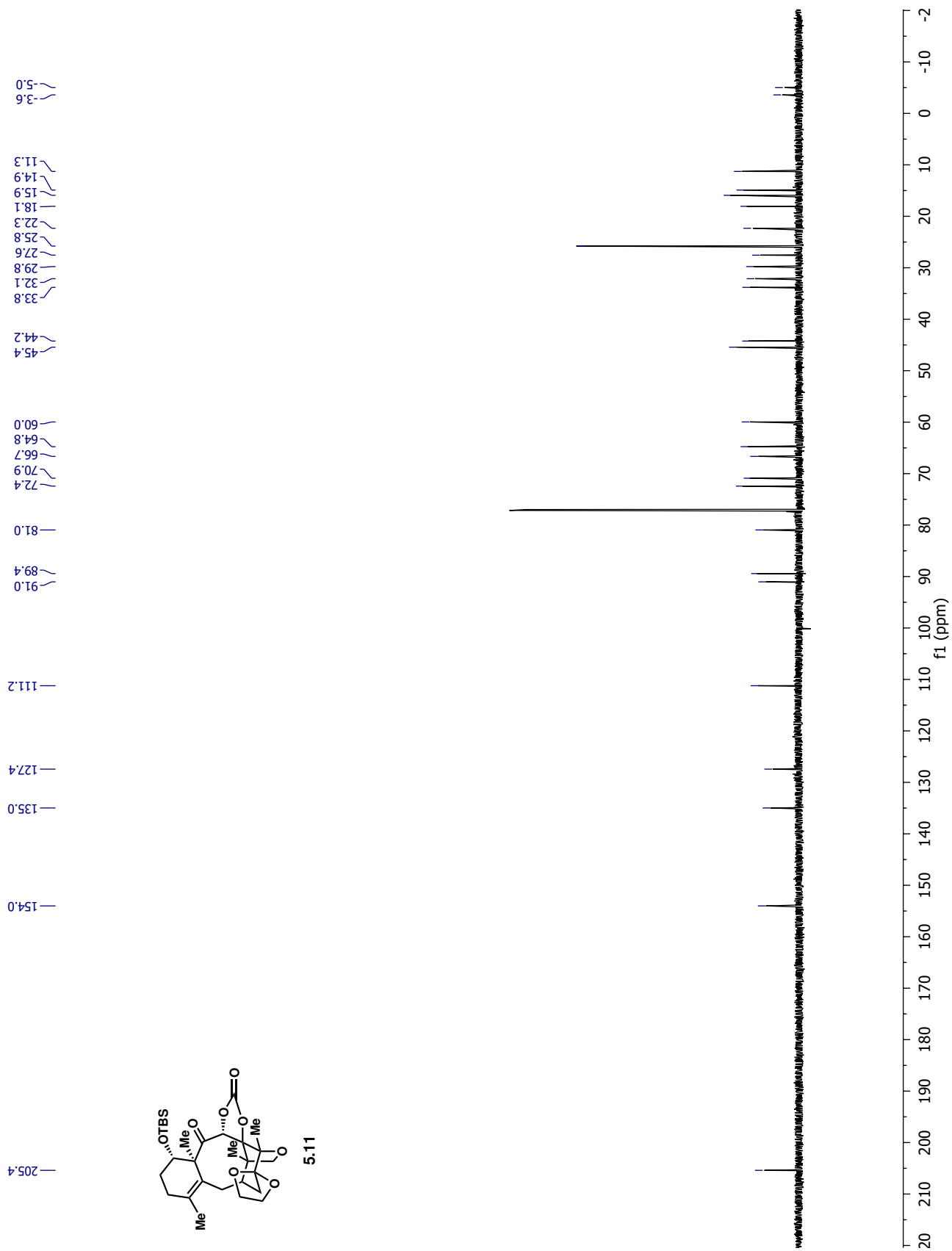
4.61



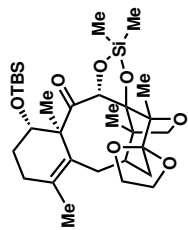


5.11

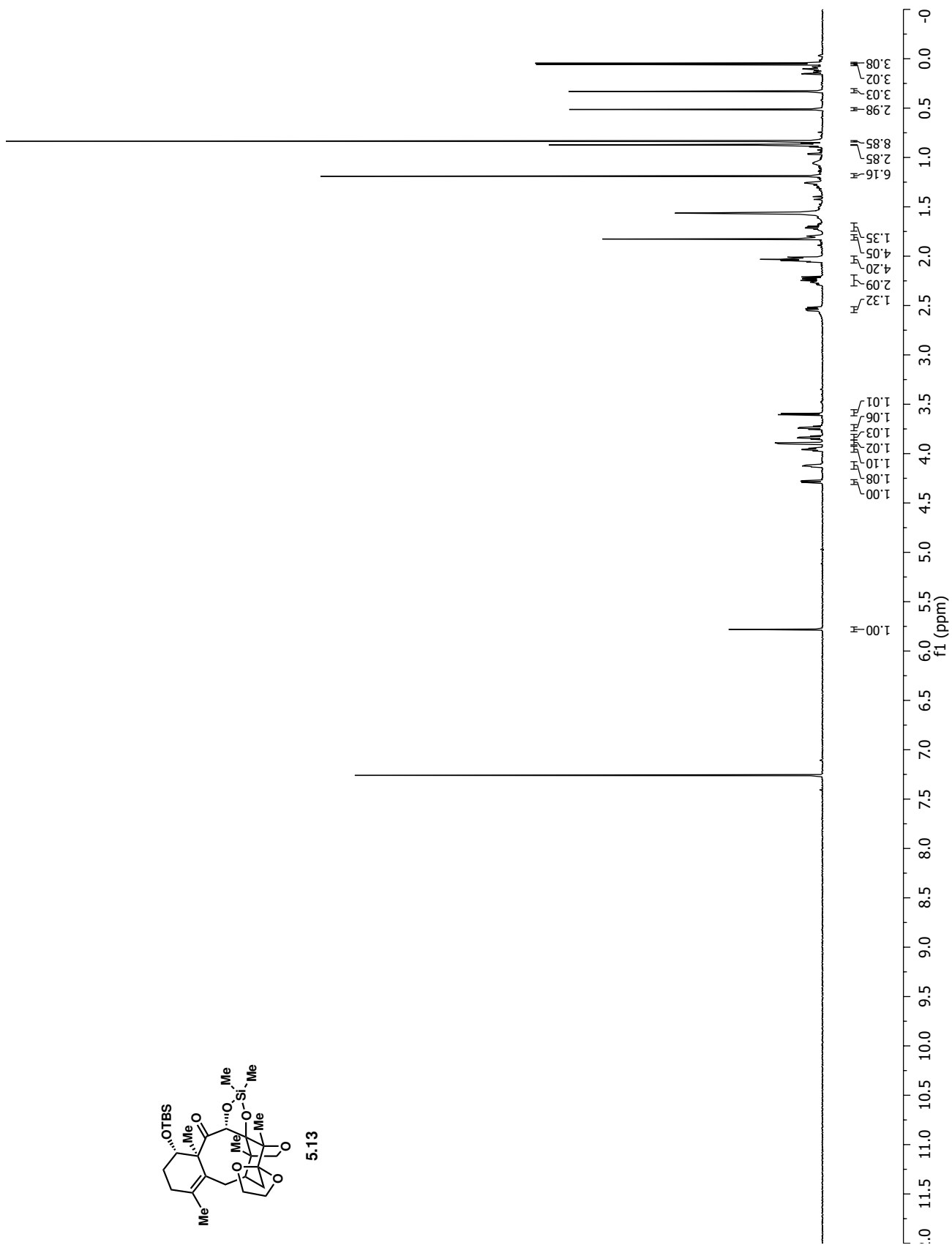


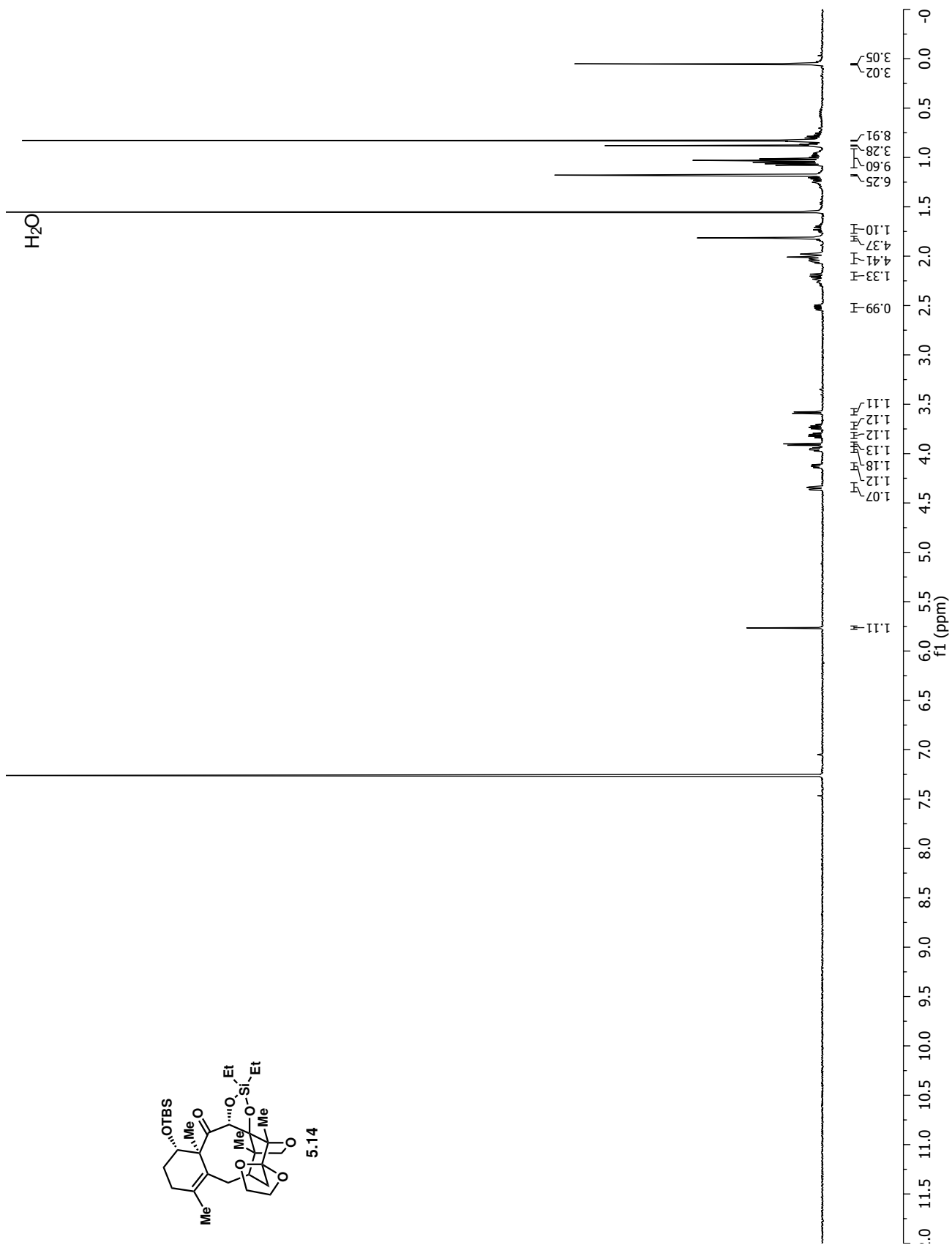
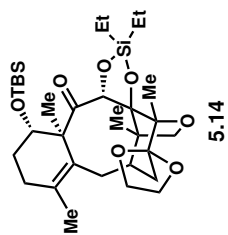


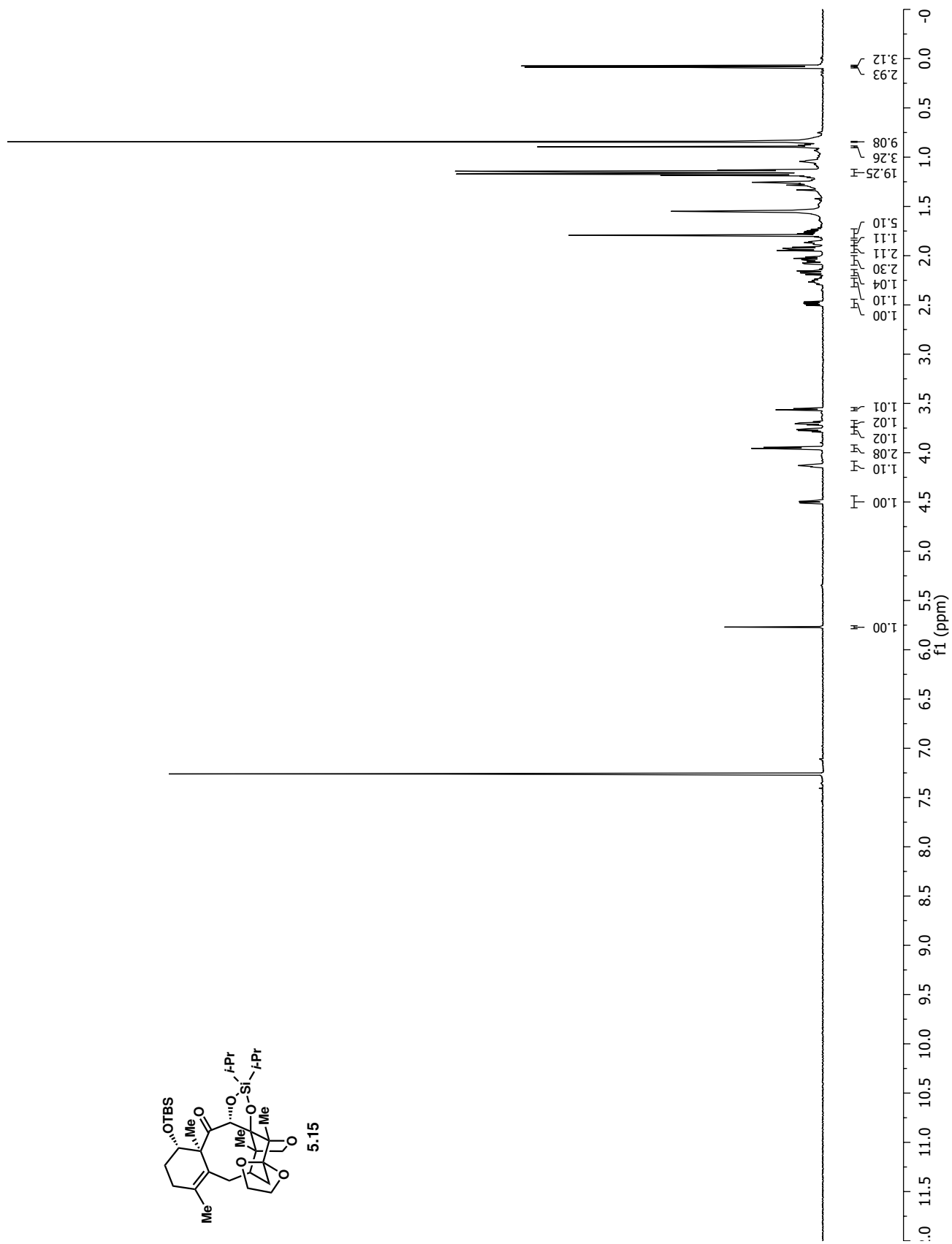
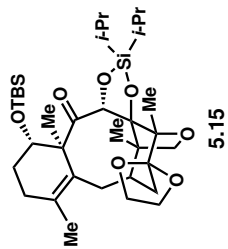
5.11



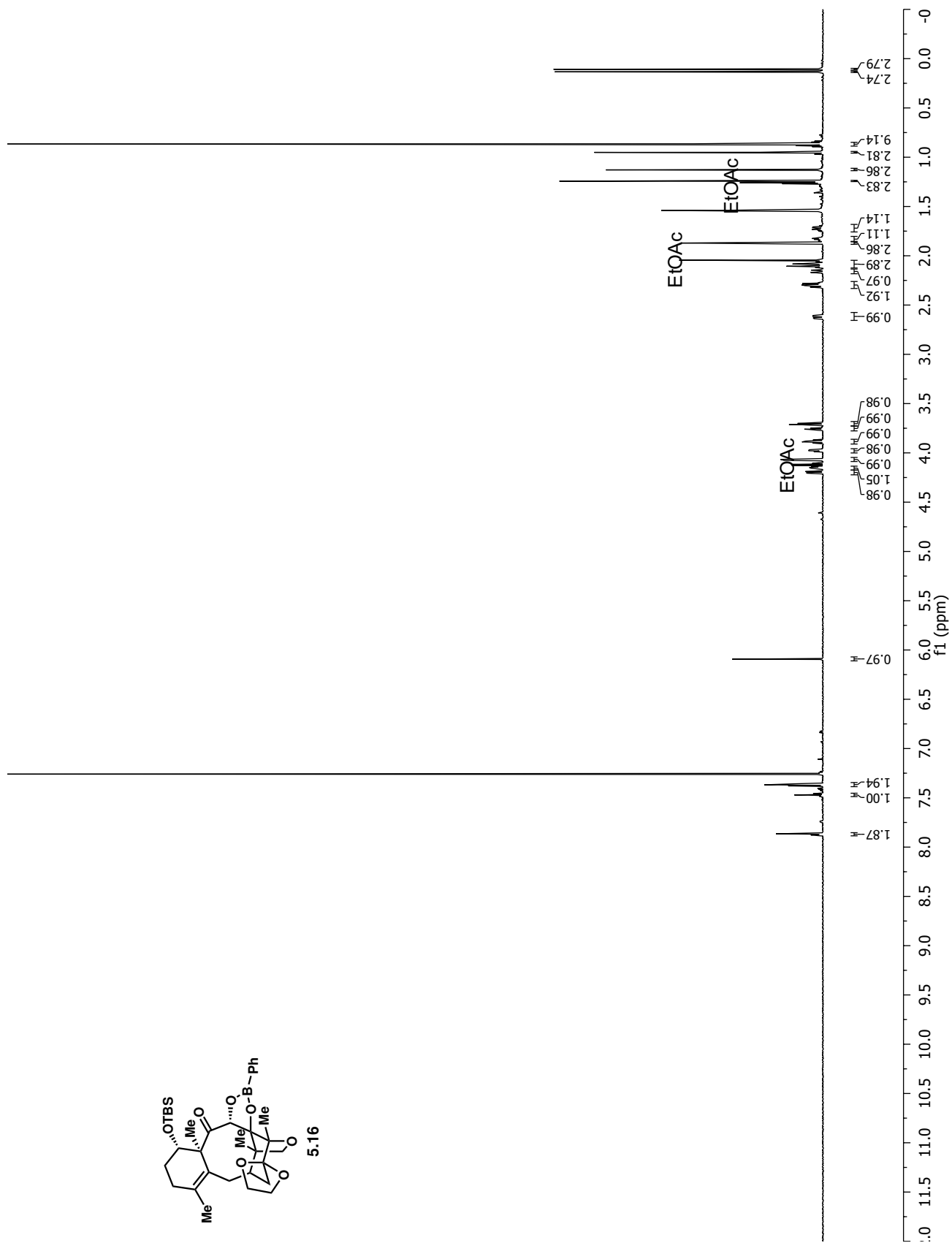
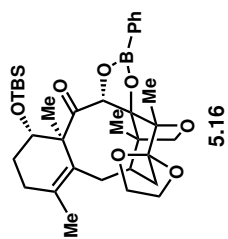
5.13

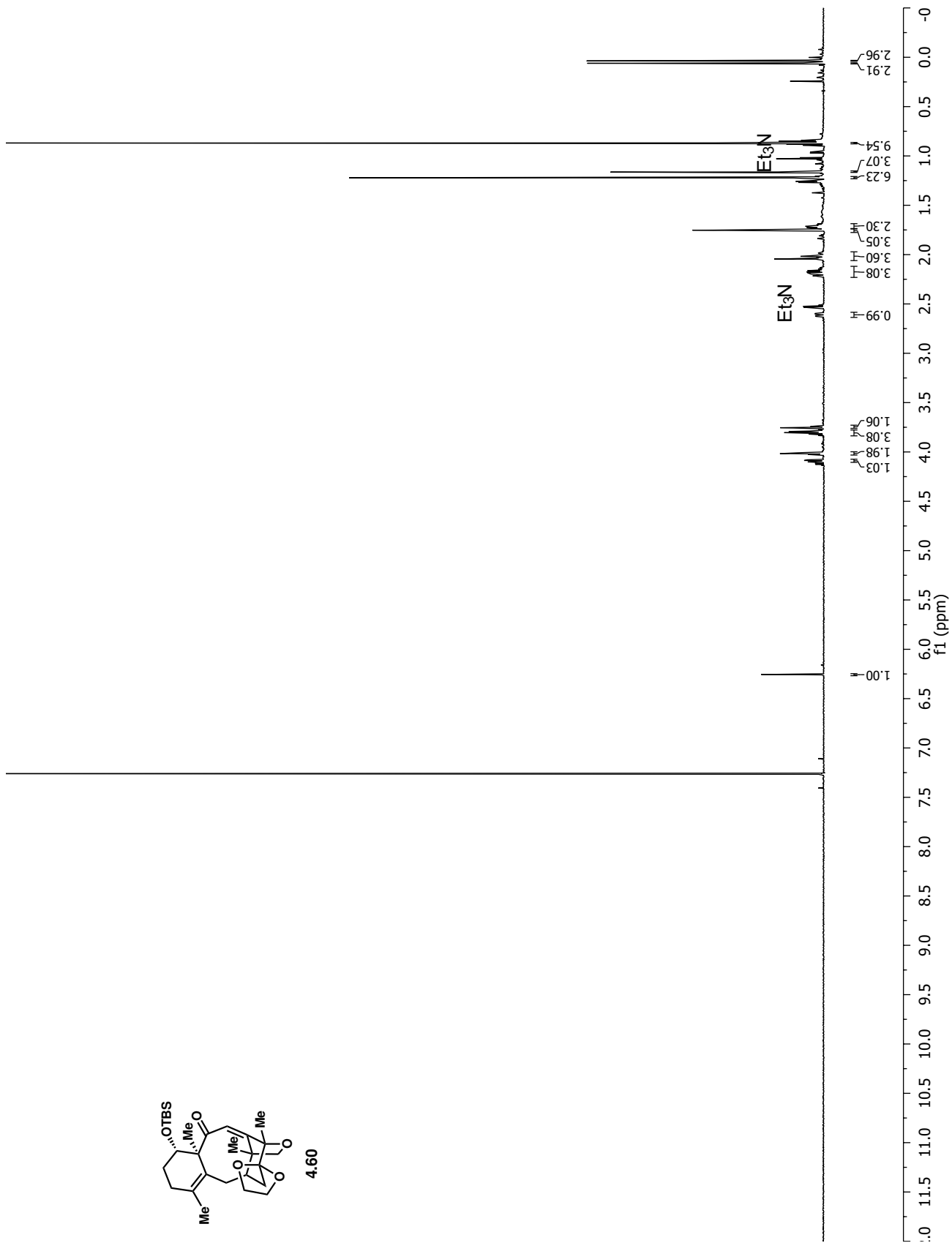
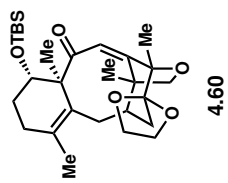


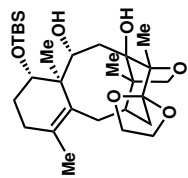




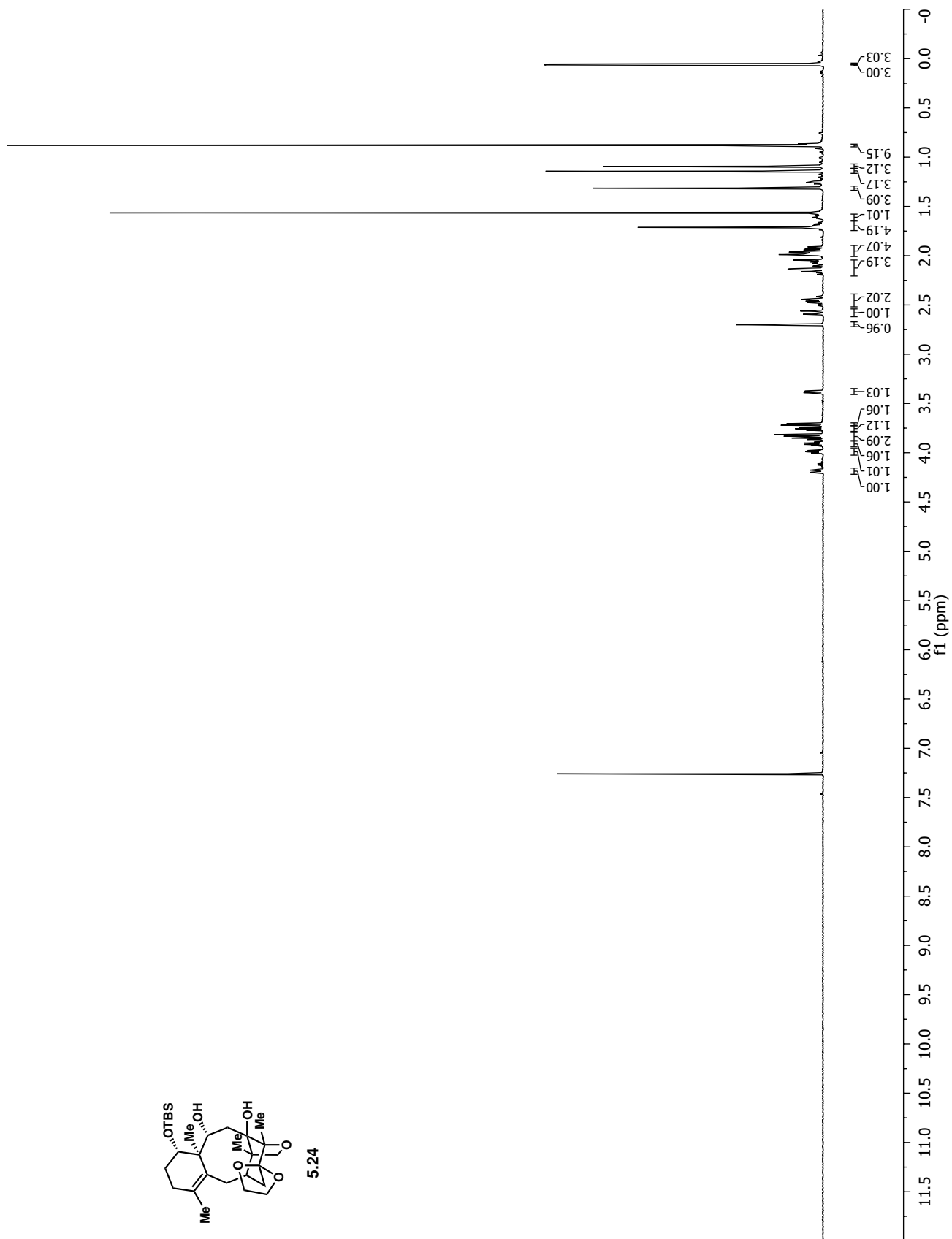


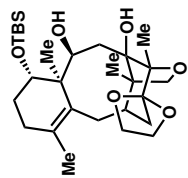




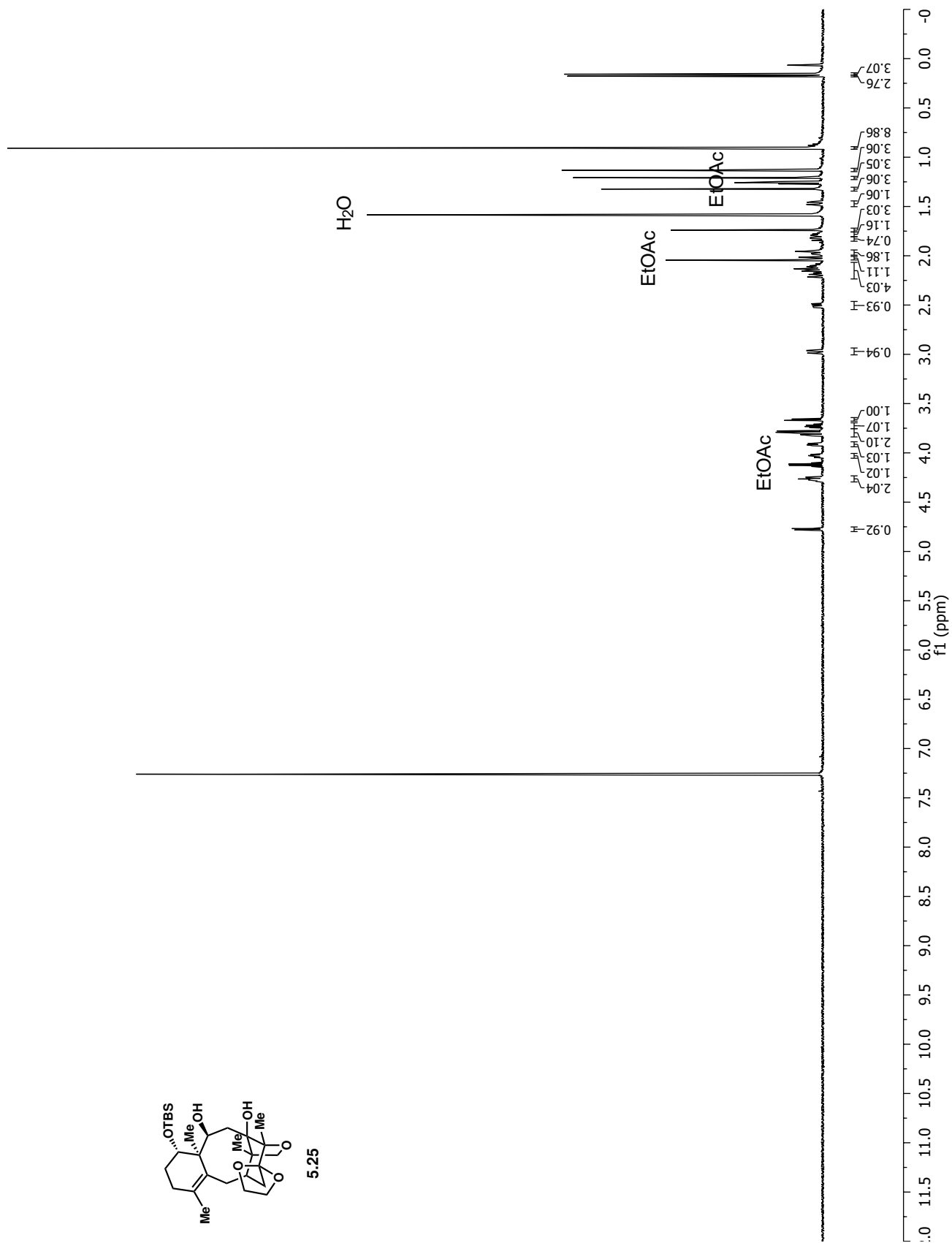


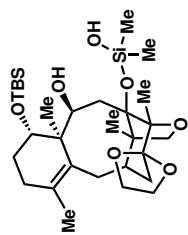
5.24



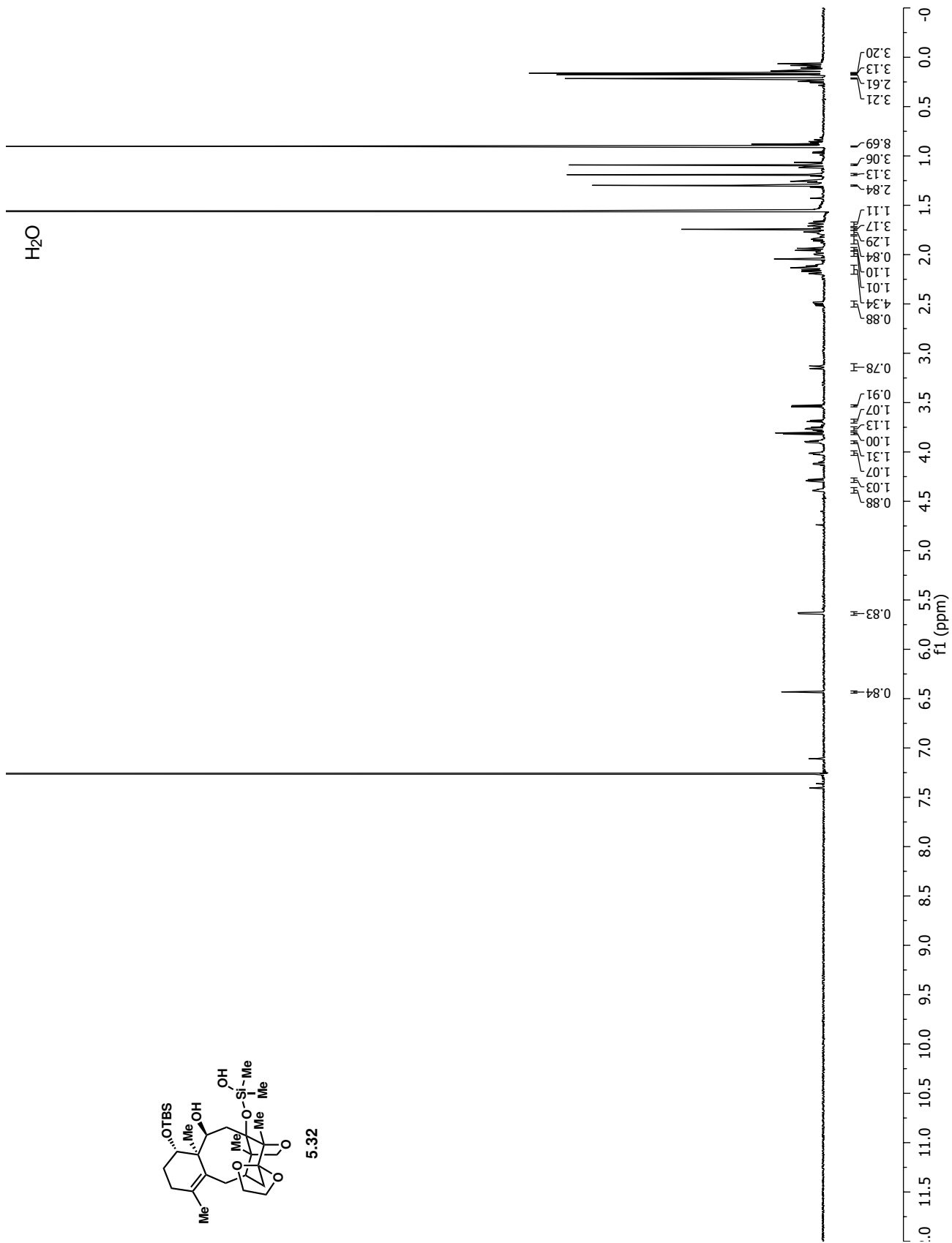


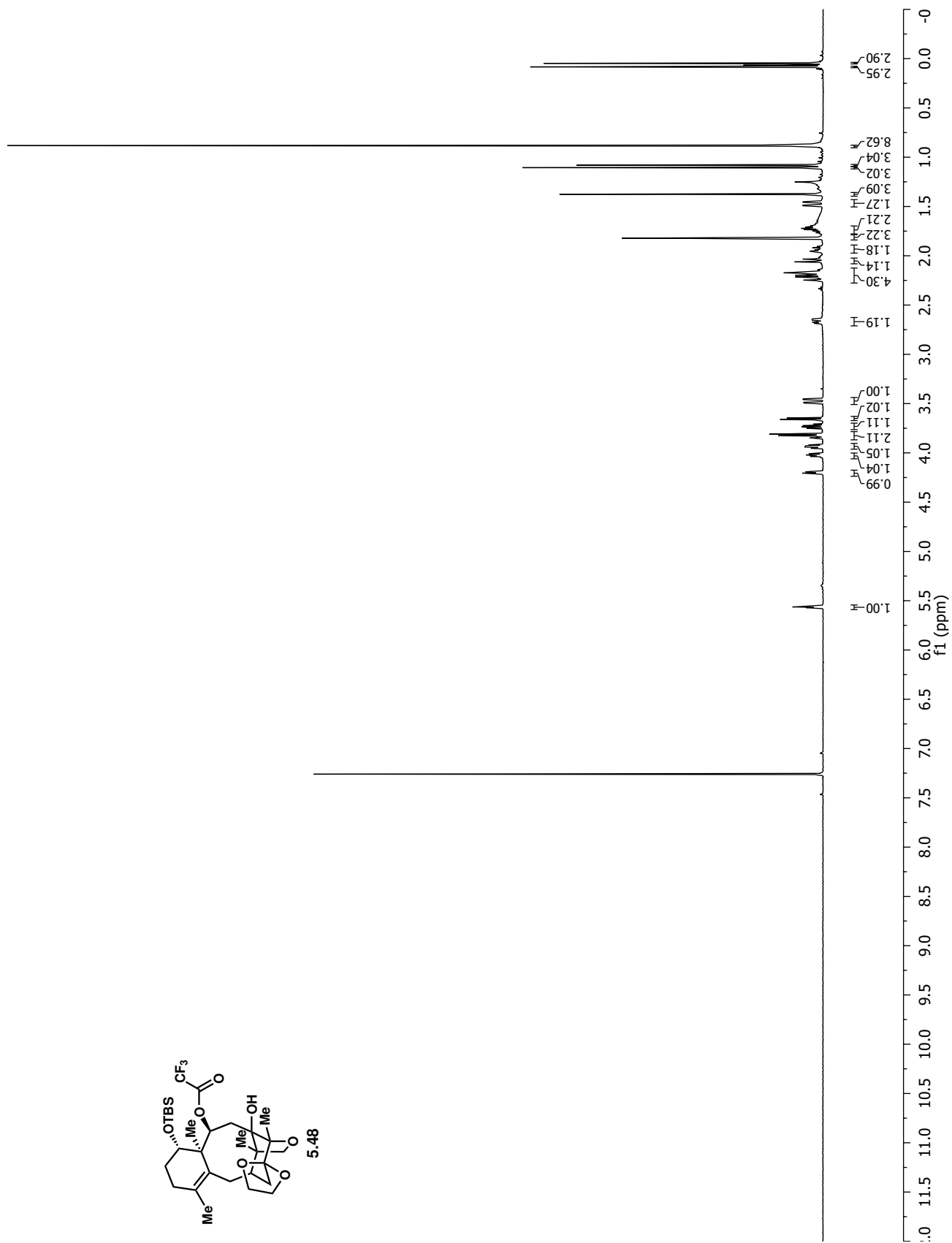
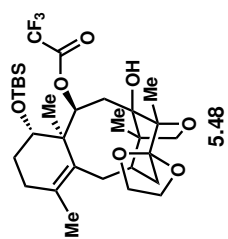
5.25

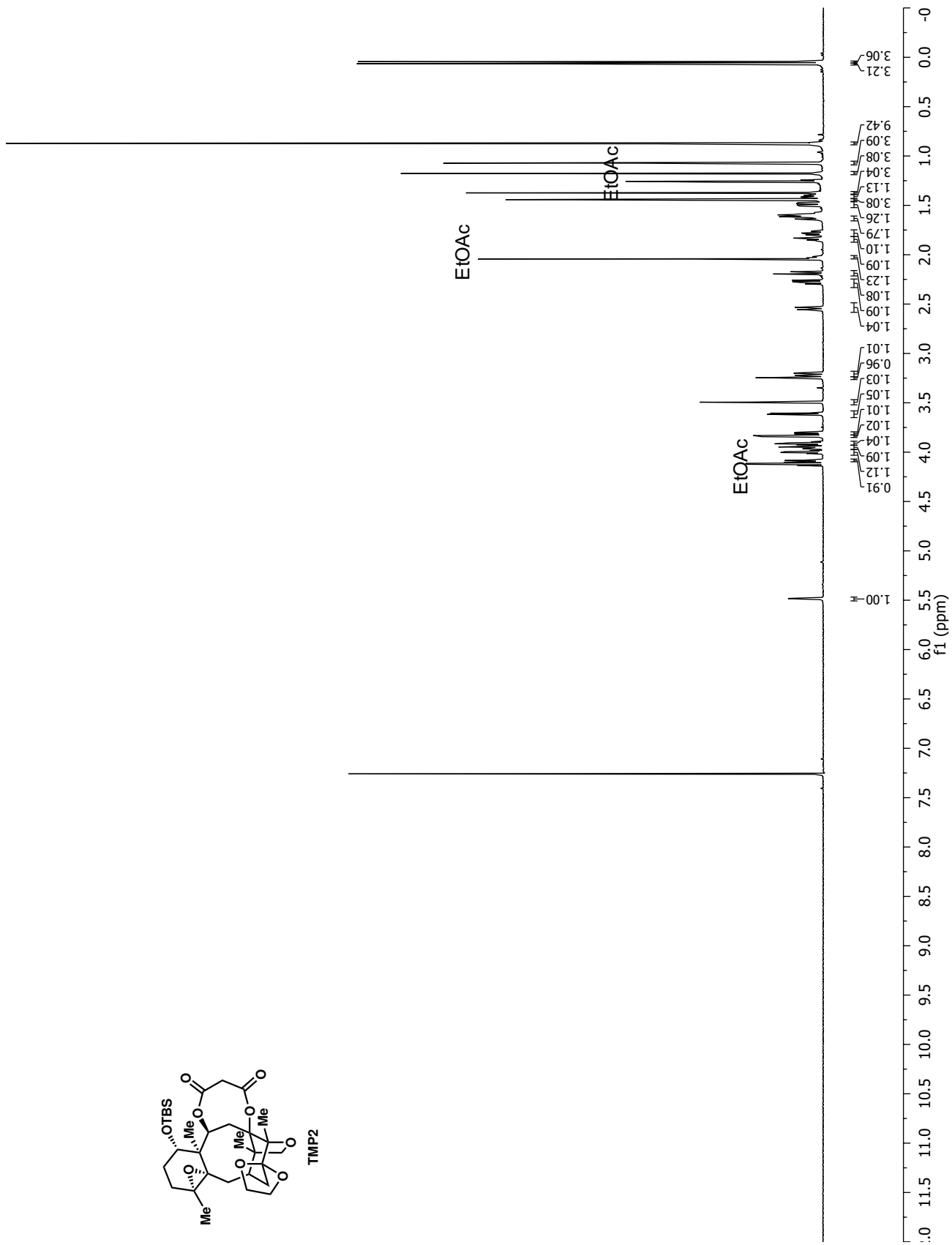
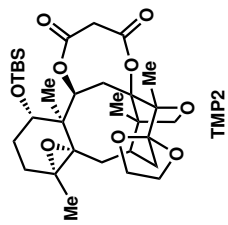


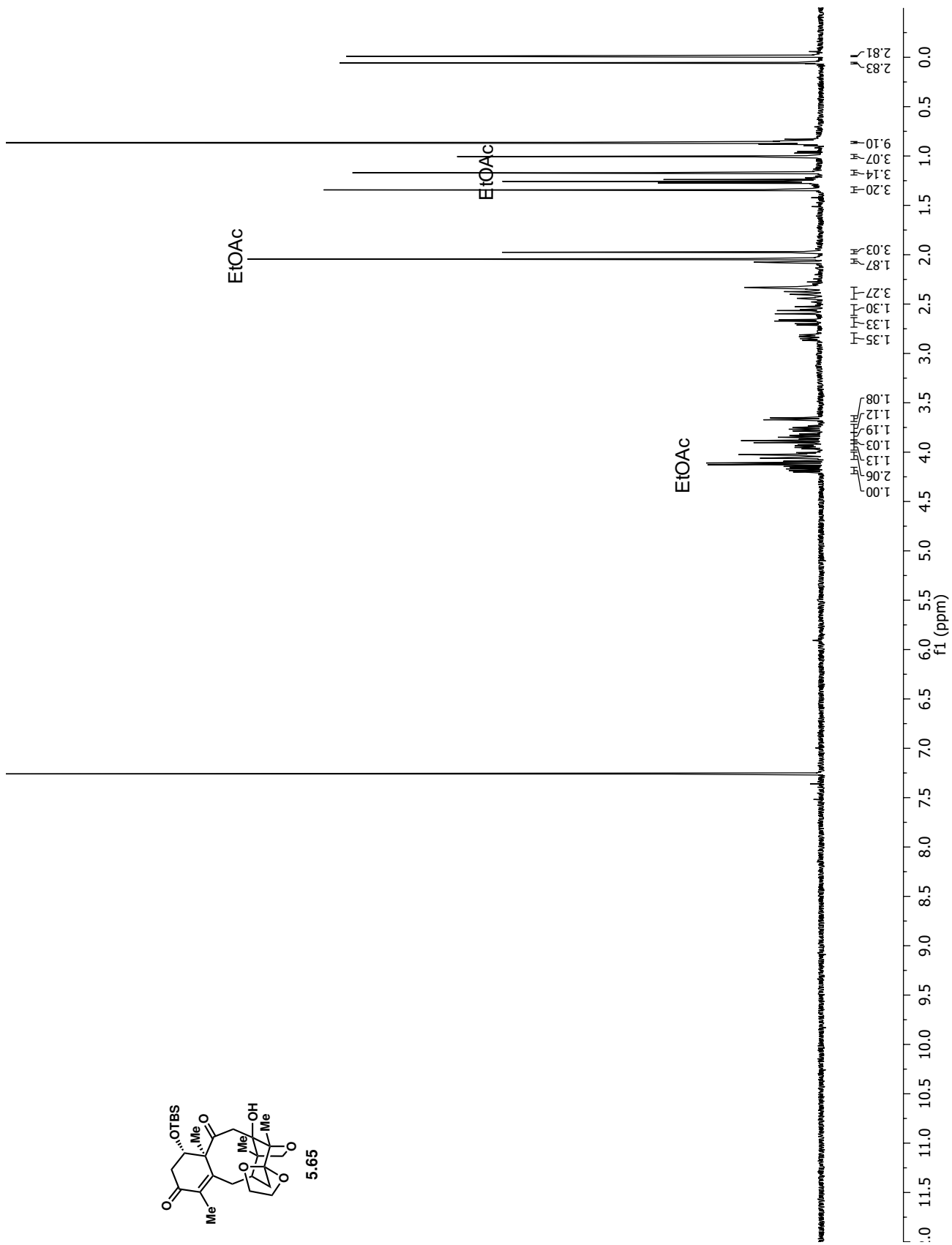
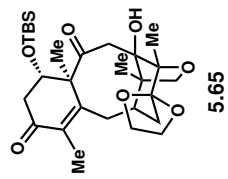


5.32

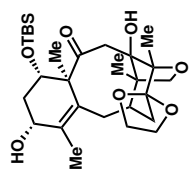




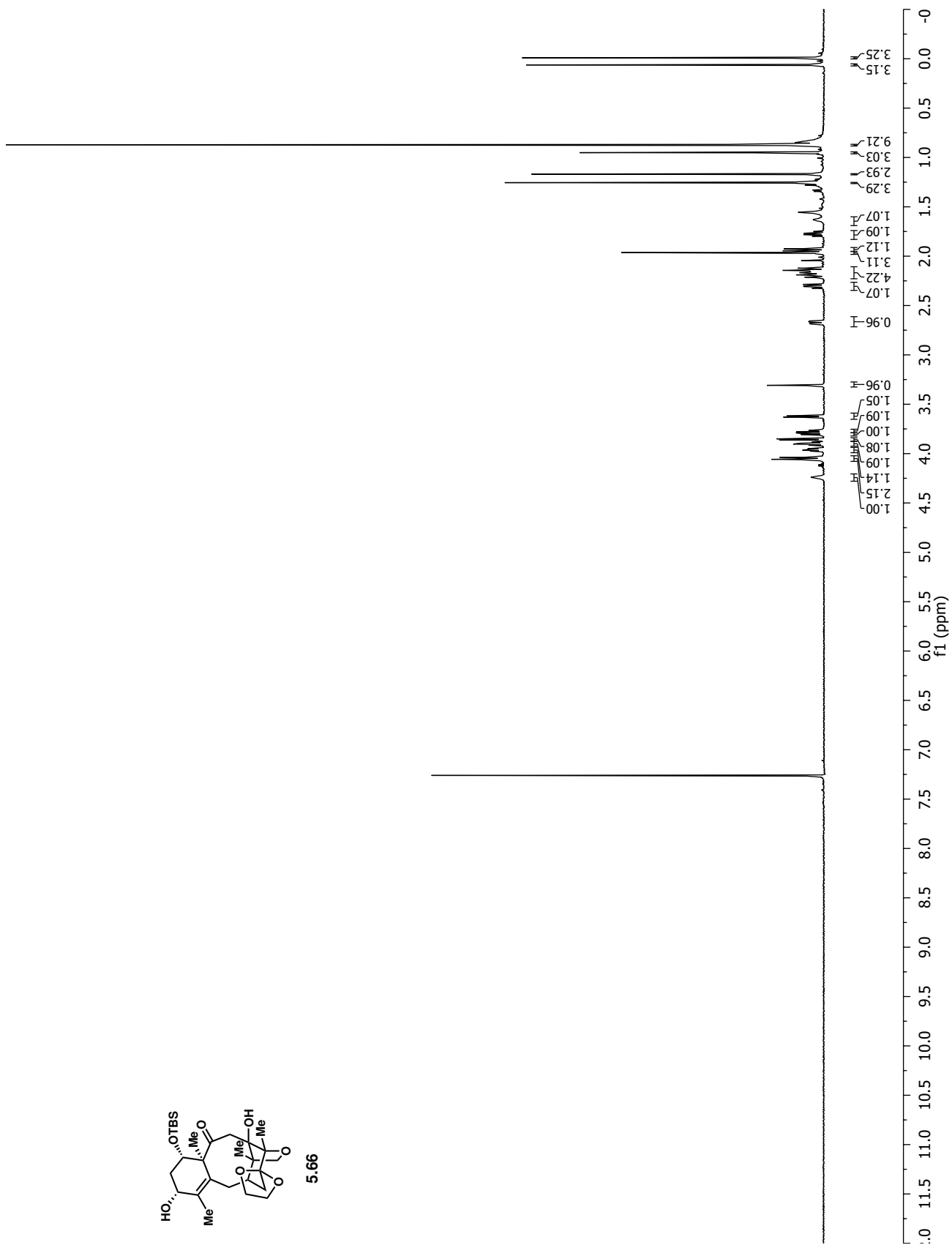


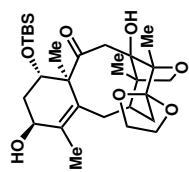




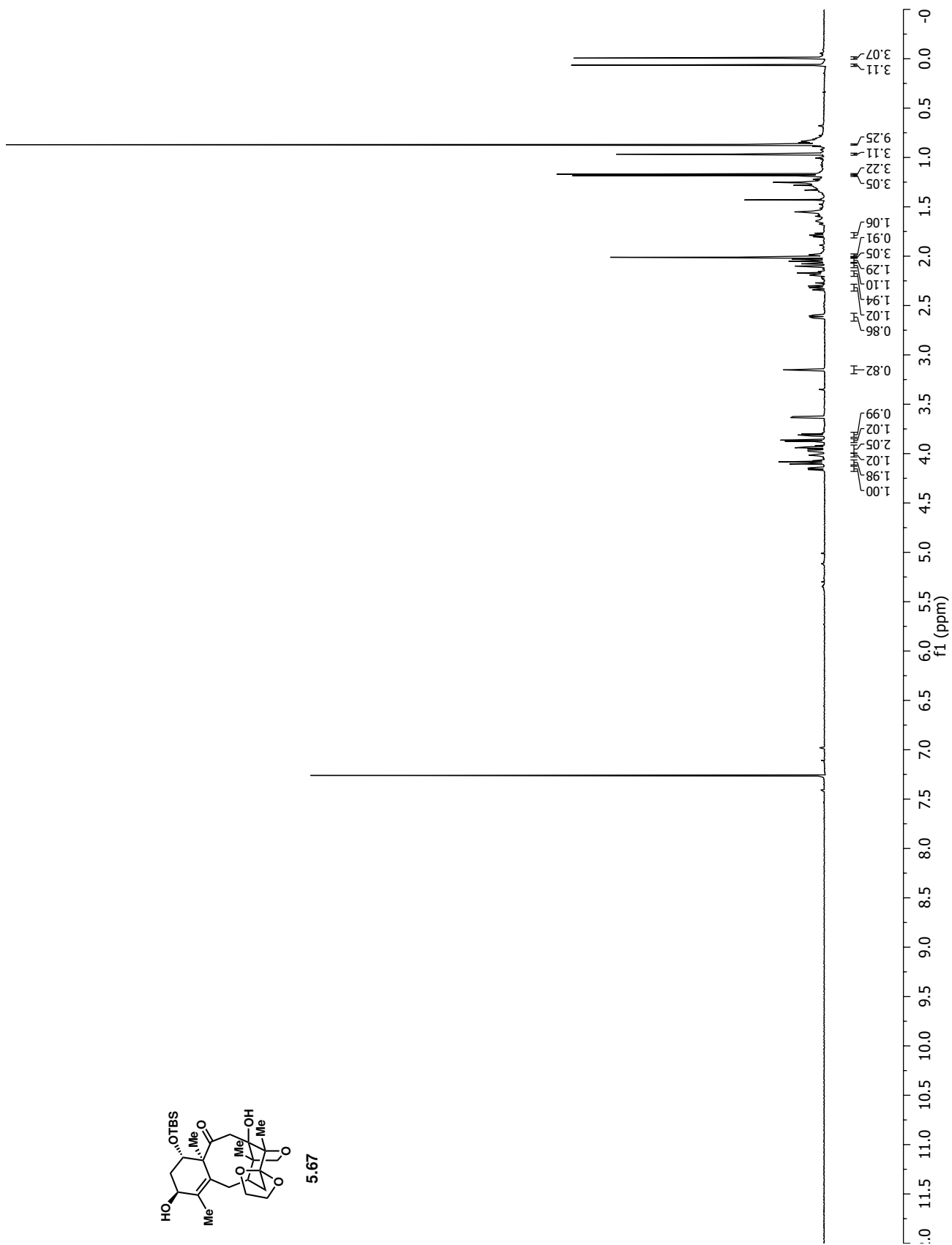


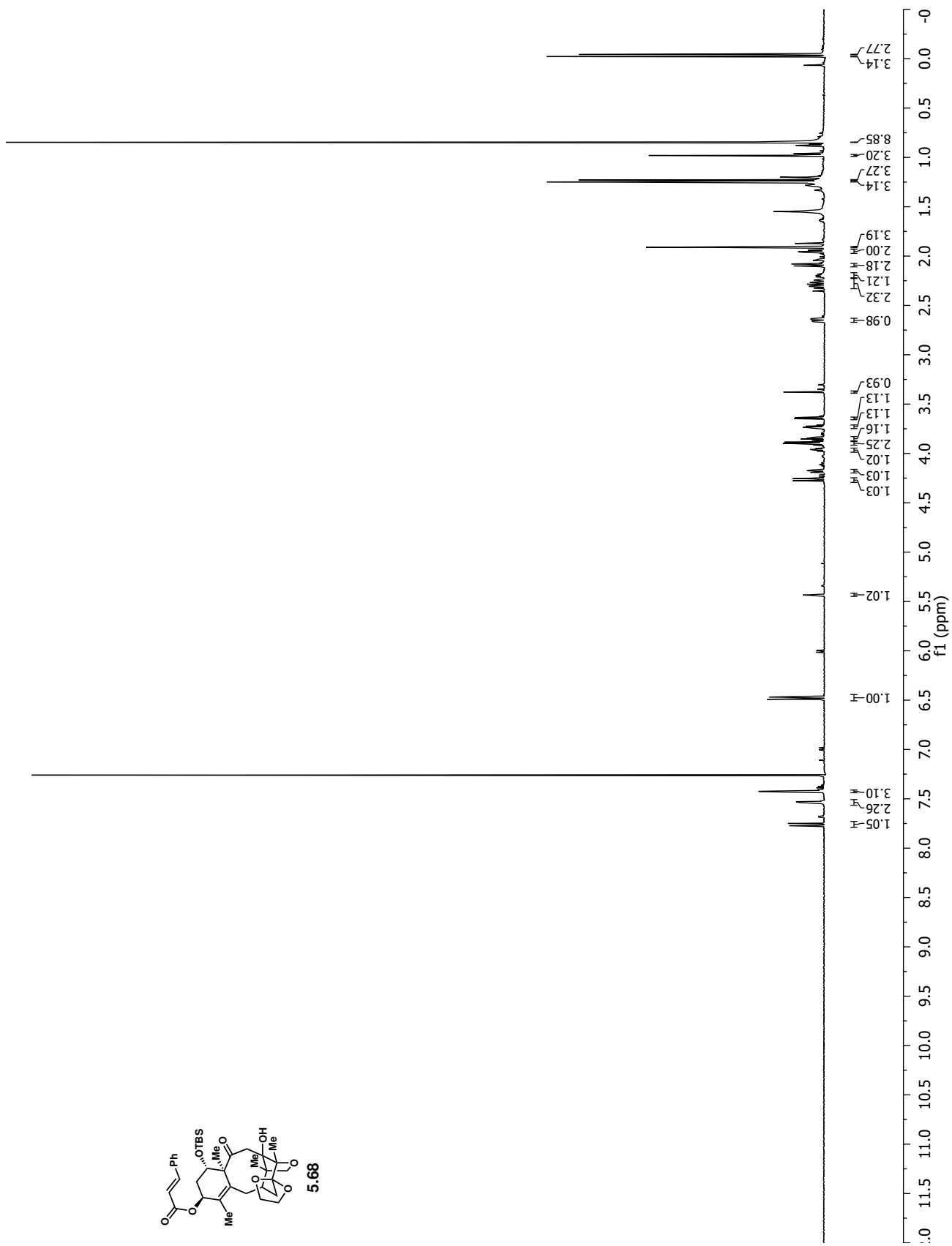
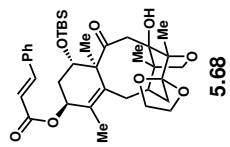
5.66

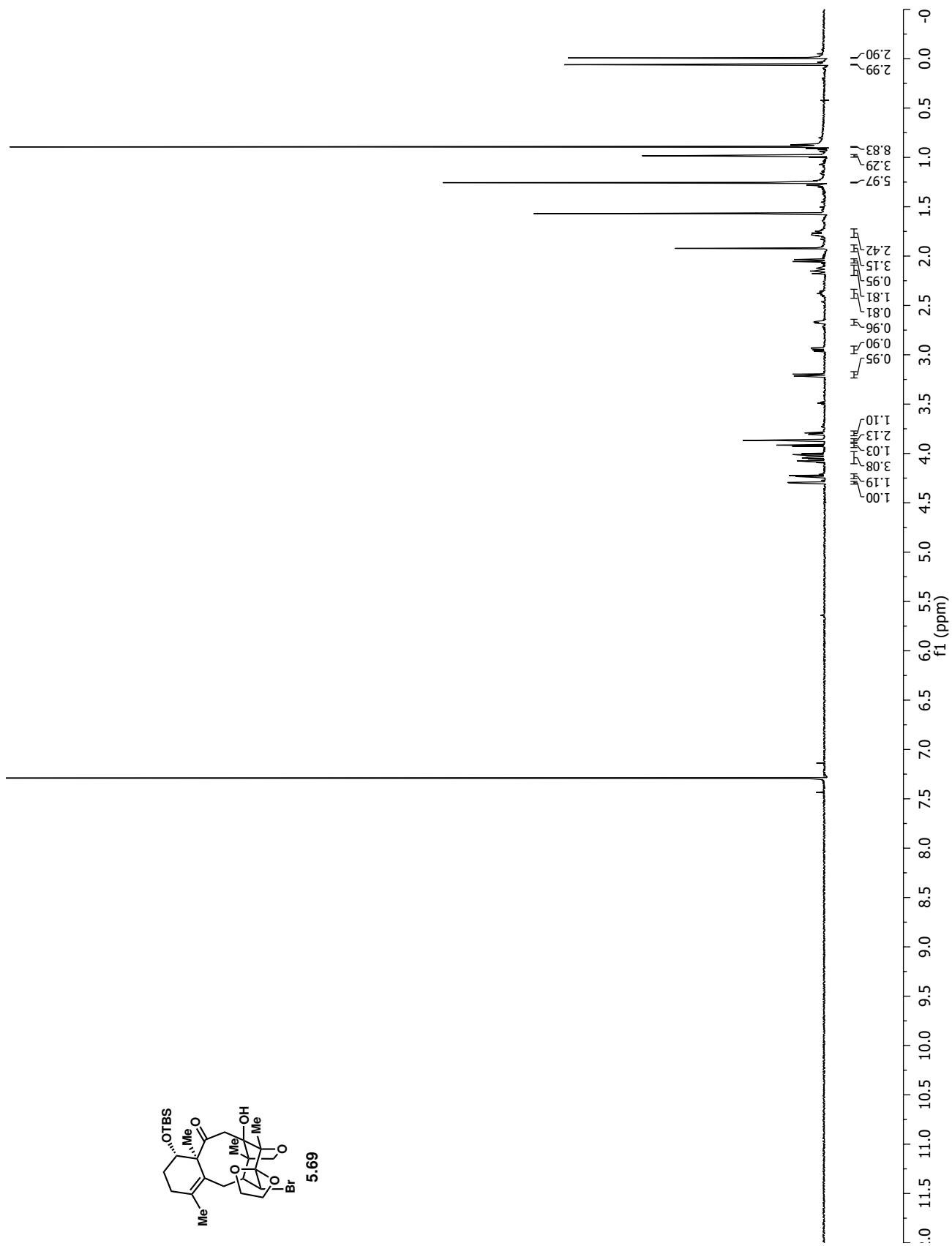
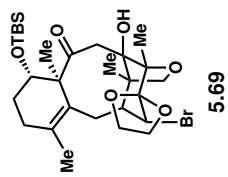


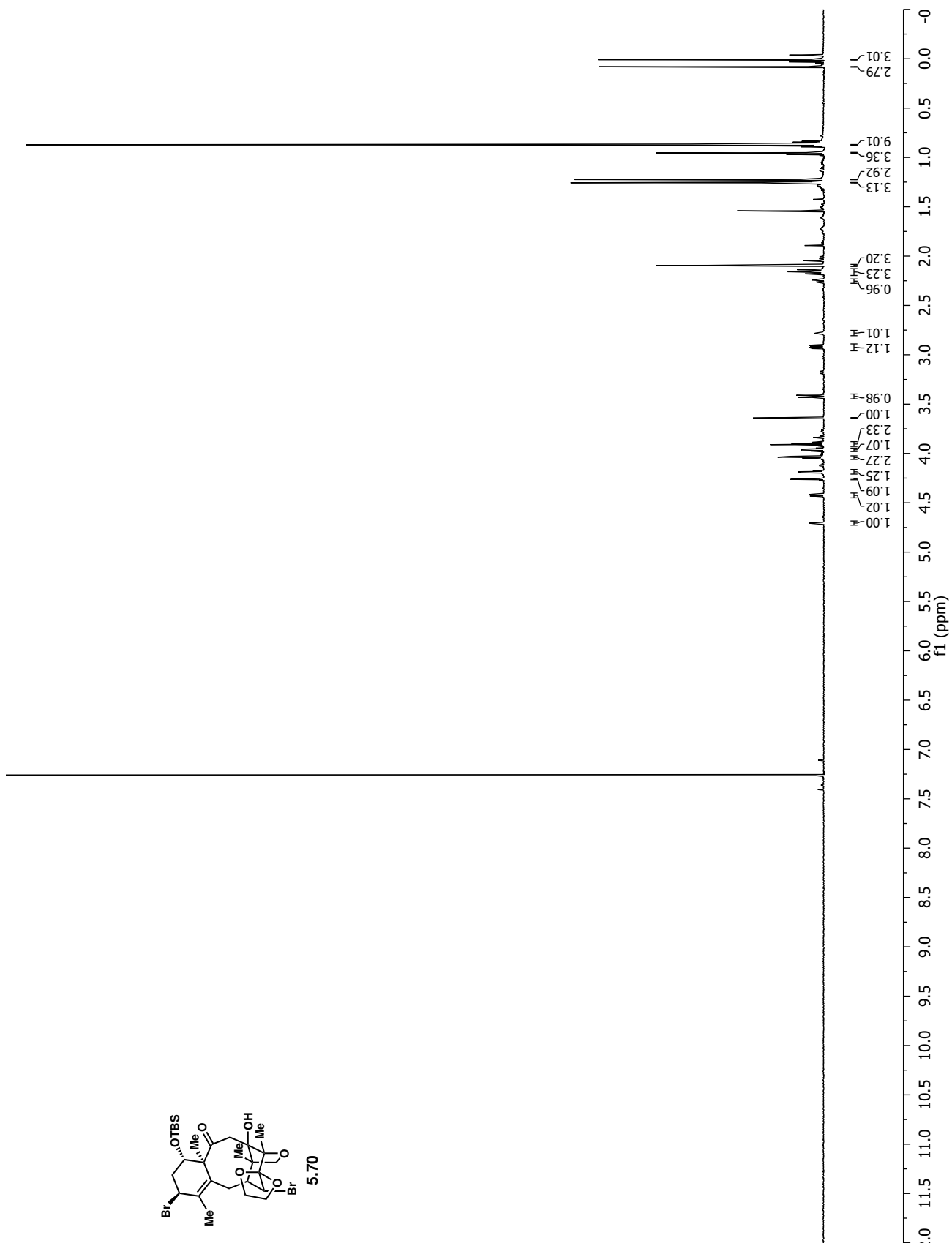
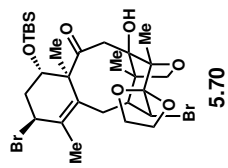


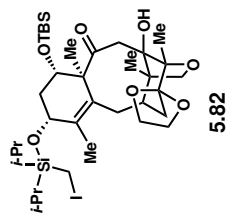
5.67



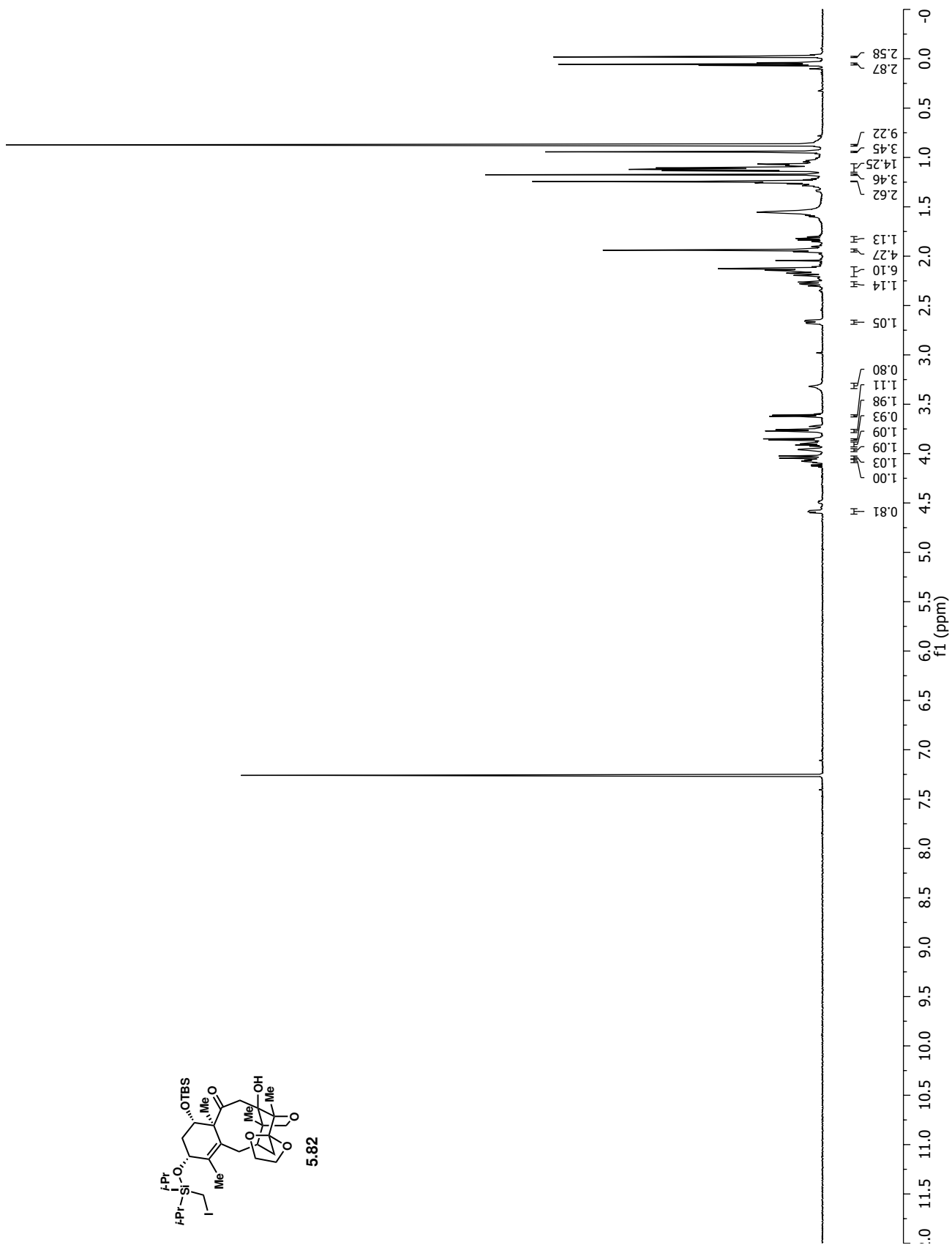


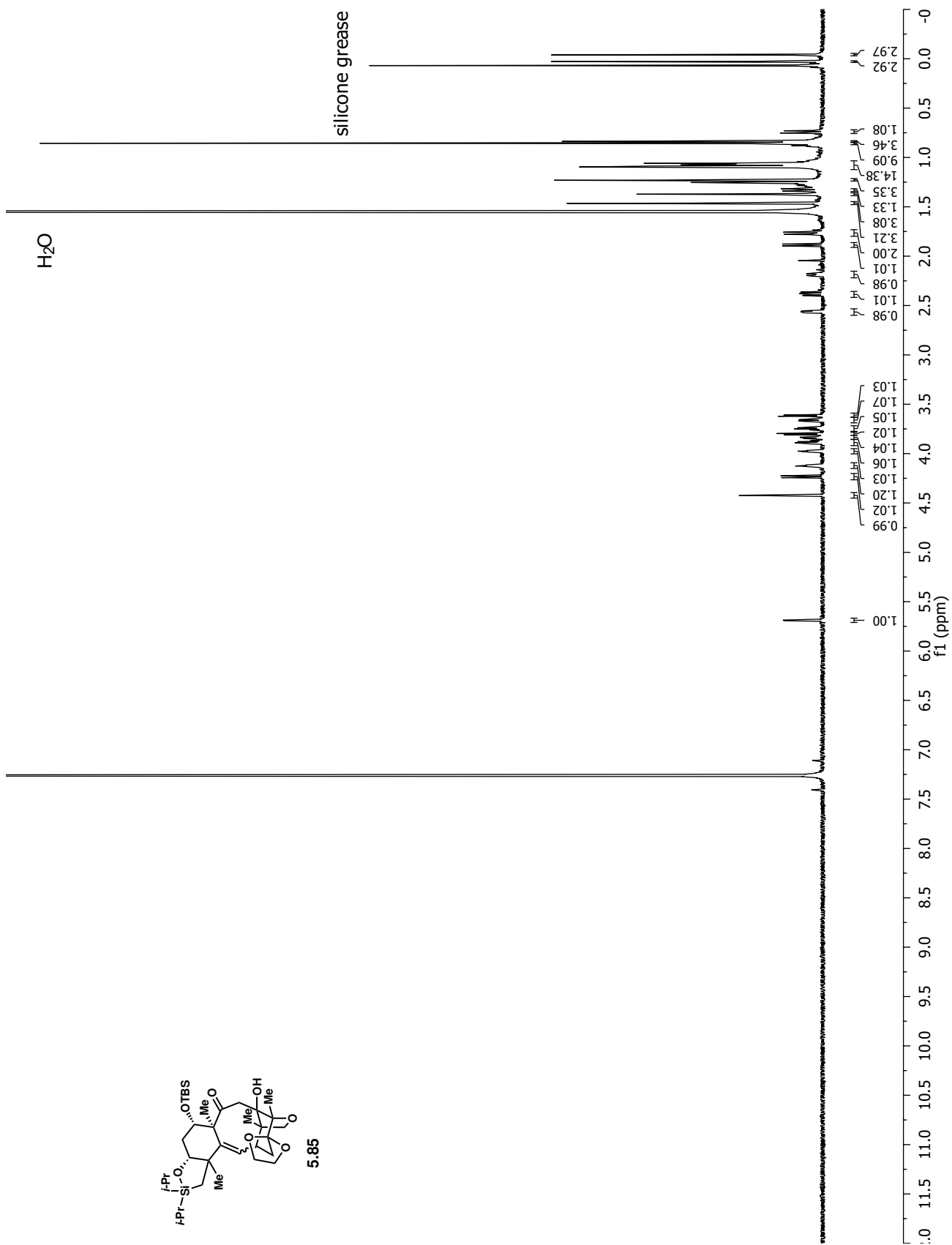
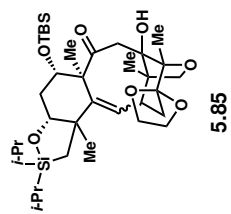


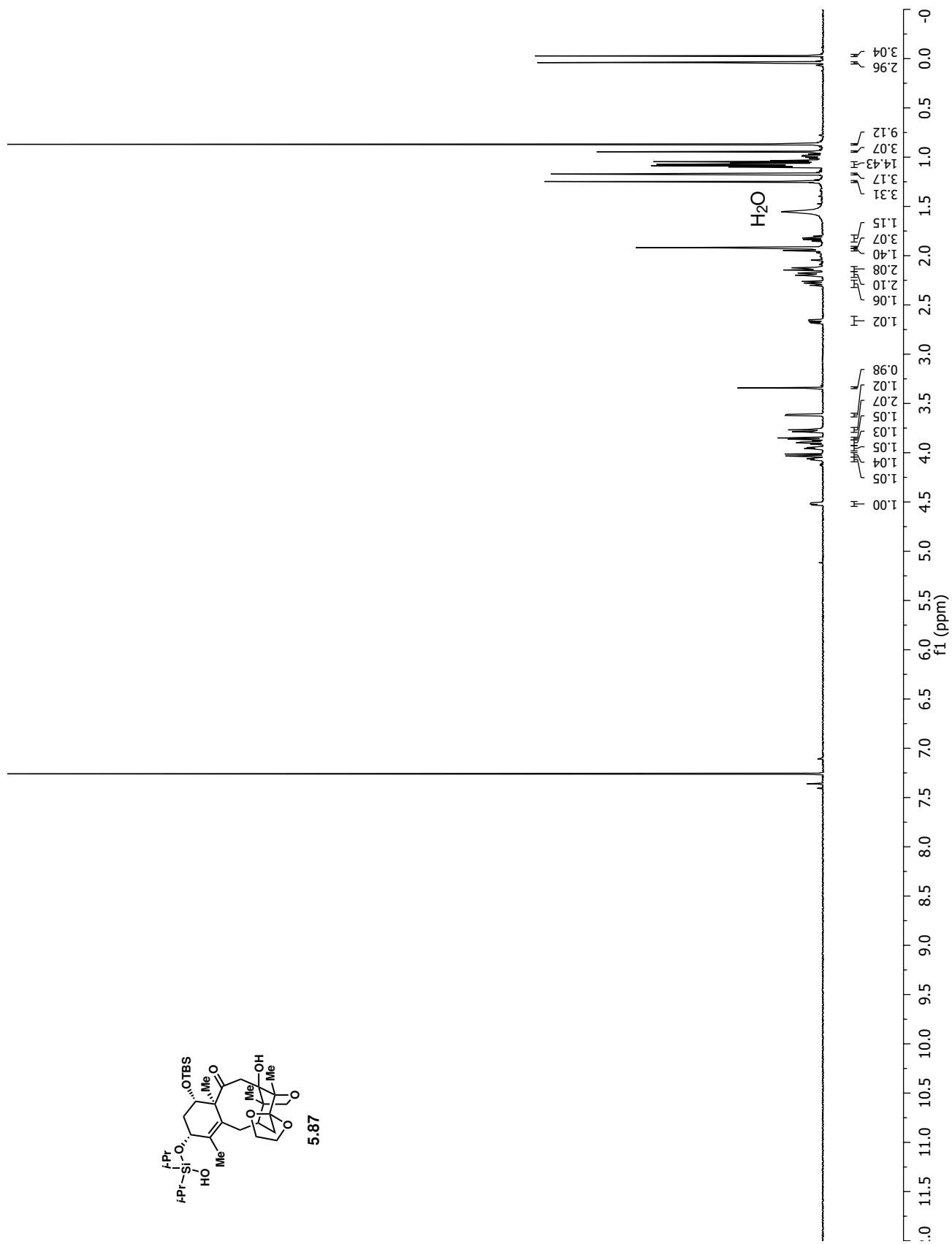
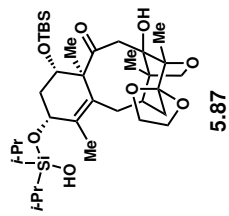




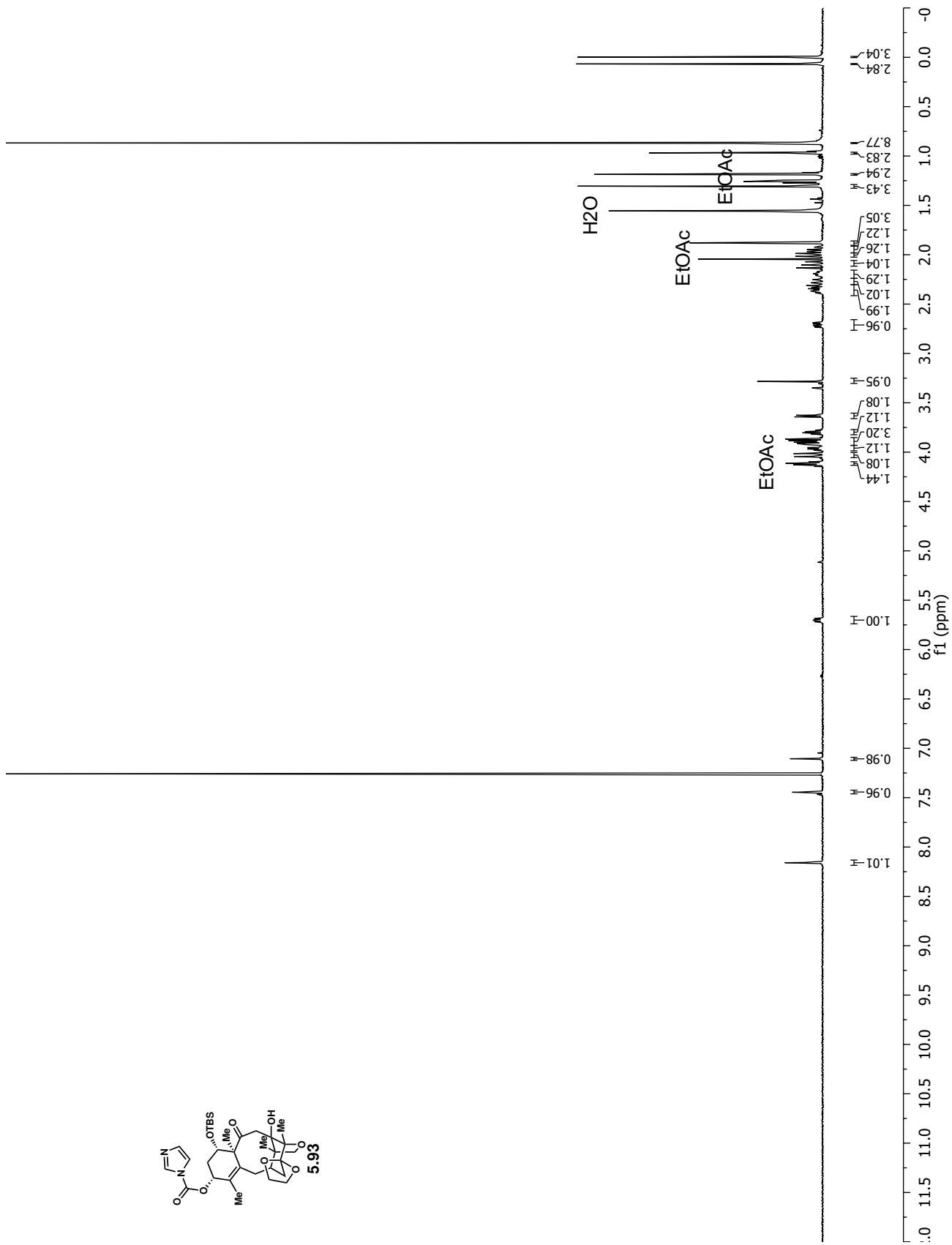
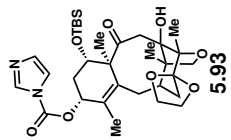
5.82

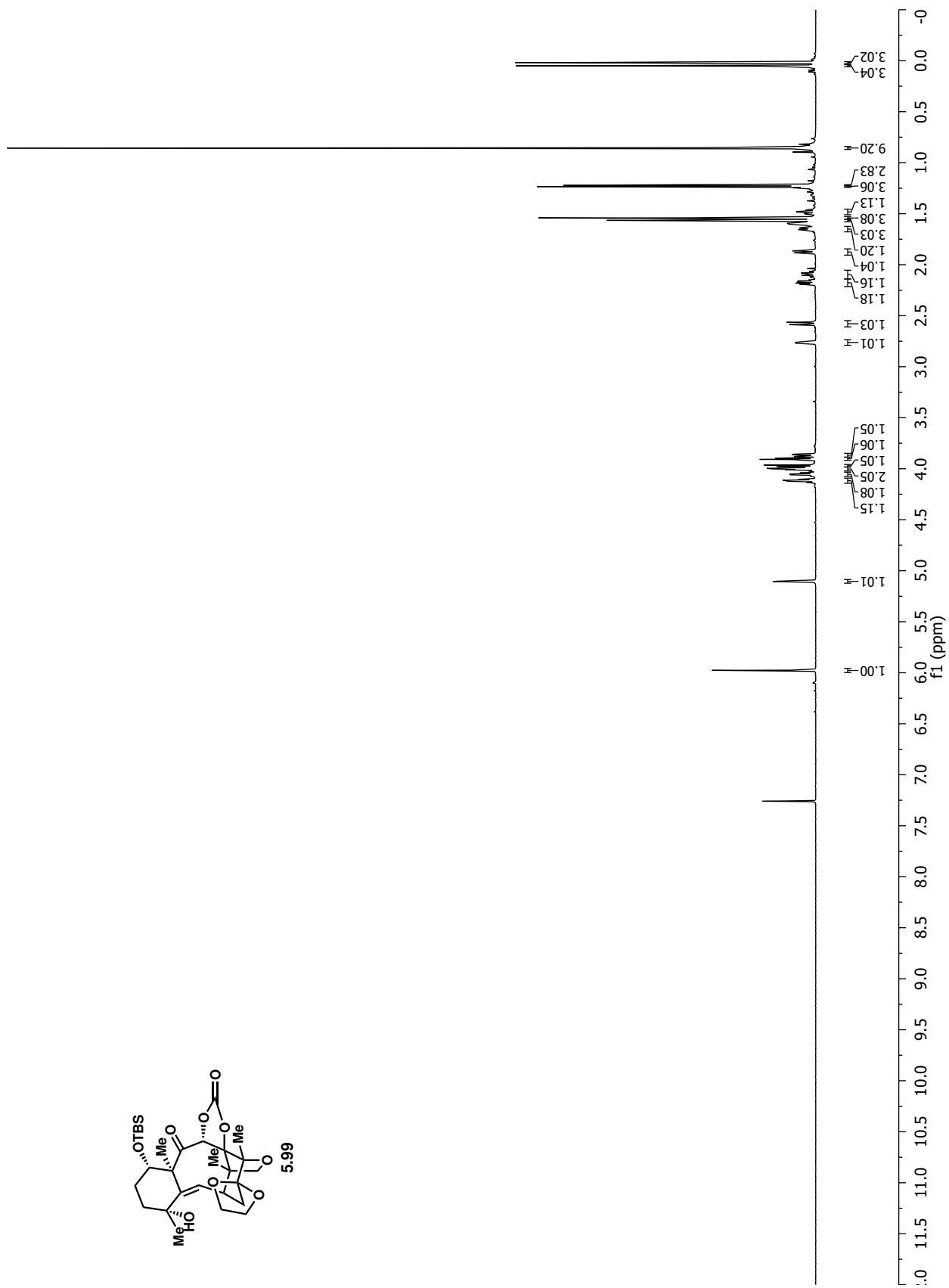
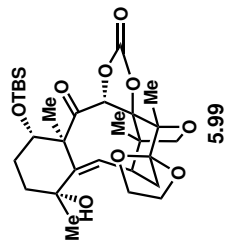


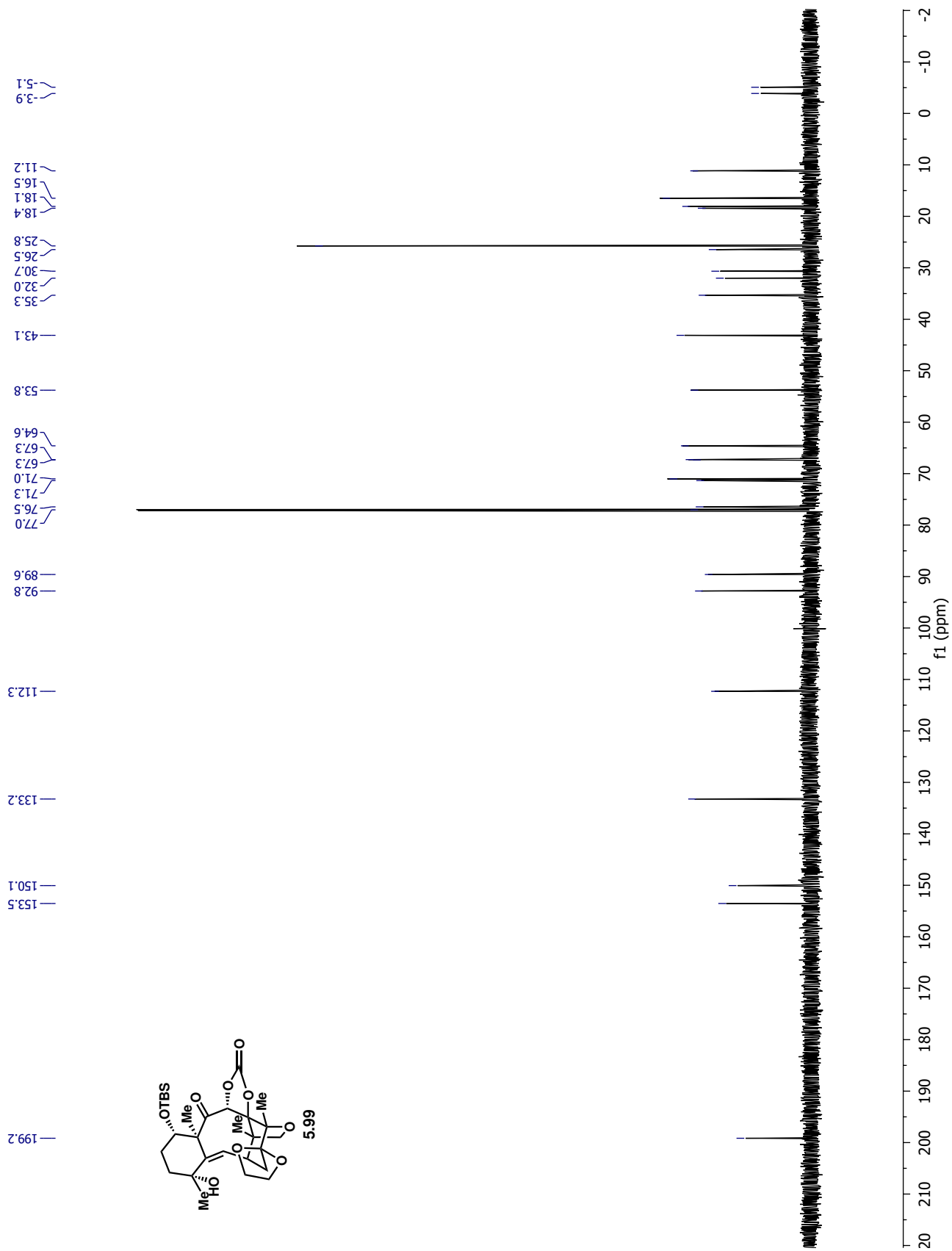


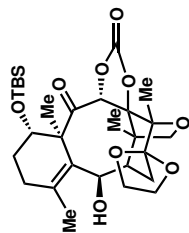




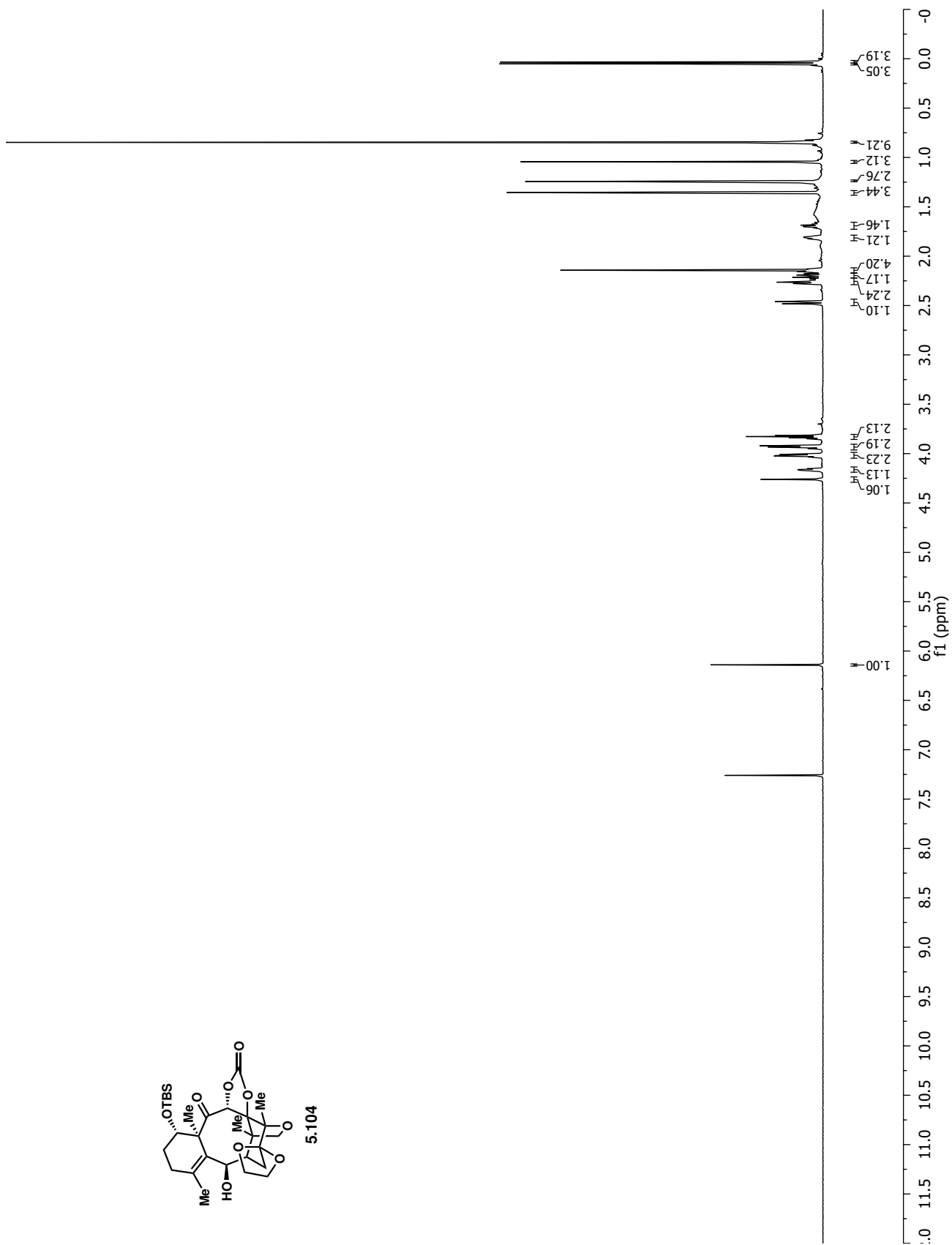


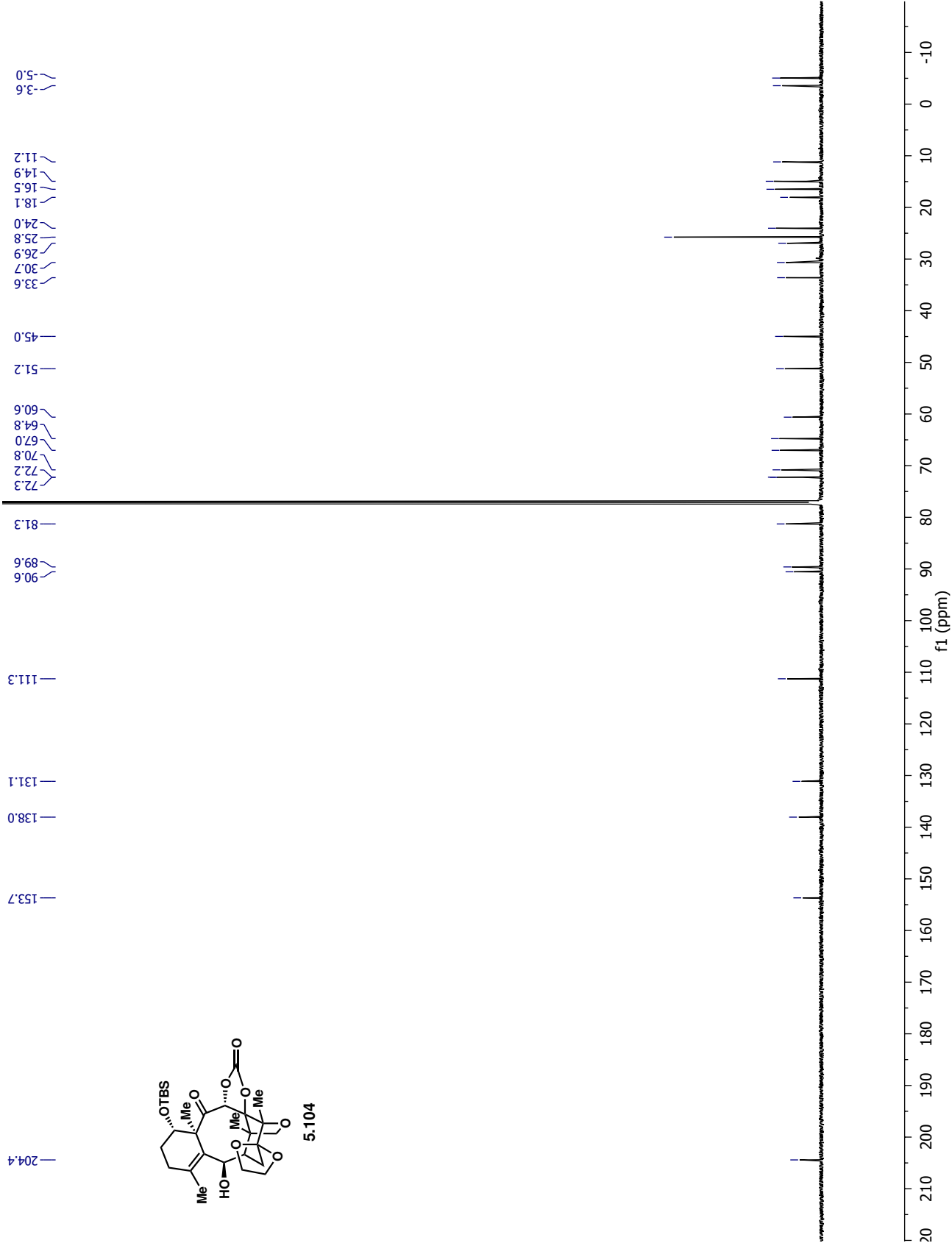


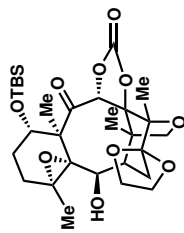




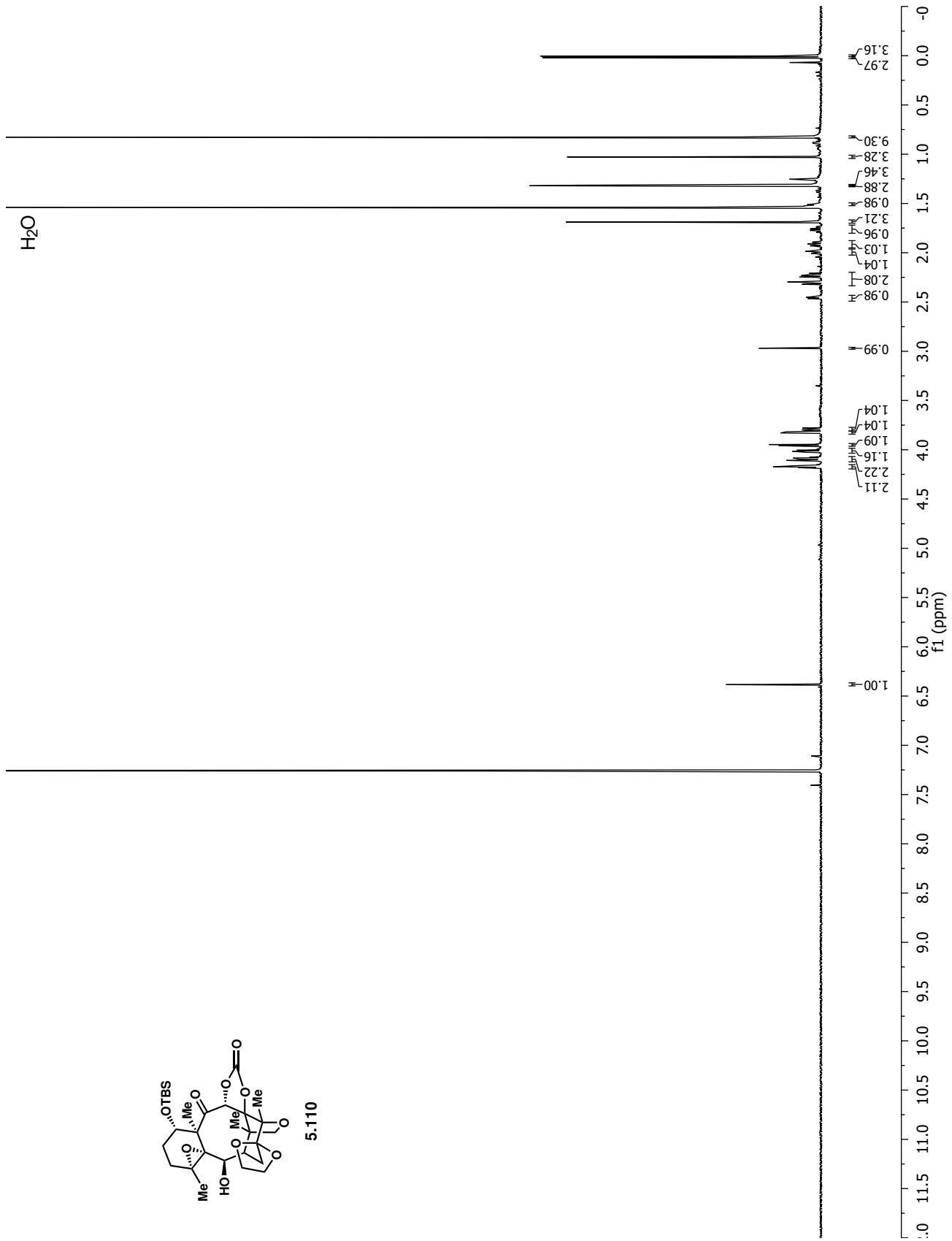
5.104

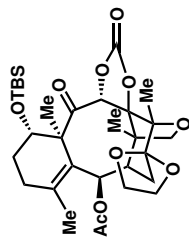




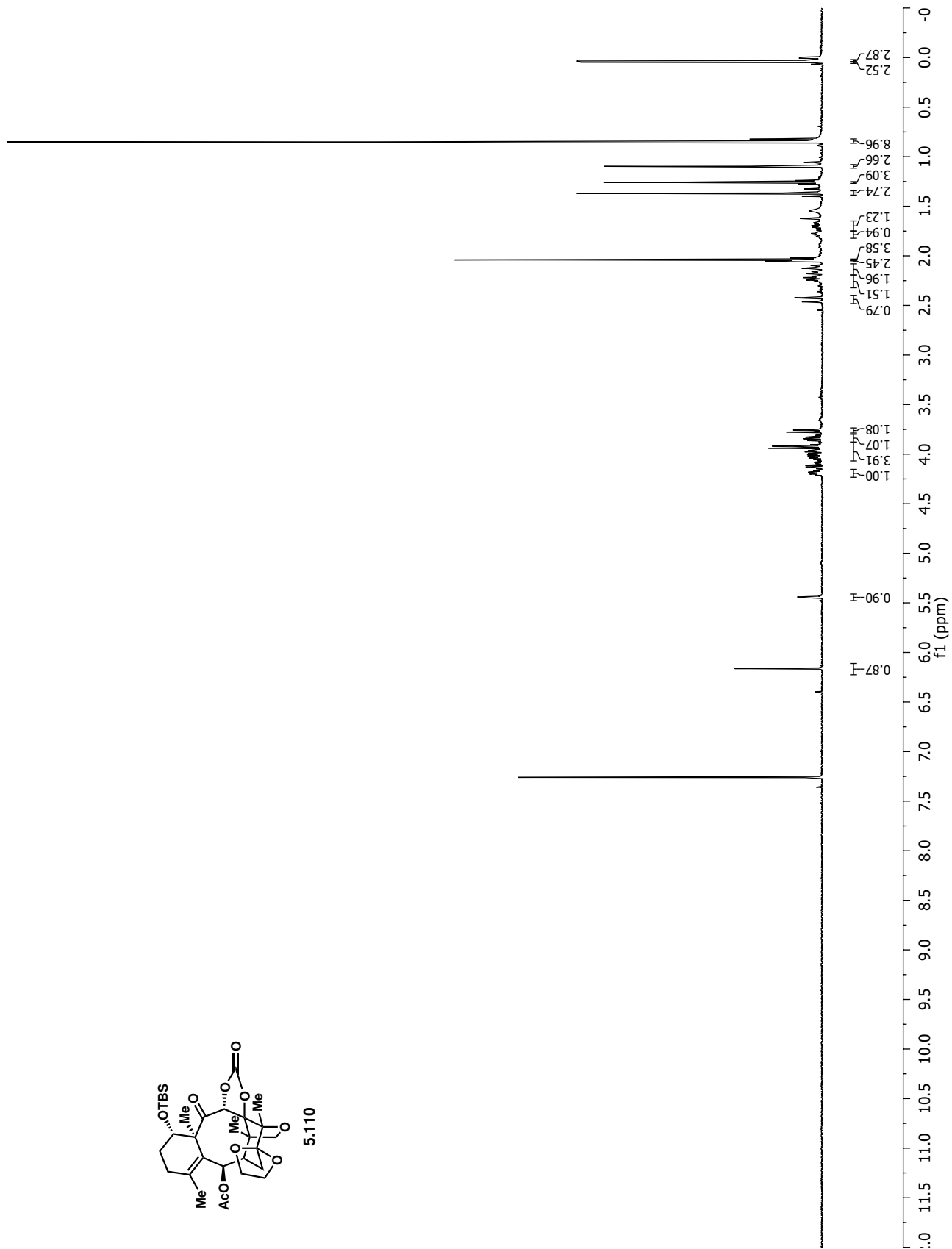


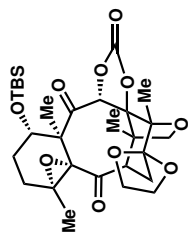
5.110



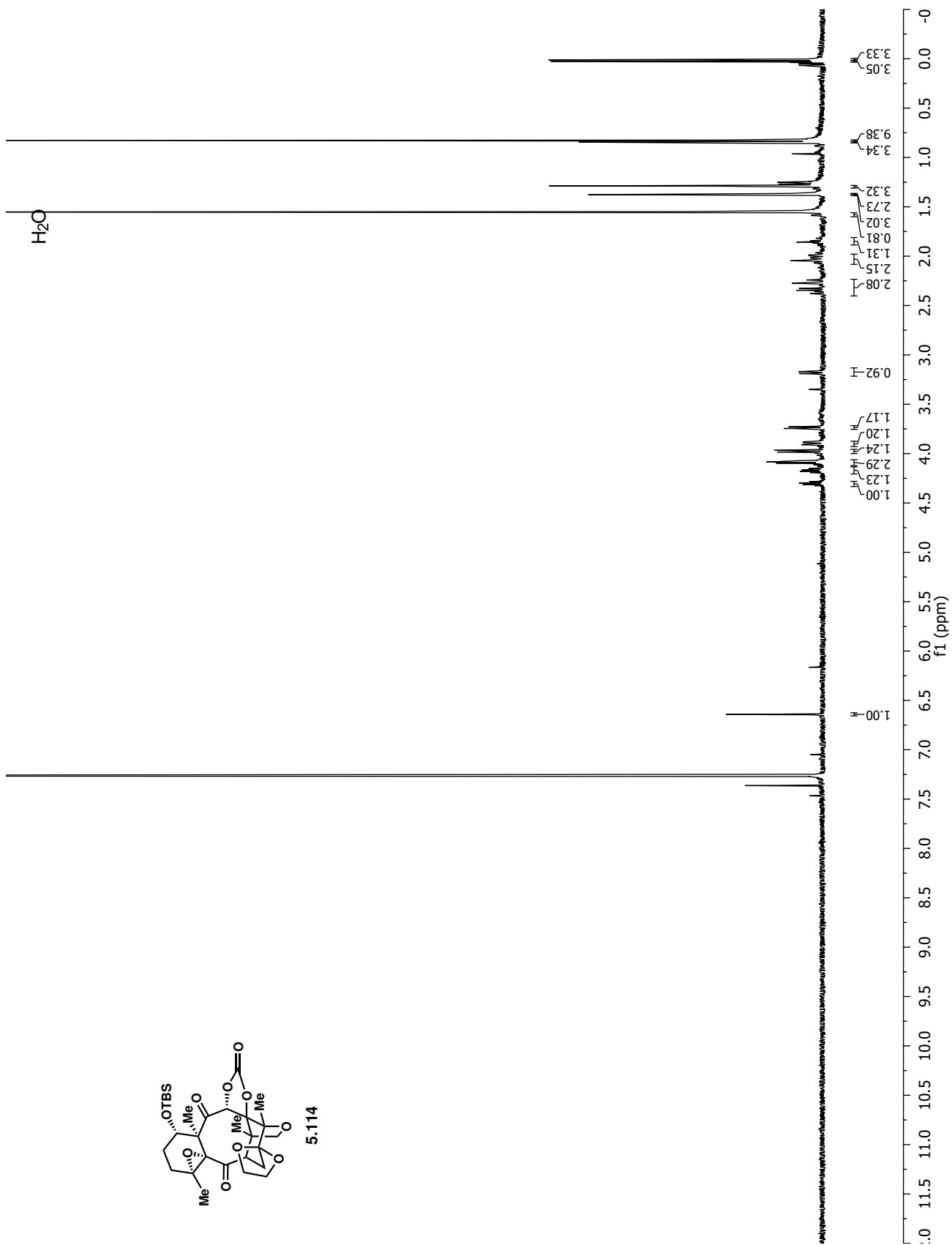


5.1110



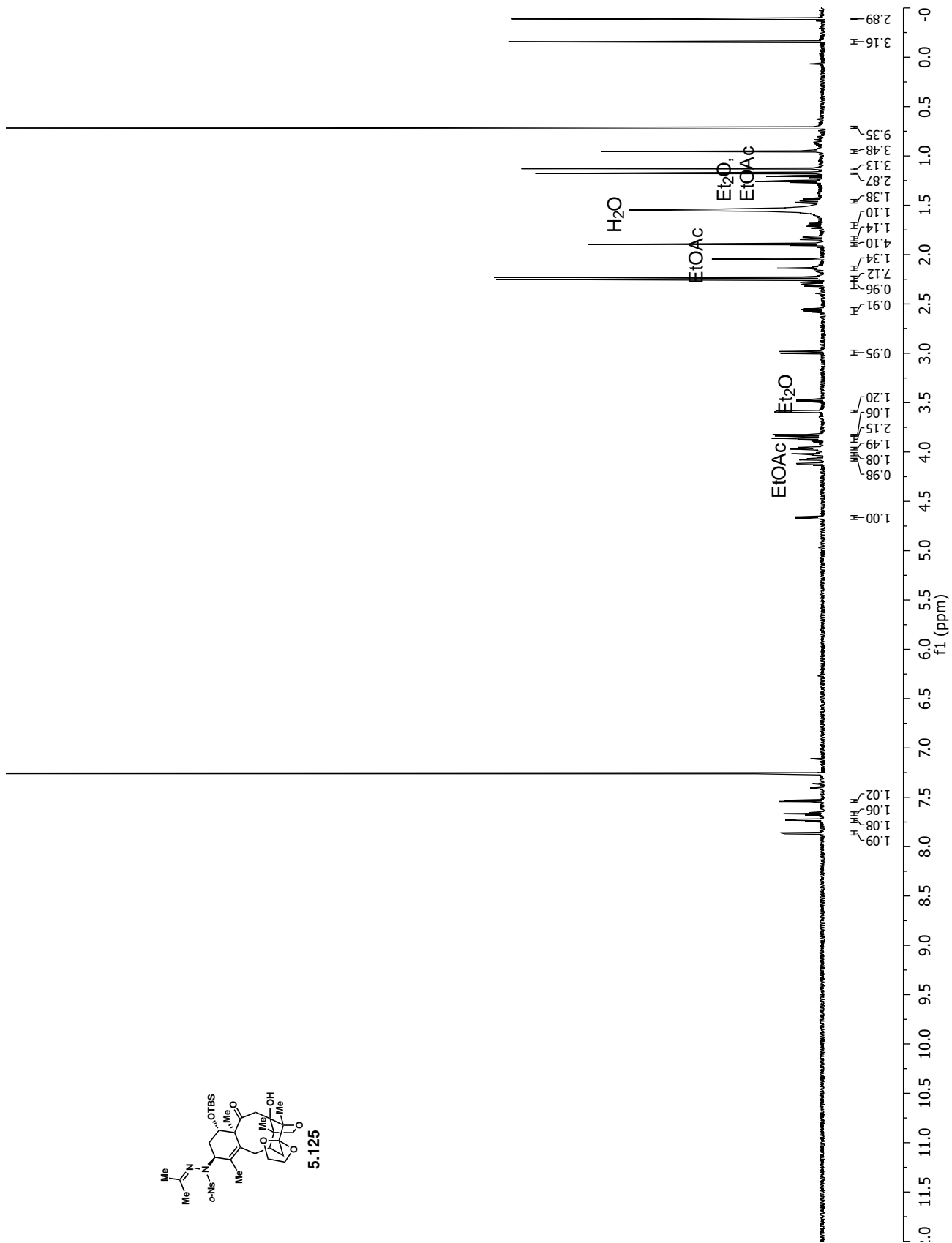
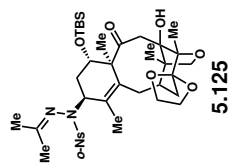


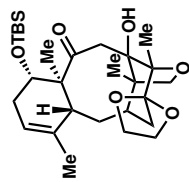
5.1114



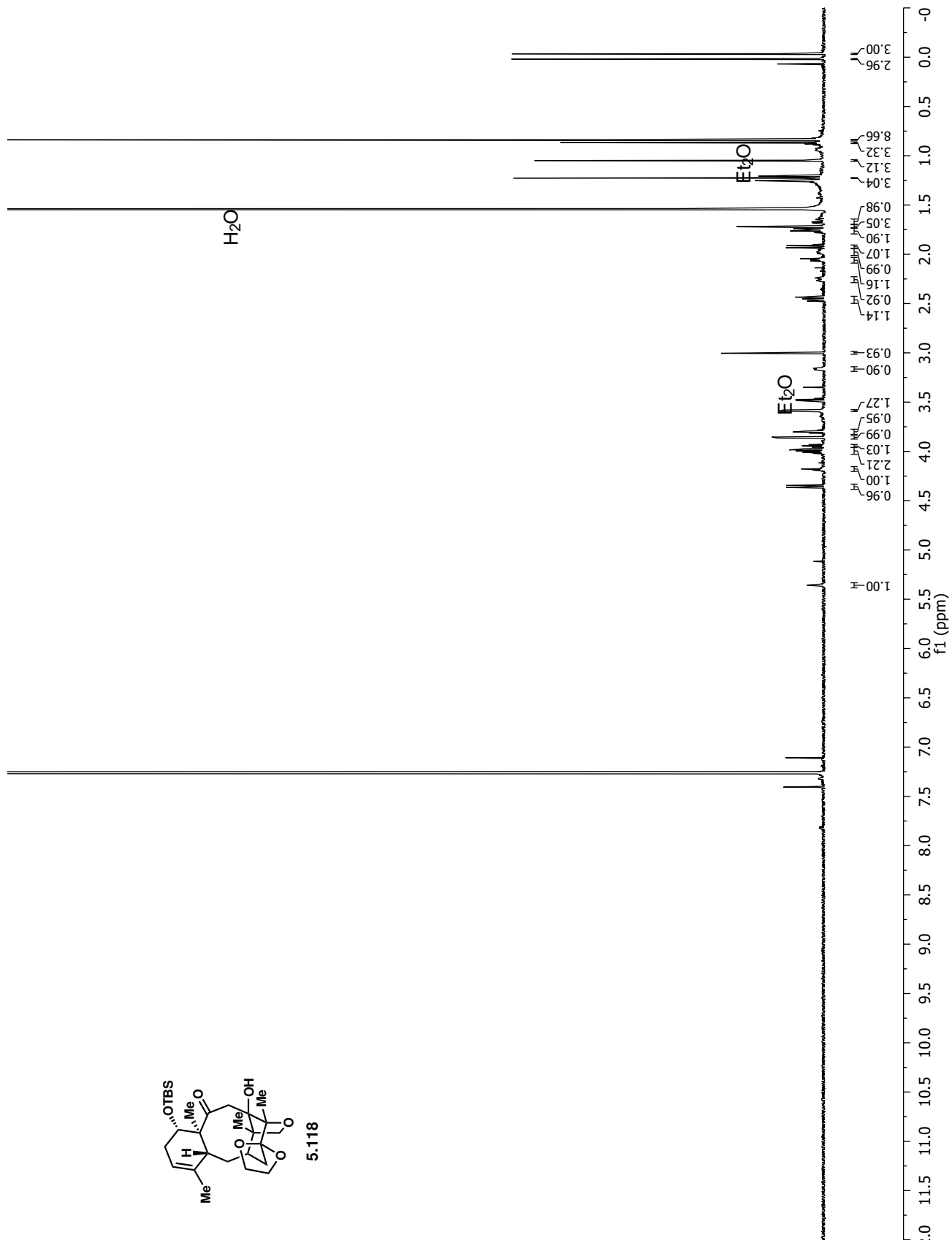


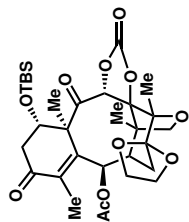




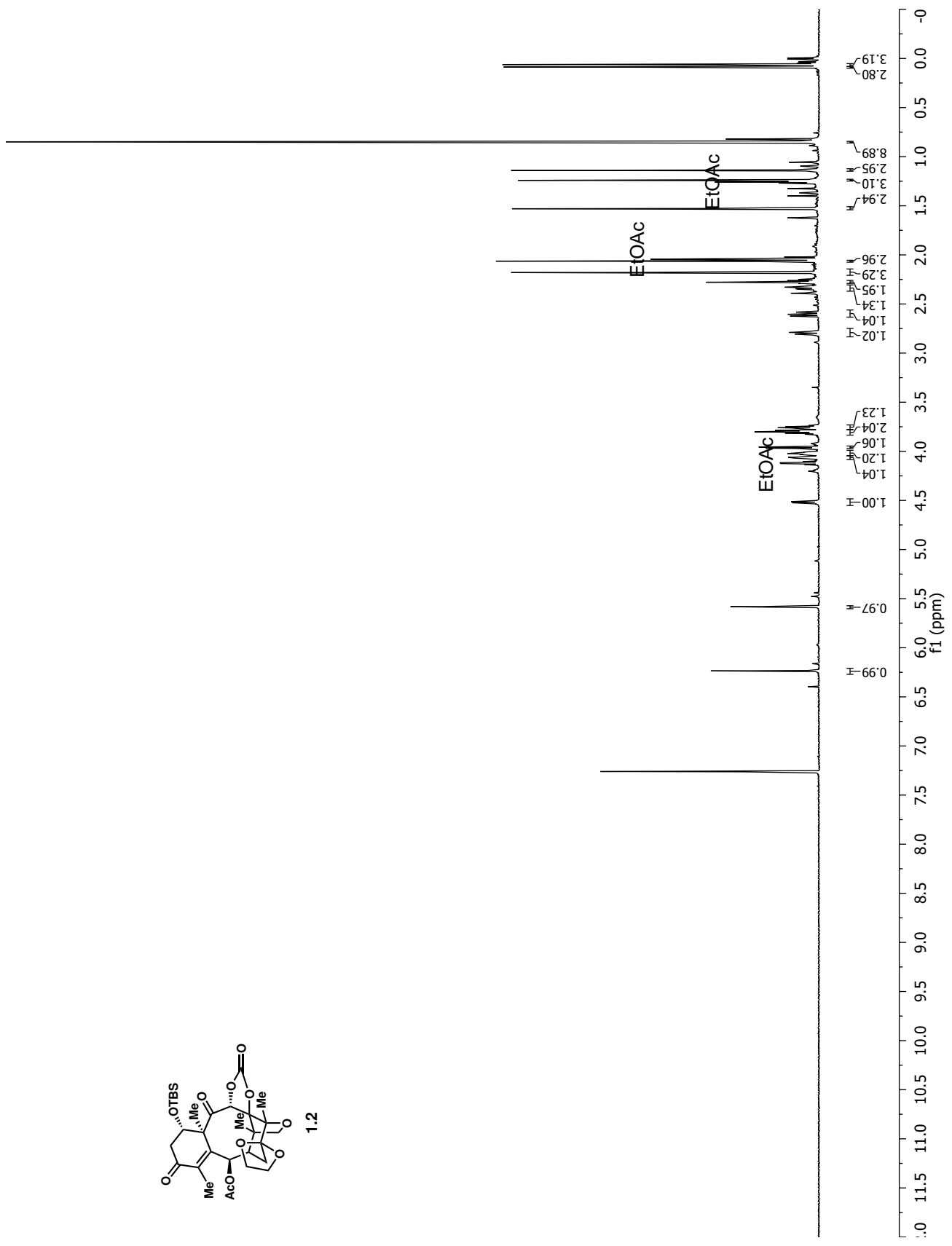


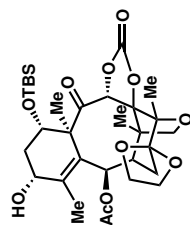
5.118



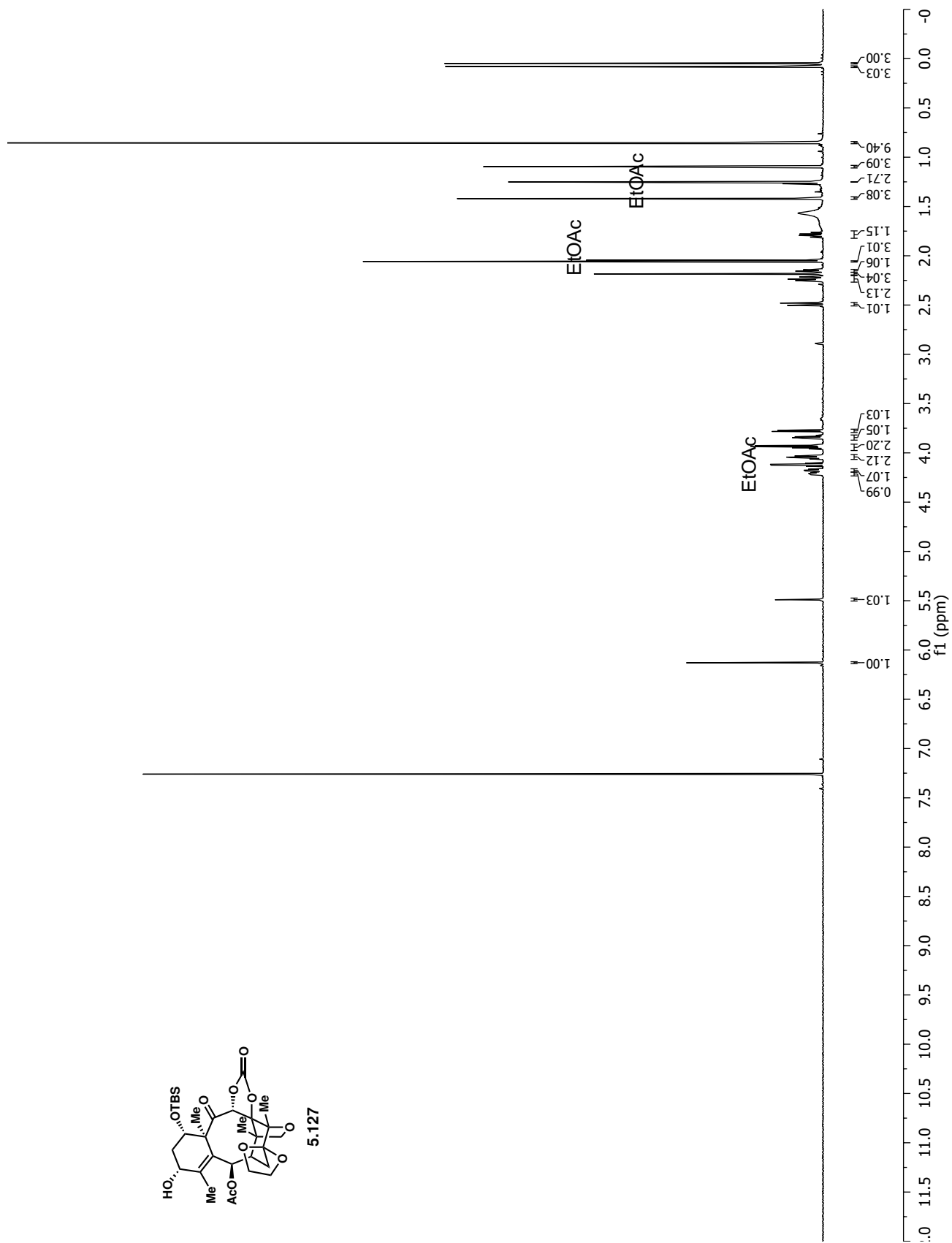


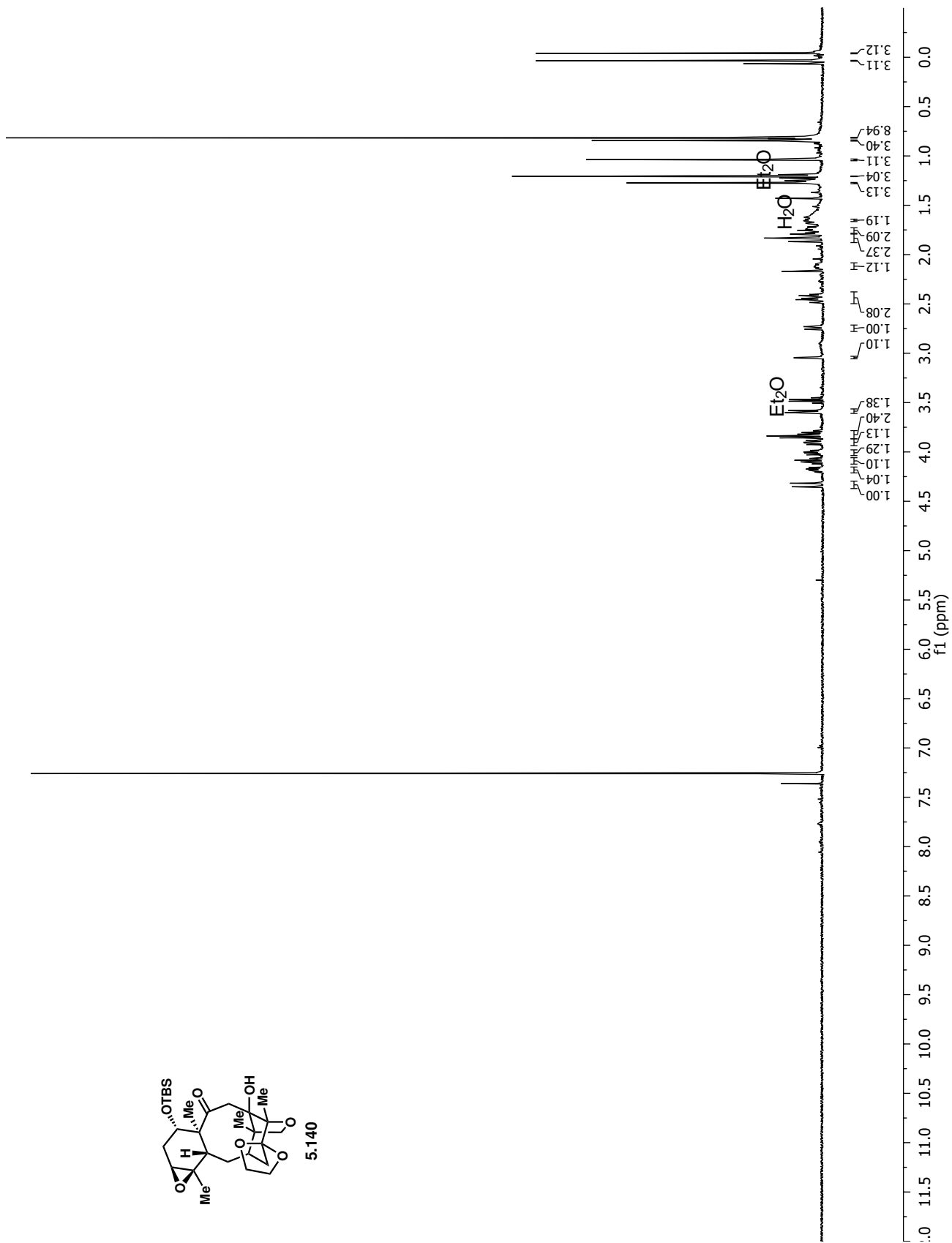
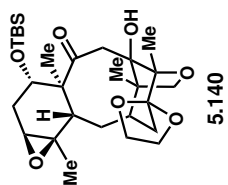
1.2

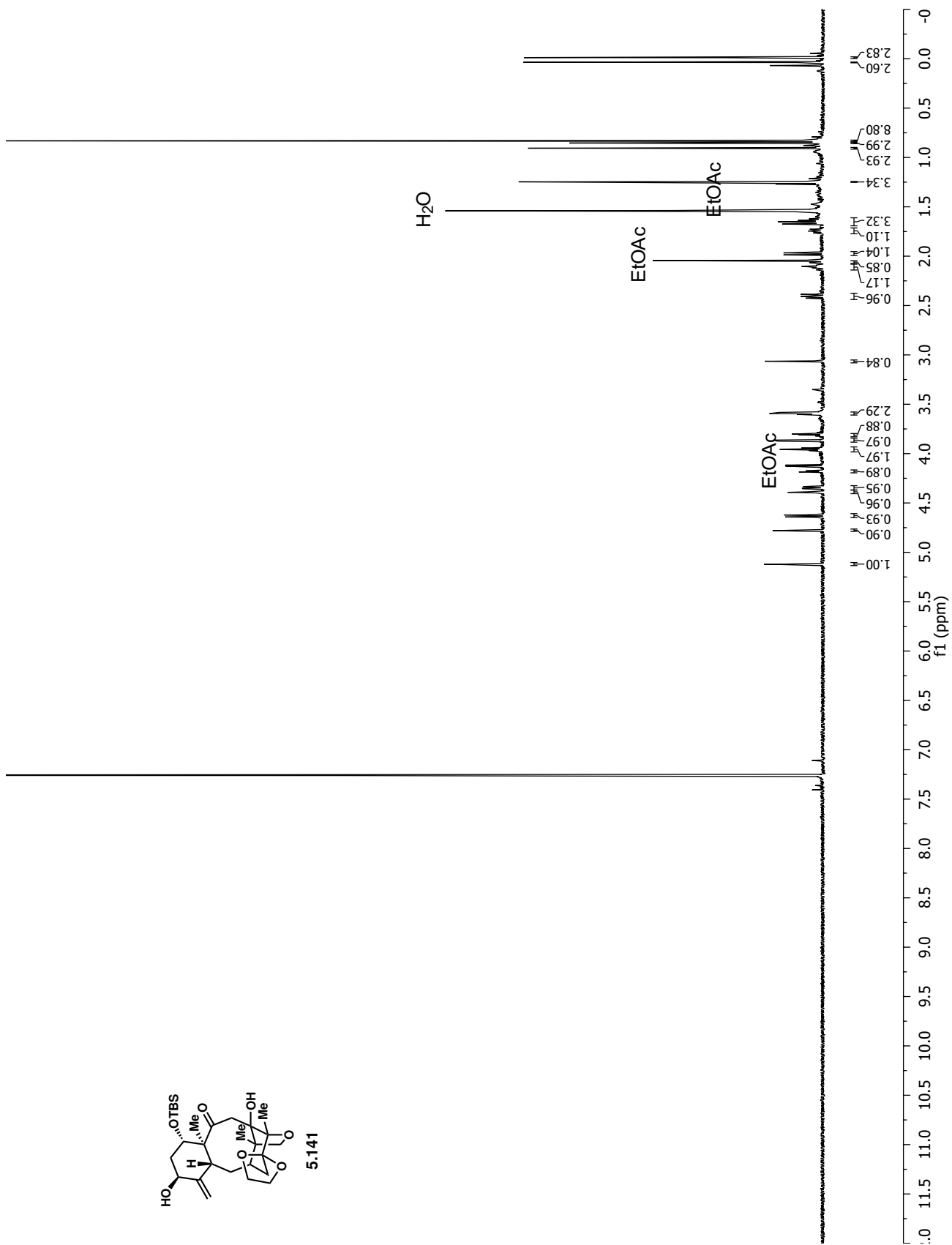
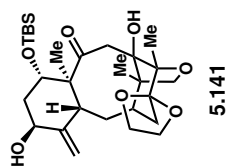


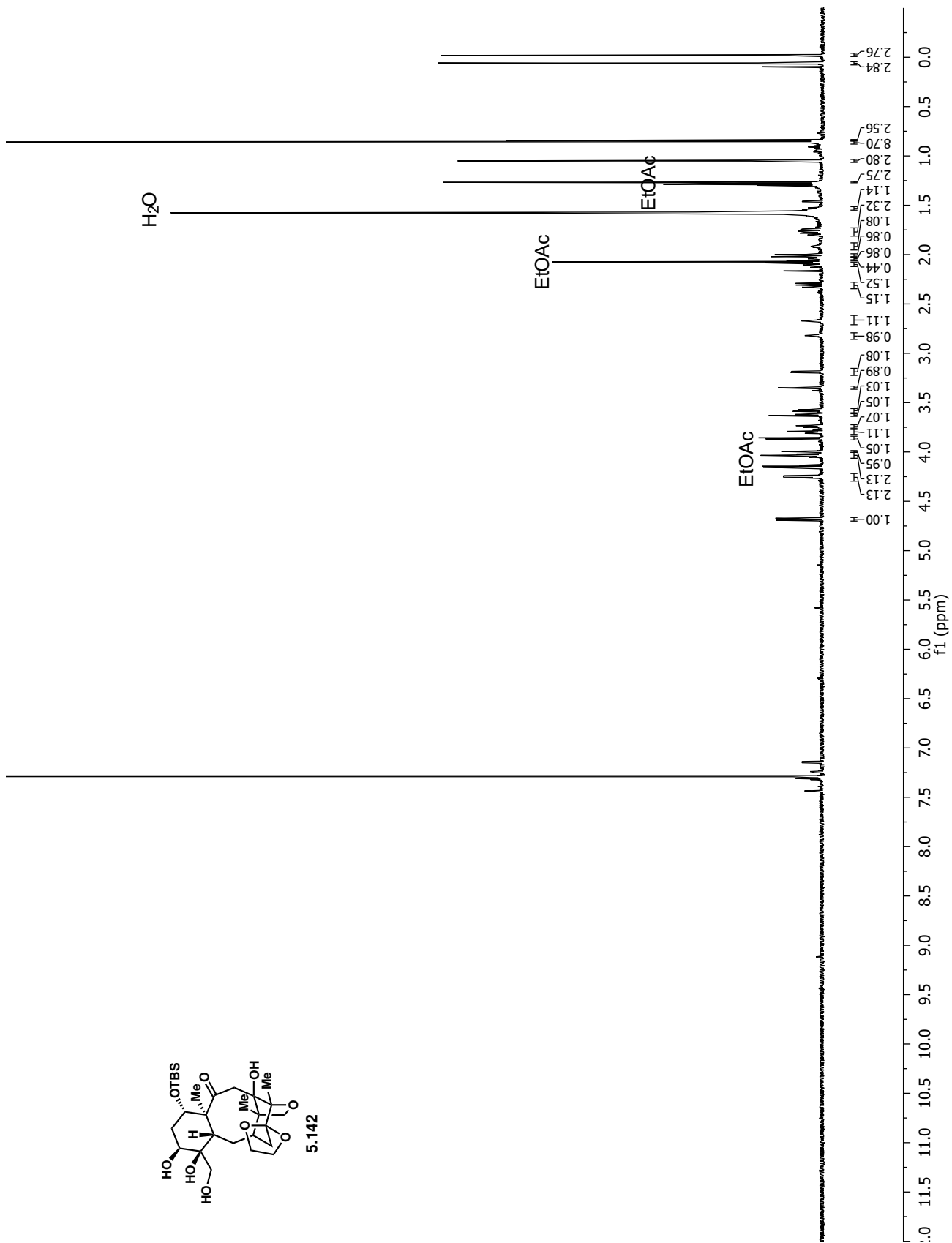
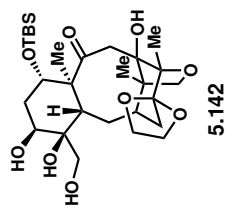


5.127

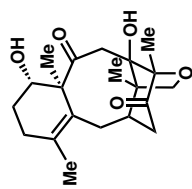




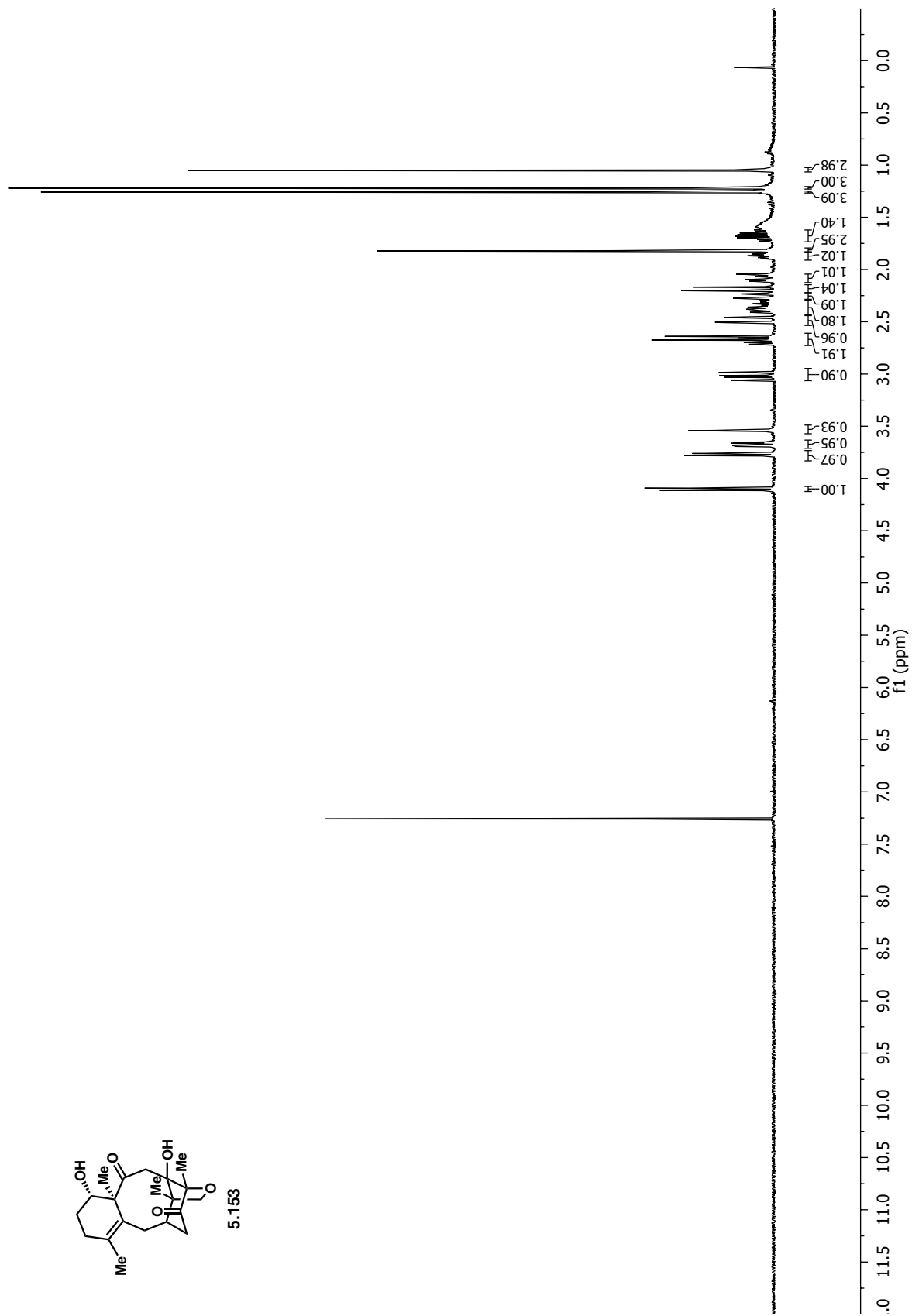




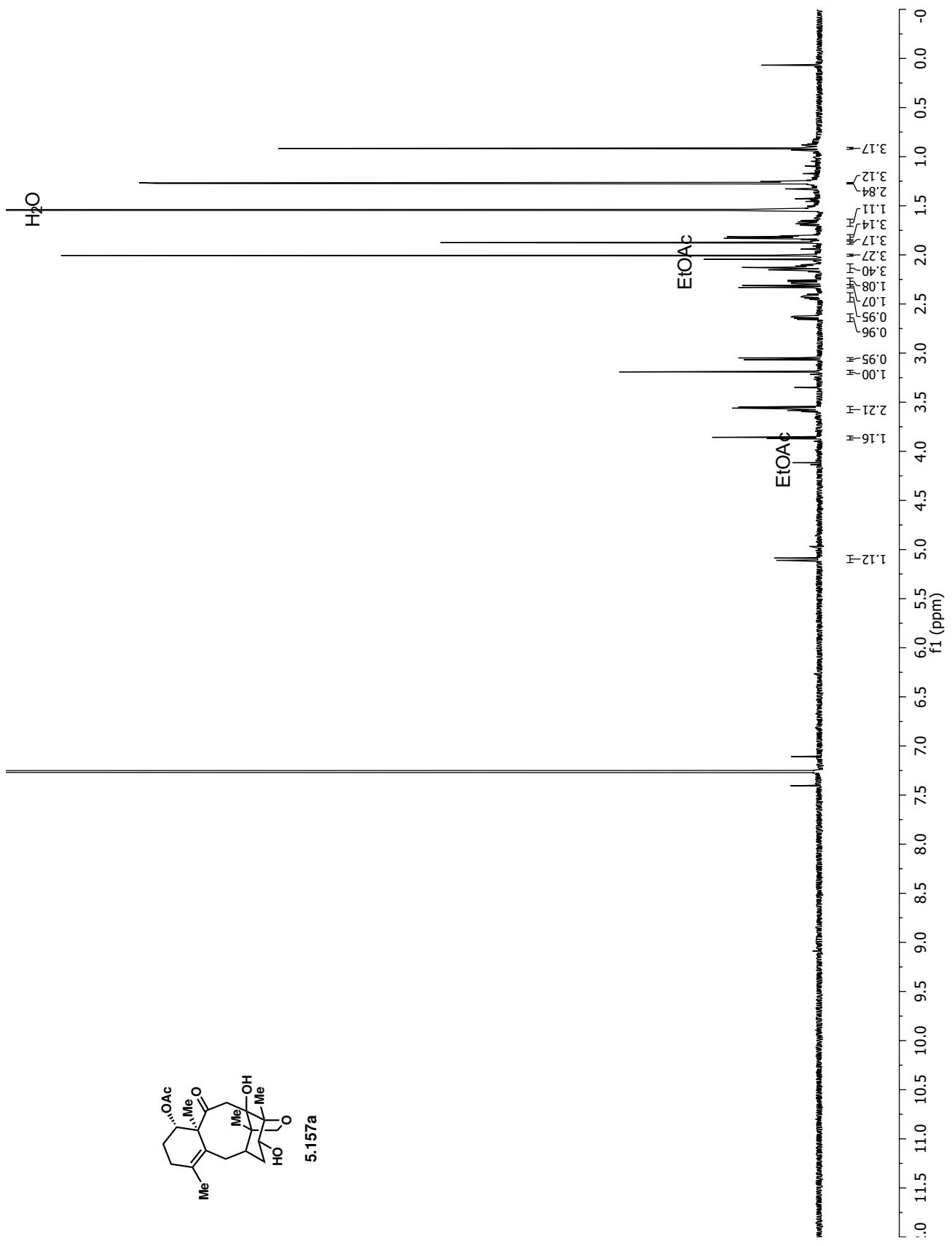
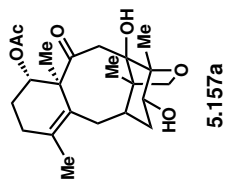


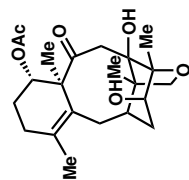


5.153

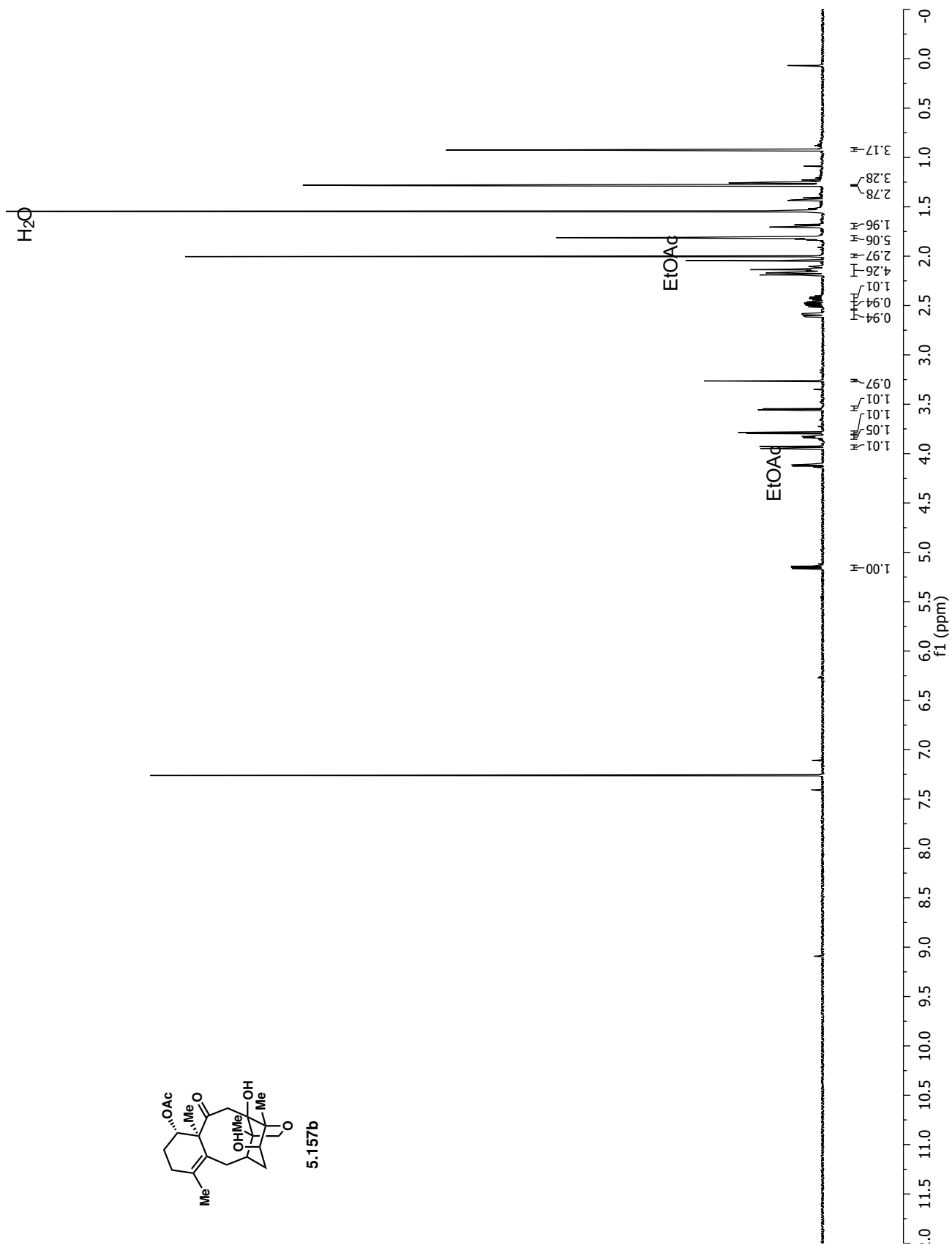


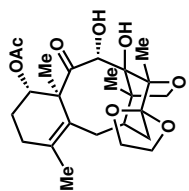




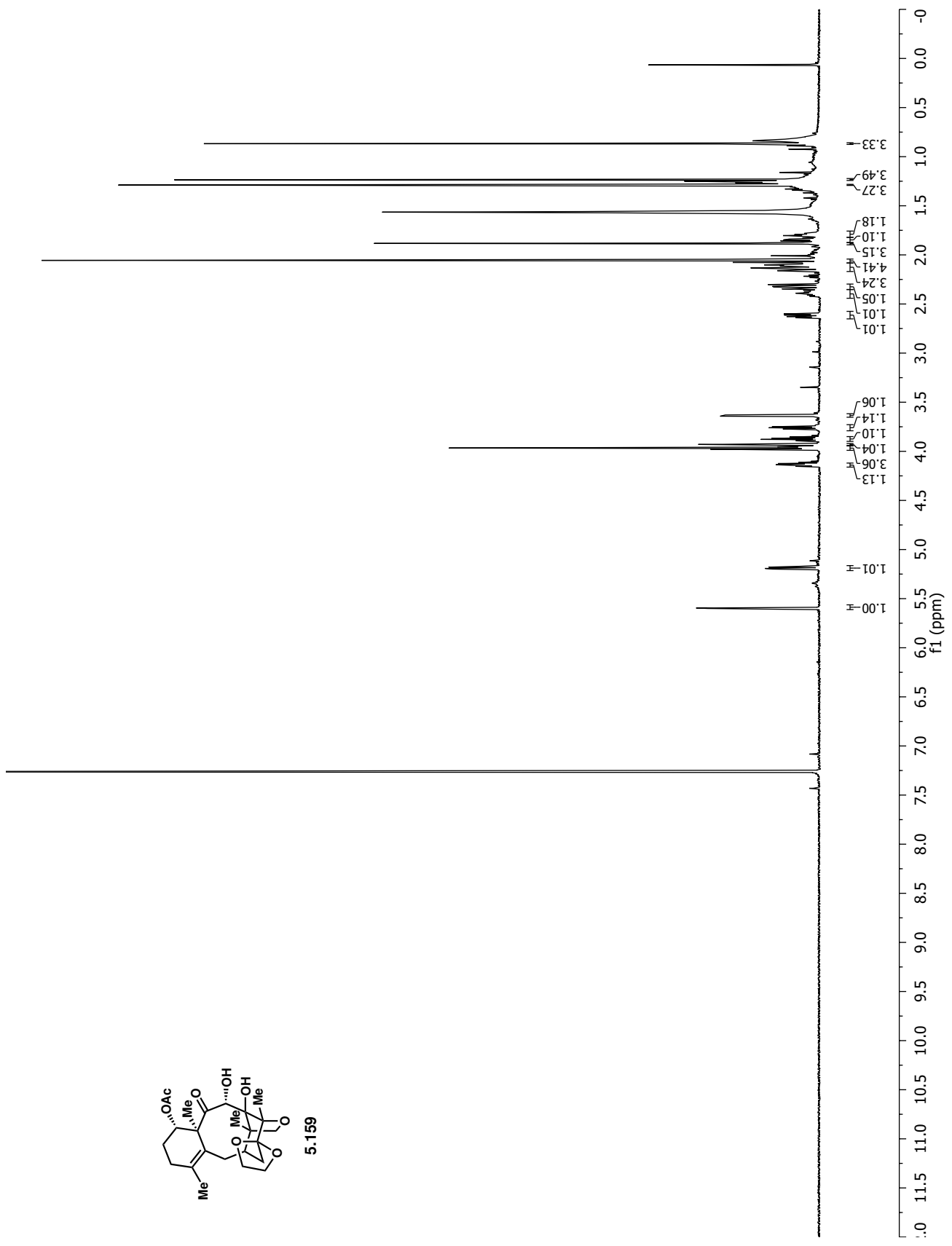


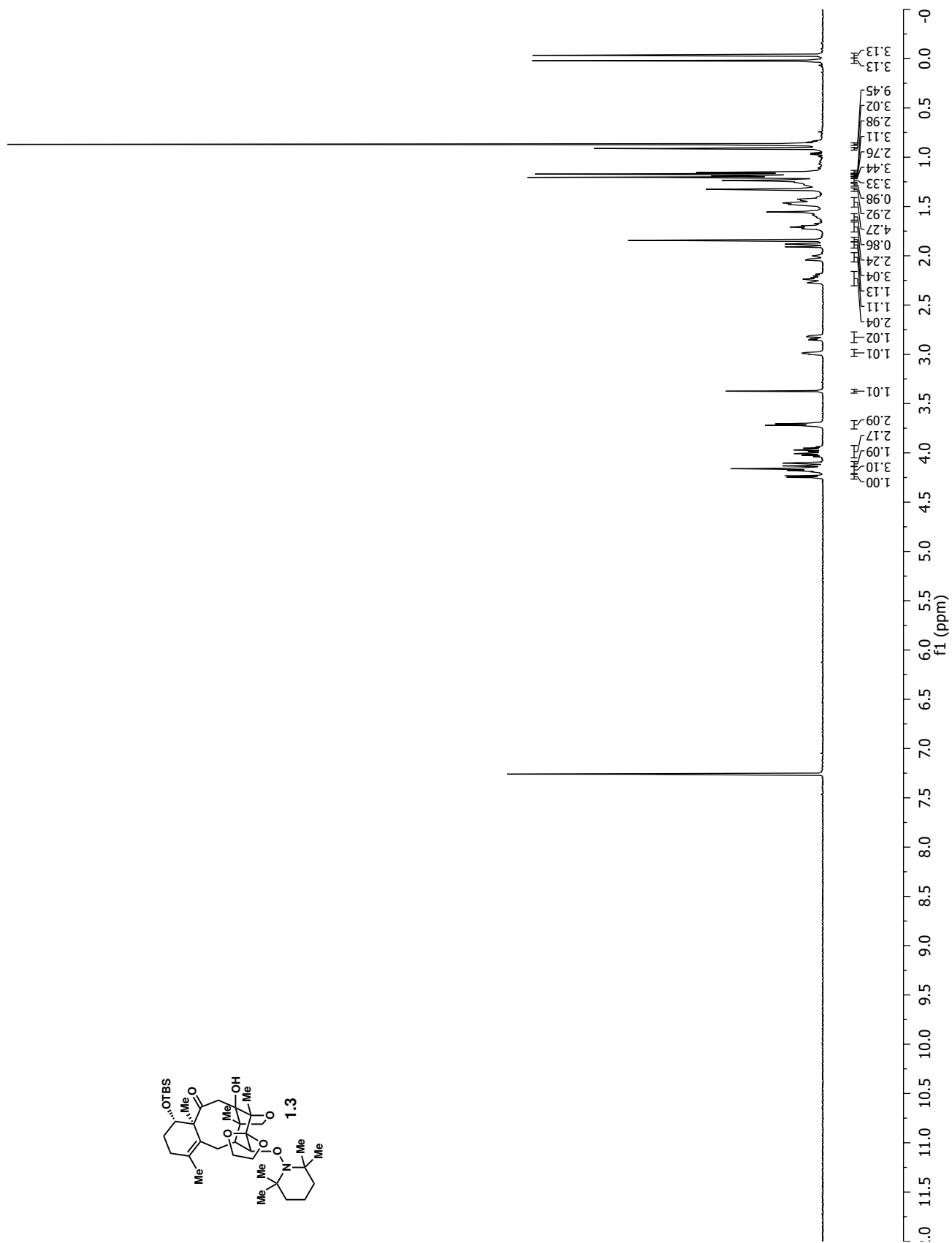
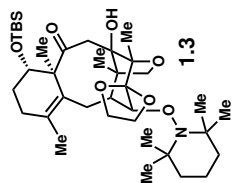
5.157b

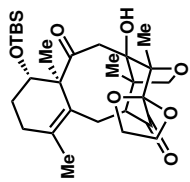




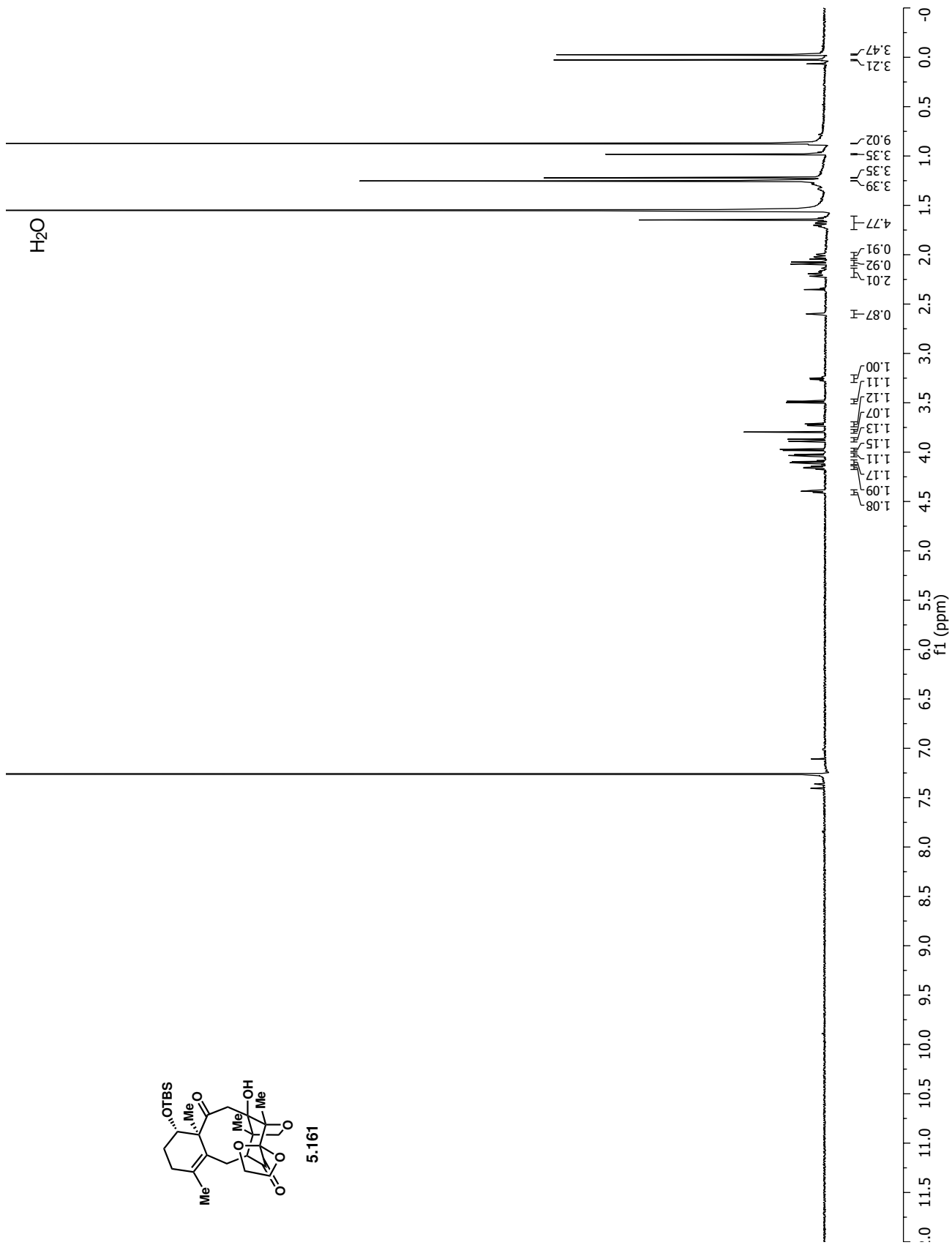
5.159

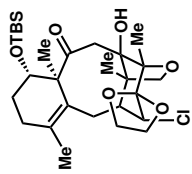




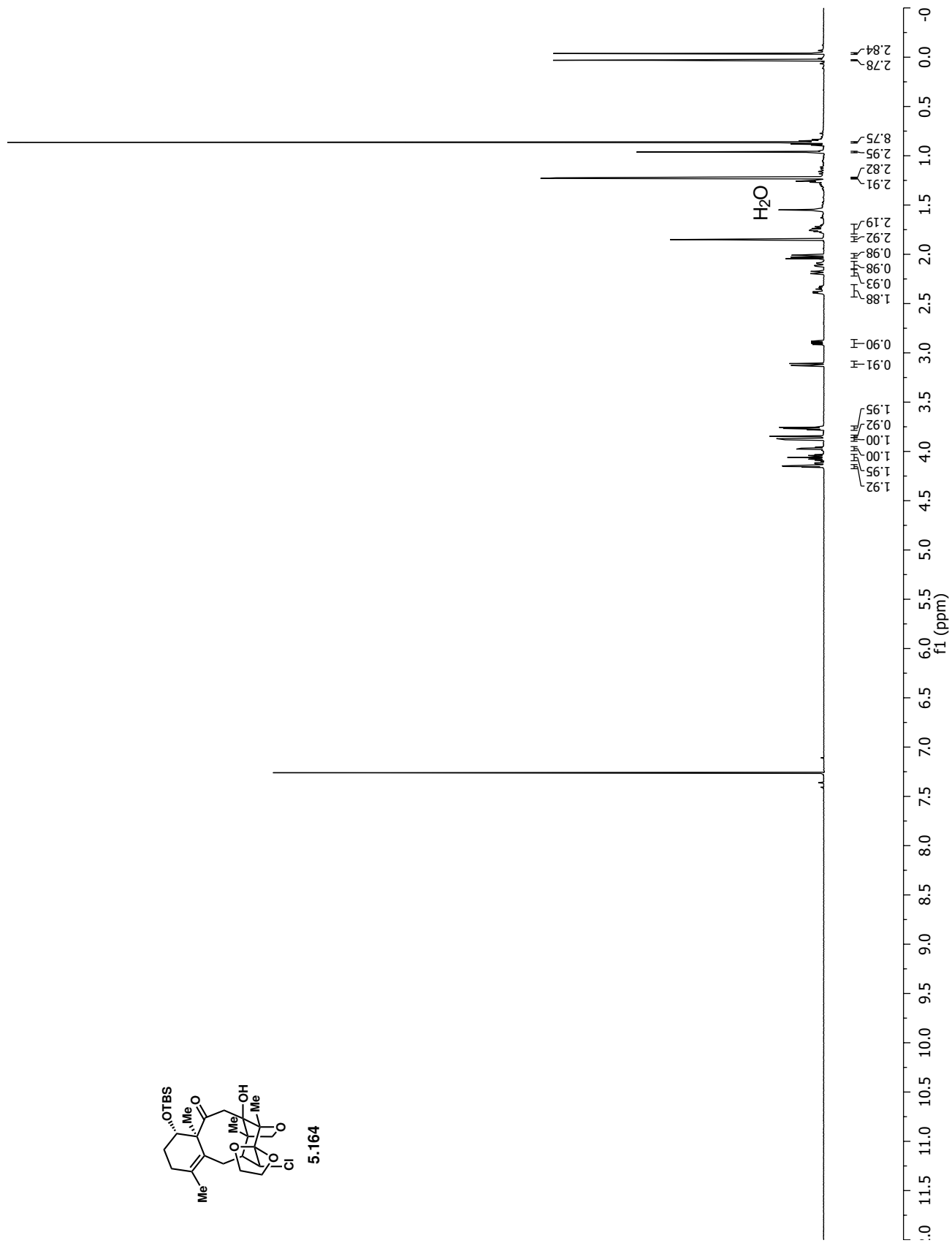


5.161

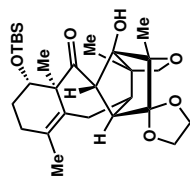




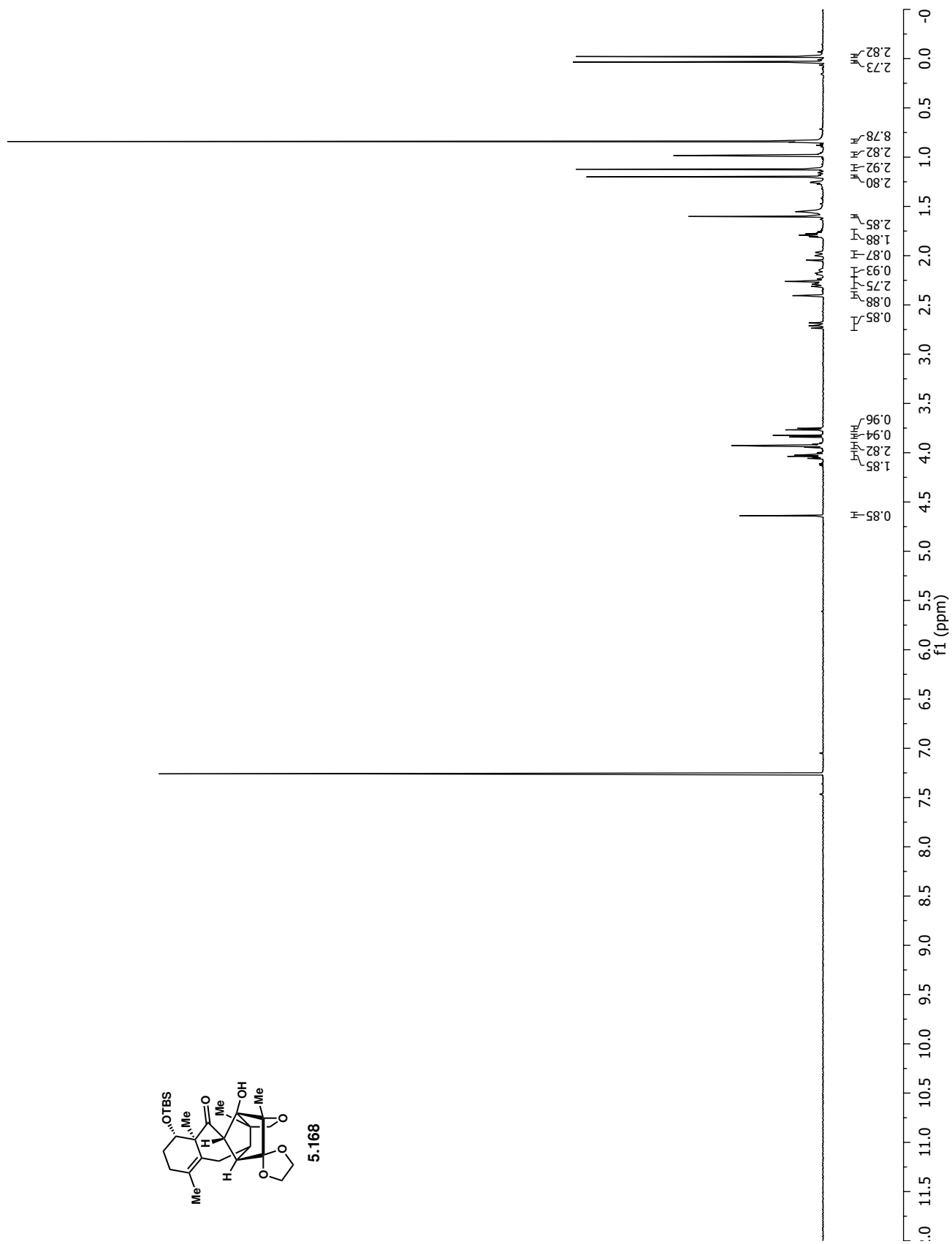
5.164

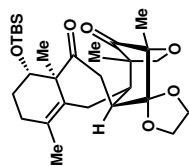




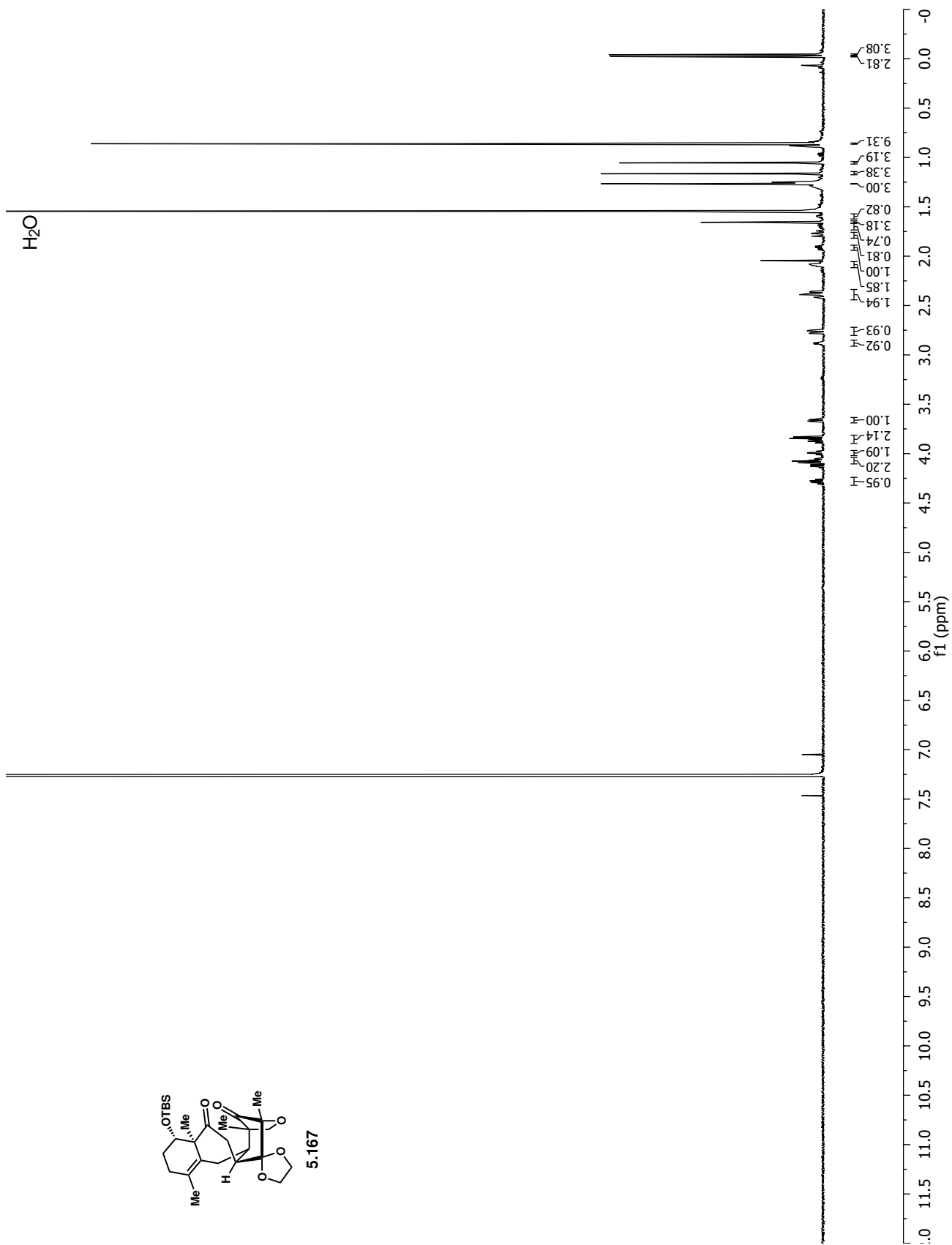


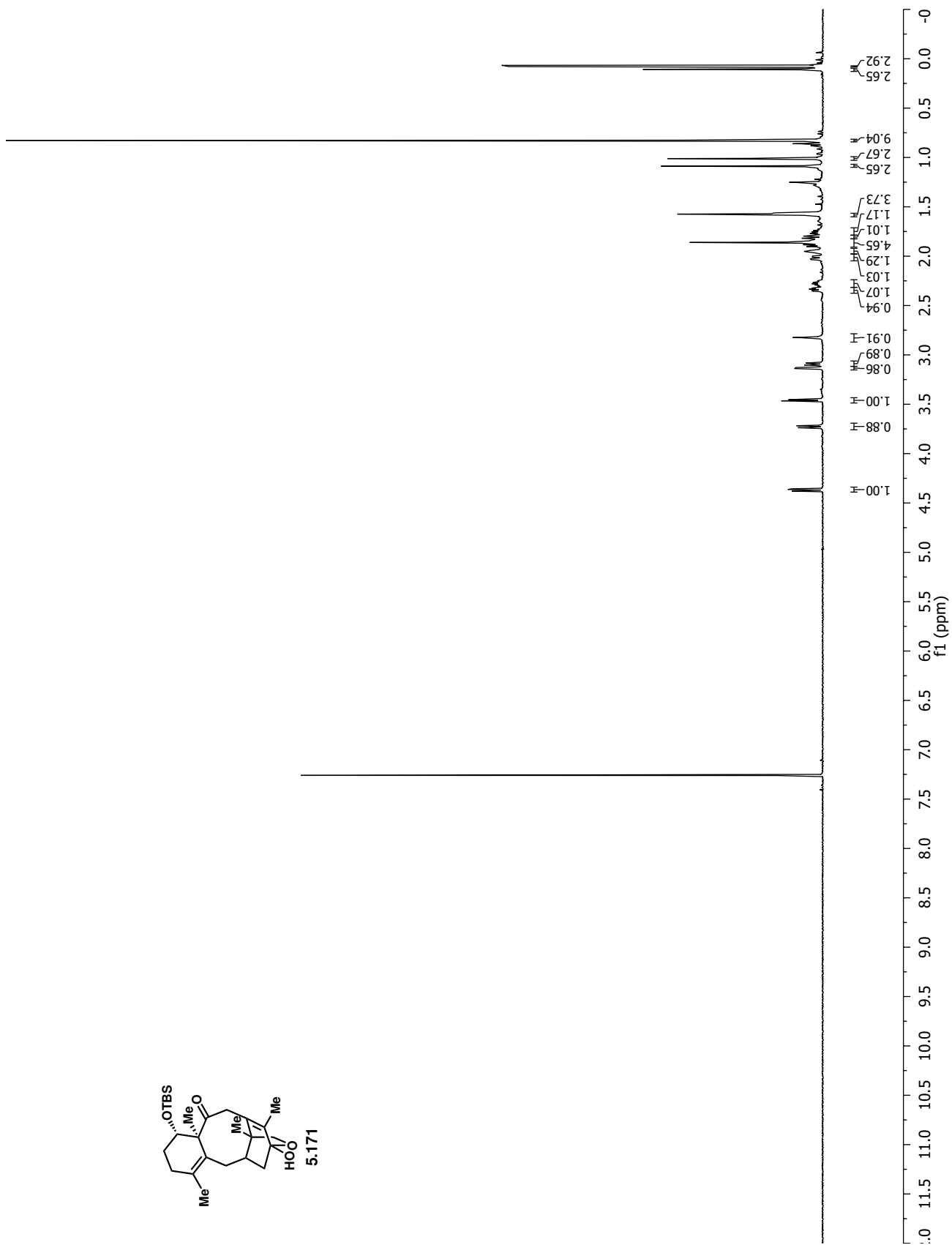
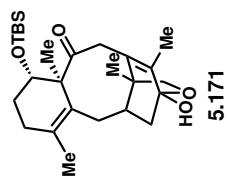
5.168

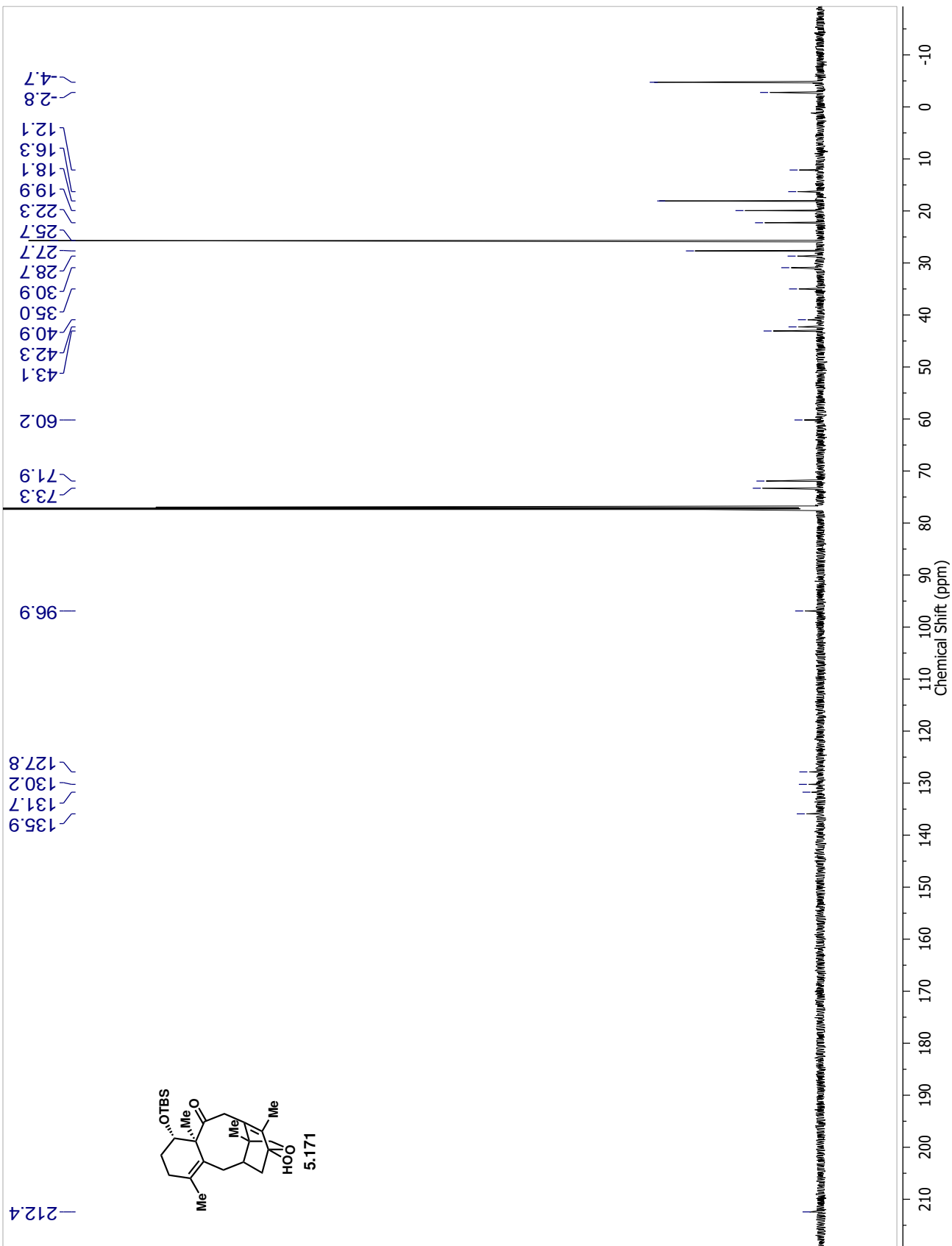




5-167

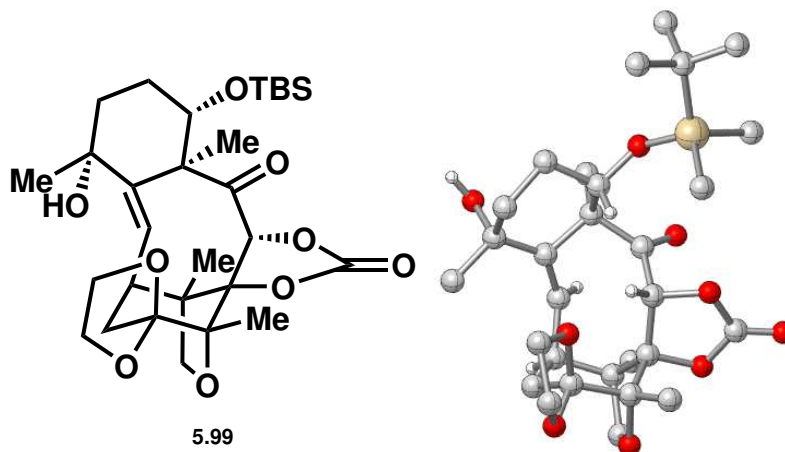






## Appendix 5b: X-Ray Crystallographic Data Relevant to Chapter 5

X-ray crystallographic analysis of C4 allylic alcohol 5.99



A colorless block 0.35 x 0.17 x 0.07 mm in size was mounted on a Cryoloop with Paratone oil. Data were collected in a nitrogen gas stream at 100(2) K using omega scans. Crystal-to-detector distance was 30.23 mm and exposure time was 0.50 seconds per frame at low angles and 1.00 seconds at high angles, using a scan width of 0.5°. Data collection was 100% complete to 74.000° in  $\theta$ . A total of 36433 reflections were collected covering the indices  $-10 \leq h \leq 10$ ,  $-18 \leq k \leq 18$ ,  $-29 \leq l \leq 29$ . 6025 reflections were found to be symmetry independent, with an  $R_{\text{int}}$  of 0.0465. Indexing and unit cell refinement indicated a primitive, orthorhombic lattice. The space group was found to be P 21 21 21 (No. 19). The data were integrated using the CrysAlis<sup>Pro</sup> 1.171.40.54a software program and scaled using the SCALE3 ABSPACK scaling algorithm. Solution by intrinsic phasing (SHELXT-2015) produced a heavy-atom phasing model consistent with the proposed structure. All non-hydrogen atoms were refined anisotropically by full-matrix least-squares (SHELXL-2014). All hydrogen atoms were placed using a riding model. Their positions were constrained relative to their parent atom using the appropriate HFIX command in SHELXL-2014.

Table 2. Atomic coordinates ( $\times 10^4$ ) and equivalent isotropic displacement parameters ( $\text{\AA}^2 \times 10^3$ ) for mperea001\_sarpong.  $U(\text{eq})$  is defined as one third of the trace of the orthogonalized  $U^{ij}$  tensor.

	x	y	z	U(eq)
C(1)	-980(3)	6716(2)	2678(1)	22(1)
C(2)	702(3)	6608(2)	2420(1)	18(1)
C(3)	1466(3)	7534(2)	2319(1)	18(1)
C(4)	3101(3)	7593(1)	1999(1)	18(1)
C(5)	4122(3)	9014(2)	2016(1)	21(1)
C(6)	3249(3)	7957(1)	1381(1)	17(1)
C(7)	1927(3)	7956(2)	914(1)	18(1)
C(8)	550(3)	8633(2)	986(1)	23(1)
C(9)	2964(3)	8254(2)	408(1)	22(1)
C(10)	4660(3)	7520(2)	1047(1)	18(1)
C(11)	6323(3)	7679(2)	1293(1)	23(1)
C(12)	4323(3)	6511(2)	927(1)	19(1)
C(13)	6553(3)	5572(2)	894(1)	31(1)
C(14)	5454(3)	5263(2)	1357(1)	27(1)
C(15)	2726(3)	6391(2)	615(1)	21(1)
C(16)	1332(3)	6966(2)	840(1)	20(1)
C(17)	658(3)	6754(2)	1420(1)	19(1)
C(18)	715(3)	6141(2)	1839(1)	18(1)
C(19)	675(3)	5126(2)	1835(1)	20(1)
C(20)	948(3)	4680(2)	1267(1)	25(1)
C(21)	1799(3)	4723(2)	2278(1)	21(1)
C(22)	1524(3)	5125(2)	2860(1)	21(1)
C(23)	1876(3)	6117(2)	2835(1)	19(1)
C(24)	5222(3)	6829(2)	3446(1)	29(1)
C(25)	2726(4)	8053(2)	3985(1)	29(1)
C(26)	3181(4)	6148(2)	4453(1)	28(1)
C(27)	3772(5)	5208(2)	4325(1)	45(1)
C(28)	1449(5)	6071(2)	4678(2)	50(1)
C(29)	4236(7)	6577(3)	4902(1)	67(1)
O(1)	902(2)	8218(1)	2513(1)	26(1)
O(2)	4029(2)	8249(1)	2313(1)	22(1)

Table 2. Atomic coordinates ( $\times 10^4$ ) and equivalent isotropic displacement parameters ( $\text{\AA}^2 \times 10^3$ ) for mperea001\_sarpong.  $U(\text{eq})$  is defined as one third of the trace of the orthogonalized  $U^{ij}$  tensor.

	x	y	z	U(eq)
C(1)	-980(3)	6716(2)	2678(1)	22(1)
C(2)	702(3)	6608(2)	2420(1)	18(1)
C(3)	1466(3)	7534(2)	2319(1)	18(1)
C(4)	3101(3)	7593(1)	1999(1)	18(1)
C(5)	4122(3)	9014(2)	2016(1)	21(1)
C(6)	3249(3)	7957(1)	1381(1)	17(1)
C(7)	1927(3)	7956(2)	914(1)	18(1)
C(8)	550(3)	8633(2)	986(1)	23(1)
C(9)	2964(3)	8254(2)	408(1)	22(1)
C(10)	4660(3)	7520(2)	1047(1)	18(1)
C(11)	6323(3)	7679(2)	1293(1)	23(1)
C(12)	4323(3)	6511(2)	927(1)	19(1)
C(13)	6553(3)	5572(2)	894(1)	31(1)
C(14)	5454(3)	5263(2)	1357(1)	27(1)
C(15)	2726(3)	6391(2)	615(1)	21(1)
C(16)	1332(3)	6966(2)	840(1)	20(1)
C(17)	658(3)	6754(2)	1420(1)	19(1)
C(18)	715(3)	6141(2)	1839(1)	18(1)
C(19)	675(3)	5126(2)	1835(1)	20(1)
C(20)	948(3)	4680(2)	1267(1)	25(1)
C(21)	1799(3)	4723(2)	2278(1)	21(1)
C(22)	1524(3)	5125(2)	2860(1)	21(1)
C(23)	1876(3)	6117(2)	2835(1)	19(1)
C(24)	5222(3)	6829(2)	3446(1)	29(1)
C(25)	2726(4)	8053(2)	3985(1)	29(1)
C(26)	3181(4)	6148(2)	4453(1)	28(1)
C(27)	3772(5)	5208(2)	4325(1)	45(1)
C(28)	1449(5)	6071(2)	4678(2)	50(1)
C(29)	4236(7)	6577(3)	4902(1)	67(1)
O(1)	902(2)	8218(1)	2513(1)	26(1)
O(2)	4029(2)	8249(1)	2313(1)	22(1)

O(3)	4587(2)	9709(1)	2202(1)	28(1)
O(4)	3638(2)	8891(1)	1481(1)	20(1)
O(5)	4591(2)	7958(1)	509(1)	21(1)
O(6)	5557(2)	6166(1)	570(1)	24(1)
O(7)	4398(2)	6015(1)	1438(1)	21(1)
O(8)	-993(2)	4965(1)	1990(1)	24(1)
O(9)	1763(2)	6528(1)	3371(1)	22(1)
Si(1)	3215(1)	6873(1)	3798(1)	20(1)

---



Table 3. Bond lengths [Å] and angles [°] for mperea001\_sarpong.

---

C(1)-C(2)	1.533(3)
C(2)-C(18)	1.544(3)
C(2)-C(3)	1.545(3)
C(2)-C(23)	1.566(3)
C(3)-O(1)	1.215(3)
C(3)-C(4)	1.556(3)
C(4)-O(2)	1.453(3)
C(4)-C(6)	1.569(3)
C(5)-O(3)	1.195(3)
C(5)-O(4)	1.344(3)
C(5)-O(2)	1.347(3)
C(6)-O(4)	1.455(3)
C(6)-C(10)	1.557(3)
C(6)-C(7)	1.558(3)
C(7)-C(8)	1.536(3)
C(7)-C(9)	1.541(3)
C(7)-C(16)	1.573(3)
C(9)-O(5)	1.440(3)
C(10)-O(5)	1.435(3)
C(10)-C(11)	1.516(3)
C(10)-C(12)	1.563(3)
C(12)-O(7)	1.423(3)
C(12)-O(6)	1.425(3)
C(12)-C(15)	1.528(3)
C(13)-O(6)	1.437(3)
C(13)-C(14)	1.499(4)
C(14)-O(7)	1.441(3)
C(15)-C(16)	1.537(3)
C(16)-C(17)	1.517(3)
C(17)-C(18)	1.355(3)
C(18)-C(19)	1.521(3)
C(19)-O(8)	1.452(3)
C(19)-C(20)	1.521(3)
C(19)-C(21)	1.527(3)

C(21)-C(22)	1.522(3)
C(22)-C(23)	1.515(3)
C(23)-O(9)	1.416(3)
C(24)-Si(1)	1.864(3)
C(25)-Si(1)	1.867(3)
C(26)-C(29)	1.521(4)
C(26)-C(27)	1.521(4)
C(26)-C(28)	1.537(5)
C(26)-Si(1)	1.895(2)
O(9)-Si(1)	1.6555(18)

C(1)-C(2)-C(18)	114.27(19)
C(1)-C(2)-C(3)	109.84(19)
C(18)-C(2)-C(3)	105.46(17)
C(1)-C(2)-C(23)	111.40(18)
C(18)-C(2)-C(23)	110.05(18)
C(3)-C(2)-C(23)	105.28(18)
O(1)-C(3)-C(2)	122.7(2)
O(1)-C(3)-C(4)	118.2(2)
C(2)-C(3)-C(4)	118.87(18)
O(2)-C(4)-C(3)	104.52(17)
O(2)-C(4)-C(6)	101.60(16)
C(3)-C(4)-C(6)	122.86(19)
O(3)-C(5)-O(4)	124.4(2)
O(3)-C(5)-O(2)	124.5(2)
O(4)-C(5)-O(2)	111.08(19)
O(4)-C(6)-C(10)	108.66(18)
O(4)-C(6)-C(7)	105.78(16)
C(10)-C(6)-C(7)	99.65(17)
O(4)-C(6)-C(4)	101.55(16)
C(10)-C(6)-C(4)	112.79(18)
C(7)-C(6)-C(4)	127.47(19)
C(8)-C(7)-C(9)	108.12(18)
C(8)-C(7)-C(6)	116.35(19)
C(9)-C(7)-C(6)	99.18(18)
C(8)-C(7)-C(16)	113.6(2)

C(9)-C(7)-C(16)	111.16(19)
C(6)-C(7)-C(16)	107.50(17)
O(5)-C(9)-C(7)	107.78(18)
O(5)-C(10)-C(11)	107.78(18)
O(5)-C(10)-C(6)	103.30(17)
C(11)-C(10)-C(6)	115.05(19)
O(5)-C(10)-C(12)	105.81(17)
C(11)-C(10)-C(12)	112.6(2)
C(6)-C(10)-C(12)	111.39(18)
O(7)-C(12)-O(6)	106.56(17)
O(7)-C(12)-C(15)	112.82(19)
O(6)-C(12)-C(15)	106.99(18)
O(7)-C(12)-C(10)	110.01(18)
O(6)-C(12)-C(10)	109.32(19)
C(15)-C(12)-C(10)	110.94(19)
O(6)-C(13)-C(14)	103.4(2)
O(7)-C(14)-C(13)	103.09(19)
C(12)-C(15)-C(16)	114.72(18)
C(17)-C(16)-C(15)	118.3(2)
C(17)-C(16)-C(7)	102.24(18)
C(15)-C(16)-C(7)	109.34(19)
C(18)-C(17)-C(16)	142.6(2)
C(17)-C(18)-C(19)	132.3(2)
C(17)-C(18)-C(2)	110.30(19)
C(19)-C(18)-C(2)	117.26(19)
O(8)-C(19)-C(18)	100.68(18)
O(8)-C(19)-C(20)	107.01(19)
C(18)-C(19)-C(20)	116.1(2)
O(8)-C(19)-C(21)	110.04(19)
C(18)-C(19)-C(21)	112.15(19)
C(20)-C(19)-C(21)	110.2(2)
C(22)-C(21)-C(19)	112.02(19)
C(23)-C(22)-C(21)	108.85(19)
O(9)-C(23)-C(22)	112.19(19)
O(9)-C(23)-C(2)	108.58(18)
C(22)-C(23)-C(2)	111.38(19)

C(29)-C(26)-C(27)	110.2(3)
C(29)-C(26)-C(28)	109.0(3)
C(27)-C(26)-C(28)	107.5(3)
C(29)-C(26)-Si(1)	108.85(19)
C(27)-C(26)-Si(1)	111.27(18)
C(28)-C(26)-Si(1)	109.98(19)
C(5)-O(2)-C(4)	109.78(17)
C(5)-O(4)-C(6)	110.56(17)
C(10)-O(5)-C(9)	108.96(17)
C(12)-O(6)-C(13)	108.70(18)
C(12)-O(7)-C(14)	108.68(17)
C(23)-O(9)-Si(1)	129.49(15)
O(9)-Si(1)-C(24)	111.45(11)
O(9)-Si(1)-C(25)	106.42(11)
C(24)-Si(1)-C(25)	109.53(13)
O(9)-Si(1)-C(26)	108.14(11)
C(24)-Si(1)-C(26)	111.08(13)
C(25)-Si(1)-C(26)	110.12(12)

---

Symmetry transformations used to generate equivalent atoms:

Table 4. Anisotropic displacement parameters ( $\text{\AA}^2 \times 10^3$ ) for mperea001\_sarpong. The anisotropic displacement factor exponent takes the form:  $-2p^2 [h^2 a^{*2} U^{11} + \dots + 2 h k a^* b^* U^{12}]$

	U <sup>11</sup>	U <sup>22</sup>	U <sup>33</sup>	U <sup>23</sup>	U <sup>13</sup>	U <sup>12</sup>
C(1)	19(1)	25(1)	22(1)	2(1)	3(1)	2(1)
C(2)	19(1)	19(1)	16(1)	1(1)	1(1)	0(1)
C(3)	22(1)	17(1)	15(1)	1(1)	-2(1)	1(1)
C(4)	21(1)	15(1)	17(1)	-1(1)	-2(1)	-3(1)
C(5)	22(1)	20(1)	21(1)	0(1)	0(1)	-4(1)
C(6)	20(1)	14(1)	17(1)	0(1)	-1(1)	-1(1)
C(7)	21(1)	18(1)	16(1)	2(1)	-3(1)	0(1)
C(8)	25(1)	22(1)	24(1)	3(1)	-2(1)	3(1)
C(9)	24(1)	23(1)	19(1)	5(1)	-2(1)	1(1)
C(10)	20(1)	20(1)	15(1)	3(1)	0(1)	-1(1)
C(11)	20(1)	26(1)	24(1)	4(1)	-1(1)	-3(1)
C(12)	22(1)	20(1)	15(1)	3(1)	5(1)	2(1)
C(13)	31(1)	27(1)	34(1)	5(1)	7(1)	10(1)
C(14)	24(1)	26(1)	31(1)	5(1)	5(1)	9(1)
C(15)	25(1)	20(1)	16(1)	-2(1)	1(1)	-1(1)
C(16)	22(1)	22(1)	16(1)	0(1)	-2(1)	-1(1)
C(17)	17(1)	22(1)	19(1)	-2(1)	-1(1)	1(1)
C(18)	17(1)	18(1)	19(1)	-1(1)	1(1)	-2(1)
C(19)	20(1)	18(1)	23(1)	1(1)	-2(1)	-2(1)
C(20)	27(1)	21(1)	26(1)	-4(1)	-1(1)	-2(1)
C(21)	22(1)	17(1)	25(1)	2(1)	0(1)	-1(1)
C(22)	23(1)	20(1)	21(1)	4(1)	-1(1)	-1(1)
C(23)	20(1)	20(1)	16(1)	1(1)	1(1)	-1(1)
C(24)	27(1)	33(1)	26(1)	2(1)	-2(1)	-1(1)
C(25)	40(1)	22(1)	27(1)	1(1)	-2(1)	1(1)
C(26)	44(2)	19(1)	19(1)	3(1)	-3(1)	-1(1)
C(27)	74(2)	31(2)	31(2)	9(1)	10(2)	20(2)
C(28)	62(2)	42(2)	45(2)	21(2)	23(2)	12(2)
C(29)	116(4)	54(2)	31(2)	17(2)	-35(2)	-31(2)
O(1)	30(1)	18(1)	29(1)	-4(1)	3(1)	2(1)
O(2)	27(1)	21(1)	18(1)	2(1)	-5(1)	-8(1)

O(3)	33(1)	23(1)	28(1)	-3(1)	-2(1)	-9(1)
O(4)	25(1)	16(1)	19(1)	1(1)	-2(1)	-3(1)
O(5)	22(1)	25(1)	16(1)	6(1)	2(1)	0(1)
O(6)	26(1)	25(1)	21(1)	2(1)	8(1)	6(1)
O(7)	26(1)	19(1)	17(1)	4(1)	3(1)	4(1)
O(8)	20(1)	21(1)	30(1)	4(1)	0(1)	-5(1)
O(9)	23(1)	29(1)	15(1)	-3(1)	1(1)	1(1)
Si(1)	25(1)	18(1)	16(1)	1(1)	-1(1)	0(1)

---

Table 5. Hydrogen coordinates ( $\times 10^4$ ) and isotropic displacement parameters ( $\text{\AA}^2 \times 10^3$ ) for mperea001\_sarpong.

	x	y	z	U(eq)
H(1A)	-1667	7056	2419	33
H(1B)	-895	7037	3038	33
H(1C)	-1455	6126	2744	33
H(4)	3657	7001	2023	21
H(8A)	-123	8633	646	35
H(8B)	1002	9230	1045	35
H(8C)	-107	8466	1313	35
H(9A)	2546	7986	56	26
H(9B)	2934	8912	370	26
H(11A)	7141	7449	1032	35
H(11B)	6415	7371	1656	35
H(11C)	6489	8321	1348	35
H(13A)	7502	5889	1049	37
H(13B)	6927	5063	662	37
H(14A)	4842	4726	1241	33
H(14B)	6067	5127	1704	33
H(15A)	2407	5755	639	25
H(15B)	2895	6535	212	25
H(16)	431	6956	560	24
H(17)	-61	7218	1527	23
H(20A)	631	4051	1289	37
H(20B)	2091	4721	1165	37
H(20C)	298	4982	979	37
H(21A)	1621	4070	2296	25
H(21B)	2931	4826	2164	25
H(22A)	394	5026	2979	26
H(22B)	2242	4835	3138	26
H(23)	3002	6198	2692	22
H(24A)	5424	6221	3309	43
H(24B)	6062	6997	3716	43

H(24C)	5236	7244	3127	43
H(25A)	2706	8417	3642	44
H(25B)	3548	8285	4244	44
H(25C)	1668	8076	4169	44
H(27A)	3048	4926	4051	68
H(27B)	3784	4856	4674	68
H(27C)	4863	5236	4168	68
H(28A)	1029	6669	4761	75
H(28B)	1447	5712	5024	75
H(28C)	766	5784	4394	75
H(29A)	5340	6634	4759	100
H(29B)	4236	6203	5241	100
H(29C)	3812	7170	4994	100
H(8)	-1110(60)	4440(30)	2150(19)	68(14)

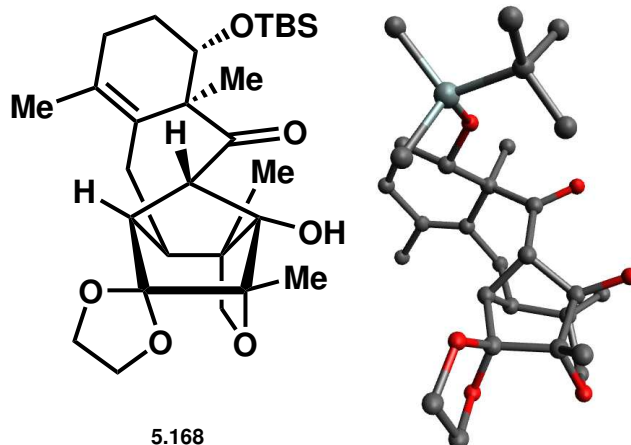
---



Table 6. Torsion angles [°] for mperea001\_sarpong.

---

## X-ray crystallographic analysis of pentacycle 5.168



A colorless needle 0.19 x 0.05 x 0.03 mm in size was mounted on a Cryoloop with Paratone oil. Data were collected in a nitrogen gas stream at 100(2) K using omega scans. Crystal-to-detector distance was 30.23 mm and exposure time was 1.42 seconds per frame at low angles and 7.00 seconds per frame at high angles using a scan width of 0.5°. Data collection was 100% complete to 74.000° in  $\theta$ . A total of 44647 reflections were collected covering the indices  $-11 \leq h \leq 9$ ,  $-9 \leq k \leq 9$ ,  $-25 \leq l \leq 25$ . 5572 reflections were founded to be symmetry independent, with an  $R_{\text{int}}$  of 0.1015. Indexing and unit cell refinement indicated a primitive, monoclinic lattice. The space group was found to be P 21 (No. 4). The data were integrated using the CrysAlis<sup>Pro</sup> 1.171.39.46e software program and scaled using the SCALE3 ABSPACK scaling algorithm. Solution by intrinsic phasing (SHELXT-2015) produced a heavy-atom phasing model consistent with the proposed structure. All non-hydrogen atoms were refined anisotropically by full-matrix least-squares (SHELXL-2014). All hydrogen atoms were placed using a riding model. Their positions were constrained relative to their parent atom using the appropriate HFIX command in SHELXL-2014.

Table 1. Crystal data and structure refinement for NRO\_III\_26\_D.

Identification code	NRO_III_26_D	
Empirical formula	C <sub>28</sub> H <sub>44</sub> O <sub>6</sub> Si	
Formula weight	504.72	
Temperature	100(2) K	
Wavelength	1.54184 Å	
Crystal system	Monoclinic	
Space group	P 21	
Unit cell dimensions	a = 9.3473(2) Å	a = 90°.
	b = 7.31740(10) Å	b = 95.153(2)°.
	c = 20.0785(3) Å	g = 90°.
Volume	1367.78(4) Å <sup>3</sup>	
Z	2	
Density (calculated)	1.226 Mg/m <sup>3</sup>	
Absorption coefficient	1.073 mm <sup>-1</sup>	
F(000)	548	
Crystal size	0.190 x 0.050 x 0.030 mm <sup>3</sup>	
Theta range for data collection	4.422 to 74.457°.	
Index ranges	-11 ≤ h ≤ 9, -9 ≤ k ≤ 9, -25 ≤ l ≤ 25	
Reflections collected	44647	
Independent reflections	5572 [R(int) = 0.1015]	
Completeness to theta = 74.000°	100.0 %	
Absorption correction	Semi-empirical from equivalents	
Max. and min. transmission	1.00000 and 0.53685	
Refinement method	Full-matrix least-squares on F <sup>2</sup>	
Data / restraints / parameters	5572 / 1 / 329	
Goodness-of-fit on F <sup>2</sup>	1.116	
Final R indices [I > 2σ(I)]	R1 = 0.0662, wR2 = 0.1848	
R indices (all data)	R1 = 0.0693, wR2 = 0.1893	
Absolute structure parameter	0.03(5)	
Extinction coefficient	n/a	
Largest diff. peak and hole	0.502 and -0.249 e.Å <sup>-3</sup>	

Table 2. Atomic coordinates ( $\times 10^4$ ) and equivalent isotropic displacement parameters ( $\text{\AA}^2 \times 10^3$ ) for nro\_iii\_26\_d.  $U(\text{eq})$  is defined as one third of the trace of the orthogonalized  $U^{ij}$  tensor.

	x	y	z	$U(\text{eq})$
C(1)	7108(4)	6180(5)	3991(2)	30(1)
C(2)	5799(4)	5941(5)	3497(2)	29(1)
C(3)	4683(4)	4681(5)	3784(2)	31(1)
C(4)	3266(4)	4582(6)	3296(2)	34(1)
C(5)	3247(4)	5866(6)	2710(2)	32(1)
C(6)	2539(4)	7457(6)	2659(2)	34(1)
C(7)	2629(5)	8779(6)	2084(2)	37(1)
C(8)	3629(4)	8219(6)	1550(2)	36(1)
C(9)	4789(4)	6922(6)	1835(2)	35(1)
C(10)	4117(4)	5228(6)	2140(2)	32(1)
C(11)	5343(4)	3988(6)	2412(2)	31(1)
C(12)	6391(4)	4681(6)	2980(2)	31(1)
C(13)	6886(4)	3188(6)	3493(2)	32(1)
C(14)	7861(4)	4240(6)	4021(2)	32(1)
C(16)	8676(5)	8494(6)	4345(2)	37(1)
C(17)	7985(5)	7606(6)	4930(2)	37(1)
C(21)	8343(5)	5471(8)	867(3)	49(1)
C(22)	9599(6)	6275(10)	513(3)	56(1)
C(23)	7538(7)	4050(12)	418(4)	74(2)
C(24)	8969(6)	4510(8)	1507(3)	56(1)
C(25)	7918(5)	8934(7)	1737(3)	47(1)
C(26)	6498(6)	8728(11)	309(3)	64(2)
C(27)	5551(4)	2844(5)	3906(2)	33(1)
C(28)	4753(5)	1069(6)	3734(2)	39(1)
C(30)	6254(4)	2727(6)	4631(2)	35(1)
C(33)	3145(5)	4149(7)	1619(2)	39(1)
C(34)	9434(4)	4246(6)	3893(2)	37(1)
C(35)	1615(5)	8174(7)	3184(2)	41(1)
O(15)	8022(3)	7552(4)	3770(1)	33(1)
O(18)	6715(3)	6787(4)	4618(1)	34(1)
O(19)	5688(3)	6305(4)	1342(2)	37(1)

O(29)	7718(3)	3330(4)	4641(1)	35(1)
O(31)	7562(3)	1634(4)	3262(2)	37(1)
O(32)	5508(3)	2461(5)	2187(1)	39(1)
Si(20)	7085(1)	7380(2)	1075(1)	39(1)

---

Table 3. Bond lengths [Å] and angles [°] for nro\_iii\_26\_d.

---

C(1)-O(18)	1.414(5)
C(1)-O(15)	1.415(5)
C(1)-C(2)	1.514(5)
C(1)-C(14)	1.584(6)
C(2)-C(12)	1.530(5)
C(2)-C(3)	1.542(5)
C(2)-H(2)	1.0000
C(3)-C(4)	1.576(6)
C(3)-C(27)	1.577(6)
C(3)-H(3)	1.0000
C(4)-C(5)	1.505(6)
C(4)-H(4A)	0.9900
C(4)-H(4B)	0.9900
C(5)-C(6)	1.339(6)
C(5)-C(10)	1.535(5)
C(6)-C(7)	1.514(6)
C(6)-C(35)	1.515(5)
C(7)-C(8)	1.541(6)
C(7)-H(7A)	0.9900
C(7)-H(7B)	0.9900
C(8)-C(9)	1.515(6)
C(8)-H(8A)	0.9900
C(8)-H(8B)	0.9900
C(9)-O(19)	1.426(5)
C(9)-C(10)	1.541(6)
C(9)-H(9)	1.0000
C(10)-C(11)	1.523(6)
C(10)-C(33)	1.541(6)
C(11)-O(32)	1.221(5)
C(11)-C(12)	1.522(5)
C(12)-C(13)	1.544(5)
C(12)-H(12)	1.0000
C(13)-O(31)	1.400(5)
C(13)-C(14)	1.541(6)

C(13)-C(27)	1.580(5)
C(14)-O(29)	1.427(5)
C(14)-C(34)	1.515(6)
C(16)-O(15)	1.434(5)
C(16)-C(17)	1.535(6)
C(16)-H(16A)	0.9900
C(16)-H(16B)	0.9900
C(17)-O(18)	1.425(5)
C(17)-H(17A)	0.9900
C(17)-H(17B)	0.9900
C(21)-C(23)	1.529(8)
C(21)-C(24)	1.535(8)
C(21)-C(22)	1.542(7)
C(21)-Si(20)	1.896(6)
C(22)-H(22A)	0.9800
C(22)-H(22B)	0.9800
C(22)-H(22C)	0.9800
C(23)-H(23A)	0.9800
C(23)-H(23B)	0.9800
C(23)-H(23C)	0.9800
C(24)-H(24A)	0.9800
C(24)-H(24B)	0.9800
C(24)-H(24C)	0.9800
C(25)-Si(20)	1.866(5)
C(25)-H(25A)	0.9800
C(25)-H(25B)	0.9800
C(25)-H(25C)	0.9800
C(26)-Si(20)	1.867(6)
C(26)-H(26A)	0.9800
C(26)-H(26B)	0.9800
C(26)-H(26C)	0.9800
C(27)-C(28)	1.522(6)
C(27)-C(30)	1.545(5)
C(28)-H(28A)	0.9800
C(28)-H(28B)	0.9800
C(28)-H(28C)	0.9800

C(30)-O(29)	1.436(5)
C(30)-H(30A)	0.9900
C(30)-H(30B)	0.9900
C(33)-H(33A)	0.9800
C(33)-H(33B)	0.9800
C(33)-H(33C)	0.9800
C(34)-H(34A)	0.9800
C(34)-H(34B)	0.9800
C(34)-H(34C)	0.9800
C(35)-H(35A)	0.9800
C(35)-H(35B)	0.9800
C(35)-H(35C)	0.9800
O(19)-Si(20)	1.655(3)
O(31)-H(31)	0.93(7)
O(18)-C(1)-O(15)	105.6(3)
O(18)-C(1)-C(2)	111.1(3)
O(15)-C(1)-C(2)	110.6(3)
O(18)-C(1)-C(14)	113.4(3)
O(15)-C(1)-C(14)	111.7(3)
C(2)-C(1)-C(14)	104.6(3)
C(1)-C(2)-C(12)	101.2(3)
C(1)-C(2)-C(3)	111.0(3)
C(12)-C(2)-C(3)	101.0(3)
C(1)-C(2)-H(2)	114.1
C(12)-C(2)-H(2)	114.1
C(3)-C(2)-H(2)	114.1
C(2)-C(3)-C(4)	110.8(3)
C(2)-C(3)-C(27)	102.2(3)
C(4)-C(3)-C(27)	116.7(3)
C(2)-C(3)-H(3)	108.9
C(4)-C(3)-H(3)	108.9
C(27)-C(3)-H(3)	108.9
C(5)-C(4)-C(3)	114.0(3)
C(5)-C(4)-H(4A)	108.7
C(3)-C(4)-H(4A)	108.7



C(5)-C(4)-H(4B)	108.7
C(3)-C(4)-H(4B)	108.7
H(4A)-C(4)-H(4B)	107.6
C(6)-C(5)-C(4)	125.0(4)
C(6)-C(5)-C(10)	120.0(4)
C(4)-C(5)-C(10)	115.0(3)
C(5)-C(6)-C(7)	123.5(4)
C(5)-C(6)-C(35)	123.9(4)
C(7)-C(6)-C(35)	112.5(4)
C(6)-C(7)-C(8)	116.1(4)
C(6)-C(7)-H(7A)	108.3
C(8)-C(7)-H(7A)	108.3
C(6)-C(7)-H(7B)	108.3
C(8)-C(7)-H(7B)	108.3
H(7A)-C(7)-H(7B)	107.4
C(9)-C(8)-C(7)	111.2(3)
C(9)-C(8)-H(8A)	109.4
C(7)-C(8)-H(8A)	109.4
C(9)-C(8)-H(8B)	109.4
C(7)-C(8)-H(8B)	109.4
H(8A)-C(8)-H(8B)	108.0
O(19)-C(9)-C(8)	112.5(3)
O(19)-C(9)-C(10)	107.9(3)
C(8)-C(9)-C(10)	110.5(3)
O(19)-C(9)-H(9)	108.6
C(8)-C(9)-H(9)	108.6
C(10)-C(9)-H(9)	108.6
C(11)-C(10)-C(5)	110.2(3)
C(11)-C(10)-C(33)	108.5(3)
C(5)-C(10)-C(33)	110.0(3)
C(11)-C(10)-C(9)	107.5(3)
C(5)-C(10)-C(9)	108.3(3)
C(33)-C(10)-C(9)	112.2(3)
O(32)-C(11)-C(12)	119.2(4)
O(32)-C(11)-C(10)	121.9(4)
C(12)-C(11)-C(10)	118.9(3)

C(11)-C(12)-C(2)	117.5(3)
C(11)-C(12)-C(13)	113.5(3)
C(2)-C(12)-C(13)	94.5(3)
C(11)-C(12)-H(12)	110.1
C(2)-C(12)-H(12)	110.1
C(13)-C(12)-H(12)	110.1
O(31)-C(13)-C(14)	112.2(3)
O(31)-C(13)-C(12)	118.1(3)
C(14)-C(13)-C(12)	103.3(3)
O(31)-C(13)-C(27)	116.5(3)
C(14)-C(13)-C(27)	99.4(3)
C(12)-C(13)-C(27)	105.0(3)
O(29)-C(14)-C(34)	108.5(3)
O(29)-C(14)-C(13)	105.8(3)
C(34)-C(14)-C(13)	114.0(3)
O(29)-C(14)-C(1)	112.1(3)
C(34)-C(14)-C(1)	115.2(3)
C(13)-C(14)-C(1)	100.9(3)
O(15)-C(16)-C(17)	103.6(3)
O(15)-C(16)-H(16A)	111.0
C(17)-C(16)-H(16A)	111.0
O(15)-C(16)-H(16B)	111.0
C(17)-C(16)-H(16B)	111.0
H(16A)-C(16)-H(16B)	109.0
O(18)-C(17)-C(16)	103.4(3)
O(18)-C(17)-H(17A)	111.1
C(16)-C(17)-H(17A)	111.1
O(18)-C(17)-H(17B)	111.1
C(16)-C(17)-H(17B)	111.1
H(17A)-C(17)-H(17B)	109.0
C(23)-C(21)-C(24)	108.2(6)
C(23)-C(21)-C(22)	110.1(5)
C(24)-C(21)-C(22)	108.2(4)
C(23)-C(21)-Si(20)	110.4(4)
C(24)-C(21)-Si(20)	110.5(3)
C(22)-C(21)-Si(20)	109.5(4)

C(21)-C(22)-H(22A)	109.5
C(21)-C(22)-H(22B)	109.5
H(22A)-C(22)-H(22B)	109.5
C(21)-C(22)-H(22C)	109.5
H(22A)-C(22)-H(22C)	109.5
H(22B)-C(22)-H(22C)	109.5
C(21)-C(23)-H(23A)	109.5
C(21)-C(23)-H(23B)	109.5
H(23A)-C(23)-H(23B)	109.5
C(21)-C(23)-H(23C)	109.5
H(23A)-C(23)-H(23C)	109.5
H(23B)-C(23)-H(23C)	109.5
C(21)-C(24)-H(24A)	109.5
C(21)-C(24)-H(24B)	109.5
H(24A)-C(24)-H(24B)	109.5
C(21)-C(24)-H(24C)	109.5
H(24A)-C(24)-H(24C)	109.5
H(24B)-C(24)-H(24C)	109.5
Si(20)-C(25)-H(25A)	109.5
Si(20)-C(25)-H(25B)	109.5
H(25A)-C(25)-H(25B)	109.5
Si(20)-C(25)-H(25C)	109.5
H(25A)-C(25)-H(25C)	109.5
H(25B)-C(25)-H(25C)	109.5
Si(20)-C(26)-H(26A)	109.5
Si(20)-C(26)-H(26B)	109.5
H(26A)-C(26)-H(26B)	109.5
Si(20)-C(26)-H(26C)	109.5
H(26A)-C(26)-H(26C)	109.5
H(26B)-C(26)-H(26C)	109.5
C(28)-C(27)-C(30)	108.9(3)
C(28)-C(27)-C(3)	117.2(3)
C(30)-C(27)-C(3)	111.3(3)
C(28)-C(27)-C(13)	114.3(3)
C(30)-C(27)-C(13)	102.4(3)
C(3)-C(27)-C(13)	101.7(3)

C(27)-C(28)-H(28A)	109.5
C(27)-C(28)-H(28B)	109.5
H(28A)-C(28)-H(28B)	109.5
C(27)-C(28)-H(28C)	109.5
H(28A)-C(28)-H(28C)	109.5
H(28B)-C(28)-H(28C)	109.5
O(29)-C(30)-C(27)	108.7(3)
O(29)-C(30)-H(30A)	110.0
C(27)-C(30)-H(30A)	110.0
O(29)-C(30)-H(30B)	110.0
C(27)-C(30)-H(30B)	110.0
H(30A)-C(30)-H(30B)	108.3
C(10)-C(33)-H(33A)	109.5
C(10)-C(33)-H(33B)	109.5
H(33A)-C(33)-H(33B)	109.5
C(10)-C(33)-H(33C)	109.5
H(33A)-C(33)-H(33C)	109.5
H(33B)-C(33)-H(33C)	109.5
C(14)-C(34)-H(34A)	109.5
C(14)-C(34)-H(34B)	109.5
H(34A)-C(34)-H(34B)	109.5
C(14)-C(34)-H(34C)	109.5
H(34A)-C(34)-H(34C)	109.5
H(34B)-C(34)-H(34C)	109.5
C(6)-C(35)-H(35A)	109.5
C(6)-C(35)-H(35B)	109.5
H(35A)-C(35)-H(35B)	109.5
C(6)-C(35)-H(35C)	109.5
H(35A)-C(35)-H(35C)	109.5
H(35B)-C(35)-H(35C)	109.5
C(1)-O(15)-C(16)	108.3(3)
C(1)-O(18)-C(17)	104.6(3)
C(9)-O(19)-Si(20)	127.3(3)
C(14)-O(29)-C(30)	107.1(3)
C(13)-O(31)-H(31)	103(4)
O(19)-Si(20)-C(25)	110.42(19)

O(19)-Si(20)-C(26)	109.6(2)
C(25)-Si(20)-C(26)	109.7(3)
O(19)-Si(20)-C(21)	104.2(2)
C(25)-Si(20)-C(21)	112.2(2)
C(26)-Si(20)-C(21)	110.5(3)

---

Symmetry transformations used to generate equivalent atoms:

Table 4. Anisotropic displacement parameters ( $\text{\AA}^2 \times 10^3$ ) for nro\_iii\_26\_d. The anisotropic displacement factor exponent takes the form:  $-2p^2 [ h^2 a^{*2} U^{11} + \dots + 2 h k a^* b^* U^{12} ]$

	U <sup>11</sup>	U <sup>22</sup>	U <sup>33</sup>	U <sup>23</sup>	U <sup>13</sup>	U <sup>12</sup>
C(1)	28(2)	33(2)	28(2)	0(1)	4(1)	-1(2)
C(2)	32(2)	29(2)	26(2)	0(1)	6(1)	-1(1)
C(3)	31(2)	34(2)	27(2)	-1(2)	7(1)	-1(2)
C(4)	29(2)	41(2)	33(2)	0(2)	7(2)	-4(2)
C(5)	25(2)	41(2)	31(2)	-2(2)	4(1)	-4(2)
C(6)	26(2)	41(2)	35(2)	0(2)	5(1)	-2(2)
C(7)	32(2)	41(2)	37(2)	1(2)	2(2)	2(2)
C(8)	33(2)	44(2)	32(2)	6(2)	2(2)	-1(2)
C(9)	29(2)	45(2)	31(2)	2(2)	7(2)	0(2)
C(10)	27(2)	41(2)	29(2)	1(2)	4(1)	0(2)
C(11)	33(2)	36(2)	27(2)	-2(2)	8(1)	-3(2)
C(12)	28(2)	37(2)	29(2)	-2(2)	5(1)	1(2)
C(13)	35(2)	31(2)	29(2)	1(1)	4(2)	5(2)
C(14)	33(2)	37(2)	27(2)	5(2)	4(2)	0(2)
C(16)	34(2)	38(2)	38(2)	-3(2)	0(2)	-5(2)
C(17)	36(2)	42(2)	32(2)	-7(2)	-2(2)	-2(2)
C(21)	31(2)	71(3)	45(2)	-13(2)	13(2)	-9(2)
C(22)	38(2)	83(4)	51(3)	0(3)	18(2)	1(3)
C(23)	46(3)	102(5)	76(4)	-51(4)	16(3)	-5(3)
C(24)	48(3)	55(3)	67(3)	-2(3)	22(3)	8(2)
C(25)	39(2)	52(3)	50(3)	-5(2)	9(2)	-2(2)
C(26)	46(3)	99(5)	48(3)	27(3)	9(2)	-6(3)
C(27)	35(2)	37(2)	28(2)	1(2)	3(1)	-2(2)
C(28)	43(2)	36(2)	37(2)	-1(2)	6(2)	-3(2)
C(30)	38(2)	37(2)	30(2)	5(2)	6(2)	-3(2)
C(33)	33(2)	48(2)	34(2)	-1(2)	1(2)	-2(2)
C(34)	31(2)	41(2)	38(2)	4(2)	4(2)	2(2)
C(35)	36(2)	43(2)	44(2)	-3(2)	11(2)	-1(2)
O(15)	33(1)	34(1)	32(1)	2(1)	4(1)	-5(1)
O(18)	35(1)	41(1)	26(1)	-4(1)	6(1)	-2(1)
O(19)	33(1)	49(2)	31(1)	-2(1)	7(1)	0(1)

O(29)	38(2)	39(1)	28(1)	5(1)	2(1)	-2(1)
O(31)	42(2)	37(1)	33(1)	-1(1)	6(1)	5(1)
O(32)	42(2)	39(1)	37(1)	-7(1)	3(1)	1(1)
Si(20)	30(1)	56(1)	31(1)	3(1)	5(1)	-2(1)

---

Table 5. Hydrogen coordinates ( $\times 10^4$ ) and isotropic displacement parameters ( $\text{\AA}^2 \times 10^3$ ) for nro\_iii\_26\_d.

	x	y	z	U(eq)
H(2)	5391	7114	3308	35
H(3)	4445	5178	4224	37
H(4A)	3145	3316	3126	41
H(4B)	2437	4863	3552	41
H(7A)	2956	9976	2271	44
H(7B)	1650	8952	1862	44
H(8A)	3056	7621	1172	44
H(8B)	4080	9324	1376	44
H(9)	5399	7569	2195	41
H(12)	7242	5258	2796	37
H(16A)	8464	9819	4319	44
H(16B)	9730	8316	4390	44
H(17A)	8628	6676	5155	44
H(17B)	7751	8534	5263	44
H(22A)	9227	6826	87	84
H(22B)	10278	5300	429	84
H(22C)	10090	7211	798	84
H(23A)	6808	3455	664	111
H(23B)	8218	3132	282	111
H(23C)	7073	4653	20	111
H(24A)	9526	5388	1794	83
H(24B)	9596	3508	1391	83
H(24C)	8185	4020	1747	83
H(25A)	7255	9938	1808	70
H(25B)	8816	9431	1596	70
H(25C)	8119	8249	2154	70
H(26A)	5973	7930	-20	96
H(26B)	7342	9234	119	96
H(26C)	5869	9727	427	96
H(28A)	4399	1073	3259	58



H(28B)	3939	957	4007	58
H(28C)	5406	33	3825	58
H(30A)	5724	3510	4927	41
H(30B)	6222	1452	4794	41
H(33A)	3694	3808	1245	58
H(33B)	2326	4911	1454	58
H(33C)	2795	3043	1826	58
H(34A)	9983	4948	4245	55
H(34B)	9543	4805	3457	55
H(34C)	9792	2987	3895	55
H(35A)	604	7902	3049	61
H(35B)	1742	9499	3229	61
H(35C)	1899	7585	3614	61
H(31)	7020(70)	1380(100)	2860(40)	59(18)

---

Table 6. Torsion angles [°] for nro\_iii\_26\_d.

---

O(18)-C(1)-C(2)-C(12)	-160.5(3)
O(15)-C(1)-C(2)-C(12)	82.5(4)
C(14)-C(1)-C(2)-C(12)	-37.8(3)
O(18)-C(1)-C(2)-C(3)	-54.0(4)
O(15)-C(1)-C(2)-C(3)	-170.9(3)
C(14)-C(1)-C(2)-C(3)	68.7(4)
C(1)-C(2)-C(3)-C(4)	174.8(3)
C(12)-C(2)-C(3)-C(4)	-78.5(4)
C(1)-C(2)-C(3)-C(27)	-60.2(4)
C(12)-C(2)-C(3)-C(27)	46.5(3)
C(2)-C(3)-C(4)-C(5)	-6.3(5)
C(27)-C(3)-C(4)-C(5)	-122.7(4)
C(3)-C(4)-C(5)-C(6)	-102.0(4)
C(3)-C(4)-C(5)-C(10)	78.4(4)
C(4)-C(5)-C(6)-C(7)	175.5(4)
C(10)-C(5)-C(6)-C(7)	-4.9(6)
C(4)-C(5)-C(6)-C(35)	-1.7(6)
C(10)-C(5)-C(6)-C(35)	178.0(4)
C(5)-C(6)-C(7)-C(8)	-1.4(6)
C(35)-C(6)-C(7)-C(8)	176.1(4)
C(6)-C(7)-C(8)-C(9)	-24.7(5)
C(7)-C(8)-C(9)-O(19)	177.0(3)
C(7)-C(8)-C(9)-C(10)	56.3(5)
C(6)-C(5)-C(10)-C(11)	152.8(4)
C(4)-C(5)-C(10)-C(11)	-27.5(5)
C(6)-C(5)-C(10)-C(33)	-87.6(4)
C(4)-C(5)-C(10)-C(33)	92.1(4)
C(6)-C(5)-C(10)-C(9)	35.4(5)
C(4)-C(5)-C(10)-C(9)	-144.9(3)
O(19)-C(9)-C(10)-C(11)	56.3(4)
C(8)-C(9)-C(10)-C(11)	179.7(3)
O(19)-C(9)-C(10)-C(5)	175.4(3)
C(8)-C(9)-C(10)-C(5)	-61.2(4)
O(19)-C(9)-C(10)-C(33)	-62.9(4)

C(8)-C(9)-C(10)-C(33)	60.5(4)
C(5)-C(10)-C(11)-O(32)	125.7(4)
C(33)-C(10)-C(11)-O(32)	5.2(5)
C(9)-C(10)-C(11)-O(32)	-116.4(4)
C(5)-C(10)-C(11)-C(12)	-54.4(4)
C(33)-C(10)-C(11)-C(12)	-174.9(3)
C(9)-C(10)-C(11)-C(12)	63.5(4)
O(32)-C(11)-C(12)-C(2)	-146.2(4)
C(10)-C(11)-C(12)-C(2)	33.8(5)
O(32)-C(11)-C(12)-C(13)	-37.4(5)
C(10)-C(11)-C(12)-C(13)	142.7(3)
C(1)-C(2)-C(12)-C(11)	175.5(3)
C(3)-C(2)-C(12)-C(11)	61.2(4)
C(1)-C(2)-C(12)-C(13)	56.0(3)
C(3)-C(2)-C(12)-C(13)	-58.3(3)
C(11)-C(12)-C(13)-O(31)	58.1(4)
C(2)-C(12)-C(13)-O(31)	-179.2(3)
C(11)-C(12)-C(13)-C(14)	-177.4(3)
C(2)-C(12)-C(13)-C(14)	-54.8(3)
C(11)-C(12)-C(13)-C(27)	-73.7(4)
C(2)-C(12)-C(13)-C(27)	49.0(3)
O(31)-C(13)-C(14)-O(29)	-82.7(4)
C(12)-C(13)-C(14)-O(29)	149.0(3)
C(27)-C(13)-C(14)-O(29)	41.0(4)
O(31)-C(13)-C(14)-C(34)	36.4(5)
C(12)-C(13)-C(14)-C(34)	-91.9(4)
C(27)-C(13)-C(14)-C(34)	160.1(3)
O(31)-C(13)-C(14)-C(1)	160.4(3)
C(12)-C(13)-C(14)-C(1)	32.2(3)
C(27)-C(13)-C(14)-C(1)	-75.8(3)
O(18)-C(1)-C(14)-O(29)	12.4(5)
O(15)-C(1)-C(14)-O(29)	131.6(3)
C(2)-C(1)-C(14)-O(29)	-108.8(3)
O(18)-C(1)-C(14)-C(34)	-112.3(4)
O(15)-C(1)-C(14)-C(34)	6.9(5)
C(2)-C(1)-C(14)-C(34)	126.6(3)

O(18)-C(1)-C(14)-C(13)	124.5(3)
O(15)-C(1)-C(14)-C(13)	-116.3(3)
C(2)-C(1)-C(14)-C(13)	3.3(3)
O(15)-C(16)-C(17)-O(18)	-19.7(4)
C(2)-C(3)-C(27)-C(28)	-139.7(3)
C(4)-C(3)-C(27)-C(28)	-18.7(5)
C(2)-C(3)-C(27)-C(30)	94.0(3)
C(4)-C(3)-C(27)-C(30)	-145.0(3)
C(2)-C(3)-C(27)-C(13)	-14.4(3)
C(4)-C(3)-C(27)-C(13)	106.6(3)
O(31)-C(13)-C(27)-C(28)	-27.3(5)
C(14)-C(13)-C(27)-C(28)	-147.9(3)
C(12)-C(13)-C(27)-C(28)	105.5(4)
O(31)-C(13)-C(27)-C(30)	90.3(4)
C(14)-C(13)-C(27)-C(30)	-30.3(4)
C(12)-C(13)-C(27)-C(30)	-136.9(3)
O(31)-C(13)-C(27)-C(3)	-154.5(3)
C(14)-C(13)-C(27)-C(3)	84.8(3)
C(12)-C(13)-C(27)-C(3)	-21.8(4)
C(28)-C(27)-C(30)-O(29)	132.7(4)
C(3)-C(27)-C(30)-O(29)	-96.5(4)
C(13)-C(27)-C(30)-O(29)	11.4(4)
O(18)-C(1)-O(15)-C(16)	25.4(4)
C(2)-C(1)-O(15)-C(16)	145.6(3)
C(14)-C(1)-O(15)-C(16)	-98.4(4)
C(17)-C(16)-O(15)-C(1)	-3.2(4)
O(15)-C(1)-O(18)-C(17)	-38.4(4)
C(2)-C(1)-O(18)-C(17)	-158.3(3)
C(14)-C(1)-O(18)-C(17)	84.2(4)
C(16)-C(17)-O(18)-C(1)	35.4(4)
C(8)-C(9)-O(19)-Si(20)	82.8(4)
C(10)-C(9)-O(19)-Si(20)	-155.0(3)
C(34)-C(14)-O(29)-C(30)	-158.5(3)
C(13)-C(14)-O(29)-C(30)	-35.8(4)
C(1)-C(14)-O(29)-C(30)	73.2(4)
C(27)-C(30)-O(29)-C(14)	14.6(4)

C(9)-O(19)-Si(20)-C(25)	27.0(4)
C(9)-O(19)-Si(20)-C(26)	-94.0(4)
C(9)-O(19)-Si(20)-C(21)	147.7(4)
C(23)-C(21)-Si(20)-O(19)	50.5(5)
C(24)-C(21)-Si(20)-O(19)	-69.2(4)
C(22)-C(21)-Si(20)-O(19)	171.8(4)
C(23)-C(21)-Si(20)-C(25)	170.0(4)
C(24)-C(21)-Si(20)-C(25)	50.3(4)
C(22)-C(21)-Si(20)-C(25)	-68.7(4)
C(23)-C(21)-Si(20)-C(26)	-67.2(5)
C(24)-C(21)-Si(20)-C(26)	173.2(4)
C(22)-C(21)-Si(20)-C(26)	54.1(5)

---

Symmetry transformations used to generate equivalent atoms: